Vol 1

STUDIES OF HETEROGENEOUS TWO PHASE FLOW IN LARGE DIAMETER HORIZONTAL PIPELINES

A thesis presented for the Degree of

Doctor of Philosophy

by

FARIS ABDUL AZIZ AL-SAMARRA'E, B.Sc., M.Sc.

Department of Thermodynamics
and Fluid Mechanics,

Mechanical Engineering Group,

UNIVERSITY OF STRATHCLYDE.

November 1977.

To my family at home

and

awrra freens 'n Glesga

ABSTRACT

The work presented in this thesis consists of two parts. The first part deals mainly with the problems associated with flow patterns, pressure drops, settling lengths, void fractions, and their prediction. The second part describes methods evolved to define flow patterns from the characteristics of the pressure and void fraction fluctuations.

A test rig was designed and constructed from transparent tubing with the main test section horizontal. The working fluids were air and water, at pressures and temperatures close to atmospheric, and the test conditions covered a range of air and water superficial velocities respectively of

0 → 28 m/s and 0 → 5.1 m/s in a 127 mm nominal bore tube.

0 → 8.6 m/s and 0 → 1.7 m/s in a 216 mm nominal bore tube.

The experimental observations indicated asymmetric flows in general with a stratification effect superimposed on the normal flow patterns. Comparison with existing flow pattern maps showed an effect of tube diameter. The inadequacies of flow pattern maps are discussed.

The experimental data relating to pressure drops and void fractions showed a strong flow pattern dependency, and correlations are presented for three main groups of flow patterns. These groups are (i) Annular Flows - incorporating annular, annular mist, rough wavy, etc. (ii) Intermittent Flows - incorporating bubble, plug and

slug, (iii) Separated Flows - incorporating stratified and smooth wavy.

Transition equations, defining the changes from one flow pattern group to another, were developed to enable predictions of flow patterns for particular sets of conditions to be made. These were essentially based on a wave stability criterion.

Comparisons were made between the experimental friction pressure drop and void fraction data and several well known correlations available in the literature. These showed poor agreement, in general.

Pressure and void fraction probes were developed and tested with the object of obtaining more objective flow pattern measurements. These were used in conjunction with a high speed data acquisition system with a view to relating the statistical behaviour of the pressure and void fraction fluctuations to flow patterns. The results confirm the usefulness of these probes for this purpose.

TABLE OF CONTENTS

ACKNOWLEDGEMENTS

The author wishes to express his sincere thanks and gratitude to Professor Hugh C. Simpson, S.M., Sc.D., F.Inst.P., A.M.A.I.Ch.E., C.Eng., F.I.Mech.E., F.R.S.E., Dean, School of Mechanical, Chemical and Naval Architecture for affording the opportunity to conduct this work in his Department and for his critical discussion and advice during the development of the theoretical models. The author has greatly benefited from being associated with Professor Simpson and from his methods of approach to scientific and engineering problems.

The author is very much indebted to Dr. David H. Rooney, B.Sc., Ph.D., F.I.Mech.E., A.R.C.S.T., C.Eng., M.I.E.D. , for his encouragement, help and advice throughout the project and also for his critical examination of the manuscript and suggested improvement. The author is grateful to have been associated with Dr. Rooney and has greatly benefited from his experience.

Thanks are also due to Mr. Edward Grattan, B.Sc., C.Eng., M.I.Mech.E., for his assistance and suggestions during the building and running of the experimental work.

The author would like to thank Dr. R.J. Henery of the Mathematics Department for his comments and advice during the development of the statistical analysis.

Thanks are also due to Mr. R.A. Crawford for his assistance in building the crystal oscillator, and also to Mr. R. Hoare for helping the author become acquainted with

the data acquisition system and for providing the various binary tapes.

The author is grateful to the technical staff of the Heat Engine and Hydraulics Laboratories who helped with the construction and testing of the experimental plant, and also to the staff and operators of the Computer Centre for their help during the development and running of the computer programs.

The author wishes to thank the Government of Iraq for the opportunity and the financial support it has given for the author's higher studies.

The author would like to thank Miss A. Whyte for tracing some of the graphs and Mrs. G. Stewart for typing the manuscript.

Thanks are due to the members of the Multiphase Research Group for showing interest and for their fruitful discussions during the group meetings.

Finally, the author wishes to thank the National Engineering Laboratory (N.E.L.) for financing the project.

LIST OF APPENDICES

LIST OF APPENDICES
(continued)

NOMENCLATURE

SYMBOL	DESCRIPTION	DIMENSION
A	c/s area of channel	m^2
A_j	c/s area of the j phase	m^2
A	dimensionless c/s area = A_j/D^2	
B	Channel width (rectangular)	m
B	parameter used in eq. (2.46)	
B_e	Band width	s^{-1}
C	velocity of sound	m/s
C_o	distribution parameter, eq. (2.87)	
D	diameter	m
D	weighting factor	
d	orifice diameter (Appendix B)	m
d	average core diameter	m
E	velocity of approach coeff. (Appendix B)	
f	friction factor = $\frac{1}{4}\lambda$	
f	frequency	s^{-1}
f_c	Nyquist frequency = 1/sampling interval	s^{-1}
F	force	
Fr	Froude No. = $\frac{U}{\sqrt{gD}}$	
G	mass velocity	Kg/m^2s
Ga	Galileo no. = $\frac{gD^3}{\nu^2}$	
g	acceleration due to gravity	m/s^2
h_j, H_j	depth of the j phase in separated flows	m
H	channel height (rectangular)	m
h	head loss (Appendix C)	

SYMBOL	DESCRIPTION	DIMENSIONS
I	γ - ray intensity	
K	flow parameter (eq. 2.79)	
L	settling length	m
L/D	settling length to diameter ratio	
M	mass flowrate	Kg/s
M	number of points averaged (Ch. 7)	
m	(orifice diameter/pipe diameter)^2 used in Appendix B	
N	total no. of points per record	
P	pressure	N/m^2
P	probability distribution function	
p	probability density function	
Q	volume flowrate	m^3/s
Q	heat input	kjoule
R	pipe radius (Appendix D)	m
Re	Reynold's no. $= \frac{UD\rho}{\mu}$	
R, R_x	auto correlation function	
R_{xy}	cross correlation function	
S	slip factor $= U_g/U_f$	
S	circumferential distance	
S, S_x	auto power density	
S_{xy}	cross power density	
t	time	s
T	period	s
T	temperature	
U	velocity	
U_j	dimensionless velocity $= U_j/U_{sj}$	

SYMBOL	DESCRIPTION	DIMENSION
U_R	relative velocity	
u	spectral window	
v	specific volume = $1/\rho$	m^3/kg
W	work	joule
We	Weber no. = $\frac{U^2 \rho D}{\sigma}$	
w	angular frequency = $2 \pi f$	rad/s
x	mass dryness fraction	
x(t)	a given time series (Ch. 7)	
x_i	the ith data point in a given record (Ch. 7)	
X	Lock.-Mart. multiplier	
y	distance measured radially from tube wall	m
Z	axial distance in the direction of motion	m
Z_R	Reynold's no. correction factor (Appendix B)	
Z_D	pipe diameter correction factor (Appendix B)	

GREEK

ρ	density	Kg/m^3
σ	surface tension	N/m
σ	standard deviation (Ch. 7)	
λ	$(\frac{\rho_g}{0.075} \frac{\rho_f}{62.3})^{\frac{1}{2}}$	
λ	friction factor = 4 f	
λ	parameter defined by eq. (2.45)	
ψ	$\frac{73}{\sigma} \left[\mu_f (\frac{62.3}{\rho_f})^2\right]^{1/3}$	
ψ	parameter defined by eq. (2.43)	

GREEK	DESCRIPTION	DIMENSION
ψ^*	$(\frac{k_{gl}}{k_{fl}})\ (\frac{\rho_{gl}}{\rho_f})\ \frac{F_{rg}}{\alpha^3}\ \left[\frac{\rho_{gl}}{\rho_{g2}}\ (\frac{1}{k_1})^2 - 1\right]$	
$\overline{\psi}$	Choe et al parameter = $(\frac{\rho_g}{\rho_f})\ (\frac{U_g}{U_f})$	
μ	viscosity	Ns/m
μ	linear absorption coefficient	
β	input volume fraction	
α	void fraction	
$\overline{\alpha}$	average void fraction using single shot method (Ch. 7)	
α_{loc}	Local void fraction using a pencil beam of γ-ray (Ch. 7)	
ϕ_f	two phase friction multiplier based on liquid flowrate alone	
ϕ_{fo}	two phase friction multiplier based on total mixture flowrate and liquid properties	
ϕ_g	two phase multiplier based on gas flowrate alone	
ϕ_{go}	two phase multiplier based on mixture flowrate and gas properties	
τ	time lag (Ch. 7)	
τ	shear stress	
ν	kinematic viscosity = $\frac{\mu_f}{\rho_f}$	
ν	slug frequency	s^{-1}
γ	Gamma ray	
γ^*	$(\frac{2}{k_{fl}})^2\ (1 - k_1)$ used in Ch. 8	
Γ	parameter used in eq. (2.82)	
θ	angle	

GREEK	DESCRIPTION	DIMENSION
δ	film thickness	
δ	channel wall thickness (Appendix E)	
ϵ	standard error	
ϵ	Expansibility factor (Appendix B)	
ϵ_o	normalised standard error	
χ^2	ki-square variable	

SUBSCRIPT	
s	superficial
g,G	gas
f,F,L	liquid
tp	two phase
t,tot	total
H	homogeneous
H	Hamming
m	mixture
m	max. lag (Ch. 7)
i	interface
loc.	local
R	relative
wf	wall friction
gr	gas relative to mixture

SUPERSCRIPT	
$\sim$	dimensionless
-	average
*	complex multiplication
*	convolution
^	estimated

FLOW PATTERN SYMBOLS	FLOW PATTERN	CODE
	Bubble	1
	Slug	2
	Stratified	3
	Annular	5
	Wavy	4
	Plug	6
T	Transition	24,62,etc.

LIST OF TABLES

I. TEXT TABLES

LIST OF TABLES (Continued)

II. APPENDICES TABLES

LIST OF FIGURES

I. TEXT FIGURES

LIST OF FIGURES (Contd)

LIST OF FIGURES (Contd)

LIST OF FIGURES

LIST OF FIGURES (Contd)

LIST OF FIGURES (Contd)

LIST OF FIGURES (Contd)

LIST OF FIGURES (Contd)

LIST OF FIGURES (Contd)

LIST OF FIGURES (Contd)

LIST OF FIGURES (Contd)

CHAPTER 1

INTRODUCTION

CHAPTER 1 INTRODUCTION

Many gaps exist in the present state of knowledge of fluid mechanics, particularly in areas such as turbulence and two-phase flow. Apart from scientific curiosity, there are strong technological demands for information in these areas and this has resulted in a rapid expansion in research over the last two decades, particularly in two phase flow.

Typical applications where two phase flow problems are encountered include boilers, condensers, water-cooled nuclear power reactors, chemical process plants, oil pipelines, etc.

Early work on two phase flow produced many correlations, often empirical, to produce a quick answer to industrial needs for design. Many were based on simulations of well established techniques used in single phase flow especially for items such as pressure drop and heat transfer evaluation.

However, the unsatisfactory nature of general correlations has been illustrated on several occasions. For example, Dukler et al (D1) compared several well known pressure drop correlations and found that an early one by Lockhart and Martinelli (L 1) was as good as any although the agreement with experiment was still not satisfactory. A similar situation arose in correlations involving heat transfer coefficients. Perhaps this is not too surprising, since it is unreasonable to expect

that the parameters which might be important in correlating, say, the heat transfer coefficient in a disturbed or turbulent two phase flow, such as bubbly flow, would also be important when the two phases flowed separately, such as a stratified type flow.

The inherent weaknesses of such techniques have led workers in the field to recognise the logical physical divisions between the various flow configurations encountered. For horizontal flows these could range from a perfectly stable, stratified flow at low liquid and gas flow rates to a homogeneous dispersion of one phase in another as in bubbly flow (high liquid and low gas flow rates) or droplet flow (high gas and low liquid flow rates). Between these flow pattern extremes, a variety of geometrical configurations are encountered which combine, to various degrees, the two properties of stratification and homogeneity.

Once the existence and variety of two phase flow patterns were recognised, it became obvious that they played a determining role in the heat, mass and momentum transfer behaviour of the flow. In addition, the occurrence of certain flow patterns under certain conditions posed serious problems to the design engineer. For example, slug flow is undesirable in a line where sudden changes in the flow direction cannot be avoided. The slug impact due to the high momentum at the point of flow direction change, can seriously fatigue equipment. Also the

formation of a dry surface in a heated horizontal tube as in wavy or stratified type flows, could result in tube overheating and failure.

This recognition of flow pattern differences and the consequent physical effects led to the requirement for prediction of the range of occurrence of the various flow patterns and their transition boundaries. Once the flow pattern was known, or specified, attention could be devoted to the development of the conservation equations for that system based on a realistic physical model that accounted for the predominant transport mechanisms of that specific pattern.

A number of flow patterns maps and correlations were constructed, mostly as a result of experimental and visual observations (e.g. S1, G1, C1), with seldom any attempt made to justify the map coordinates used. In general, none of the existing maps proved satisfactory over a wide range of two phase flow conditions and there was poor agreement between them (S1, C1). This is hardly surprising since at least 78 different flow patterns have been labelled in the literature on the basis of visual observation - an indication of the subjectiveness of the process of identification. This uncertainty in predicting flow pattern is probably the main reason why empirical type correlations are still in wide use, despite their proven inadequacy.

A flow pattern should not be completely characterised by its visual appearance only, since, even if the flow

structure may look different, the pressure drop behaviour, for example, may be the same. Hence an attempt should be made to identify such similarities and, accordingly, divide the complete flow field into a reasonable number of patterns, or regimes. A study of the flow field fluctuations, e.g. pressure or void fraction, could be a starting point which, when coupled with the average pressure gradient or void fraction, could provide the means of identifying the flow regimes and their boundaries. Indeed this constitutes one of the main objects of this project.

Most of the overall correlations for pressure drop, void fraction and flow patterns were derived from experimental data taken in small diameter tubes, usually less than 50 mm diameter. The engineer is often faced with designs involving much larger diameter tubes, etc. and, because of lack of data and correlations for such tube sizes, scaling up is usually adopted. This is a doubtful procedure since, for example, bubbles do not scale up with the tube size. Also, there is more scope for gravity forces to produce more separated type of flows such as stratified or wavy. However, no other methods are available, at present, and large errors cannot be avoided. The need for data in large diameter tubes is thus obvious, if only to check the accuracy of the existing correlations and techniques (C2). This constitutes another aspect of this project.

Settling length data in two phase flow are also

scarce. A figure of 60 diameter, which is often quoted as being the maximum settling length necessary, was based on a few visual observations only and was probably influenced by the single phase value of $\sim$ 50 diameters. Indeed, the few data available in the literature suggest longer lengths, depending on the flow rates of the individual phases (K1, S2). More data on settling lengths are required and part of this project involves such measurements. These include the settling lengths necessary after a double horizontal 90^{o} bend and after an air-water mixing device.

Finally, it is hoped that this work will make some contribution towards a better understanding of the heterogeneous character of two phase flows in general, and large diameter tubes in particular.

CHAPTER 2

LITERATURE REVIEW

CHAPTER 2 LITERATURE REVIEW

2.1 GENERAL

The literature on two phase flow is enormous as evidenced in a number of surveys published (S1, G1, G2, C3, W1, T2, H1). Thus, because of the diverse problems investigated in this project, it is unrealistic to carry out a complete survey within the size of this report. However, an attempt will be made to discuss the various problems (concentrating on physical phenomena and behaviour) and various stages of development in the field and citing the necessary references. The chapter is divided into four parts. The first part deals with flow patterns and their predictions. The second and third parts discuss the problems of pressure drop and void fraction predictions and with existing correlations. The fourth part deals with the problems of entrance effects and settling lengths.

2.2 FLOW PATTERNS

When two phases, gas and liquid are brought together and allowed to flow in a pipe, they tend to distribute themselves in a variety of geometrical configurations called flow patterns. A flow pattern is normally identified by its visual appearance and this is subject to errors of individual interpretation of such broadly defined terms as plug, slug, froth, etc. Flow pattern designations in gas-liquid flows have not yet been standardised and, as a result, a confusing variety of

classifications exist in the literature (A1, A2, C2, C4, C5, H2, K2, K3, K4, M1, S3, W2, etc.). Similar names are used to describe different flow conditions, and different names are used to describe essentially the same flow configuration (S1). A reasonably accepted classification for horizontal flows is that of Hoogendoorn (H2) which is given in Table 2-1.

The ability to predict the flow pattern present in a conduit at a given flow condition has been the target of a large number of investigations, most of which have used empirical methods to present their data and normally in the form of a flow pattern map.

2.2.1 FLOW PATTERN MAPS

These are two dimensional plots of some chosen variables assumed to represent the occurrence of the flow patterns and their transition boundaries at the specific conditions of the experiment. An area is assigned for each flow pattern according to the experimental and visual observations. Few authors give physical explanations or reasoning for using particular combinations of dimensionless numbers or flow variables as the map coordinates (C6, E2, Q1, T1, W1).

The importance of a particular force, or combination of forces, dictates the occurrence of a given flow pattern. For example, Wallis (W1) suggested that the balance between the inertia force of the gas and the buoyancy force may scale up stratification in horizontal flows. Different

Flow Pattern	Description
Plug Flow (EB)	The gas moves in bubbles or plugs along the upperside of the pipe.
Stratified Flow (ST)	The liquid flows in the lower part of the pipe and the air over it with a smooth interface.
Wavy Flow (W)	Similar to stratified flow, except for a wavy interface due to a velocity difference between the phases. Sometimes the gas velocity is so great that a certain amount of atomisation takes place.
Slug Flow (SL)	Splashes or slugs of liquid occasionally pass through the pipe with a higher velocity than the bulk of the liquid. Pressure fluctuations are typical for this type of flow.
Mist-Annular Flow (A)	The liquid is partly atomised in the gas phase and partly flowing in an annular film along the pipe wall.
Froth Flow (B)	The gas is dispersed in fine bubbles through the liquid phase.

Table 2-1 Flow Pattern Classification According to Hoogendoorn (H2)

mechanisms are involved in the different transitions and hence it is difficult to imagine that a single set of coordinates could represent adequately the conditions at which the different flow patterns or their transitions exist.

Al-Sheikh et al (A3) used the AGA-API data bank to test more than ten sets of correlations. They concluded that no single correlation can predict to any acceptable degree the boundaries of all flow patterns. The best correlations were the mass flow rates (M_g, M_f) and the Reynold's numbers (Re_g, Re_f).

The coordinates of gas volume fraction against the mixture superficial velocity used by some authors (H2, H3, K2, M1) is not convenient because an important range of flow behaviour tends to be squeezed into a small area of the plot. On the other hand maps with coordinates based on mass flow rates (A3, B2, J1, R1), or mass velocities (C6, G3, W2) without incorporating a gas density correction term lack the possibility of using it at pressure conditions different from those upon which the map was constructed. Volume flow rates are probably better but they are not general as far as tube diameter is concerned. Superficial velocities are a reasonable choice (A1, G1, M2, S4), although such terms as superficial velocity, superficial mass velocity, etc. could obscure or distort diameter effects.

Baker (B3, B4) used the data of Kosterin (K2), Berglin and Gazley (B2) and Alves (A1) to produce a flow

patterns map for horizontal flows. The map is shown in Fig. 2.1 with the lines of the Schicht (S5) map superimposed. Considerable discrepancy exists between the Backer transition lines and the data (B4). The Alves (A1) data show definite entrance effects (he was unable to obtain stratified flow because of a vertical bend in the line), and the wavy-slug transition line has a positive slope when plotted on Baker's map contrary to most data (C1).

Baker used the parameters λ and ψ combined with the mass velocities of the phases as the map coordinates in the form

$$\text{Ordinate } \frac{\rho_g \, U_{sg}}{\lambda} \quad , \quad \text{Abscissa } \frac{\rho_f}{\rho_g} \frac{U_{sf}}{U_{sg}} \lambda \psi$$

where

$$\lambda = \left[\frac{\rho_g}{.075} \frac{\rho_f}{62.3} \right]^{\frac{1}{2}} \quad , \quad \psi = \frac{73}{\sigma} \left[\mu_f \left(\frac{62.3}{\rho_f} \right)^2 \right]^{1/3} \tag{2.1}$$

The ordinate of the map is not dimensionless and does not have any physical meaning apart from the fact that it contains the term $\rho_g^{\frac{1}{2}} U_{sg}$ which represents the inertia of the gas. Wallis (W1) suggested that a dimensionless group of the form

$$U_{sg} \left(\frac{\rho_g}{gD(\rho_f - \rho_g)} \right)^{\frac{1}{2}} \simeq U_{sg} \left(\frac{\rho_g}{\rho_f \, gD} \right)^{\frac{1}{2}} \qquad \rho_g \ll \rho_f$$

may scale up stratification effects in horizontal flows. The abscissa is more complicated but can be arranged in the form

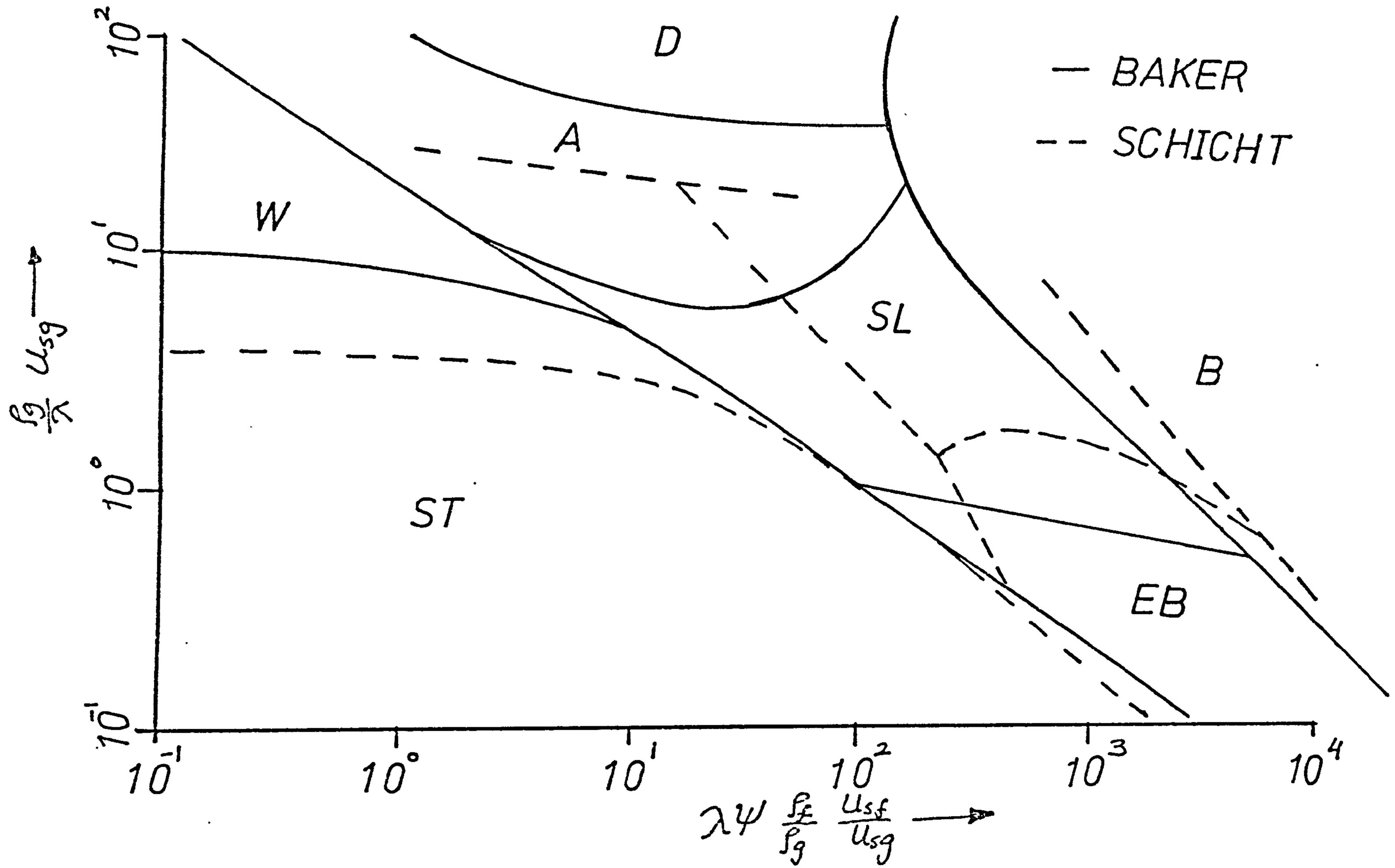

FIG. 2.1 BAKER (B3) AND SCHICHT (S5) FLOW PATTERN MAPS

$$K\ \left(\frac{U_{sf}}{U_{sg}}\right)\left(\frac{\rho_f}{\rho_g}\right)^{\frac{1}{2}} \quad \left(\frac{\mu_f\ \rho_f}{\sigma}\right)^{1/3}, \qquad K = \text{constant}$$

The first term exerts the major influence and is similar to the Martinelli parameter X if the friction factors for the gas and liquid flowing alone in the pipe are assumed equal.

Scott (S6) widened the transition boundaries to improve somewhat the agreement with Hoogendoorn (H2) and Govier and Omer (G3) data.

Reid et al (R2) observed slug flow only in their 101.6 mm (4") and 152.4 mm (6") lines while, according to Baker's map, they should have been in the annular flow region.

Schicht (S5) flow pattern data, from a 101.6 mm (4") line using air-water mixtures at atmospheric pressure (shown in Fig. 2.1), agreed with the observations of Reid et al (R2) and the transition from slug to annular flow was shifted to higher gas mass velocities and wavy flow occupied a bigger area.

The Travis and Rohsenow (T3) results for condensing flows in small diameter pipes (7.6 mm) suggested that the slug to semi-annular (assymetric annular) occurred at lower gas mass velocities. The observations suggested that pipe diameter does influence the accuracy of a map drawn to Baker's coordinates.

Deganse and Atherton (D2) pointed out that the Baker map coordinates are linearly dependent and that the

slope of any operating line* on the map is always near -1. Although this may be true for isothermal flows, it is certainly not correct for diabatic flows (boiling and condensing) since this may obscure some of the patterns that occur naturally.

The Baker map is still widely used in industry with the recommendation to work away from the transition boundaries (A4). The main reason for its publicity, so to speak, is probably the inherent flexibility of the coordinates in spite of the fact that there is no evidence that the mass velocities, or the parameters λ and ψ are the correct scaling factors.

Hoogendoorn (H2) carried out an extensive study on flow patterns and pressure drops in horizontal two phase flows and presented his results in terms of a flow pattern map, and flow pattern dependent pressure drop correlations. In general, the effects of diameter and liquid viscosity were found to be small, but noticeable on a Kosterin diagram (β vs $U_{sf} + U_{sg}$).

Hoogendoorn and Buitelaar (H3) found that such a diagram was not seriously influenced by the gas density in the range 1-12 Kg/m^3, except that atomisation occurred at lower mixture velocities for higher densities.

---

* The operating line is defined as follows:- As the two phases flow in the conduit, temperature, pressure and consequently all the physical properties change. Hence the map coordinate can be calculated for every physical situation along the conduit. By plotting these points on the map, an operating line is produced.

Eaton et al (E2) carried out experiments in 50.8 mm (2") and 101.6 mm (4") horizontal pipelines using mixtures of either water, distillate or crude oil as the liquid phase with natural gas as the gas phase. The map coordinates were developed using dimensional analysis and were a form of two phase Reynolds and Weber numbers.

Govier and Aziz (G1) suggested a revised version of the map originally produced by Govier and Omer (G3) drawn to superficial velocity coordinates.

A completely different method of flow pattern map comparison was presented recently by Mandhane et al (M2), who included the general flow pattern map for use in horizontal flows as shown in Fig. 2.2. Their comparison was made using a data bank of 5935 flow pattern observations which included the AGA-API Two Phase Flow Data Bank material augmented by data from other sources, and was statistically based. Existing flow pattern maps were evaluated using two parameters A and B defined as follows

$$A_i = \frac{\text{no. of points predicted to lie in flow pattern i}}{\text{no. of points which were observed in flow pattern i}} \times 100$$

i.e. percentage success of a given flow pattern map with respect to particular flow regime.

and

$$B = \frac{\text{total no. of observations correctly predicted to lie in their respective flow patterns}}{\text{total no. of observations}} \times 100$$

i.e. the overall percentage success for a given flow pattern map.

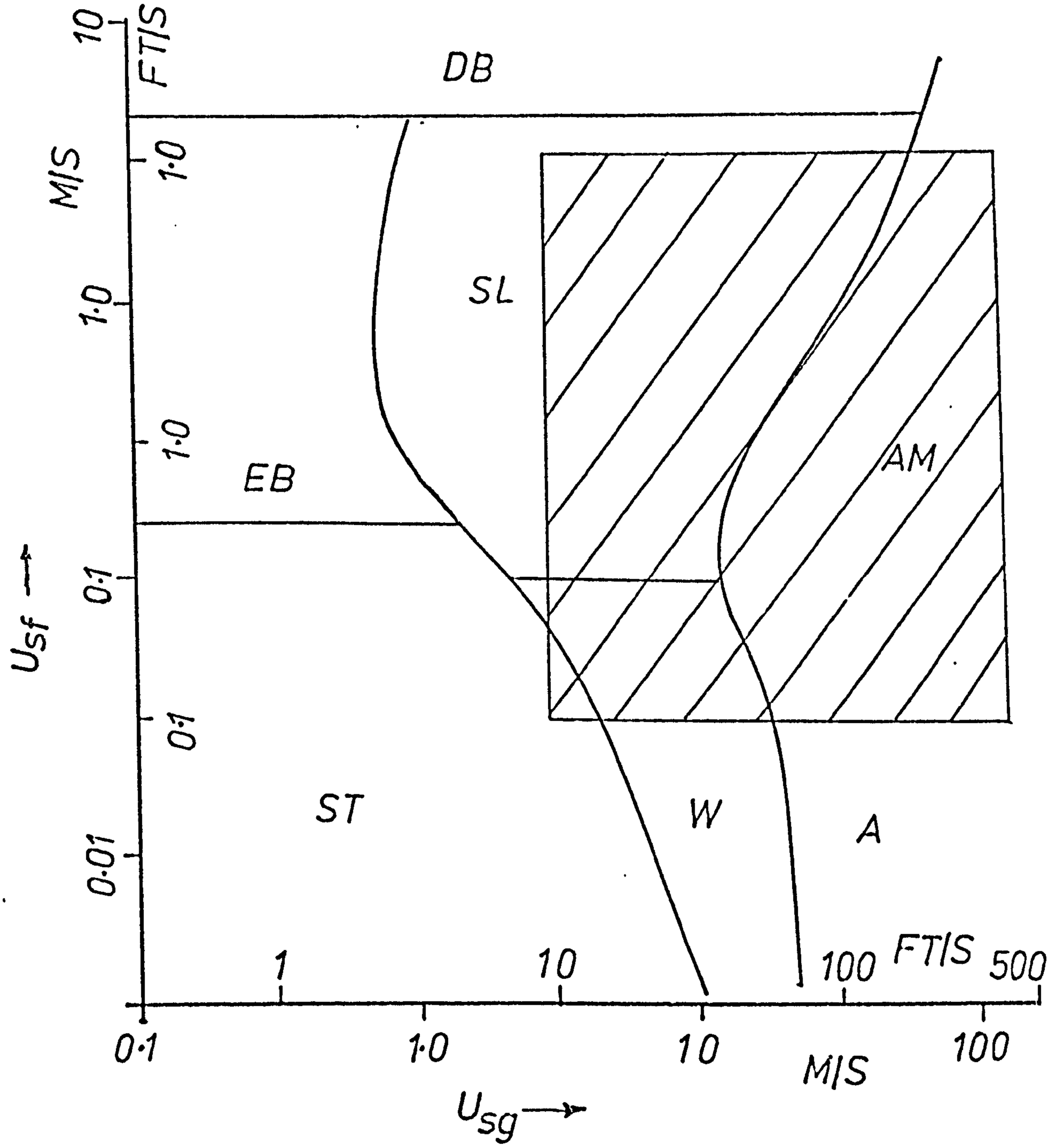

FIG. 2.2 MANDHANE et al (M2) FLOW PATTERN MAP

All the data were analysed, but in addition a separate examination was made of air-water data only (for which there were 1178 data points). In addition to their own flow pattern map, those of Baker (B3), Hoogendoorn (H2) and revised Govier and Omer (G1) were selected for comparison. The results are given in Tables 2-2 and 2-3 for air-water data and all data respectively. Also shown in Fig. 2.3 are the lines of Baker and Hoogendoorn superimposed on Mandhane et al map. These results favour the Hoogendoorn (H2) map as the best of those considered (apart from Mandhane et al map) and indicate that flow patterns in air-water flows are much better predicted than flows in general. However, the proposed map gives the best performance which is hardly surprising since it was constructed to fit the Data Bank requirements.

This author has reservations about such methods of comparison especially when the data cover a wide range of physical parameters and properties which are not equally, or at least fairly, weighted. For example, it would be difficult to distinguish a diameter effect if only 100 large diameter data points were used against 5000 small diameter ones. In fact, some deterioration in performance was observed for large diameter tubes data.

The shaded area in Fig. 2.2 is enlarged and the results of other investigators for the transition boundaries of slug-annular flows are superimposed and shown in Fig. 2.4. The scatter is large and highlights the problem of flow pattern maps.

Flow Pattern	No. of Observations	Values of A%			
		Baker (B3)	Hoogendoorn (H2)	Govier and Omer (G1)	Proposed Map
Bubble and plug	12	58.4	91.6	58.4	83.3
Stratified	229	72.1	89.1	52.8	78.6
Wavy	162	9.9	64.2	43.2	71.6
Slug	453	49.0	57.8	73.7	79.7
Annular-Mist	320	97.5	94.1	95.0	92.8
Dispersed bubble	2	0.0	0.0	0.0	0.0
Total	1178				
B%		61.3	74.9	71.0	81.8

Table 2-2 Comparison of Flow Pattern Maps Using Air-Water Data

Flow Pattern	No. of Observations	Values of A%			
		Baker (B3)	Hoogendoorn (H2)	Govier and Omer (G1)	Proposed Map
Bubble and Plug	758	20.4	64.4	32.4	64.5
Stratified	397	54.7	80.9	51.6	73.0
Wavy	783	16.0	41.5	17.5	55.2
Slug	2020	24.0	58.7	63.4	73.9
Annular-mist	1746	84.7	90.5	91.0	76.9
Dispersed bubble	231	2.2	0.0	0.0	0.0
Total	5935				
B%		41.5	65.7	58.3	68.2

Table 2-3 Comparison of Flow Pattern Maps Using All Available Data

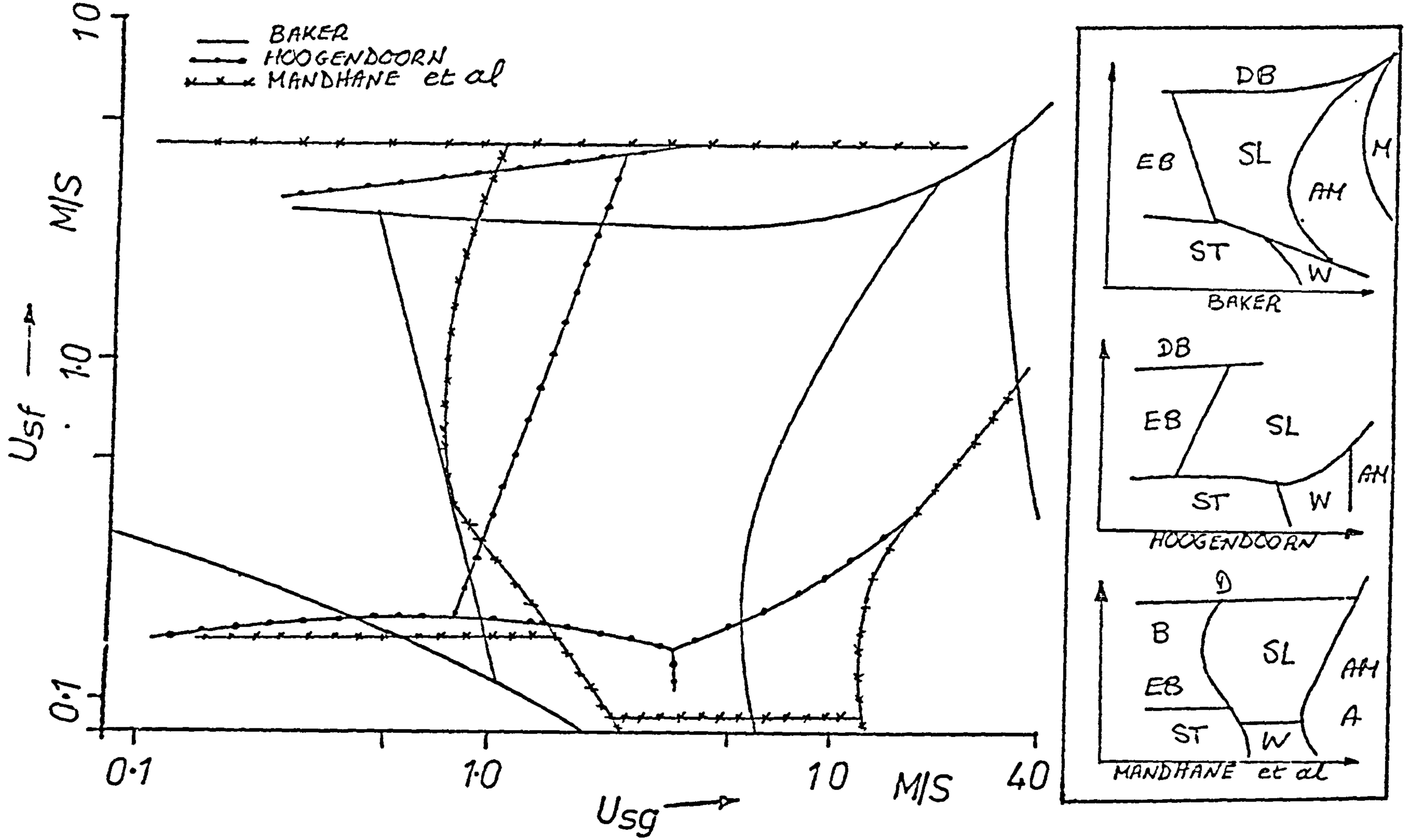

FIG. 2·3 BAKER(B3), HOOGENDOORN(H2) AND MANDHANE et al (M2) MAPS

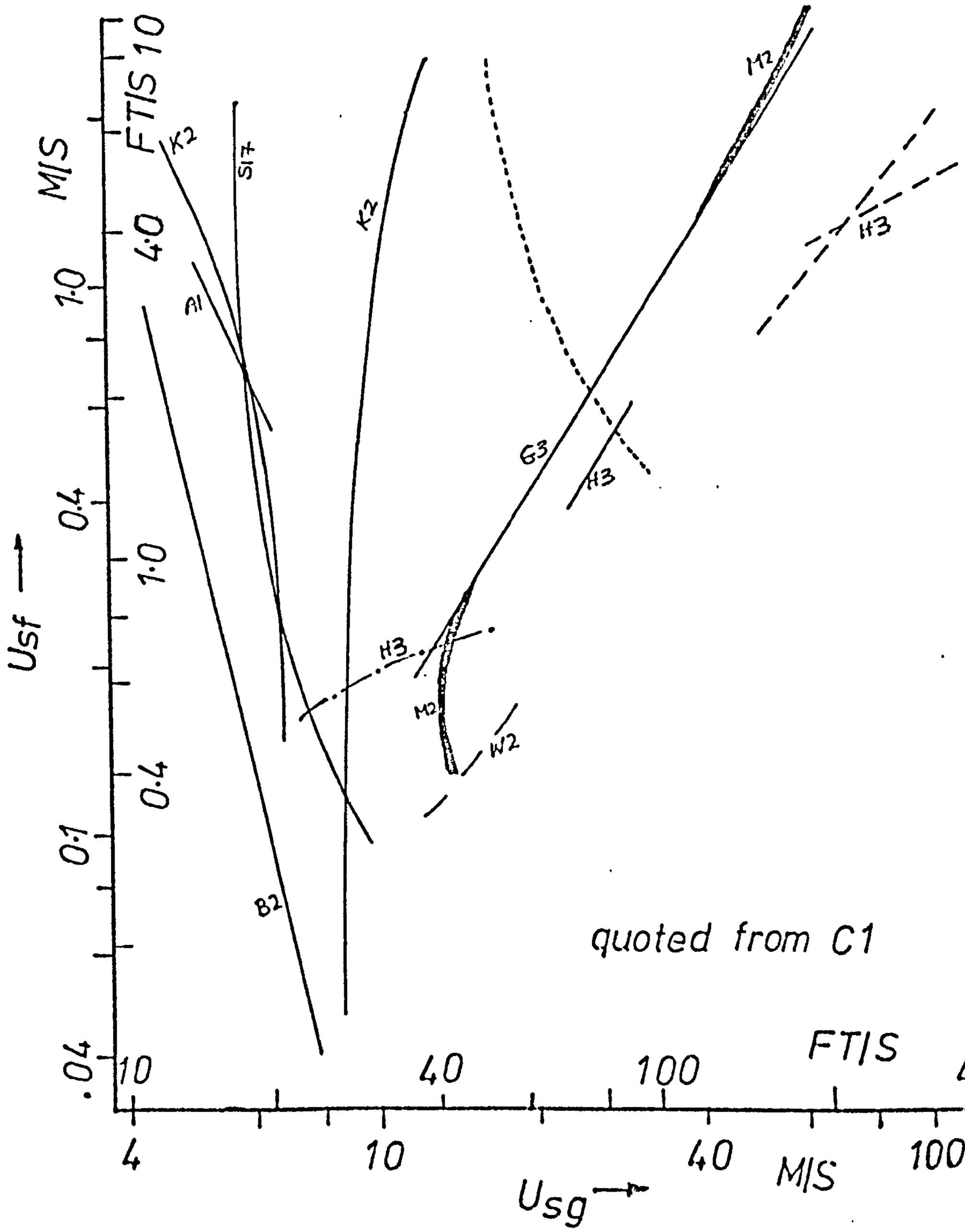

FIG. 2.4 SLUG - ANNULAR BOUNDARY

Recently, Choe et al (C6) presented a flow patterns map based on coordinates of mass velocity of each phase, using their air-water data in 12.7 mm ($\frac{1}{2}$"), 25.4 (1") and 50.8 mm (2") diameter pipe. Visual observations were supplemented by traces of pressure drop fluctuations which were used to identify slug flows. The map, shown in Fig. 2.5, is effectively a superposition of three maps, each for a given diameter, and highlights the inadequacy of the coordinates for scaling up diameter. The slug-annular boundary is shifted to higher gas mass velocities with increasing diameter in accordance with the observations of Reid et al (R2) and Schicht (S5). Fig. 2.6 is a comparison between the Mandhane et al (M2) and Choe et al (C6) maps for a 25.4 mm (1") pipe and for air-water mixtures at atmospheric pressure and 15°C. The striking feature of the comparison is the disagreement in the prediction of slug-annular boundary.

Taitel and Dukler (T1) presented a map based on the dominant force criteria. Unfortunately the most important transition i.e. slug-annular was empirically assumed to occur whenever the equilibrium liquid level in the pipe was half the tube diameter and that the flow conditions were such that slug flow would develop. Lower liquid level would result in annular flow, otherwise slug flow would develop. This disagrees with some experimental observations (R2, S5, C6).

Gould et al (G7) presented a flow pattern map for horizontal, vertical and inclined (45°) pipes based on

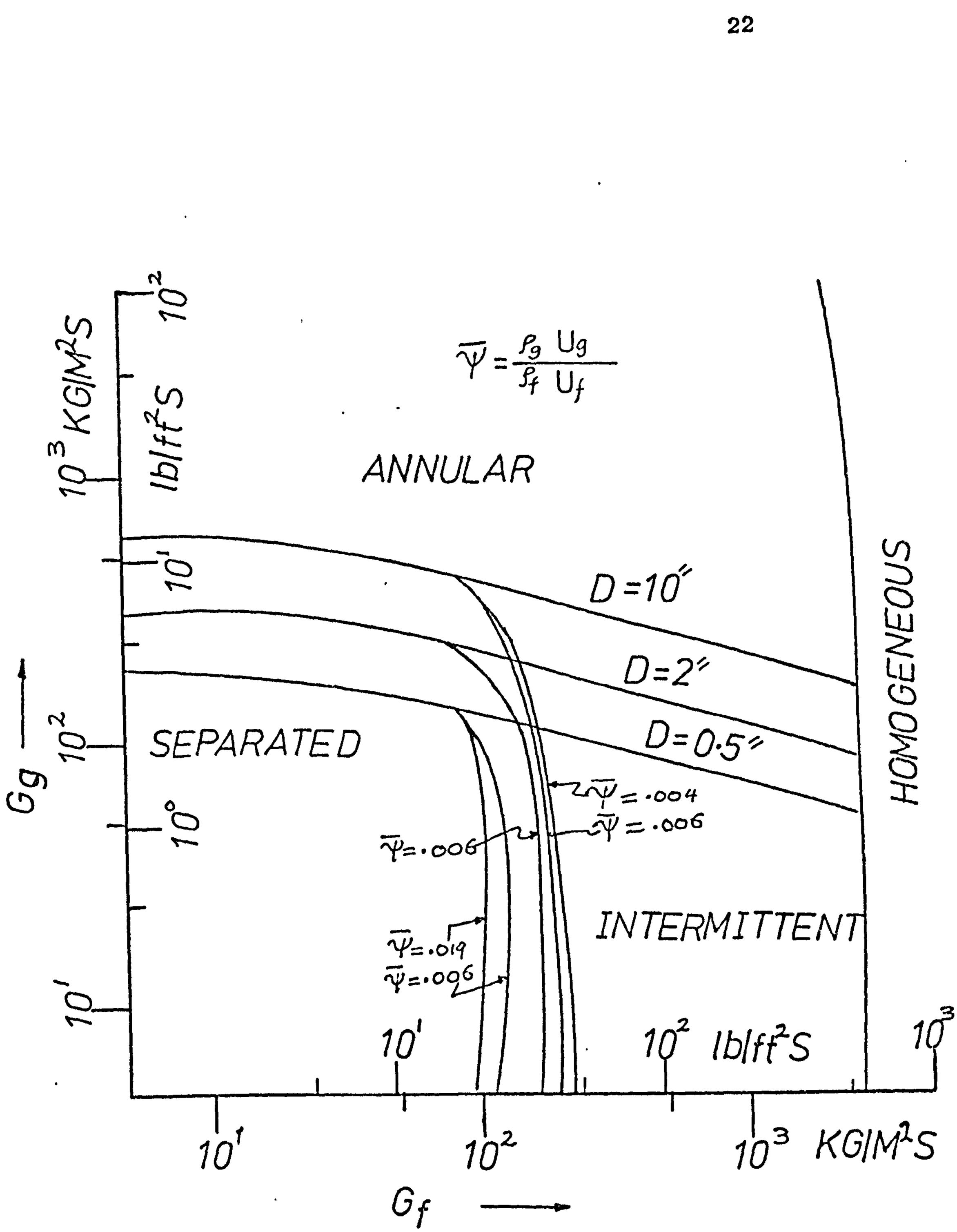

FIG·2·5 CHOE et al FLOW PATTERN MAP

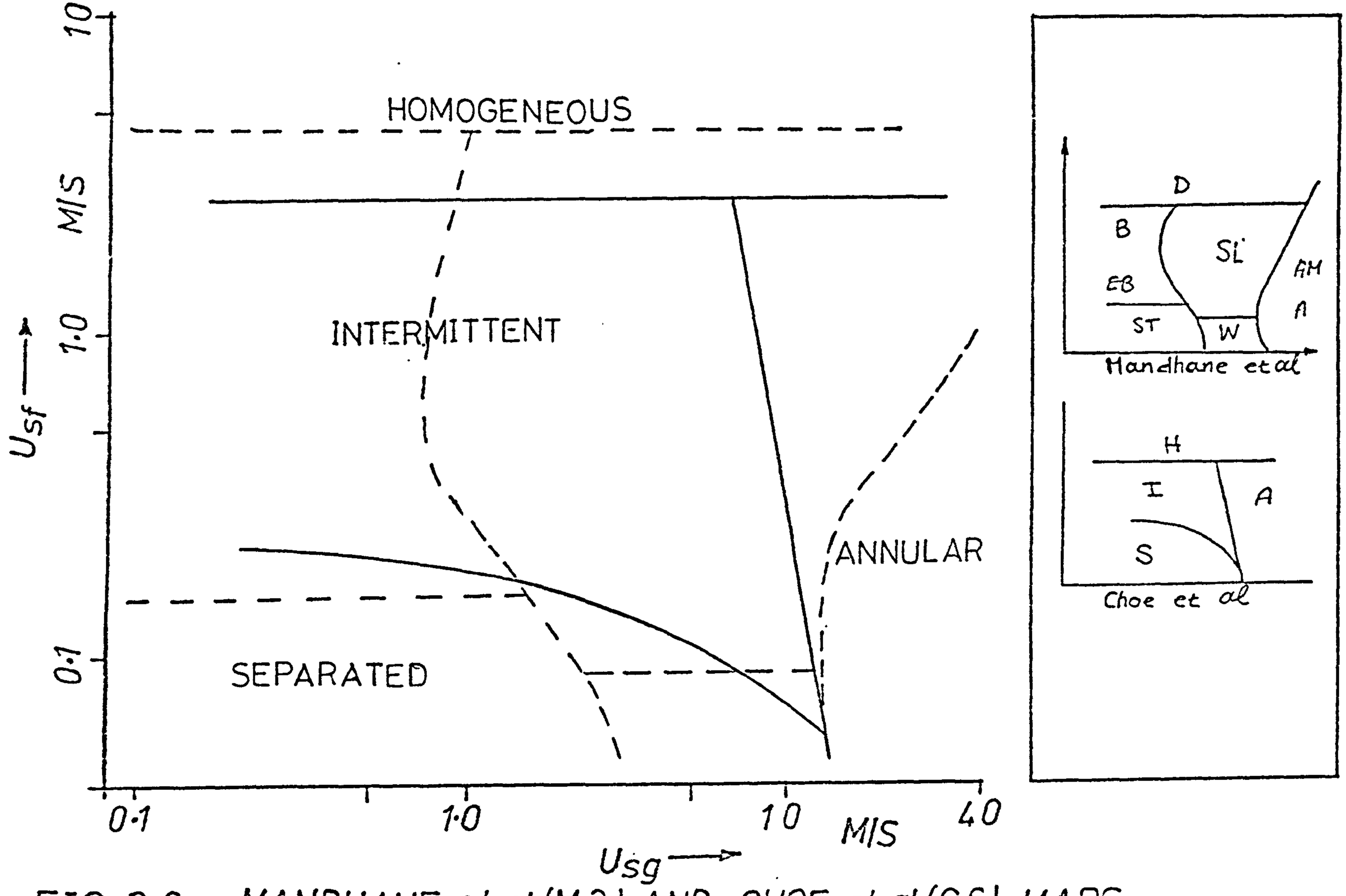

FIG. 2.6 MANDHANE et al (M2) AND CHOE et al (C6) MAPS

two dimensionless numbers which were liquid property weighted superficial velocities, i.e.

$$U_{sg}\left(\frac{\rho_f}{\sigma}\right)^{\frac{1}{4}} \quad \text{and} \quad U_{sf}\left(\frac{\rho_f}{\sigma}\right)^{\frac{1}{4}}$$

Good agreement was obtained with Hoogendoorn (H2) map if froth and slug flows, bubble and plug flows were grouped in two areas only. Their experimental results showed no significant effect of inclination on the slug-annular boundary and bubble-slug boundary, while the slug-wavy boundary was drastically affected.

Sakaguchi et al (S4) investigated steady state and transient behaviour of air-water two phase flow in horizontal pipe and proposed a flow pattern map for both cases. The tests were carried in 40 mm acrylic tubes and covered low air and water flow rates. The transient state was initiated by a step increase in either flowrate. They observed that flow patterns transition occur at lower flowrates in transient condition than in steady state condition.

In diabatic two phase flows, the flow is always transitional and a flow pattern never develops in the sense of adiabatic flows. When boiling flows are compared to adiabatic flows, the local existence of a given flow pattern is dependent on other factors such as, the heated length, heat flux, inlet subcooling temperature, etc. Hence one would expect that the flow pattern maps based on adiabatic flows data are not adequate for boiling flows. This is confirmed by the experimental results (S7, B5, H4).

Hosler (H4) and Zhan (Z1) pointed out that the Quandt (Q1) map, based on the dominant force criteria, predicted the largest fraction of the data as compared to Baker (B3) and Kozlov (K5). Flow patterns maps for boiling flows were developed, usually with the coordinates of mass velocity versus quality (S7, B5, H4, Z1) and results showed that such factors as pressure (H4, B5), heat flux (S7) heated length (S7, B5) and inlet subcooling temperature (B5) influenced the flow pattern boundaries to a certain extent. Bergles et al (B5) suggested that many of the trends in the heat flux data can be related to the flow pattern instability caused by slug flow. They also found that bubbly to slug and slug to annular transitions shift to lower qualities as pressure or mass flux increase and heated length or inlet temperature decrease.

Condensing flows, on the other hand, have only recently received some attention but the data are too sparse to draw any definite conclusions. As in boiling flows, other factors influence local flow patterns, factors such as cooling rate, inlet superheat and the condenser length. Soliman and Azer (S3, S8) could not observe stratified or bubbly flows and concluded that Baker's map was not adequate for condensing flows. Instead they developed a new flow patterns map to the coordinates of liquid velocity against gas to liquid volume fraction. They pointed out that with such coordinates they were able to correlate their data for the three diameters tested

(5-15 mm) and for the two refrigerants R12 and R113. Other coordinates such as U_{sf} vs U_{sg}, F_r vs β , G_g vs G_f and G_t vs x failed to correlate. On the other hand, Travis and Rohsenow (T3) pointed out that the modified Baker map recommended by Scott (S6) did represent their flow pattern data fairly well. More work is needed in this area.

In conclusion, it can be said that no two flow patterns maps are identical and this lack of agreement may be due to one or more of the following:

(i) Personal judgement and lack of subjectiveness in distinguishing between flow patterns. The multiple reflections, refractions, and the limited response of the human eye tend to obscure the actual appearance of the flow structure.

(ii) Not enough length allowed for the flow to develop and settle.

(iii) The transition from one flow pattern to another is gradual, making the judgement based on visual observations alone uncertain.

(iv) Flow patterns are subject to hysteresis effects (D2, F1, R1). The development of a flow pattern at a given part of the conduit is not only a function of the physical conditions there, but also of the history of the flow. The flow patterns boundaries observed with increasing flowrates may not match

those observed with decreasing flow rates, because, at the transition boundaries, instabilities of one kind or another can be present and persist over a band of flow rates.

A more realistic method of defining flow patterns may be to draw a map for each flow pattern transition, using the appropriate coordinates (Sl, C3).

2.2.2 CALCULATIONAL METHOD

Al-Sheikh et al (A3) proposed a complicated method of flow pattern prediction which required a maximum of twenty parameters to be calculated per test point. The method was unique in that

(i) a line separating two flow patterns was not drawn but rather the entire flow area considered for each pattern

(ii) different correlations were used to separate any two flow patterns

(iii) the analysis was based on a large number of data points utilizing the AGA-API Dukler data bank.

The prediction procedure utilised two major correlations i.e.

M_f vs M_g, and Re_f vs Re_g

in conjunction with another 8 auxiliary correlations.

The authors claimed accuracy of better than 5%. The method had deficiencies in that most of the data used

were taken in small diameter pipes ($\sim$25.4 mm ID) and this probably explains why one of the major correlations used was based on mass flowrates.

2.3 FLOW PATTERNS CHARACTERISATION

The transition from one flow pattern to another is gradual and hence a large number of names can be used if visual appearance alone is the discriminating criterion. A survey carried out by Strathclyde University Multi-Phase Flow Group (S1) quoted over 60 flow pattern lables for horizontal flow alone. This is hardly advantageous to the design engineer. A change in the spatial distribution of the two phases does not necessarily mean a change in the basic mechanisms by which heat, mass and momentum are transferred. It was suggested that flow pattern identification be linked to other physical and statistical phenomena of the flow through the effects it produces on such parameters as heat and mass transfer coefficients, pressure gradient and pressure fluctuations, void fraction and its fluctuation, etc. This would lead to a reduction in the number of flow patterns by grouping flow pattern names under a given category and make comparison of data from different laboratories possible with minimum uncertainty.

2.3.1 PRESSURE DROP

An early paper by Martinelli et al (M12), reporting experiments using air-water mixtures, showed that a lowering of the surface tension by adding Nekal BX resulted in different flow patterns. They indicated, however, that the

effect of flow pattern variation on pressure gradient, using the additives, was not significant. Hence they concluded that the two phase pressure drop data (in terms of friction multipliers) could be correlated without introducing flow pattern dependency. However in the discussion of a subsequent paper (L1), Gazley and Berglin pointed out that the two phase flow multiplier showed a mass velocity dependency and that sharp changes in the slope were related to changes in the flow pattern present. Armand (A2) also found horizontal flow data, when plotted as ϕ_f^2 vs $(1-\alpha)$, to fall into three distinct regions.

Baker (B3), Hoogendoorn (H2), White and Huntington (W2), Beattie (B6), etc. reported peculiar trends which were recognised as being associated with certain flow patterns.

Beattie (B6) pointed out that the two phase friction data in general could be plotted as straight lines on the log (ϕ_{fo}^2-1), log (x) plane. A transition from one flow pattern to another was indicated by a step change in the slope of the lines which could be expressed in the form

$$\phi_{fo}^2 = 1 + a\, x^b \qquad (2\text{-}2)$$

where 'x' was the quality and 'a' and 'b' were representative of the different slopes. Three groupings were identified:

(i) 'b', a multiple of 1/6

(ii) 'a', equal to (ϕ_{fo}^2-1) and $x^a = (x/x_c)^{b(G)}$ with x_c, $(\phi_{fo}^2-1)_c$ defining a common point in the plot through which all lines of different mass velocity passes.

(iii) 'b', slightly less than unity.

Plug, slug and froth flows were correlated by

$$\phi_{fo}^2 = 1 + a\, x^{5/6} \qquad (2.3)$$

where 'a' could be a function of diameter, physical properties and mass velocity. Hoogendoorn (H2) gave an expression very close to

$$\phi_{fo}^2 = 1 + 230\, x^{5/6} \qquad (2.4)$$

Wave and stratified flows could be correlated by

$$\phi_{fo}^2 = 1 + a\, x^{9/6} \qquad (2.5)$$

Annular flows showed trends that could be correlated by a form of group (iii). For high flow rates, Beattie calculated the acceleration component using the homogeneous flow model.

Baker (B3, B4) suggested similar expressions for the behaviour of the gas two phase multiplier with flow pattern, i.e.

$$\phi_g = K(G_f)\, x^n \qquad (2.6)$$

where $n \leqslant 1$ depending on the flow pattern present, K(G) was some function of liquid mass velocity. A remarkable change in the slope of one of the curves was attributed to transition from annular to slug flow in large tubes (also discussion on C7).

Hoogendoorn (H2) found that some flow patterns showed identical pressure drop behaviour and hence were correlated by one equation. These were

(i) plug, slug and froth

(ii) stratified and wavy

(iii) mist-annular.

Rooney et al (R3) suggested the presence of a flow pattern effect on the liquid two phase multiplier although no visual observations were made since the tests involved steam-water mixtures at high pressures. Based on the Baker map, three flow patterns should have been covered by the data, namely bubbly, slug and annular. The data showed two trends approximately correlated by,

$$\phi_f = \frac{C_1}{(1-\alpha)^{n_1}} \qquad 0 < \alpha < .5 \qquad (2.7)$$

and

$$\phi_f = \frac{C_2}{(1-\alpha)^{n_2}} \qquad .55 < \alpha < .9 \qquad (2.8)$$

where C_1, C_2 were constants and n_1 and n_2 functions of single phase factor and diameter.

Eaton et al (E2) claimed that no flow pattern effect was observed on their energy loss correlation. However, close examination of their curvesuggested such a dependoncy.

The mass velocity correction factors suggested by Baroczy (B7) vary with mass velocity in a rather unusual way suggesting a possible flow pattern dependency. Similar trends could be seen in the correlation proposed by Hughmark (H7).

Johannessen (J2) examined the stratified flow pattern, based on a separated flow model, and arrived at a

set of equations for the void fraction and pressure drop. His results could be correlated by C = 2 in the equation originally suggested by Chisholm and Laird (C7), i.e.

$$\phi_f^2 = 1 + \frac{C}{X} + \frac{1}{X^2} \qquad (2.9)$$

For bubbly and froth flows, the parameter C was given by

$$C = \left(\frac{\rho_f}{\rho_g}\right)^{\frac{1}{2}} + \left(\frac{\rho_g}{\rho_f}\right)^{\frac{1}{2}} \qquad (2.10)$$

Collier (C3) presented a modified Baker's map with the lines of constant C superimposed, as shown below to highlight its connection with flow patterns. He suggested

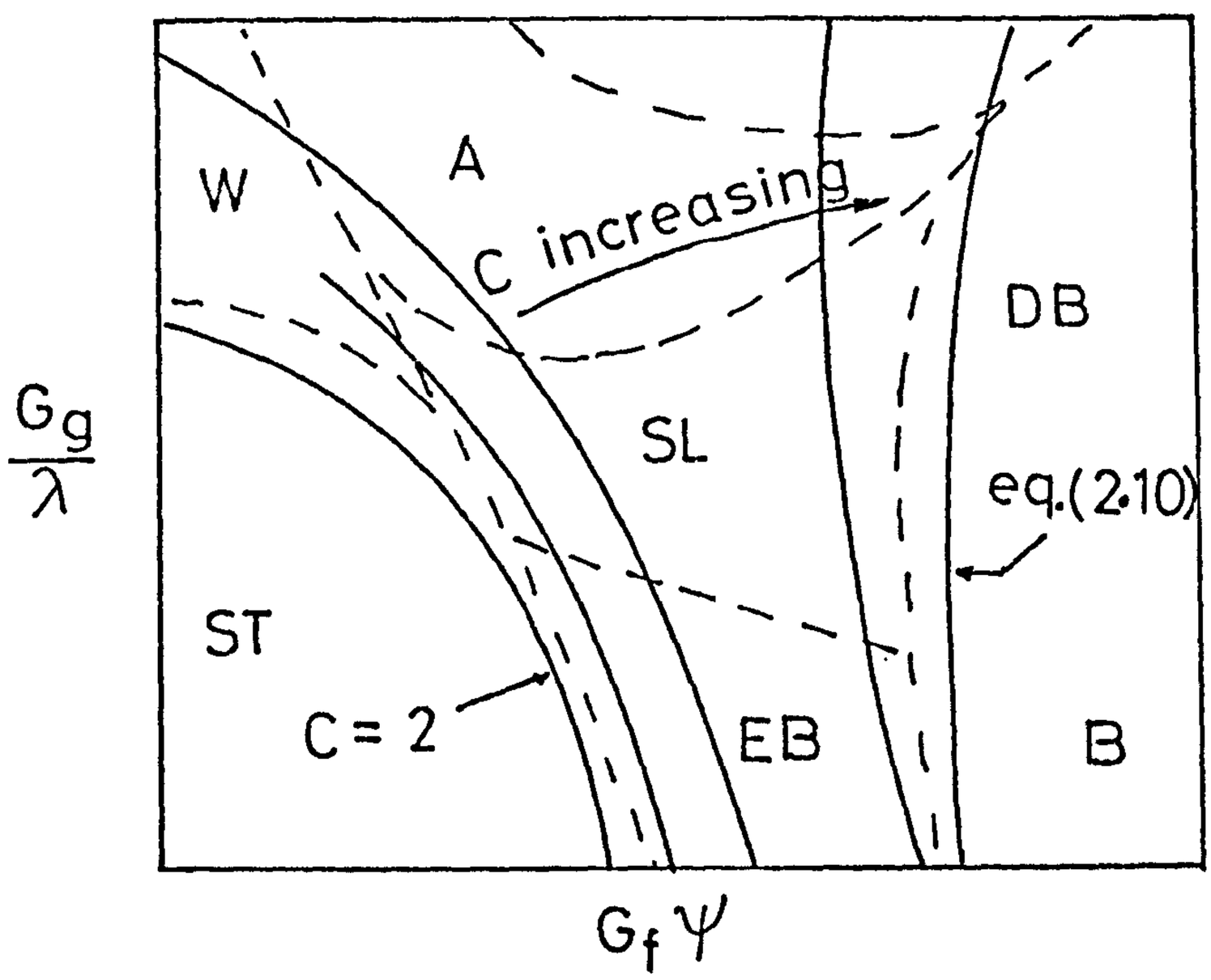

that C_2, rather than C, may prove more convenient. Chisholm and Sutherland (C8) presented an expression relating C and C_2,

$$C = \lambda + (C_2 - \lambda)\left(\frac{\rho_f - \rho_g}{\rho_f}\right)^{\frac{1}{2}}\left[\left(\frac{\rho_g}{\rho_f}\right)^{\frac{1}{2}} + \left(\frac{\rho_f}{\rho_g}\right)^{\frac{1}{2}}\right] \quad (2.11)$$

where $\lambda = 0.5(2^{2-n} - 2)$, and n was defined by a Blasius type friction factor equation.

Flow pattern effects on pressure drop in vertical flows are easier to notice (G4, R4).

Comment: the important groups of flow patterns are

(i) Plug, Slug and Froth

(ii) Wavy and Stratified

(iii) Annular.

2.3.2 VOID FRACTION

The recognition of the effect of flow pattern transitions on void fraction is quite old, although perhaps not very clear. Johnson and Abou-Sabe (J1) attributed a change in the behaviour of their liquid volume fraction data to such effects.

Chisholm (C10) developed a correlation for predicting void fraction for the flow of gas-liquid mixtures in a horizontal pipe. The data, plotted as the slip ratio against the ratio of volumetric flow rates, were found to lie in three distinct flow regimes. No information was given about the flow patterns, however a flow pattern effect cannot be ruled out.

The hold up data of Govier and Omer (G3) showed strange changes in slope when plotted against superficial gas velocity (G1). These were attributed to transitions from one flow pattern to another, namely stratified and ripply flows to wavy and annular flows.

Zuber and Findlay (Z2), in a well presented theoretical analysis, arrived at expressions relating the weighted average gas velocity to the total average velocity of the mixture through a distribution parameter C_o and a weighted mean drift velocity term. Zuber et al (Z3) observed a flow pattern effect on the distribution parameter C_o. For annular flows, C_o = 1.0, while for slug flows, C_o = 1.2. Bubbly flows showed values in the range 1.2 - 1.5. Most of their data were in vertical flows.

Graskovich et al (G5) observed that a plot of α vs β for horizontal flows showed an S-shaped structure with a big scatter. This was due to transition from slug to stratified type of flow.

Comment: the important flow patterns affecting void fractions are

(i) Stratified, Ripply

(ii) Annular and probably Wavy-misty

(iii) Slug and probably Bubbly.

2.3.3 PRESSURE WAVE PROPAGATION

It is known that the speed of acoustic waves is dependent on the density of the medium in which the wave is propagated. A two phase mixture in the simplest approach can be looked at as being a medium of variable density whose value depends on the flow structure present.

Henry et al (H5) analytically derived the following relations for the propagation velocity of the pressure waves C_{tp} in two phase horizontal flows.

For bubbly flow

$$\left(\frac{C_{tp}}{C_g}\right)^2 = \left[\alpha^2 + \frac{\alpha(1-\alpha)}{\rho_g}\ \rho_f\right]^{-1} \qquad (2.12)$$

For stratified, annular and droplet dispersed flows,

$$\left(\frac{C_{tp}}{C_g}\right)^2 = 1 + \frac{1-\alpha}{\alpha}\left(\frac{\rho_g}{\rho_f}\right) \qquad (2.13)$$

and for slug flow

$$\left(\frac{C_{tp}}{C_g}\right) = \frac{C_f}{C_f + (1-\alpha)C_g} \qquad (2.14)$$

Good agreement was found with the experimental results covering bubbly, slug and stratified flows. The suggestion that equation (2.13) was valid for annular flows is doubtful, because of the phase discontinuities present in the core. Evans et al (E3) found that, in their annular-mist, semi-annular and slug flows, the axial density in homogeneities in the core structure governed the propagation phenomena.

Comment: the important flow patterns affecting wave propagation are

(i) Bubbly

(ii) Stratificd, Wavy

(iii) Probably Annular

(iv) Slug.

2.3.4 HEAT AND MASS TRANSFER COEFFICIENTS

Two phase heat transfer coefficients are usually several times larger than the single phase ones. The introduction of gas in a flowing liquid stream causes an increase in the liquid velocity, and also an increase in the level of turbulence.

Grothuis and Hendal (G6) found that the occurrence of maxima in their two phase heat transfer coefficient was connected to transition from froth or slug flow into mist-annular flow.

Degans and Atherton (D4) pointed out that the variation in heat transfer coefficient can certainly be attributed to the flow pattern present as whether bubbly, slug, annular or mist flows.

Collier (C3) quoted the results of experiments carried out by Kodirka (K6) on the air-water heat transfer characteristics in vertical flows. Changes in the behaviour were found to coincide with transitions in flow patterns, namely bubble to slug or froth, and to annular.

Apart from a few papers, e.g. Lunde (L1), most two phase heat transfer problems were tackled by assuming models based on some particular flow pattern present (O1, H12).

The mass transfer coefficient may be expected to behave in a similar manner because the transfer mechanisms depend largely on such factors as the distribution of the phases, the interfacial interactions, etc., and hence on

the flow pattern present. Cichy and Russel (C9) emphasized such effects and attempted to develop a theoretical model based on flow patterns models.

Jepsen (J4) carried out mass transfer measurements in 25.4 mm (1") and 101.6 mm (4") horizontal pipelines near the annular-slug boundary. The data showed two distinct trends which could be attributed to flow pattern effects. Only one of the trends showed a clear diameter effects.

Comment: the important flow patterns affecting heat and mass transfer are

(i) Annular

(ii) Slug, Froth

(iii) Probably Stratified, Wavy.

(iv) Bubbly.

It is clear that flow patterns do influence the fluid mechanics, heat and mass transfer, etc. of two phase flow, and that only few major patterns, or group of patterns, appear to have such remarkable and distinguishable effects.

2.4 THE FLUCTUATING NATURE OF TWO PHASE FLOW

The presence of one phase or the other at a given point in a steady state two phase flow field fluctuates randomly, and sometimes near periodically. Accordingly, one might expect the flow variables, e.g. pressure, void fraction, mass flux, etc. to fluctuate in a similar manner. The magnitude of the fluctuations and the frequency of the

presence of each phase at a given point is dependent on the location of the point in the flow field, geometry, flow pattern, etc.

2.4.1 PRESSURE FLUCTUATIONS

It has long been recognised that certain flow patterns (e.g. slug) are accompanied by unusual, and sometimes severe, pressure pulsations. Ishagai et al (I1) indicated the importance of studying the varying component of pressure and void fraction in describing the heterogeneity of two phase flow.

Hubbard and Dukler (H6) attempted to relate the pressure fluctuations to the flow pattern present in a horizontal air-water, flow line. The character of the pressure trace was distinguished by two variables: the amplitude of the fluctuations and their frequency of occurrence. A flow pattern could then be characterized in terms of how the amplitude of the fluctuations was distributed among the existing frequencies. This involved the calculation of the power spectral distribution of the wall pressure fluctuations defined as the Fourier cosine transformation of the autocorrelation function, or

$$S(f) = \int_{-\infty}^{\infty} R(\tau)\ \mathrm{Cos}\ 2\pi f \tau\ \ dt \qquad (2.15)$$

where f is the frequency and $R(\tau)$ is the autocorrelation function of the pressure pulsations assumed random which is given by

$$R(\tau) = \lim_{T \to \infty} \int_{-T}^{+T} P(t)\, P(t+\tau)\, dt \qquad (2.16)$$

In equation (2.16), P(t) is the pressure at time t, T is the sampling time and τ is a time lag between two pressure signals which for statistical reliability should not exceed 5-10% of the sampling time (using what is known now as Blackman-Tukey method). With the aid of visual observations the flow patterns were grouped into three general classes,

(i) Separated flows: The distributions were centred about zero frequency with the amplitudes dropping off rapidly with increasing frequency. These correspond to stratified, wavy and cresting flow patterns.

(ii) Dispersed flows: The spectra showed more or less uniform distribution of power density over the entire frequency band. Bubbly and dispersed patterns lay in this grouping.

(iii) Intermittent flows: The spectra displayed sharp energy peaks at frequencies other than zero. Slug and plug were identified as belonging to this category.

Nishikawa et al (N1) studied the pressure fluctuations in vertical upward concurrent flow of air-water mixtures. The frequency distribution of static pressure showed normal distribution (single peak) for bubbly flow and nearly normal distribution for annular flow. Froth flow showed double peaked distribution while for slug flow both

normal and double peaked distributions were detected, depending on whether low or high air flowrates were involved. Definite discrimination was not possible between bubbly and annular flows.

Akagawa et al (A5) studied the pressure fluctuations which accompanied slug flow in vertical pipes. They showed quantitatively that the fluctuations of pressure drop were due to void fraction fluctuations.

Davis (D8) studied the pressure fluctuations in a heated channel using two pressure transducers. Cross-correlation technique was employed and the results indicated that the pressure fluctuations travelled at a convective velocity of 1.4-1.6 times the mixture velocity. No flow pattern observations were made.

Kutateladze et al (K7) studied the flow field fluctuations in vertical two phase flow using an electrochemical method for measuring the frictional wall shearing stress. They concluded that bubbly, slug and annular flows could be characterised by the spectral density behaviour of the fluctuations.

Comment: More effort is required to collect and analyse information on pressure pulsations to arrive at more precise and definite conclusions. Generally speaking the flow patterns which can be identified are

(i) Wavy, Stratified

(ii) Slug, plug

(iii) Bubble and Dispersed

(iv) Annular

2.4.2 VOID FRACTION FLUCTUATIONS

Void fraction fluctuations were studied by different workers in connection with different aspects of two phase flow. Among these are Neal and Bankoff (N2), Lanchme (L3) and Akagawa et al (A6). Although these studies showed the inherent unsteadiness of the flow field, no real attempt was made to relate these fluctuations to flow patterns.

Jones and Zuber (J3) were more objective when they attempted to use void fraction fluctuations to characterise three main flow patterns in vertical upward two phase flow. Such characterization depended on the behaviour of the probability density function (PDF) of the fluctuations in void fraction, defined as

$$\bar{p}(\alpha) = \frac{1}{K} \sum_{K=1}^{K} p^{K}(\alpha) \qquad K = \text{no. of runs taken} \tag{2.17}$$

where

$$p^{1}(\alpha) = \lim_{\Delta\alpha \to 0} \frac{1}{\Delta\alpha_1} \sum_{J=1}^{N} \frac{\Delta n_j}{N} \tag{2.18}$$

and N is the number of sampling intervals per run. $p^{1}(\alpha)$ is the probability that the void fraction lies inside the given interval $\Delta\alpha_1$.

For bubbly flow it was expected that the PDF would show a low void peak, while a high void peak was expected in annular flow. Slug flow would show both low and high void peaks because at one instant a given section of the pipe is full of water with some entrained bubbles and

would show a PDF characteristic of bubbly flow. The next instant the major bubble would be filling the same section of the pipe presenting a thin film on the wall and a centre core free of liquid. The result is a PDF characteristic of annular flow.

No such work was carried out for horizontal flow although the above argument could be extended to include stratified and wavy flows.

Comment:

The flow patterns which could be detected through void fraction fluctuations are:

(i) Bubbly

(ii) Slug, Plug

(iii) Annular

(iv) Stratified, Wavy

2.5.1 FLOW REGIMES IDENTIFICATION

It was shown in previous sections that the number of acceptable flow patterns could be reduced by grouping the patterns that show similar trends or behaviours into one flow area.

Gould et al (G7) recommended that the flow patterns be identified as

(i) liquid phase continuous (bubbly)

(ii) gas phase continuous (annular)

(iii) alternating phases (slug)

(iv) both phases continuous (wavy and stratified)

independent of pipe inclination. However, the 1st and

3rd patterns are common in that the phases are mixed with undefined and complex interfaces. A homogeneous model with the correct weighting of the properties may be used for such flows.

It is suggested that only two flow regimes manifest themselves in vertical two phase flows, vis.

(i) Homogeneous type flow

(ii) Annular type flow

For horizontal flows various attempts were made to reduce the number of acceptable flow patterns. Armand (A2) suggested the groups

(i) slug, plug, bubble

(ii) wavy, stratified

(iii) annular

(iv) annular-mist

Knowles (K4) suggested only three stable flow patterns. His classification was,

(i) Stratified type

a - Laminar stratified b - wave one

c - wave two d - ripple one

(ii) Slug types

a - slug one b - slug two

c - slug three

(iii) Homogeneous

a - stratified mist b - full mist

c - segregated froth d - full froth

Mandhane et al (M2) grouped bubble and plug flow into one area, also annular and annular-mist.

Dukler (D9) extended the results of Hubbard and Dukler (H6) to include annular and froth flows. Annular flow was grouped with stratified and wavy flows (both phases continuous) in what he called segregated flows. Froth flow was included in the category of homogeneous flows which was called distributed flows. The grouping of annular flow in the same area as stratified and wavy flows certainly needs examination.

It is suggested that only three flow regimes manifest themselves in horizontal two phase flows, vis

(i) Separated type flow

(ii) Homogeneous type flow

(iii) Annular type flow

This is in line with the recommendations of Simpson et al (S1), Choe et al (C6) and the findings of Hoogendoorn (H2).

2.5.2 GENERAL CRITERIA FOR FLOW REGIMES TRANSITIONS

As a starting point the flow regimes boundaries could be determined from the existing flow patterns maps by grouping the flow patterns into their respective flow regimes. In the literature, more information is given about the transition boundaries in terms of expressions based on either theoretical or empirical analysis. These are given in Table 2-4.

In two recent papers, Taitel and Dukler (T1) and Choe et al (C6) presented expressions based on experimental and/or theoretical analysis for the transitions from one

Table 2-4 Flow Pattern Transition Correlations

Transition	Correlation	Reference
bubble to plug and slug	min. water flow $\sim 4882 \frac{kg}{m^2 s}$ for onset of bubble flow.	H8
	bubble to plug $0.2 < \frac{\beta}{1-\beta} < 3.3$	
	plug to slug $\frac{\beta}{1-\beta} > 3.3$	
	Onset of dispersed bubble $G_f \sim 4296 \frac{kg}{sm^2}$	M2
	Onset of homogeneous flow $G_{tot} \sim 2712 \frac{kg}{sm^2}$	C6
	Bubble flow when $\frac{x}{1-x} = \frac{\rho_g}{\rho_f}$	Q1
	Dispersed bubble $\frac{G_{tot}}{\beta\rho_g + (1-\beta)\rho_f}$ $\simeq$ 4-6 m/s	K2
Stratified to wavy	$U_{sg} = \left[\frac{\rho_g}{g(\rho_f - \rho_g)\sigma}\right]^{\frac{1}{4}} \text{fun}(\frac{U_{sf}}{gD})$	S11
Wavy to plug and slug	$(U_g - U_f)^2 \geq \frac{\rho_f}{\rho_g} \frac{g}{K} \frac{1}{y + 0.45\, y^2}$	
	$y = \coth (K h_g - 0.9)$	K8
	K = wave number	
	h_g = depth of channel occupied by gas	

Transition	Correlation	Reference
	$1.35 \frac{U_c^2}{gh_c} \frac{\rho_g}{\rho_f - \rho_g} = 1$ U_c = average velocity at the wave crest h_c = distance from wave crest to top of channel	K9
Stratified to plug and slug	$F_r = \frac{a}{1-\beta} \left(\frac{gD^3}{\nu_f^2}\right)^{1/3}$ $a = 2.42 \times 10^{-4} - 2.33 \times 10^{-4}$ $F_r = \frac{U_H^2}{gD}$, ν_f = kinematic viscosity a = dimensionless constant	M1
	$(U_g - U_f) = 0.5 \left(\frac{gA(\rho_f - \rho_g)}{\rho_g}\right)^{\frac{1}{2}} \propto^{\frac{1}{2}}$	W3
wavy to annular	$\frac{\rho_g U_{sg}^2}{(\rho_f - \rho_g)gD} = \text{fun}\left(\frac{U_{sf}}{\sqrt{gD}}\right)$	S11
slug to annular	$F_r = \frac{(U_{sf}+U_{sg})^2}{gD} > \frac{2}{f}$ f = single phase friction factor	Q1
	for $1 - \beta \geqslant 0.06$ $\gamma^2 = \frac{\left(\frac{\partial Y}{\partial r}\right)_{r=r_m}}{Y_{r=r_m}} (1-K^2 r_m^2) \frac{\sigma}{\rho r_m^2}$	G8

Contd.

Transition	Correlation	Reference
	γ = growth coeff. in velocity potential r_m = radius to mean position of liquid-vapour interface Υ = fun(D, λ) where λ is the wavelength	
slug to froth	$\frac{D \rho_f U_{sf}(U_{sf} + U_{sg})}{\sigma} = 750$	S11
annular to mist	$F_r > \frac{2}{f_{tp}} \left(\frac{\rho_f}{\rho_m}\right)$ $F_r = \frac{U_{sf} + U_{sg}}{gD}$, $\rho_m = \left[\frac{x}{\rho_g} + \frac{1-x}{\rho_f}\right]^{-1}$	Q1
Spray to annular	$W_e = 163\ Re^{0.275}$ $We = \frac{U_m^2 \rho_m D}{\sigma}$ $\rho_m = \left[\frac{x}{\rho_g} + \frac{1-x}{\rho_f}\right]^{-1}$ $Re = \frac{U_m \rho_m D}{\mu_f}$, $U_m = U_{sf} + U_{sg}$	S3
Annular to semi-annular	For $Re_f < 50$ $Re_f = 1.38\ Ga_f^{0.31}\ Fr_f^{0.68}$ $\left[F(X_{tt})\right]^{-0.94}$	

Contd.

Transition	Correlation	Reference
	For $50 < Re_f < 1125$ $Re_f = 0.474\ Ga_f^{0.38}\ Fr_f^{0.68} \left[F(X_{tt})\right]^{-1.02}$ For $Re_f > 1125$ $Re_f = 0.0442\ Ga_f^{0.44}\ Fr_f^{0.88} \left[F(X_{tt})\right]^{-1.33}$ $Ga_f = \frac{gD^3}{\nu_f^2}$, $\nu_f = \frac{\mu_f}{\rho_f}$ $F(X_{tt}) = 0.15\left[\frac{1}{X_{tt}} + \frac{2.85}{X_{tt}^{0.476}}\right]$ $Re_f = \frac{(1-x)\ G_{tot}\ D}{\mu_f}$ $Fr_f = \frac{U_{film}}{\sqrt{g\delta}}$, δ = film thickness U_{film} = mean film velocity.	T3
Annular to annular-mist	inception of entrainment for $Re_f < 1635$ $\frac{\mu_f\ U_{sg}}{\sigma}\sqrt{\frac{\rho_g}{\rho_f}} \geqslant 11.78\ Nu^{0.8} Re_f^{-1/3}$ $Nu \leqslant 15$ $\geqslant 1.35\ Re_f^{-1/3}$, $Nu > 1/15$	

Contd.

Transition	Correlation	Reference
	For $Re_f > 1635$ $\frac{\mu_f \cdot U_{sg}}{\sigma}\sqrt{\frac{\rho_g}{\rho_f}} \geq Nu^{0.8}$, $Nu < 1/15$ ≥ 0.1146 , $Nu > 1/15$ $Nu = \frac{\mu_f}{\left[\rho_f \sigma \sqrt{\frac{\sigma}{g(\rho_f - \rho_g}}\right]^{\frac{1}{2}}}$	I2
	is a viscosity number. $Re_f = \frac{4\Gamma}{\nu_f}$, Γ = liquid volume flow rate per unit wetted perimeter	

flow regime into another. These are given in Table 2-5..

2.6 PRESSURE DROP PREDICTIONS

Previous work on pressure drop predictions can be grouped into three categories

(i) Theoretical approach

(ii) Overall empirical and semi-empirical approach

(iii) Flow pattern approach.

2.6.1 THEORETICAL APPROACH

Progress in the derivation of basic theoretical models has been slow mainly because of the complexity and unsteadiness of the flow field and the difficulty in defining boundary conditions. An added difficulty is the lack of knowledge about interfacial interactions and their contribution to the transfer processes.

One simple way to tackle the problem was to regard the mixture as a continuum of average properties, i.e. a homogeneous model, and the predictions of such models are largely dependent on the weighting precedures used. The general conservation equations are (S9, S10),

continuity

$$\frac{\partial \rho_m}{\partial t} + \frac{\partial}{\partial Z} (G_g + G_f) = 0 \qquad (2.19)$$

momentum

$$-\frac{\partial p}{\partial Z} - \frac{F}{A dZ} - g \rho_m \cos \Theta = \frac{1}{A}\left[\frac{\partial}{\partial Z} (M_g U_g + M_f U_f) + \frac{\partial}{\partial t} (M_g + M_f)\right] \qquad (2.20)$$

Table 2-5 Flow Regimes Transition Correlations

Transition	Correlation	Reference
Separated to homogeneous	$F_r^2 = \frac{1}{C^2} \frac{\tilde{U}_g^2}{\tilde{A}_g} \frac{d\tilde{A}_f}{d\tilde{h}_f} \geqslant 1$ $X > 1.6$ $F_r = \left(\frac{\rho_g}{\rho_f - \rho_g}\right)^{\frac{1}{2}} \frac{\tilde{U}_{sg}}{(Dg\cos\theta)^{\frac{1}{2}}}$ $\frac{d\tilde{A}_f}{d\tilde{h}_f} = 1 - (2\tilde{h}_f - 1)^{\frac{1}{2}}$ $\tilde{h}_f = \frac{h_f}{D}$ = dimensionless liquid level	T1
	$\left(\frac{\rho_g}{gD(\rho_f - \rho_g)}\right)^{\frac{1}{2}} \tilde{U}_{sg} = 2.5\ e^{-12(1-\alpha)} + 0.03\alpha$ or $= 4.7\alpha^{\frac{1}{4}} + 0.015$	C6
Separated to annular	$F_r^2 \frac{1}{C^2} \frac{\tilde{U}_g^2}{\tilde{A}_g} \frac{d\tilde{A}_f}{d\tilde{h}_f} \geqslant 1,$ $X < 1.6$ F_{rf}, $\frac{d\tilde{A}_f}{d\tilde{h}_f}$ and $\tilde{h}_f$ are defined above	T1
	$\left[\frac{\rho_g}{gD(\rho_f - \rho_g)}\right]^{\frac{1}{2}} \tilde{U}_{sg} = 2.5\ e^{-12(1-\alpha)} + 0.03$	C6

Contd.

Transition	Correlation	Refefence
Annular to homogeneous	provided that $F^2 \cdot \frac{1}{C^2} \frac{\tilde{U}_g^2}{\tilde{A}g} \frac{d\tilde{A}_f}{\tilde{dh}_f} \geqslant 1$ transition occurs at $X = 1.6$	T1
	onset of annular flow $G_g = 10\, G_f^{-0.285} \left(\frac{D}{D_c}\right)^{0.38}$ $D_c = 1.5$ inch	C6

energy

$$Q-W = \frac{\partial}{\partial Z}\left[M_g h_g + \tfrac{1}{2} M_g U_g^2 + M_f h_f + \tfrac{1}{2} M_f U_f^2\right] + (M_f + M_g) g \cos\Theta + \frac{\partial}{\partial t}\left[\rho_g A_g \upsilon_g + \tfrac{1}{2}\rho_g A_g U_g^2 + \rho_f A_f \upsilon_f + \tfrac{1}{2}\rho_f A_f U_f^2\right] \quad (2.21)$$

where h refers to enthalpy.

For steady state, no slip condition

$$G = \rho_m U_{Ho_m.} = \text{constant} \quad (2.22)$$

and

$$-\frac{\partial p}{\partial Z} = \frac{g\rho_m \cos\Theta + \frac{\lambda_H}{2D}\frac{G^2}{\rho_m} + G^2\left(\frac{\rho_f - \rho_g}{\rho_f \rho_g}\right)\frac{dx}{dZ}}{1 + G^2\left(x\frac{d\upsilon_{fg}}{dp} + \frac{d\upsilon_f}{dp}\right)} \quad (2.23)$$

For steady state, with slip condition

$$G = \alpha\rho_g U_g + (1-\alpha)\rho_f U_f = \text{const.} \quad (2.24)$$

and $-\frac{\partial p}{\partial Z} =$

$$g\rho_m \cos\Theta + \frac{\lambda_H}{2D}\frac{G^2}{\rho_m} + G^2\frac{dx}{dZ}\left[2\left(\frac{x}{\alpha\rho_g} - \frac{1-x}{(1-\alpha)\rho_f}\right) - \frac{d\alpha}{dx}\left(\frac{x^2}{\alpha^2\rho_g} - \frac{(1-x)^2}{(1-\alpha)^2\rho_f}\right)\right] \quad (2.25)$$

$$\frac{}{1 + G^2\left[\frac{x^2}{\alpha}\frac{d\upsilon_g}{dp} + \frac{(1-x)^2}{1-\alpha}\frac{d\upsilon_f}{dp} - \frac{d\alpha}{dp}\left(\frac{x^2}{\alpha^2\rho_g} - \frac{(1-x)^2}{(1-\alpha)^2\rho_f}\right)\right]}$$

and requires a void fraction correlation.

The above equations highlight the complexities normally encountered even after simplifications. For horizontal two component flow, neglecting compressibility and slip effects, eqs. (2.23) and (2.25) reduce to

$$-\frac{dP}{dZ} = \frac{\lambda_H}{2D} \frac{G^2}{\rho_m} \tag{2.26}$$

which is equivalent to a single phase pressure drop relationship for a fluid with density ρ_m and friction factor λ_H. The mean density can be expressed in various ways. In terms of input volume fraction,

$$\rho_m = \beta\rho_g + (1 - \beta)\ \rho_f \tag{2.27}$$

whereas in terms of quality x,

$$\frac{1}{\rho_m} = \frac{x}{\rho_g} + \frac{1 - x}{\rho_f} \tag{2.28}$$

The viscosity of the mixture is also required to enable calculating λ_H. Some common expressions for μ_m are (M3),

$$\frac{1}{\mu_m} = \frac{x}{\mu_g} + \frac{1-x}{\mu_f} \tag{2.29}$$

and (D10)

$$\mu_m = \beta\mu_g + (1 - \beta)\mu_f \tag{2.30}$$

Levy (L4) indicated that eq. (2.30) underestimated the mixture viscosity and resulted in lower pressure drop predictions. This was confirmed in a recent publication by Weisman and Choe (W4) for homogeneous flows.

The steam-water data of Rooney et al (R3) at 10-70 bars were predicted reasonably well by the homogeneous model when compared to that of Martinelli correlation (M4). The model also predicted well the data of Baldina and Petersen (B9).

More sophistication is included by adopting a separated flow model whereby each fluid may be treated separately, possibly with suitable matching or slip conditions at the interface. Here, each phase maintains its identity and properties and velocity profiles are completely independent. Separate equations are written for the conservation laws and solved simultaneously together with rate equations describing how the phases interact with each other and with the channel wall. In most cases, simplifying assumptions were introduced and still the resulting model gave encouraging results, Smith (S12), Johannessen (J2), Turner and Wallis (T4), Taitel and Dukler (T5), Agrawal et al (A9), etc.

A completely different approach was suggested by Levy (L4) and Beattie (B10) based on the application of Prantdl mixing length theory to two phase flows.

It is encouraging to see that the well established single phase flow techniques can be used to tackle some two phase flow problems, however, it is doubtful, considering the complexities of such flows, that such 'lumped model' approaches will give a satisfactory general solution.

2.6.2 EMPIRICAL AND SEMI-EMPIRICAL APPROACH

One of the earliest and now well established methods of correlating the frictional pressure drops in two phase flow system is by means of friction multipliers. If the pressure drop which would occur if either fluid was allowed to flow alone in the pipe can be calculated, then the two phase friction multipliers are given by

$$\phi_f^2 = \frac{(dP/dZ)_{tp}}{(dP/dZ)_f} \quad , \quad \phi_g^2 = \frac{(dP/dZ)_{tp}}{(dP/dZ)_g} \qquad (2.31)$$

where subscripts f, g and tp stand for fluid, gas and two phase respectively.

This method was originally suggested by Martinelli and co-workers (L1). They empirically correlated the two phase friction multipliers based on their data (taken in pipes up to 25.4 mm I.D.) in terms of the variable X (known now as the Martinelli parameter) defined as

$$X = \left(\frac{(dP/dZ)_f}{(dP/dZ)_g}\right)^{1/2} = \left(\frac{G_f}{G_g}\right)^{\frac{2-n}{2}} \left(\frac{\mu_f}{\mu_g}\right)^{\frac{n}{2}} \left(\frac{\rho_g}{\rho_f}\right)^{0.5} \qquad (2.32)$$

where n is the power of Reynolds number in a Blasius type friction factor relation.

Since the single phase pressure drop can be calculated from laminar or turbulent flow theory, for both gas and liquid, four different combinations are possible. The above definition of the two phase friction multipliers, however, cannot be used in one component flows because of the mass transfer between the phases. Instead,

Martinelli and co-workers (M4) used a more general definition based on either phase flowing alone with a mass flowrate equal to the total mass flowrate of the mixture, i.e.

$$\phi^2_{f_o} = \frac{(dP/dZ)_{tp}}{(dP/dZ)_{fo}} \quad , \quad \phi^2_{g_o} = \frac{(dP/dZ)_{tp}}{(dP/dZ)_{go}} \qquad (2.33)$$

Armand (A2) assumed a separated flow model (annular) with a 1/7th power law applicable to the liquid film and arrived at

$$\left(\frac{dP}{dZ}\right)_{tp} = \left(\frac{dP}{dZ}\right)_{f} \frac{H_1}{(1-\sqrt{\alpha})^2 (1+\frac{8}{7}\sqrt{\alpha})^{7/4}} \qquad (2.34)$$

where H_1 is a constant.

Good agreement was obtained with data (26 mm ID pipe) for $\alpha > 0.8$, as being the region of occurrence of annular flow on which the model was developed. He further suggested that the entire region of flow could be correlated by an equation of the form

$$\left(\frac{dP}{dZ}\right)_{tp} = \left(\frac{dP}{dZ}\right)_{f} \frac{H_2}{(1-\alpha)^n} \qquad (2.35)$$

with the constants H_2 and n being a function of α, or

n	H_2	range of α
1.42	1.0	$6 \leqslant \alpha < 0.65$
2.2	0.478	$0.65 \leqslant \alpha < 0.9$
1.64	1.73	$0.9 \leqslant \alpha \leqslant 0.999$

The void fraction was calculated from the input volume fraction β as

$$\alpha = 0.833\,\beta \qquad \beta \leqslant 0.9 \qquad (2.36)$$

For higher values of β, Armand recommended a more complicated expression.

Chenoweth and Martin (C11) developed an empirical correlation for their air-water data in horizontal pipes (38.1 mm and 76.2 mm ID). They presented the two phase friction multiplier in graphical form against the liquid volume fraction, with k as a parameter, or

$$\phi_{f_o}^2 = \text{fun}\ (1-\beta, k) \quad , \quad k = \frac{(dP/dZ)_{g_o}}{(dP/dZ)_{f_o}} \qquad (2.37)$$

Most of the predicted data were within 50% of the measured ones.

Chisholm and Laird (C7) and, later, Chisholm (C12,C13) proved analytically that the friction multiplier was related to Martinelli parameter by

$$\phi_{f_o}^2 = 1 + \frac{C}{X} + \frac{1}{X^2} \qquad (2.38)$$

with the following values of C predicting the Martinelli correlation curves fairly accurately

Liquid	Gas	Values of C
turbulent	turbulent	20
viscous	turbulent	12
turbulent	viscous	10
viscous	viscous	5

However, these values are only true for mixtures with gas-liquid density ratio equal to that of air-water mixtures at atmospheric pressures.

Turner and Wallis (T4) used a separate cylinder model with no interaction and no gravity effects (horizontal) to show that

$$\left(\frac{1}{\phi_f^2}\right)^{\frac{1}{n}} + \left(\frac{1}{\phi_g^2}\right)^{\frac{1}{n}} = 1 \quad , \quad 2 \leqslant n \leqslant 3.5 \qquad (2.39)$$

Wallis (W1) pointed out that good agreement with the Martinelli tt curve was obtained for n = 4.

Levy (L5) introduced a momentum exchange model based on separate phase equations and showed that the frictional and head losses of the liquid phase must equal the frictional and head losses of the vapour phase. Experimental results showed some deviations from the predictions of the model and were explained as due to non equilibrium effects.

Muscettola (M5) compared his steam-water data in horizontal pipes at pressures of 70 Kg/cm^2 with Levy's model and also with the Martinelli correlation. The former model predicted the data to within 15% for $x < 0.2$, while the latter always overestimated the data.

Bankoff (B8), by assuming the local gas and liquid velocities to be identical but with a gas concentration and velocity profiles that peaked at the centre of the tube, arrived at the following expression for the two phase friction multiplier

$$\phi_{f_o}^2 = \left[1 - \alpha\left(1 - \frac{\rho_g}{\rho_f}\right)\right]^{\frac{3}{4}} \left[1 - x\left(1 - \frac{\rho_f}{\rho_g}\right)\right]^{7/4} \qquad (2.40)$$

and the average void fraction

$$\alpha = k\beta \qquad (2.41$$

Using k = 0.89, reasonable agreement was obtained with the Martinelli correlation (M4) for qualities up to 0.6. Armand (A2) suggested a value of 0.833 for β values less than 0.9.

Thom (T6) modified and extended the Martinelli calculational procedure for the three pressure drop components for steam-water mixtures by including the density term and a constant slip factor for a given pressure.

Hughmark (H7) proposed a pressure drop correlation for horizontal and vertical two phase flow for pipe sizes up to 254 mm (10"). The correlation was based on 1379 data points but with only 163 points taken in pipes greater than 50.8 mm (2") ID. When compared with its own large diameter data, the correlation did not perform better than that of Chenoweth-Martin (C11), with the performance becoming worse on increasing diameter.

Dukler et al (D1) compared the predictions of Baker (B3), Bankoff (B8), Chenoweth-Martin (C11), Lockhart-Martinelli (L1) and Yagi (Y1) correlations against some 5000 data points carefully selected from the literature. The Martinelli correlation gave the best performance. The same group developed a semi-empirical method for pressure predictions based on a similarity analysis approach. Their results with slip (known as Dukler case II) were written as,

$$\phi_f^2 = \frac{\rho_f}{\rho_m} \lambda \psi \qquad (2.42)$$

$$\psi = \frac{\rho_f}{\rho_m} \frac{(1-\alpha)^2}{1-\beta} + \frac{\rho_g}{\rho_m} \frac{\alpha^2}{\beta} \qquad (2.43)$$

$$\rho_m = \alpha \rho_g + (1-\alpha) \rho_f \qquad (2.44)$$

$$\lambda = 1 + \frac{y}{1.281 - 0.478y + 0.444y^2 - 0.094y^3 + 0.00843y^4}$$

and (2.45)

$$y = -\ln(\alpha)$$

Using Hughmark (H9) void fraction correlation the above method gave better predictions than did the Martinelli correlation. However, the weakness of the method lay in its dependency on a void fraction correlation.

Recently, Van Thanh and Spedding (V1) re-examined the assumptions made by Dukler and showed it to be true for symmetrical systems.

It has long been recognised that the two phase friction multipliers showed a mass velocity dependency, whether two component flow (A8, B2, H2, J1, L1, P1, etc.) or one component steam-water flow (S13, M5).

Baroczy (B7) proposed a general correlation which could be used for different fluids over a wide range of mass velocities. The two phase liquid multiplier was expressed as a function of quality and a property index, i.e. $(\mu_f/\mu_g)^{0.2}$ (ρ_g/ρ_f), for a mass velocity of 1356 Kg/m^2S (10^6 lb /ft^2 hr). A correction multiplier could be obtained for mass velocities other than this value,

again in terms of quality and property index. The correlation is widely used in the American literature although only 129 points were used to develop the correlation which covered five different sets of data, mostly taken in small diameter tubes.

Eaton et al (E2) presented a pressure drop correlation based on data for crude oil-natural gas mixtures flowing in 50.8 mm (2"), 101.6 mm (4") and 431.8 mm (17") ID pipelines. The correlation was based on the total energy balance equation obtained by adding the separate energy equations of the two phases in addition to an energy loss factor correlation. An iterative procedure was suggested which required a hold up correlation in case of appreciable acceleration effects.

Chisholm (C13) suggested the following design equation for evaporating flows, viz.

$$\phi_{f_o}^2 = 1 + (\Gamma^2 - 1)\left[B\, x^{\frac{2-n}{2}}\,(1-x)^{\frac{2-n}{2}} + x^{2-n}\right] \qquad (2.46)$$

with

$$\Gamma = \left(\frac{\rho_f}{\rho_g}\right)^{0.5}\left(\frac{\mu_g}{\mu_f}\right)^{\frac{n}{2}} \quad \text{smooth tubes}$$

$$= \left(\frac{\rho_f}{\rho_g}\right)^{0.5} \quad \text{rough tubes}$$

The parameter B was given in terms of total mass velocity and a property index Γ, viz.

Γ	$G\ (kg/m^2s)$	B
$\leqslant 9.5$	$\leqslant 500$	4.8
	$500 < G < 1900$	$2400/G$
	$\geqslant 1900$	$55/G^{0.5}$
$9.5 < \Gamma < 28$	$\leqslant 600$	$520/(\Gamma G^{0.5})$
	> 600	$21/\Gamma$
$\geqslant 28$		$15000/(\Gamma^2 G^{0.5})$

These values were chosen as a compromise between Baroczy (B7), Martinelli (L1) and Chisholm and Laird (C7) such that the greatest estimate of pressure gradient was obtained. However, one of the shortcomings of this procedure is the discontinuities at $\Gamma = 9.5$ and $\Gamma = 28$.

Borshansky et al (B11) pointed out a shortcoming in using the two phase multipliers as defined by Martinelli and co-workers (M4),

$$\phi_{f_o}^2 = \frac{(dP/dZ)_{tp}}{(dP/dZ)_{fo}}$$

At zero vapour content ($x = 0$), the multiplier converges to a value equal to 1 independent of the flow variables. However, this is not true for the other extreme, i.e. zero liquid content ($x = 1$). In this case

$$\phi_{f_o}^2 = \left(\frac{\mu_g}{\mu_f}\right)^n \left(\frac{\rho_f}{\rho_g}\right) \qquad \text{smooth tubes}$$

and

$$\phi_{f_o}^2 = \left(\frac{\rho_f}{\rho_g}\right) \qquad \text{rough tubes}$$

where n is the exponent of Reynold's number in a Blasius type friction equation.

The dependence of the multiplier at the extreme condition of zero liquid content on system pressure for steam-water mixtures is given below

Pressure (atm)		1	30	70	100	150
$\phi^2_{f_o}$	rough n=0	1650	56	21	12.8	6.5
	smooth n=0.25	745	35	14	9	4.9

The authors suggested the following definition for the multiplier

$$\bar{\phi}^2_{f_o} = \frac{\Delta P_{tp} - \Delta P_{fo}}{\Delta P_{go} - \Delta P_{fo}} \qquad (2.47)$$

which gives

$$\bar{\phi}^2_{f_o} = 0 \qquad \text{at } x = 0$$

$$\bar{\phi}^2_{f_o} = 1 \qquad \text{at } x = 1$$

Alves (A4) reviewed experiences in the prediction of pressure drop in large diameter steam strippers (190 mm and 400 mm ID) and transport lines (300 mm and 4 mm ID). The pressure drop components were calculated using the Martinelli correlation (L1) for the frictional term, Hughmark and Pressberg (H10) for the static head term and Andeen and Griffith (A7) for the acceleration term. The calculated pressure drop was between -13% to + 3% from the actual one, almost too good to be true (C2).

Lawson and Brill (L6) compared the predictions of several correlations for vertical two phase flows against 729 data point from the literature on oilfields tests or tests on experimental wells only. The correlations tested were those of Poettman and Carpenter (P2), Baxandell and Thomas (B1), Duns and Ros (D11), Fancher and Brown (F2), Hagedorn and Brown (H11) and Orkiszewski (02). Each of these correlations was proposed specifically for predicting pressure losses in vertical oil well tubing for the upward flow of multiphase well fluids. No correlation performed well over the range tested, however, the Hagedorn and Brown correlation performed best.

2.6.3 FLOW PATTERN APPROACH

With the increasing doubt about the ability of the overall correlation technique to predict reasonably accurately the required design parameters, e.g. pressure drop, attention was diverted to the more sophisticated approach of using flow pattern models. The theoretical approach is still in its infancy, but steady progress has been made over the past twenty years. Empirical correlations based on flow patterns approach were used even at early stages, Baker (B3), Hoogendoorn (H2).

In this complicated approach, the two phases are considered to be arranged in one of three or more definite prescribed geometries. These geometries are based on the various configurations or flow patterns found when

gas-liquid mixtures are allowed to flow together in a pipe. The basic conservation equations are solved within the framework of each of these idealised representations. Obviously, the progress in this direction is linked to that of being able to develop a sound flow patterns map which will enable accurate predictions of the transition boundaries of each flow pattern.

In the following paragraphs, a brief indication of the state of the art is given in addition to a discussion of the flow mechanisms involved in each pattern.

(a) Separated Flows:

In such flows, interfacial interaction may be small or even negligible (stratified) with a smooth interface, or it may be appreciable giving rise to wave and ripple formation (wavy). Berglin and Gazley (B2), and Gazley (G9) presented the earliest extensive studies of such flows.

Ellis and Gay (E4) found that the air velocity profile near the interface were distorted supporting the suggestion that a rippled liquid behaves as a rough solid surface. Gazley (G9) also arrived at a similar conclusion and found that the onset of wave formation showed a sharp increase in the interfacial gas phase friction factor.

Cohen and Hanratty (C14) on the other hand pointed out that gas velocity profiles obtained over a wavy interface were different from what had been reported for

roughened solid surfaces, because of the existence of a direct exchange of mechanical energy from one phase to another in the former case.

The pressure drop is wholly frictional and yet errors as much as 200% were observed using the Martinelli correlation (L1, A9). Berglin and Gazley (B2, L1) suggested that this discrepancy was due to the presence of a hydraulic gradient in stratified flows (liquid layer decreases downstream).

Hoogendoorn (H2) recommended the following

$$\left(\frac{dP}{dZ}\right)_{tp} = C \frac{G_t^2}{2D \rho_g} x^{1.45}, \quad C \simeq 0.022 \qquad (2.48)$$

for wave flow. The parameter C was found to depend slightly on pipe diameter and liquid viscosity.

Johannessen (J2) assumed a simple separated flow model and solved for the friction multiplier and void fraction. His results predicted the data well, except at low values of the Martinelli parameter. This was attributed to the strong interaction between the phases (wavy flow) which was not accounted for in the theory.

The more recent theoretical analysis of stratified flows were carried out by Govier and Aziz (G1), Agrawal et al (A9), Russel et al (R5) and Taitel and Dukler (T5).

The first two models used empirical correlation for the interfacial shear stress and were almost identical except in the definitions of the hydraulic diameter of the liquid phase. Agrawal et al (A9) was found superior

to those of Martinelli (L1), Dukler no slip model (D10), Govier and Aziz (G1) and Etchells (E5) using data taken near atmospheric and in 25.4 mm (1") ID transparent.tube.

Russel et al (R5) developed a model for the laminar liquid flow only. The conservation equations were written for both cases (laminar and turbulent gas) and solved by an iterative procedure. The model gave better predictions than those of Martinelli (L1) and Agrawal (A9) for data taken in tubes 25.4 mm, 38.1 mm and 50.8 mm (1", 1.5" and 2") diameter using air-water and air-glycerine.

Taitel and Dukler (T5) used a simple stratified model and, by assuming that $U_f \ll U_g$, arrived at the following relationships for the two phase multipliers,

$$\phi^2_{g_o} = \frac{1}{4} \frac{f_g}{f_{sg}} \frac{\tilde{U}^2_g}{\tilde{A}_g} \left(\tilde{S}_g + \frac{f_i}{f_g} \tilde{S}_i\right) \qquad (2.49)$$

$$\phi^2_{f_o} = \frac{1}{4} \frac{\tilde{U}^2_f}{\tilde{A}_f} \frac{f_f}{f_{sf}} \tilde{S}_f - \frac{f_i}{f_{sg}} \left(\frac{\tilde{A}_f}{\tilde{A}_g}\right)^2 \frac{\tilde{S}_i}{X^2} \qquad (2.50)$$

where the tild stands for dimensionless numbers, viz.

$$\tilde{U}_j = \frac{U_j}{U_{sj}} \quad , \quad \tilde{A}_j = \frac{A_j}{D^2} \quad , \quad \tilde{S}_j = \frac{S_j}{D}$$

letter S refers to circumferential distance and subscripts i, s, to interfacial and superficial respectively.

The authors recommended that $f_i = f_g$. However Davis (D12), Smith and Tait (S14) and Kordyban (K10) found that $f_i > f_g$ always. To test the dependency of the model

on f_i, the following relationship was used

$$\frac{f_i}{f_g} = 1 + 4 \frac{h_f}{D} \qquad (2.51)$$

i.e. the interfacial friction factor increases linearly with the liquid level h_f. The results are plotted in Fig. (2.7) and clearly show such a dependency. An exact solution of the model was carried out (Appendix P) which showed the predictions to be dependent on the mixture properties. The solution was obtained by an iterative technique using a digital computer.

Recently Weisman and Choe (W4) compared the predictions of different correlations for separated flows and found that the correlation of Hoogendoorn (H2) and Agrawal et al (A9) performed best and recommended the earlier one for its simplicity.

All the models discussed so far have ignored the presence of hydraulic gradients in such flows. Although this effect could probably be ignored in small diameter pipes (frictional pressure drop is high compared to the hydraulic gradient), it may be more significant as the diameter increases and should be accounted for in the momentum equation.

(b) Annular Flows:

One of the earliest models for such flows was that of Armand (A2). Levy (L7), however was the first to present a rather complete analysis of the horizontal

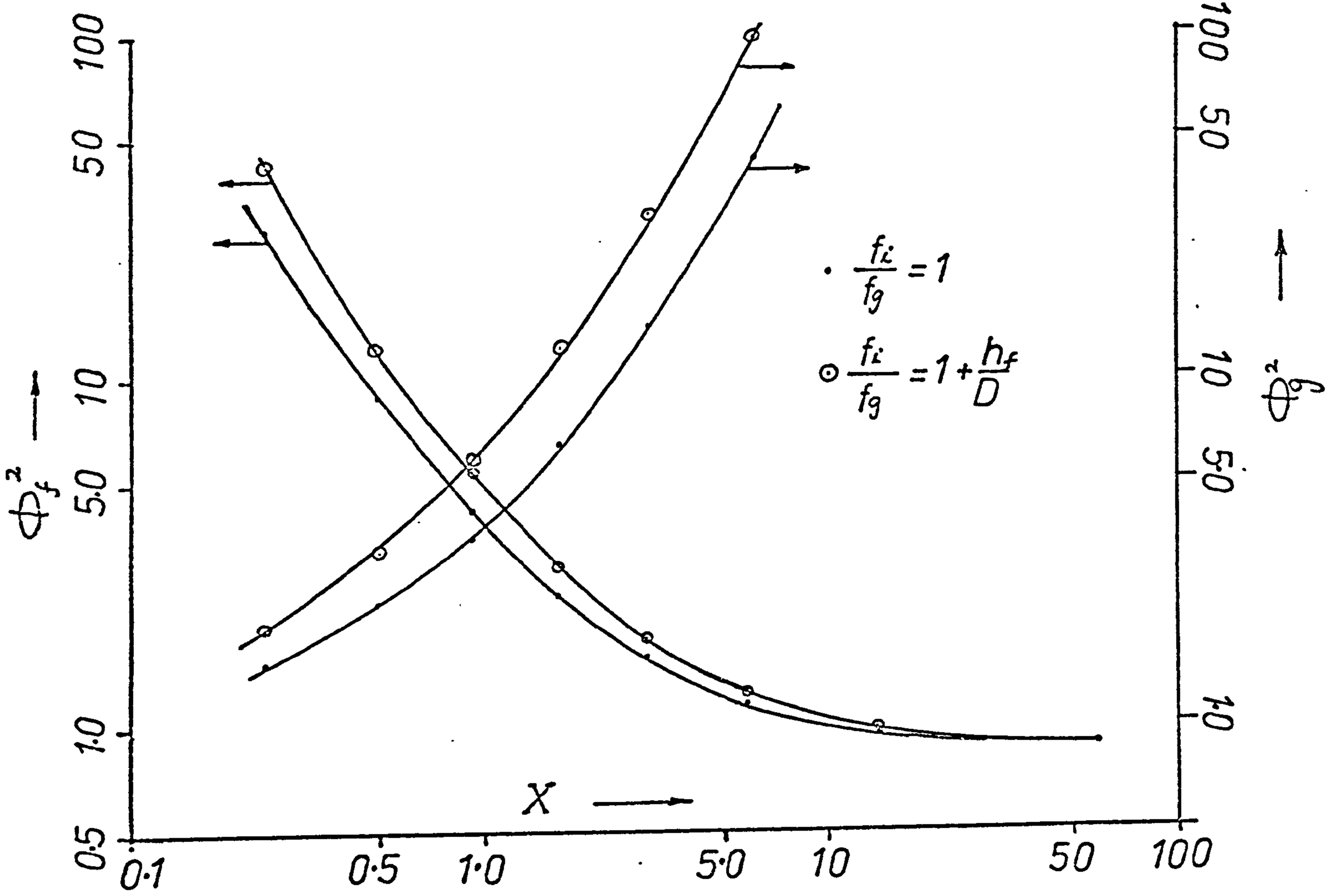

FIG·2·7 DUKLER MODEL PREDICTIONS (Ref. T1)

annular two phase flow problem but his predictions always fell below the Martinelli correlation (G1).

Baker (B3) recommended

$$\phi_g = (4.8 - 0.3125D)\, X^{0.343 - 0.021D} \qquad (2.52)$$

where D is the diameter in inches.

With an average deviation of $\sim \pm 10\%$, Hoogendoorn (H2) suggested the following

$$\left(\frac{dP}{dZ}\right)_{tp} = 0.06\ \frac{G_g^{1.75}}{D\,\rho_g}, \quad 30 < G_f\ \frac{Kg}{m^2 s} < 200 \qquad (2.53)$$

The experimental findings when compared to the Martinelli predictions showed under prediction by the correlation in contradiction to Levy's analysis (L7).

It is interesting to note that the above correlations showed clearly the influence of diameter on such pattern.

Wicks and Dukler (W5) carried out experiments in horizontal 25.4 mm diameter tube and presented their entrainment results in a form of graphical correlation in terms of the Martinelli multiplier.

McManus (M6) carried out measurements in horizontal annular flow in pipe sizes 25.4 mm, 50.8 mm and 76.2 mm (1", 2" and 3") and presented his results of mean film thickness, maximum wave height, etc., in graphical form. These results showed clearly the importance of such parameters as film thickness and entrainment concentration in the flow mechanism. The gravity forces on the film

distort the uniformity of the film thickness and resulted in a thicker film at the bottom of the tube than at the top. This is expected to be even more observable in bigger pipes.

Turner (T7) based his treatment on application of the momentum equation and used Prantdl mixing length concept to relate the shear stress to the velocity profile. His result for the tt case was (W1),

$$\phi_g = 1 - (1-\sqrt{\alpha})^{8/7}(1 + \frac{8}{7}\sqrt{\alpha}) - \frac{\alpha(1-\sqrt{\alpha})^{1/7}}{0.817}$$

$$\left[1 - (\frac{\rho_g}{\rho_f})^{5/7}(\frac{\mu_f}{\mu_g})^{1/7}\right]^{-7/8} \qquad (2.54)$$

Levy (L8) derived a model using mixing length concepts and presented a semi-empirical correlation based on CISE group data. The model predicted reasonably well the data of Wicks and Dukler (W5) for horizontal flows, also that of McManus (M6) in 25.4 mm (1") pipe at high pressure drops. However, the comparison was poor with McManus 50.8 mm (2") ID pipe data where the pressure drop was low and considerable asymmetry existed.

Russel and Lamb (R6) used salt tracer with electrical conductivity probes to measure the film and core velocities. The time average film flow was downwards (in their 25.4 mm and 50.8 mm ID tubes) and the film velocity at the top of the pipe was less than that at the bottom.

Hewitt (H13) observed the disturbance waves associated with vertical annular two phase flow and found two distinct

types, namely

1. Waves with amplitude several times the mean film thickness. These had milky appearance and were the main source of entrainment.
2. Ripples occurred in the region between the disturbance waves and are of smaller amplitude and are continuously regenerated as the disturbance waves traverse the surface.

Anderson and Russell (A10) studied circumferential droplet interchange between film and core by reducing the film thickness (suction through porous wall) and then observe the film growth. The interchange was found to be a monotonically increasing function of circumferential position (angle is 0^{o} at the top of the pipe). The ratio of the value at the bottom of the pipe to that at the top was $\sim$10. These findings are in agreement with those of Hutchinson and Whalley (H20) who showed the entrainment flux from an interface to increase rapidly with the group ($\tau_i \delta/\sigma$) where δ is the film thickness, τ_i interfacial shear stress and σ is surface tension.

Butterworth and Pulling (B12) carried out visual studies with the help of a dye tracer and suggested the following mechanisms for the film formation

1 - secondary flow due to circumferential variation in roughness
2 - net entrainment deposition.
3 - wave mixing
4 - wave spreading

In general a net downward flow in the film was observed.

Moeck and Stachiewicz (M7) proposed a droplet interchange model between the film and the core and its associated momentum transfer which agreed well with Wicks and Dukler (W5) entrained data.

Hughmark (H14) presented an empirical correlation to determine the film thickness, entrainment and pressure drop in upwards annular flow, in terms of dimensionless film thickness, based on phase shear velocity and kinematic viscosity. The correlation was based on data with tubes up to 40 mm ID and viscosities up to 5cp.

Ishii and Grolmes (I2) suggested the following mechanisms for entrainment formation

1. shear of roll waves
2. wave undercut
3. bubble burst
4. liquid impingement

Based on the first mechanism, they developed a criteria for the inception of droplet entrainment in annular flow.

Fisher and Hopley (F3) presented axial view studies of air-water mixtures in horizontal, vertical and at exit of a 90^{o} vertical bend. Excellent photographs were given supporting some of the mechanisms mentioned earlier.

Weisman and Choe (W4) found that out of the correlations they compared, the Martinelli correlation predicted the compiled annular flow data reasonably well which is rather interesting.

(c) Homogeneous flows:

Such flows cover all the intermixed flow patterns e.g. slug, bubble, plug, etc. However, slug flow was treated separately in the literature and mostly on a mechanistic approach.

(c.1) Slug Flows:

Because of the inherent instability of such flows and the lack of axial symmetry, a mechanistic approach becomes difficult and complicated.

Hoogendoorn (H2) suggested the following empirical correlation

$$\phi_{f_o}^2 = \left[1 + 230 \left(\frac{G_g}{G_f}\right)^{0.84}\right] \left[0.00138 \frac{\rho_f}{\rho_g}\right]^Z \qquad (2.55)$$

$$Z = 9.5 \left(\frac{G_g}{G_f}\right)^{0.5} - 62.6 \left(\frac{G_g}{G_f}\right)^{1.3} \qquad (2.56)$$

Hughmark (H15) proposed a graphical correlation for the liquid hold up, R_f, and used it to calculate the pressure gradient as though the pipe was carrying the liquid only (a form of homogeneous model) at the average actual liquid velocity, i.e.

$$\left(\frac{dP}{dZ}\right)_{tp} = \frac{2f \rho_f U_{sf}^2}{D R_f^2} \qquad (2.57)$$

Gregory and Scott (G10) have shown that the Hughmark correlation underpredicted their data (carbon dioxide and water mixtures) by 15-20%.

Kordyban (K11) was the first to propose a mechanistic model for slug flow in horizontal pipe. He assumed that part of the liquid flowed along the bottom of the pipe whereas the remainder of the liquid flowed as truncated disc-shaped slug which alternated with the gas bubble in the upper part of the pipe. The model was an over-simplified approach and the results were not satisfactory.

Hubbard (H16) and Hubbard and Dukler (H17) presented another model based on their visual and quantitative studies. The basic difference from that of Kordyban (K11) was the assumption that the fast moving liquid slug extended over the full area of the pipe, picking up and shedding liquid from and to the liquid film, also that the model provided for gas saturation in the liquid slug. However, the model required information on such parameters as slug frequency and slug density.

Gregory and Scott (G11) presented data on slug velocity and frequency for the system carbon dioxide-water in 19 mm ($\frac{3}{4}$") ID tube. The slug velocity was correlated reasonably well by

$$U_{slug} \simeq 1.35(U_{sg} + U_{sf}) \qquad (2.58)$$

A form of slug Froude number correlated the slug frequency data for 19 mm and 35.1 mm ($\frac{3}{4}$" and $1\frac{3}{8}$") ID tubes, viz.

$$\nu_f = 0.0226 \ (N_{fr})^{1.2}_{slug} \quad sec^{-1} \qquad (2.59)$$

$$(N_{fr}) = \frac{U_{sf}}{gD}\left[\frac{19.75}{U_{sg}+U_{sf}} + \left(U_{sg} + U_{sf}\right)\right]$$

Vermeulen and Ryan(V2) proposed a simple model for horizontal and inclined pipes. The model also required a slug frequency correlation and for the inclined case a hold up correlation to determine the gravity head. The frequency was measured mostly visually and used in the calculation of the pressure drop.

Greskovich and Shrier (G12) presented a graphical correlation for slug frequency based on mixture Froude number with the input liquid volume fraction as a parameter. They used this in conjunction with the holdup correlation of Greskovich et al (G5) combined with Hubbard and Dukler (H12) to calculate pressure drop. In general this method overpredicted the pressure drop data by sometimes as much as 100%.

Weisman and Choe (W4) found that the Martinelli correlation gave reasonable predictions when compared to other correlations tested, such as Baker (B3), Hoogendoorn (H2) and Hughmark (H15).

(c.2) Bubbly Flows:

For such flows a homogeneous model with the correct weighted properties should provide reasonable predictions. Bankoff's model (B8) is one of those approaches. He assumed the local velocity and local void fraction to

follow power low distributions and that the liquid and gas velocities were equal at any point. In mathematical form,

$$\frac{\alpha}{\alpha_{max}} = \left(\frac{2y}{D}\right)^{\frac{1}{n}} \tag{2.60}$$

$$\frac{U}{U_{max}} = \left(\frac{2y}{D}\right)^{\frac{1}{m}} \tag{2.61}$$

Assuming the one seventh velocity profile (m = 7), the following relation emerged for the friction multiplier,

$$\phi_{f_o}^2 = \left[1 - \alpha\left(1 - \frac{\rho_g}{\rho_f}\right)\right]^{\frac{3}{4}} \left[1 - x\left(1 - \frac{\rho_f}{\rho_g}\right)\right]^{7/4} \tag{2.62}$$

For the average void fraction,

$$\alpha = k\beta \tag{2.63}$$

where

$$k = \frac{2(m + n + mn)(m + n + 2mn)}{(n+1)(2n+1)(m+1)(2m+1)}$$

The exponents m and n are the two unknowns in the model.

Moussalli and Chawla (M8) suggested that m = 7 → 10 and analytically arrived at the following expression for n

$$n = \frac{0.671}{R} + \left[\left(\frac{0.671}{R}\right)^2 + \left(\frac{0.4083}{R}\right)\right]^{\frac{1}{2}} \tag{2.64}$$

$$R = \frac{Q_f}{Q_g}$$

Weisman and Choe (W4) recommended the following weighting procedure for the mixture properties for the

whole range from bubble to mist, viz

$$\frac{1}{\rho_m} = \frac{x}{\rho_g} + \frac{1-x}{\rho_f} \tag{2.65}$$

for $\alpha \geqslant 0.5$

$$\mu_m = \mu_g + (\mu_c - \mu_g)\left(\frac{1}{\alpha} - 1\right)^3 \tag{2.66}$$

$$\mu_c \simeq 36\,\mu_f$$

for $\alpha < 0.5$

$$\mu_m = \mu_f \exp\left(\frac{2.5}{1 - \frac{39\,\alpha}{64}}\right) \tag{2.67}$$

The Chisholm correlation (C8) provided results which were nearly as good as the above approach if C was taken to be equivalent to a truly homogeneous flow,

$$C = \left(\frac{\rho_f}{\rho_g}\right)^{0.5} + \left(\frac{\rho_g}{\rho_f}\right)^{0.5} \tag{2.68}$$

as suggested by Chisholm.

2.7 VOID FRACTION PREDICTIONS

In two phase flow systems, void fraction and pressure drop are inter-related through the conservation equations. In general, discussions on pressure drop predictions also involve void fraction predictions. The author has attempted to separate the two subjects in this chapter because of the large number of literature items available and the diversity of methods of approach which could have

caused some confusion. Void fraction data can also be divided into three categories similar to the pressure drop predictions.

2.7.1 THEORETICAL APPROACH

For a homogeneous model, where the two phases are assumed to move with identical velocities, we have

$$\alpha = \beta = \frac{Q_g}{Q_g + Q_f} = \frac{1}{1 + (\frac{1-x}{x}) \frac{\rho_g}{\rho_f}} \qquad (2.69)$$

On the other hand for a two phase flow with slip

$$\alpha = \frac{1}{1 + (\frac{1 - x}{x}) \frac{\rho_g}{\rho_f} S} \qquad (2.70)$$

where S is the slip factor defined by

$$S = \frac{U_g}{U_f} = \frac{1 - \alpha}{\alpha} \frac{U_{sg}}{U_{sf}} \qquad (2.71)$$

For homogeneous flow, S = 1 and eq. (2.70) reduces to eq. (2.69). Generally the slip factor and void fraction are inter-related and either could be used to describe the relative movement of the phases and hence be used in a pressure drop correlation.

Separated flow models, however, are expected to produce more sophisticated relationships depending largely on such parameters as the geometry of the model, the degree and mechanisms of interaction between the phases, etc.

Levy's (L4) approach through mixing length theory predicted reasonably well some of the published void fraction data. Beattie (B10) also used the mixing length concepts and arrived at expressions for the void fraction profiles for bubbly and droplet flows. Good agreement with the data in the region of bubbly and dispersed annular flows was obtained.

2.7.2 EMPIRICAL AND SEMI-EMPIRICAL APPROACH

One of the earliest attempts to correlate void fraction data probably were those of Armand (A2) and Martinelli (L1). Both correlations showed clearly the inter-dependency of void fraction and pressure drop. However, the Martinelli correlation was presented in graphical form while Armand suggested for $\beta > 0.9$,

$$\alpha = \frac{4 + \frac{8}{7} m}{5 + m(\frac{\beta}{1-\beta} + \frac{8}{7})} \qquad (2.72)$$

with

$$m = 4\ a \sqrt{\frac{\rho_g}{\rho_f}} \left(\frac{G_f D}{\mu_f}\right)^{1/8}$$

$$a = 0.69 + (1 - \beta)\ (4 + \frac{M_f}{M_o})$$

$$M_o = 4.35 \text{ Kg/hr.}$$

For smaller values of β,

$$\alpha = 0.833\ \beta$$

Johnson and Abou-sabe (J1) produced a graphical correlation for liquid holdup (air-water in 25.4 mm ID pipe) which consistently fell below that of Martinelli.

On the other hand, Bakers (B3) data in large diameter pipes were higher than the Martinelli predictions.

Isbin et al (I3) presented a comprehensive survey on void fraction data and showed that neither Martinelli (L1) nor the homogeneous model proved satisfactory in correlating the available data. They also stressed the inter-dependency of friction multipliers and void fraction.

Chisholm and Laird (C7) indicated that they were able to correlate their data in rough and smooth tubes by an equation

$$\frac{K}{(1-\alpha)^n} = 1 + \frac{21}{X} + \frac{1}{X^2} \qquad (2.73)$$

where K, and n are constants whose values were respectively 0.8, 1.75 for smooth tubes and 1.0, 2.0, for rough tubes.

Yagi (Y1) recommended the following correlation for upward vertical flow of air-water and air-oil mixtures near atmospheric pressure

$$\frac{1-\alpha}{\alpha} = \text{const.} \left(\frac{U_{sf}}{U_{sg}}\right)^{0.88} G_f \, \mu_f^{0.3} \qquad (2.74)$$

Hoogendoorn (H2) and Hoogendoorn and Buitlaar (H3) correlated their data by the equation

$$\frac{\alpha}{1-\alpha} = \text{const.} \; U_{sg}^{0.85} \left(1 - \frac{\alpha}{1-\alpha} \frac{U_{sf}}{U_{sg}}\right)^{0.85} \qquad (2.75)$$

Levy (L5) arrived at complex expressions for the void fraction in terms of quality which reduced to

$$x = \left(\frac{\rho_g}{\rho_f}\right)^{0.5} \frac{\alpha}{1-\alpha} (2\alpha)^{0.5} \qquad (2.76)$$

for small qualities. The slip factor was given by,

$$S = \frac{U_g}{U_f} = \left(\frac{\rho_f}{\rho_g}\right)^{0.5} (2\alpha)^{0.5} \qquad (2.77)$$

Bankoff's (B8) variable density model produced the following relationship for the slip factor in terms of the average void fraction,

$$S = \frac{\text{mean gas velocity}}{\text{mean liquid velocity}} = \frac{1-\alpha}{K-\alpha} \qquad (2.78)$$

and

$$\alpha = K\beta$$

The flow parameter K was assumed to depend on the pressure in the form,

$$K = 0.71 + 0.0001\ P \qquad (2.79)$$

where P is the system pressure in psia.

Hugmark (H9) suggested a correlation based on the equation derived by Bankoff (B8), viz

$$\frac{1}{x} = 1 - \frac{\rho_f}{\rho_g}\left(1 - \frac{K}{\alpha}\right) \qquad (2.80)$$

With the flow parameter K empirically correlated in terms of the quantity Z defined by

$$Z = \left[\frac{D\,G}{(1-\alpha)\,\mu_f + \alpha\,\mu_g}\right]^{1/6} \left[\frac{U_{s_f} + U_{s_g}}{\sqrt{gD}}\right]^{1/4} (1-\beta)^{-1/4} \qquad (2.81)$$

Hugmark recommended this correlation for both vertical and horizontal flows and indicated that the deviations observed at high pressures were comparable to those observed in the original pressure dependency model of Bankoff.

Chisholm (C10) developed equations for the prediction of the phase velocities during the flow of two phase mixtures in horizontal tubes (25.4 mm ID) and over a wide range of liquid viscosities. Three distinct flow regimes were observed, viz.

Regime I $$S = 1.2\left(\frac{\mu_f}{\mu_r}\right)^{0.22} + 0.22\left(\frac{\mu_f}{\mu_r}\right)^{0.22} \Gamma \qquad (2.82)$$

Regime II $$S = 2.1\left(\frac{\mu_f}{\mu_r}\right)^{0.5} + 0.155\left(\frac{\mu_f}{\mu_r}\right)^{0.22} \Gamma \qquad (2.83)$$

Regime III $$S = 258\,Re_f^{-1/3} - 3.5\left(\frac{\mu_f}{\mu_r}\right)^{0.5} \qquad (2.84)$$

where $S = \frac{U_g}{U_f}$ and $\Gamma = \frac{Q_g}{Q_f} = \frac{x}{(1-x)}\frac{\rho_f}{\rho_g}$

The regime boundaries were given by the intersection of the above equations.

Dukler et al (D1) compared the correlations of Hoogendoorn (H2), Martinelli (L1) and Hughmark (H9) against some 700 data point and concluded that the Highmark was the best.

The CISE group (A11) summarised the results of an extensive study on liquid volume fraction in adiabatic two phase vertical upflow, and were able to correlate the in situ liquid hold up, in terms of input liquid volume fraction and other variables, in the form

$$1 - \alpha = (1 - \beta)\left[1 + \frac{1.35\ \beta^{n}}{1 + 0.335\ \frac{GD^{\frac{1}{2}}}{\sigma}}\ \left(\frac{1}{\rho_g}\right)^{\frac{1}{4}}\right] \qquad (2.85)$$

$$n = 0.9 + 0.05\,\sigma$$

and σ is the surface tension.

Zuber and Findlay (Z2) showed analytically that

$$\frac{U_{sg}}{\alpha} = C_o\ U_{smix} + \frac{\langle \alpha\, U_{gr} \rangle}{\langle \alpha \rangle} \qquad (2.86)$$

where

$$C_o = \frac{\frac{1}{A}\int \alpha\, U_{mix}\ d\ A}{(\frac{1}{A}\int \alpha\, dA)(\int U_{mix}\ dA)} = \text{distribution parameter} \qquad (2.87)$$

Linear relationships were obtained when U_{sg}/α was plotted against U_{sm} for most of the data tested, which indicated that C_o was constant. However, Zuber et al (Z3) observed a flow pattern dependency. In general

C_o	Profile
=1	concentration profile is uniform.
>1	concentration at centre line is greater than that at the wall.
<1	concentration at centre line is smaller than that at the wall.

Nothing was said about horizontal flows although one would expect the same argument to hold.

Baroczy (B13) used air-water and mercury-nitrogen mixture data and an upper limit for the liquid volume fraction (calculated assuming critical conditions) to arrive at a general correlation for the liquid hold up. It was expressed graphically in terms of a property index, C and the Martinelli parameter, X, i.e.

$$C = \left(\frac{\mu_f}{\mu_g}\right)^{0.2} \left(\frac{\rho_g}{\rho_f}\right) \quad , \quad X = \left(\frac{M_f}{M_g}\right)^{0.9} \left(\frac{\rho_g}{\rho_f}\right)^{0.5} \left(\frac{\mu_f}{\mu_g}\right)^{0.1} \qquad (2.88)$$

Smith (S12) assumed an annular type flow with a homogeneous core such that the velocity heads (i.e. ρU^2) of the mixture in the core and that of the liquid film were equal. An empirical factor K, where

$$K = \frac{\text{mass of liquid flowing in homogeneous mixture}}{\text{total mass of water flowing}} \quad ,$$

appeared as an important parameter in the correlation. A constant value of 0.4 produced good agreement with the data tested and indeed performed better than Martinelli (M4), Bankoff (B2), Levy (L4), and Thom (T6) correlations. However an underprediction of more than 50% was observed at low voidages ($\alpha < 0.2$).

Simpson and Rooney (S19) proposed an empirical correlation in terms of input volume fraction and the quantity U_R/U_{MH}, where

U_g = no-slip mean velocity + relative velocity = $U_{MH}+U_R$

and

$$U_R = k(\sigma g \frac{\rho_{fg}}{\rho_f^2})^{\frac{1}{4}} \qquad (2.89)$$

Good agreement was obtained ($\pm$ 5%) over a fairly wide range of natural circulation conditions.

Chisholm (C15) used homogeneous model considerations to arrive at a simple relationship for the slip factor S which he showed to be valid for $\beta < 0.9$,

$$S = \frac{U_g}{U_f} \simeq (\frac{\rho_f}{\rho_m})^{\frac{1}{2}} = \left[1 + x(\frac{\rho_f}{\rho_g} - 1)\right]^{\frac{1}{2}} \qquad (2.90)$$

The conditions were that the liquid was no more viscous than water and that in horizontal flow the phases were not stratified.

Gregory (G15) tested four holdup correlations for use in inclined pipelines against data from the literature for pipe sizes up to 50.8 mm (2"). The commonly used correlations of Baker (B14, B4) and Flanigan (F4) were found to be subject to large errors whilst the Martinelli (L1) correlation for horizontal flows provided reasonable predictions over a wide range of flow rates for inclined pipes. The Guzhov (G16) correlation was recommended for hold up values down to 0.25 and the Martinelli correlation for lower values.

Recently Greskovich and Cooper (G17) proposed a new holdup correlation based on data in large diameter tubes

(up to 79.4 mm). In mathematical form

$$1 - \alpha = 1 - \frac{\beta}{1 + 0.671 \left(\frac{\text{Sin } \theta^{0.263}}{F_{r_m}^{0.5}}\right)} \qquad (2.91)$$

over the range

$$0.1 \leqslant F_{r_m} \leqslant 4.0 \quad , \qquad 1^{\circ} \leqslant \theta \leqslant 10^{\circ}$$

and

$$0.1 \leqslant 1 - \beta < 0.7$$

The correlation predicted the data reasonably well (5-10%) for the ranges quoted above. However the correlation was based on air-water data only and extrapolation to different mixtures should be made with caution.

2.7.3 FLOW PATTERN APPROACH

This approach is still in its early stages of development. This lack in progress is largely due to the deliberate neglect of flow pattern effects as in the case of pressure drop. Indeed as shown above these two variables i.e. pressure drop and void fraction are interrelated and that a lack in progress in one is directly reflected in the other. No further review is given as this will largely be a repetition of section 2.6.3.

2.8 SETTLING LENGTHS AND BEND EFFECTS

In single phase flows, the distance from an entrance required for the development of a stabilised flow has been found to depend on the nature of the motion upstream

of the entrance, the nature of the entrance and whether the final flow is laminar or turbulent. The theoretical analysis of McComas (M9) for laminar flow predicted that

$$\frac{L}{D} = 0.026\ Re \qquad (2.92)$$

Experimental results (M9, M10) showed the constant to be ranging from 0.03 to 0.035. As can be seen for $Re \simeq 2300$ (transition to turbulent flows); $L/D \simeq 60$.

No exact theoretical solution is available for turbulent flow but settling lengths are in general smaller than that of laminar flow. Knudsen and Katz (K12) and Schlichting (S15) quote experimental results which show the distance to be,

$$\frac{L}{D} \simeq 50 - 100 \qquad (2.93)$$

Obviously much higher lengths are expected near the transition zone from laminar to turbulent flows.

In two phase flows one would expect the inlet devices to have similar effects on the resulting gas-liquid flow pattern and pressure drop and hence dictate the length required for their development and stabilization. Unfortunately the data in these areas are scarce and one has to depend largely on few scattered individual and accidental observations.

Alves (A1) found that stratified flow was not possible in his horizontal pipe with a vertical return bend and that such a bend caused slugging in the pipe preceded by

the bend. Later on Alves (Al2) pointed out that the length necessary for the establishment of a flow pattern could be over 100D.

Hoogendoorn (H2) suggested that beyond a length of 60D, the influence of the inlet device (mixer) on the flow pattern was negligible. However, near the transition from one flow pattern to another (wave to slug) he was able to produce either of them by changing the mixing device only.

Wicks and Dukler (W5) used a tee shaped mixer in their study of entrainment and pressure drop in annular flow. They found that the entrainment was higher and the pressure drop lower with air on the run of the entrance tee at given flow conditions (water introduced at right angles to flow direction).

Gill et al (G13) used two different injectors; the multijet and the annular or slot injector. A difference of pressure readings of up to 40% was recorded by interchanging the injectors only.

Sekoguchi et al (S2) conducted what was probably the only systematic study of inlet effects. In addition to visual flow pattern observations the pressure distribution along the test section was recorded for pipe sizes 18 mm, 25.7 mm and 34.8 mm diameter. It was found that at any given water flowrate an increase in gas flowrate generally caused an increase in the inlet settling length sometimes up to 150D. The outlet or exit settling lengths could be as high as 100D. In general the larger diameters required

smaller settling length ratio (L/D).

The same authors conducted a study on the effect of a 90^{o} horizontal bend and found that the bend did not change the flow pattern, but rather changed the mode of flow, particularly downstream the bend. Settling lengths of up to 150D downstream and 35D upstream the bend were recorded.

Gardner and Neller (G14) studied the effect of a 90^{o} bend situated at the exit of a vertical pipe 76 mm in diameter. Visual observations showed that the bend acted as an effective agglomerator of bubbles and that where spray was present, it might be effective in separating the spray at the bend wall to form larger water masses.

Anderson and Hill (A13) carried out measurements of film thickness, entrainment and pressure drop in annular two phase air-water mixtures in 25.4 mm diameter tube. They concluded that the film thickness was always relatively high on the inside of the bend due to lower interfacial shear stress and drainage of the film. Deposition of entrained droplets kept the film on the outside of the bend supplied with liquid. They also noticed that the secondary flow in the gas, so noticeable in single phase flow in a bend, appeared to be hindered by the presence of the second phase once the tube wall was completely covered with liquid, although it remained a very significant feature of the flow pattern.

Maddock et al (M11) conducted measurements of different flow parameters in air-water annular flow at the exit of bends of different radii (2" to 10") and different angles (30^{o} to 90^{o}). These parameters included local film thickness and flowrate, static pressure and the distribution of local gas and water velocities over the exit cross-section of the bend. On the basis of these measurements a flow structure was suggested for the developing region of a bend.

Coney and Fisher (C4) and Fisher and Hopley (F3) carried out visual and photographic (using axial view technique in the latter one) studies on the effect of a vertical 90^{o} bend. Their results supported the phase separation effect of the bend in accordance with the observation and measurements mentioned above.

CHAPTER 3

EXPERIMENTAL APPARATUS AND INSTRUMENTATION

CHAPTER 3 EXPERIMENTAL APPARATUS AND INSTRUMENTATION

3.1 INTRODUCTION

The experimental work in this project involved the measurements of gas and liquid flow rates, void fractions, pressures, pressure distributions and visual and photographic studies of the flow pattern.

In the latter part of the test program flow pattern sensors were developed and used whereby pressure and void fraction pulsations were recorded at comparatively high speeds in an attempt to identify flow patterns more objectively.

To allow comparison between the flow pattern observations and recordings, the test section was transparent and took the form of acrylic resin (perspex) tubes. Still photographs of the flow patterns were taken with the help of a specially constructed viewing box, while cine´ films were used to record the effects of a 90^{o} bend on the flow structure.

Air and water were used as the components of the two phase mixture under test for reasons of availability and comparatively low costs; also for reasons of safety (non-toxic) and fire hazard (non-inflammable). Tests were carried out at near atmospheric conditions using tubes of different diameters, namely 127 mm (5") and 215.9 mm (8.5") nominal bore. Almost all of the measurements were taken manually except for the pulsations

data where a fast response data acquisition system was used.

3.2 EXPERIMENTAL CIRCUIT

The layout of the experimental circuit is shown diagrammatically in Fig. 3.1 and in photographs illustrated in Figs. 3.2 and 3.3. Water flowed from the separation tank into a centrifugal pump (type Worthington-Simpson, 35 HP) where it was pumped around the circuit. The water flow rate was controlled by the valves 'V_1' and 'V_3' through the by-pass arrangement shown. Valve 'V_2' was normally kept fully open except when starting or closing the pump.

The water flow rate was measured in terms of the pressure difference across a 76.2 mm (3") diameter orifice plate situated at a distance of $\sim$ 4m (32 pipe diameter) downstream of valve 'V_2' and bend 'A'. Details of the orifice plate are given later. The water then entered the mixing device 'M' via the control valve 'V_3' which was located $\sim$ 3m (24 pipe diameter) downstream of the orifice plate. At the mixing chamber, air was injected and the emergent air-water mixture flowed through the transparent test section after traversing two 90^{o} bends, 'B' and 'C'. The air entering the mixing device was metered by rotameters (low flow rates) or by a 41 mm (1.625") diameter orifice plate (high flow rates).

Transparent viewing lengths were inserted into the circuit:

(i) immediately after bend 'A' in order to ensure no air

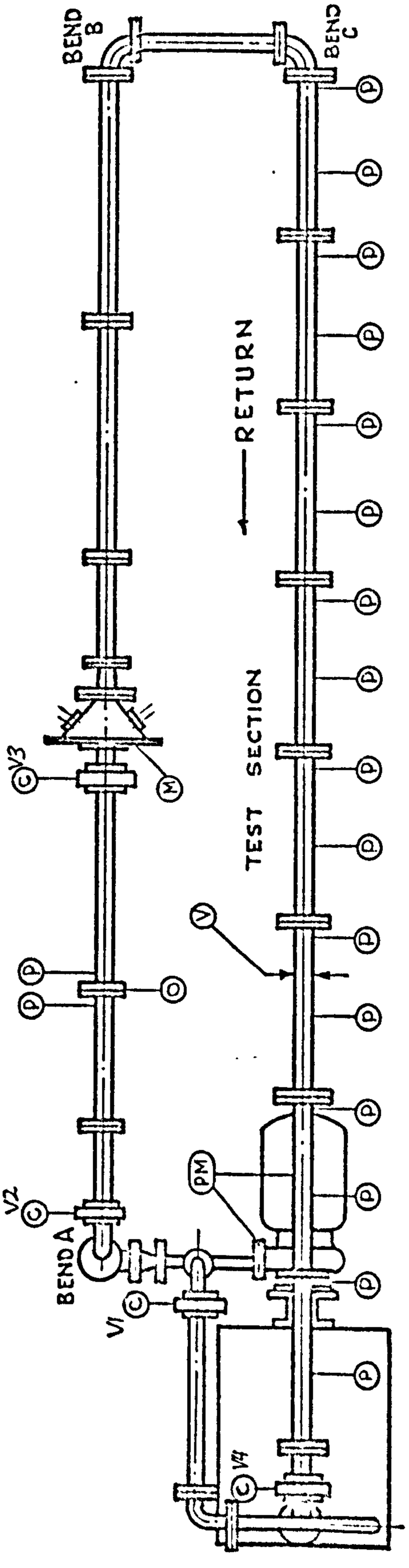

CODE

- C CONTROL VALVES
- M MIXING DEVICE
- O ORIFICE PLATE
- P PRESSURE SENSING POINT
- PM PUMP AND MOTOR
- V VOID FRACTION APPARATUS

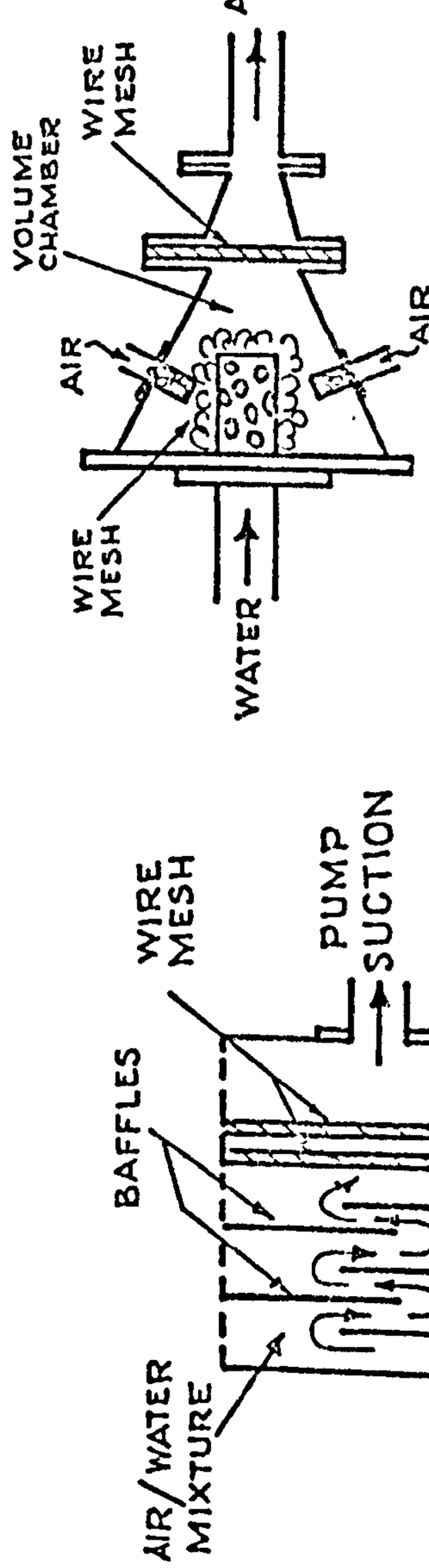

DETAIL OF MIXING DEVICE

DETAIL OF SEPARATION TANK
(ELEVATION)

FIG.3.1 LAYOUT OF TEST RIG SHOWING DETAILS OF SEPARATION TANK AND MIXING DEVICE

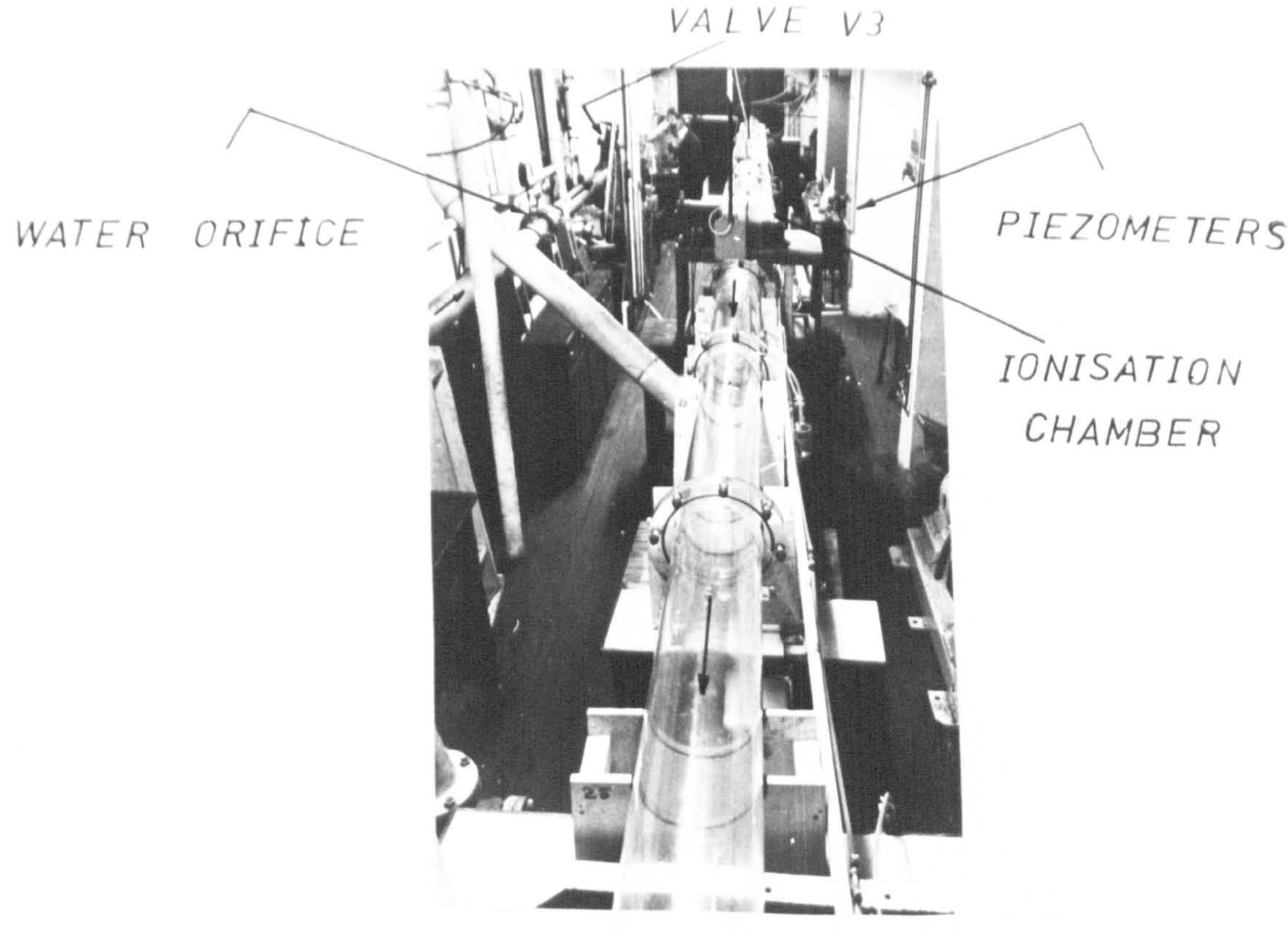

FIG 3·2 LAYOUT OF TEST SECTION

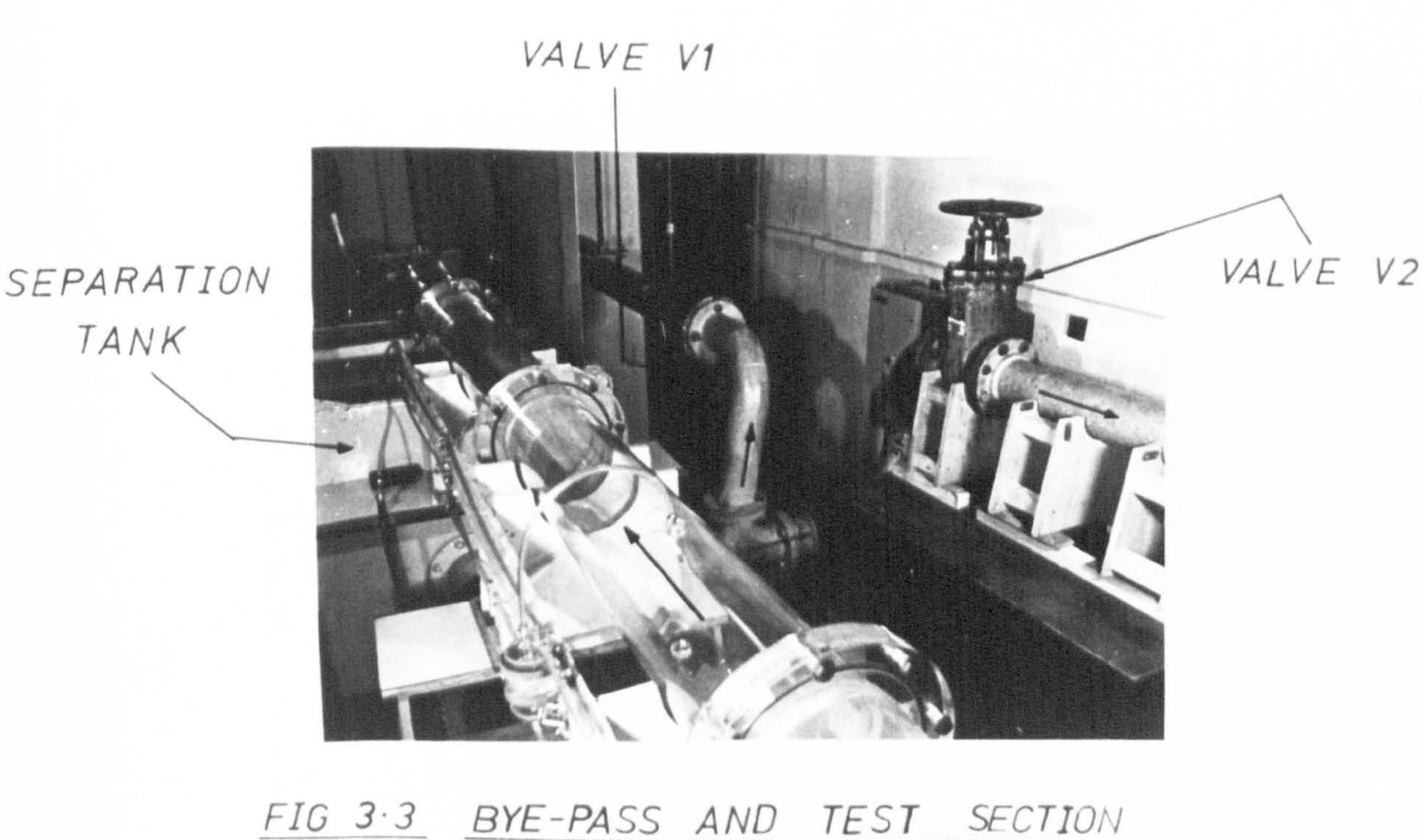

FIG 3·3 BYE-PASS AND TEST SECTION DISCHARGE ARRANGEMENT

carry-over from the separation tank.

(ii) before bend 'B' to check the flow pattern in the line before entering the 90^{o} bend.

(iii) between bends 'B' and 'C' to observe the effect of the 90^{o} bend on the flow pattern.

The test section was 16m (52 ft) in length, completely transparent and manufactured from 127mm (5") nominal bore perspex tubing (Phase 1 and Phase 2 tests) or 215.9mm (8.5") nominal bore perspex tubing (Phase 3 tests). Bosses containing 1.6 mm ($^{1}/16$") pressure tapping holes were located at intervals of 1 m along the centre line of the test section, and connections made to a manometric device through transparent plastic tubing. The air-water mixture was discharged from the test section, via the valve 'C_4' into the separation tank where its temperature was measured.

In Phase 2 and Phase 3 tests, the mixing device was situated at the start of the test section, just after bend 'C'. Appendix L details the differences in the experimental arrangement between the three phases.

3.2.1 SEPARATION TANK

Details of the separation tank are shown in Fig. 3.1. The tank was constructed from 6.35 mm ($\frac{1}{4}$") steel plate and was open at the top. It contained a series of vertically offset baffles to lengthen the mixture flow path and hence encourage separation of the air. Two wire mesh filters were inserted after the baffles to trap air bubbles carried over. The baffles and meshes were

jointly supported and fixed to the tank walls. Pieces of hardboard were attached to the sides of the tank to a height exceeding 1.8 m (6 ft) above the top of the tank to prevent water splashing to the surroundings.

3.2.2 MIXING SECTION

In designing the mixing section (see also Fig. 3.6) the main object was to thoroughly mix the air and water before leaving the unit, thus allowing the flow conditions to determine the flow pattern.

Water entered the mixer via a series of circumferential holes drilled in a length of flow pipe (blocked at the end) protruding into the volume chamber of the device. The total c/s area of the holes was made about twice the tube c/s area to avoid excessive head losses. The air entered the mixer via four injection lines equally spaced around the volume chamber with, again circumferential holes drilled in the injection pipes to break up the air jets and promote mixing. The mixing of the air and water was further assisted by wire mesh packing in the volume chamber and near the exit. The chamber took the form of a convergent circular channel made from 6.35 mm ($\frac{1}{4}$") thick steel plate, the exit diameter being equal to the main tube diameter.

3.2.3 MANUFACTURE AND ASSEMBLY OF TEST SECTION

The test section was made from 8 pieces of perspex tube 2m in length (for the 216 mm tube, the pieces were 1.2m long). The tubes were cut to the required length

and machined flanges cemented to each end (Tensol cement No. 7 was used). The cemented parts were annealed for 24 hrs. for stress relief. The flanges were designed to avoid using rubber joints which could introduce disturbances to the flow; instead, a circular groove was cut in one flange of each pair and an O-ring used to seal the connection. This also allowed the tube ends to be joined with a minimum of offset.

The tubes were supported by wooden stands with thin sponge rubber strips separating the tubes from the stands and acting as a vibration dampers. Great care was taken in the assembly of the test section to ensure matching of the tube inside diameters at joints and to ensure that the test section was strictly horizontal and straight. Spirit levels and theodolite were used in the alignment.

Near the tube exit, the valve, bend and the exit pipe were bolted to the tank and supported from the ceiling. The exit pipe had a blocked end (to safeguard the tank base) but was circumferentially perforated, the area of the perforations being more than four times the pipe c/s area to minimise losses and exit effects disturbances. Double layers of 9.5 mm x 9.5 mm (3/8" x 3/8") mesh was wrapped around the pipe to promote separation of the phases.

3.2.4 PRESSURE TAPPING POINTS

The pressure tapping points consisted of 1.6 mm (^{1}/16") holes drilled in perspex bosses welded to the

test tube. Careful examination was made to ensure that no burrs existed at the inside edges which could disturb the flow.

Further comments and the background to the design used are given in appendix A.

3.3 INSTRUMENTATION AND CALIBRATION

A schematic diagram of the instrumentation used is shown in Fig. 3.4. In the following sections the calibration and operation of each unit is discussed.

3.3.1 WATER FLOW RATE MEASUREMENTS

A stainless steel sharp edged orifice plate, 76.2 mm (3") in diameter, was used for measuring the water flow rate. The plate was designed and manufactured according to B.S. 1042 with D and D/2 pressure tappings. The plate was inserted in the line far from any upstream disturbances (Figs. 3.1 and 3.5). For low water flow rates, an air-water manometer was used to measure the pressure drop across the orifice; for high flow rates a water-mercury manometer was used. Transparent reinforced polythene tubings were used as the pressure connecting lines to facilitate purging. The orifice plate was calibrated in situ with the pipework in a standard test facility in the Department of Hydraulics laboratory. Further details are given in Appendix B.

3.3.2 AIR FLOW RATE MEASUREMENTS

For low air flow rates, i.e. up to $\sim .04\ m^3/sec.$,

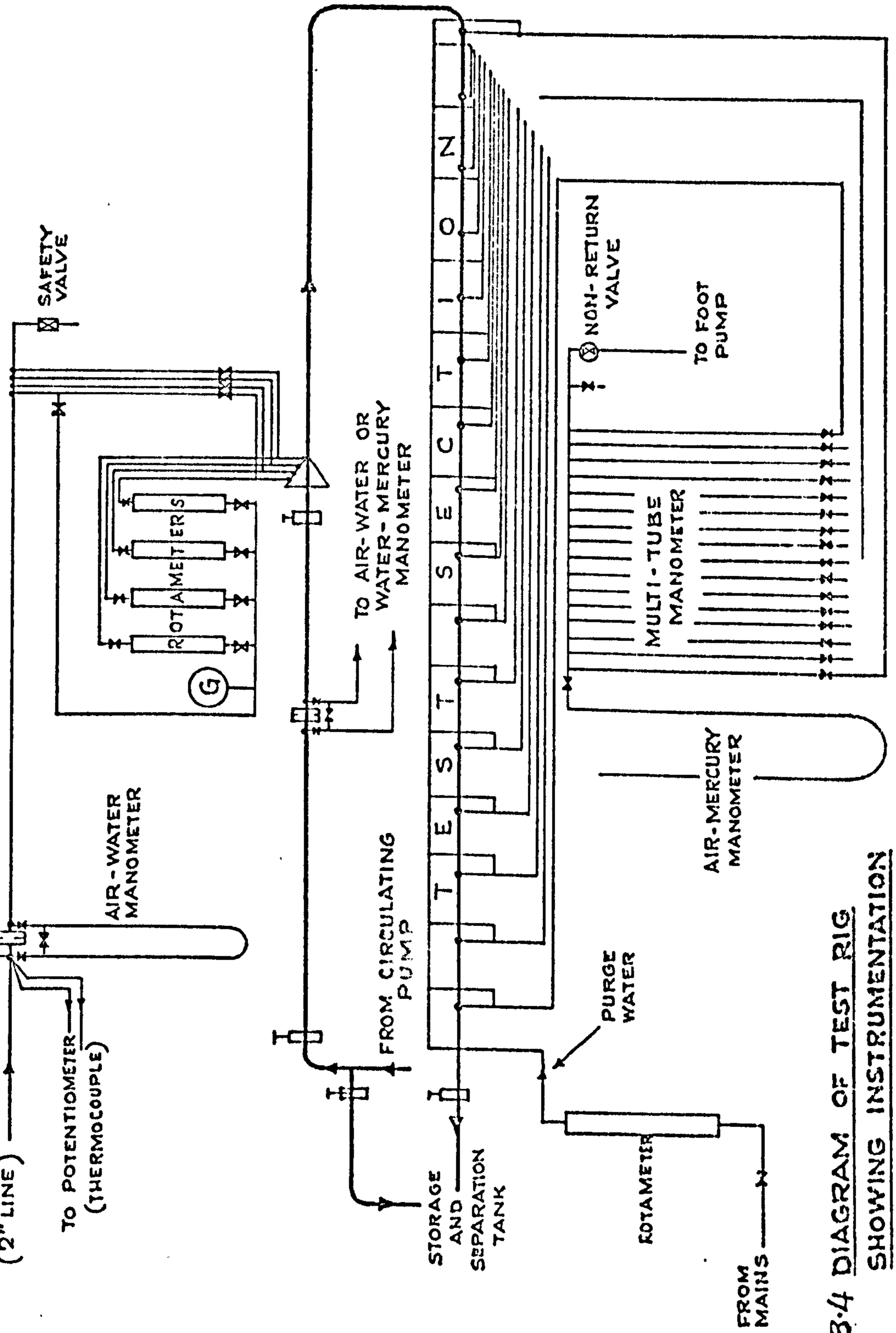

FIG. 3.4 DIAGRAM OF TEST RIG SHOWING INSTRUMENTATION

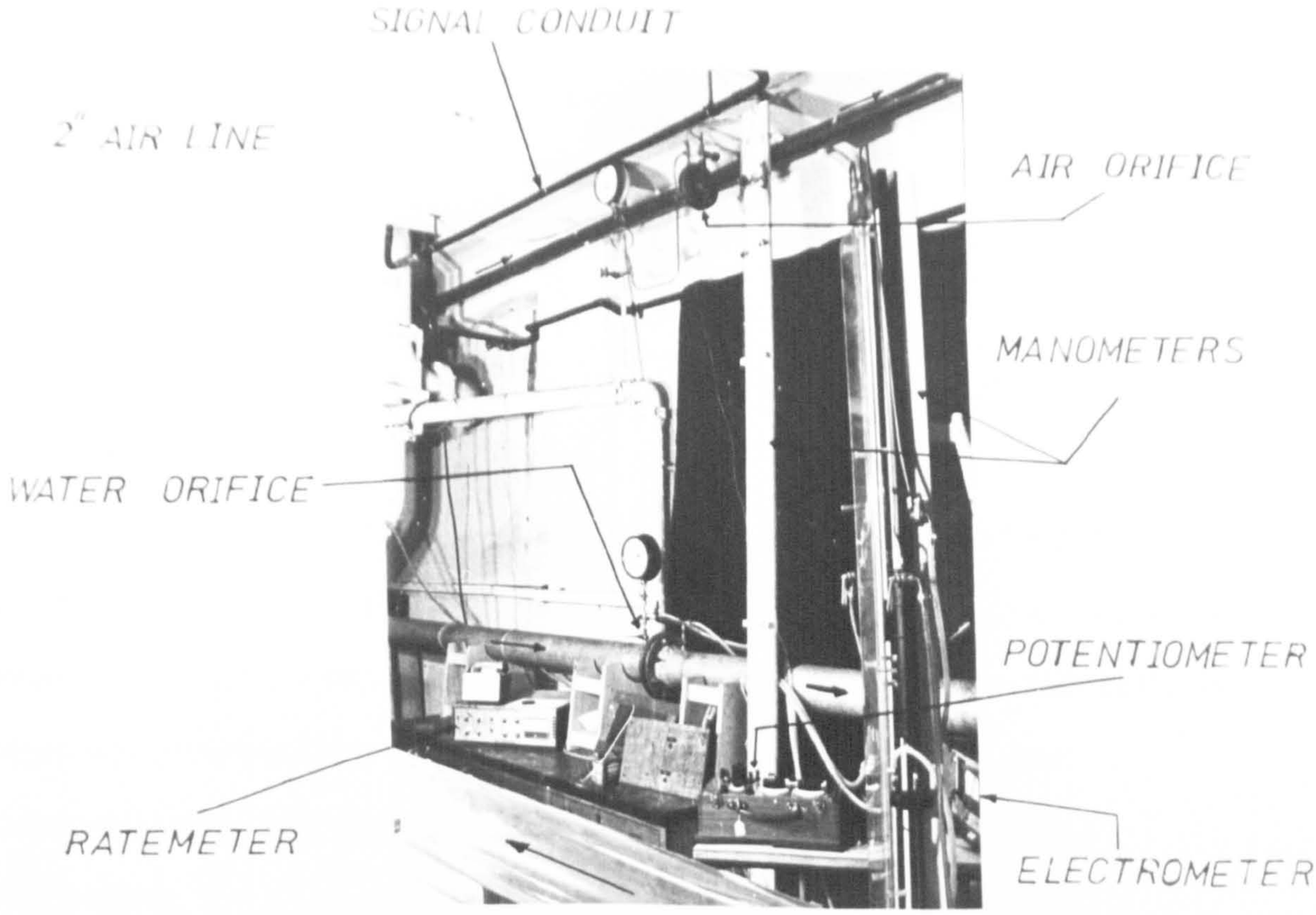

FIG 3·5 AIR AND WATER ORIFICE ASSEMBLIES

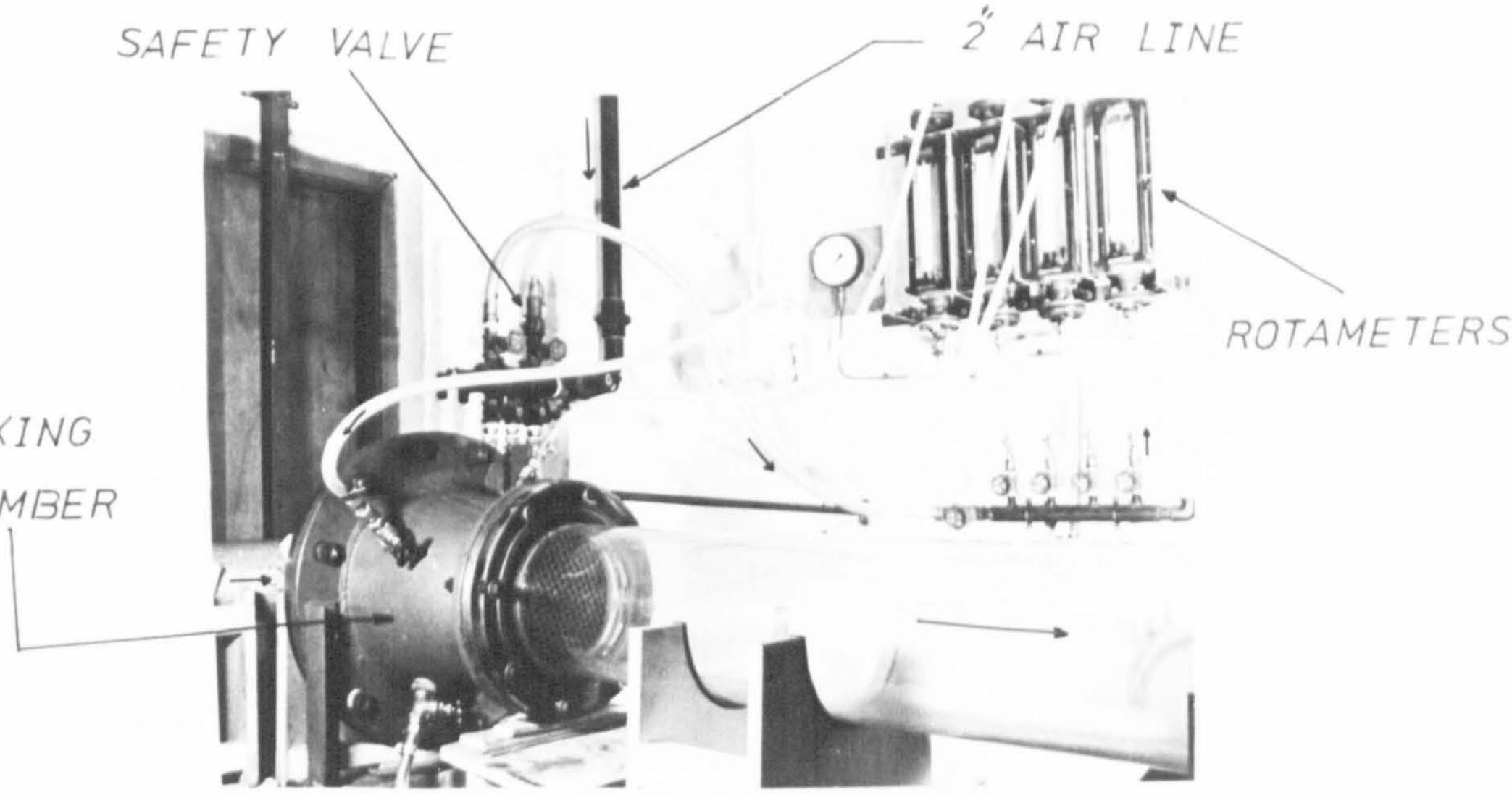

FIG 3·6 MIXING SECTION AND ROTAMETERS ASSEMBLIES

four rotameters (type 'Metric 35') were used to meter the air flow, one for each air injection point. The arrangement is shown in Fig. 3.6. For high air flow rate an orifice meter was used.

In the rotameter system, the operating pressure was measured in the manifold at the inlet to the rotameters using a Bourdon gauge of range 0-6 bar (frequently checked using a Budenberg dead weight gauge tester). With the orifice meter, the pressure was measured upstream of the orifice plate. For both systems the air temperature was measured upstream of the orifice plate using a calibrated copper-constantan thermocouple. Corrections for temperature and pressure deviations could then be obtained.

Full details of the design, installation and calibration of the flowmeters are given in Appendix B.

In the interest of safety, a perspex shield was built around the rotameters and a safety valve inserted into the inlet manifold as shown in Fig. 3.6.

3.3.3 PRESSURE AND PRESSURE DIFFERENCE MEASUREMENTS

The pressure distribution along the test section was measured using sixteen pressure tapping points, distributed at 1 m intervals along the test section and connected to a multi-tube, manometer-piezometer system. This is shown schematically in Fig. 3.4. The manometer and purging system are shown in Fig. 3.7. The pressure tapping points were located initially at the tube centre line since the tube diameters were comparatively large

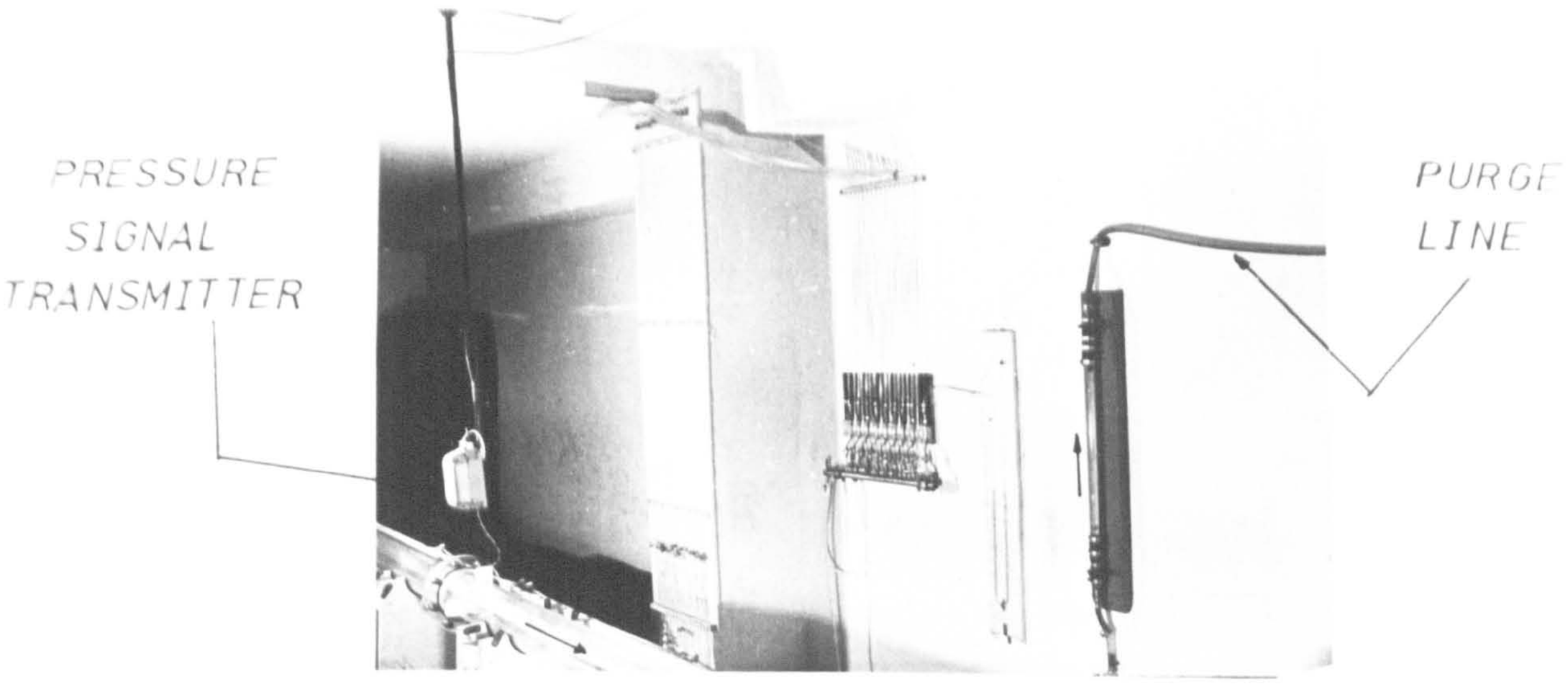

FIG 3·7 MULTI-TUBE PIEZOMETER ASSEMBLY

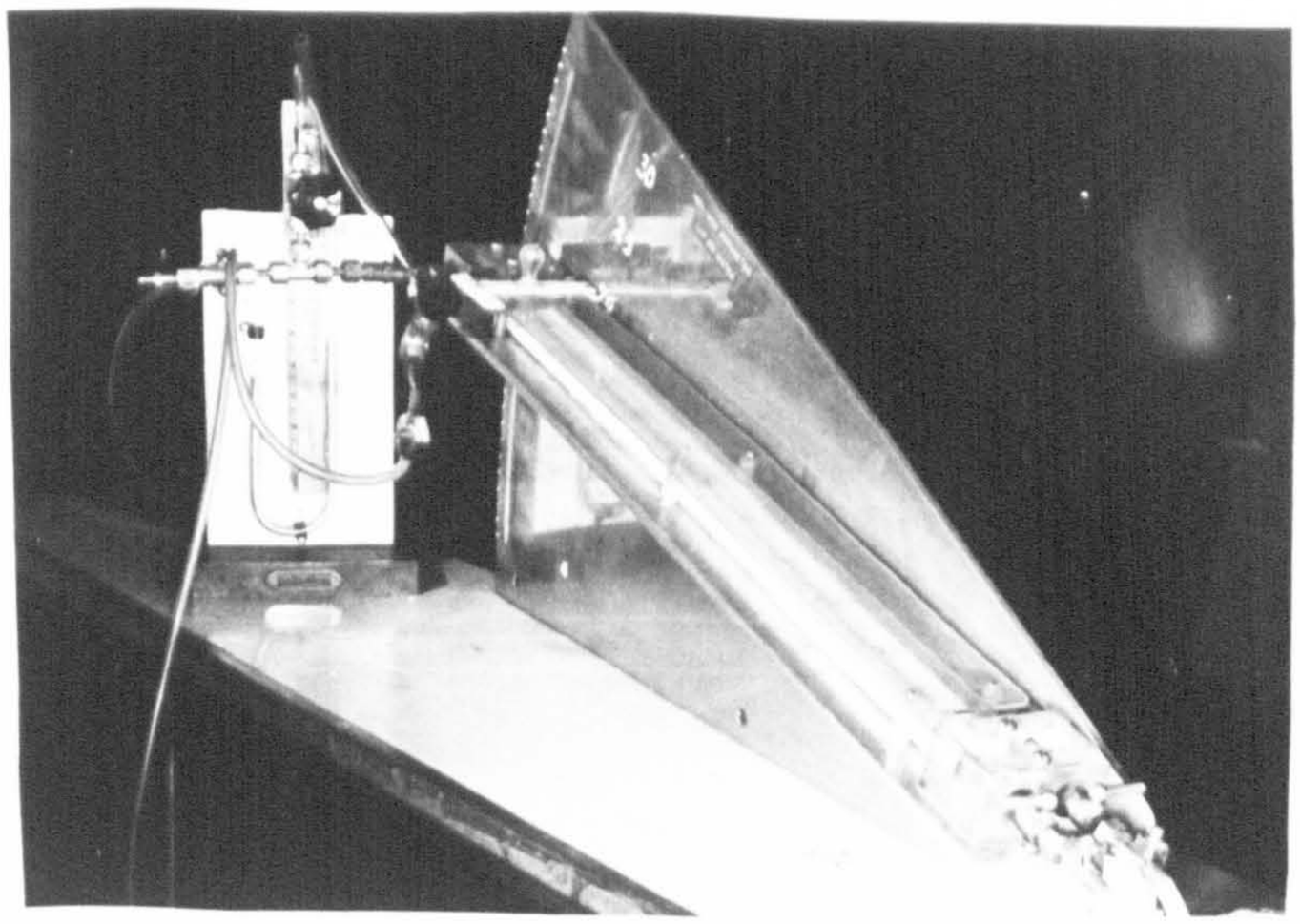

FIG 3·8 INCLINED MANOMETER

and gravity might have had some effect.

To avoid the possibility of air being forced into the connecting lines and trapped there, the lines were purged continuously using water from the mains. The purging flow rate was metered using a rotameter and was kept below 1% of the lowest water flow rate in the test section. The purge lines were pressurised sufficiently to force the purging water into the test section even when the pressure in the test section was comparatively high (max. $\sim$ 12 psig). Further discussion on purging is given in Appendix C. The pressure lines were made of 6.35 mm ($\frac{1}{4}$") bore transparent plastic tubing. The piezometers were made of 4 mm bore glass tubes and connected to the pressure lines through needle valves. The top of the glass tubes were connected to a common header by plastic tubing. Provisions were made for pressurising the header (through a non-return valve) using an air foot pump, and for measuring the pressure using an air-mercury, U-tube manometer. Valves were installed at each branch point from the header and these, in conjunction with the valves at the inlet to the piezometers, allowed flexibility and isolation of any of the pressure lines without affecting the whole unit. The pressure pulsations on the manometer-piezometer unit were throttled using clamps on the plastic tubing at the inlet to the piezometers.

Small pressure differences ($<$ 10 mm H_2O) were measured at two points only using an inverted U-tube air-

water inclined manometer as shown in Fig. 3.8. The upstream tapping was located at approximately 8 m from the bend and the pressure difference was measured over a 6 m length of test section. The angle of inclination was measured by an inclinometer with checks made against a vertical air-water manometer at an angle of 25^{o}. No corrections were required. For each test the zero reading was noted for correction purposes. Fig. 3.9 shows a special arrangement which was found necessary to obtain pressure drop measurements in the gas phase when stratified type flow existed in the 216 mm (8.5") tube.

3.3.4 VOID FRACTION MEASUREMENTS

Void fraction measurements were made at a point in the test section $\sim$ 12 m from the inlet, where the flow conditions were generally settled.

The measurements were obtained using the gamma ray attenuation technique and the apparatus consisted of a radioactive source, a large ionisation chamber, two lead collimators, an electrometer unit and an amplifier/ indicating unit arranged as shown in Fig. 3.11.

The technique is based on the principle that the attenuation of a beam of gamma rays in passing through a medium (in this case an air-water mixture in a tube) is dependent on the density (or void fraction) of the medium. Thus, by measuring the intensity of the beam after passing through the tube, the degree of attenuation can be obtained which enables the mean density, and hence the

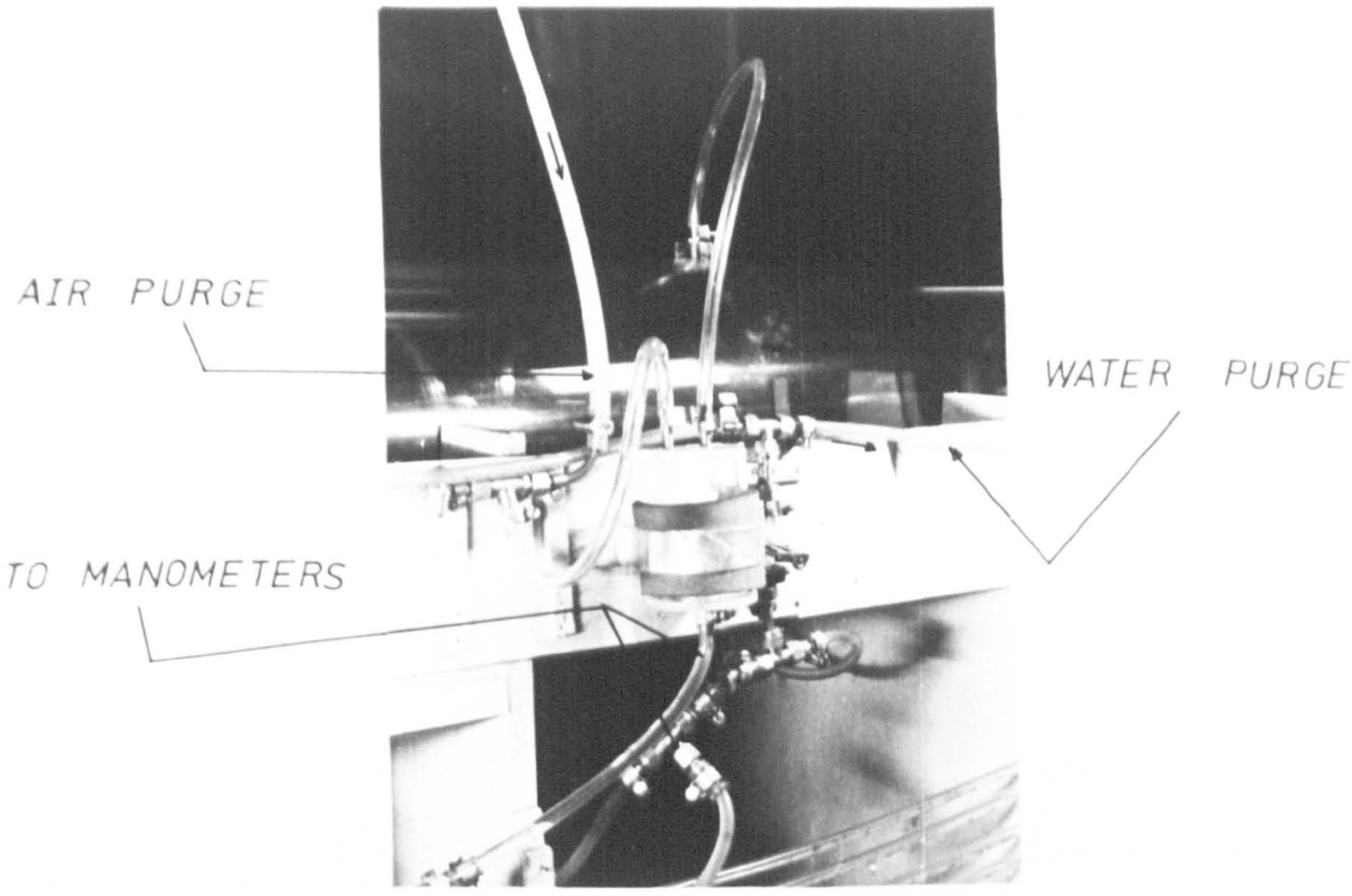

FIG 3·9 A SEPARATOR ARRANGEMENT FOR THE TOP TAPPING POINT

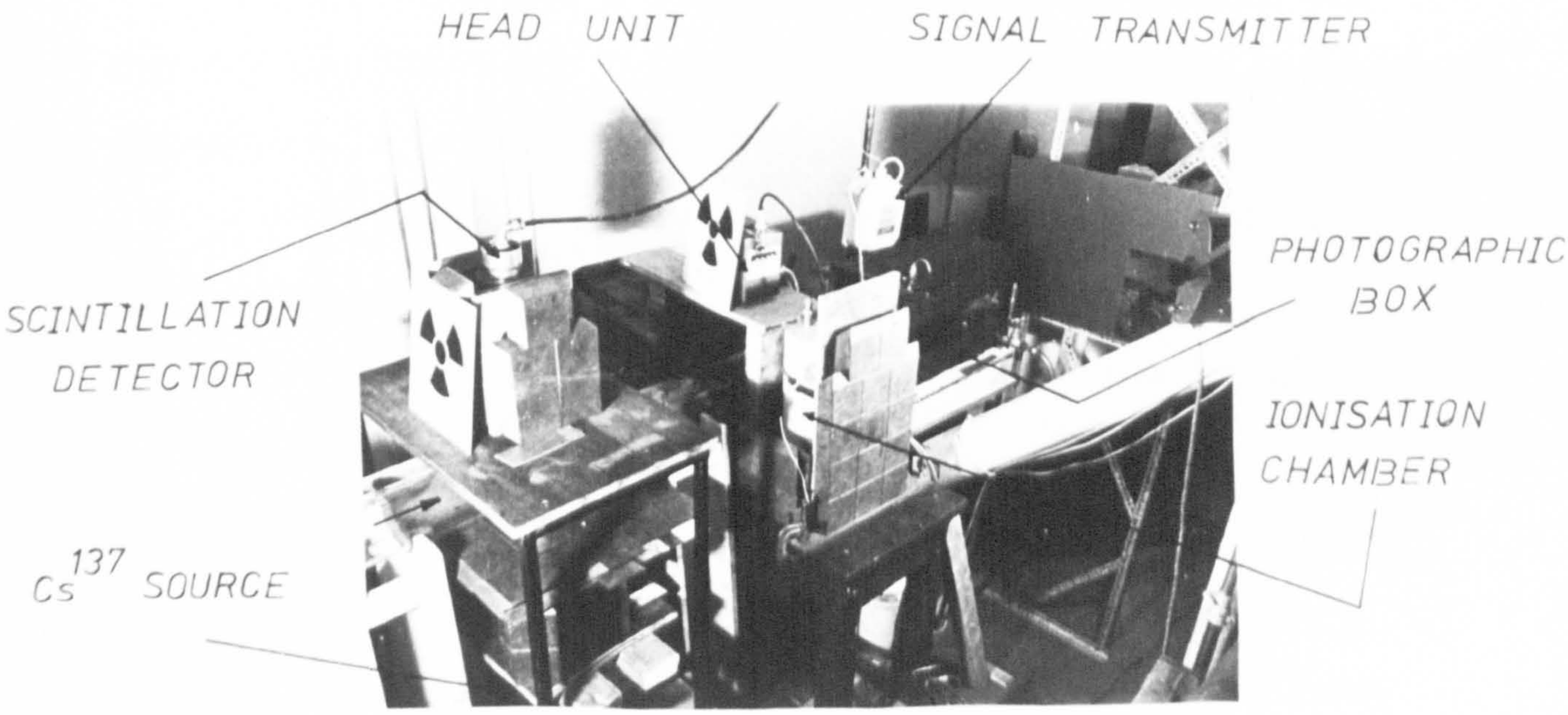

FIG 3·10 VOID FRACTION DETECTING UNITS

void fraction, to be obtained.

The radioactive source used was Cs^{137} of strength 125 mC and half life 33 years. The lead collimators were arranged such that the divergent beam of gamma rays emitted from the source scanned the total tube contents before passing into the ionisation chamber.

The ionisation chamber took the form of a hemi-spherical ended cylinder 185 mm dia, 400 mm long, filled with argon gas at a pressure of 20 bar. It contained two electrodes maintained at different potentials so that the gamma rays which entered the chamber, ionised the gas and set up a small current flow between the electrodes. The current was detected in terms of a voltage across a high resistor, passed to a vibrating reed electrometer for conversion from d.c. to a.c., then suitably amplified and displayed by an indicating unit.

Fig. 3.10 shows the experimental arrangement for the 127 mm (5") tube. Fig. 3.11 illustrates the principle and gives an abbreviated version of the underlying theory.

The apparatus was calibrated in-situ before each day's testing under conditions of

(a) tube containing air only, i.e. density ~ 1 Kg/m^3.
    void fraction = 1

(b) tube containing water only, i.e. density ~ 1000 Kg/m^3,
    void fraction = 0.

For each condition, the intensity of the gamma ray beam after passing through the tube 'I_x' was measured in terms of a millivoltage on the display meter. To improve the

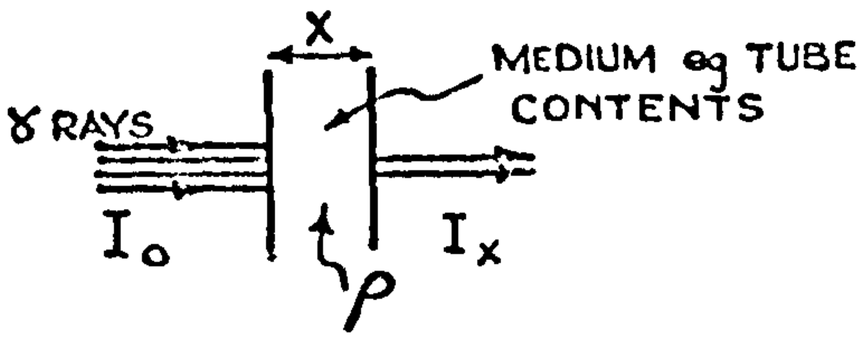

INTENSITY OF γ RAYS ATTENUATED BY MEDIUM OF DENSITY ρ ACCORDING TO

$$I_x = I_o e^{-(K_1 + K_2 \rho)}$$

WHERE K_1 ALLOWS FOR ATTENUATION EFFECTS BY OTHER THAN MEDIUM CONSIDERED

K_2 = CONSTANT FOR GIVEN GEOMETRY

SINCE K_1, K_2, I_o CONSTANTS

HENCE $\log_e I_x = K_3 - K_4 \rho$

BUT VOID FRACTION $\alpha = \dfrac{\rho_f - \rho}{\rho_f - \rho_g}$

$\therefore \log_e I_x = K_5 + K_6 \alpha$

ie. STRAIGHT LINE RELATIONSHIP BETWEEN $\log_e I_x$ AND α

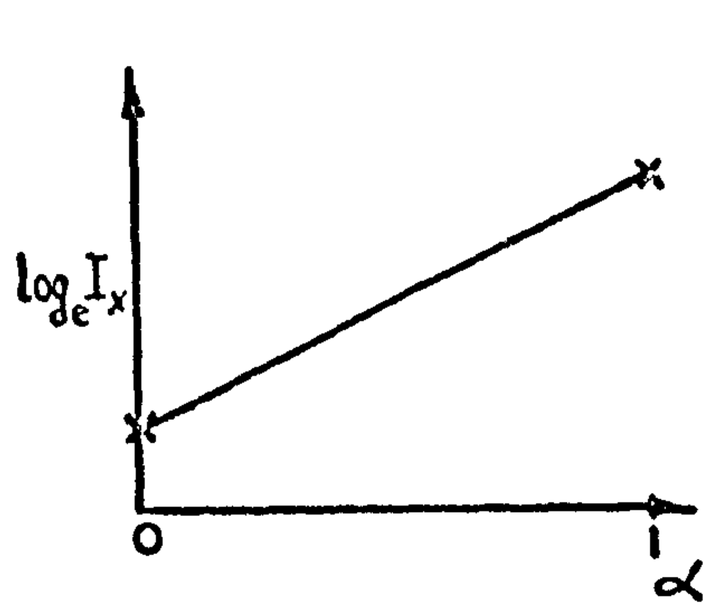

CALIBRATION LINE OBTAINED BY MEASURING I_x (IN m V.)

FOR:-

(I) TUBE WITH AIR ONLY ie $\alpha = 1$

(II) TUBE WITH WATER ONLY ie $\alpha = 0$

AND PLOTTING AS ABOVE

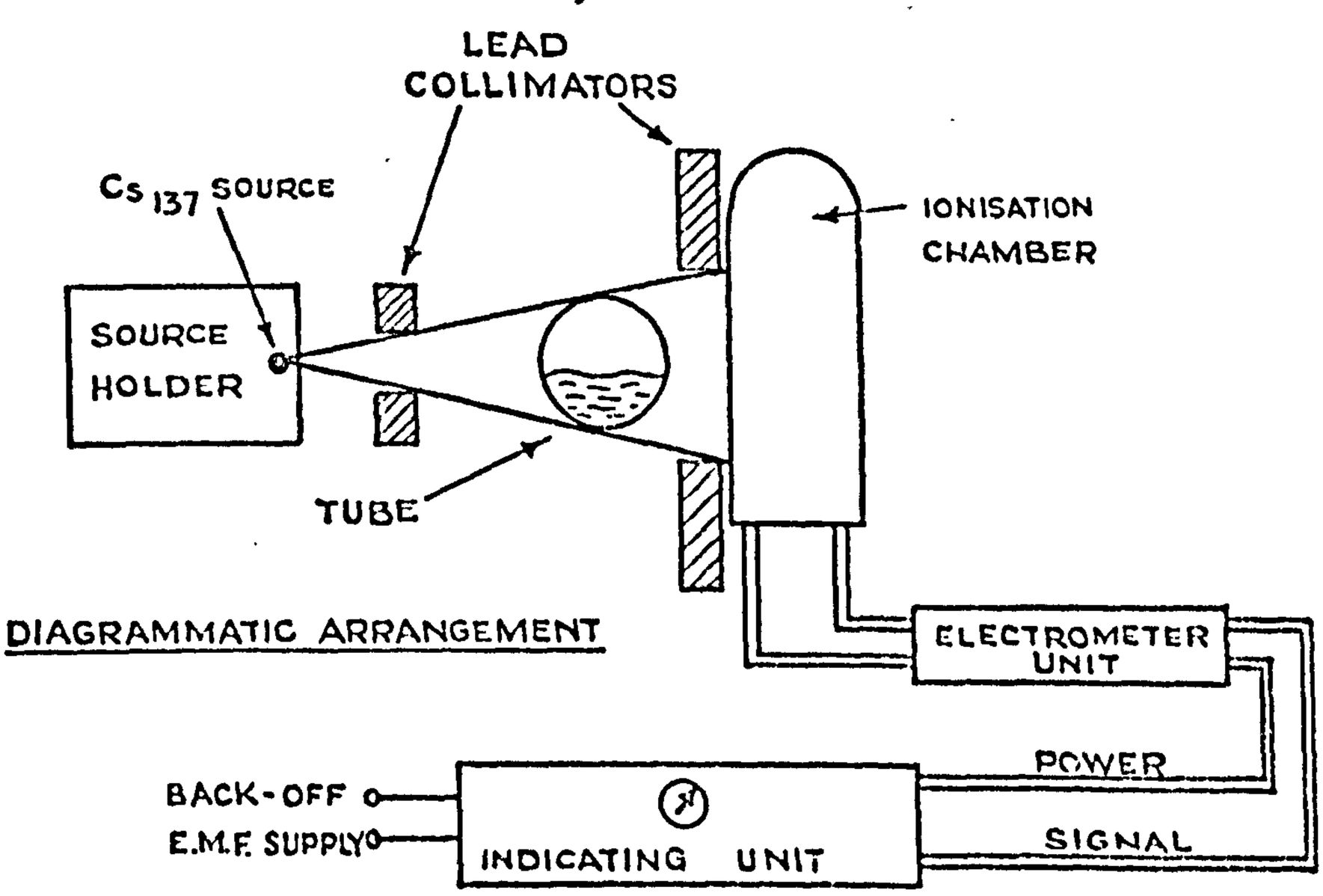

DIAGRAMMATIC ARRANGEMENT

FIG. 3-11 PRINCIPLE AND ARRANGEMENT OF VOID FRACTION APPARATUS.

accuracy of the measurements, the difference between the readings obtained from (a) and (b) was kept as large as possible and the difference measured on the most possible sensitive scale of the indicating unit. This was made possible by introducing a back (or negative) emf to the meter of approximately the same value as the milli-voltage obtained from (b), or from (a), or in between depending on the void fraction measured.

From the calibration readings, a straight line calibration characteristic was obtained for analysing subsequent readings. The co-ordinates of the calibration characteristic were

(i) $Log_e I_x$ versus α - if the two phase flow being analysed was uniformly distributed, or if the gamma ray beam was shone normal to the plane of phase separation in an asymmetrical two phase flow. See Fig. (i) below.

(ii) I_x versus α - if the gamma ray beam was shone parallel to the plane of phase separation in an asymmetrical two phase flow. See Fig. (ii) below.

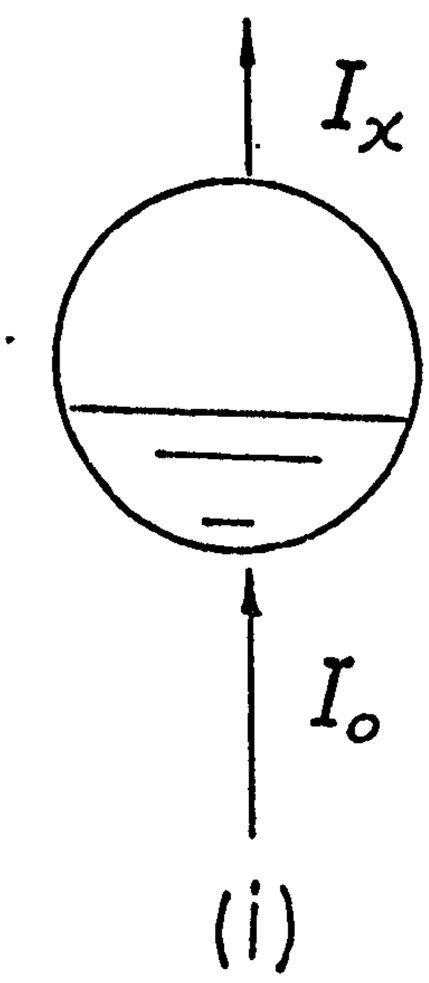

(i)

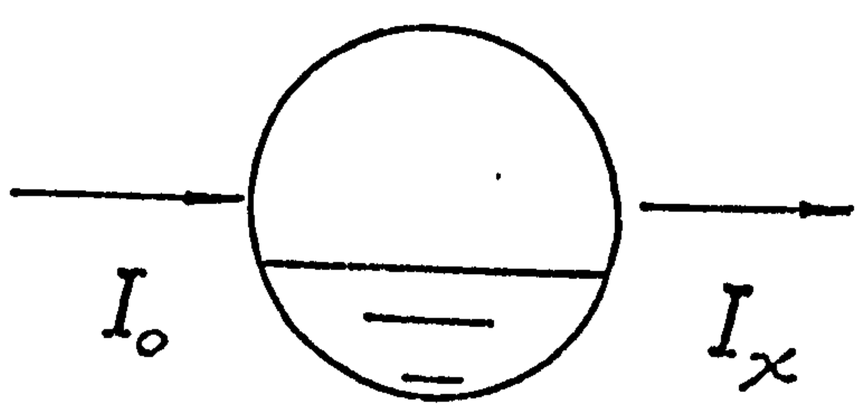

(ii)

In this project a horizontal gamma ray beam was used for the Phase 1 and Phase 2 tests (127 mm bore tube) and a vertical upwards gamma ray beam for the Phase 3 tests (216 mm bore tube).

Further details of the principles, procedures, calibrations etc. are given in Appendices D and E.

The background radiation in the working area, beyond the lead shielding around the apparatus, was continuously monitored, for safety reasons, and a zero reading on the indicating unit was frequently checked for background effects and drift.

3.4 PHOTOGRAPHIC MEASUREMENTS

Still photographs of the flow structures obtained during some of the tests were taken at a point $\sim$ 12.5 m downstream of the test section entry. The camera used was an EXAKTA type (SLR) with a maximum speed of 1/1000 sec., loaded with high speed KODAK film (400 ASA), and a fine grain paper was employed in the printing.

In order to minimize reflections and refractions caused by the perspex tube surfaces, a perspex box 610 mm x 305 mm x 305 mm was made to encase the test tube at the viewing station. The box was filled with water and the surfaces covered with black paint or cardboard except for suitable viewing and lighting apertures, as shown in Fig. 3.10.

Full details are given in Appendix F.

A few ciné-photographs were also taken using a ciné camera running at 16 frames per second and covering

a range of flow patterns.

3.5 FLOW PATTERN SENSORS

In an attempt to obtain more objective flow pattern measurements (other than visual), some effort was expended in the development of flow pattern sensors. Two types were considered (i) a pressure sensor, (ii) a void fraction sensor, each being developed on the possibility of relating fluctuations in the pressure or void fraction readings to a particular flow pattern type. Both sensors depended on a fast rate of data collection and this was made possible by the use of a high speed data acquisition system (up to 100,000 pieces per second), located in the thermodynamics laboratory, which had a mini-computer associated with it.

In general, the system involved

(i) Inserting pressure transducers into the test tube and a void fraction apparatus (γ-ray) around the tube, and obtaining from each of these an electrical signal output.

(ii) Transmitting the signals from the experimental apparatus to the data acquisition system which was housed some 100 m away.

(iii) Conditioning the signals for acceptance by the data acquisition system and mini-computer.

(iv) Develop a time base generator to actuate the collection of relevant data at required time intervals.

These items are briefly dealt with below. More detailed information being given in Appendices D, E, G, H and J.

3.5.1 CONVERTING PRESSURE FLUCTUATIONS INTO ELECTRICAL SIGNALS

Two flush mounted diaphragm type pressure transducers (Bell and Howell type 4-312) were used to measure variations in pressure and convert these into electrical signals. They had a frequency response of range 0-5 kHz which exceeded the test requirements. The signal from each transducer was conditioned and amplified to produce 0-5 V over the range 0-50 psia by a Bell and Howell transmitter type 1-375. One transducer was located ~8m downstream from the test section entry and the other ~14 m from entry. This encouraged short time pressure signals to die out before reaching the second transducer and also afforded the opportunity of cross-correlating the two signals. The 6 m distance between the transducers was an arbitrary choice.

Further information on the transducers, particularly the calibration, are given in Appendix G.

3.5.2 CONVERTING VOID FRACTION FLUCTUATIONS INTO ELECTRICAL SIGNALS

The gamma ray attenuation technique using a scintillation counter and NaI crystal was used for the void fraction measurements.

This method has not been used before for flow

pattern sensing although Jones and Zuber (J3) used an X-ray void fraction measuring technique. The main limitation of the void fraction method is the low response time of the instruments (minimum time constant 0.1 sec) but this disadvantage is partly offset by the fact that the void fraction value itself gives some indication of probable flow patterns (e.g. bubble flow at low voidage, annular flow at high voidage).

The arrangement of the apparatus was such that a Cs^{137} radioactive source shone a thin pencil beam of gamma rays vertically upwards through the centre line of the test section tube into the NaI crystal, which was affixed to the scintillation counter. The dimensions of the beam were controlled by lead collimators, on either side of the test section tube, having holes of 12.5 mm diameter. The apparatus was located $\sim$ 11.5 m downstream of the test section inlet, and is shown in Fig. 3.10.

Details of the principle of this method with instrumentation involved are given in Appendix D, which also defines methods for obtaining optimum operating conditions.

An electrical signal, which could be related to the void fraction, was available from the scintillation counting ratemeter. This covered the range 0-5 V and corresponded to full scale deflection of the ratemeter for any particular scale chosen.

3.5.3 TRANSMITTING THE SIGNALS

Co-axial cables enclosed in an earthed metal conduit

were used to transmit the signals from the apparatus to the data acquisition system . The effectiveness of this shielding and the degree of attenuation of the signal were checked by inputing a known signal at the apparatus end and monitoring the output at the data acquisition system location. No noise or attenuation of signal was detected for frequencies up to 1 kHz.

3.5.4 CONDITIONING THE SIGNALS

The analogue to digital converter (ADC) in the data acquisition unit could only accept signals in the range $\pm$ 1 V, thus the output signals from the pressure and void fraction sensors had to be brought down to within these limits. This was done after transmission, i.e. at the input to the data acquisition system as follows:

(i) The void fraction signal ranged from 0-5V, hence a simple potential divider (Fig. 3.12) was used to reduce the signals.

(ii) The pressure signals ranged from $\sim$ +1 V at zero pressure to +5 V at a higher pressure than the maximum operating pressure of the apparatus. Hence a back emf in conjunction with a variable potential divider (see Fig. 3.13) was used to condition these signals.

3.5.5 TIME BASE GENERATOR

This unit was essential to the data collection. The computer responds to a given triggering pulse and reads the values of the signals at the input channels; thus

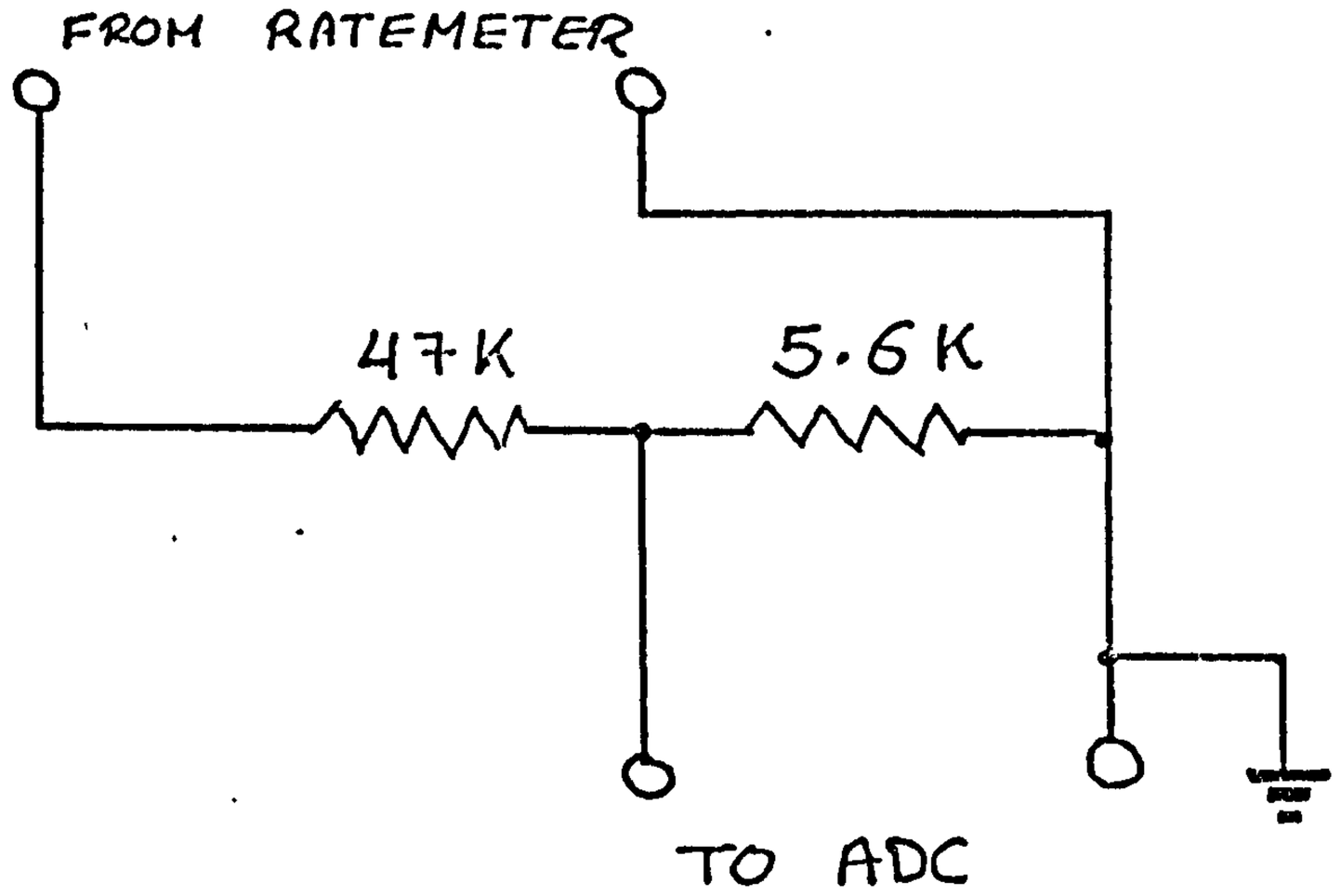

FIG. 3·12 VOID SIGNAL POTENTIAL DIVIDER

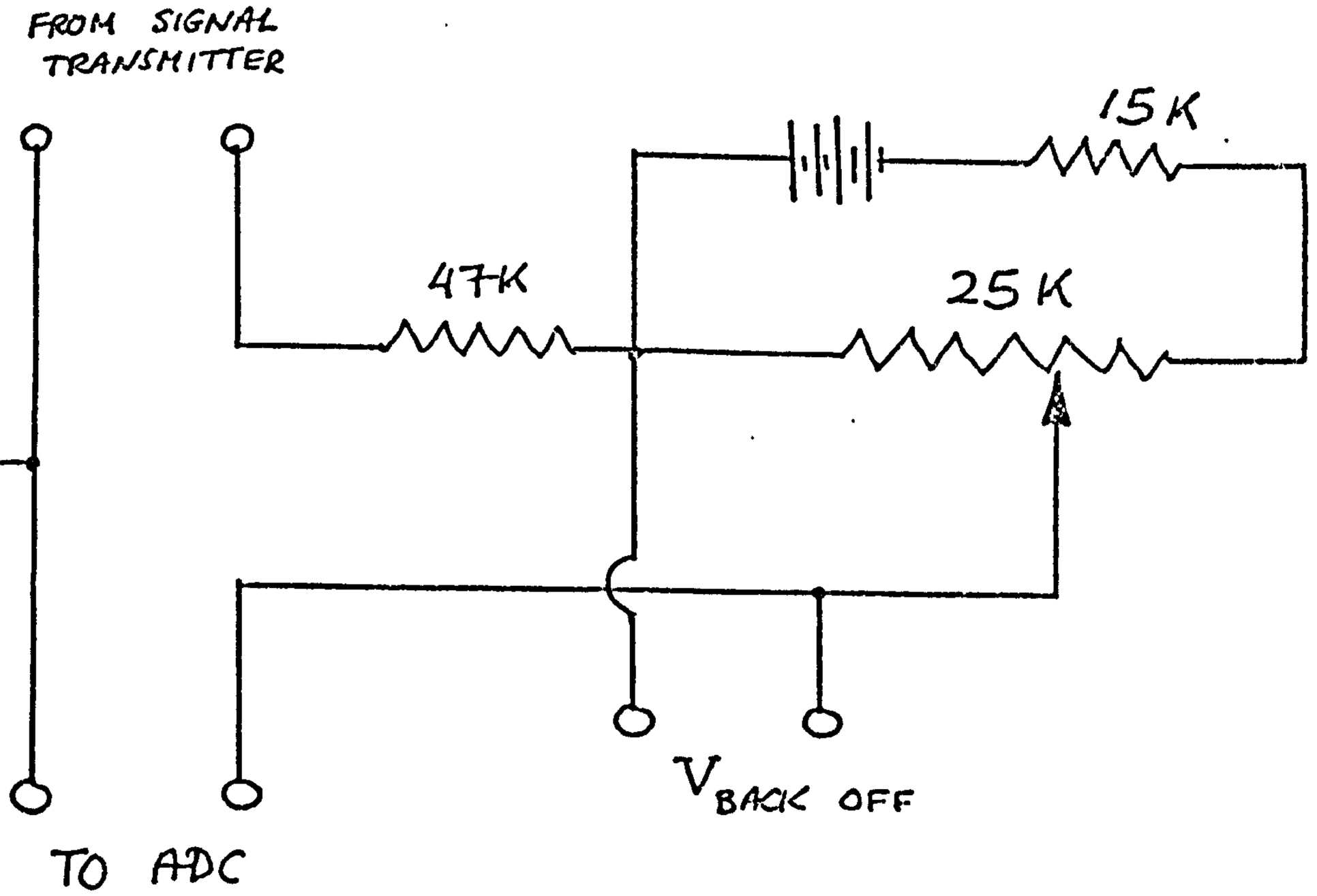

FIG. 3·13 PRESSURE SIGNAL POTENTIAL DIVIDER

pulses must be supplied at the appropriate times. This was done by a time base generator which took the form of a crystal oscillator circuit incorporating a 100 kHz Quartz crystal. Different frequencies of data collection could be obtained by using different combinations of dividing counters (multivibrator integrated circuits) as explained in Appendix H. The frequencies were checked with a calibrated oscilloscope and found to be exact.

3.5.6 COMPUTER CONTROLLED DATA ACQUISITION SYSTEM

A photograph of the data acquisition system is shown in Fig. 3.14. The main constituent being a Hewlett-Packard 2100 mini-computer with a 16 K memory. In addition, 1000 K of back up store from a cartridge disc system were available. The peripherals to the mini-computer were standard Hewlett-Packard or Tektronix items. The speed of operation was limited by the speed at which the analogue signal from each channel was converted to digital form. The analogue to digital converter (ADC) was rated at 100,000 signals per sec with a sensitivity of $\sim \pm$ 2 mV (i.e. 1000/512). A schematic diagram of the hardware is shown in Fig. 3.15. As can be seen, analogue signals were allowed to pass through the multiplexer unit and the ADC to the computer core by the 'Direct Memory Access' and then stored in the core. This enabled about 5000 words of store to be allocated to each of the three channels. The data was then transferred to a permanent store in the cartridge subsystem as explained in Appendix J.

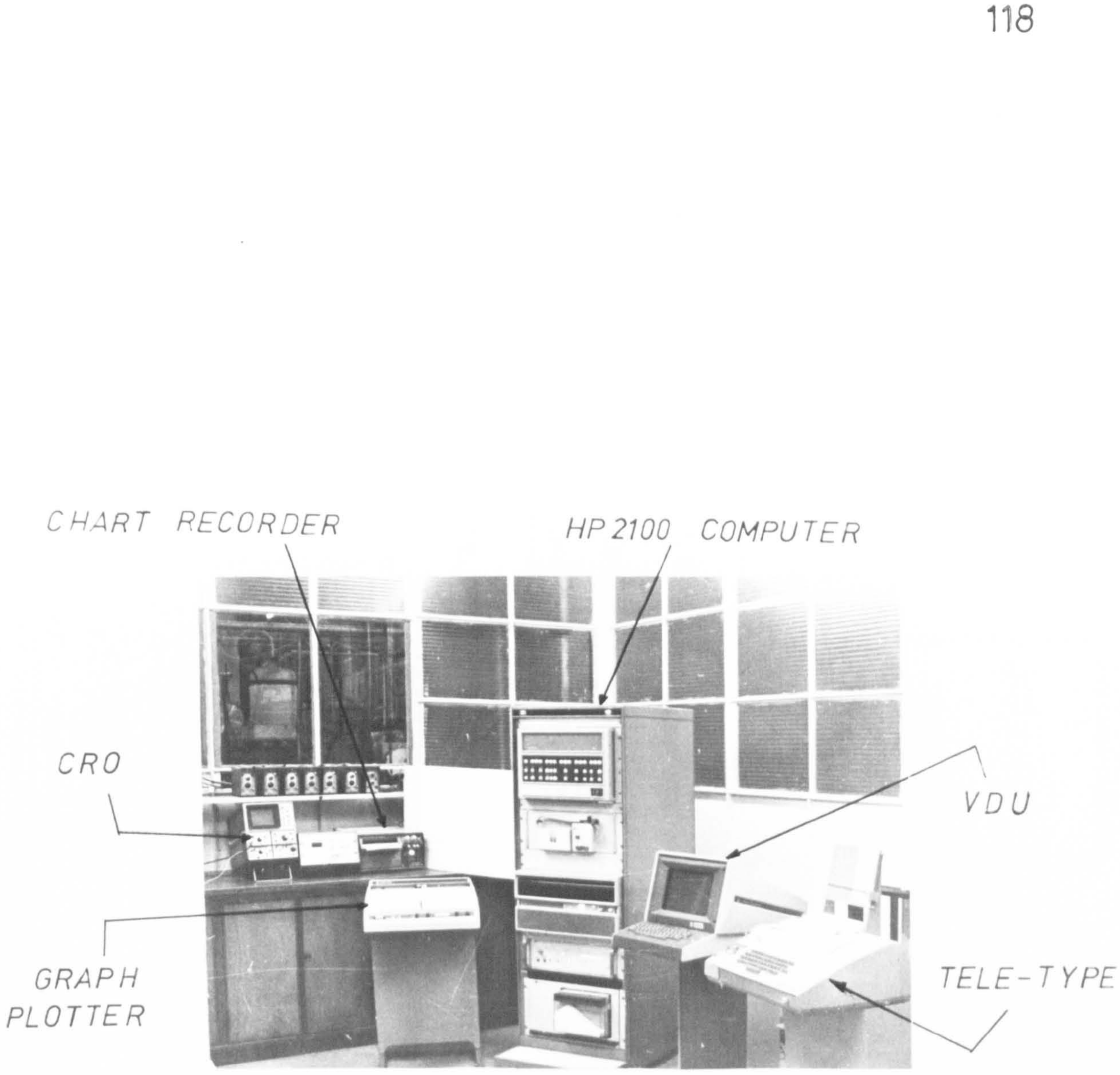

FIG 3·14 HIGH SPEED DATA ACQUISITION SYSTEM

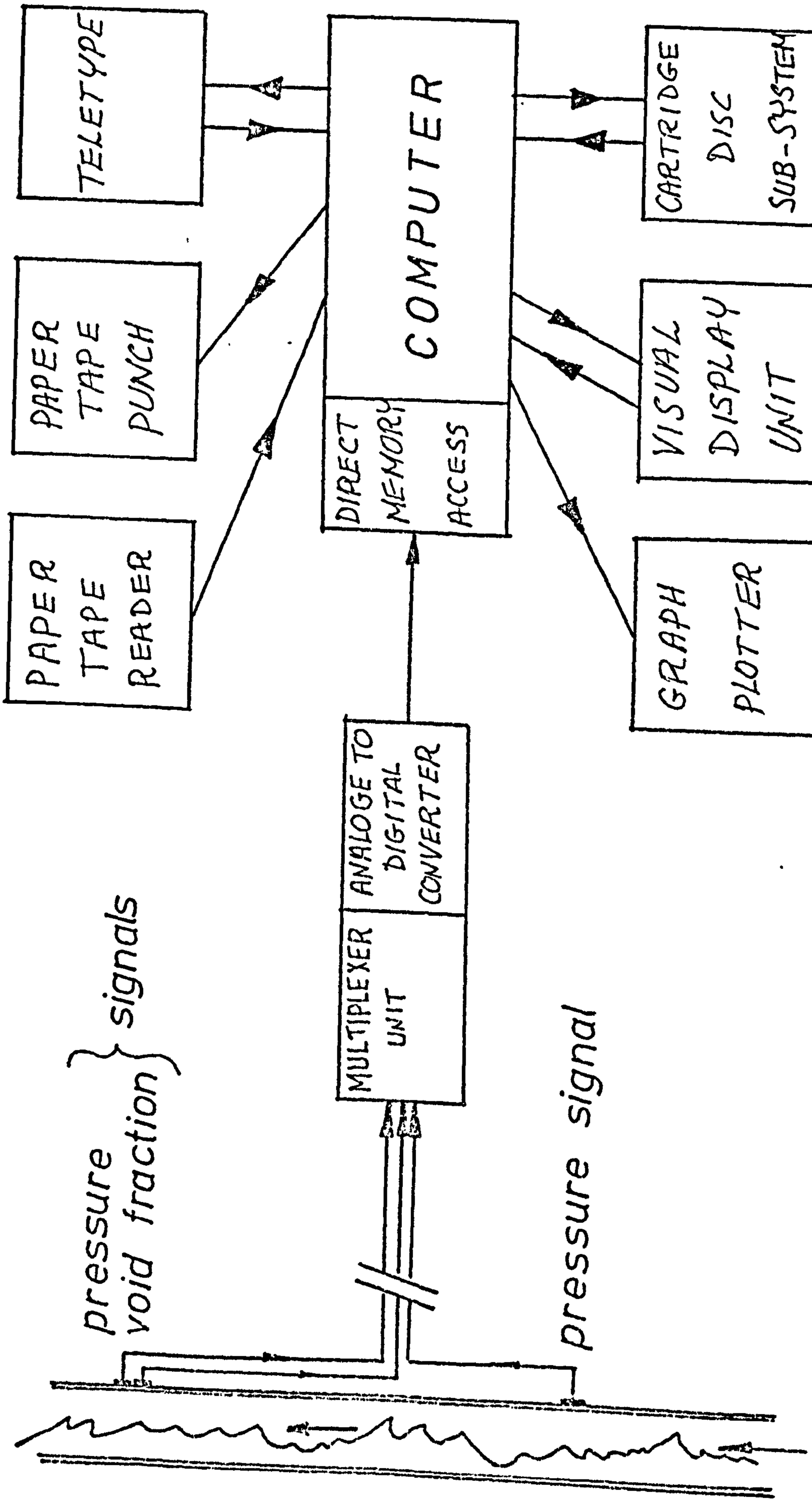

FIG. 3.15 SCHEMATIC DIAGRAM OF DATA ACQUISITION SYSTEM

The stored data could either be:

(i) Printed on the teletype to provide a permanent hard copy in digital form.

(ii) Displayed on the visual display unit (VDU) in either digital or graphical form (which could be photographed to provide a permanent record).

(iii) Presented in graphical form by graph plotter.

(iv) Transferred to paper tape for processing on a larger computer.

The system was checked out using known input signals and found to be completely satisfactory.

More detailed information is given in Appendix J.

CHAPTER 4

TEST PROGRAM AND PROCEDURE

CHAPTER 4 TEST PROGRAM AND PROCEDURE

4.1 RANGE OF CONDITIONS

The flow conditions investigated covered the complete range of air and water flow rates up to the maximum possible values of 0.33 m^3/s and 0.065 m^3/s respectively. The flow field was divided into four major areas to coincide with the flow rate instrumentation required. These are detailed below. In addition each area was divided into a grid of air and water flow rate test conditions. The tests were conducted in the following order:

(i) Series 'A' Tests - high water flow rates, low air flow rates.

Water flow rates measured using orifice plate and $Hg-H_2O$ manometer.

Air flow rates measured using rotameters.

(ii) Series 'B' Tests - low water flow rates, low air flow rates.

Water flow rates measured using orifice plate and $air-H_2O$ manometer.

Air flow rates measured using rotameters.

(iii) Series 'C' Tests - low water flow rates, high air flow rates.

Water flow rates measured using orifice plate and $air-H_2O$ manometer.

Air flow rates measured using orifice plate and $air-H_2O$ manometer.

(iv) Series 'D' Tests - high water flow rates, high air flow rates.

Water flow rates measured using orifice plate and Hg-H_2O manometer.

Air flow rates measured using orifice plate and air-H_2O manometer.

Figs. 4.1, 4.2 and 4.3 show the overall range of conditions for Phases 1, 2 and 3 respectively and Tables 4-1 and 4-2 give further details.

4.2 TEST PROCEDURE

At each test condition, i.e. each setting of air and water flow rate, measurements were taken relating to air and water flow rates, void fraction, pressure distribution (16 tapping points) and mixture temperature, in addition to visual observations and comments on the flow structure. Fig. 4.4 shows the 'data sheet' used to record these raw data, together with a sample of such data. The test procedure involved setting the water flow rate to the required value and then adjusting the air flow rate.

The detailed procedure was as follows:

(i) The purging rate was adjusted and the sixteen piezometer zero readings (mm H_2O) and purging rates (gal/hr) noted.

(ii) The water flow rate was set to the required value and measured using the appropriate instrumentation detailed earlier.

(iii) Tube full of water readings of the void fraction

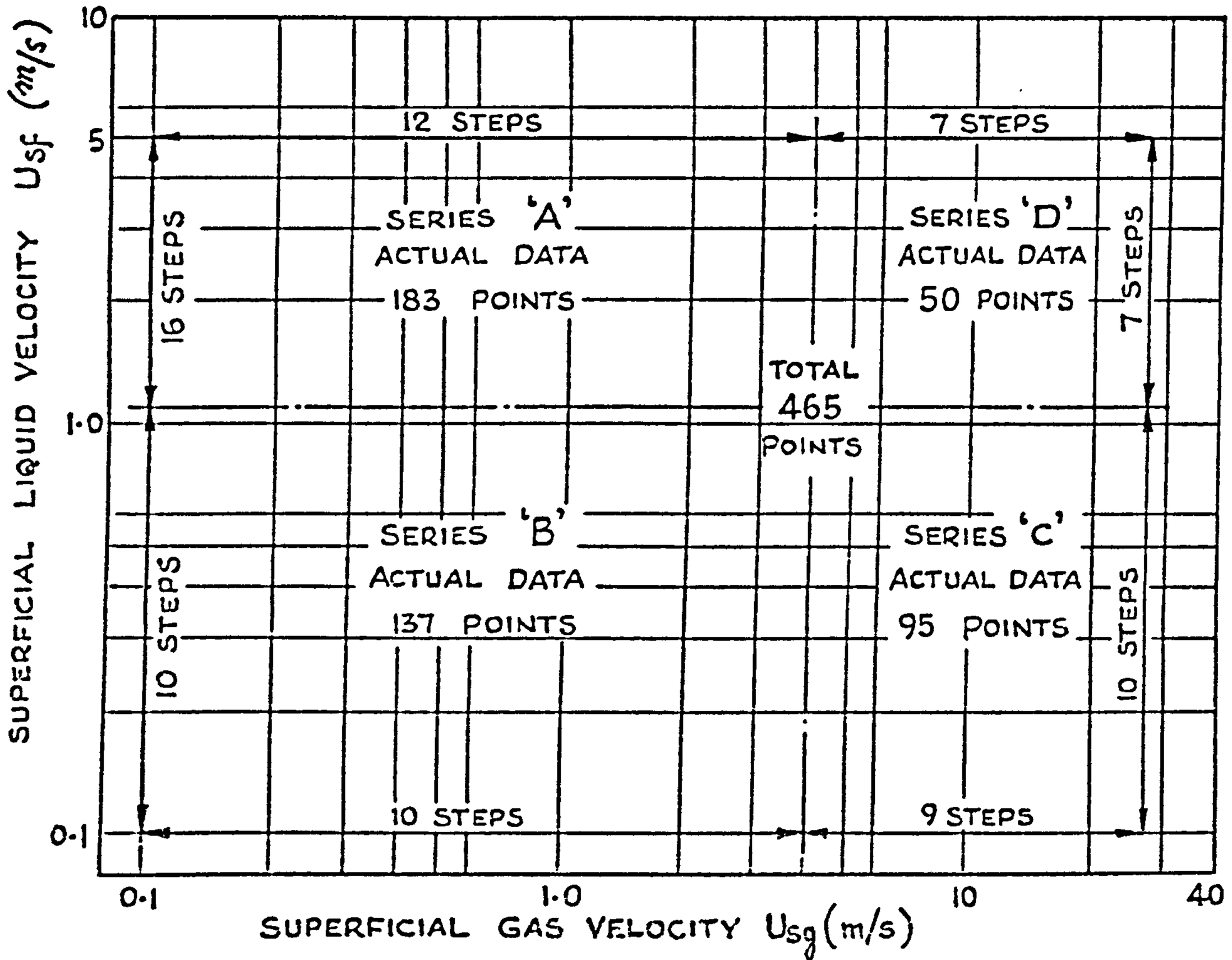

SERIES 'A' WATER FLOW - $Hg-H_2O$ MANOMETER AIR FLOW - ROTAMETERS
SERIES 'B' WATER FLOW - $AIR-H_2O$ MANOMETER AIR FLOW - ROTAMETERS
SERIES 'C' WATER FLOW - $AIR-H_2O$ MANOMETER AIR FLOW - ORIFICE
SERIES 'D' WATER FLOW - $Hg-H_2O$ MANOMETER AIR FLOW - ORIFICE

(PHASE 1 TESTS)

FIG. 4·1 TEST PROGRAM (MIXER BEFORE BEND)

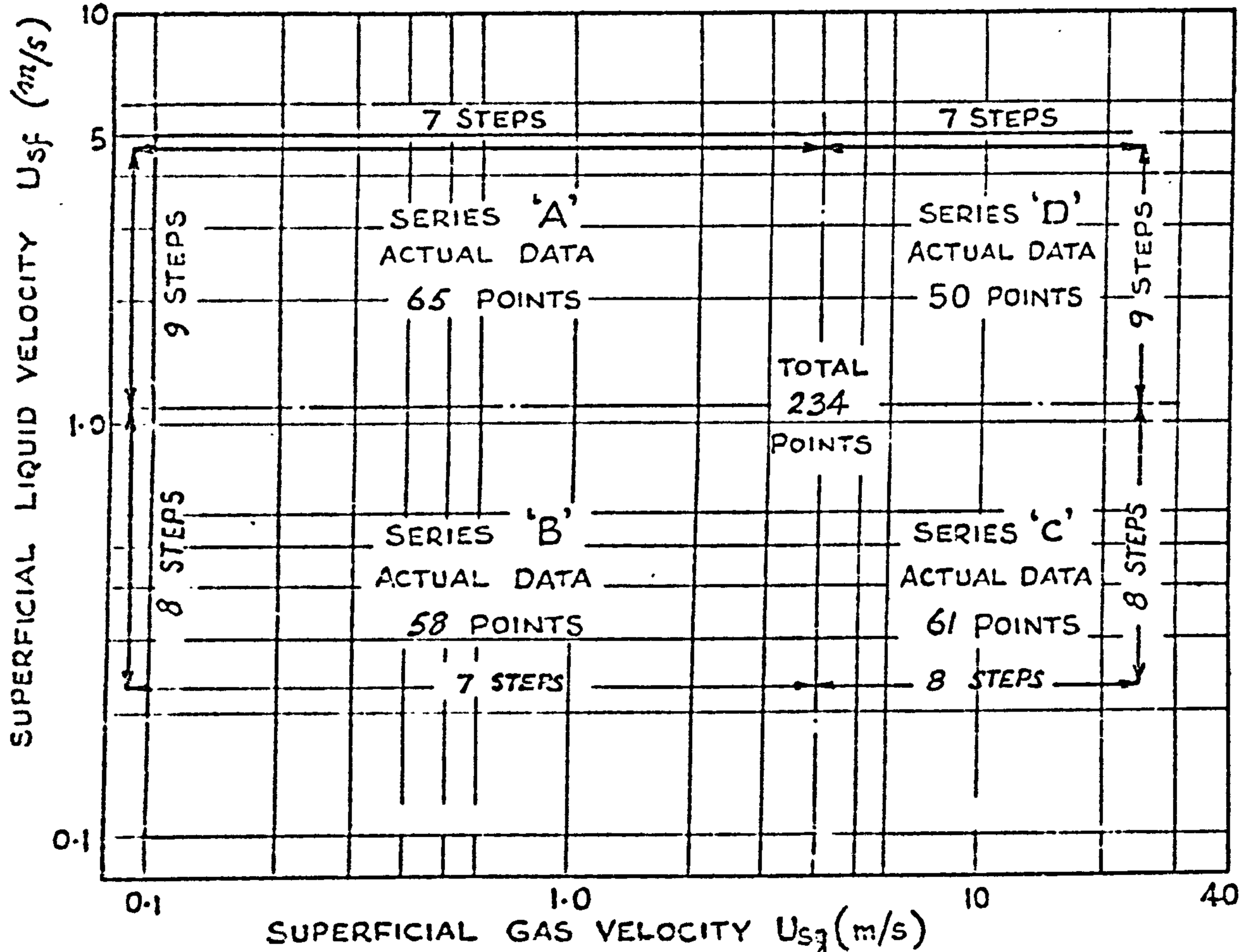

SERIES 'A' WATER FLOW - $Hg-H_2O$ MANOMETER AIR FLOW - ROTAMETERS
SERIES 'B' WATER FLOW - AIR-H_2O MANOMETER AIR FLOW - ROTAMETERS
SERIES 'C' WATER FLOW - AIR-H_2O MANOMETER AIR FLOW - ORIFICE
SERIES 'D' WATER FLOW - $Hg-H_2O$ MANOMETER AIR FLOW - ORIFICE

FIG. 4·2 TEST PROGRAM (MIXER AFTER BEND) (PHASE 2)

SERIES 'A'	SERIES 'B'	SERIES 'C'	SERIES 'D'
WATER FLOW- Hg-H O MANOMETER	WATER FLOW- AIR-H O MANOMETER	WATER FLOW- AIR-H O MANOMETER	WATER FLOW- Hg-H O MANOMETER
AIR FLOW- ROTAMETERS	AIR FLOW- ROTAMETERS	AIR-FLOW- ORIFICE	AIR-FLOW- ORIFICE

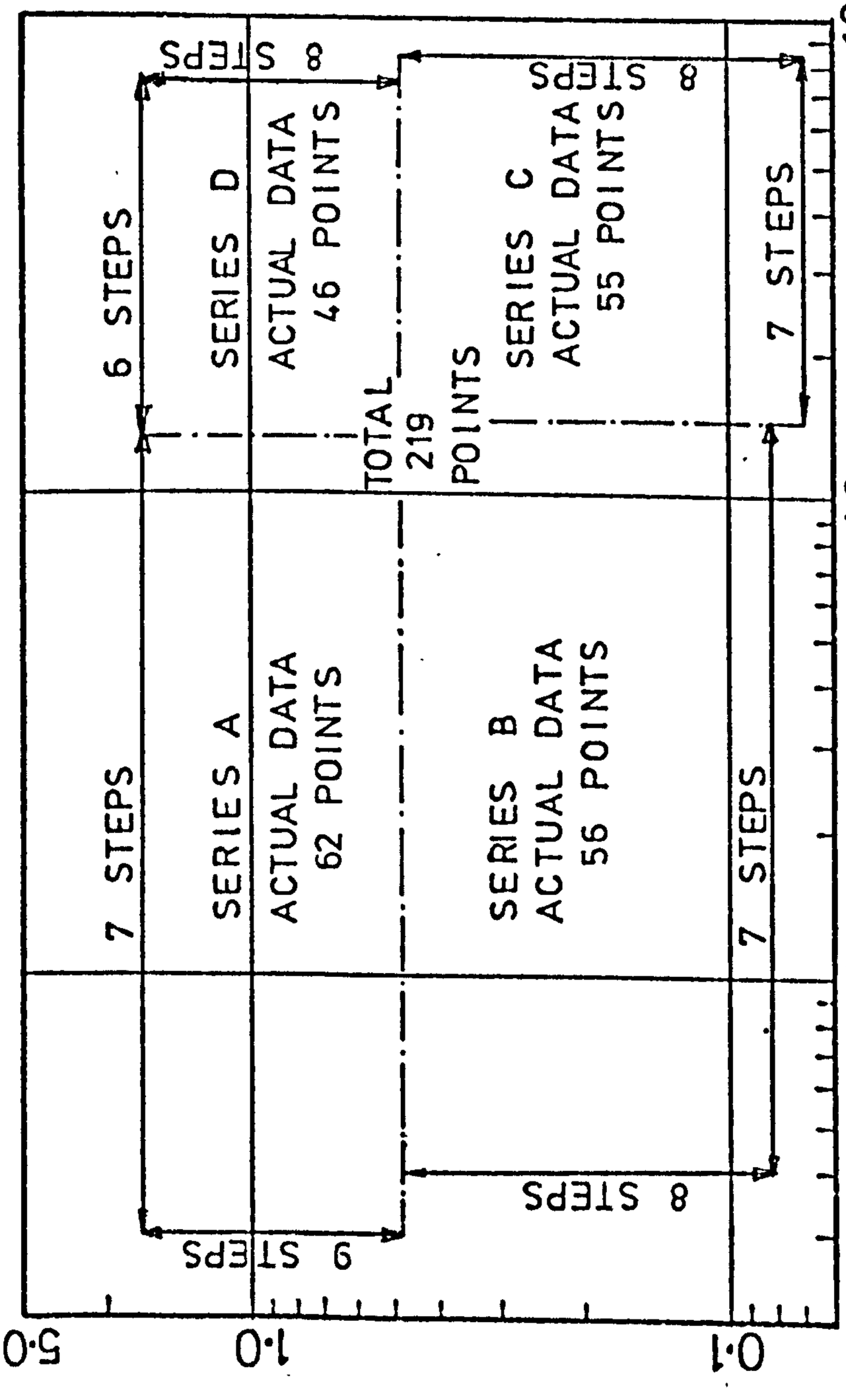

TEST PROGRAM (PHASE 3 TESTS)

FIG.4·3

	Phase 1 and 2	Phase 3
Tube diameter (nominal bore)	127 mm (5")	216 mm (8.5")
Test section length	16 m (52 ft) ≡ 125 diameters	16 m (52 ft.) ≡ 74 diameters
Water volume flow rate	0 to 0.065 m^3/s (2.3 ft^3/s)	0 to 0.062 m^3/s (2.18 ft^3/s)
Air volume flow rate	0 to 0.33 m^3/s (12.4 ft^3/s)	0 to 0.316 m^3/s (11.2 ft^3/s)
Water superficial velocity	0 to 5.1 m/s (16.7 ft/s)	0 to 1.68 m/s (5.5 ft/s)
Air superficial velocity	0 to 26 m/s (92 ft/s)	0 to 8.63 m/s (28.2 ft/s)
Water mass flow rate	0 to 64 Kg/s (141 lb/s)	0 to 61.3 Kg/s (135 lb/s)
Air mass flow rate	0 to 0.45 Kg/s (1 lb/s)	0 to 0.39 Kg/s (0.86 Kg/s)
Number of test conditions	465 (over 350 tests with static pressure distribution) for phase 1. 234 for phase 2.	219 (plus over 100 repeat tests)
Flow patterns covered	Bubbly, plug, slug, stratified, wavy, annular	plug, slug, stratified, wavy

TABLE 4-1 RANGE OF TEST CONDITIONS COVERED IN THIS PROJECT

	Phase 2	Phase 3
Total number of tests	28	31
Type of data collected per reading	2 pressure 1 void fraction	2 pressure 1 void fraction
Number of data collected per channel per test	4,800	4,800
Speed of acquisition used (sec^{-1}) and number of tests covered	10 (1 test) 40 (23 tests) 100 (4 tests)	10 (2 tests) 40 (29 tests) 100 (-)
Total number of data collected	403,200	446,400
Flow patterns covered	Bubbly, slug, plug, stratified, wavy, annular	Stratified, wavy, plug, slug

TABLE 4-2 DETAILS OF PULSATIONS DATA COLLECTED IN THIS PROJECT

FIG. 4.4 DATA SHEET

						NUMBER
					24/2	DATE
		0·49		0·58	0·71	EMF mV
		18·5		14·5	11·0	TEMP. °C
						WATER FLOW cm h_{H_2O}
		106·4		107·3	107·3	h_{Hg}
		1·79		1·87	1·65	AIR FLOW cm P_{BAR}
		30·1		14·7	6·2	h_1
						h_2
						h_3
						h_4
145		666		450	200	VOID FRACTION ELE
34·27		43·49		43·74	44·06	POT
		—		—	1673	TEST SECTION PRESSURE mm H_2O h_1
		1693		1550	1498	h_2
		1515		1404	1372	h_3
		1428		1342	1313	h_4
		1204		1161	1137	h_5
		1042	1481	1003	1023	h_6
		754	1258	783	862	h_7
	1686	466	1043	565	711	h_8
	1390	157	825	358	565	h_9
	1125	-110	649	160	425	h_{10}
	882	-365	472	-13	279	h_{11}
	600	-643	247	-237	117	h_{12}
	333		51		-30	h_{13}
	5		-200		-223	h_{14}
	-284		-416		-380	h_{15}
	-580		-618		-531	h_{16}
	258		223		178	MAN. PRESS. cm Hg
8	8		8		8	PURGE RATE GAL/HR
	13		13		13	CALMING LENGTH m
ZERO READING		SLUG		SLUG	SLUG	FLOW PATTERN

apparatus were taken which involved

(a) an electrometer reading (mv)

(b) a potentiometer reading (mv)

(iv) Air was then admitted to the mixing chamber and the flow rate adjusted to the required value.

When using rotameters, the measurements involved,

(a) float height in each of the four rotameters (cm)

(b) operating pressure of the rotameters (bar, gauge)

(c) emf of thermocouple (mv)

When using the orifice plate, the measurements involved,

(a) head difference across orifice (cm H_2O)

(b) upstream pressure (bar, gauge)

(c) emf of thermocouple (mv)

(v) The mixture temperature was taken as that of the water in the separation tank and was measured by a thermometer (^oC).

(vi) To obtain measurements of the static pressure along the test section, the following readings were taken

(a) the water level in the sixteen piezometer lines (mm H_2O)

(b) the manifold pressure (mm Hg, gauge).

When the pressure drop across the test section was more than 2.5 m H_2O (i.e. greater than the height of the piezometer tubes), only the first ten piezometer readings were taken. After this, the last ten readings were taken so that the two sets of readings overlapped over more than three piezometer readings

to determine the normalising factor accurately.

(vii) Visual observations and comments on the flow pattern and its settling length were recorded.

(viii) The air flow rate was changed keeping the water flow rate constant, and steps (ii) to (vii) repeated.

When collecting the pressure and void fraction pulsation data, the same general procedure was followed with the exception that steps (i) and (vi) were omitted. In addition, the process involved setting the instruments and checking the signals at the computer end. The procedure followed was:

(i) The ratemeter 'pulse per second' switch was set to the appropriate value to obtain a reasonable reading within the scale of the meter movement. the 'pps' switch position was noted.

(ii) The signals were monitored at the input to the computer using a calibrated oscilloscope. Adjustments of the back off voltages were made to bring the pressure signals to within $\pm$ 1 volt.

(iii) The required speed of acquisition was set by selecting an appropriate frequency from the crystal oscillator.

(iv) The acquisition binary tape was loaded into the photoreader and run in accordance with the procedures outlined in the HP2100A computer manual.

(v) The data was then transferred to the disc and stored in a pre-selected tracks (3 tracks per test). The track numbers were noted.

(vi) To check that the whole process was successful; the stored data was displayed on the VDU, and if necessary steps (iv) to (vi) repeated. At this stage communication with the mini-computer was made through the DOS-M system, by feeding in the DOS-M binary tape.

Each test condition was identified by a six character 'Test Run Number', composed of, from left to right the test number (2 characters), day (2 characters) and month (2 characters) respectively.

4.3 CONVERSION INTO MEANINGFUL DATA

The number of readings collected per test was comparatively large and the conversion into meaningful and useful data involved repetitive calculations such as those detailed in Appendix (M).

Over 1000 test conditions were examined and in order to eliminate manual conversion, a computer program was developed to convert the measured quantities into meaningful results. This reduced the manual procedures to:

(i) A plot of the static pressure distribution along the test section (to determine the pressure gradient and settling lengths).

(ii) A conversion of the head difference across the water orifice into units of cm H_2O when the Hg-H_2O manometer was used at high water flow rates (density difference was taken as 12.55).

(iii) A calculation of the static pressure in the settled part of the test section, in units of cm H_2O, for property corrections.

More detailed information on the computer program used is given in Appendix (N).

Air and water properties were determined from standard tables of properties for dry air and distilled water respectively. Measurements of water properties before, and after four hours of testing showed no significant difference from those given in the standard tables as can be seen from table 4-3.

4.4 ESTIMATED EXPERIMENTAL ACCURACY

The accuracy of the water flow rate measurements was dependent on the manometer head readings and the calibration characteristics. From Fig. B5, the calibration characteristic was consistent to within $\pm$ 2% of the data points (and was 3% higher than the characteristic obtained by calculation using B.S. 1042). The in-situ calibration involved errors in manometer readings, hence the estimated accuracy of the flow rate readings is $\pm$ 2%.

For air flow rates, the rotameter float height reading and the orifice head difference reading were measured to the nearest mm, and the accuracy is estimated to be within $\pm$ 2%.

The manometers and piezometers used in measuring the test section pressures and pressure differences could be read to the nearest mm water (relative to inclined or vertical manometers). Since the minimum pressure

Temperature °C	Density Kg/m^3			Viscosity C poise		
	Tables	Measured		Tables	Measured	
		Before	After		Before	After
25	997.07	1000.38	1000.73	0.8960	0.83470	0.89880
30	995.67	998.78	999.08	0.7975	0.74456	0.79720
35	994.06	997.05	997.44	0.7150	0.68020	0.75588
Total dissolved solids	None					

Table 4-3 Water Properties as a Function of Temperature

difference over the settled length of test section was 80 mm water, this gave the maximum error of pressure gradient measurement as approx. 1%. Since a number of pressure readings were used to determine the gradient, this is conservative and most errors are likely to be much less than 1%. The errors due to purging were estimated to be less than 1% making a total possible error in the measurement of less than 2%.

It is difficult to assess the errors associated with void fraction measurements, but from previous tests carried out on a larger diameter (18") steel pipe, they were found to be within $\pm$ 10%, except perhaps at very low void fractions (Fig. 4.5). In this project a modified in-situ calibration was also employed which should improve the accuracy of stratified flow values.

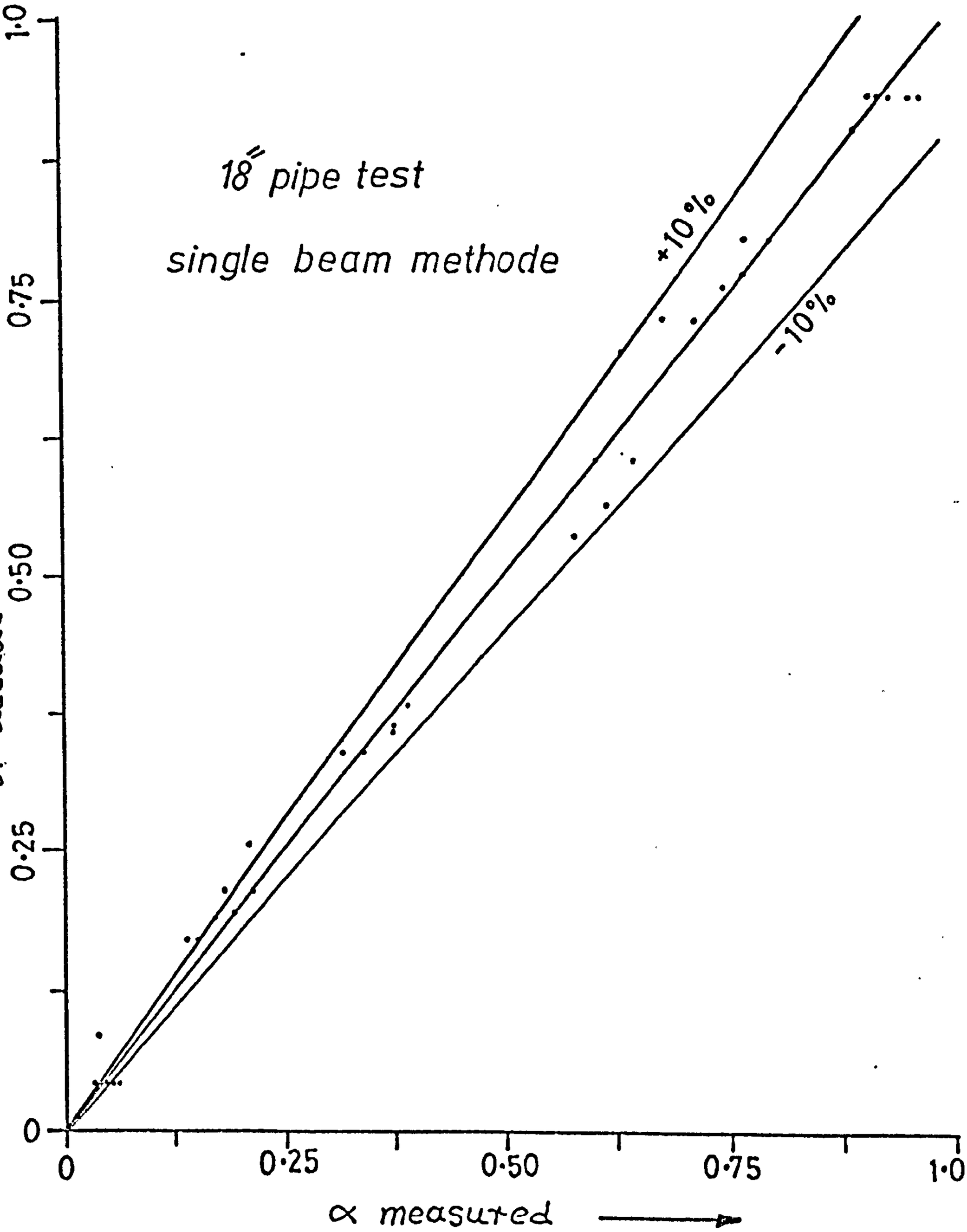

FIG 4·5 VOID FRACTION CALIBRATION

CHAPTER 5 EXPERIMENTAL RESULTS

CHAPTER 5 EXPERIMENTAL RESULTS

5.1 PRESSURE DROP DATA

The first step in the conversion of the raw data (a sample was given in Fig. 4.4) into useful information was to plot the static pressure distribution along the test section, as shown in Fig. 5.1. The slope of the linear part of the graph determined the pressure gradient, whilst deviations from linearity determined the region where the flow was unsettled. Families of these graphs are given in Appendix R for Phases 1, 2 and 3. The pressure drop data for particular air and water flowrates, under settled conditions, are given in Appendix S with a specimen shown in Fig. 5.2 which corresponds to the raw data shown previously in Fig. 4.4.

5.2 SETTLING LENGTH DATA

The settling length required, whether after a return U-bend (Phase 1) or after a mixing chamber (Phases 2 and 3), at inlet to the test section was obtained from

(i) the static pressure distribution graphs given in Appendix R,

(ii) visual observations of the flow pattern stabilising.

The settling lengths required at the test section exit were also determined from the static pressure distribution graphs and these, together with other useful data, are also presented in Appendix S with a specimen in Fig. 5.2.

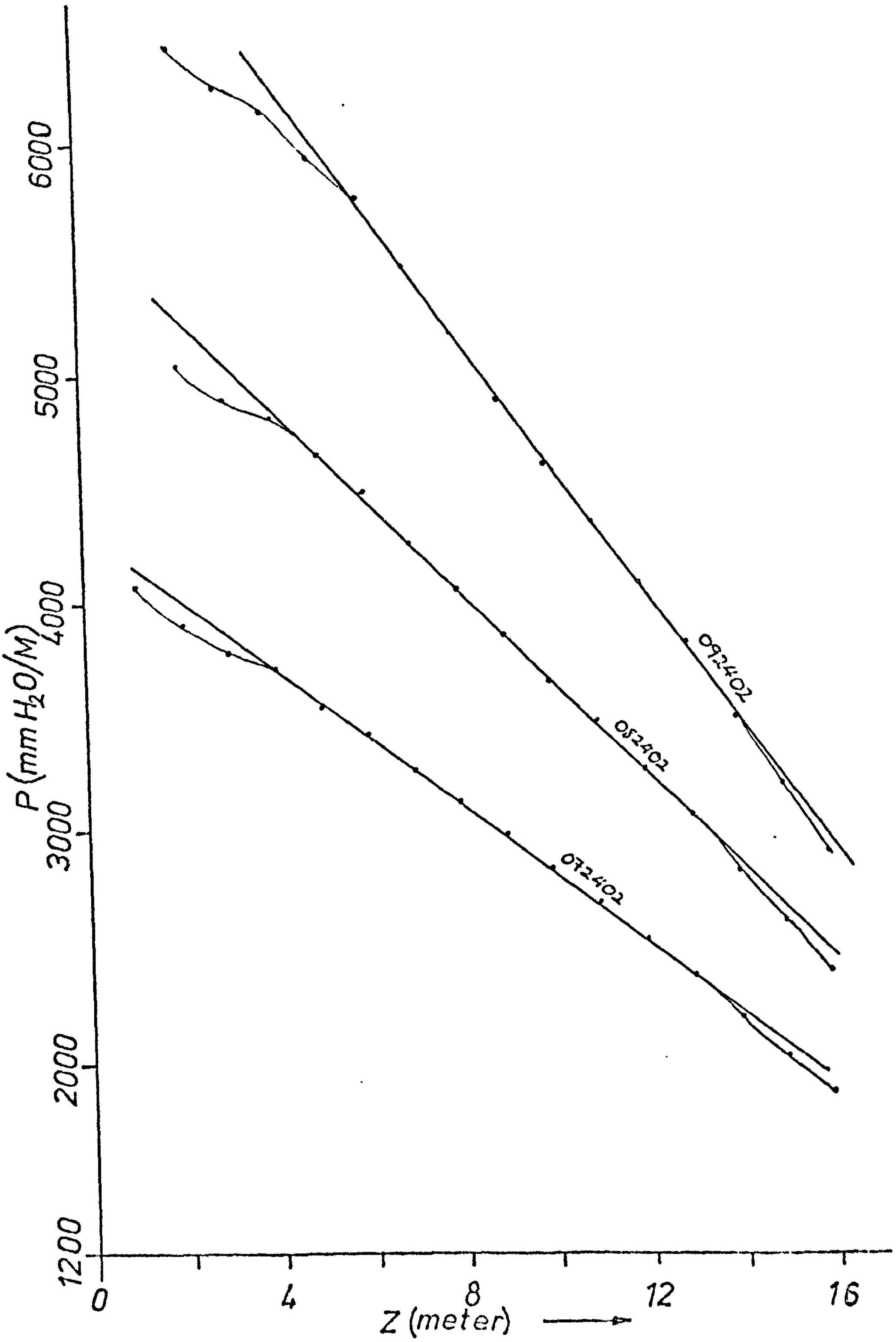

FIG. 5·1 STATIC PRESSURE DISTRIBUTION PLOT

TEST RUN NO	TEMP C	P MEAN KN/M2	VOID FRCTN	WATER FLOW RATE M3/SEC	AIR FLOW RATE M3/SEC	DENSITY WATER KG/M3	DENSITY AIR KG/M3	SETTLING LENGTH,L INLET L	INLET L/D	OUTLET L	OUTLET L/D	METRE FLOW PATRN L	PATRN L/D	PR-GRAD KN/M3	FLOW PATTERN
22402	13.5	128.75	0.505	0.045224	0.070136	999.34	1.5705	3.75	29.5	4.25	33.5			1.51187	2
32402	16.5	137.36	0.581	0.045146	0.097850	998.89	1.6340	7.25	57.1	3.75	29.5			2.09753	2
42402	20.5	142.01	0.644	0.045172	0.119646	998.13	1.6910	4.75	37.4	3.75	29.5			2.75133	2
52402	23.0	151.06	0.681	0.045328	0.146012	997.37	1.7834	5.25	41.3	3.75	29.5			3.47591	2
72402	11.0	126.11	0.420	0.050212	0.044862	999.63	1.2719	3.25	25.6	3.75	29.5			1.65432	2
82402	14.5	133.32	0.565	0.050224	0.068818	999.20	1.6206	3.75	29.5	3.75	29.5			1.94069	2
92402	18.5	141.41	0.576	0.050013	0.092676	998.53	1.6953	5.25	41.3	3.25	25.6			2.72181	2
12302	12.0	127.23	0.371	0.053005	0.039879	999.32	1.5678	3.25	25.6	3.75	29.5			1.47100	2
22302	14.0	135.94	0.452	0.053069	0.061371	999.27	1.6334	4.25	33.5	3.75	29.5			2.18366	2
32302	19.0	146.09	0.573	0.053003	0.089728	998.44	1.7183	5.25	41.3	3.75	29.5			3.16179	2
12602	11.5	130.28	0.362	0.059461	0.037582	999.58	1.6004	0.75	5.9	4.5	35.4			1.79902	2
22602	19.0	141.91	0.507	0.058485	0.067042	998.44	1.6984	4.25	33.5	3.5	27.6			2.36963	2
32602	22.5	148.35	0.540	0.059126	0.083258	997.88	1.7344	4.25	33.5	3.75	29.5			3.24637	2

FIG. 5.2 PRESSURE DROP, SETTLING LENGTH AND OTHER DATA DERIVED FROM EXPERIMENTAL READINGS

5.3 FLOW PATTERN DATA

The flow patterns observed visually in the settled part of the test section are also given in Appendix S in terms of one of the six flow pattern types (on their transitions) detailed in Table 5-1. Flow pattern data are also shown in Figs. 5.3, 5.4 and 5.5, for Phase 1, 2 and 3 respectively, on a nominal co-ordinate system of superficial water velocity versus superficial air velocity. These co-ordinates are used simply as a means of presentation and to facilitate comparison with some of the existing flow pattern maps. Photographs of some of the flow patterns encountered are shown in Figs. 5.6 to 5.9, these covering some of the pressure and void fraction pulsation data given in Table 5-2 and plotted against time in Figs. 5.10 to 5.13.

5.4 PRESSURE AND VOID FRACTION PULSATION DATA

The pressure and void fraction pulsation data collected were stored on two magnetic discs, one for the Phase 2 tests and the other for the Phase 3 tests. These discs are stored in the Department of Thermodynamics and Fluid Mechanics, University of Strathclyde.

Specimen results are shown in Figs. 5.10 to 5.13 the remainder being given in Appendix Y. These curves are shown plotted to a base of time, on each figure. These are, reading from top to bottom, local void fraction, pressure near the end of the test section ($\sim$ 14 m from

Table 5-1

Flow Pattern	Code	Description
Bubbly	1	The gas is dispersed in fine bubbles through the liquid phase such that the bubble concentration near the top of the tube is much higher than anywhere else.
Plug	6	The gas moved as long bubbles or plugs along the upper side of the tube. The plugs could be of fair size and length.
Slug	2	At moderate liquid and low gas flow rates, the slug front appears to roll on the wavy liquid ahead feeding bubbles to the liquid slug. The air plugs could occupy up to $\frac{3}{4}$ of tube diameter. At low gas and liquid flowrates, a wave grows and blocks the pipe to form a slug which traverse the whole tube leaving a thin stratified-wavy layer. The layer thickness builds up until slug is formed. At high flowrates, the slug frequency increases, and the slugs become very frothy and milky in appearance making it difficult to distinguish the flow structure.

Flow Pattern	Code	Description
Stratified	3	Liquid flows in the lower part of the pipe and the air on top with a smooth interface. A hydraulic gradient exists such that the liquid level decreases downstream.
Wavy	4	Same as above but with wavy interface, and with the hydraulic gradient less obvious. The waves range from small to long wavelengths, small amplitude to large ones, and, at high air flow rates, three dimensional waves appear (rough interface). Higher air flow-rates cause atomisation indicating the start of transition to annular flows.
Annular	5	A film is sustained around the inside of the tube, much thicker at the bottom, with a frothy appearance. The core is foggy and at high flowrates the structure becomes milky and foggy making visual identification of the flow structure difficult.

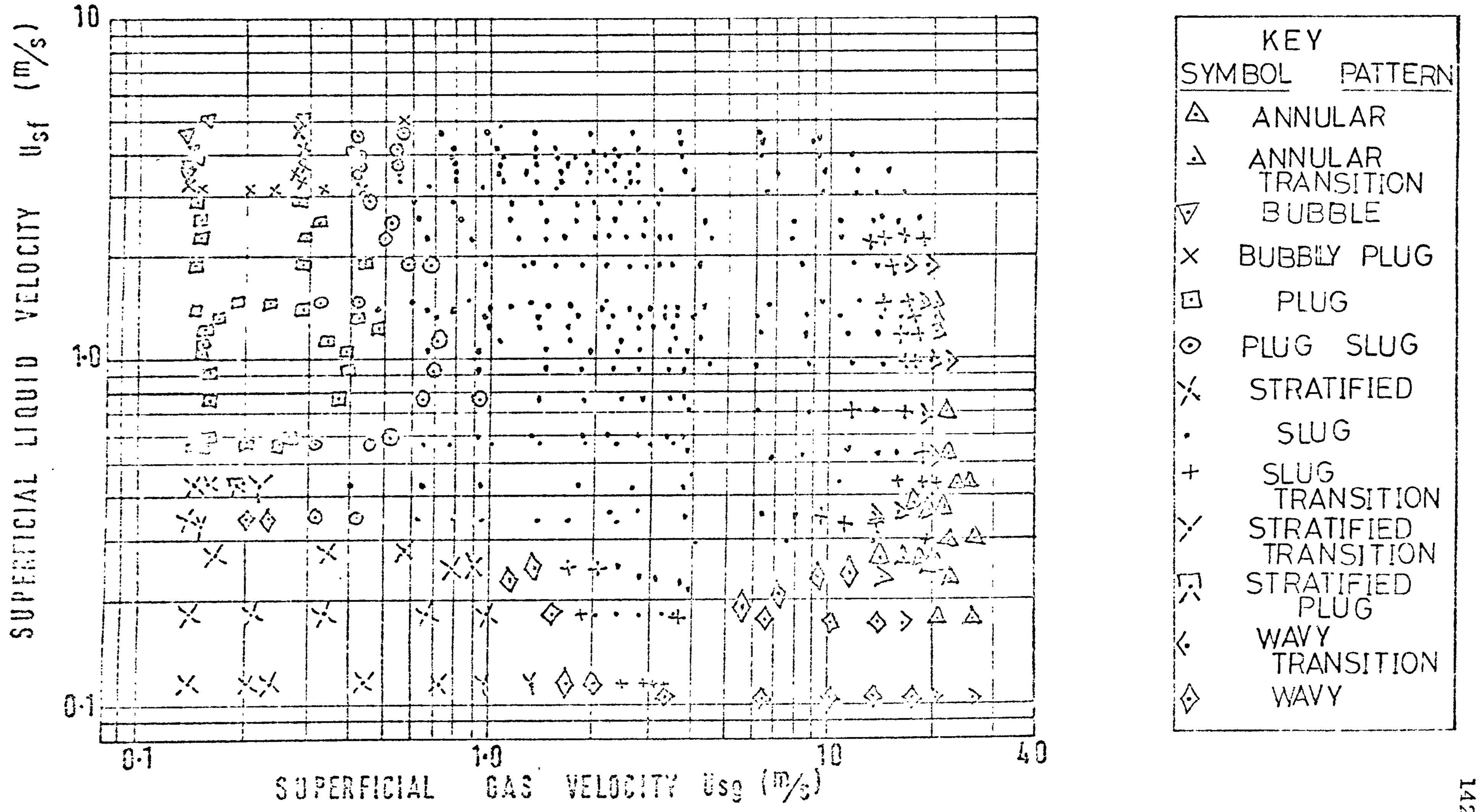

FIG. 5·3 EXPERIMENTAL FLOW PATTERN RESULTS (PHASE 1)

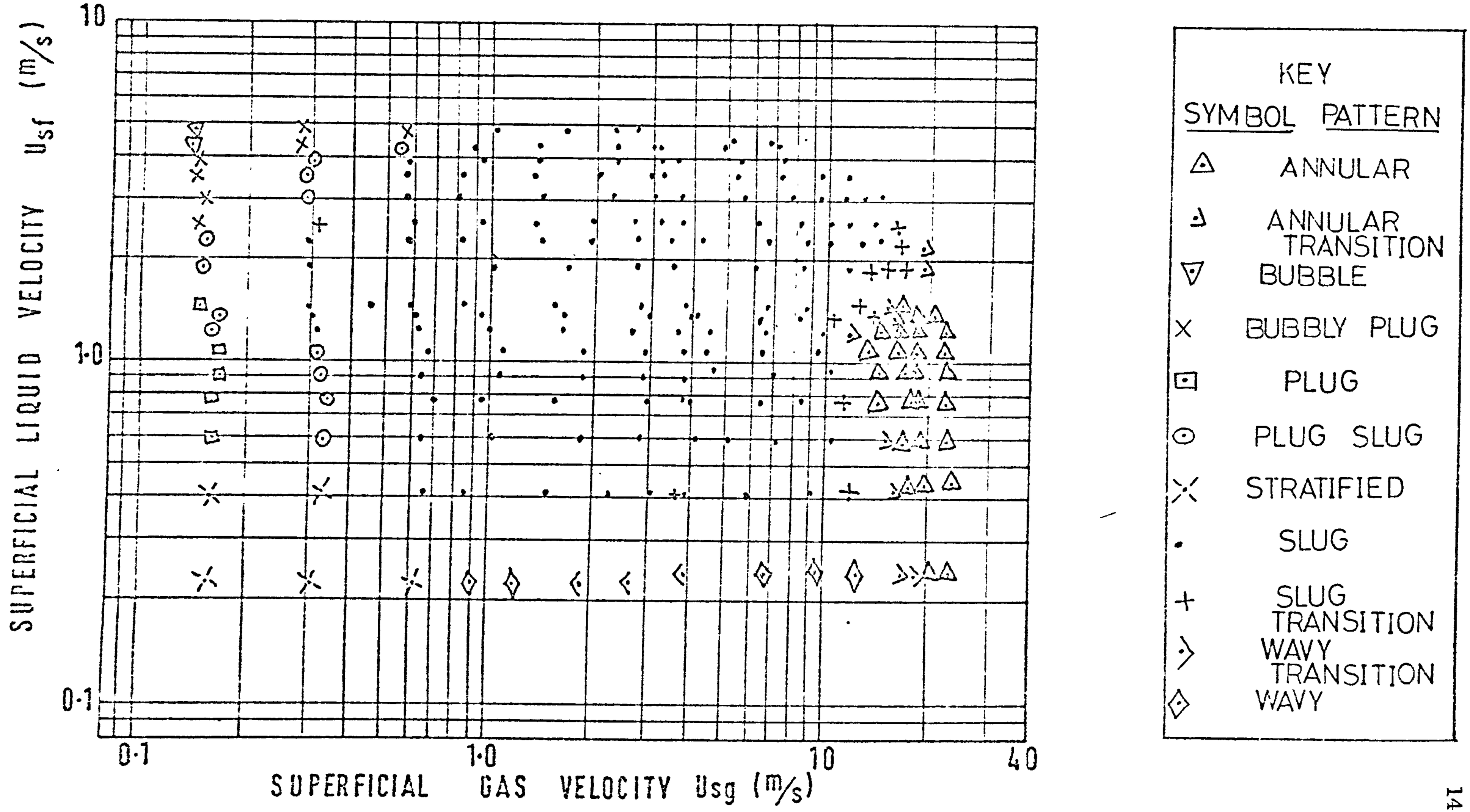

FIG. 5.4 EXPERIMENTAL FLOW PATTERN RESULTS (PHASE 2)

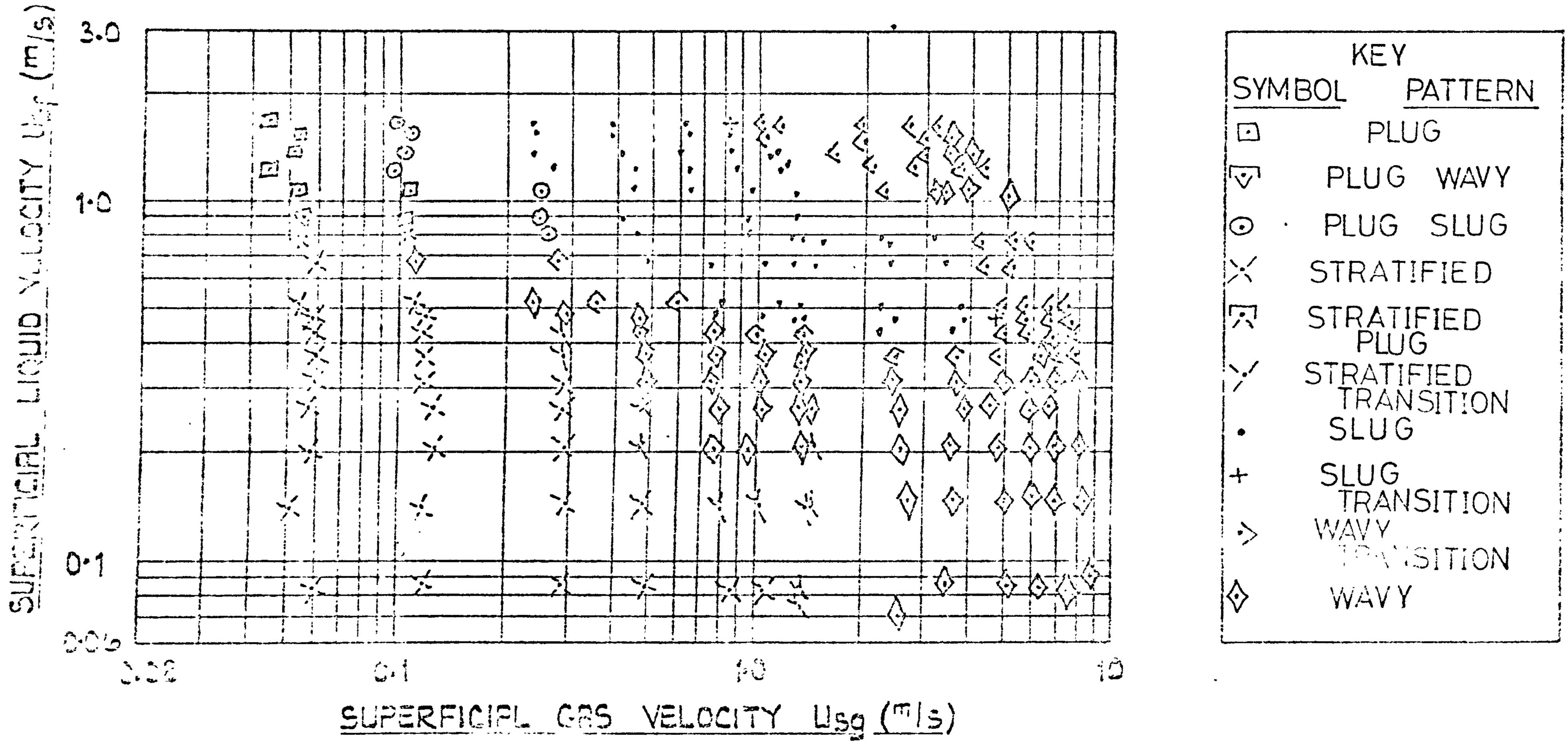

FIG. 5.5 EXPERIMENTAL FLOW PATTERN RESULTS (PHASE 3)

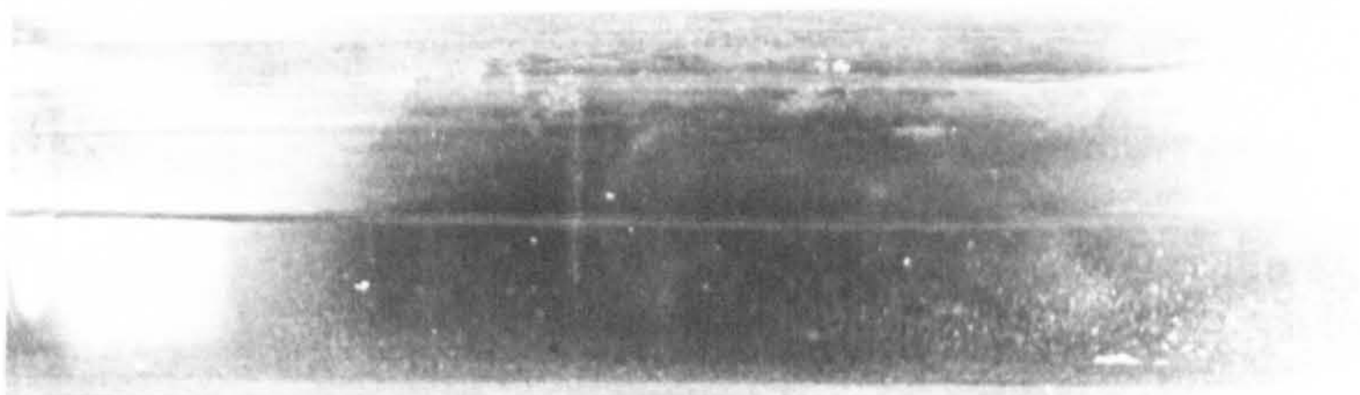

STRATIFIED (081305)

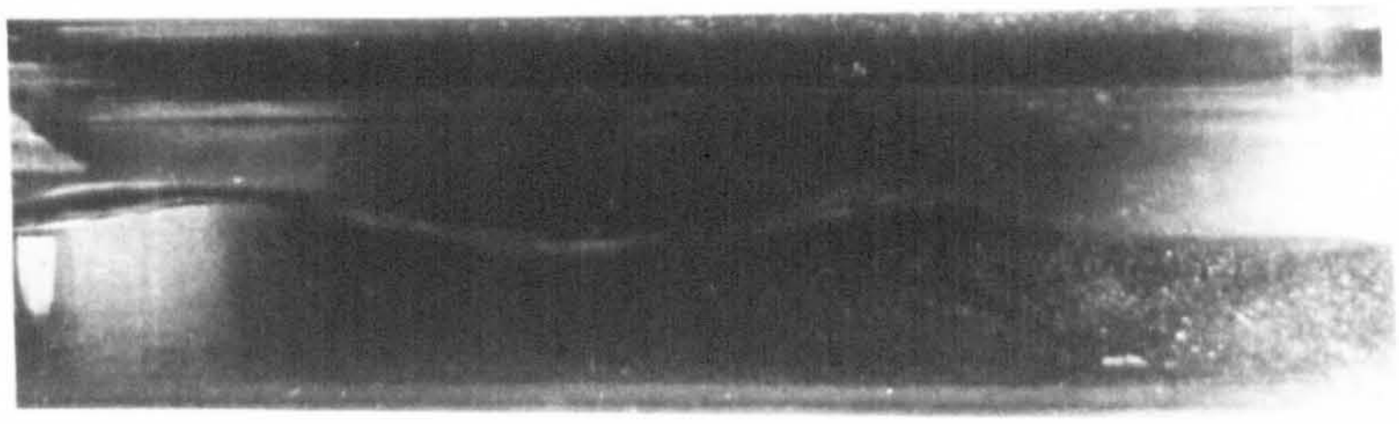

WAVY (091305)

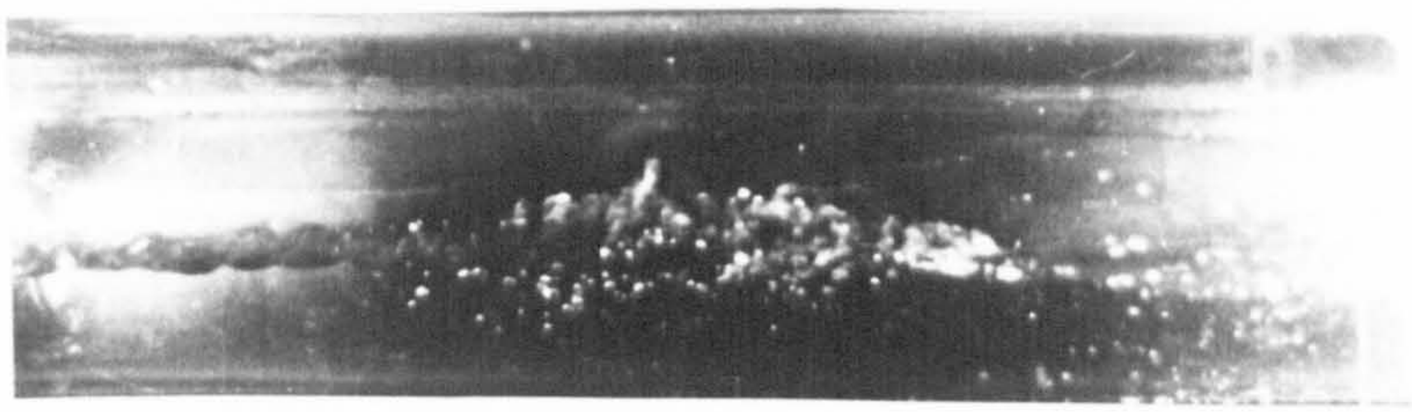

ROUGH WAVY (011405)

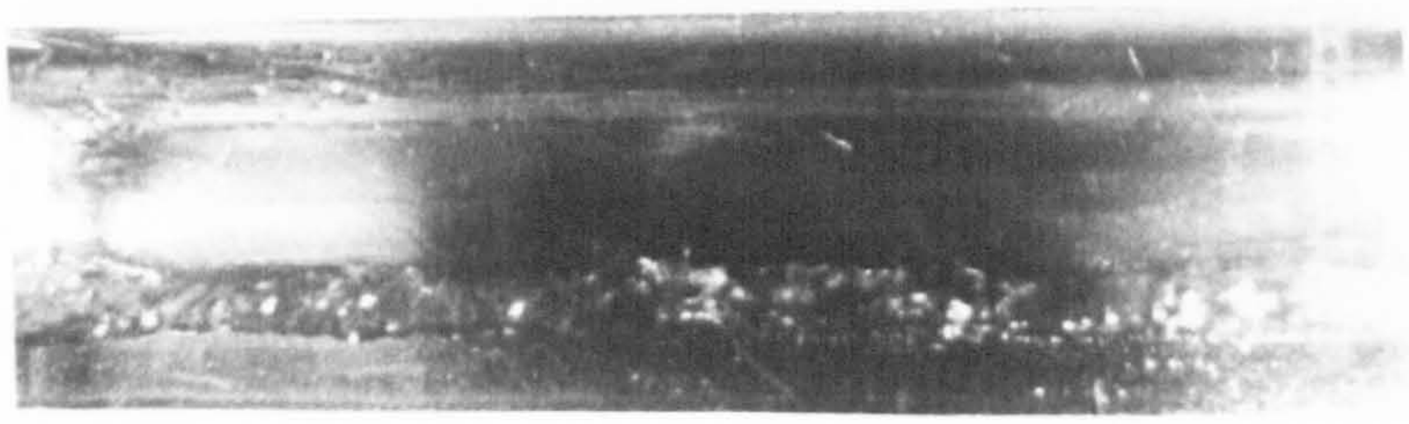

ROUGH WAVY (021405)

FIG. 5.6

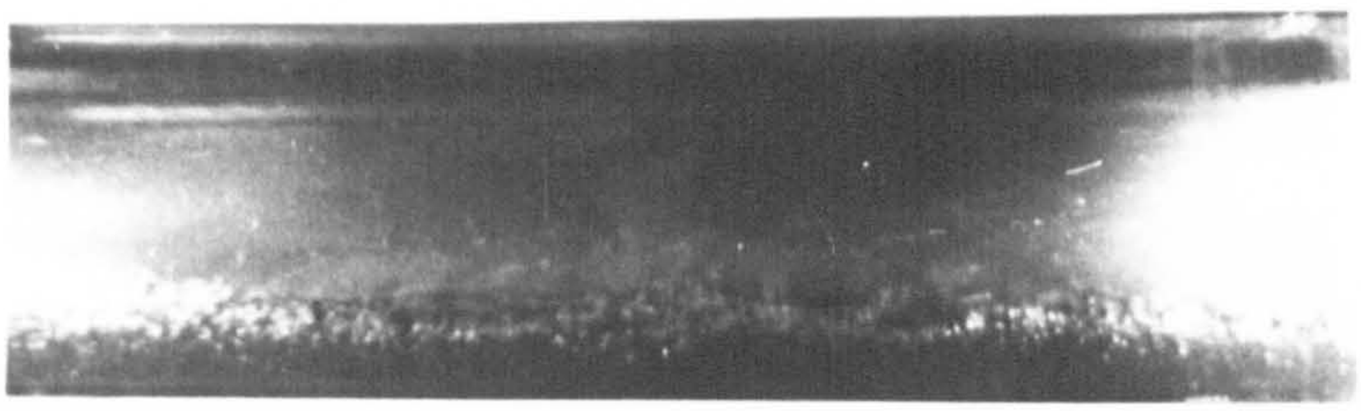

ANNULAR (061405)

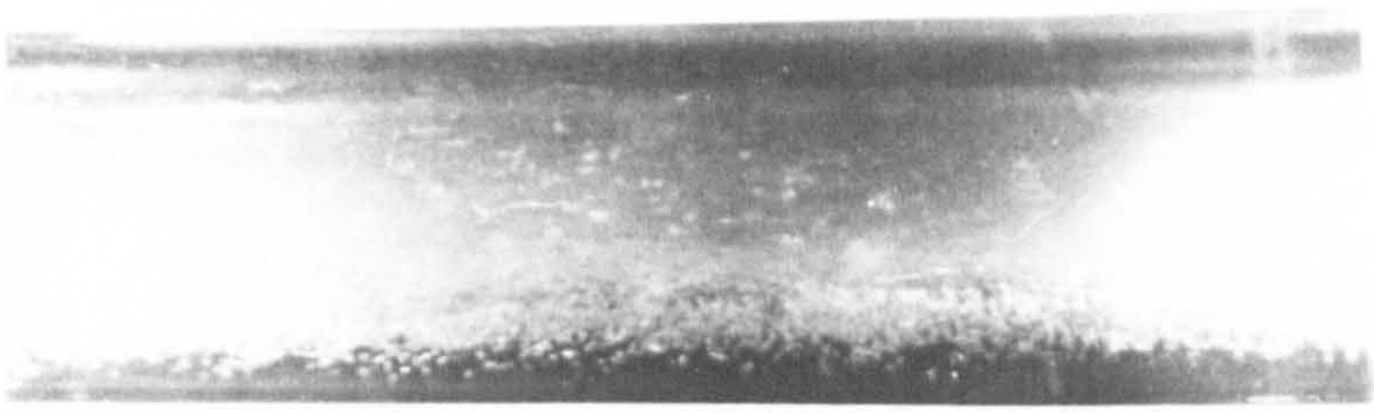

ANNULAR (081405)

ANNULAR (091405)

ANNULAR (111405)

FIG. 5·7

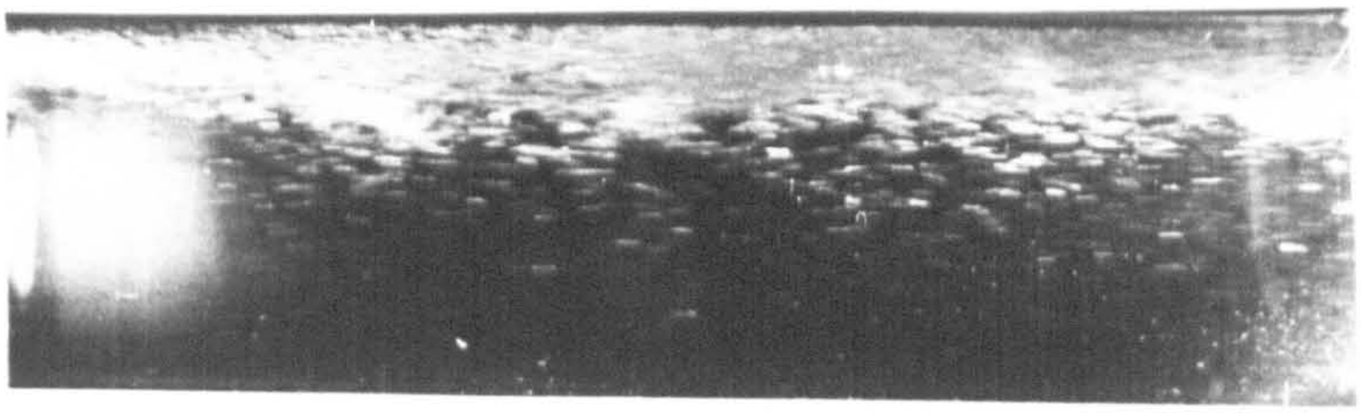

BUBBLY (041305)

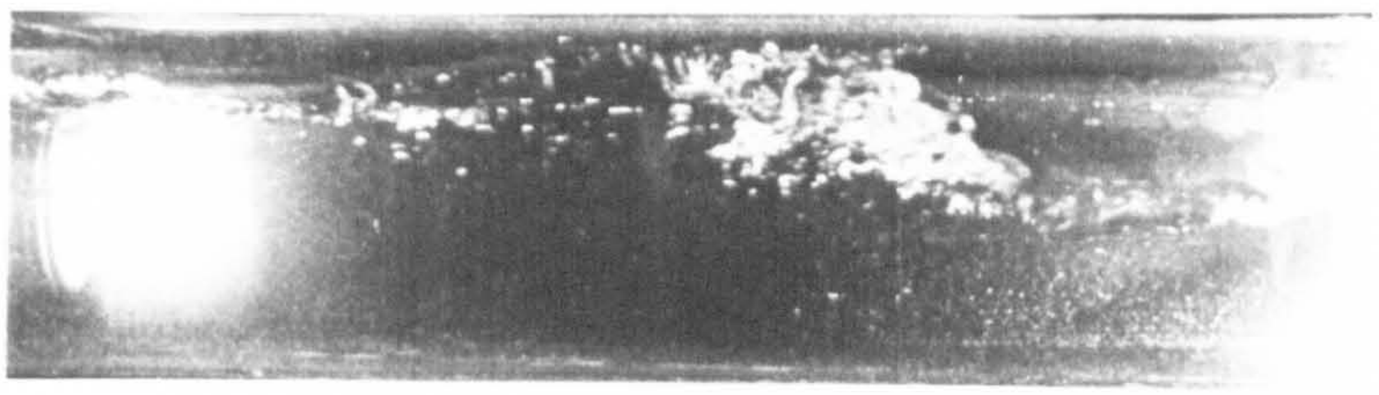

PLUG (021205)

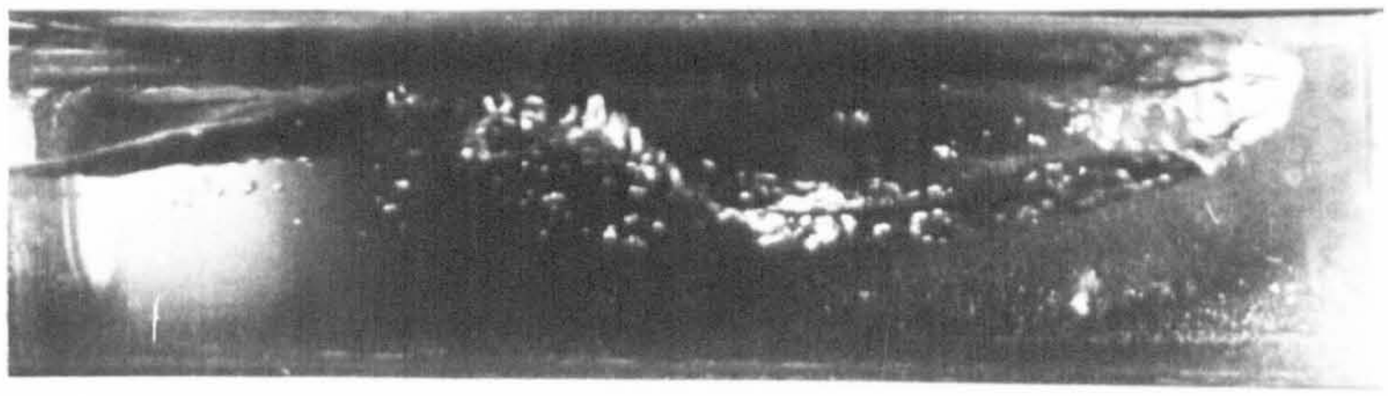

PLUG (021205)

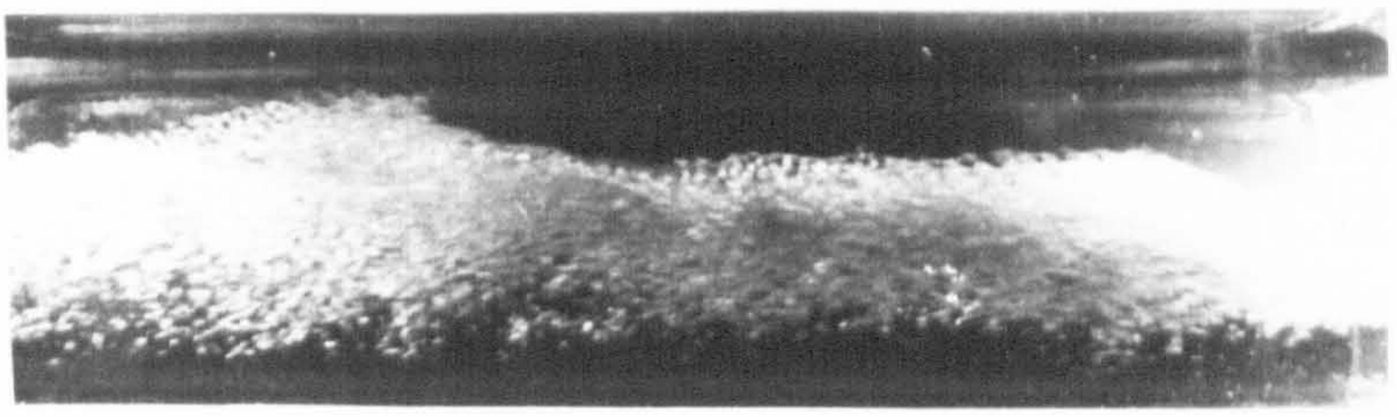

SLUG (111305)

FIG. 5·8

SLUG (031305)

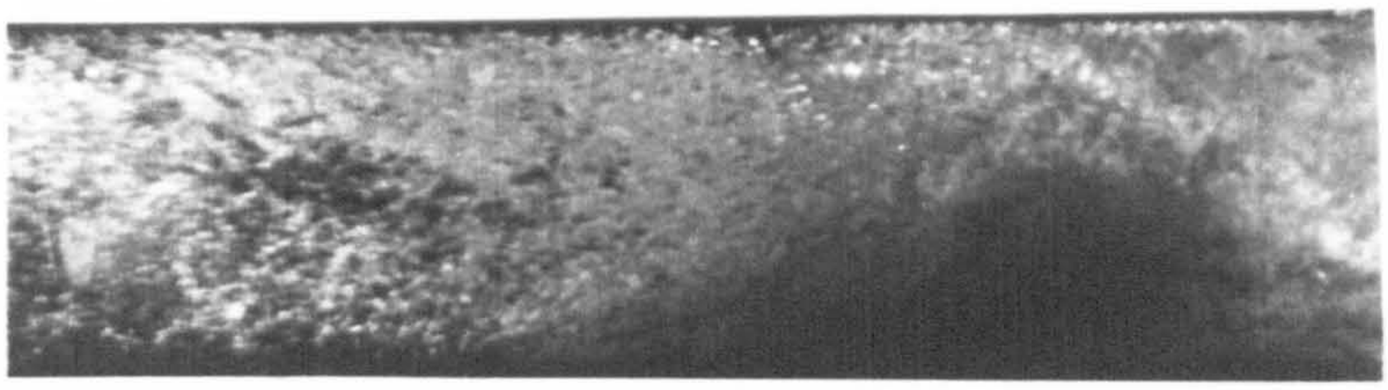

SLUG (031305)

SLUG (101305)

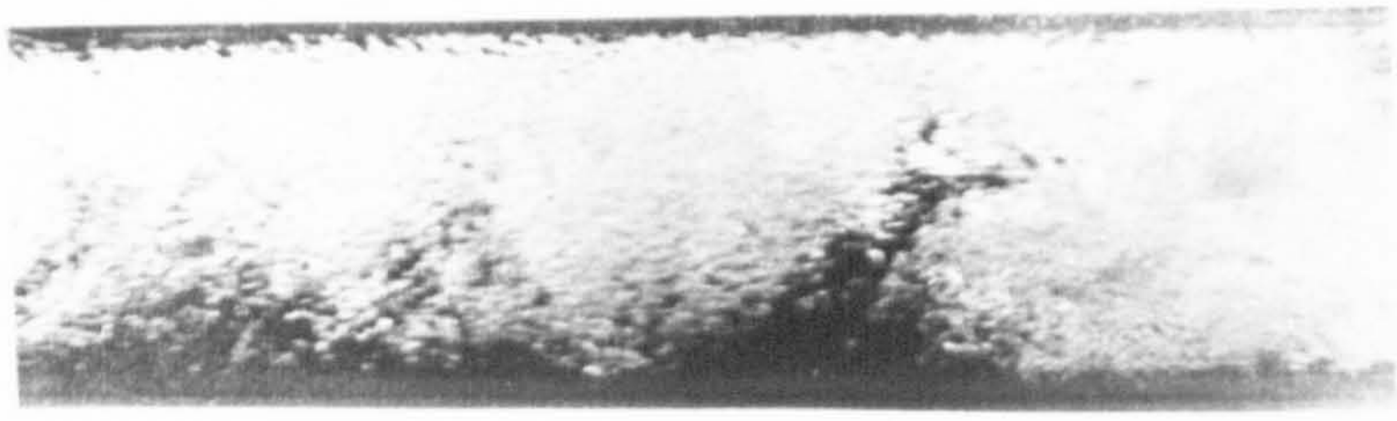

SLUG (101305)

FIG. 5·9

Code	Test Number	Temp.	α	Q_f m^3/sec	Q_g m^3/sec	ρ_f kg/m^3	ρ_g kg/m^3	F*	Flow Pattern	Camera Speed Sec
A	011205	29.5	0.0	0.01768	0.0	995.8	1.171	40	9	1/500
B	021205	30.0	0.131	0.01608	0.00207	995.7	1.169	40	6	1/500
C	031305	12.0	0.567	0.02439	0.03531	999.5	1.243	40	2	1/500
D	041305	15.5	0.052	0.05550	0.00184	999.1	1.227	40	1	1/100 1/500
E	051305	19.0	0.060	0.063124	0.00176	998.4	1.213	40	1	
F	061305	22.0	0.106	0.05889	0.00529	997.8	1.200	40	12	
G	071305	24.0	0.111	0.05623	0.03927	997.3	1.192	40	2	
H	081305	15.0	0.454	0.00267	0.00380	999.1	1.230	40	3	1/500
I	091305	20.5	0.459	0.00267	0.01547	998.1	1.207	40	4	1/500
J	101305	22.5	0.677	0.00671	0.02207	997.7	1.198	40	2	1/500 1/100
K	111305	26.0	0.705	0.01254	0.04082	996.8	1.184	40	2	1/500
L	121305	30.5	0.264	0.01266	0.00398	995.5	1.167	40	6	
M	011405	16.5	0.677	0.00274	0.08572	998.9	1.223	40	4	1/500
N	021405	21.0	0.781	0.00263	0.15591	998.0	1.204	40	4	1/500

* F: Rate of data collection, i.e. reading/sec.

TABLE 5-2 RANGE OF CONDITIONS COVERED BY THE PULSATION DATA

Contd.

Code	Test Number	Temp. ^{o}C	α	Q_f m^3/sec	Q_g m^3/sec	ρ_f kg/m^3	ρ_g kg/m^3	F	Flow Pattern	Camera Speed Sec
O	031405	23.5	0.872	0.00281	0.23188	997.5	1.194	40	54	
P	041405	23.5	0.872	0.00281	0.23188	997.5	1.194	100	54	
Q	051405	14.0	1.0	0.0	0.0	999.3	1.234	40	8	
R	061405	15.6	0.871	0.00452	0.31102	999.0	1.227	40	5	1/1000
S	071405	15.6	0.871	0.00452	0.31102	999.0	1.227	100	5	
T	081405	17.5	0.840	0.00756	0.31092	998.7	1.219	40	5	1/1000
U	091405	18.5	0.771	0.01029	0.32173	998.5	1.215	40	5	1/1000
V	101405	18.5	0.771	0.01029	0.32173	998.53	1.215	100	5	
W	111405	19.6	0.793	0.01712	0.32153	998.3	1.210	40	5	1/1000
X	121405	21.0	0.664	0.01742	0.15890	998.0	1.204	40	2	
Y	131405	22.3	0.715	0.01726	0.20316	997.7	1.199	40	52	
Z	141405	23.5	0.727	0.01310	0.12213	997.5	1.194	40	2	
AA	151405	23.5	0.727	0.01310	0.12213	997.5	1.194	100	2	
BB	161405	23.5	0.727	0.01310	0.12213	997.5	1.194	10	2	

TABLE 5-2 RANGE OF CONDITIONS COVERED BY THE PULSATION DATA

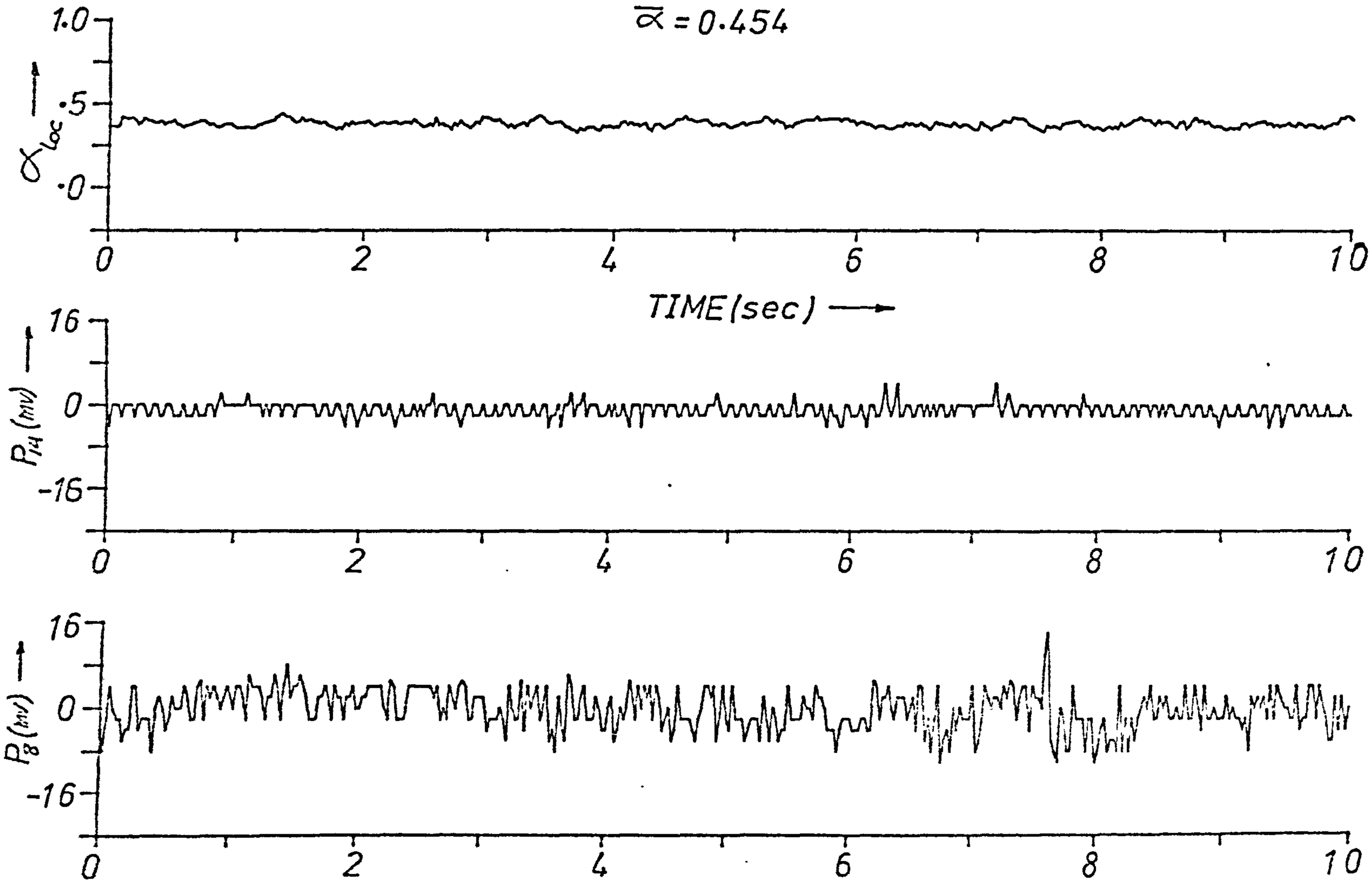

FIG. 5·10 TEST RUN 081305 (STRATIFIED) CODE(H)

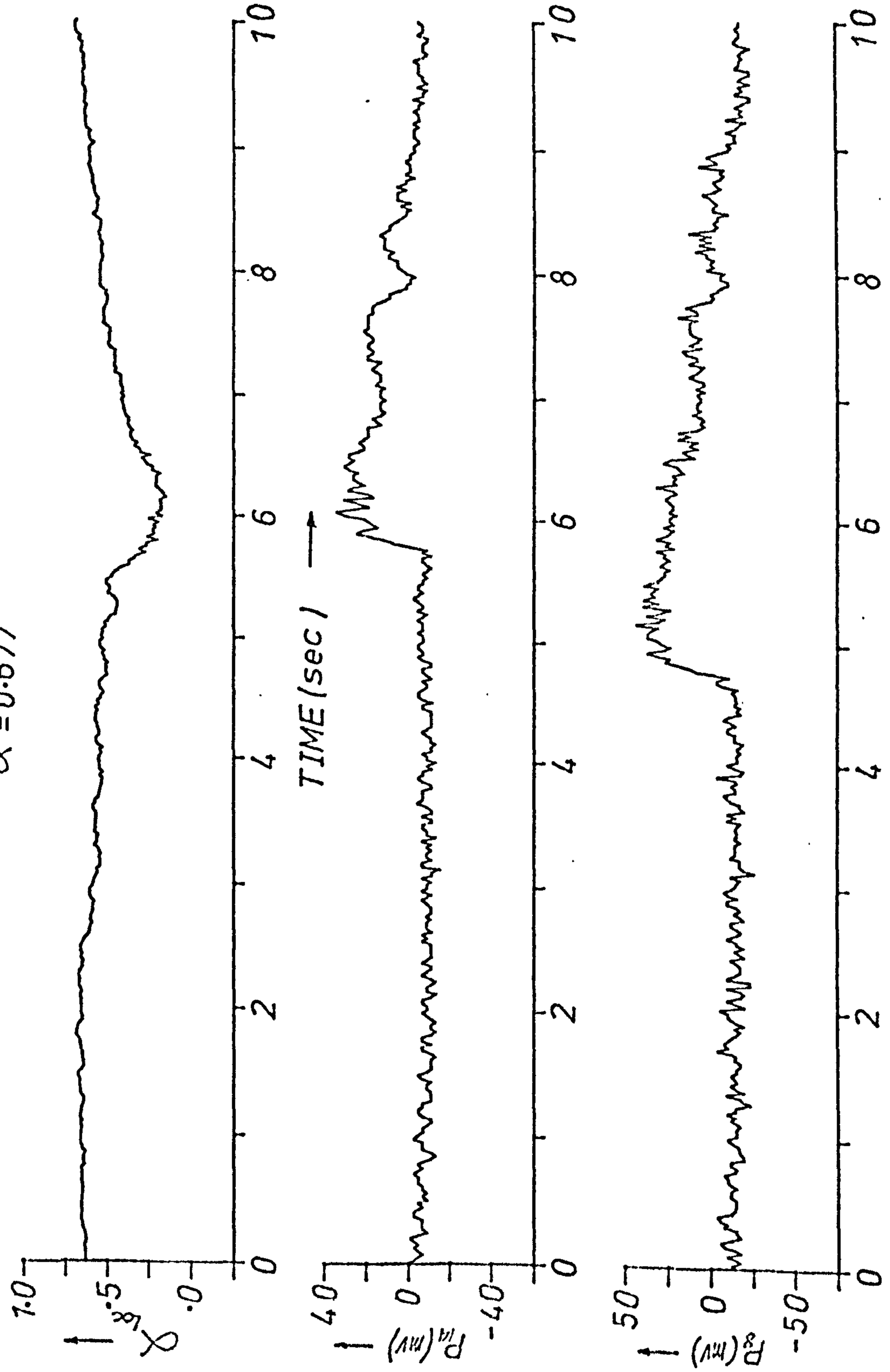

FIG. 5.11 TEST RUN 1013 CODE (J) 1305 (SLUG)

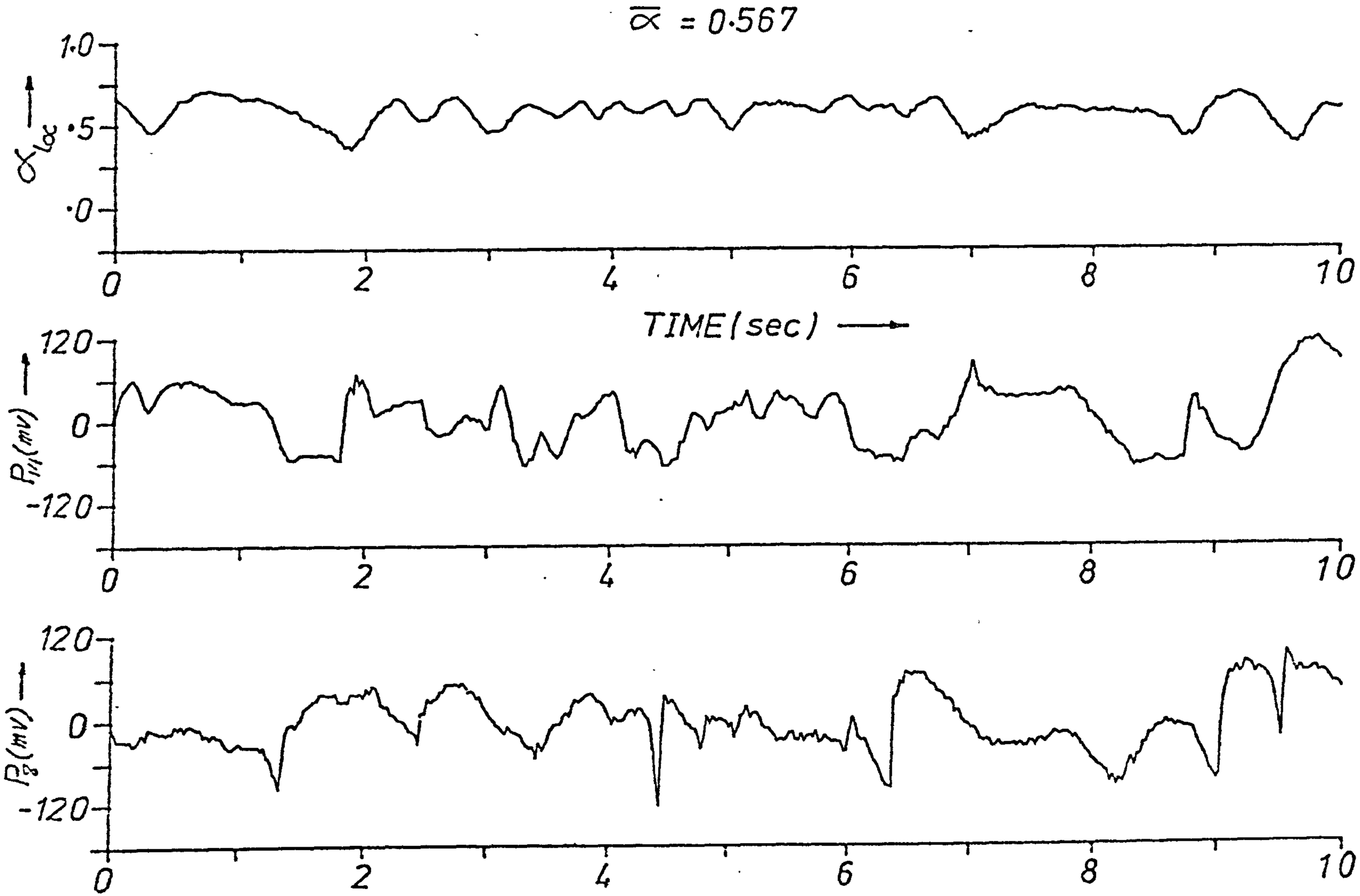

FIG. 5·12 TEST RUN 031305(SLUG) CODE(C)

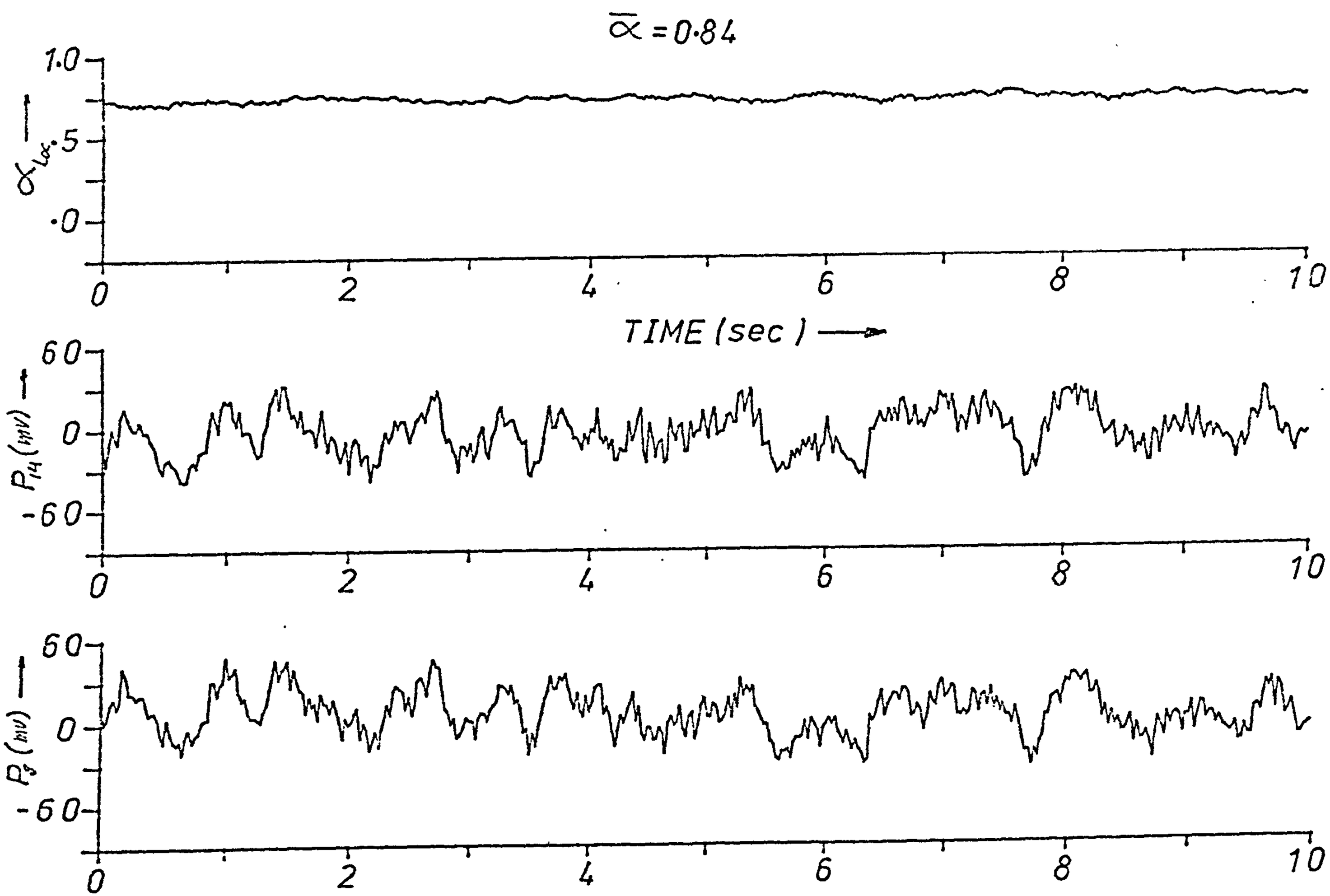

FIG. 5·13 TEST RUN 081405 (ANNULAR) CODE(T)

mixer), pressure near the inlet to the test section ($\sim$ 8m from mixer). Table 5-2 details the ranges covered and Fig. 5.15 locates these points on the flow patterns map for the Phase 2 tests. The zero signal readings for both transducers are shown in Fig. 5.14.

5.5 PHOTOGRAPHIC OBSERVATIONS BEFORE AND AFTER A 90° BEND

The effects of a 90° bend on the flow pattern of an Air-Water mixture was recorded photographically using a ciné camera running at a speed of 16 frames/sec. The films are stored in the Department of Thermodynamics and Fluid Mechanics, University of Strathclyde. The effect of the bends on the flow structure depended largely on the type of flow pattern present. Bubbly, annular and wavy were clearly affected as follows:

(a) Bubbly Flow: A swirl effect was observed which tended to throw the bubbles towards the bottom of the pipe, i.e. promoting mixing. In the Phase 2 tests, less bubbly flow points were observed compared to Phase 1 (two 90° bends) and were developed at lower water flowrates in the latter case.

(b) Wavy Flow: At low flowrates where long wavelengths and high amplitude waves appeared, the bend encouraged slugging and in some cases it occurred at the bend itself. At high air flowrates where some atomisation occurred, the bend separated the droplets which appeared as a thin film at the bend exit and disappeared soon after the bend.

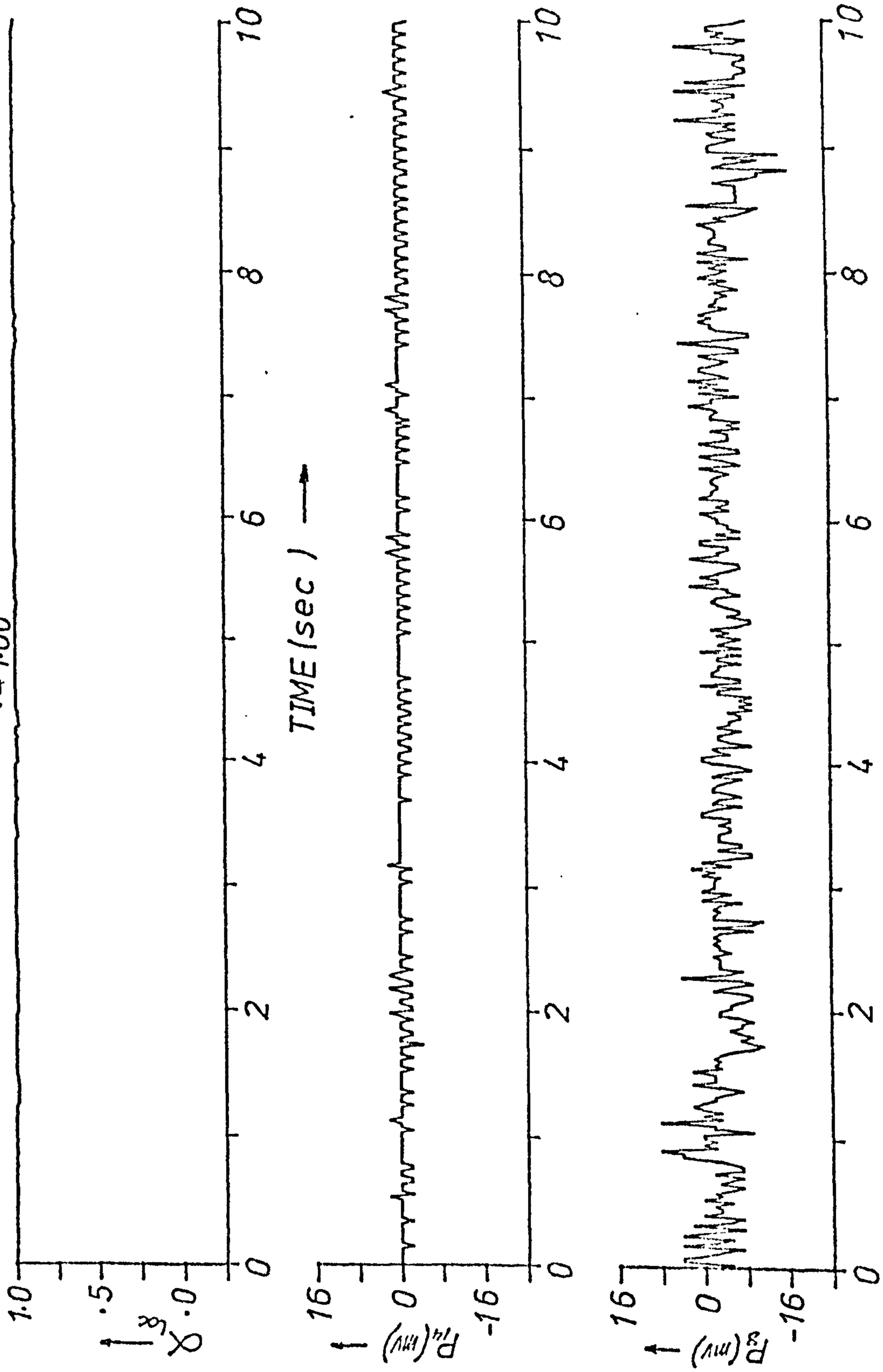
$\overline{\alpha}$ = 1.00
α
1.0
.5
0.0
0
2
4
6
8
10
TIME (sec) →
P_{14} (mv)
16
0
-16
P_3 (mv)
051405 (ALL GAS)
TEST RUN
CODE (Q)

FIG. 5.14

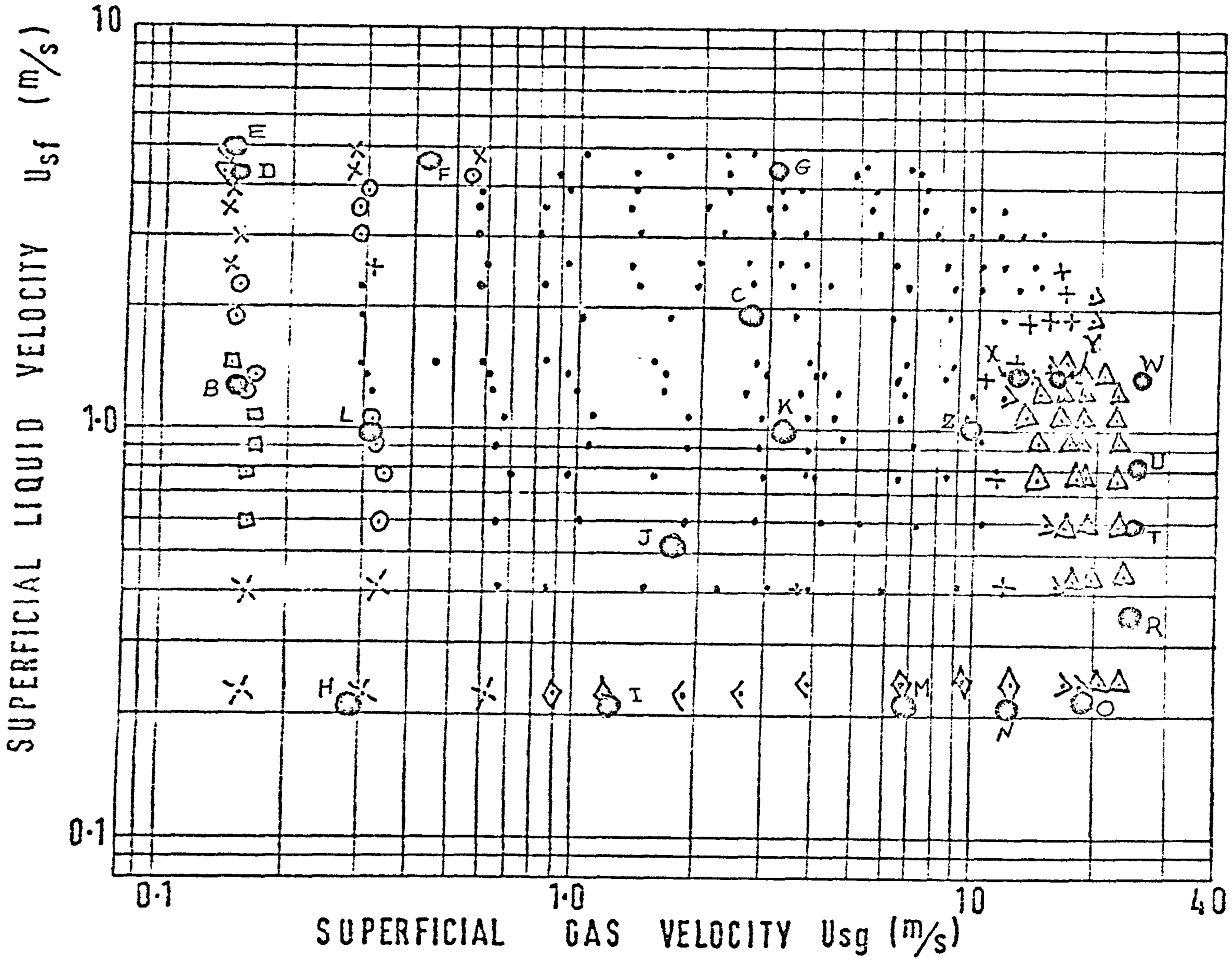

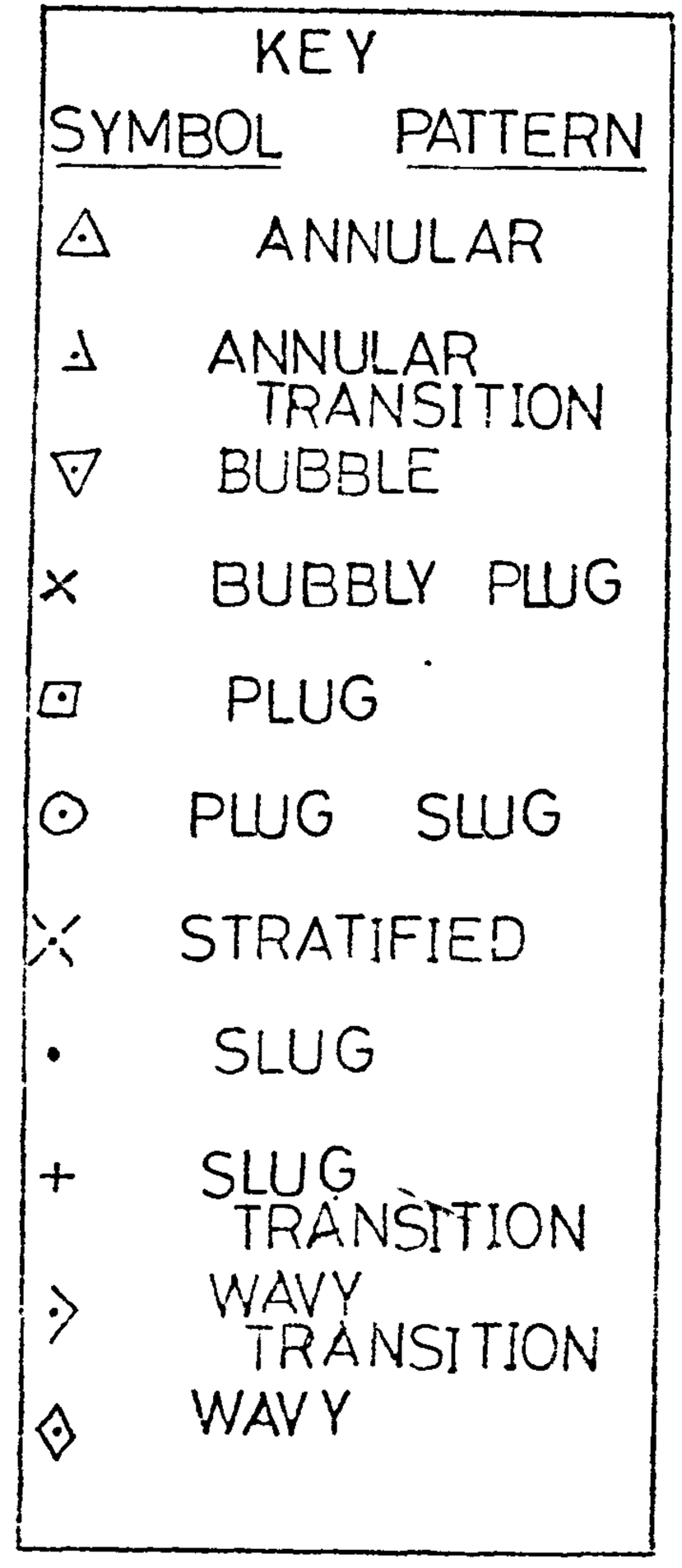

FIG. 5·15 FLOW PATTERN CONDITIONS COVERED BY THE PULSATION DATA

(c) Annular Flow: The effect of phase separation was very clear whereby droplets were agglomerated into larger liquid masses. At higher liquid flowrates, slugging occurred and a burst of milky structure traversed the pipe. Slugs were found to form after the first or second bend although the flow before the bend was completely annular. Thus less annular flow points were observed in Phase 1 tests when compared to Phase 2 tests. Annular flow developed at lower air flowrates in the latter case.

5.6 TEST SECTION FRICTION CHARACTERISTICS

The single phase friction characteristics for the two test sections (127 mm and 219 mm ID), obtained by in-situ calibration using water as the flowing fluid, are shown in Figs. 5.16 and 5.17. As can be seen from Fig. 5.16, the data for the 127 mm (5") pipe cannot be represented over the complete range of Reynolds numbers by a single relationship of the form $\lambda = K\ Re^{-n}$. Hence the data is represented by two equations, namely

$$\lambda = 0.212\ Re^{-0.222} \qquad Re > 10^5$$

$$\ln \lambda = \sum_{n=0}^{4} a_n (\ln Re)^n$$

where $a_o = 1084.06$ $\quad a_1 = -381.55$

$a_2 = 50.261$ $\quad a_3 = -2.946$

$a_4 = 0.0648$

and for laminar flow

FIG 5·16 SINGLE PHASE FRICTION CHARACTERISTIC FOR TEST SECTION

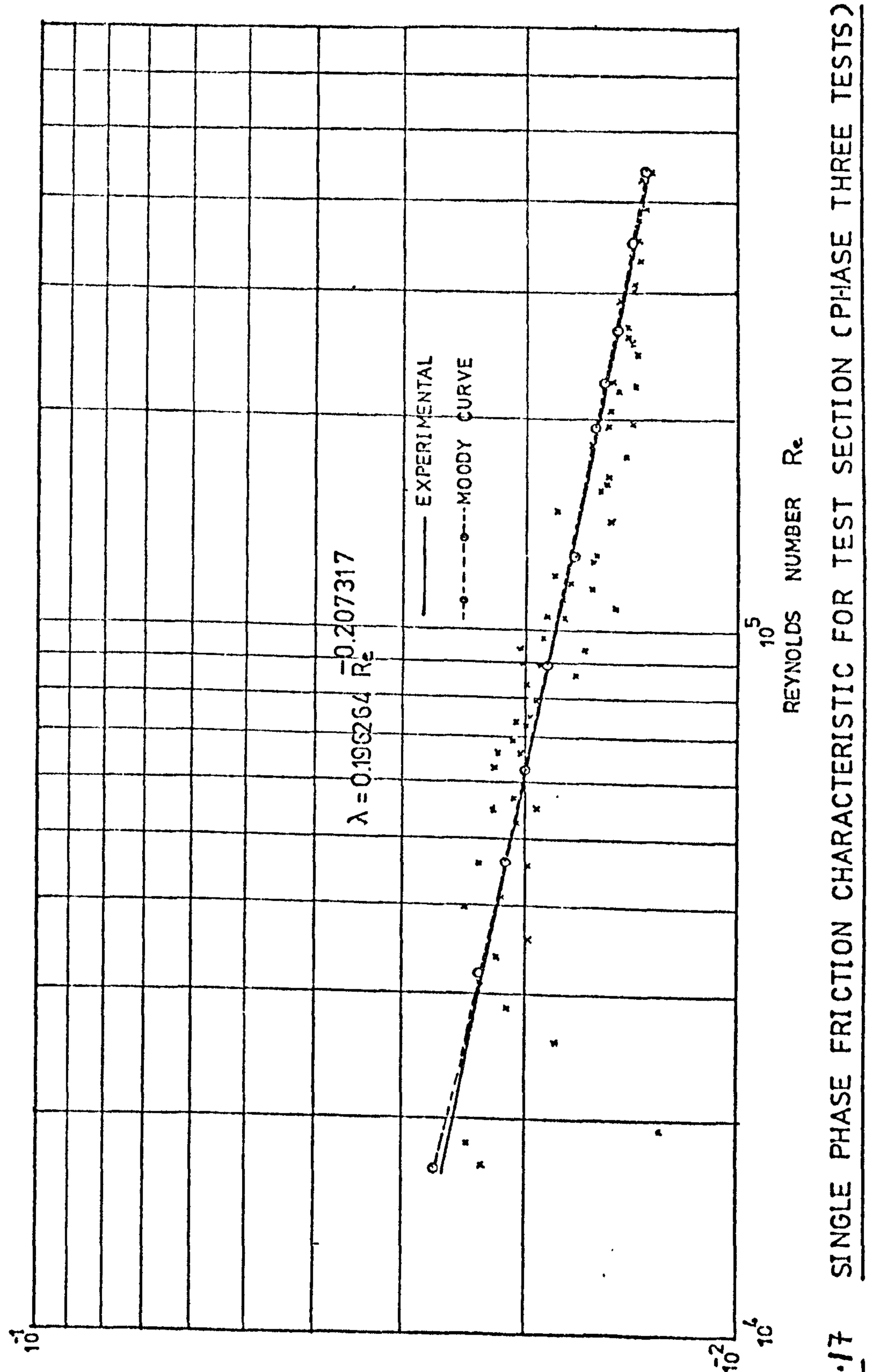
SINGLE PHASE FRICTION CHARACTERISTIC FOR TEST SECTION (PHASE THREE TESTS)
FRICTION FACTOR λ
REYNOLDS NUMBER Re
λ = 0.192264 Re^-0.207317
EXPERIMENTAL
MOODY CURVE
10^-1
10^-2
10^4
10^5

FIG. 5.17

$$\lambda = \frac{64}{Re} \qquad Re \leqslant 2 \times 10^3$$

For the 219 mm (8.5") pipe, however, the following equation represented the data reasonably well.

$$\lambda = 0.1963\ Re^{-0.2073} \qquad Re > 15 \times 10^3$$

and for laminar flow

$$\lambda = \frac{64}{Re} \qquad Re \leqslant 2 \times 10^3$$

It is worth emphasising that because of the scatter in the λ values observed at low Reynold's numbers, extrapolation of the correlation outside the range tested is not recommended; also the variations of λ with Re must be taken into account when evaluating the different friction multipliers later.

5.7 VOID FRACTION DATA

The void fraction data for Phases 1, 2 and 3 are given in Appendix S together with the other information shown previously in the specimen table shown in Fig. 5.2.

The effects (previously mentioned) of phase disposition and the direction of the γ-ray beam on the accuracy of the void fraction measurements are shown quantitatively in Figs. 5.18, 5.19 and 5.20. The figures correspond to the case of stratified type of flow. As can be seen, the results support the recommendations presented earlier about the use of different equations to determine the void fraction depending on whether the rays

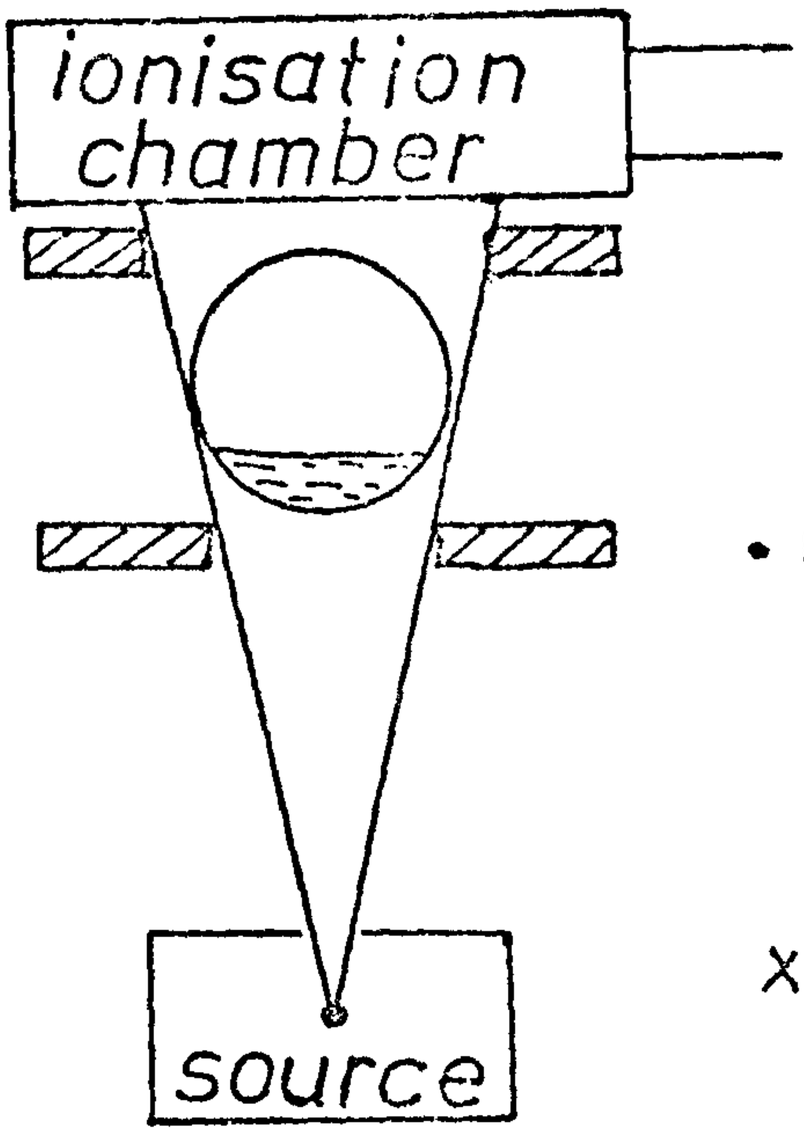

127 mm (5") bore

• using $\alpha = \dfrac{\log_e(I_m/I_f)}{\log_e(I_g/I_f)}$

x using $\alpha = \dfrac{(I_m - I_f)}{(I_g - I_f)}$

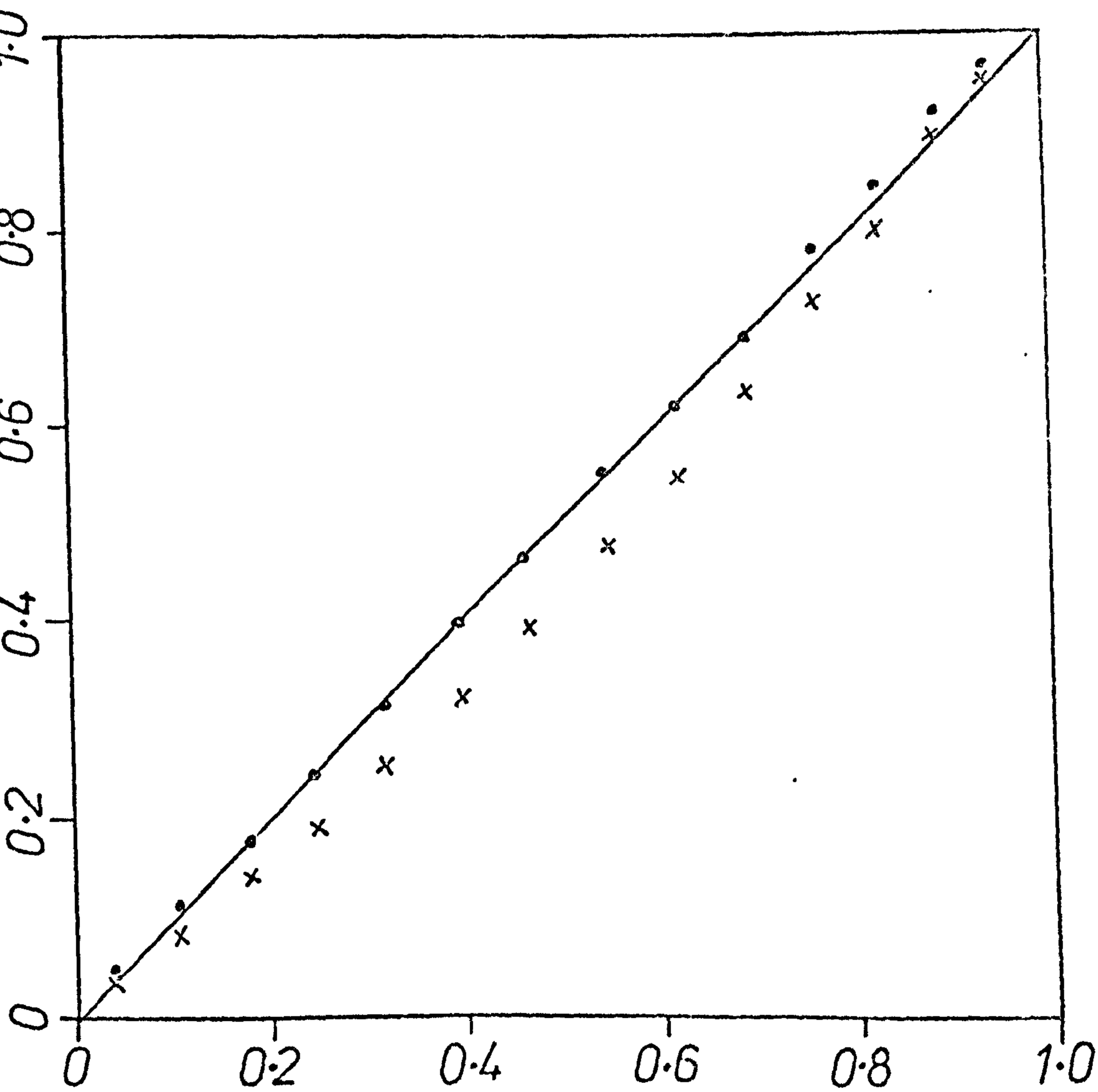

FIG. 5.18 VOID FRACTION MEASUREMENTS IN STRATIFIED FLOW

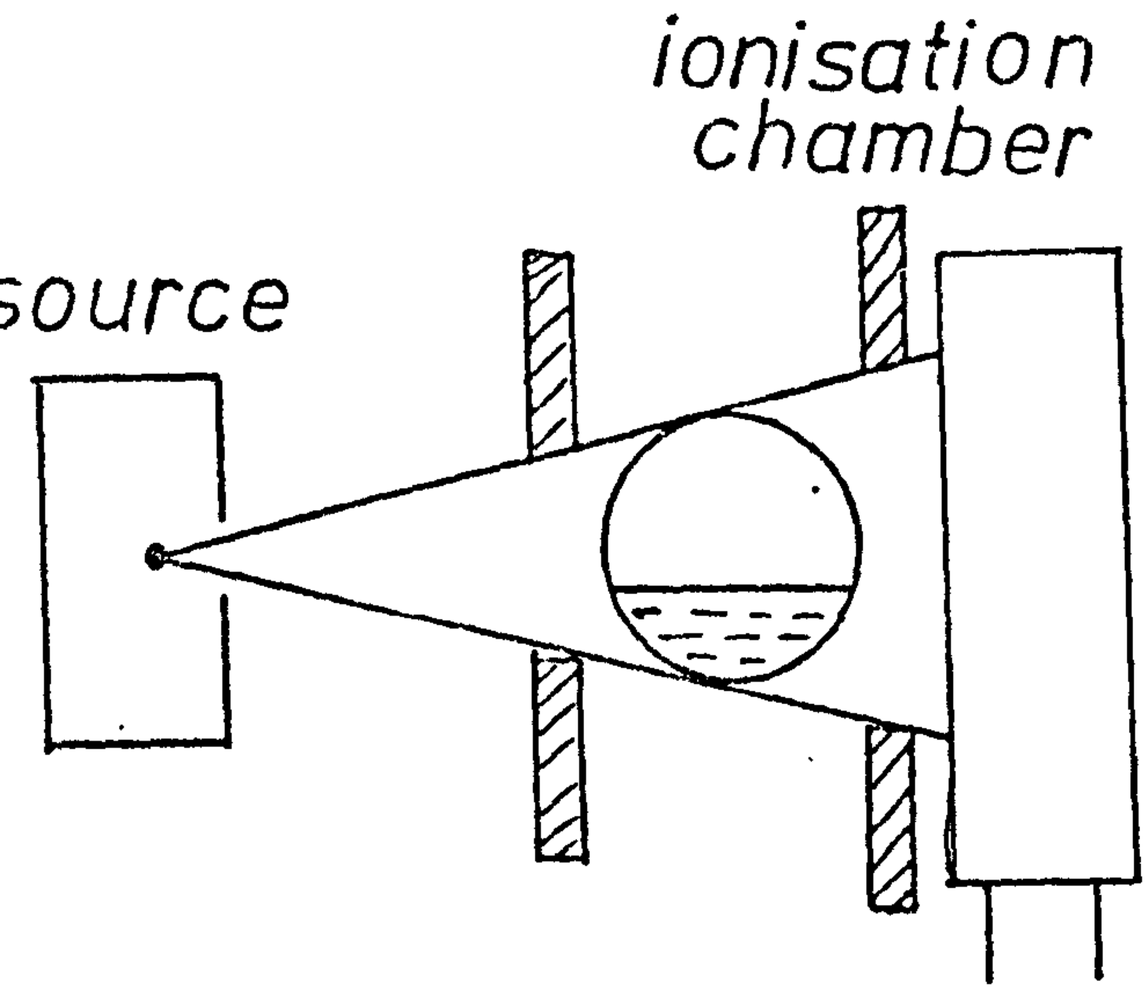

127 mm (5") bore

• using $\alpha = \dfrac{\log_e(I_m/I_f)}{\log_e(I_g/I_f)}$

x using $\alpha = \dfrac{(I_m - I_f)}{(I_g - I_f)}$

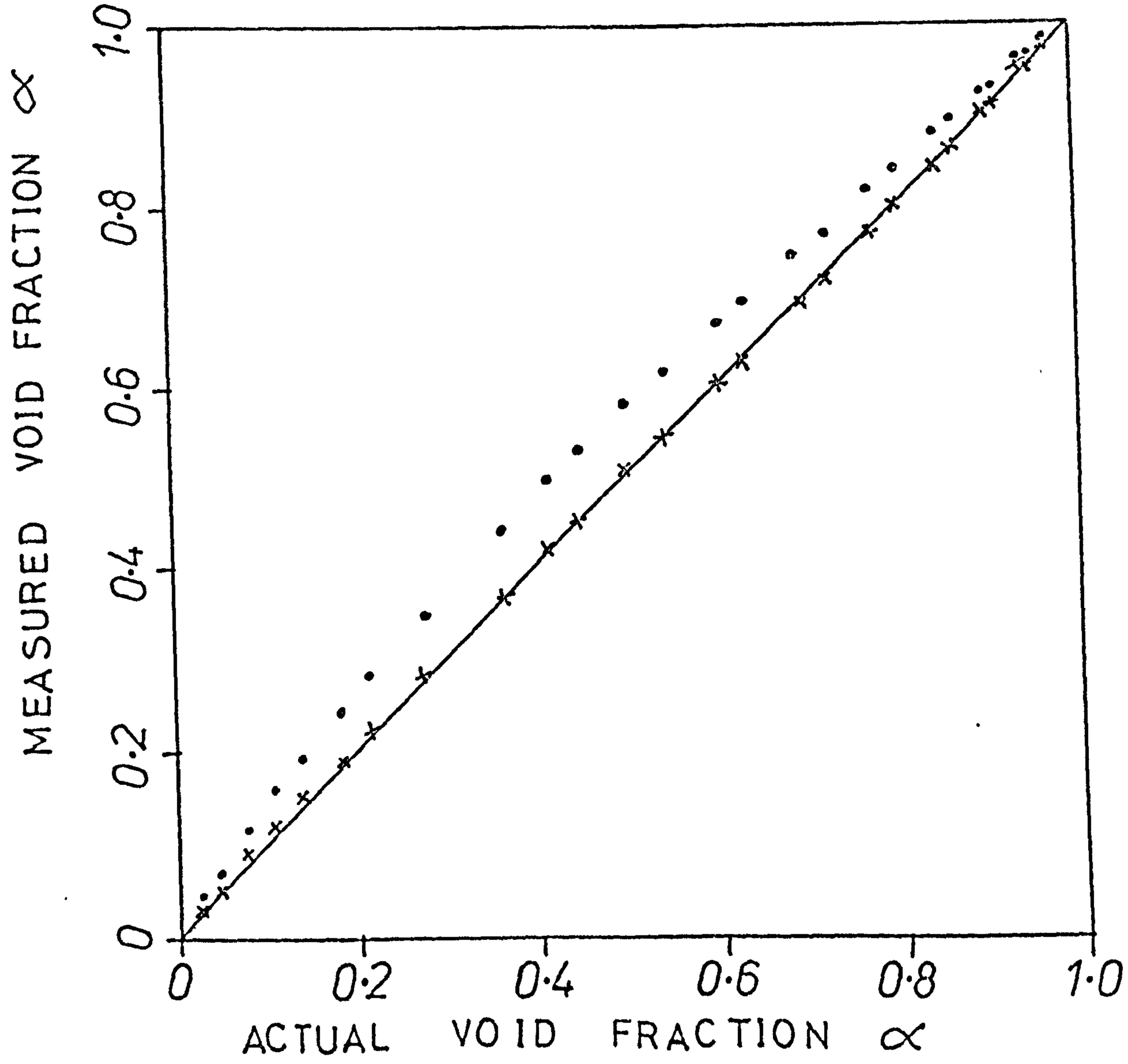

FIG.5.19 VOID FRACTION MEASUREMENTS IN STRATIFIED FLOW

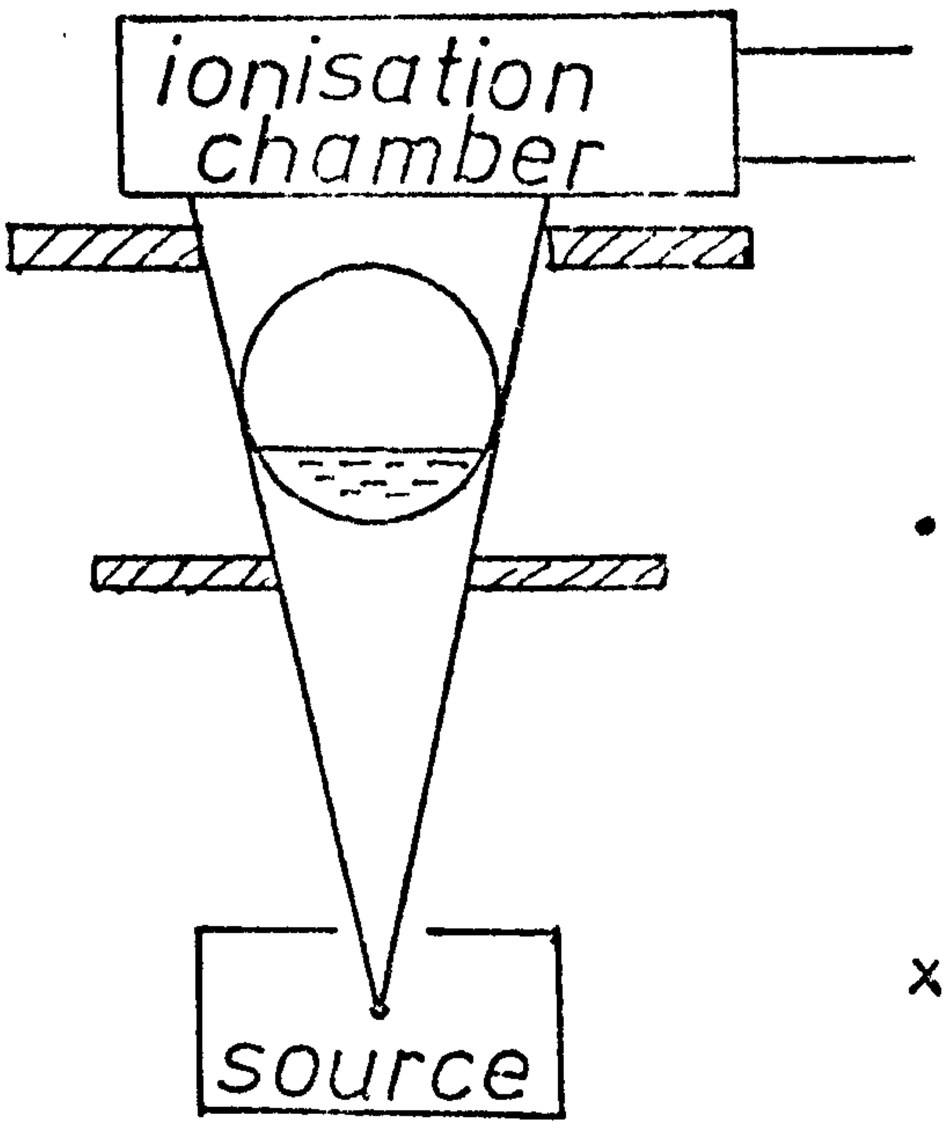

216 mm (8·5") bore

• using $\alpha = \dfrac{\log_e(I_m/I_f)}{\log_e(I_g/I_f)}$

x using $\alpha = \dfrac{(I_m - I_f)}{(I_g - I_f)}$

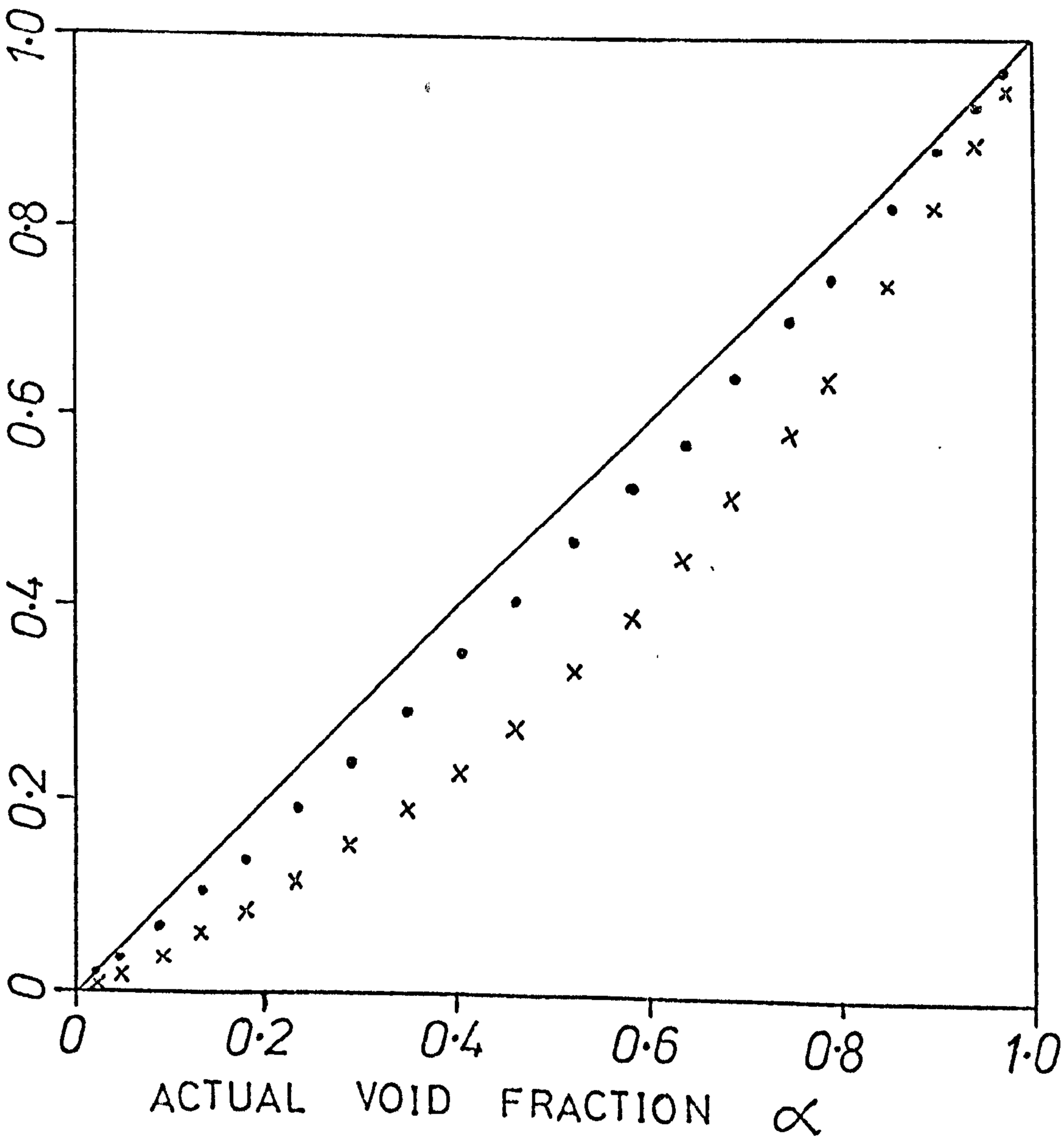

FIG. 5.20 VOID FRACTION MEASUREMENTS IN STRATIFIED FLOW

are normal or parallel to the plane of phase separation. The results also show that, for such conditions, the equations originally derived for the ideal case of parallel rays in rectangular channels (Appendix E.2) apply reasonably well to a round tube geometry and for reasonable beam divergence. The results for the 219 mm (8.5") pipe do show some deviation, even when the recommended equation is used, and this could be due to the large divergent beam needed to scan the tube.

CHAPTER 6

COMPARISON OF EXPERIMENTAL RESULTS WITH EXISTING CORRELATIONS

CHAPTER 6 COMPARISON OF EXPERIMENTAL RESULTS WITH EXISTING CORRELATIONS

6.1 PRESSURE DROP

To facilitate comparison with some existing correlations, the pressure drop data were converted into the two phase friction multipliers, $\phi^2_{f_o}$ and $\phi^2_{g_o}$ (i.e. the ratios of the two phase friction pressure drop to the corresponding single phase friction pressure drop calculated on the basis that the total mass flowrate was water or air respectively). The total pressure gradient was taken as the friction pressure gradient since check calculations based on the homogeneous flow model revealed the momentum component always less than 1% of the total.

The two phase friction multipliers were predicted using six well known correlations available in the literature, these being

(i) Homogeneous Flow Model - simplest to use.

(ii) Lockhart-Martinelli (L1) - earliest correlation allowing for slip - widely used.

(iii) Chenoweth-Martin (C11) - suitable for "large diameter" tubes.

(iv) Baroczy (B7) - general correlation allowing for property and mass velocity variations.

(v) Chisholm (C13) - extension of Lockhart-Martinelli and Baroczy which allows for mass velocity effects and dispenses with graphical procedures.

(vi) Dukler Case II (D1O) - suitable for separated flows but requires a void fraction correlation.

Details of these correlations are given in Appendix T with a sample calculation in Appendix U. The determination of these multipliers involved repetitive calculations and hence a computer program was developed whereby the graphical plots or tables used in the correlations were expressed in polynomials of the form

$$y = f(x) = \sum_{n=0}^{N} a_n x^n$$

as explained in Appendix K. The program is listed in Appendix V.

Comparison between the experimental and deduced values of the two phase friction multipliers are given in Appendix W for Phases 1, 2 and 3 respectively with a specimen shown in Fig. 6.1 (corresponding to the data sample shown in Fig. 5.2). Comparisons between the experimental and predicted two phase friction multipliers were plotted as follows:

(i) Experimental versus homogeneous model predictions for $\phi^2_{f_o}$ - Figs. 6.2 to 6.4.

(ii) Experimental versus homogeneous model predictions for $\phi^2_{g_o}$ - Figs. 6.5 to 6.7.

(iii) Experimental versus Lockhart-Martinelli model predictions for $\phi^2_{f_o}$ - Figs. 6.8 to 6.10.

TEST RUN NO	VOID FRCTN	TWO-PHASE FRICTION PRES-GRAD KN/M3	VALUES OF TWO-PHASE FRICTION MULTIPLIER									
			EXPERIMENTAL		HOMOG MODEL		LOCK-MART		CH-MRT	BAROCZY	CHLSM	CUCKLR
22402	0.5053	1.51187	2.456	0.009800	2.078	0.008290	2.655362	0.009766	2.252	2.372	2.573	3.146
32402	0.5911	2.09754	3.475	0.014146	2.463	0.010026	3.156491	0.011972	2.714	3.041	3.171	3.895
42402	0.6437	2.75133	4.652	0.019130	2.754	0.011326	3.536760	0.013650	3.071	3.353	3.652	4.624
52402	0.6815	3.47691	5.910	0.025273	3.090	0.013216	4.023664	0.016304	3.492	3.654	4.255	5.252
72402	0.4205	1.45432	1.935	0.007758	1.643	0.006598	2.131428	0.007761	1.752	1.918	1.951	2.393
62402	0.5051	1.94869	2.645	0.010817	1.962	0.008023	2.531841	0.009517	2.115	2.379	2.431	3.042
92402	0.5757	2.72181	3.806	0.015877	2.269	0.009469	2.950221	0.011620	2.479	2.774	2.929	3.713
12502	0.3712	1.47100	1.676	0.006741	1.530	0.006156	1.995180	0.007253	1.622	1.737	1.798	2.125
22502	0.4513	2.18366	2.310	0.010321	1.794	0.007320	2.332629	0.008937	1.921	2.170	2.199	2.675
32502	0.5730	3.16178	3.745	0.016068	2.130	0.009138	2.793607	0.011083	2.312	2.630	2.745	3.575
12602	0.3624	1.79902	1.779	0.007330	1.483	0.006038	1.912673	0.007102	1.549	1.649	1.709	2.030
22602	0.5066	2.66950	2.840	0.011836	1.816	0.007558	2.384706	0.009898	1.945	2.224	2.252	2.905
32602	0.5398	3.24537	3.451	0.014538	1.999	0.008434	2.642166	0.010272	2.157	2.486	2.567	3.256

FIG. 6.1 COMPARISON OF FRICTION PRESSURE DROP DATA

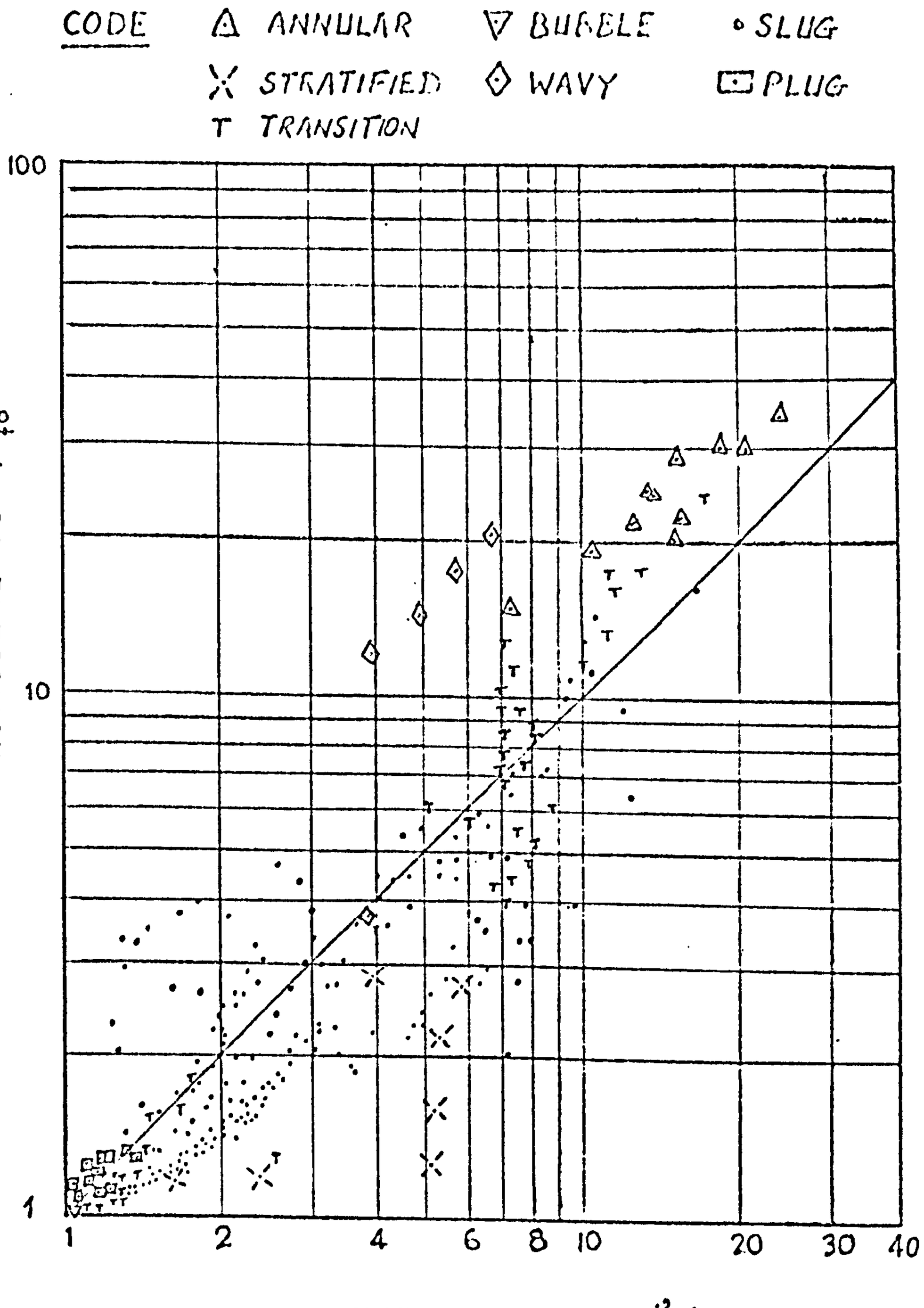

EXPERIMENTAL ϕ^2_{fo} (PHASE 1 TESTS)

FIG. 6·2 COMPARISON OF EXPERIMENTAL AND HOMOGENEOUS TWO PHASE FRICTION MULTIPLIERS ϕ^2_{fo}

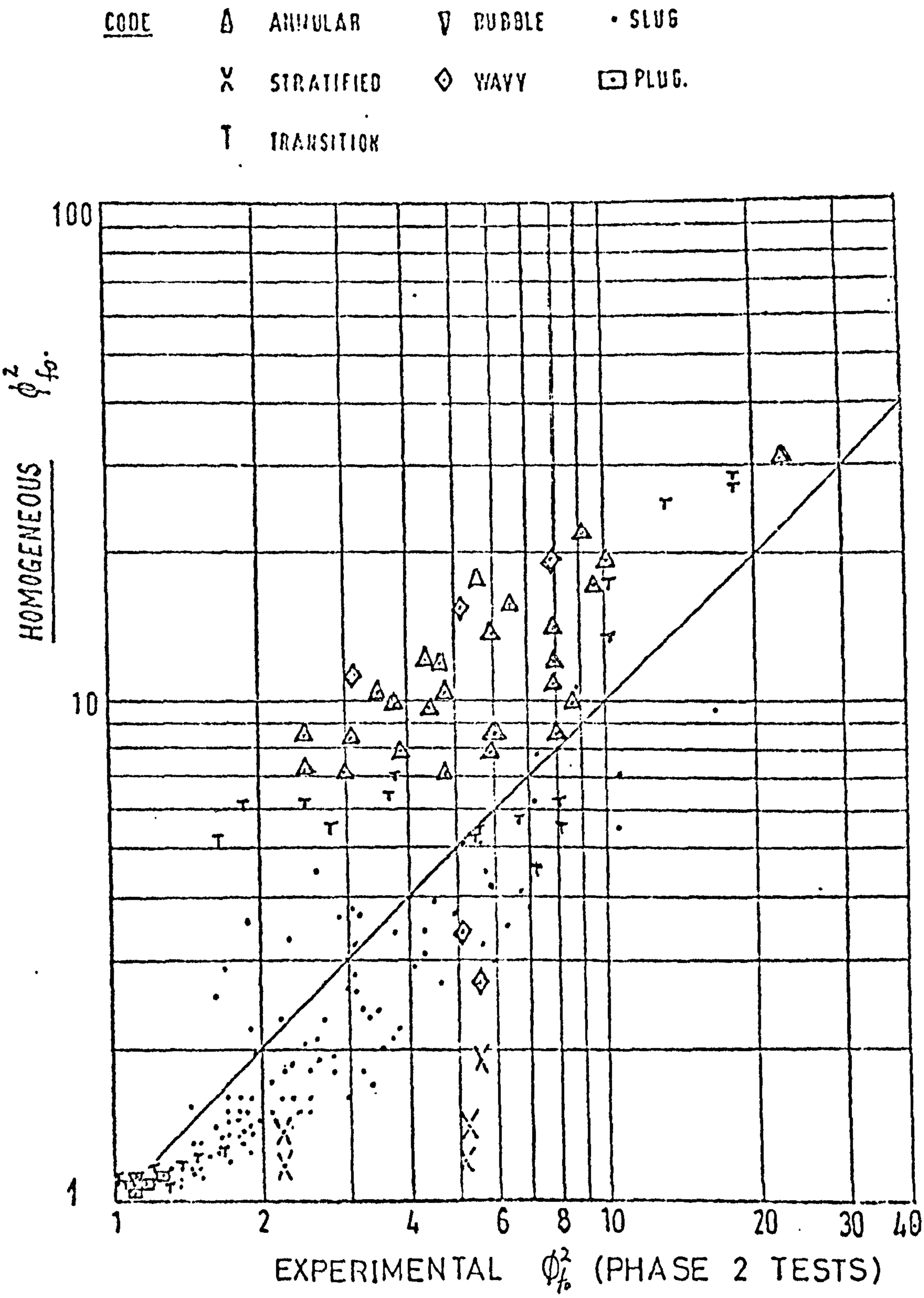

FIG. 6·3 COMPARISON OF EXPERIMENTAL AND HOMOGENEOUS TWO PHASE FRICTION MULTIPLIERS ϕ_{fo}^2

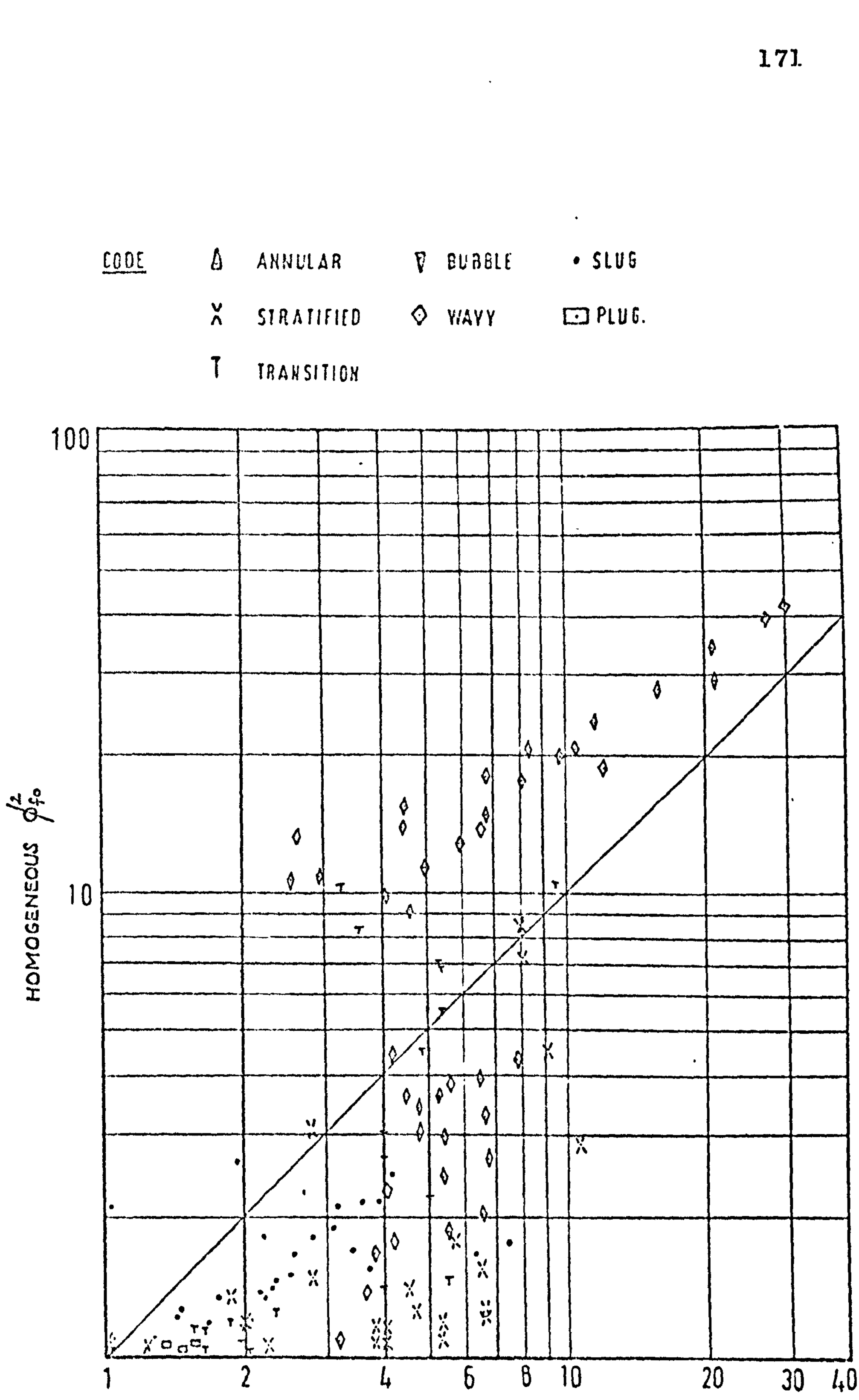

FIG. 6.4 COMPARISON OF EXPERIMENTAL AND HOMOGENEOUS TWO PHASE FRICTION MULTIPLIERS ϕ^2_{fo}

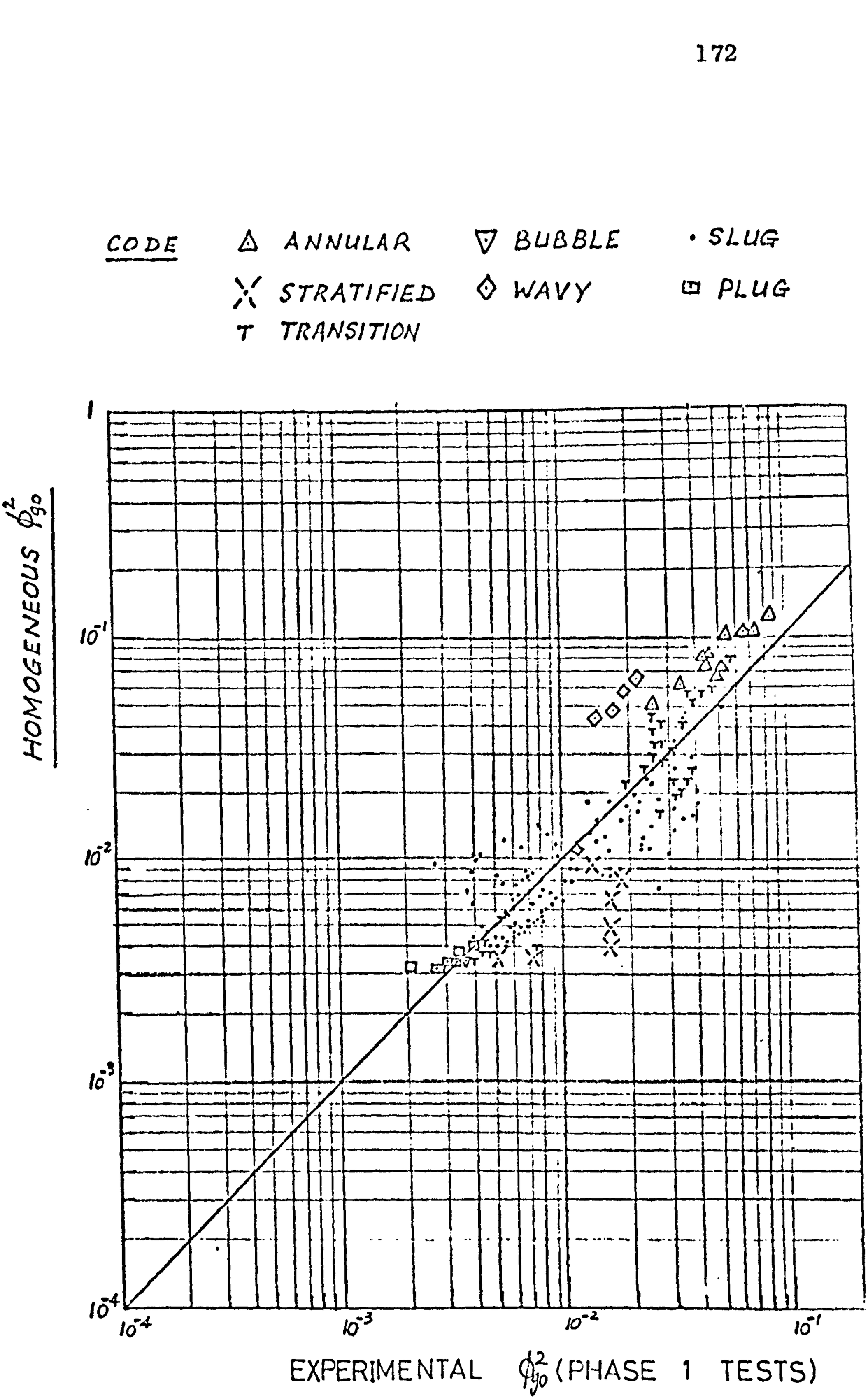

FIG. 6.5 COMPARISON OF EXPERIMENTAL AND HOMOGENEOUS TWO PHASE FRICTION MULTIPLIERS ϕ_{fo}^2

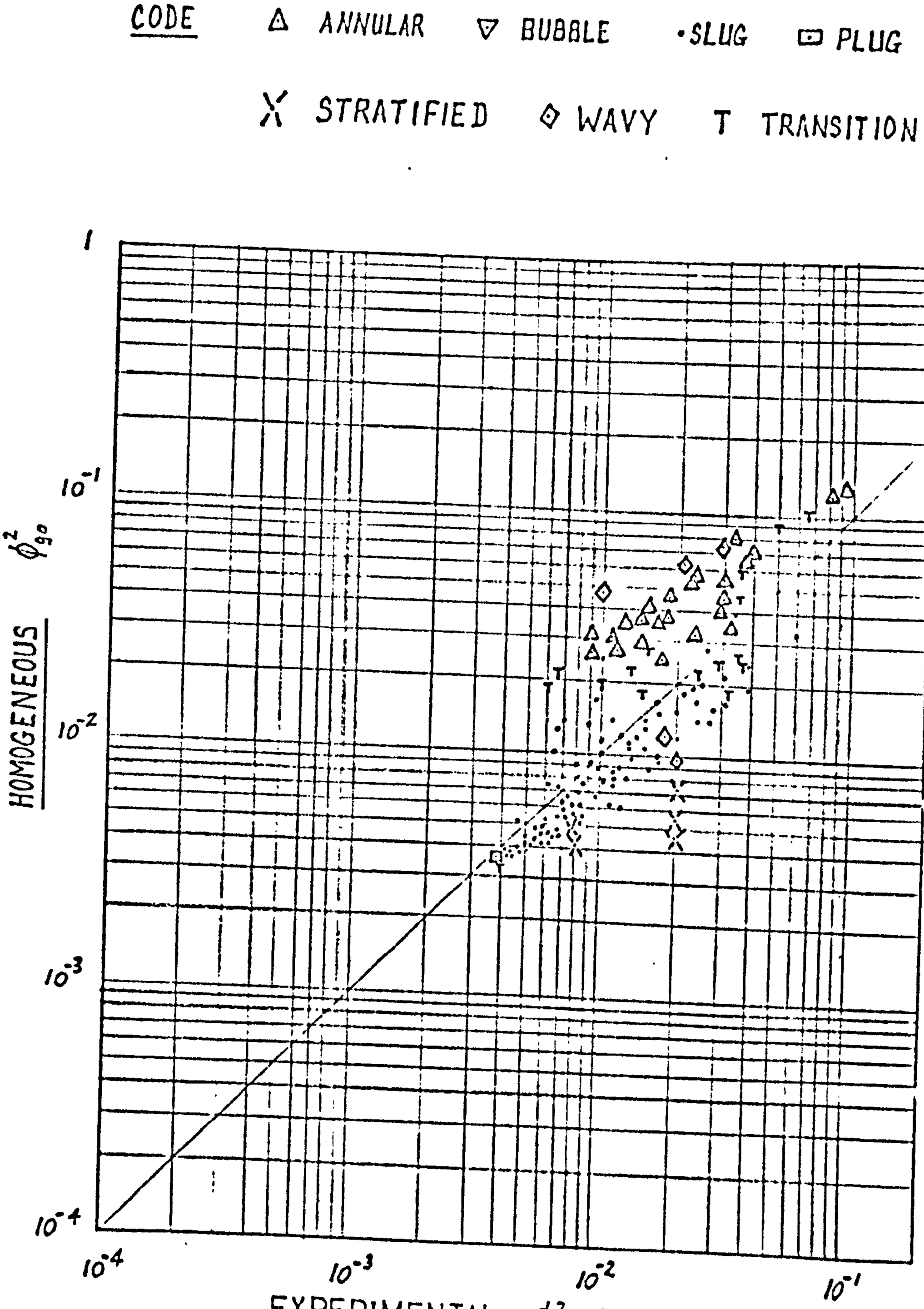

FIG. 6.6 COMPARISON OF EXPERIMENAL AND HOMOGENEOUS TWO PHASE FRICTION MULTIPLIERS ϕ_{go}^2

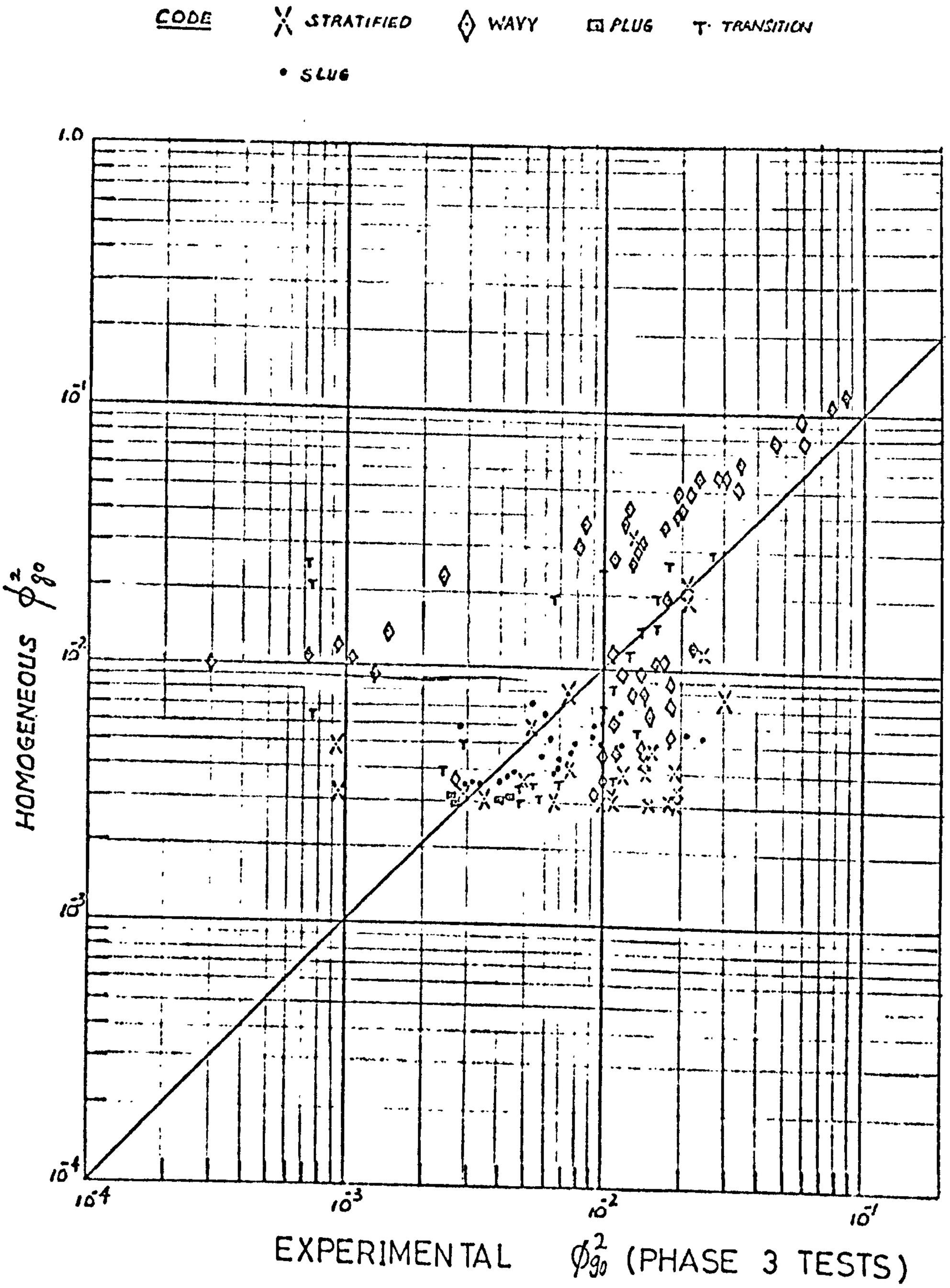

EXPERIMENTAL ϕ_{go}^2 (PHASE 3 TESTS)

FIG.6·7 COMPARISON OF EXPERIMENTAL AND HOMOGENEOUS TWO PHASE FRICTION MULTIPLIERS ϕ_{go}^2

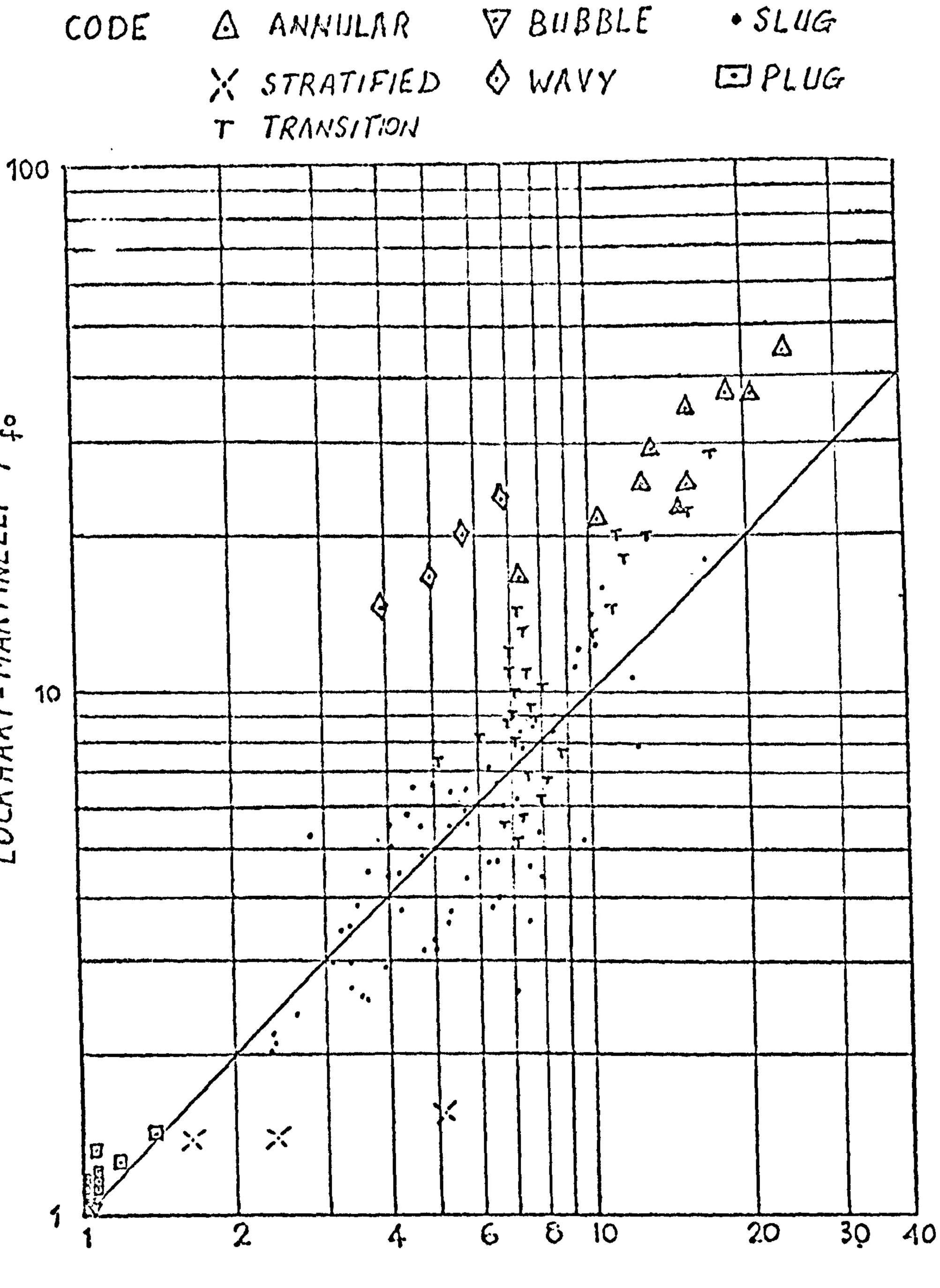

EXPERIMENTAL ϕ^2_{fo} (PHASE 1 TESTS)

FIG. 6·8 COMPARISON OF EXPERIMENTAL AND LOCKHART & MARTINELLI TWO PHASE FRICTION MULTIPLIERS ϕ^2_{fo}

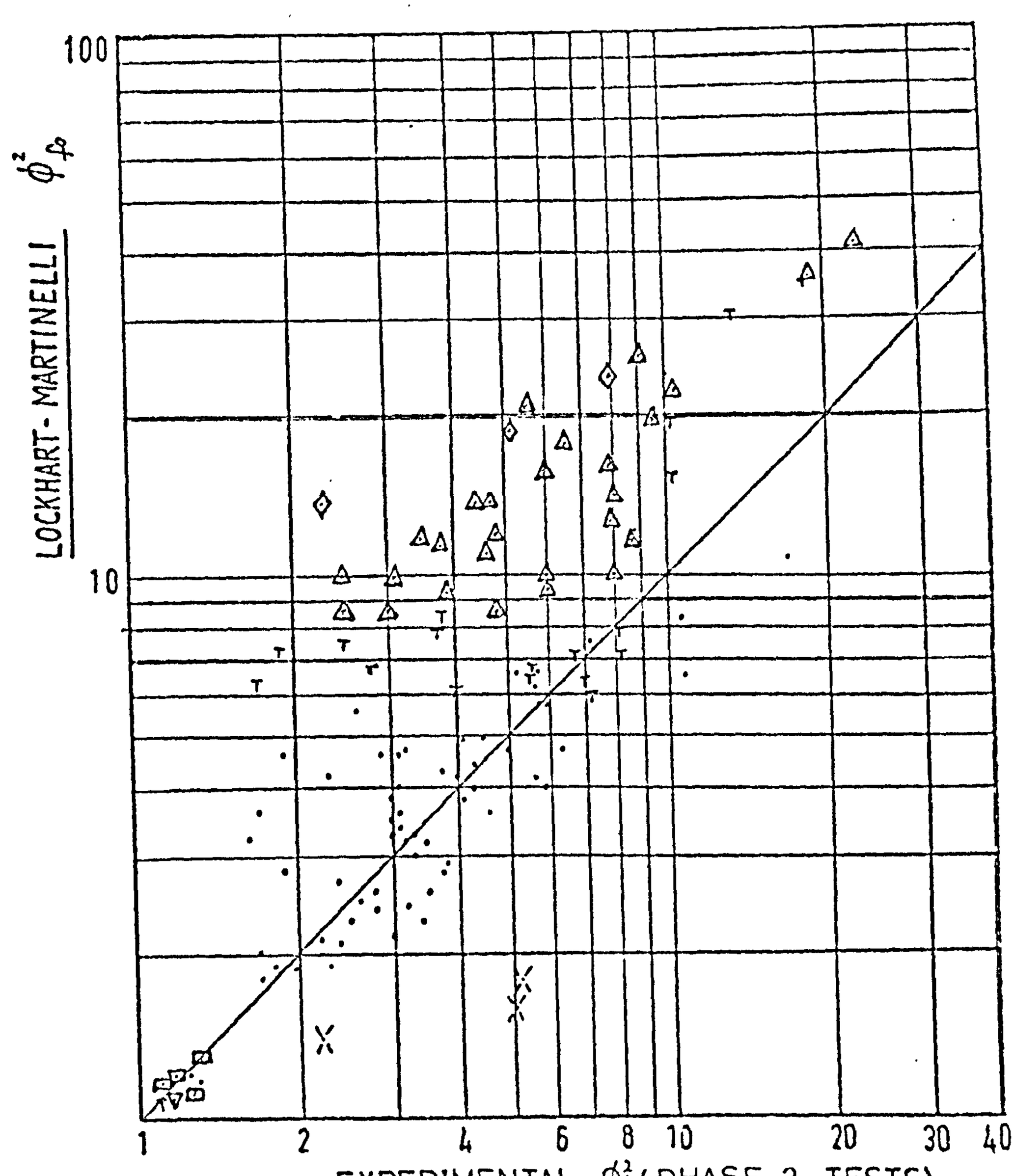

FIG. 6·9 COMPARISON OF EXPERIMENTAL AND LOCKHART-MARTINELLI TWO PHASE FRICTION MULTIPLIERS ϕ_{fo}^2

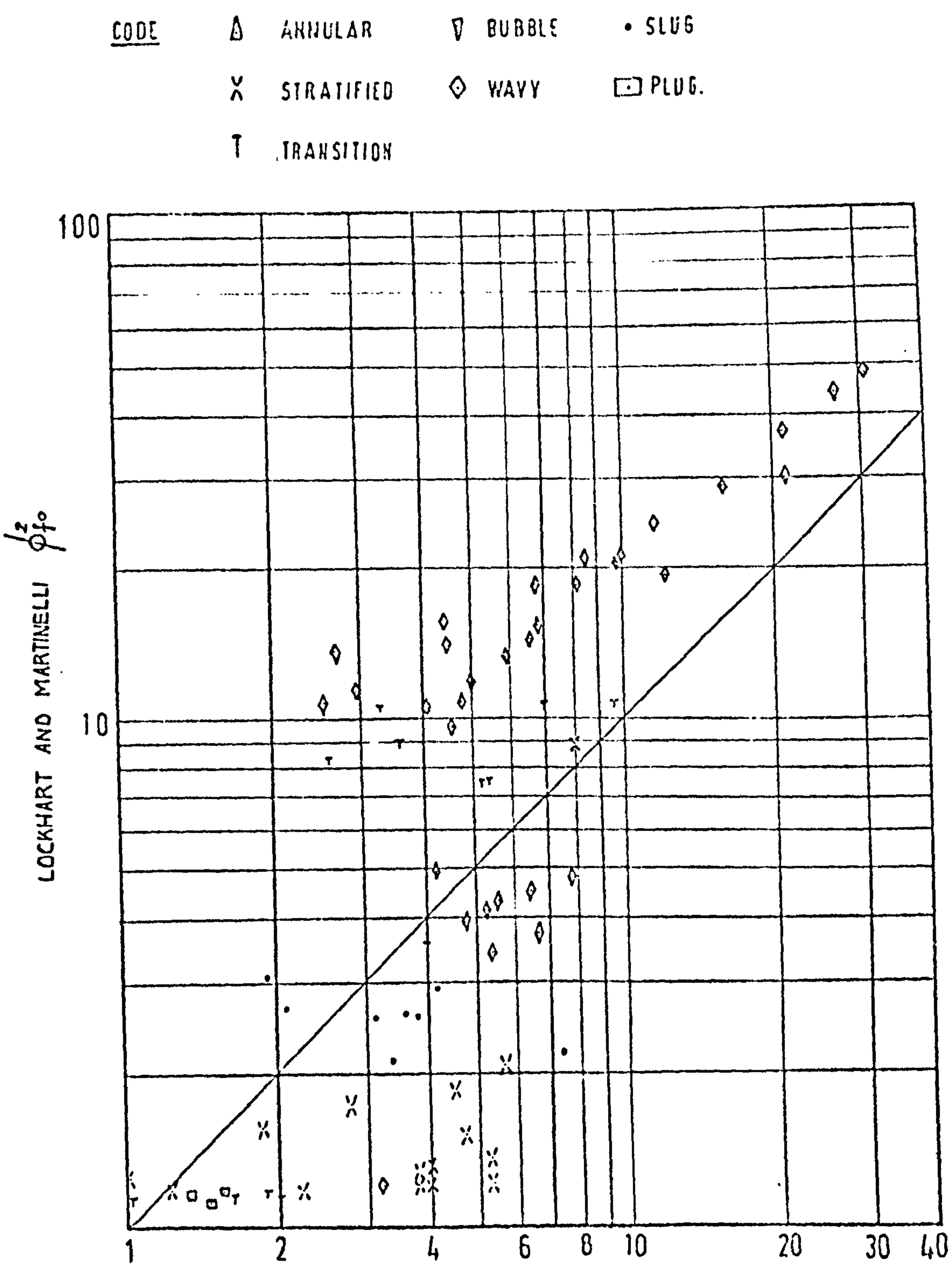

FIG. 6.10 COMPARISON OF EXPERIMENTAL AND LOCKHART AND MARTINELLI 2-PHASE FRICTION MULTIPLIERS ϕ_{fo}^2

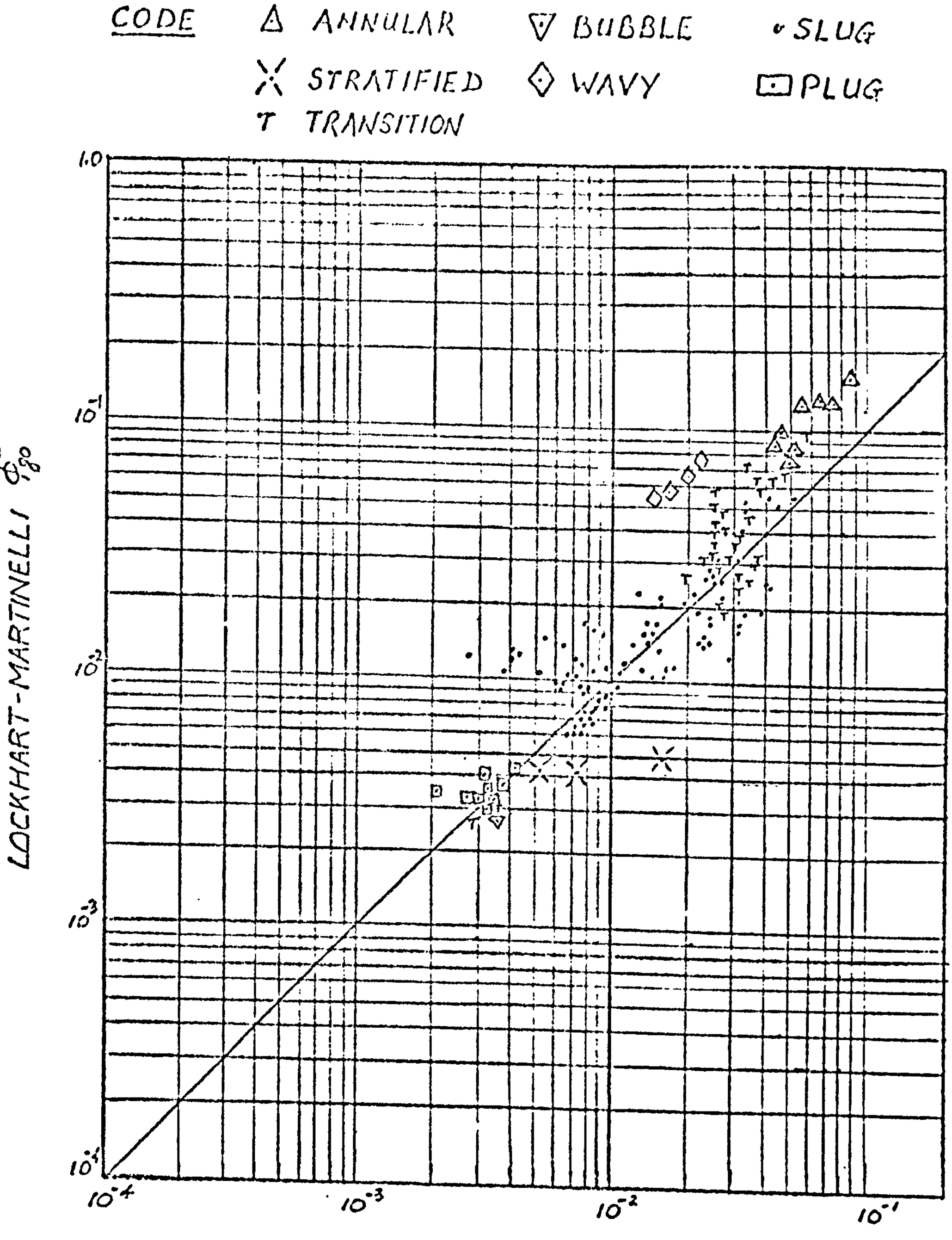

FIG.6.11 COMPARISON OF EXPERIMENTAL AND LOCKHART & MARTINELLI TWO PHASE FRICTION MULTIPLIERS ϕ_{go}^2

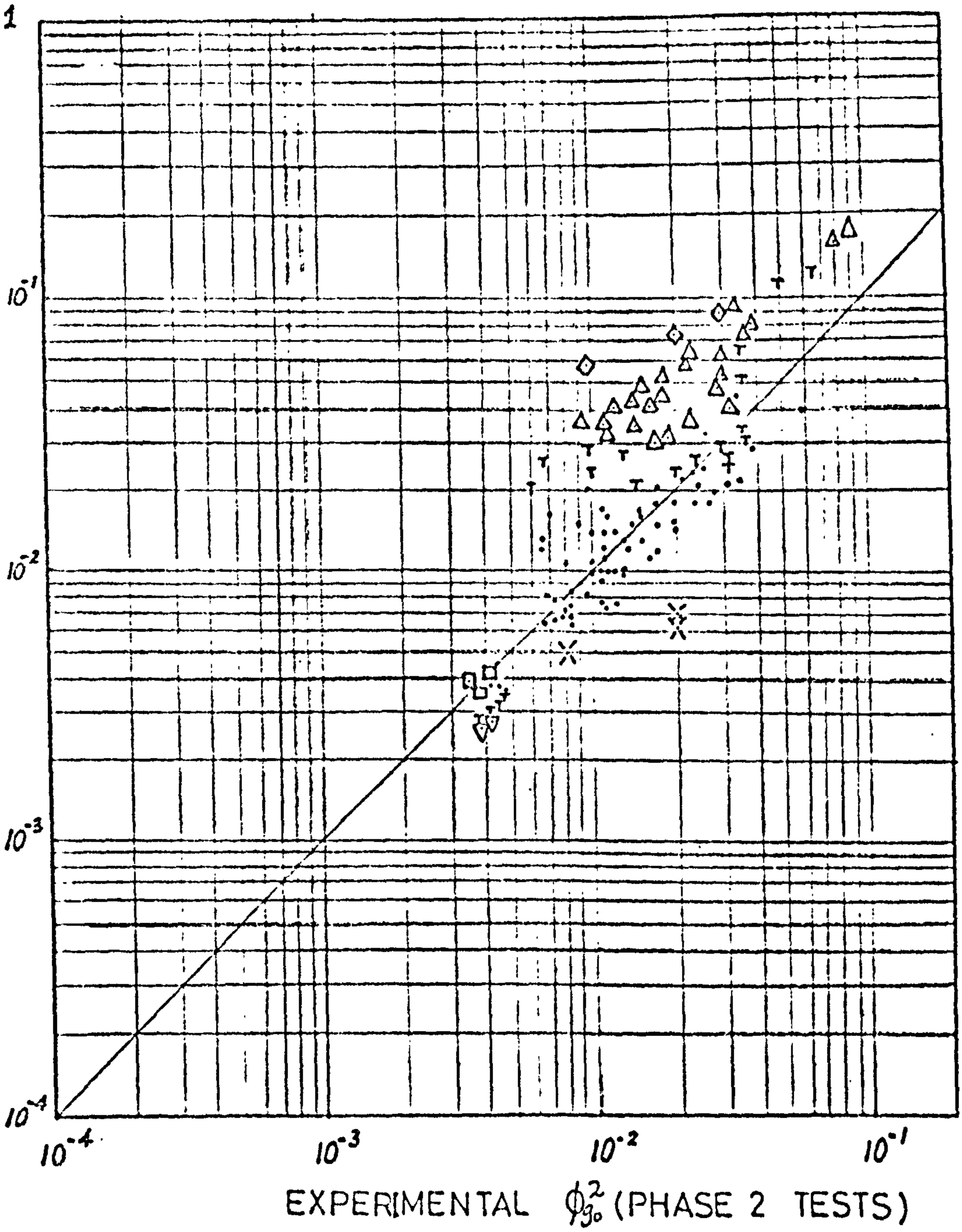

FIG. 6.12 COMPARISON OF EXPERIMENTAL AND LOCKHART-MARTINELLI TWO PHASE FRICTION MULTIPLIERS ϕ_{go}^2

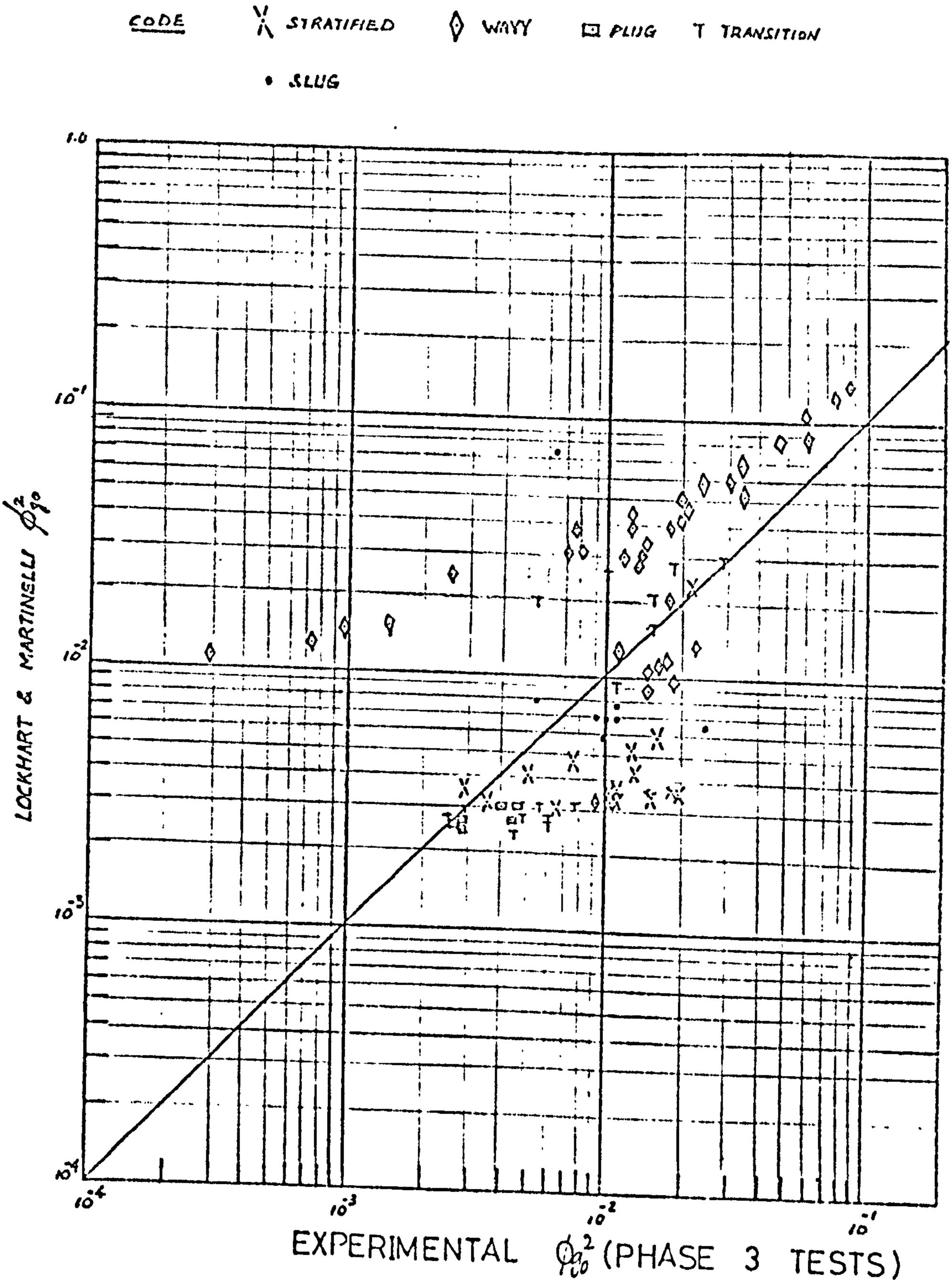

FIG.6·13 COMPARISON OF EXPERIMENTAL AND LOCKHART & MARTINELLI TWO PHASE FRICTION MULTIPLIERS ϕ_{lo}^2

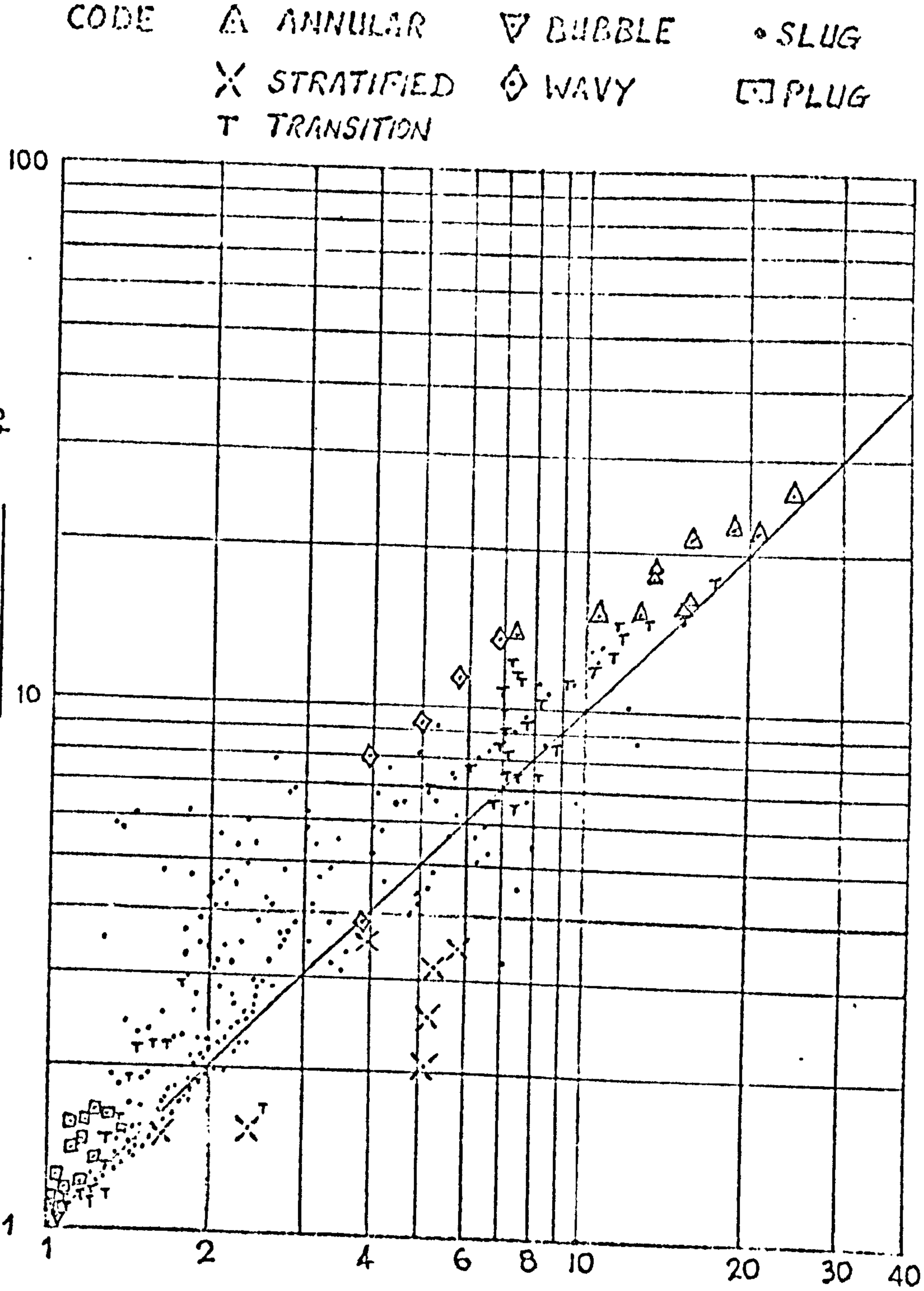

FIG. 6.14 COMPARISON OF EXPERIMENTAL AND DUKLER TWO PHASE FRICTION MULTIPLIERS ϕ^2_{fo}

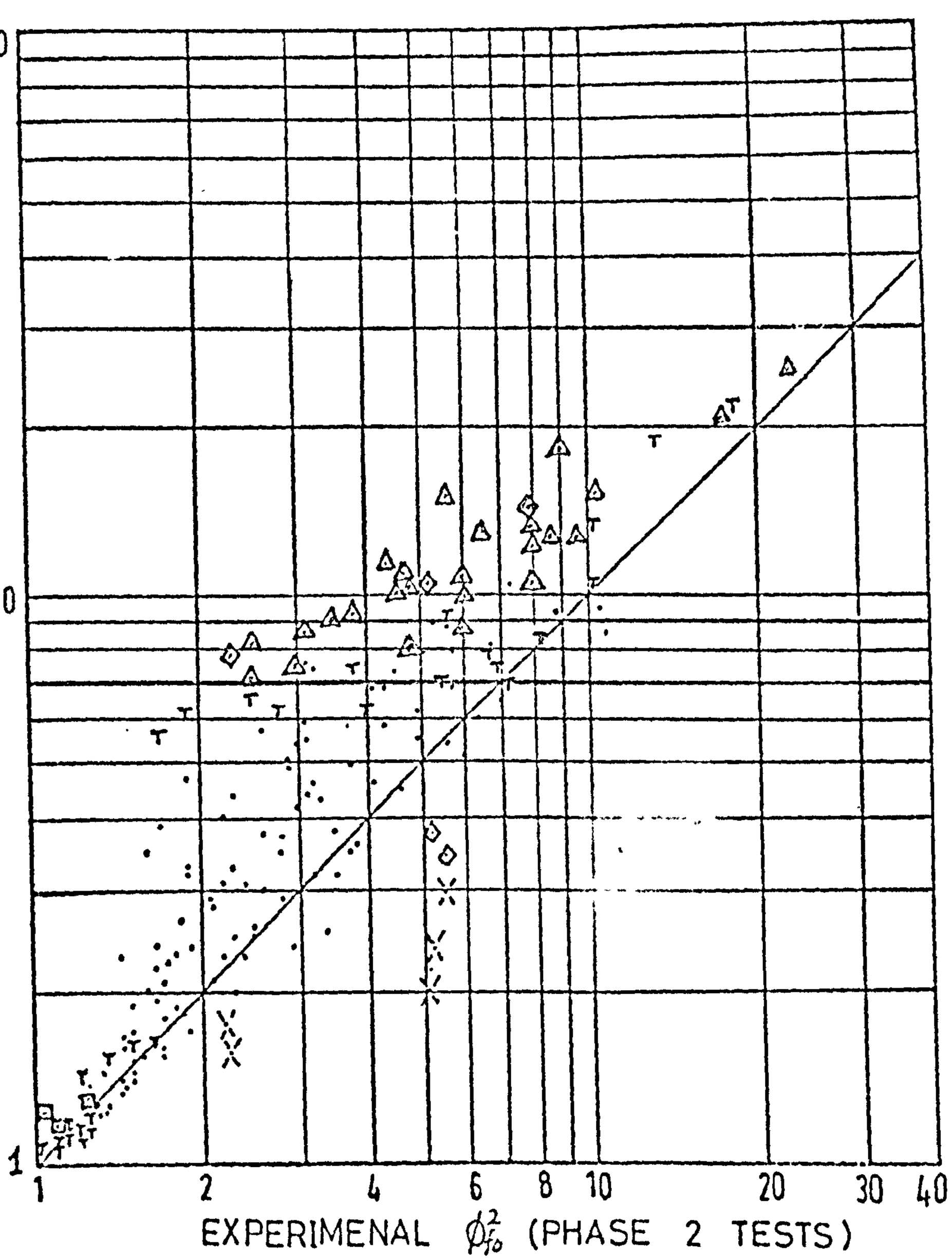

FIG. 6.15 COMPARISON OF EXPERIMENTAL AND DUKLER TWO PHASE FRICTION MULTIPLIERS ϕ_{fo}^2

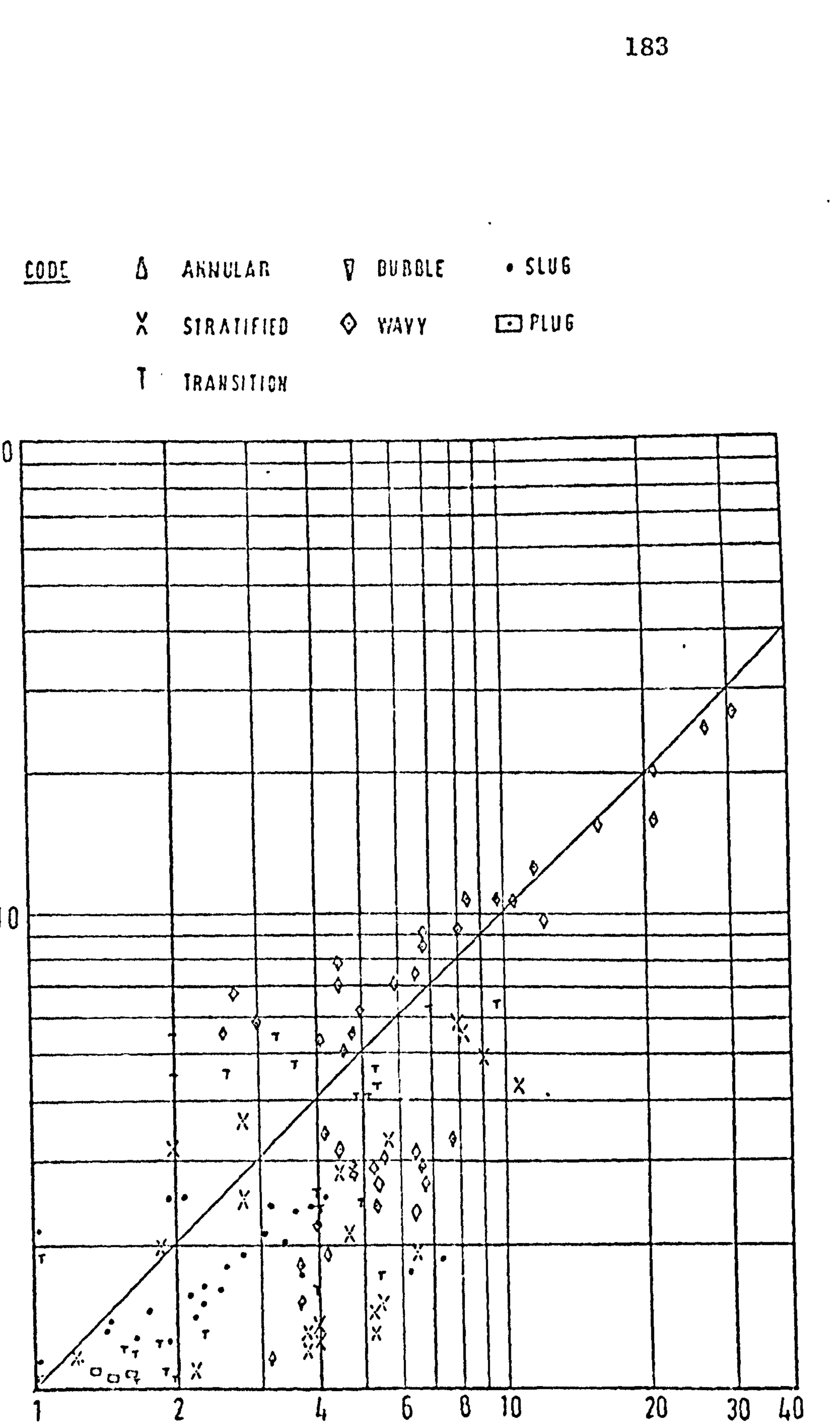

FIG. 6·16 COMPARISON OF EXPERIMENTAL AND DUKLER CASE II MODEL TWO PHASE FRICTION MULTIPLIERS ϕ^2_{fo}

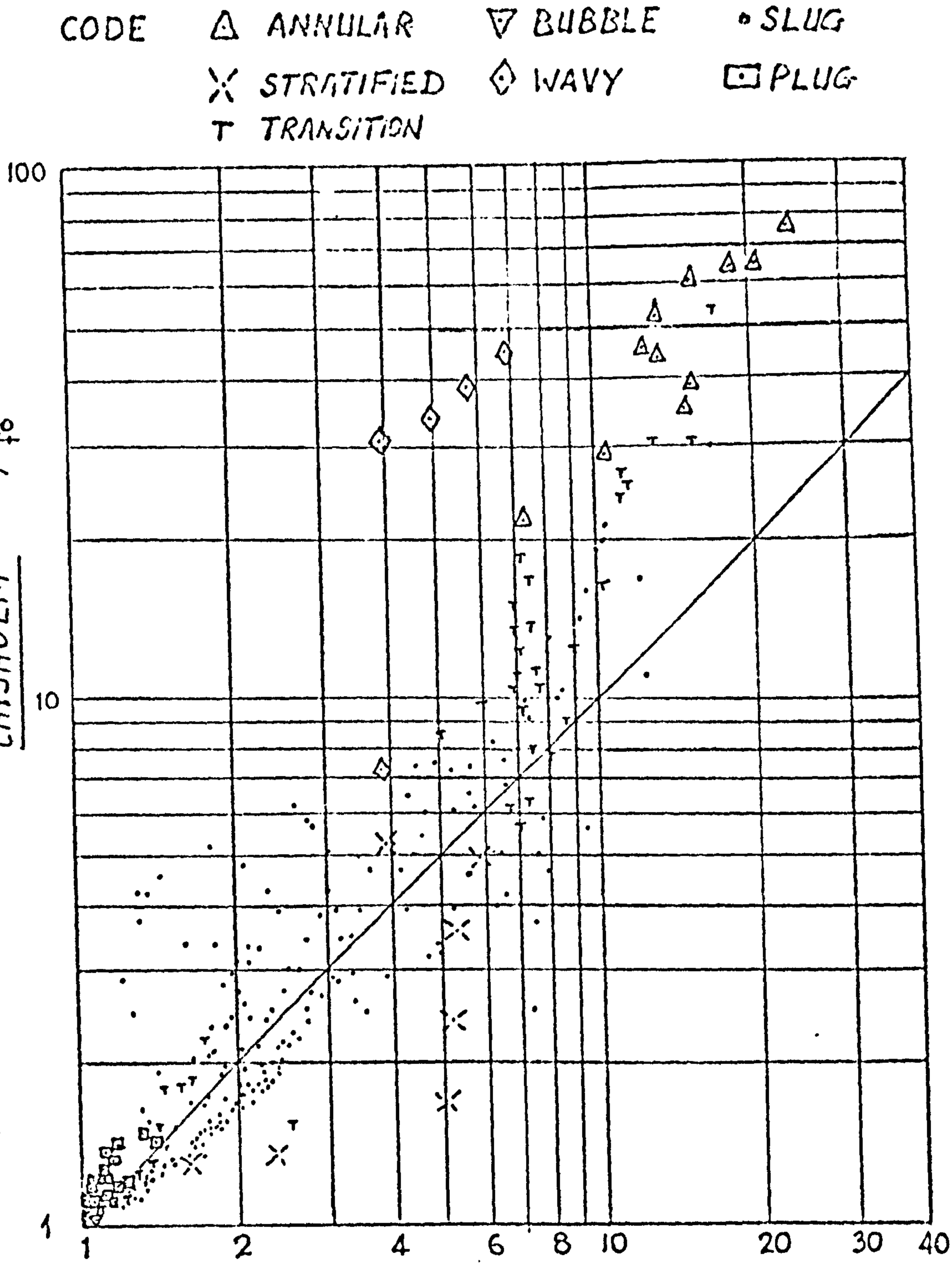

FIG. 6·17 COMPARISON OF EXPERIMENAL AND CHISHOLM TWO PHASE FRICTION MULTIPLIERS ϕ^2_{fo}

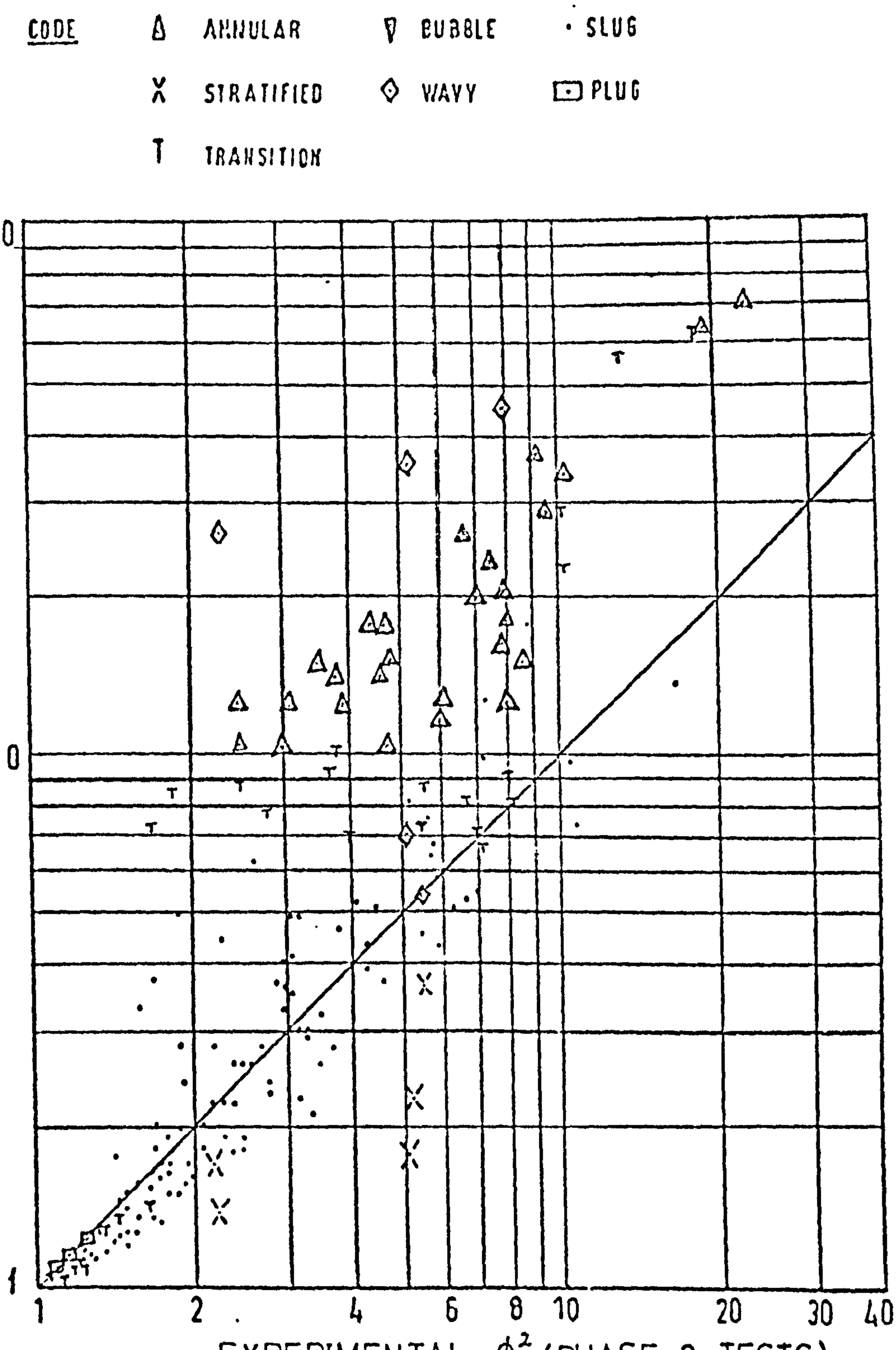

FIG. 6·18 COMPARISON OF EXPERIMENTAL AND CHISHOLM TWO PHASE FRICTION MULTIPLIERS ϕ_{fo}^2

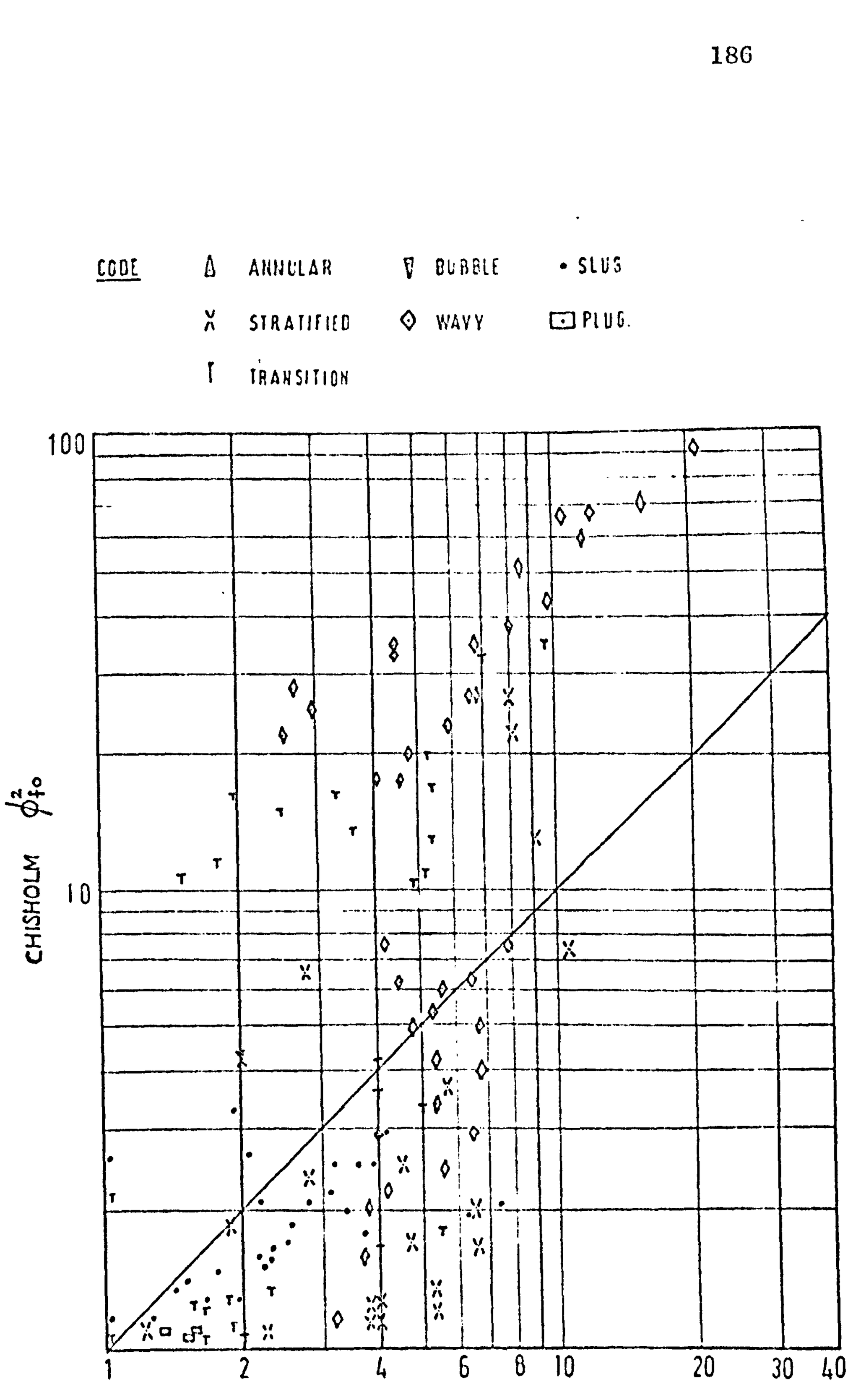

FIG.6.19 COMPARISON OF EXPERIMENTAL AND CHISHOLM TWO PHASE FRICTION MULTIPLIERS ϕ^2_{fo}

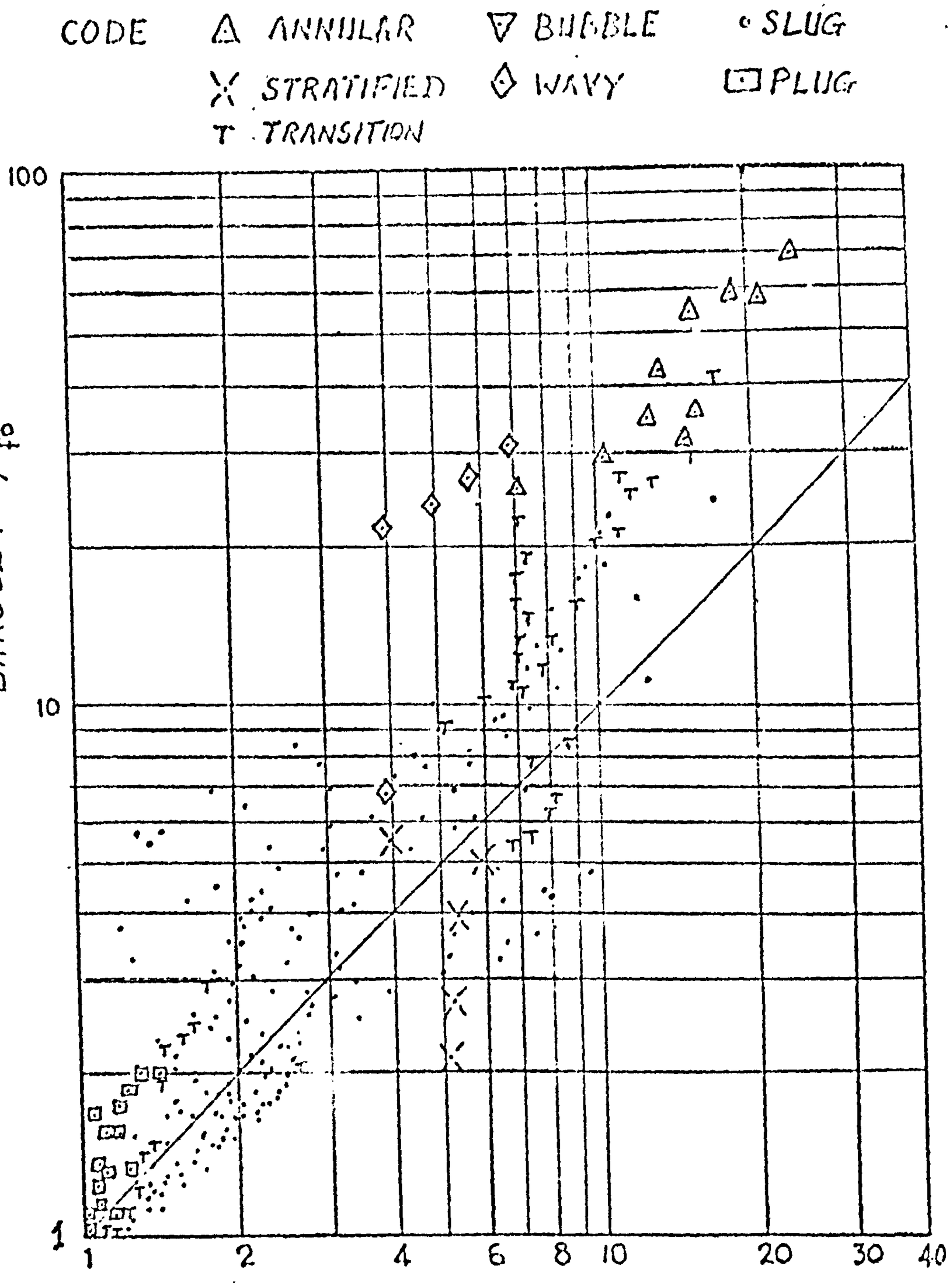

EXPERIMENTAL ϕ^2_{fo} (PHASE 1 TESTS)

FIG. 6·20 COMPARISON OF EXPERIMENTAL AND BAROCZY TWO PHASE FRICTION MULTIPLIERS ϕ^2_{fo}

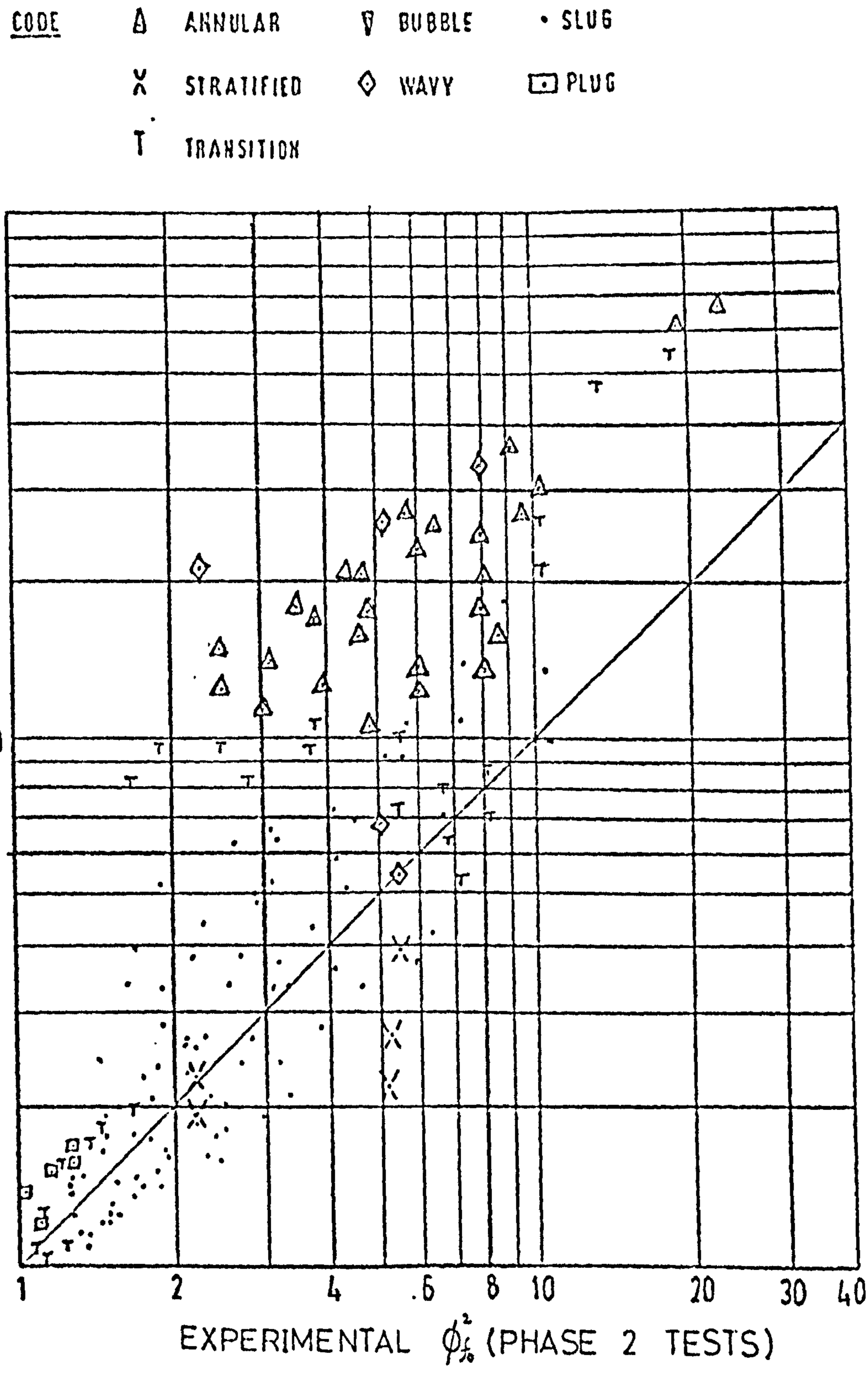

FIG. 6·21 COMPARISON OF EXPERIMENTAL AND BAROCZY TWO PHASE FRICTION MULTIPLIERS ϕ_{fo}^2

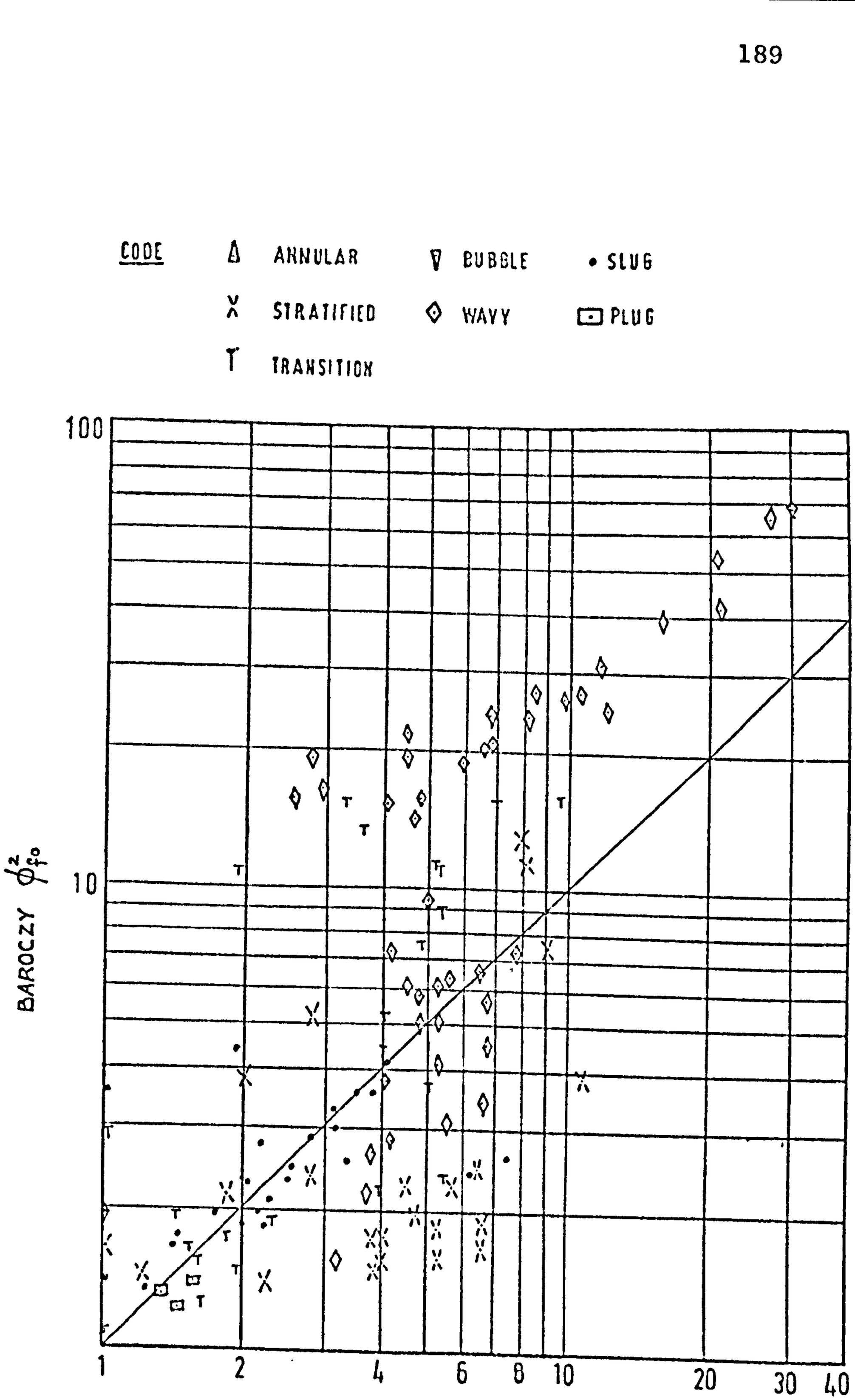

FIG. 6·22 COMPARISON OF EXPERIMENTAL AND BAROCZY TWO PHASE FRICTION MULTIPLIERS ϕ^2_{fo}

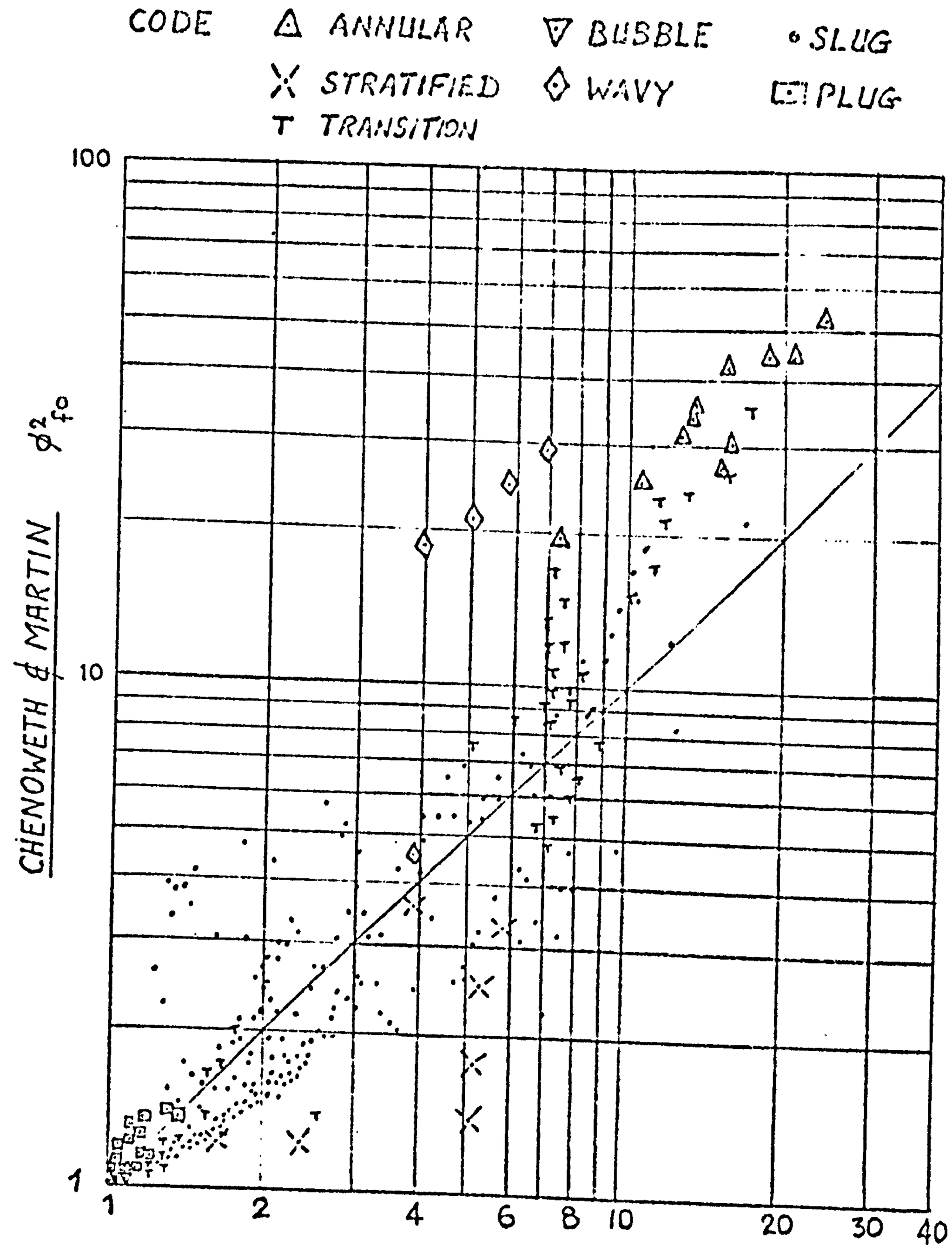

FIG. 6·23 COMPARISON OF EXPERIMENTAL AND CHENOWETH-MARTIN TWO PHASE FRICTION MULTIPLIERS ϕ^2_{fo}

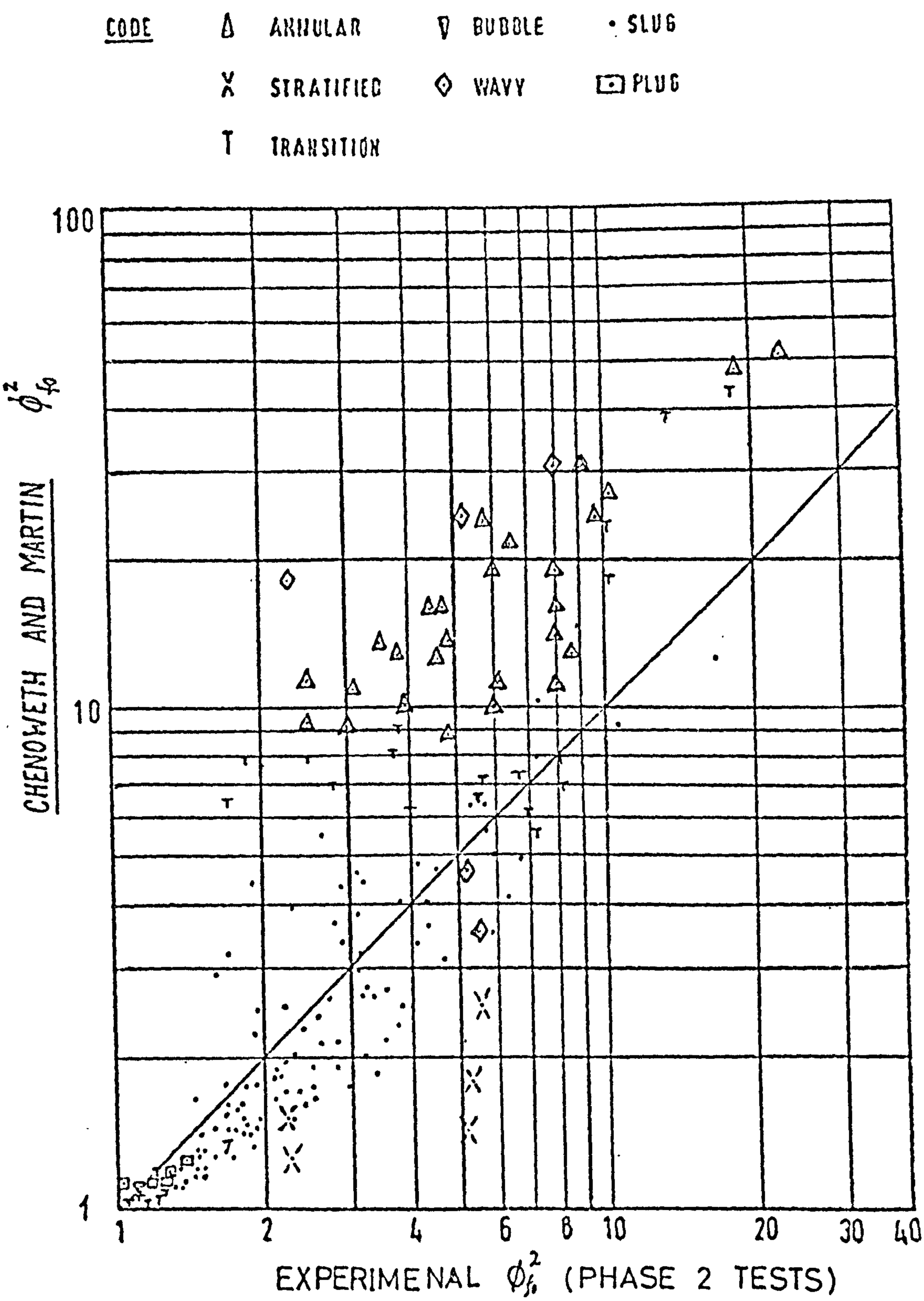

FIG. 6·24 COMPARISON OF EXPERIMENTAL AND CHENOWETH-MARTIN TWO PHASE FRICTION MULTIPLIERS ϕ_{fo}^2

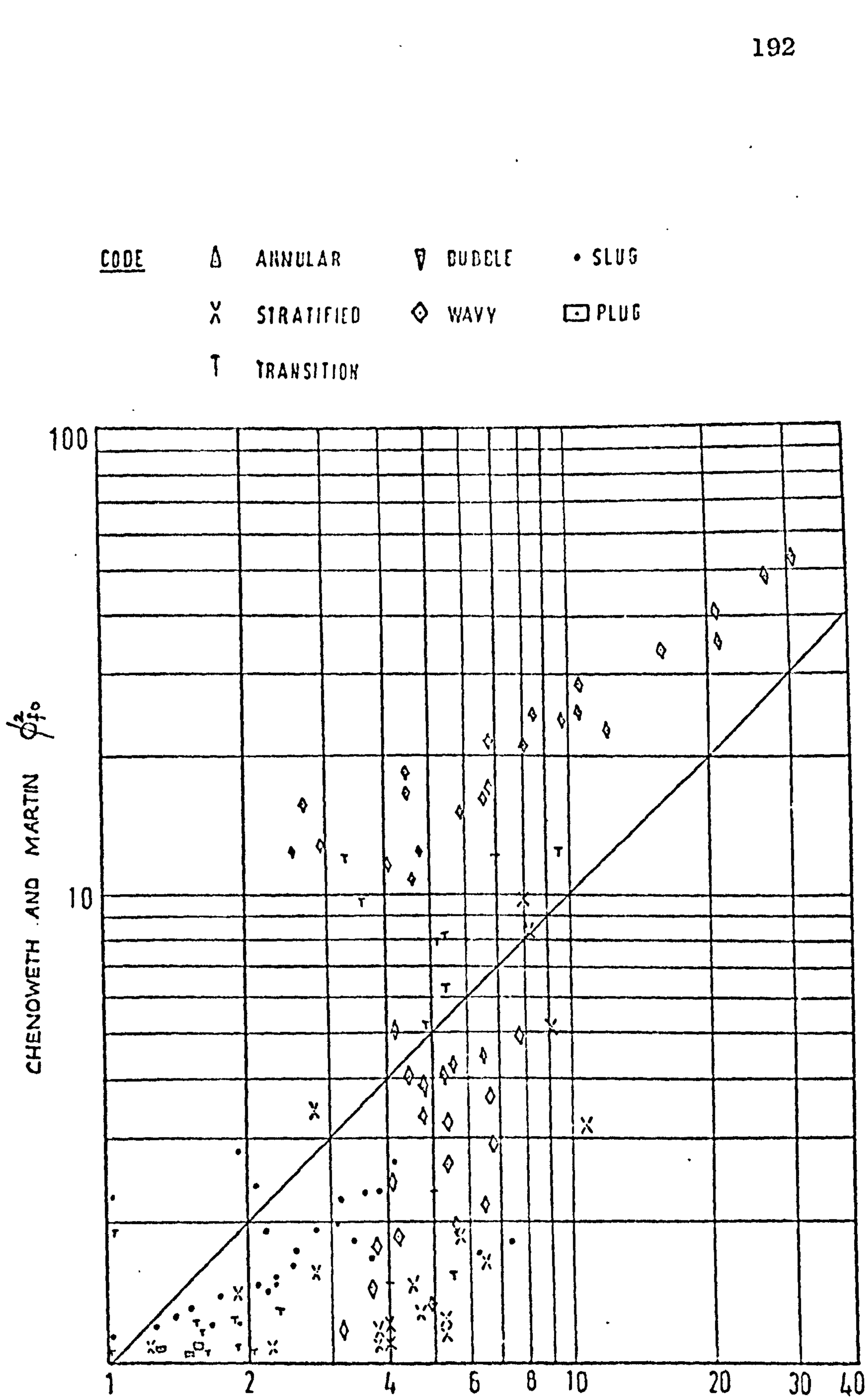

FIG. 6·25 COMPARISON OF EXPERIMENTAL AND CHENOWETH & MARTIN TWO PHASE FRICTION MULTIPLIERS ϕ^2_{fo}

(iv) Experimental versus Lockhart-Martinelli model predictions for $\phi^2_{g_o}$ - Figs. 6.11 to 6.13.

(v) Experimental versus Dukler model predictions for $\phi^2_{f_o}$ - Figs. 6.14 to 6.16.

(vi) Experimental versus Chisholm model predictions for $\phi^2_{f_o}$ - Figs. 6.17 to 6.19.

(vii) Experimental versus Baroczy model predictions for $\phi^2_{f_o}$ - Figs. 6.20 to 6.22.

(viii) Experimental versus Chenoweth-Martin model predictions for $\phi^2_{f_o}$ - Figs. 6.23 to 6.25.

Each set of 3 graphs represents Phase 1, Phase 2 and Phase 3 comparisons.

The data plotted in Figs. 6.2 to 6.25 were identified in terms of different flow patterns to detect any flow pattern effects present and to facilitate comparison. It was not considered necessary to indulge in the usual statistical commentaries and comparisons involving mean errors, standard deviations etc., but to confine the comments to general points and impressions since the predictions are generally poor.

The results of the comparison cannot be considered satisfactory. The scatter is appreciable and suggests that either the existing correlations are inadequate for predicting the friction pressure drop in large diameter tubes or that the comparisons are unfair, or perhaps both. However, this conclusion, although rather disturbing, is perhaps not too surprising if one remembers that

(i) many of the correlations compared were developed from data taken in small diameter tubes and/or for other fluid combinations and sometimes with no mass velocity effects corrections.

(ii) for a given mass or volume flowrate, the friction pressure drop in these large tubes is much less than in smaller tubes, hence large differences do not necessarily constitute large pressure drops in absolute terms, and hence small uncertainties in the correlation could be amplified.

(iii) there is more scope in large diameter tubes for flow separation and stratification and hence for variations in liquid level along the tube.

Item (iii) is very important since, if variations in liquid level do exist, questions arise as to whether the measured pressure gradient equals the friction pressure gradient and whether the comparisons with other correlations in terms of friction multipliers are fair. This mostly applies to stratified and wavy type flows. This stratified effect however, could affect other flow patterns, e.g. annular, where the film thickness at the bottom of the tube is so thick as to give the effect of a stratified type flow superimposed on a symmetrical annular flow.

The Dukler case II correlation gives the best overall agreement (although large differences with experiment still exist) and is generally conservative,

i.e. the predicted pressure drop is higher than the experimental. It should be pointed out that this correlation is the only one requiring a void fraction correlation and that experimental values of void fraction were used in the analysis. However, any bias towards the Dukler correlation in using these experimental void fraction values could be insignificant compared with the magnitude of the differences in the $\phi_{f_o}^2$ term between the various correlations and experiment. The relatively bad performance may be attributed to the empiricism introduced into the correlation in evaluating the λ_2 term (Appendix T).

In relative terms of general agreement, perhaps the Lockhart-Martinelli and homogeneous flow correlations come next to Dukler, appreciating that differences between theory and experiment of over 100% are common. The Lockhart-Martinelli predictions are generally conservative whereas the homogeneous flow model often underpredicts $\phi_{f_o}^2$, which is undesirable, keeping in mind that less points were examined by the Lockhart-Martinelli correlation (as explained later).

The Chenoweth-Martin, Baroczy and Chisholm correlations all give poorer general agreement although the latter is fairly good at low friction multipliers. The Chisholm correlation requires the exponent of the Reynolds number in a Blasius type friction factor equation. This was taken as 0.222 for Phase 1 and 2 tests which

should introduce some (but fairly negligible) uncertainty at low liquid flowrates where a higher value ($\sim$ 0.4) fitted the single phase friction characteristic data better.

Before commenting further on the relative merits of the various correlations tested, it is perhaps worth stressing that an appreciable amount of stratification and phase separation occurred in these large tubes, whereby the air was displaced off centre towards the top of the tube. This tended to produce lower slip factors (slip $<$ 1 in some instances) than a flow symmetrically disposed about the tube centreline, due to the low velocity regions at the top of the tube being almost permanently occupied by air.

This combination of inhomogeneity and low slip may explain why the homogeneous model compares more favourably with experiment than do some of the correlations with slip built into them.

The Lockhart-Martinelli model admits to separated or inhomogeneous flow but was developed from small tube diameter data and is deficient in respect of not accounting for either interfacial effects or mass flow effects. The Chisholm correlation does account for these items and it is perhaps disappointing that it did not give better agreement. However, this correlation is very dependent on the values of the 'B' factor used, which were not obtained from large diameter tube data.

The Chenoweth-Martin correlation is based on data obtained from "large diameter" (40 mm and 78 mm) steel pipes, but since the uncertainty between their correlation and data was $\sim \pm$ 60% for the 78 mm tube, perhaps an extrapolation of the tube diameter exaggerates the error. The comments in their paper suggest a diameter effect does exist and indeed that a pressure effect exists, since tests at 100 psi produced uncertainties of the order of + 250%, i.e. overpredicted $\phi^2_{f_o}$ values similar to those shown in Figs. 6.23, 6.24 and 6.25.

The Baroczy correlation was based on data obtained from different experiments over a range of fluids and conditions. These data included the air-water data of Johnson and Abu-Sabe (J1), which were obtained from a 22 mm horizontal tube and are thus subject to previous comments regarding extrapolation to larger tube diameters. The data base for this correlation was biased towards steam-water mixtures and may give better agreement in that field of application.

The comparisons between experiment, homogeneous flow and the Lockhart-Martinelli correlations in terms of the gas friction multipliers $\phi^2_{g_o}$ are reflections of the $\phi^2_{f_o}$ comparisons as can be seen from Figs. 6.2 to 6.13.

The unsatisfactory performance of the correlations reflect the disagreement among them and, possibly, the different void fraction behaviour in large diameter tubes. This can be seen in Fig. 6.26, which is a plot of the

results of Chisholm correlation against Dukler case II correlation for Phase 2 data with flow pattern and air and water flowrates effects shown. The agreement is poor and the comparison changes from underprediction by Chisholm of the Dukler values at low voidages and for mixed flows (bubbly, plug and slug) to overprediction at high voidages and for annular type flows.

In general, less data points appear in the Lockhart-Martinelli comparisons, Figs. 6.8 to 6.13, than in the other comparisons. This is because the evaluation of the Lockhart-Martinelli multipliers required evaluation of the parameter X which in turn required values of the single phase friction factor λ . It was considered unwise to extrapolate the experimental values of λ outwith the turbulent flow range tested and shown in Figs. 5.16 and 5.17.

Considering the measured pressure gradient equal to the friction pressure gradient inherently assumes that the gravity and acceleration contributions to the pressure gradient are zero, and that the pressure is constant over the tube cross-section at any axial position. The latter effect was found negligible and for one dimensional flow, the gravity component in a horizontal tube should be zero. However, for an asymmetrical two phase flow such as stratified flow, if there is a variation in the liquid level along the tube, this could be reflected in different pressure gradients being obtained depending upon whether

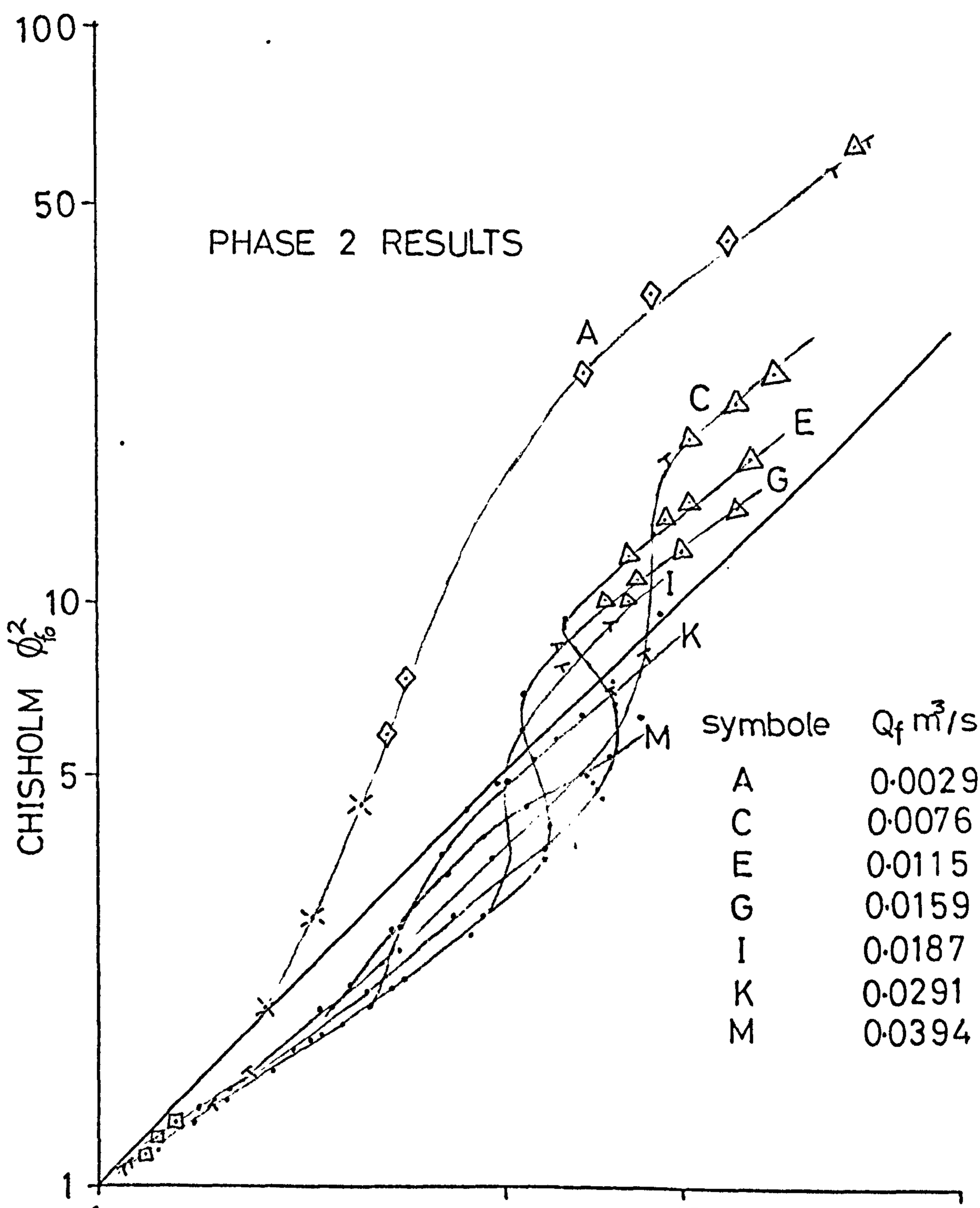

FIG. 6·26 COMPARISON OF DUKLER AND CHISHOLM CORRELATIONS

the pressure tapping points were located in the liquid or the gas, i.e. the pressure is not constant over the tube cross section at any axial position. This is indeed what was observed clearly during Phase 3 tests and, to a lesser extent, in Phases 1 and 2 tests (fewer stratified conditions encountered). This effect will be much more apparent with large diameter tubes (where the scope for variation in liquid level is large whilst the friction pressure gradient is small) than with small diameter tubes (where the scope for variation in liquid level is small and the friction pressure gradient is much larger). Hence the often quoted assumption in the literature on friction pressure drop evaluation that 'the pressure is constant over the tube cross-section' is unreasonable with asymmetrical two phase flow in large diameter tubes.

A quantitative assessment of the effect of using pressure tapping points in different circumferential locations may be obtained from Figs. 6.27 to 6.32 (Fig. 6.33 locates these repeat tests on the flow pattern map) where the experimental friction multipliers are deduced from,

(i) pressure tappings on top of tube, i.e. in air.

(ii) pressure tappings on bottom of tube, i.e. in water.

As can be seen the difference is appreciable especially at low $\emptyset_{f_o}^2$ values (low flowrates) and indicates significant changes in liquid level. Figs. 6.27 to 6.32

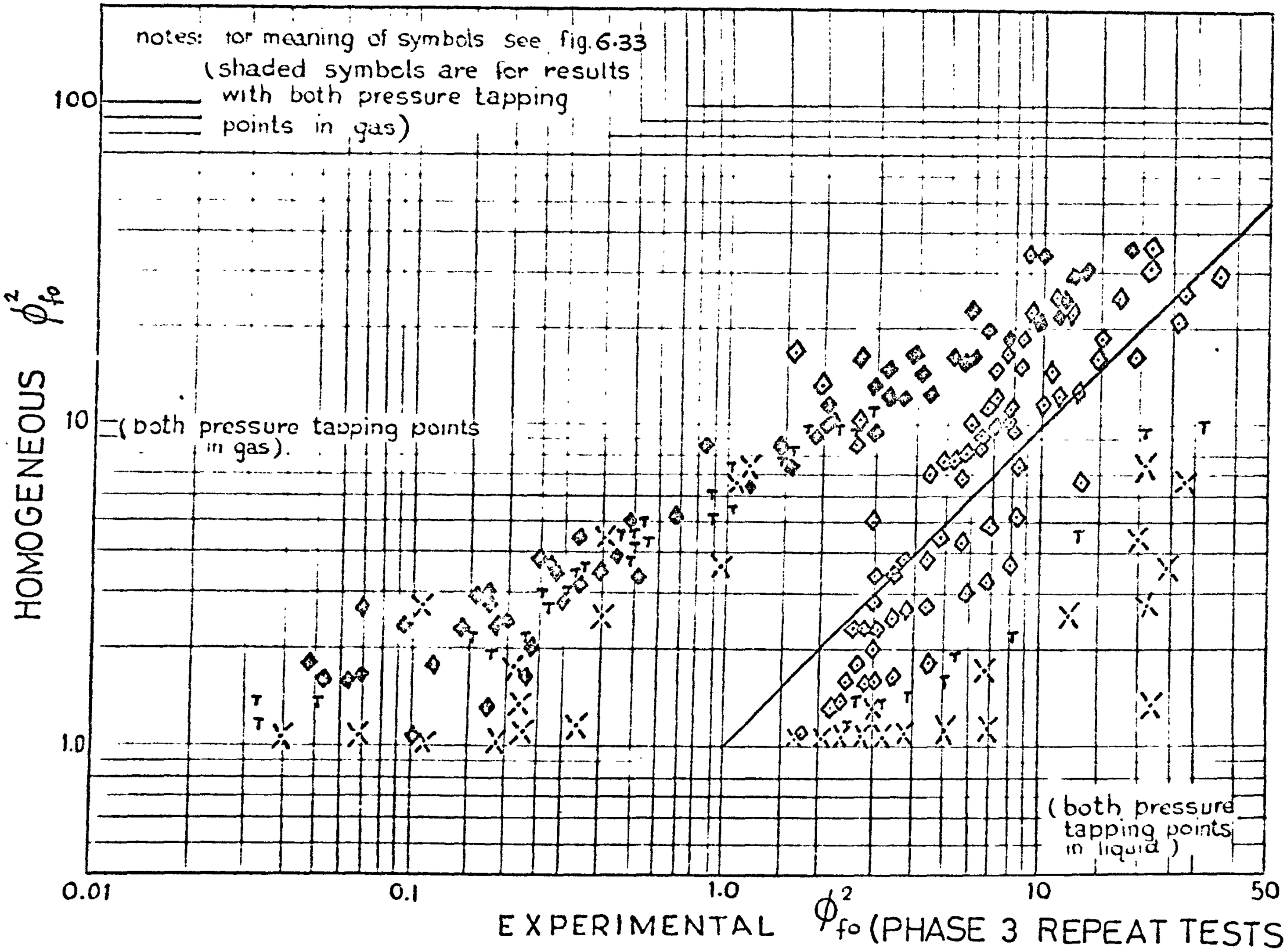

FIG.6·27 COMPARISON OF EXPERIMENTAL AND HOMOGENEOUS TWO PHASE FRICTION MULTIPLIERS ϕ^2_{fo}

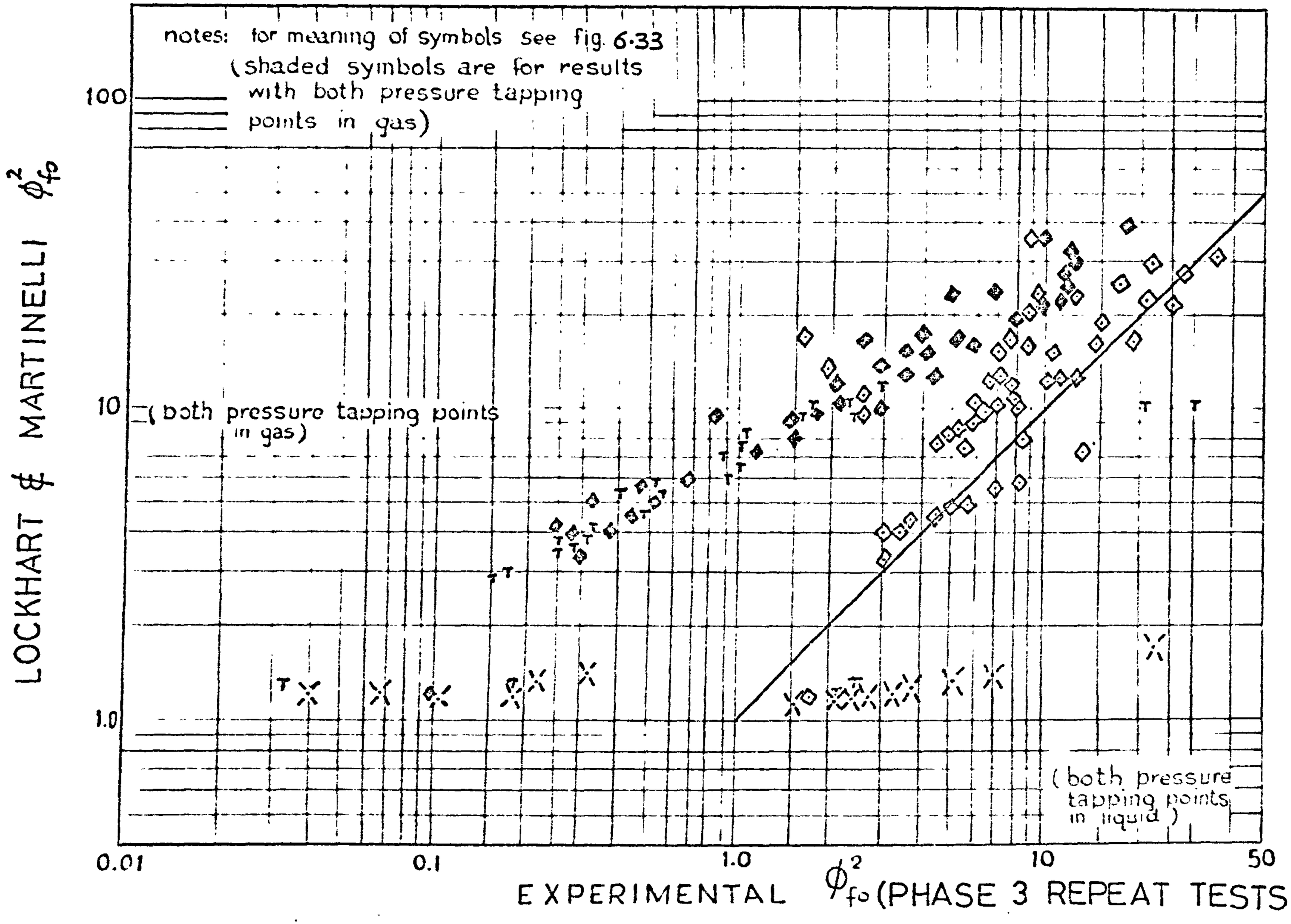

FIG.6·28 COMPARISON OF EXPERIMENTAL AND LOCKHART & MARTINELLI TWO PHASE FRICTION MULTIPLIERS ϕ_{fo}^2

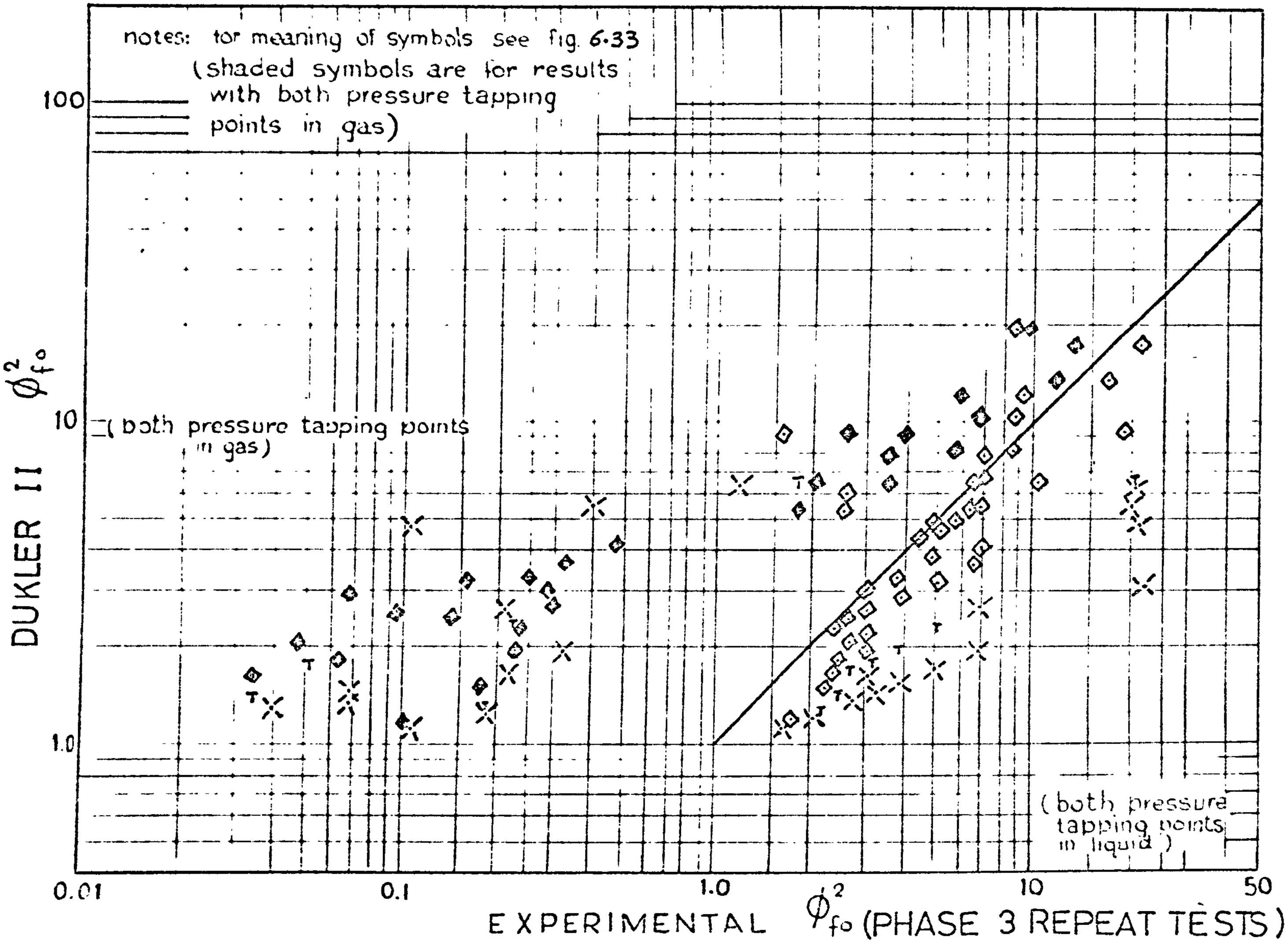

FIG.6·29 COMPARISON OF EXPERIMENTAL AND DUKLER II TWO PHASE FRICTION MULTIPLIERS ϕ^2_{fo}

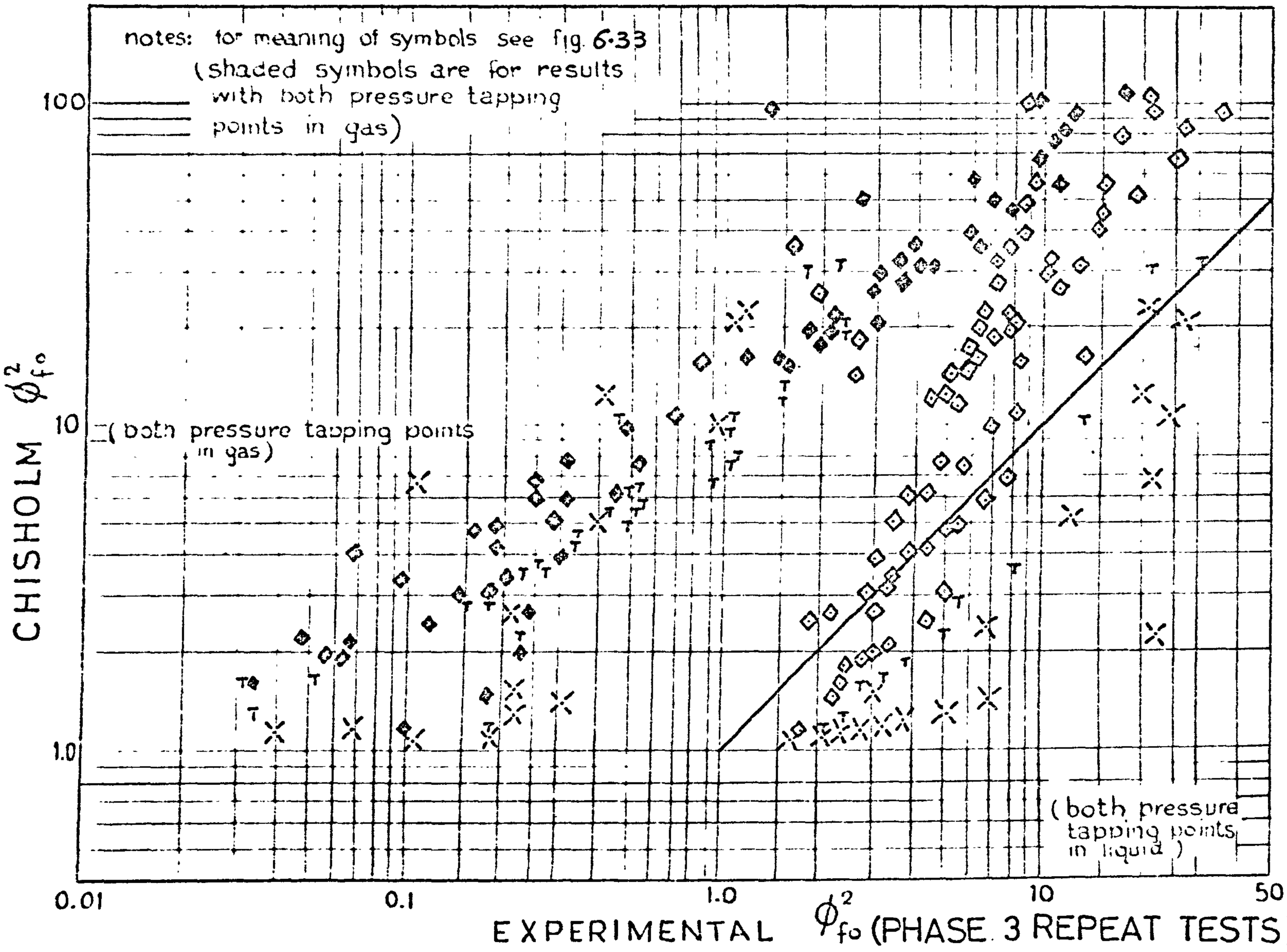

FIG 6·30 COMPARISON OF EXPERIMENTAL AND CHISHOLM TWO PHASE FRICTION MULTIPLIERS ϕ^2_{fo}

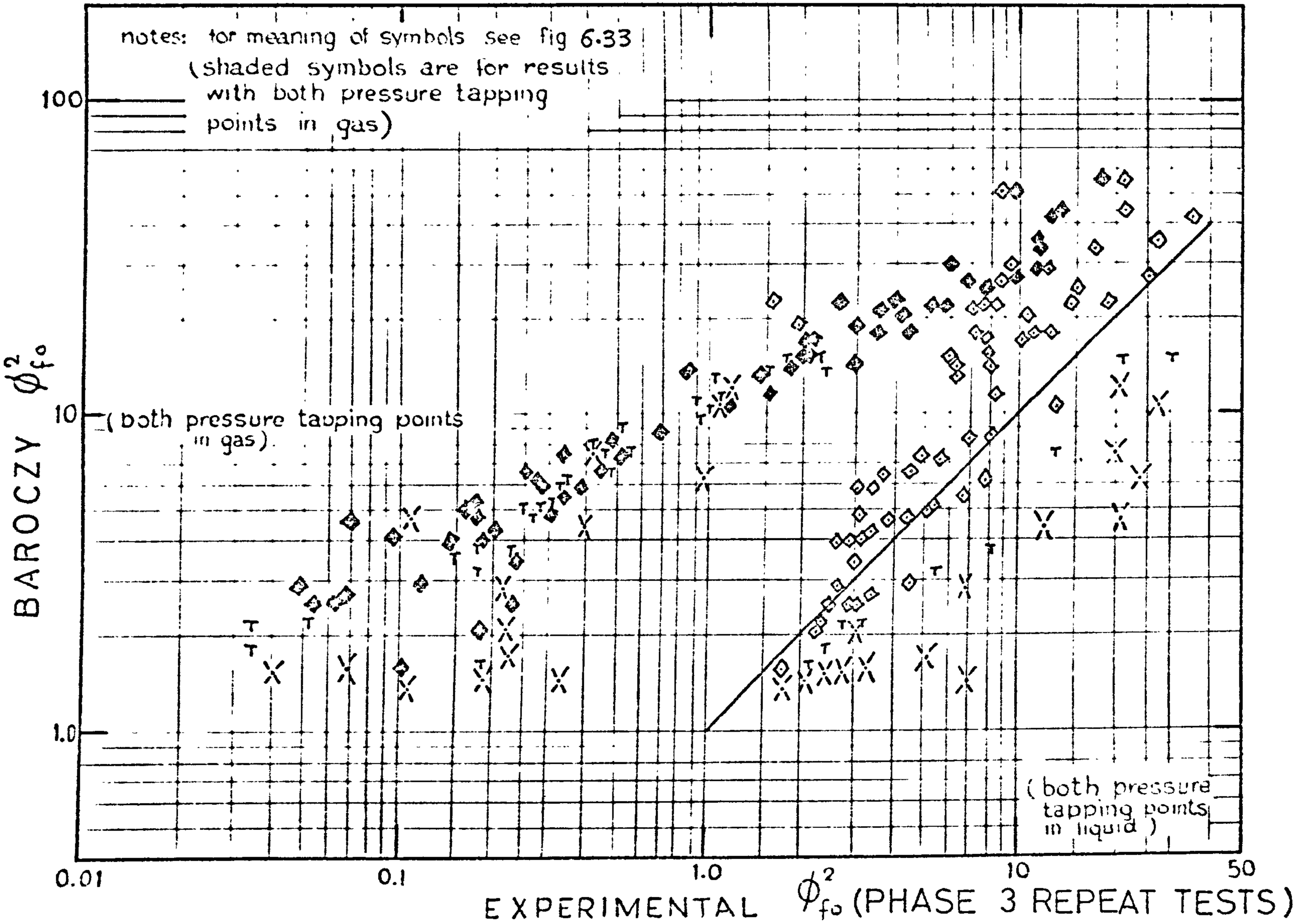

FIG.6·31 COMPARISON OF EXPERIMENTAL AND BAROCZY TWO PHASE FRICTION MULTIPLIERS ϕ^2_{fo}

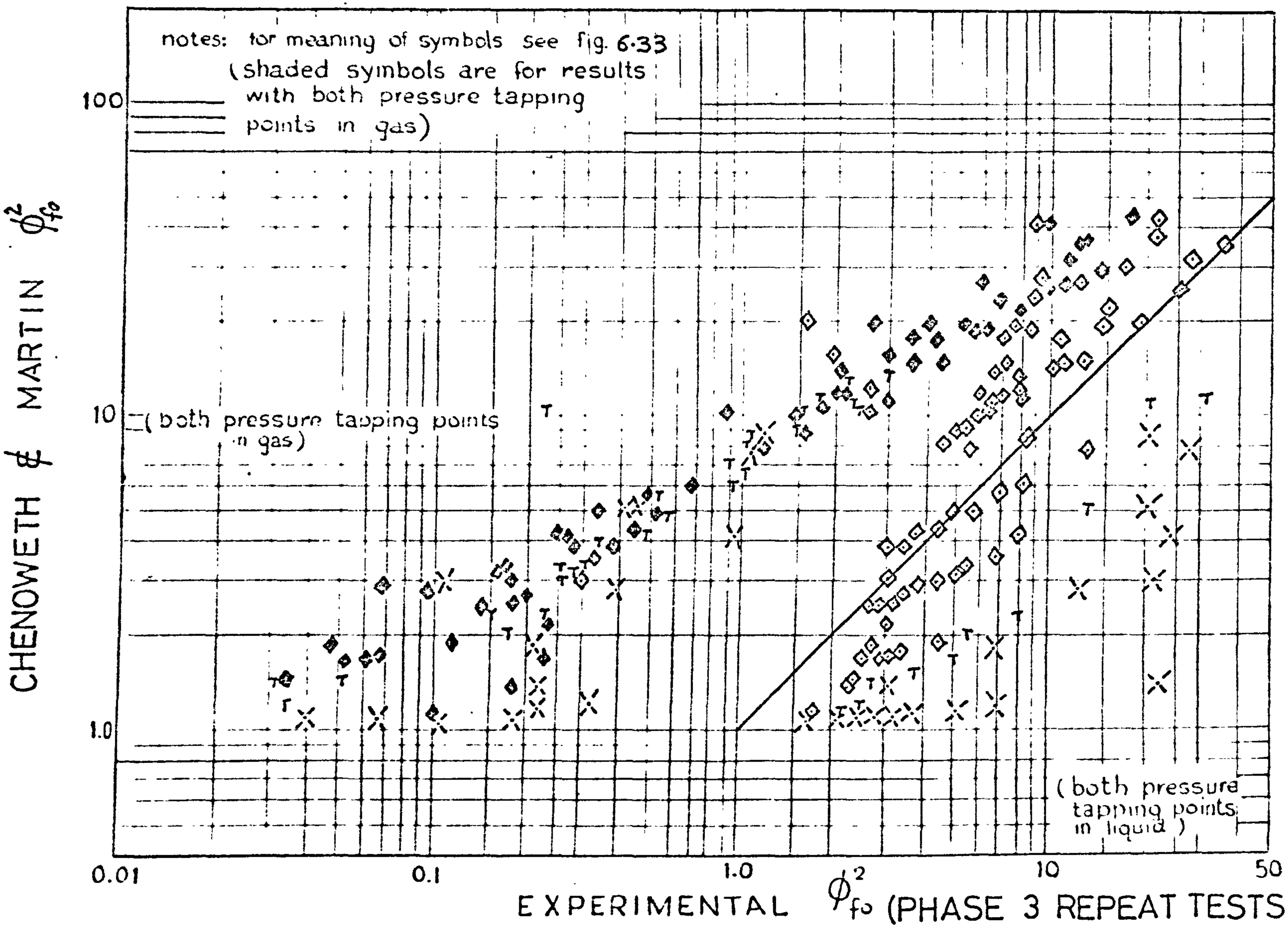

FIG.6·32 COMPARISON OF EXPERIMENTAL AND CHENOWETH & MARTIN TWO PHASE FRICTION MULTIPLIERS ϕ_{fo}^2

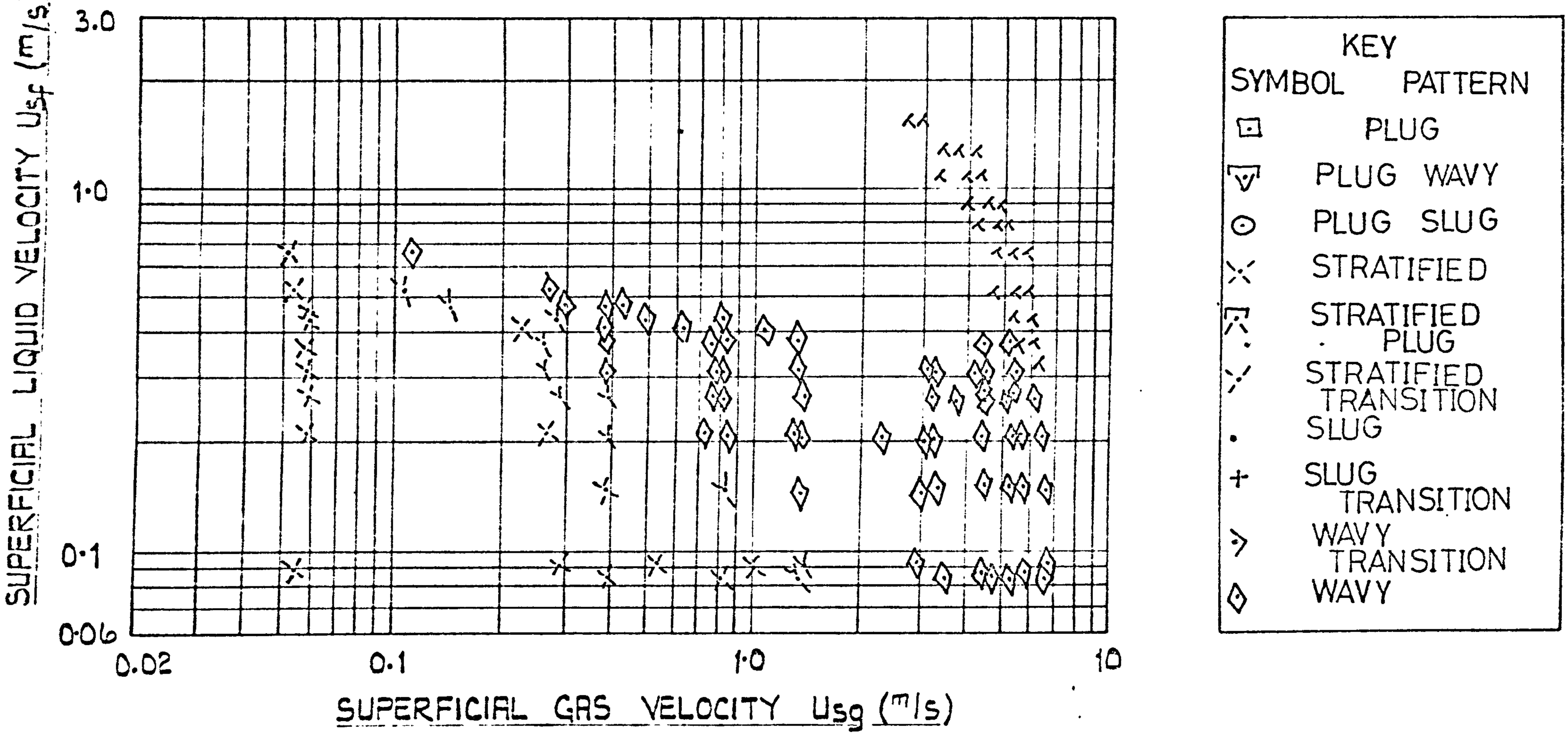

FIG. 6·33 FLOW CONDITIONS COVERED BY THE REPEAT TESTS (PHASE 3)

can also be compared with Figs. 6.4, 6.10, 6.16, 6.19, 6.22 and 6.25 where the experimental friction multipliers were deduced from centreline pressure tappings. It is to be expected that in the stratified (and some wavy) type of flows where the liquid level is always above the tube centreline the pressure gradients obtained from bottom and centreline pressure tappings will coincide; where the liquid level is always below the tube centreline the pressure gradients obtained from top and centreline pressure tappings will coincide, but where the liquid level is such that one centreline tapping is above the liquid level and the other is below it, then the centreline tapping measured pressure gradient becomes virtually meaningless.

This suggests that centreline tappings should not be used for friction pressure drop evaluation and leaves the question as to whether top or bottom pressure tappings are best. The data shown in Figs. 6.27 to 6.32 certainly suggest bottom tapping points should be used as they give higher pressure drop.

The problem is perhaps less relevant to other flow patterns and situations, e.g. where the pressure drop is large, or variations in liquid level are negligible.

The effect of increasing tube diameter is not clear (comparing Phases 2 and 3), however, the inadequacy of the correlations appears to be exacerbated with the larger diameter tube in Phase 3, although this might be due to

there being many more test conditions in the stratified and wavy flow patterns when compared to Phase 2.

For almost all of the correlations tested, the failure to predict annular and near annular (e.g. wavy misty) data points is a common factor. This could be attributed to a flow pattern effect which is probably more apparent in large tubes.

The slug, plug and bubble points are scattered around the zero error line with probably a bias towards either overprediction or underprediction.

In conclusion, it seems unlikely that any one correlation could predict the pressure drop data over the entire range of conditions covered without taking into consideration the flow pattern effects mentioned earlier. At least three different flow pattern groups should be identified,

(i) stratified and wavy (separated flows)

(ii) bubble, plug and slug (mixed flows)

(iii) annular and wavy misty (annular)

Further analysis of the pressure drop data will be pursued in this direction.

6.2 SETTLING LENGTHS

An attempt to correlate the settling length data after a return U-bend (Phase 1), or after a mixing device (Phases 2 and 3) was made by plotting the settling lengths obtained from the pressure distribution data in the form

of an L/D ratio against mass velocity for each flow pattern. These are shown in Figs. 6.34, 6.35 and 6.36 for phase 1, 2 and 3 tests respectively. No coherent relationship appears to exist. Another attempt was carried by plotting the settling length data for Phase 2 against superficial air velocity as shown in Fig. 6.37, with superficial water velocity as a parameter. Again no coherent relationship was obtained, however, there appears to be a strong dependency on flow pattern and tube diameter effects.

The following remarks are worth mentioning,

A - Phase 1 Tests:

(i) the maximum settling length encountered was 81 tube diameter and occurred under slug flow conditions. All except 3 test conditions out of over 350 settled within 70 tube diameters.

(ii) slug flow required the longest settling lengths.

(iii) bubble flows required much shorter settling lengths, the maximum being 34 tube diameters.

(iv) annular flows settled comparatively quickly although only a few points were observed.

B - Phase 2 Tests:

(i) longer settling lengths were required for all flow patterns compared to the results after the return bend (Phase 1).

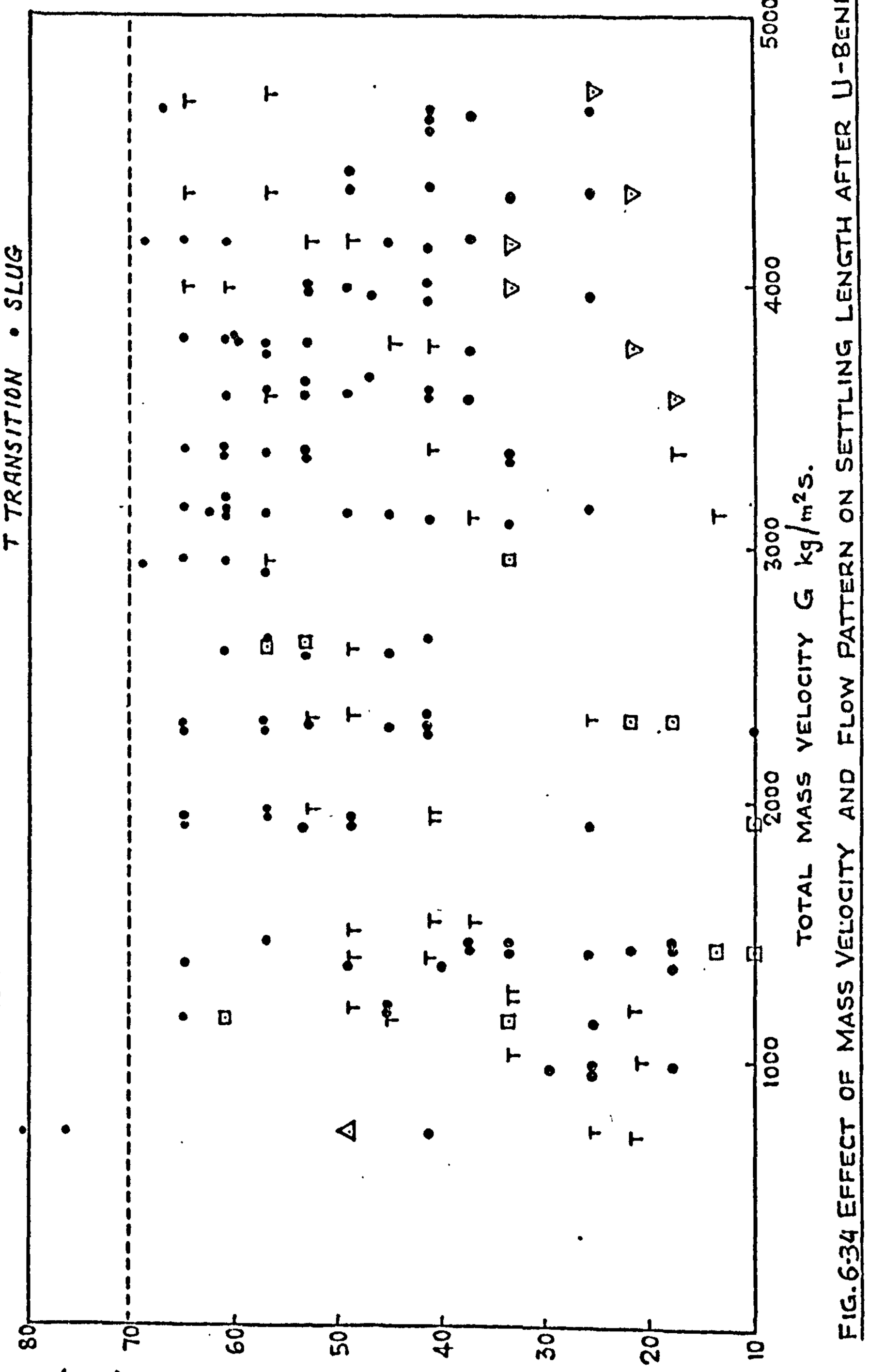

FIG. 6·34 EFFECT OF MASS VELOCITY AND FLOW PATTERN ON SETTLING LENGTH

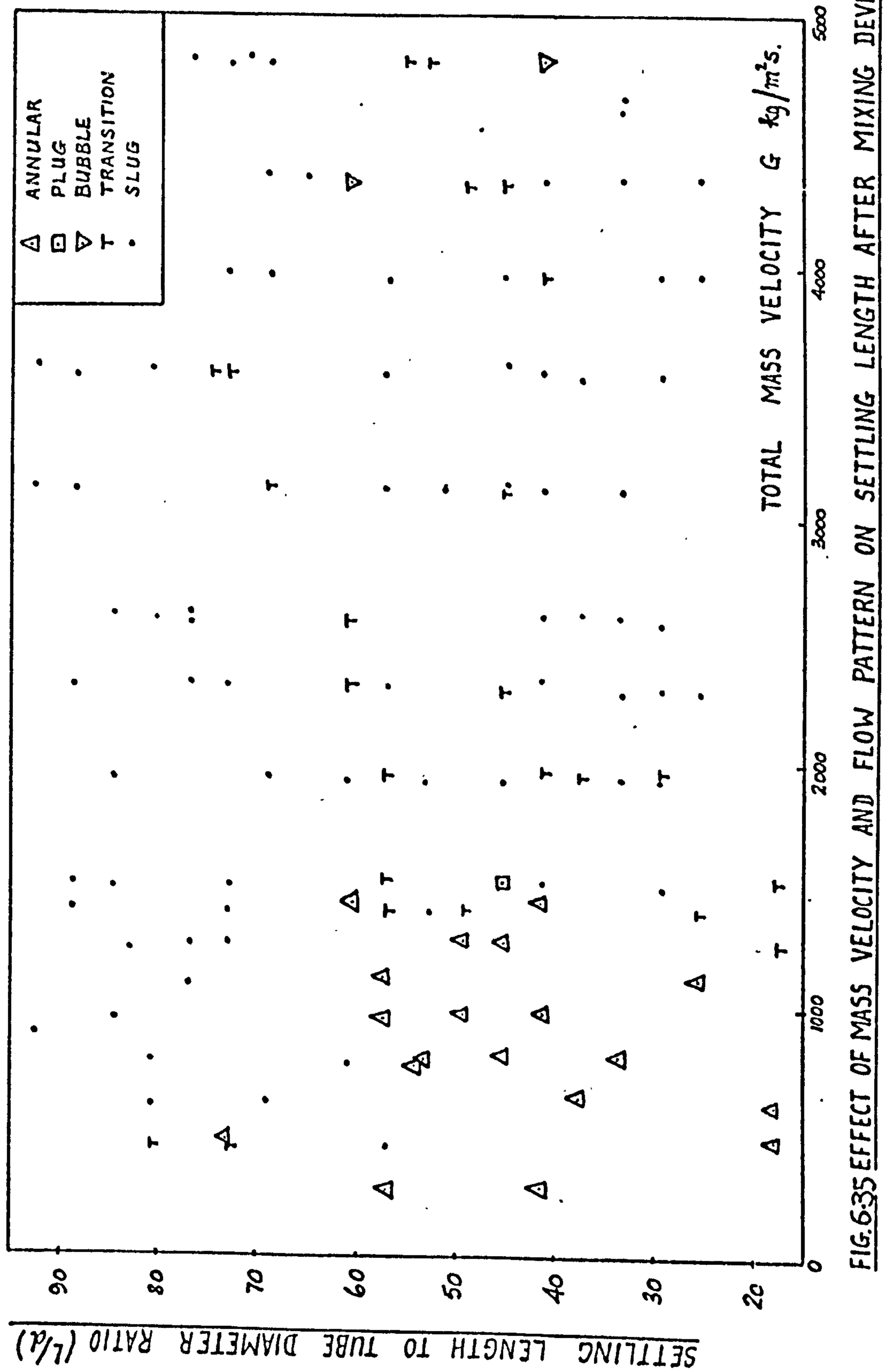

FIG.6.35 EFFECT OF MASS VELOCITY AND FLOW PATTERN ON SETTLING LENGTH AFTER MIXING DEVICE

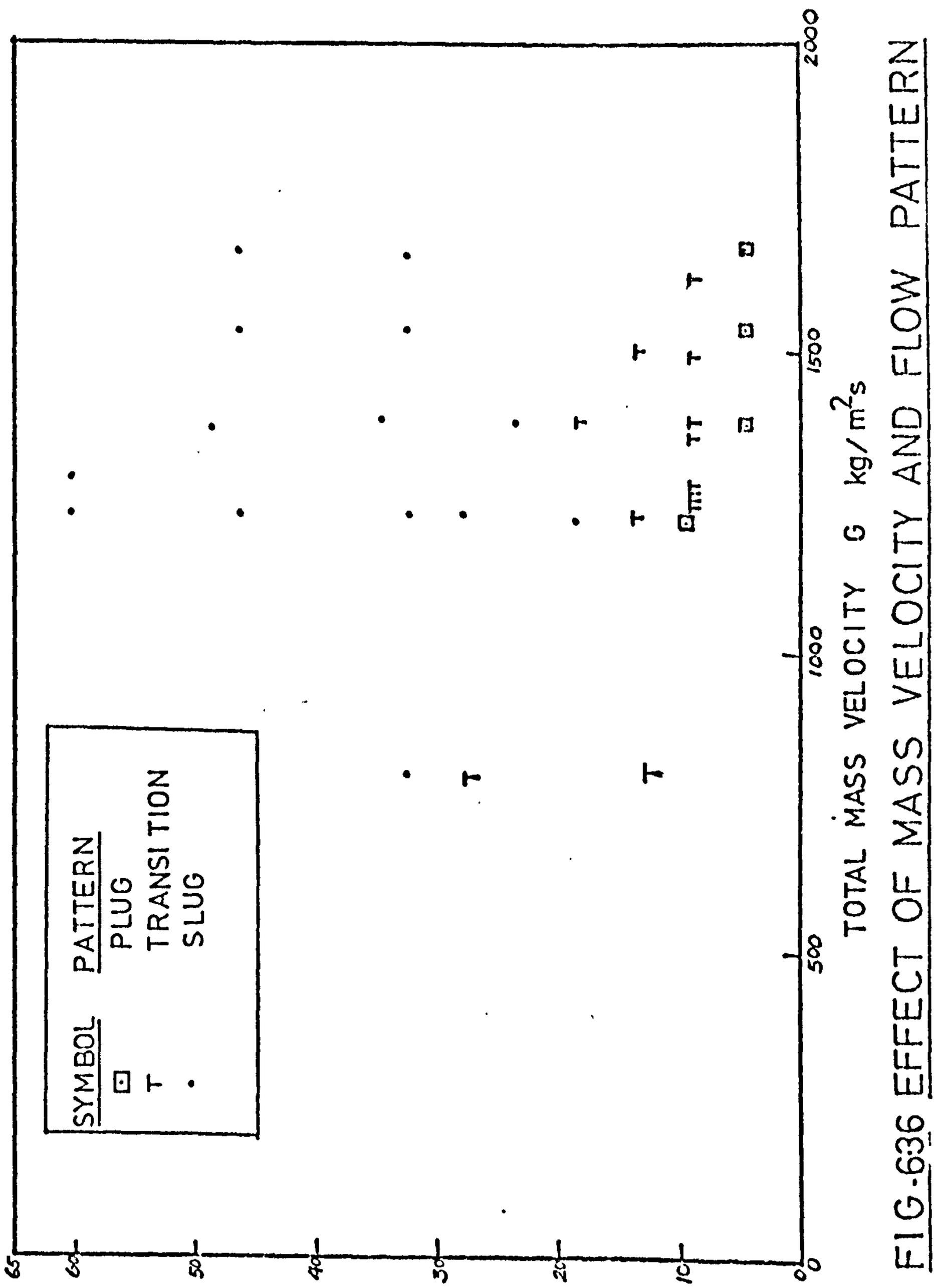

FIG-6.36 EFFECT OF MASS VELOCITY AND FLOW PATTERN ON SETTLING LENGTH (PHASE 3 TESTS)

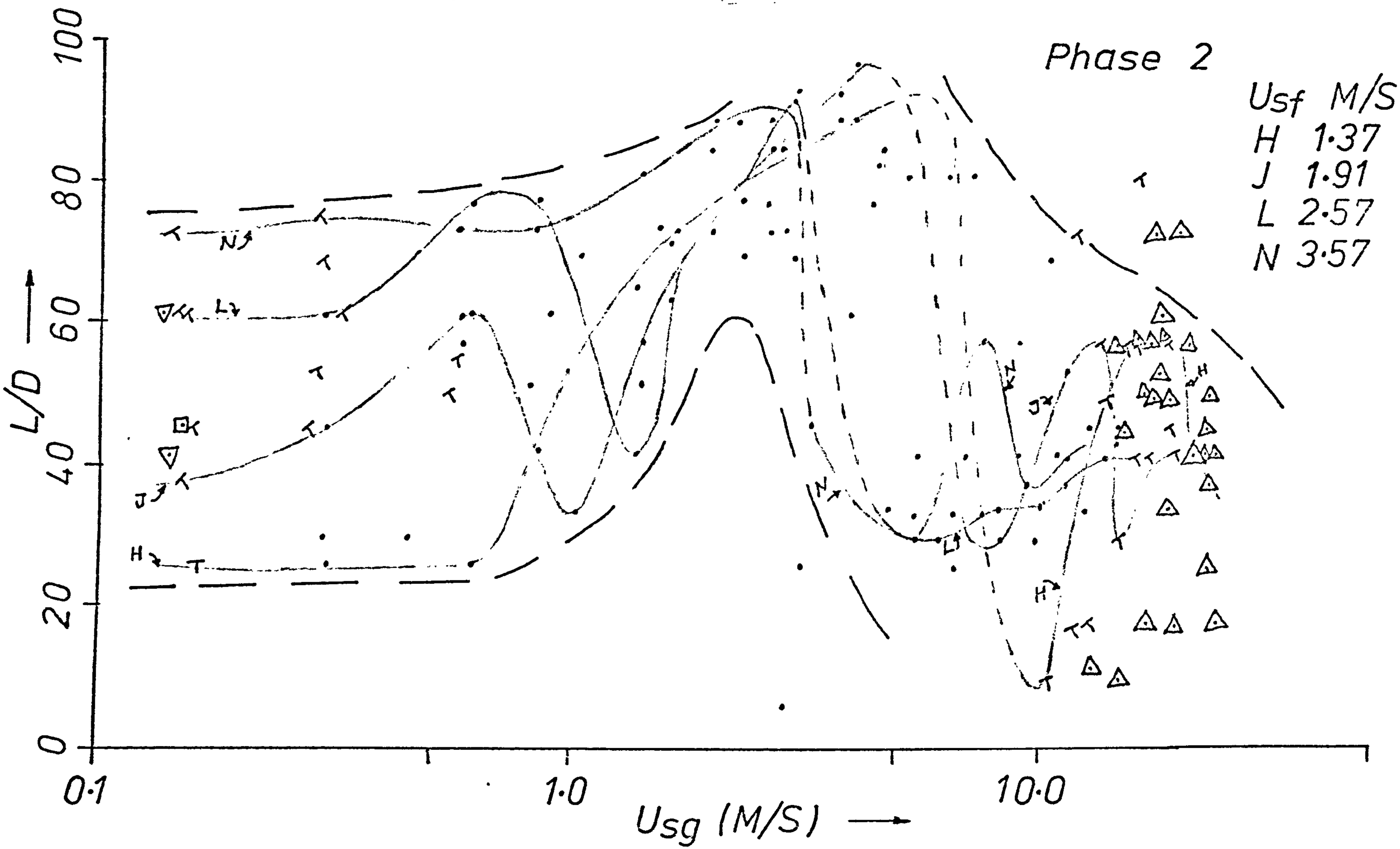

FIG. 6.37 EFFECT OF AIR AND WATER FLOWRATES, AND FLOW PATTERNS ON SETTLING LENGTH

(ii) in 20% of the test conditions, a settled flow was not obtained, slug flow again producing the most adverse conditions.

(iii) only few bubble flow points were observed and some required settling lengths up to 60 diameter.

(iv) annular flows settled quickly, although some required settling lengths up to 60 diameters.

C - Phase 3 Tests:

(i) around 40% of these tests involved stratified or wavy flow conditions where the pressure distribution settled to a uniform pressure gradient very quickly. This conclusion is based on visual observation only.

(ii) plug flows required settling lengths of under 10 tube diameters.

(iii) some slug flows did not settle within the test section length of 74 diameters.

(iv) at certain flowrates, the liquid level built up downstream, probably due to the short length of test section. These were considered transitional, and occurred near the expected slug-annular boundary.

Whilst these observations are empirical, they can be compared with the values obtained from single phase liquid flow tests carried out during phase 1. These indicated a maximum single phase settling length, after a double 90^{o} bend, of 28 diameters although most of the data were much less than this. This suggests that in general

much larger settling lengths are required in two phase flows.

There is a considerable difference in the settling length required for the various flow regimes and this emphasises the need for adequate flow pattern identification for any given set of conditions. Stratified and (slightly) wavy flows appear to be the most stable types in terms of settling very quickly after a bend or a mixer. Bubble, plug and annular flows seem relatively stable and settle in a reasonable length. On the other hand, slug type flows are most unstable and can require very long settling lengths which characterise this type of flow as a generally undesirable operating regime.

6.3 FLOW PATTERNS

The flow pattern data were compared with four flow pattern maps in common use; Baker (B3), Hoogendoorn (H2), Mandhane et al (M2), and a recent publication by Choe et al (C6). In making the comparisons, the author is not recommending the use of the flow pattern maps, nor the map coordinates employed for comparison. Indeed, it is difficult to appreciate how a two co-ordinate map can adequately represent the variety of the physical processes and instabilities involved in the different transitions. However the superficial velocities of the individual phases were used as a vehicle for comparison and accordingly the flow pattern boundaries of the different maps were transferred to these coordinates.

The comparisons with the Baker map are shown in Figs. 6.38 to 6.40, with the Hoogendoorn map in Figs. 6.41 to 6.43, with the Mandhane et al map in Figs. 6.44 to 6.46 and with the Choe et al map in Figs. 6.47 to 6.49, for Phases 1, 2 and 3 respectively.

Consider first the 127 mm pipe data (Phase 1 and 2). Comparing the experimental data with the boundaries suggested by the four maps considered, it can be seen that on the whole, and considering the disagreement between the maps themselves, the predictions are not too bad.

In all cases the boundaries between stratified and plug, wavy and slug flows are low and, perhaps more disconcerting, the boundary between slug and annular type flows is the least adequately represented, even between the maps themselves. The plug to slug boundary on the Hoogendoorn map shows poor agreement with experiment. The slug to annular boundary on the Baker map appears to have the wrong curvature while the Choe et al map has a negative slope.

It should be remembered that the transition boundaries are not lines but bands of which the lines are representative. Comparing the results for Phases 1 and 2 (also Fig. 6.50) shows that for Phase 2

(i) annular flow occurs at lower air flowrates

(ii) bubbly flow occurs at higher water flowrates

(iii) the wave-slug boundary is shifted to relatively higher water flowrate (i.e. slugging occurred at lower liquid level in phase 1).

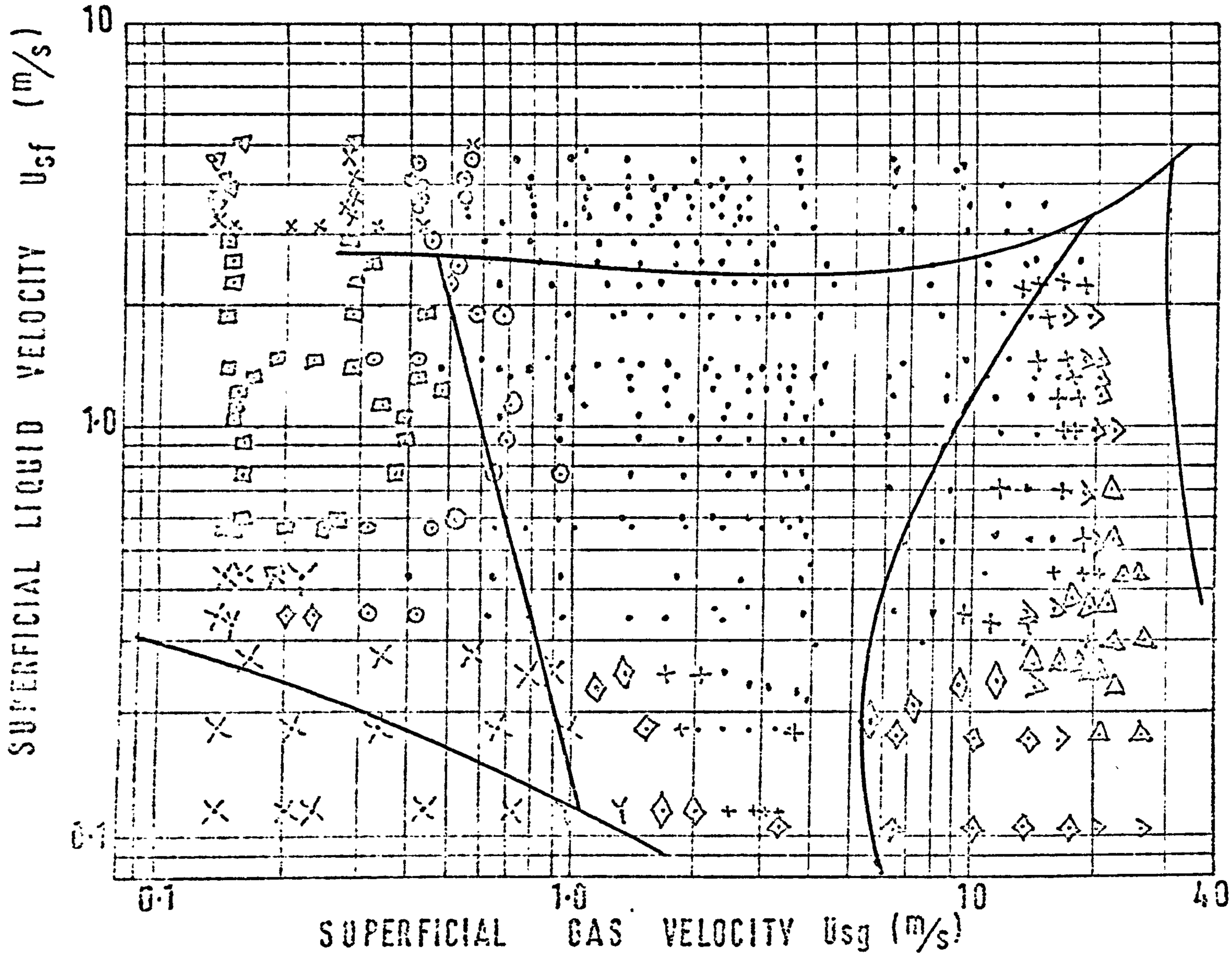

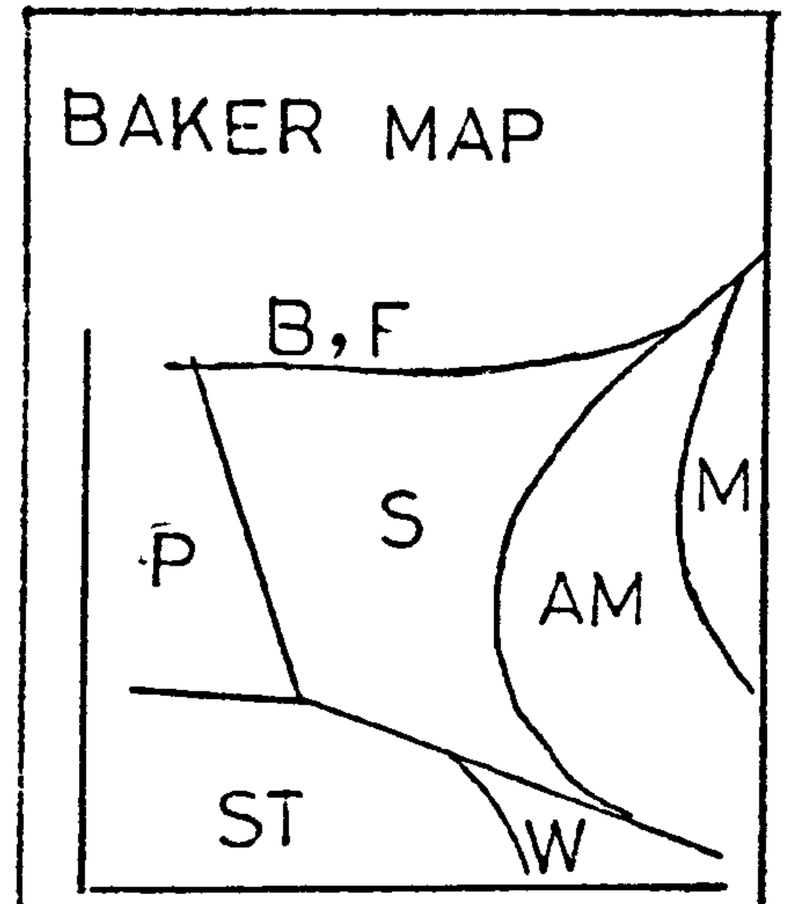

FIG. 6·38 COMPARISON OF EXPERIMENTAL AND BAKER FLOW PATTERN MAPS (PHASE 1)

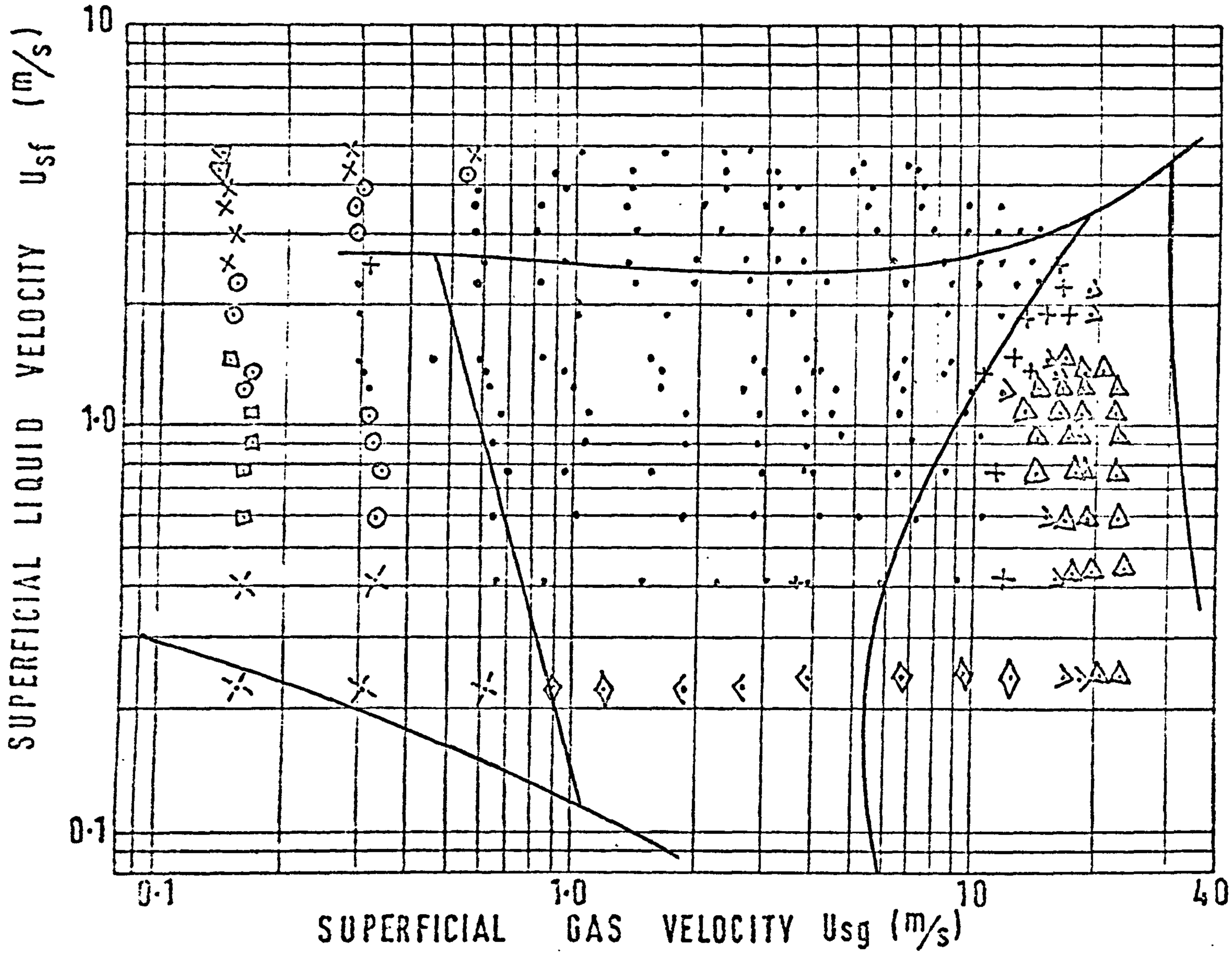

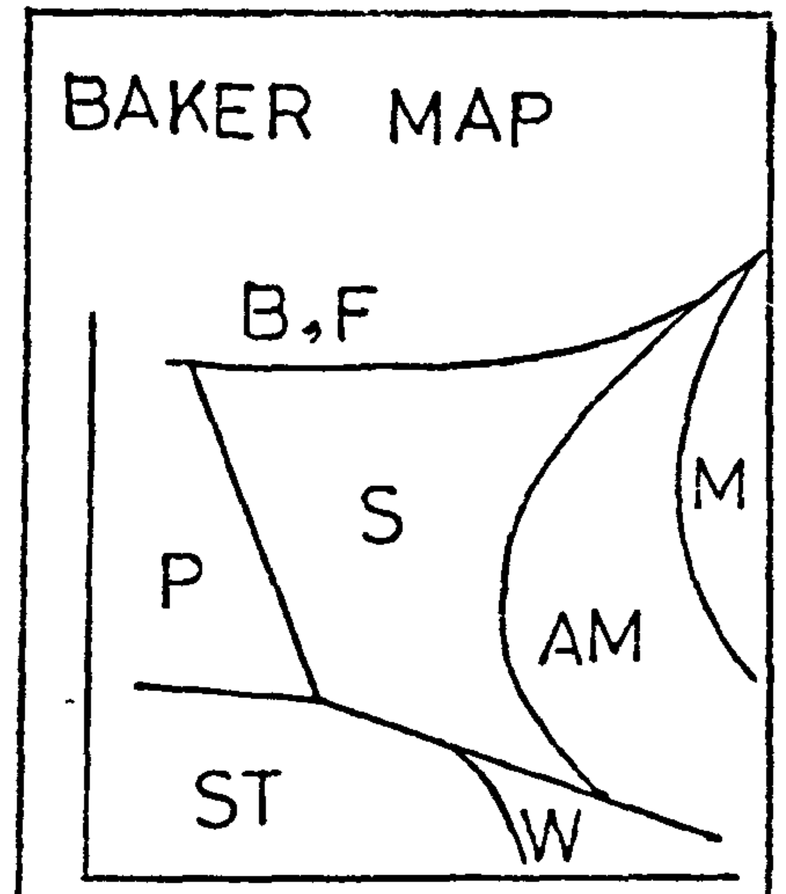

FIG. 6·39 COMPARISON OF EXPERIMENTAL AND BAKER FLOW PATTERN MAPS (PHASE 2)

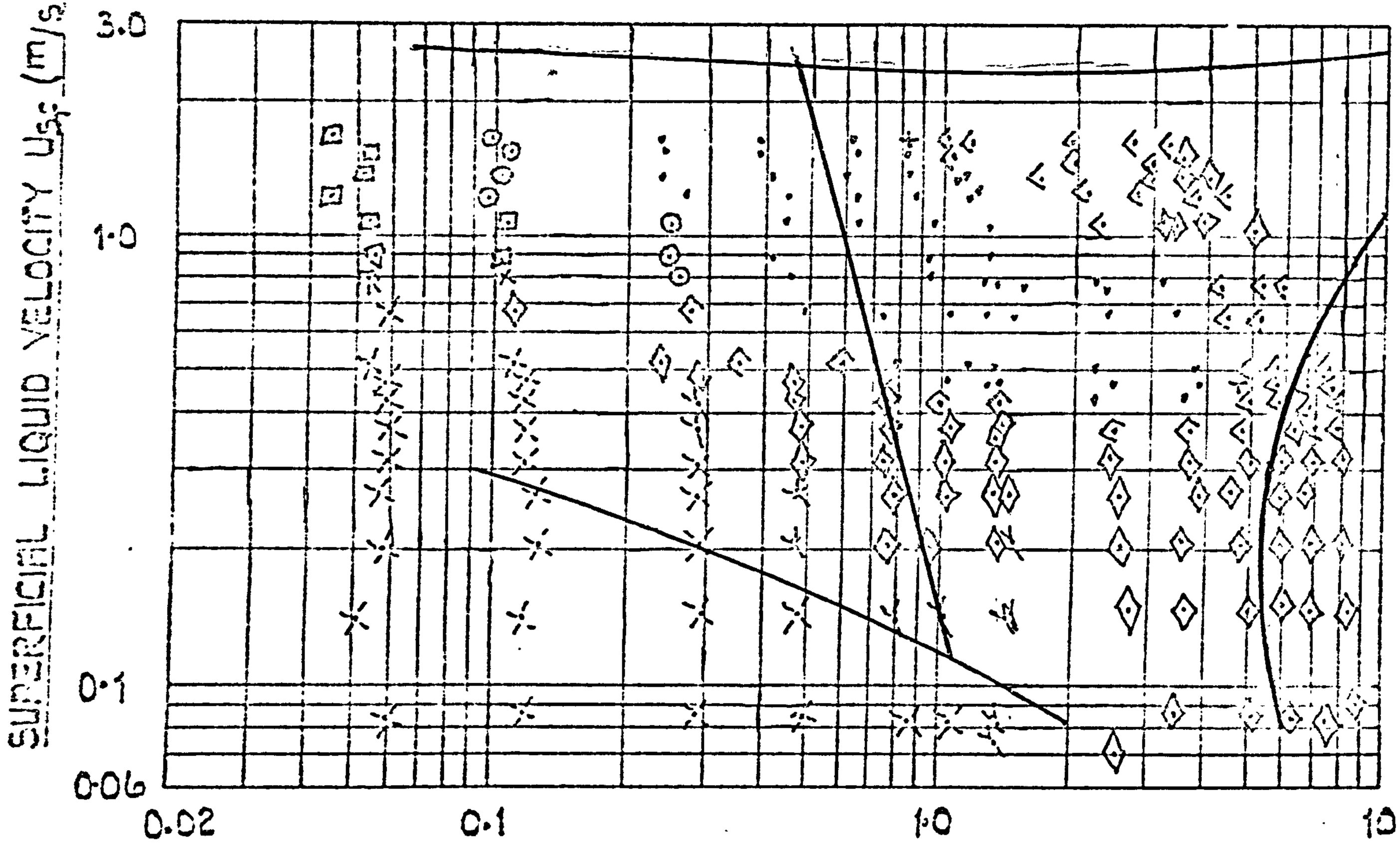

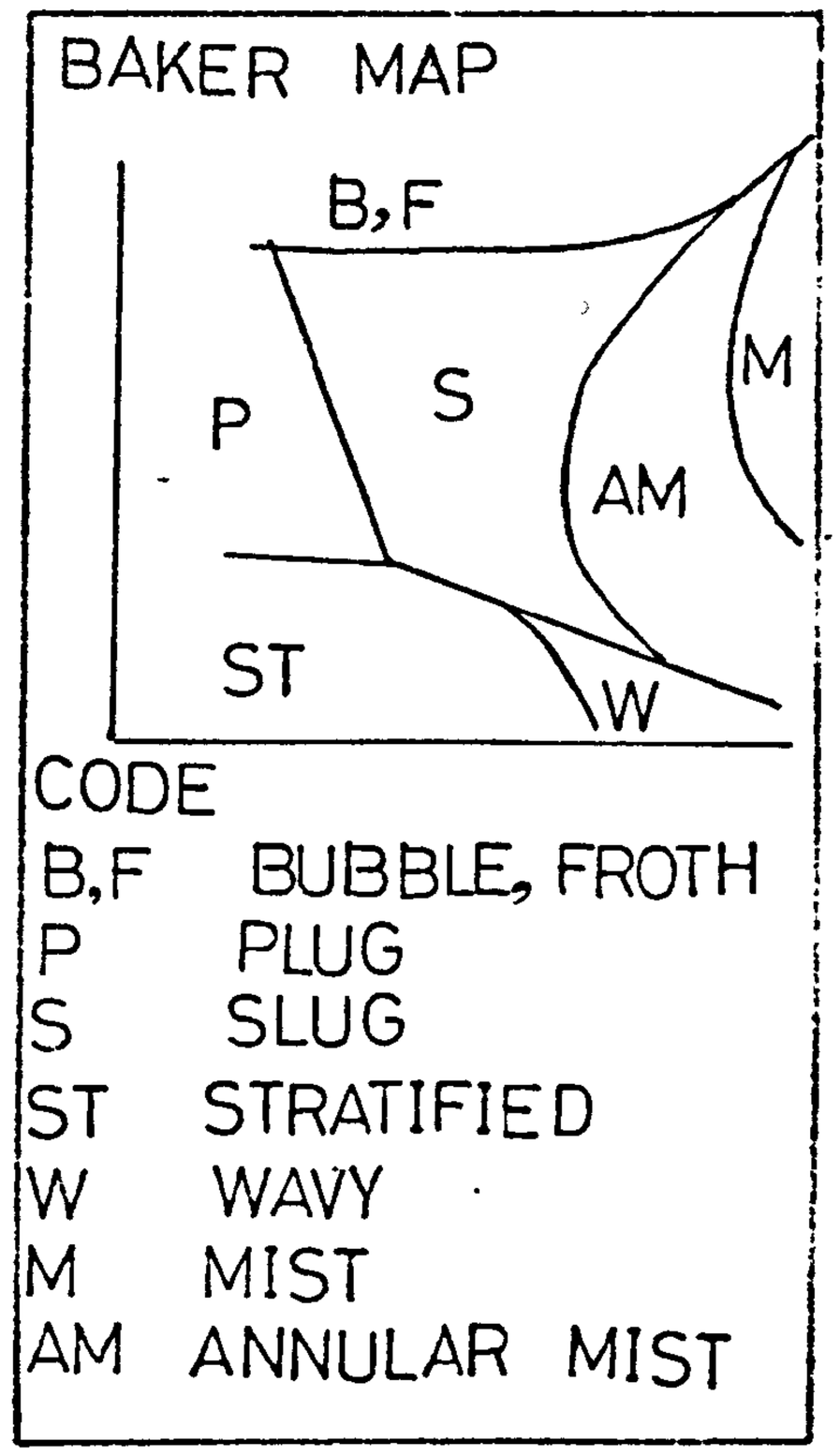

FIG. 6·40 COMPARISON OF EXPERIMENTAL AND BAKER FLOW PATTERN MAPS (PHASE 3)

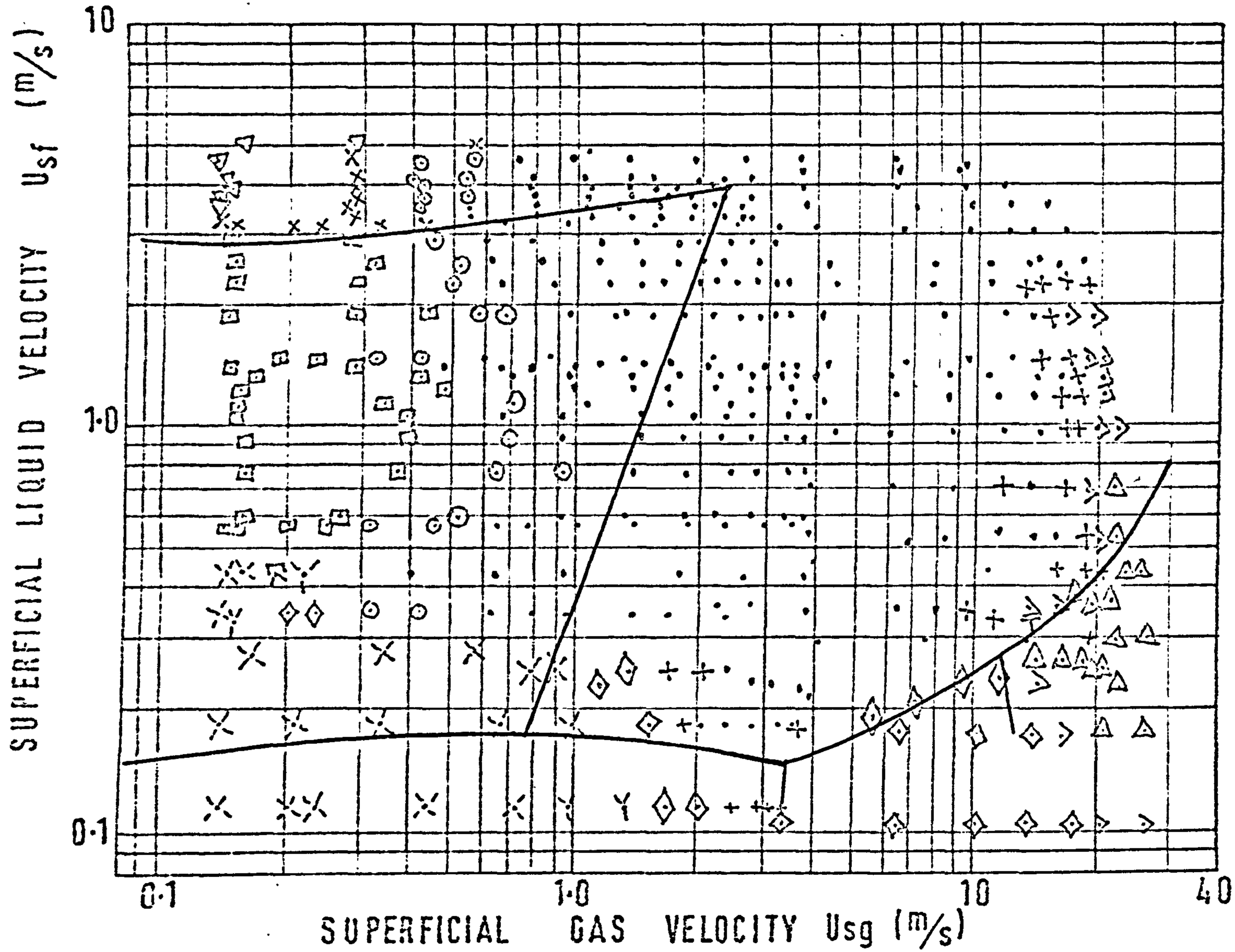

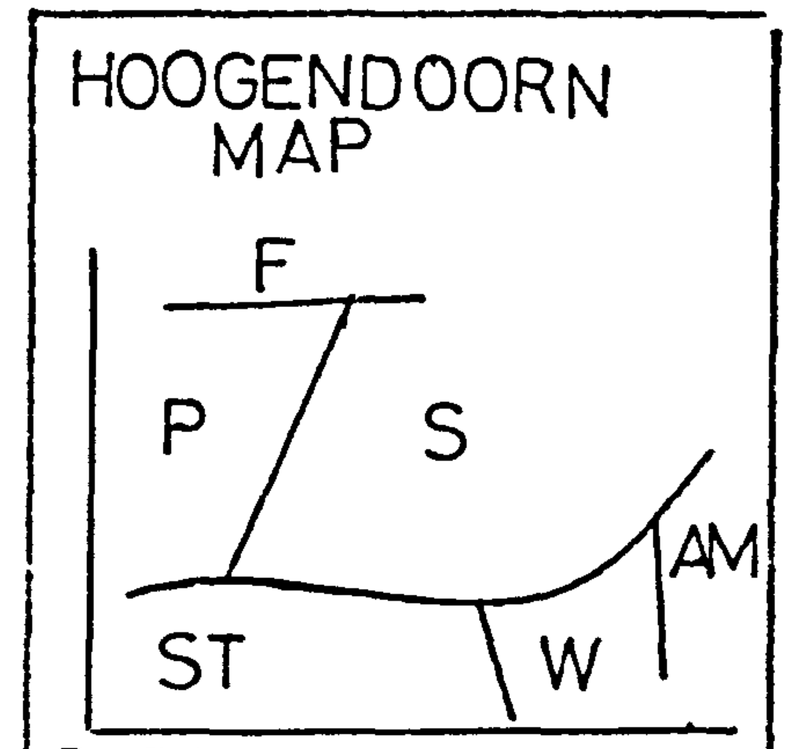

CODE

F FROTH

P PLUG

S SLUG

ST STRATIFIED

W WAVY

AM ANNULAR MIST

FIG. 6·41 COMPARISON OF EXPERIMENTAL AND HOOGENDOORN FLOW PATTERN MAPS (PHASE 1)

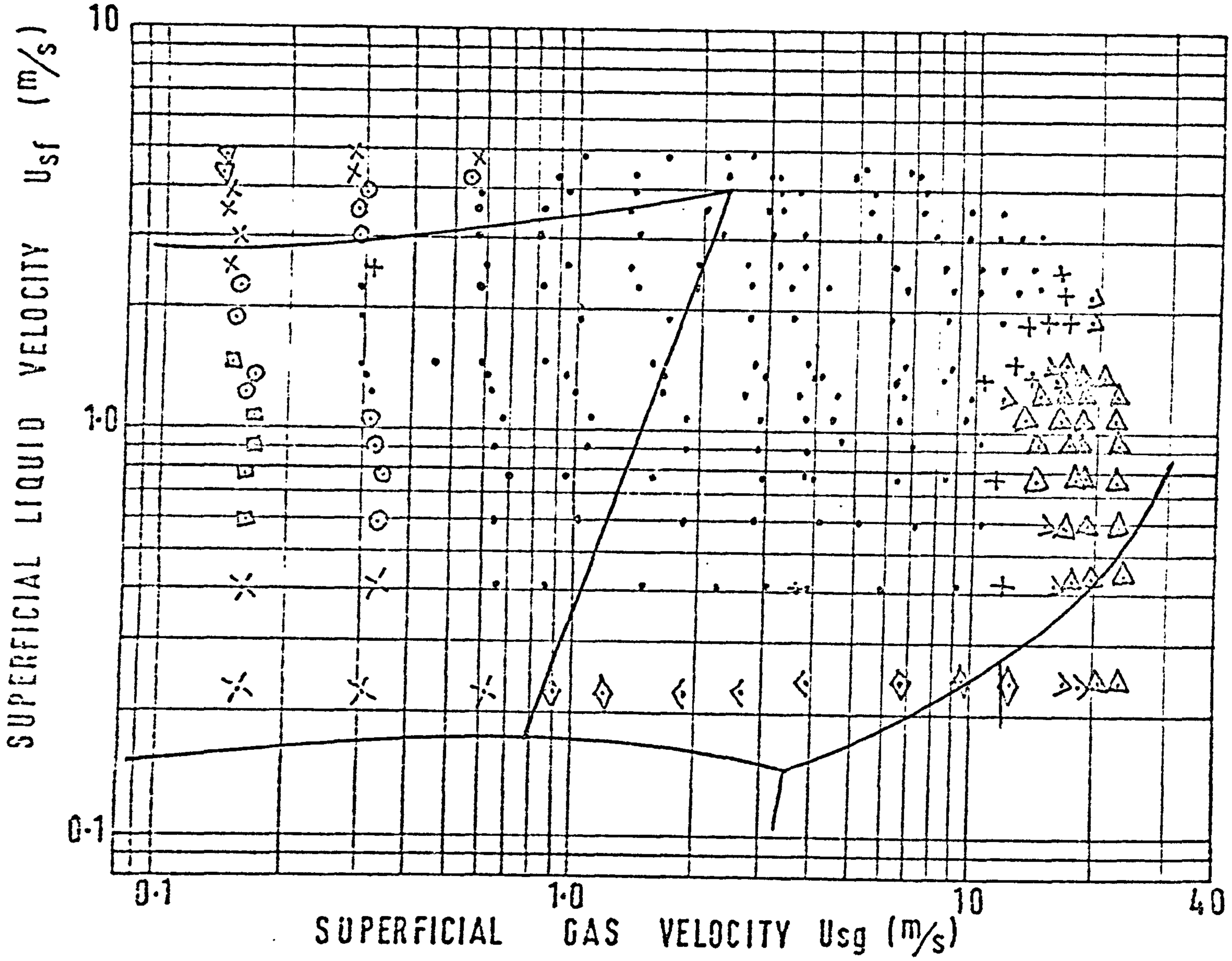

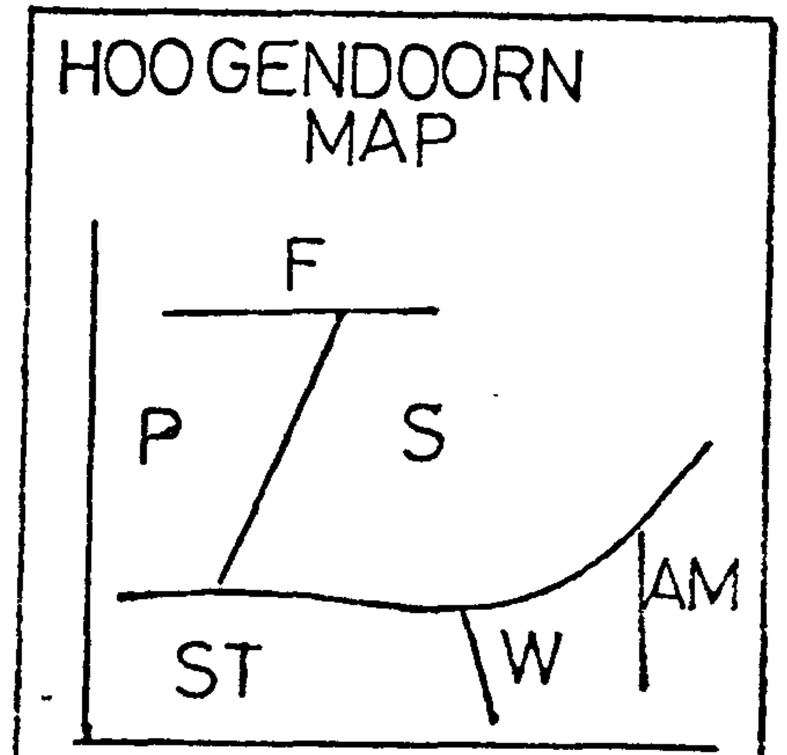

CODE

F	FROTH
P	PLUG
S	SLUG
ST	STRATIFIED
W	WAVY
AM	ANNULAR MIST

FIG. 6·42 COMPARISON OF EXPERIMENTAL AND HOOGENDOORN FLOW PATTERN MAPS (PHASE 2)

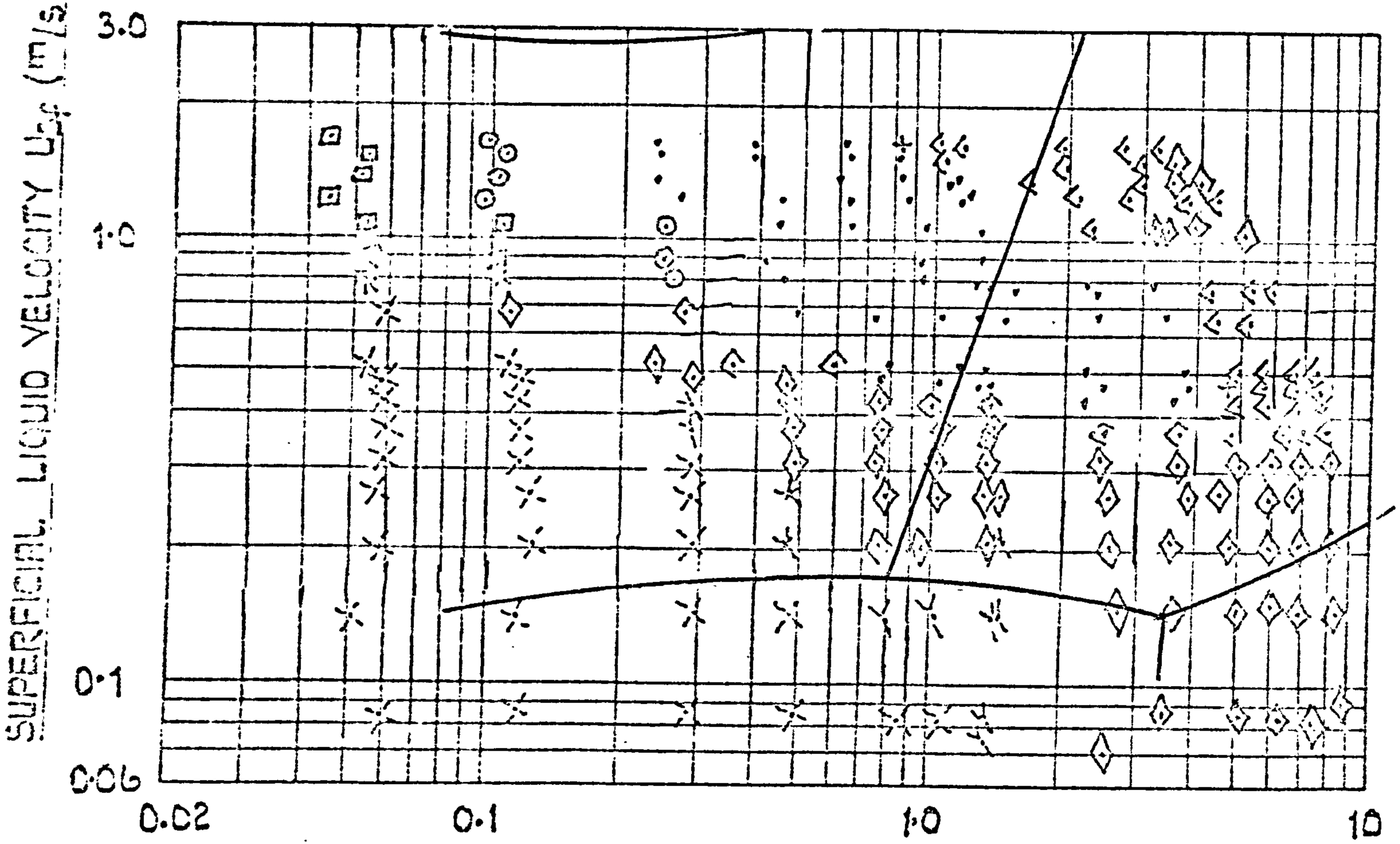

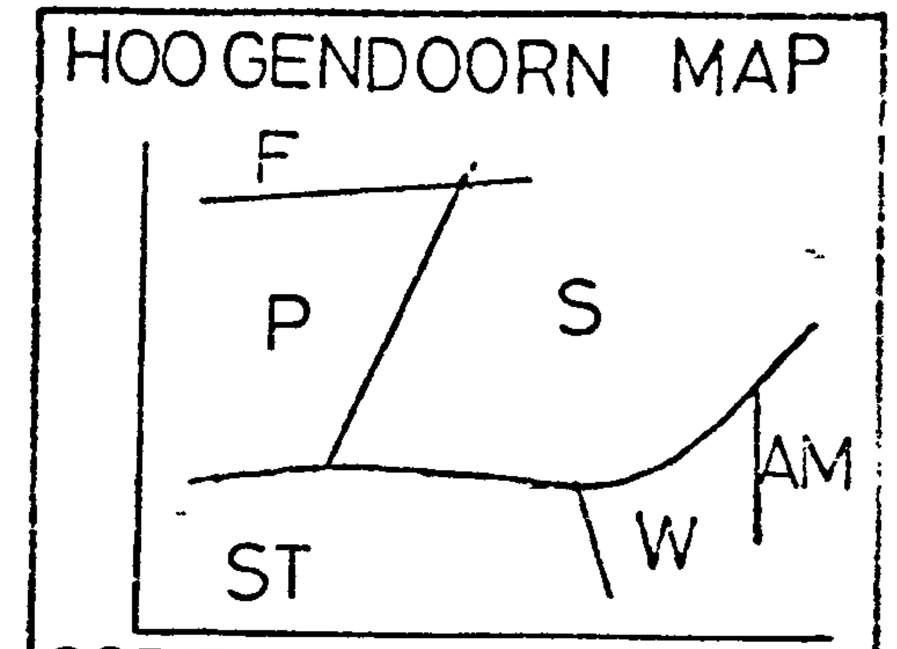

CODE

F	FROTH
P	PLUG
S	SLUG
ST	STRATIFIED
AM	ANNULAR MIST
W	WAVY

FIG. 6.43 COMPARISON OF EXPERIMENTAL AND HOOGENDOORN FLOW PATTERN MAPS (PHASE 3)

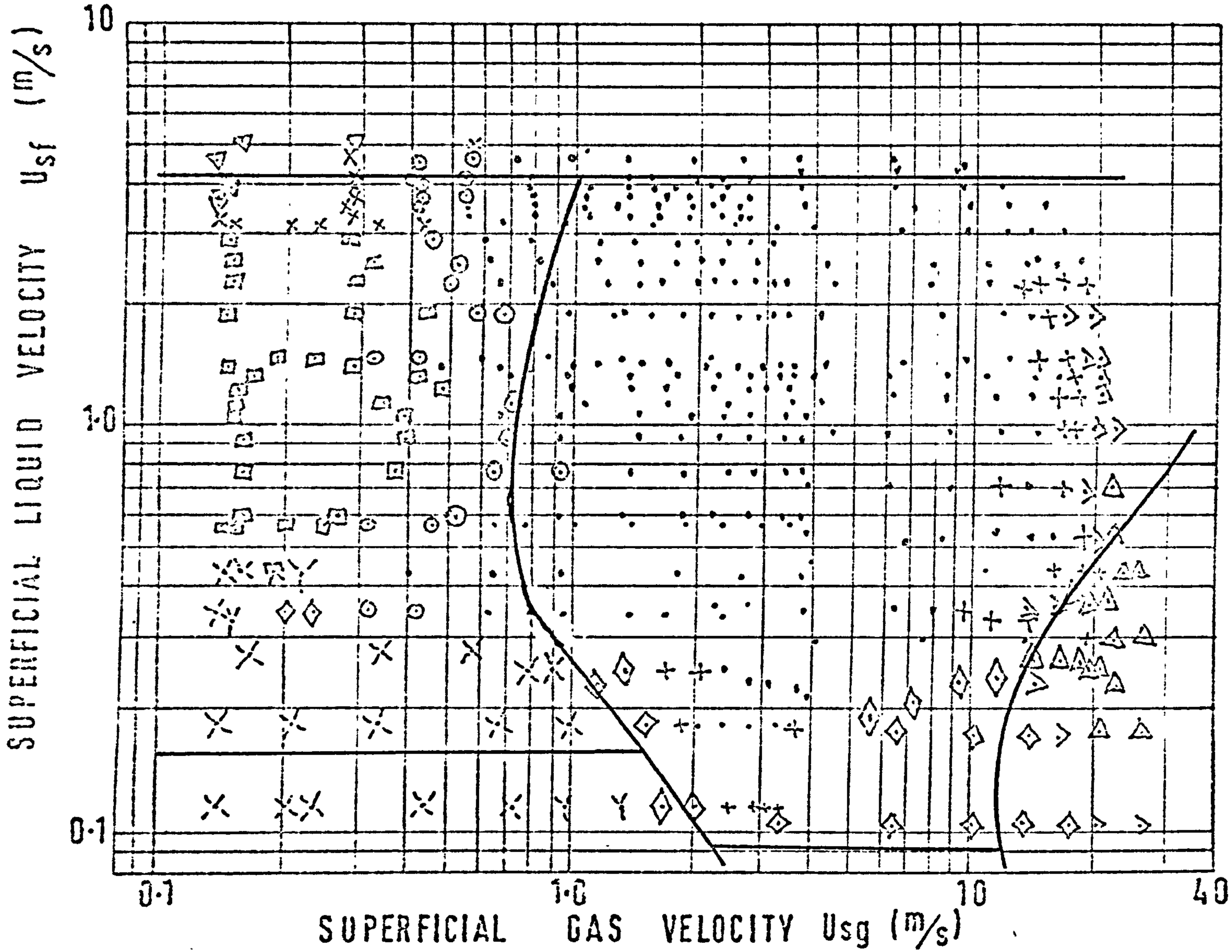

MANDHANE et al MAP

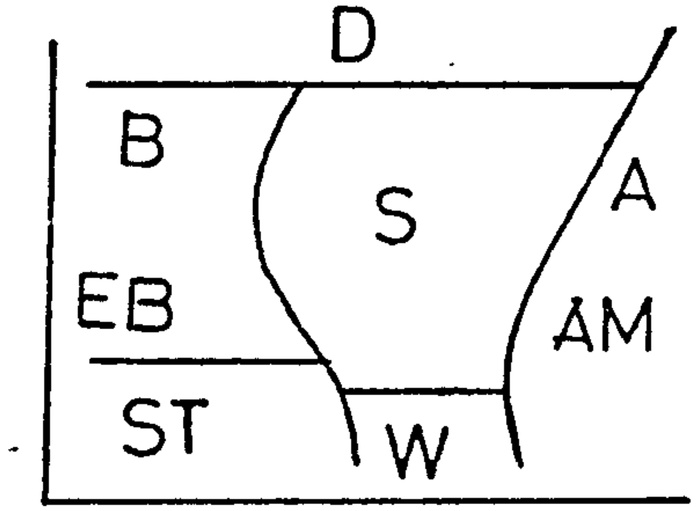

CODE

A ANNULAR
AM ANNULAR MIST
B BUBBLE
EB ELONGATED BUBBLE
D DISPERSED OR SPRAY
S SLUG
ST STRATIFIED
W WAVY

FIG. 6·44 COMPARISON OF EXPERIMENTAL AND MANDHANE et al FLOW PATTERN MAPS (PHASE 1)

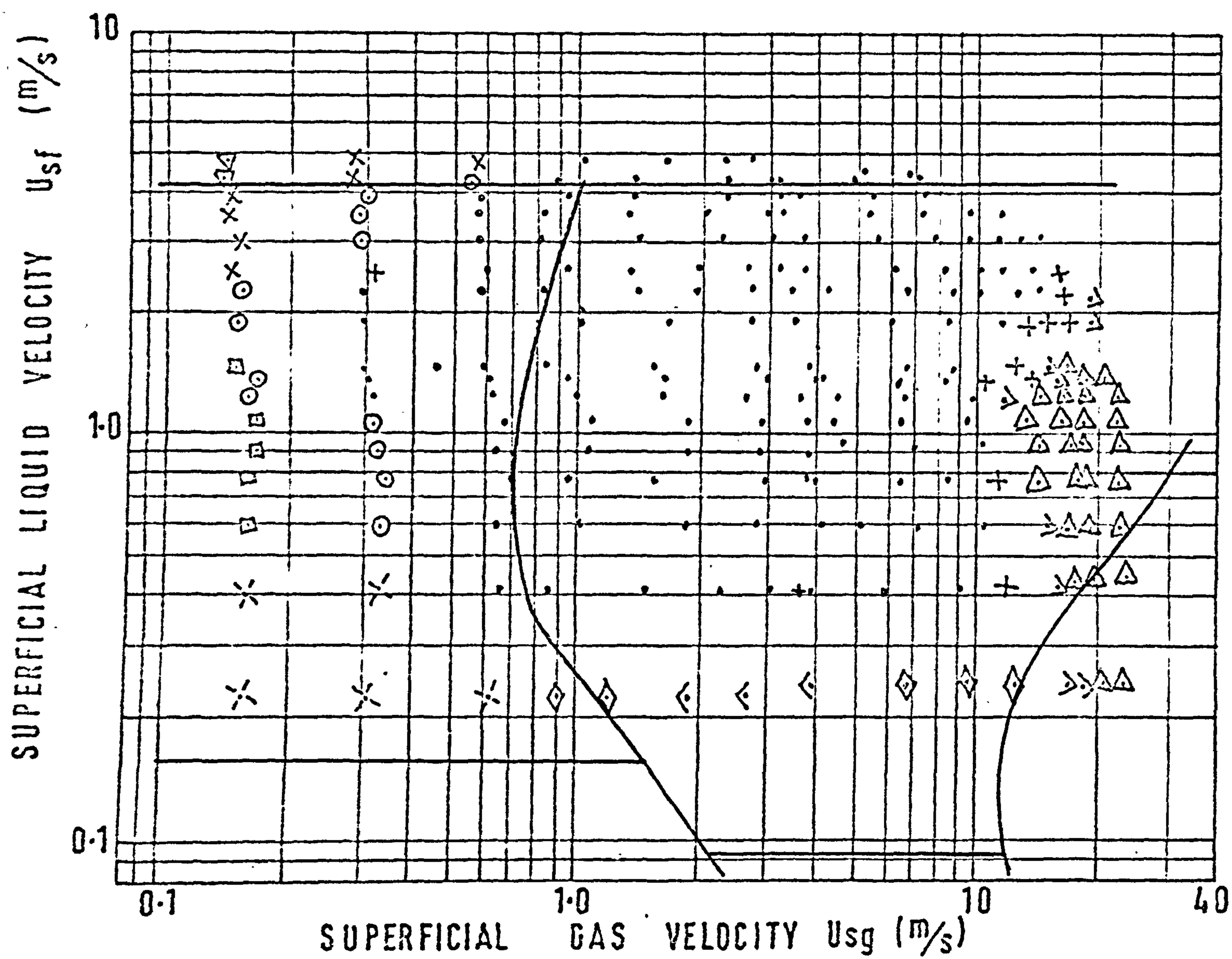

MANDHANE et al MAP

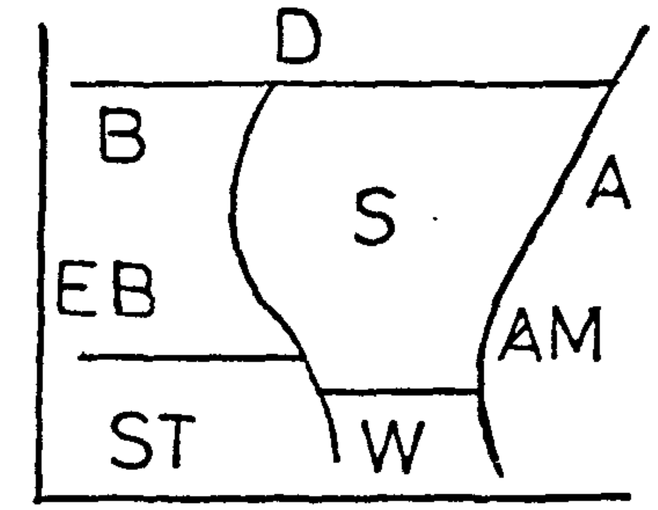

CODE

A	ANNULAR
AM	ANNULAR MIST
B	BUBBLE
EB	ELONGATED BUBBLE
D	DISPERSED OR SPRAY
S	SLUG
ST	STRATIFIED
W	WAVY

FIG. 6·45 COMPARISON OF EXPERIMENAL AND MANDHANE et al FLOW PATTERN MAPS (PHASE 2)

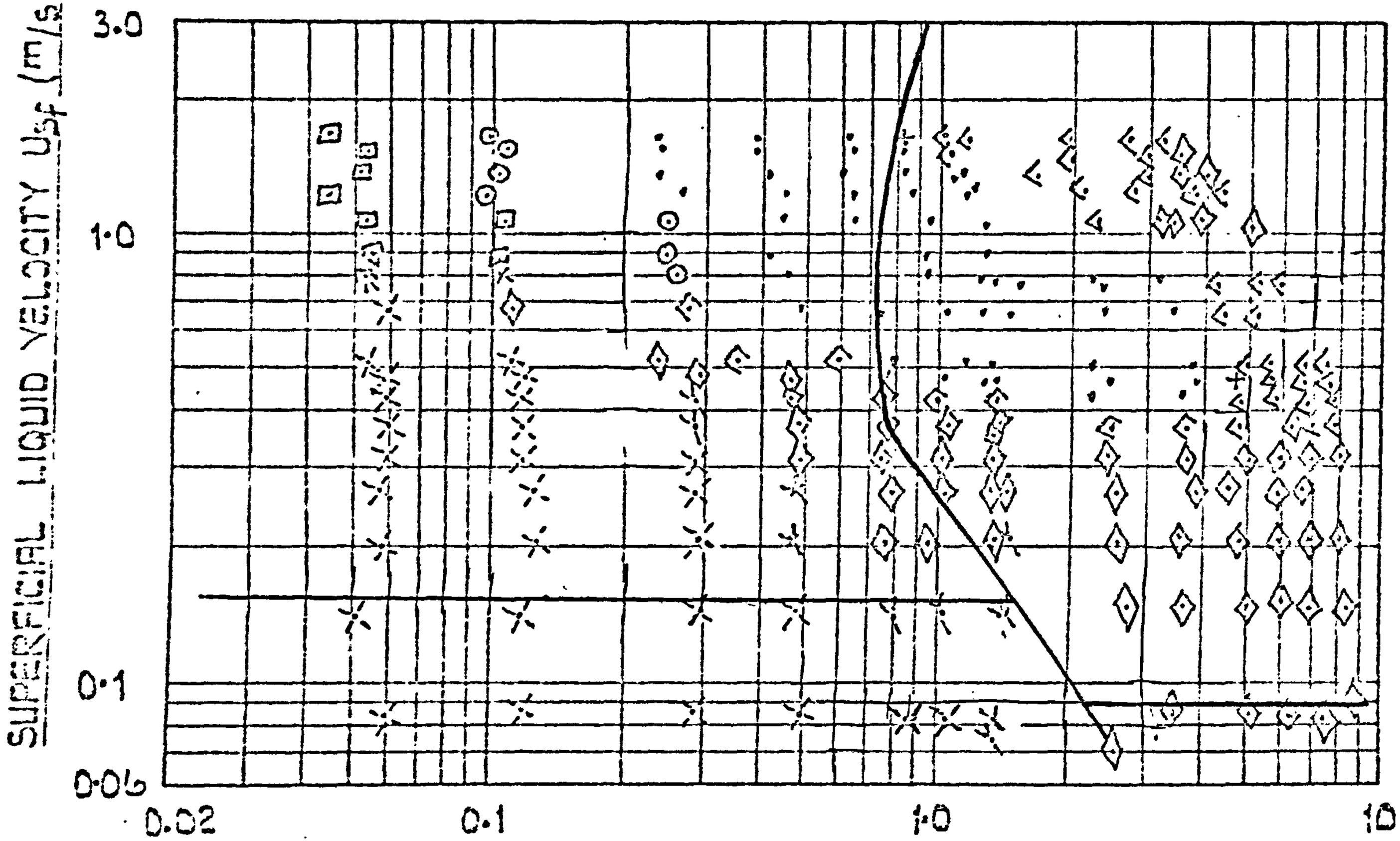

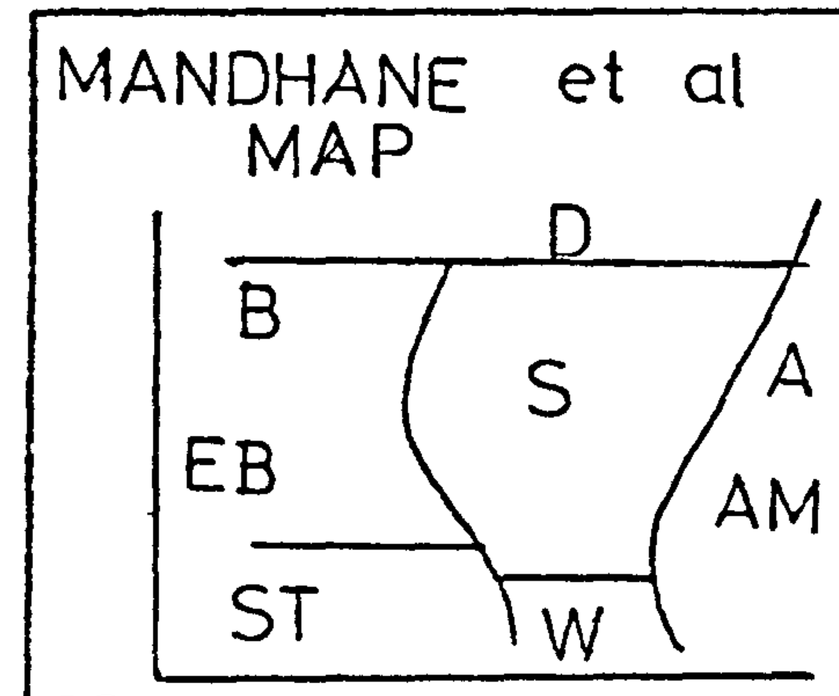

FIG. 6.46 COMPARISON OF EXPERIMENTAL AND MANDHANE et al FLOW PATTERN MAPS (PHASE 3)

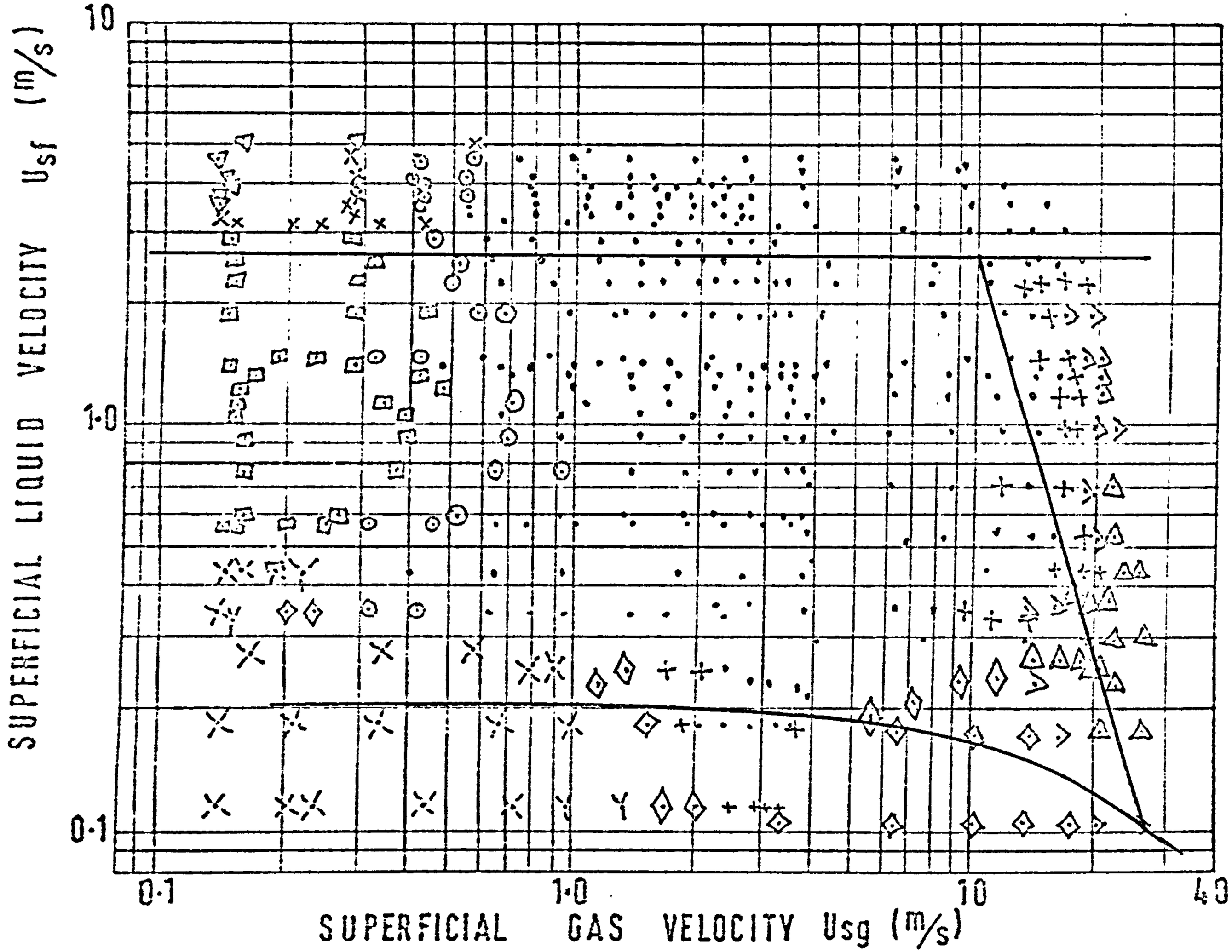

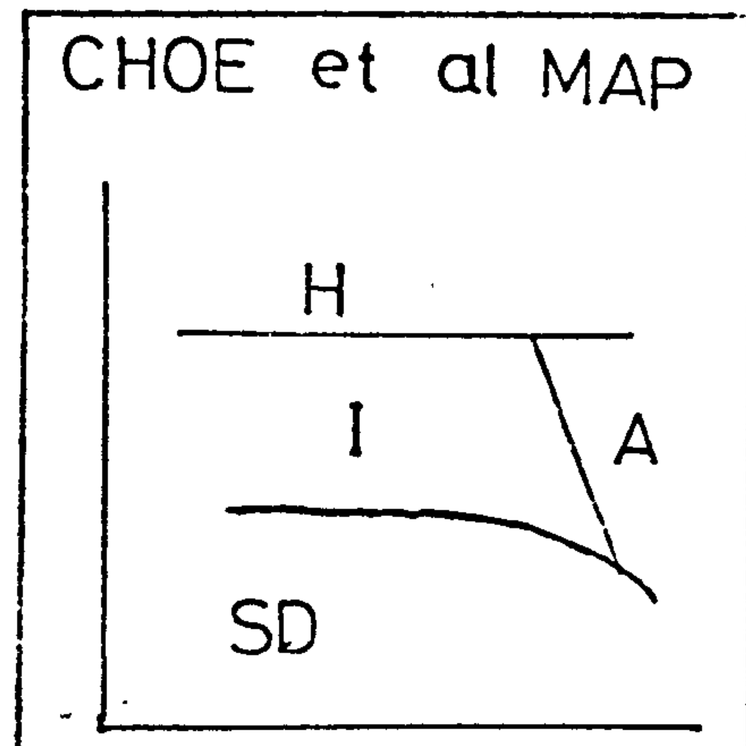

FIG.6·47 COMPARISON OF EXPERIMENTAL AND CHOE et al FLOW PATTERN MAP (PHASE 1)

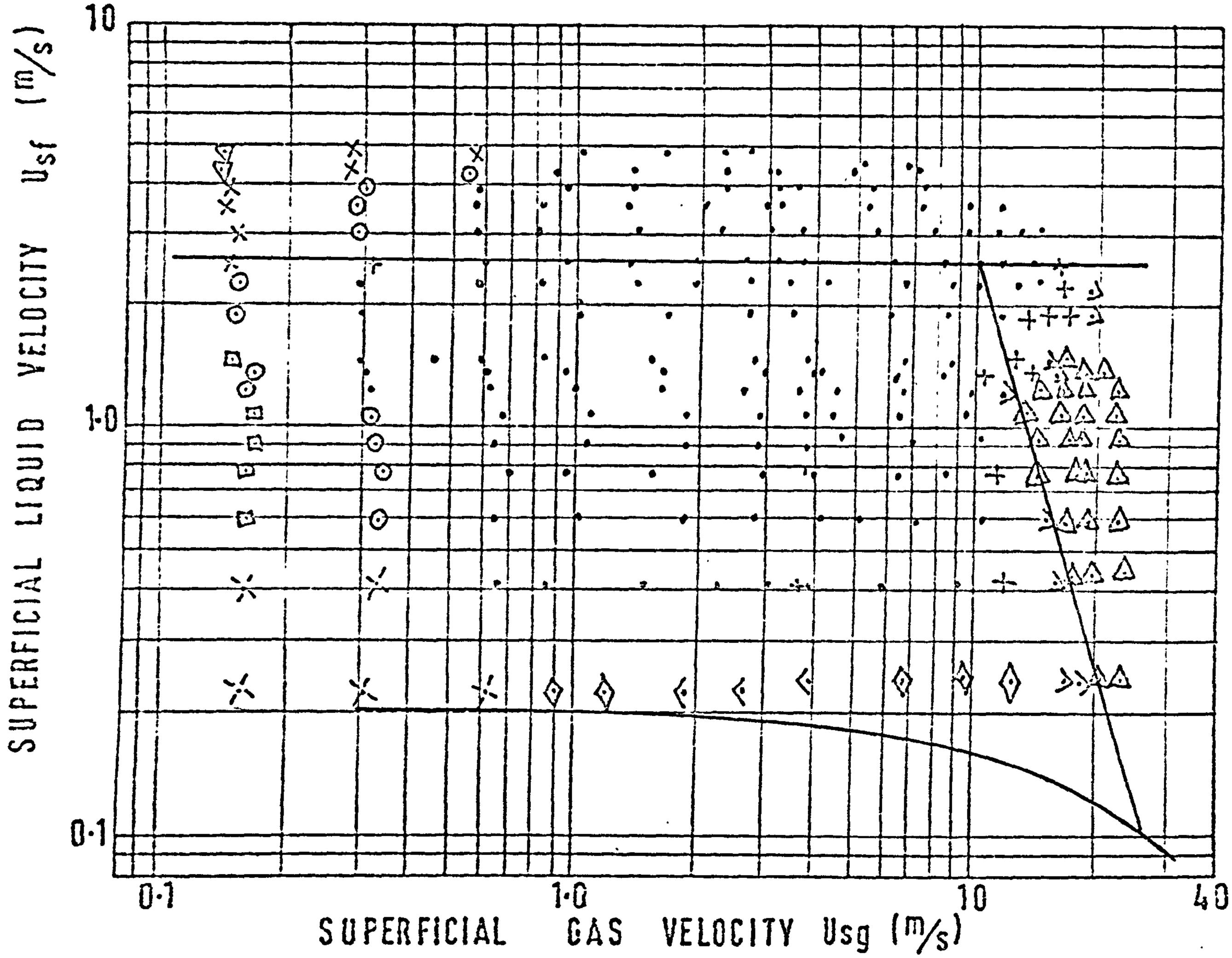

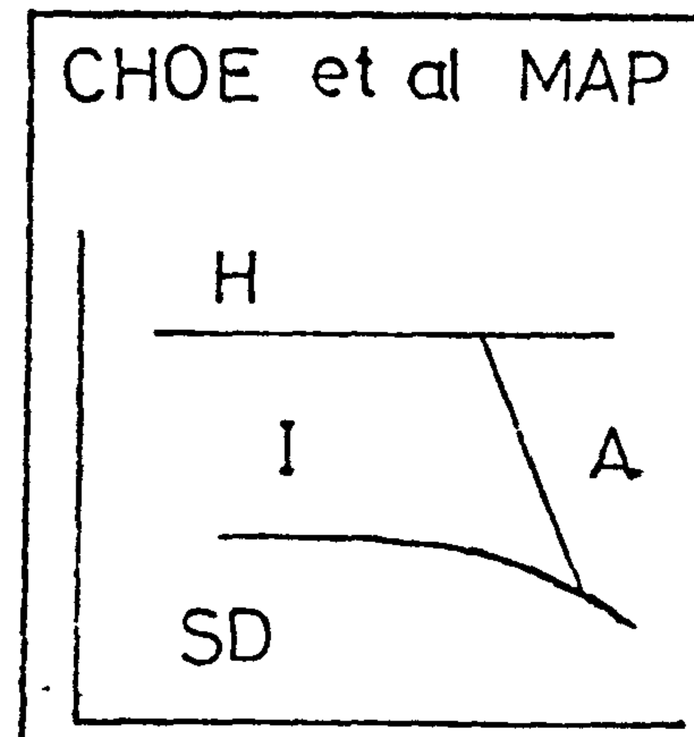

CODE

H HOMOGENEOUS

I INTERMITTENT

SD SEPARATED

A ANNULAR

FIG. 6·48 COMPARISON OF EXPERIMENTAL AND CHOE et al FLOW PATTERN MAPS (PHASE 2)

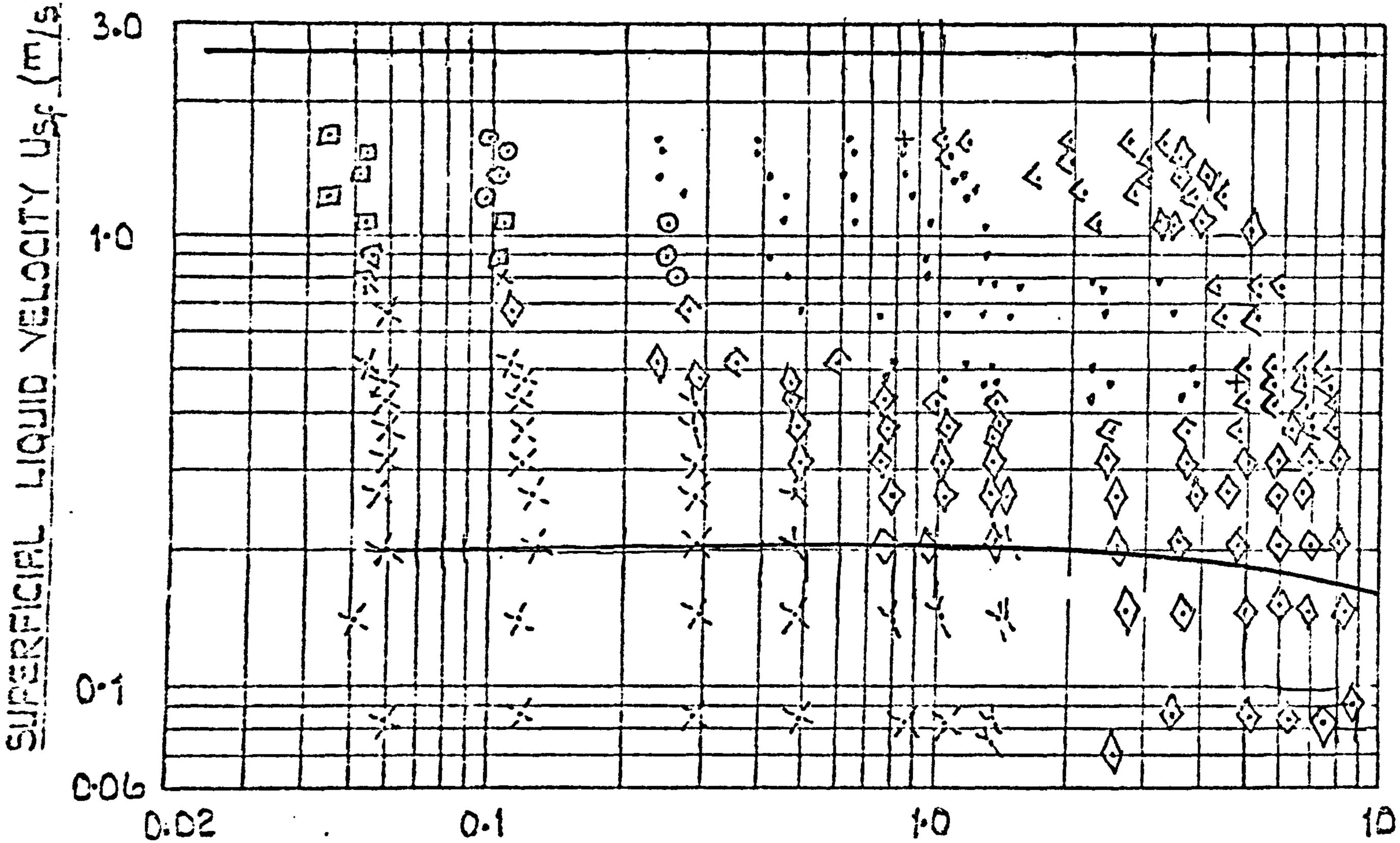

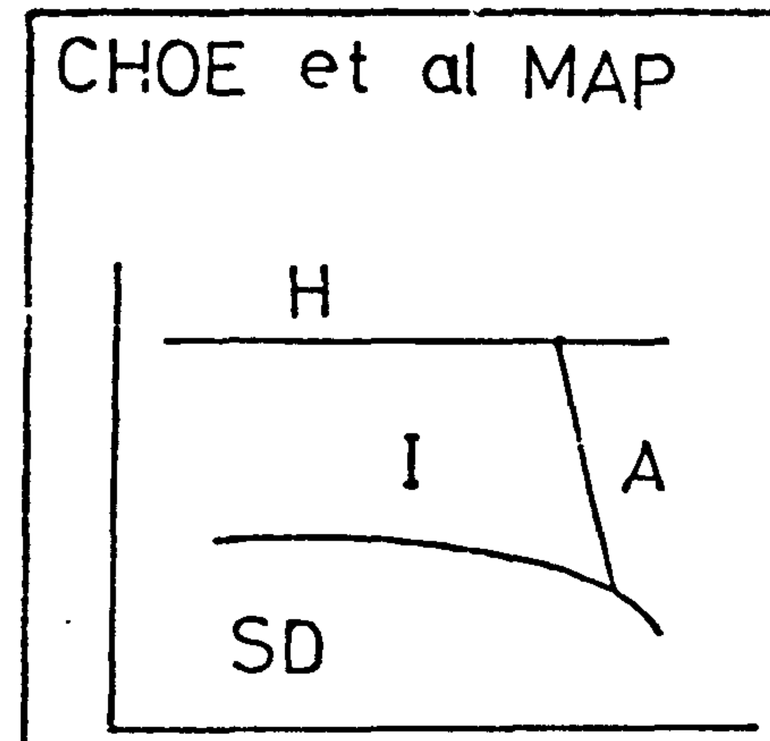

FIG. 6.49 COMPARISON OF EXPERIMENTAL AND CHOE et al FLOW PATTERN MAPS (PHASE 3)

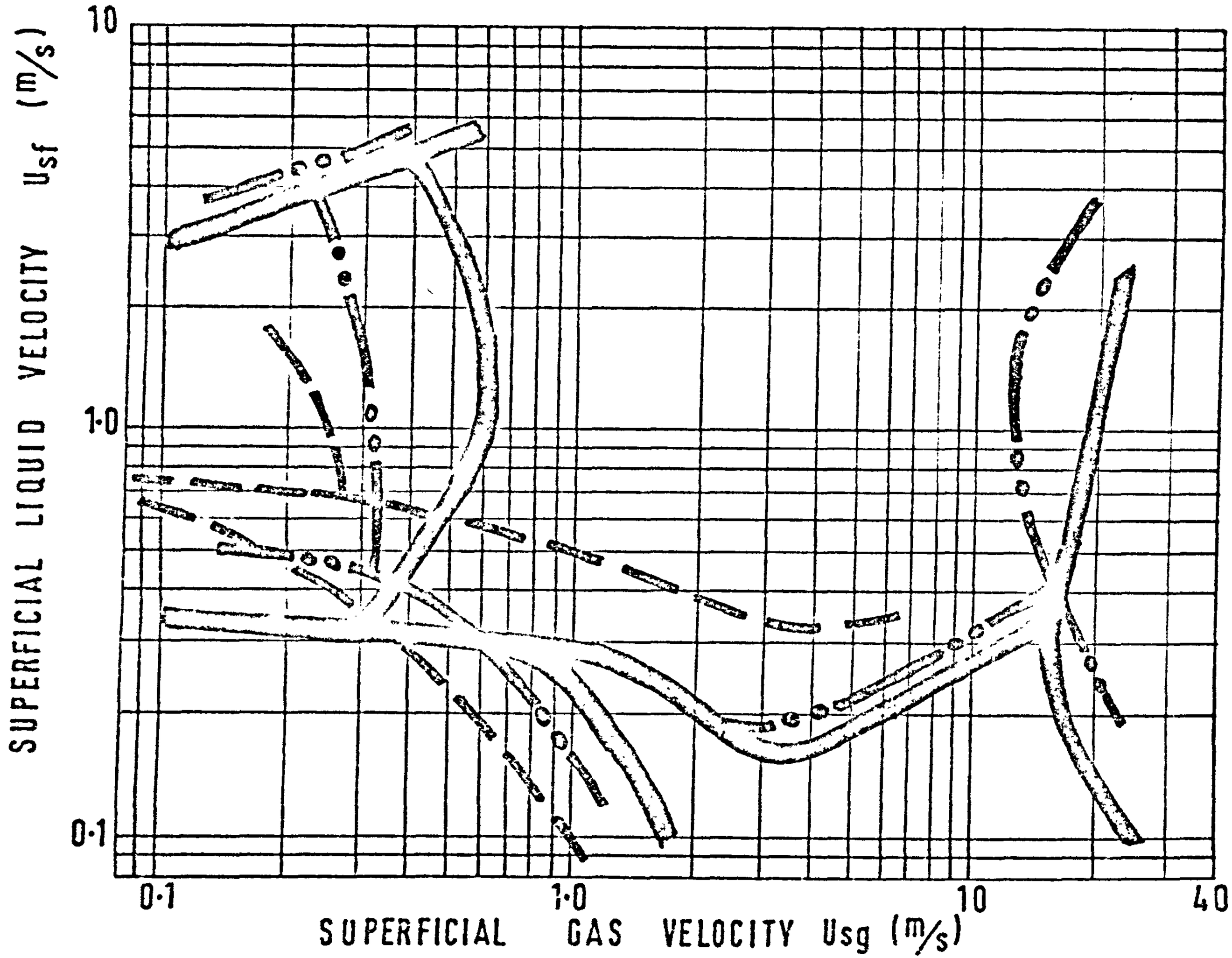

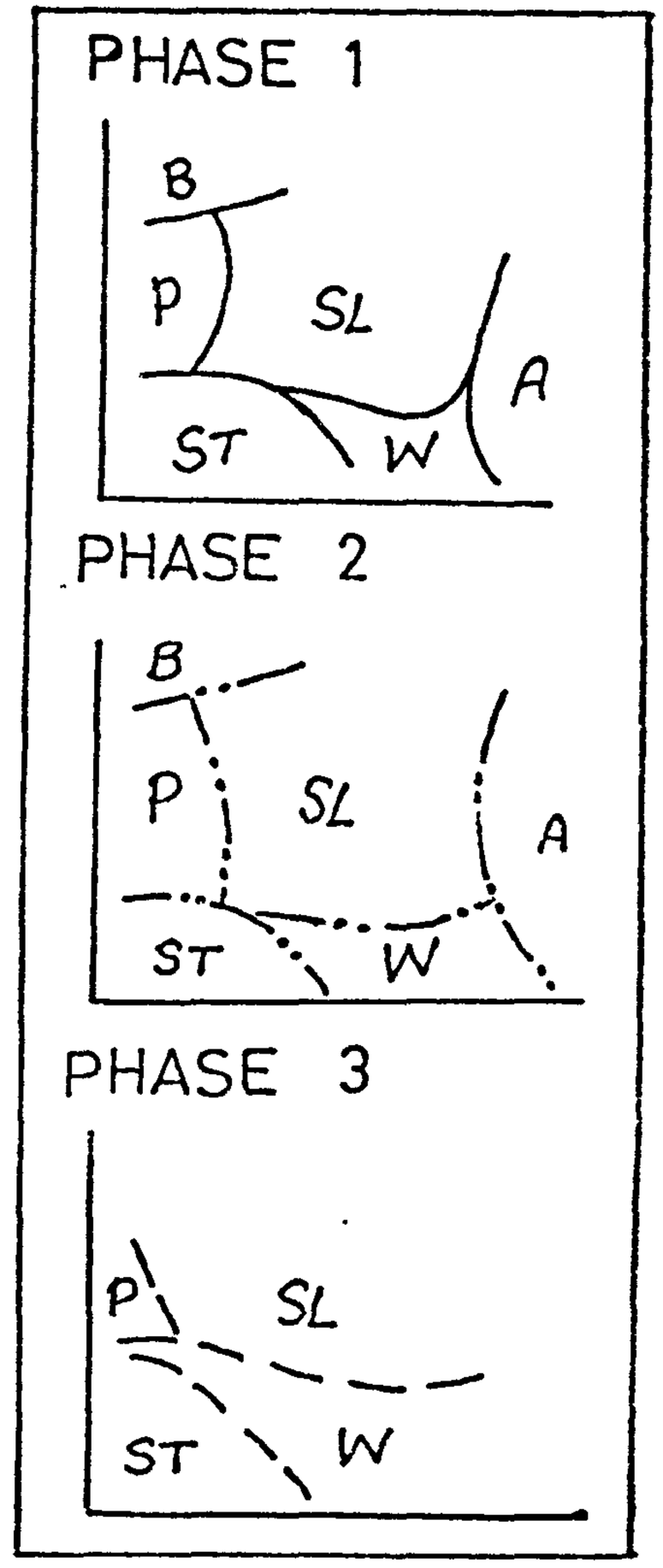

FIG. 6·50 COMPARISON OF PHASE 1,2 AND 3 FLOW PATTERN MAPS

(iv) the slug-plug boundary is shifted towards lower air flowrates.

The 216 mm pipe data confirmed the above comments, however the tests conditions did not include any annular flow pattern tests. The boundaries between stratified and plug, wave and slug flows occur at much higher water flowrates, and Baker's map suggests that the test should have covered some annular flow points. Drawing lines (they should be bands) to indicate the transition boundaries between the various flow pattern maps, the transition bands between the flow patterns for Phases 1, 2 and 3 tests are compared in Fig. 6.50. The displacement of the boundaries of Phase 2 compared to Phase 1 are not significant except perhaps for the plug-slug and slug-annular transitions, but it does show an effect of inlet conditions.

The effect of increasing tube diameter on the flow pattern transitions can be obtained by comparing Phases 2 and 3 results. In general, increasing tube diameter seems to move the transition boundaries to higher superficial water velocities and lower air velocities, and widens the wavy flow region, hence stressing the inadequacy of the coordinates U_{sf}, U_{sg} to scale up diameter.

The inadequacy of current flow patterns maps to predict these large diameter tube results is not surprising since they were based largely on data taken in smaller ducts, as indicated in Chapter 2.

6.4 VOID FRACTION

The void fraction data are plotted in Figs. 6.51, 6.52 and 6.53 for Phases 1, 2 and 3 respectively. The basis for this plot was explained in Chapter 2 and is also found in Ref. R3. In order to facilitate comparison, the data plotted were identified in terms of the different flow patterns encountered.

Let us consider first the 127 mm pipe results shown in Figs. 6.51 and 6.52. Here the data is interesting in that for volume fractions up to about 0.5, $\alpha > \beta$ which means that the slip factor < 1, i.e. the mean air velocity is less than the mean water velocity. For volume fractions greater than 0.5 approximately, the relationship changes to $\alpha < \beta$ making the slip factor >1. This indicates that at the lower air flowrate and particularly in the bubble and plug flow regimes the air is concentrated mostly in regions of low velocity (in this case the top of the tube). This agrees with the experimental observations of bubble and plug flows being disposed towards the top of the tube and can be attributed to air buoyancy effects. At higher gas flowrates, and particularly in the slug and annular flow regimes, the gas is concentrated more in the higher velocity regions, i.e. the centre of the tube, and once again this agrees with experimental observations. However this argument is not general as can be seen from the results relating to the 216 mm tube (Fig. 6.53) which were taken using a

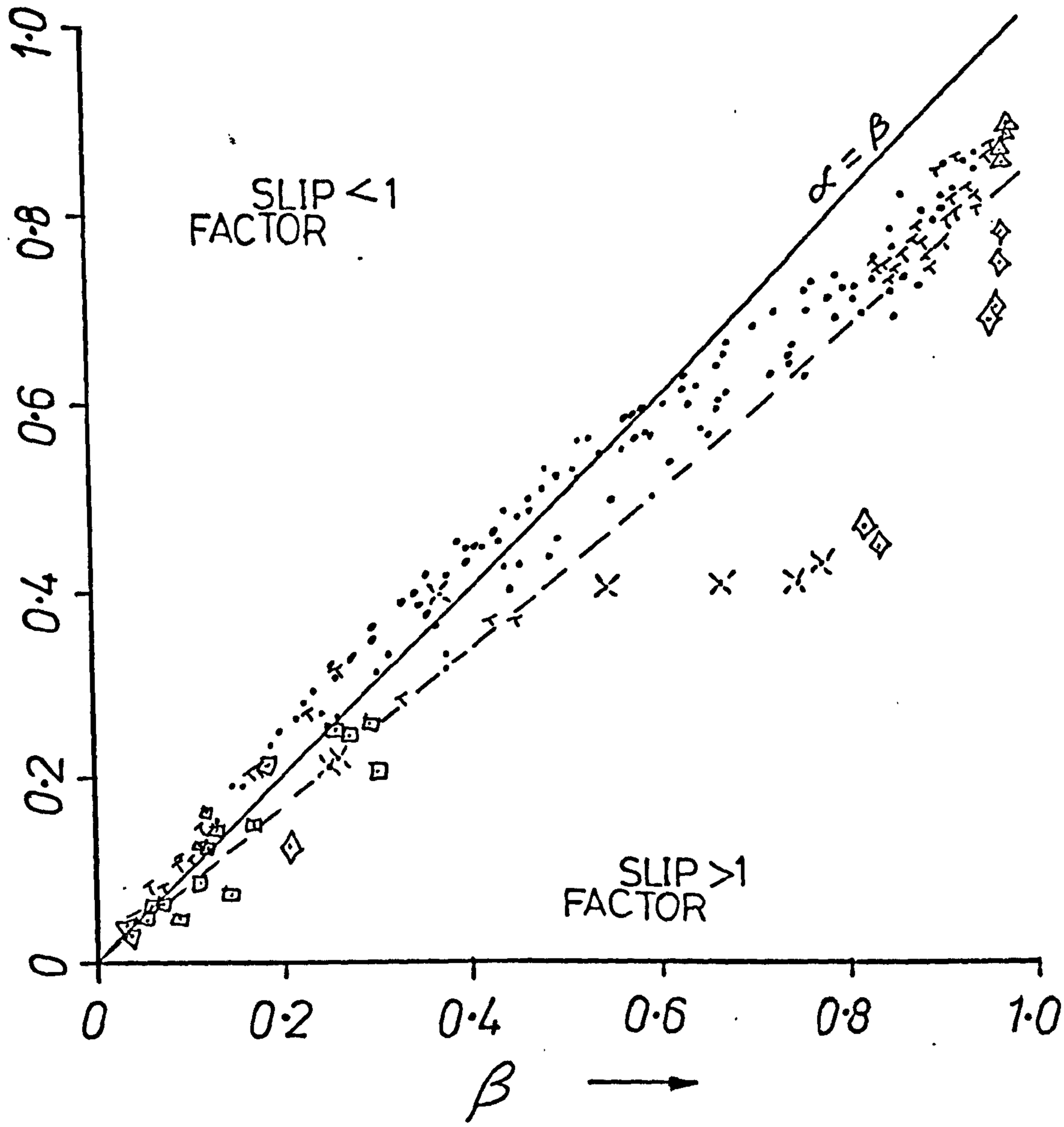

FIG. 6·51 VOID FRACTION DATA OF PHASE 1 TESTS

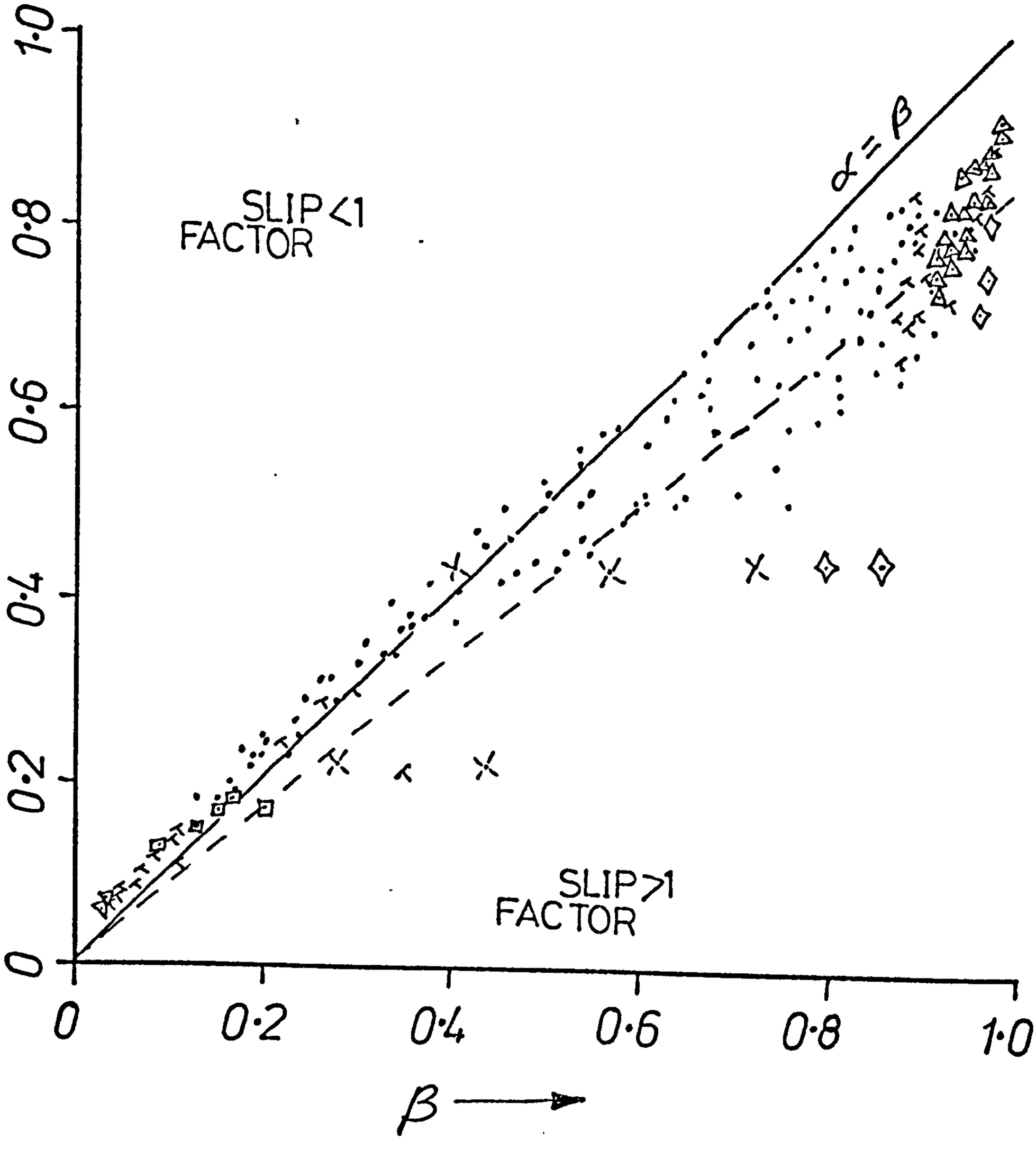

FIG. 6·52 VOID FRACTION DATA OF PHASE 2 TESTS

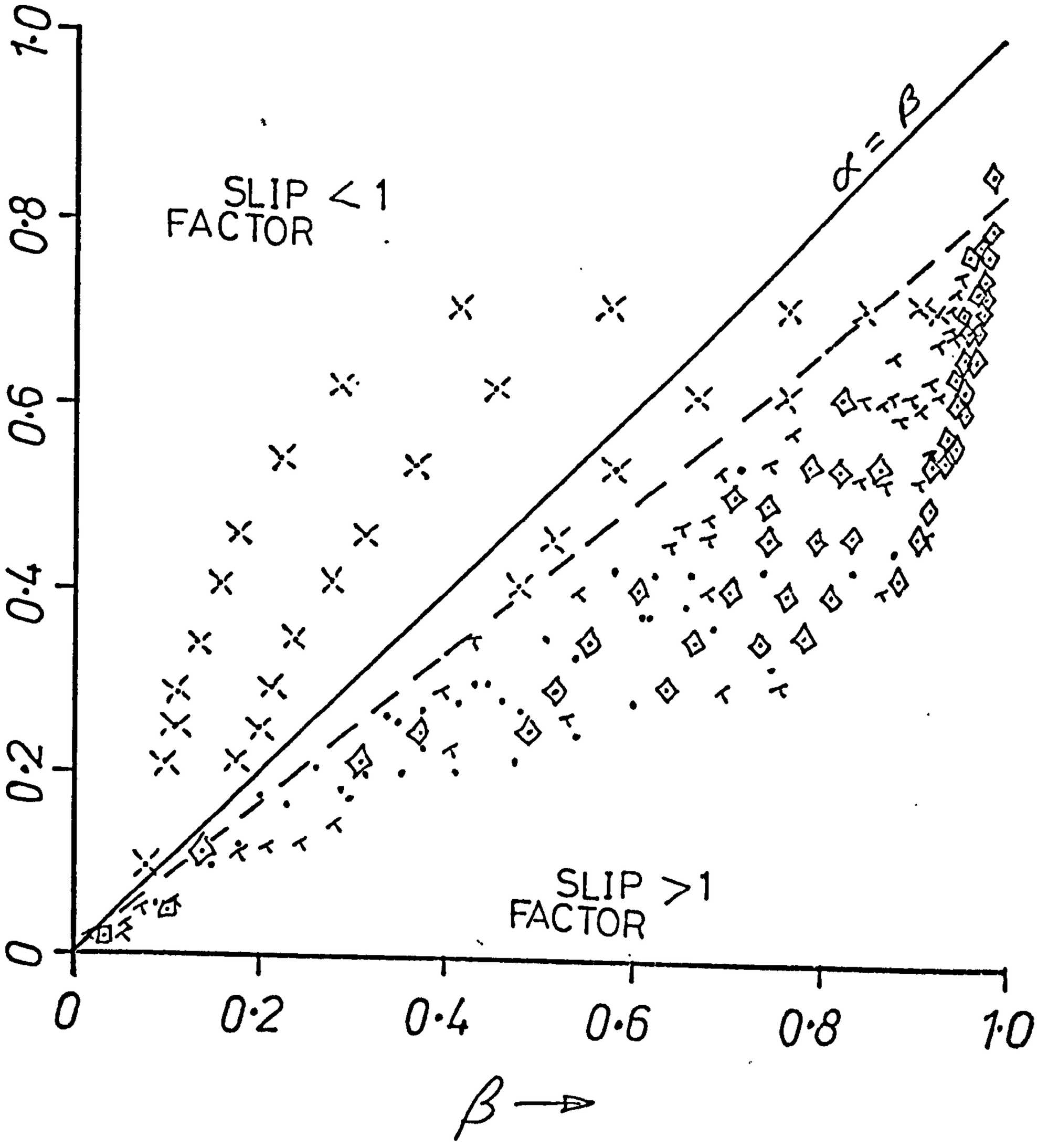

FIG. 6·53 VOID FRACTION DATA OF PHASE 3 TESTS

vertical γ-beam. The 127 mm data, however, were taken using a horizontal γ - beam (i.e. parallel to the plane of phase separation) which overpredicted the average void fraction for stratified type flows. The low β data covered bubbly, plug and slug flows which all showed some degree of stratification, and hence α could have been overpredicted a little. Fig. 6.54 shows Phase 2 results with α calculated using the stratified layer calibration relationship. As can be seen, most of the data fell below the homogeneous flow line, although it is expected that the actual α value will lie between the two extremes (shown in Figs. 6.52 and 6.54), which still suggests a small -ve slip, as might be expected.

Superimposed on these figures is the Armand (A2) relationship, $\alpha = 0.833\beta$ which was obtained from the horizontal flow of air-water mixtures in small diameter tubes. It is not too surprising that the Armand correlation does not hold for large diameter tubes particularly at low air flowrates, since bubbles, plugs and slugs cannot be scaled up as can the tube. Thus a larger bubble/tube or plug/tube diameter ratio will exist in small tubes and the air bubble or plug will be less concentrated in the low velocity region. A tube diameter effect on void fraction may be expected, therefore, at the lower air flowrates.

The behaviour of the Phase 1 data is closer to the homogeneous predictions with more scatter at low β, and

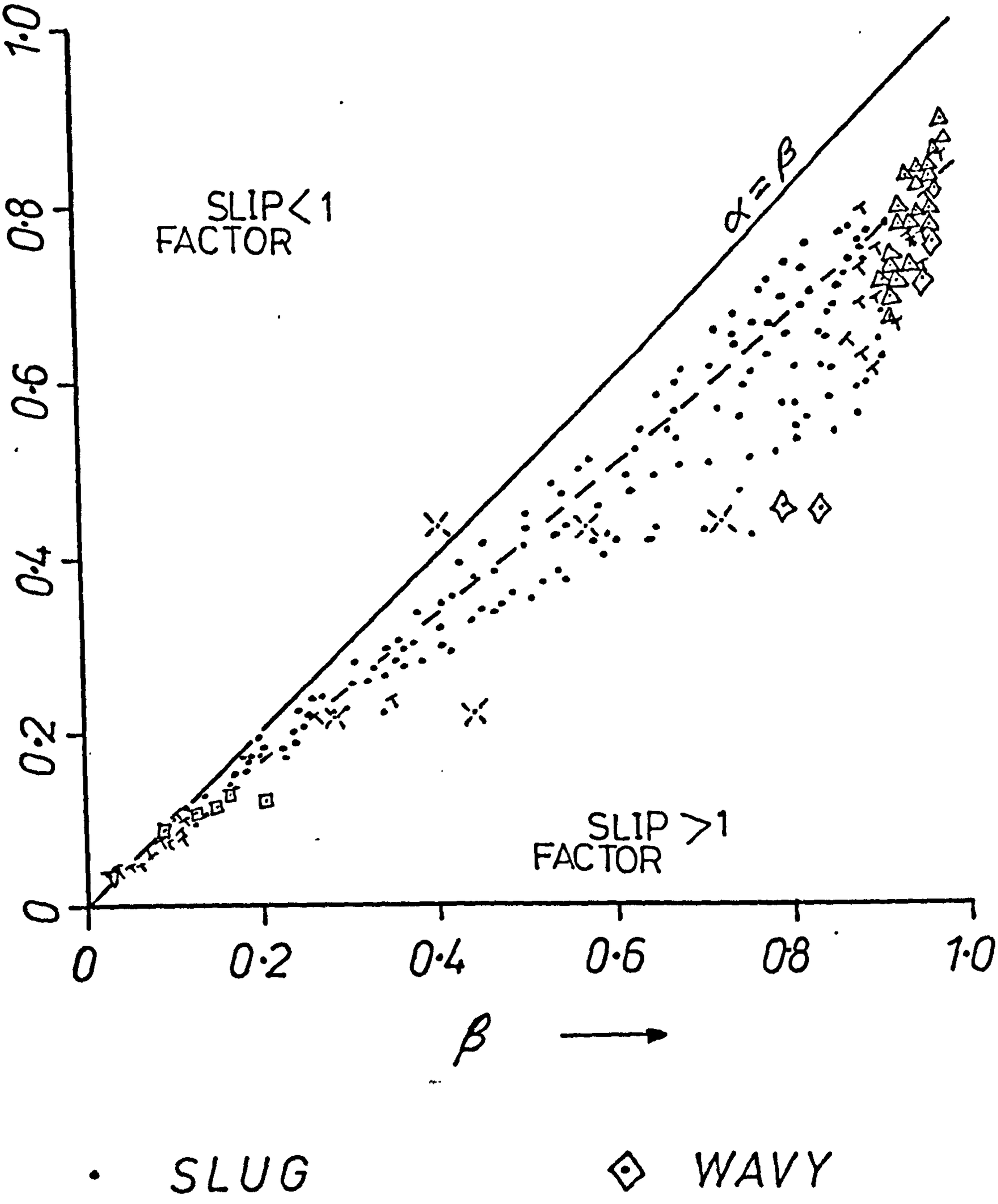

FIG. 6·54 VOID FRACTION DATA OF PHASE 2 TESTS WITH STRATIFIED LAYER CALIBRATION

less scatter at high β values. This is attributed to the mixing and instabilities introduced by the U-bend especially near the slug-annular boundary. The mixer was such as to promote less smooth transition from slug to annular in contrast to the bend in the phase 1 tests, and hence more scatter was obtained in the phase 2 data.

For the 216 mm pipe most of the data fell on or below the homogeneous line, except for the stratified flow data, indicating the gas velocity equal to or greater than the mean liquid velocity, i.e. slip factor $\geqslant 1$. It is interesting to note that most of the slug flow points, fell well into this region which was not the case with the 127 mm pipe results. This could be explained by a lack of mixing in the bigger pipe whereby the phases tended to behave independently giving rise to more stratified type of flows. In the smaller pipe, (relatively) more mixing was present which resulted in a more entrained liquid slug. The slug frequency observed in the bigger pipe was relatively small which could have affected the accuracy of the measuring device in terms of errors introduced by averaging the electrometer readings.

The stratified flow points are interesting for several reasons,

(i) many of the data indicate slip factors < 1

(ii) there seems to be less randomness about the data which appear to lie on a family of curves each representing a particular air flowrate.

(iii) at any particular void fraction level (this corresponds approximately to a particular water flowrate) increasing the air flowrate, i.e. increasing β , produces changes from slip factor < 1 to slip factors > 1. This last point is of particular significance since it suggests that the liquid flow is unaffected by changes in the air flowrate under stratified type flow conditions in large diameter tubes. This in turn suggests that the liquid behaves in a manner similar to open channel flow and that the conservation equations for stratified flow should account for this.

It is apparent that stratified and wavy flows cannot be represented by an α versus β plot. Once stratified flow was established for a particular water flowrate, increasing the air flowrate did not significantly alter the void fraction but merely increased the interfacial effects to produce wavy flow eventually.

The void fraction data in general showed a fair amount of scatter even with the same flow pattern range and especially with the larger diameter tube. This suggests that on the α versus β plot, a secondary affecting parameter (such as air or water flowrate) may be necessary to correlate the data. Since the basis of the correlation is $\alpha = k\beta$, where k is a concentration of air factor, this means that k will be a function of e.g. water flowrate and hence flow pattern.

The result as a whole suggests that void fraction should be correlated in terms of flow patterns. At least three different flow pattern groups should be identified,

(a) bubble, plug and slug flows (mixed flows),

(b) stratified and wavy flows (separated flows)

(c) annular flow.

This fits the pressure drop requirements outlined earlier.

CHAPTER 7 PRESSURE AND VOID FRACTION FLUCTUATIONS AND THE RELATION TO FLOW PATTERNS

CHAPTER 7 PRESSURE AND VOID FRACTION FLUCTUATIONS AND THE RELATION TO FLOW PATTERNS

For horizontal two phase flow systems in general, the presence of either phase at a given point fluctuates randomly, or sometimes near periodically, depending on such factors as the location of the point in the flow field, flow pattern, etc. When integrated over the whole cross section of the pipe, the net effect appears as an unsteadiness in the void fraction which due to the different properties and interfacial interactions between the phases, is reflected in the static pressure behaviour. Accordingly, one might expect severe pulsations in void fraction to be accompanied by severe pulsations in pressure (e.g. slug flow) and small variations in void fraction to be accompanied by calmer pulsations in pressure (e.g. stratified flow).

The character of a pressure or voidage signal is distinguished by two variables, the amplitude of the fluctuations and the frequency. Each flow pattern, therefore, could perhaps be characterised by the distribution of the fluctuations among the existing frequencies. If this is so, an important first step has been made in obtaining a more objective method of observing and defining flow patterns. An inspection of the pressure and local void fraction traces given in Chapter 5 (also in Appendix Y) strongly support this conclusion. Although the local void fraction traces were not as clear as the pressure traces (low response of the γ -ray detecting unit plus the fact that the scale is

limited to 0 —→ 1), nevertheless some general trends were obvious. For stratified (and some wavy) flows, the amplitude and frequency of the pressure pulsations were greatly influenced by the transducer background noise, whilst for plug flow, they were higher and more defined. Slug flows showed the most distinct characteristic of all, where large, wide pressure pulses were observed with a reasonable periodicity. Annular flow, however, showed lower amplitude, but with higher frequency components.

Once the differences between flow patterns are established, the next problem is one of characterising the two variables, i.e. the amplitude and frequency of the pulsations. The nature of the records immediately suggests the use of statistical methods of analysis.

7.1 TIME SERIES - CONCEPTS AND ASSUMPTIONS

A time series is a collection of observations made sequentially in time, and is considered discrete when the observations are taken at specific times, usually equi-spaced. If a time series can be predicted exactly it is 'deterministic' or periodic. However, most time series encountered in practice are random or 'stochastic', in that the future is only partly determined by past values. Exact predictions are impossible and must be replaced by the concept that future values have a probability distribution which is conditioned by knowledge of past values.

Broadly speaking, a time series is 'stationary' if there is no systematic change in the mean (no trend), no systematic change in the variance and if strictly periodic

variations have been removed (C16) i.e. a displacement in the time origin leaves its statistical properties unaffected. Hence given the sampled values of a stationary process, one would expect to be able to calculate the mean of the process by a straightforward integration. However it is not as simple as it may appear and the justification for such procedure constitutes the statistical 'ergodic' theorem (H21) whereby ensemble averages may be replaced by time averages.

In the following analysis, unless otherwise stated, the random processes are assumed stationary and ergodic.

It is often desirable to think of given physical data in terms of a combination of static component and dynamic or fluctuating component . The static component may be described by the mean value which, for a record of length T sec, of a process x(t), is by definition

$$\bar{x} = \frac{1}{T} \int_0^T x(t)\, dt \qquad (7.1)$$

The dynamic component may be described by the variance which is simply the mean square deviation about the mean. By definition,

$$\sigma^2 = \frac{1}{T} \int_0^T \left[x(t) - \bar{x}\right]^2 dt \qquad (7.2)$$

The root mean square deviation about the mean, known as the standard deviation is the square root of equation (7.2) or simply σ .

For a random process, the precise value of $x(t)$ at any future time t_o cannot be exactly determined. The best we can do is to find the probability that $x(t_o)$ will lie within certain limits. Given a sample time history or record of the process, then the probability that $x(t_o)$ assumes a value within the range between x_o and $x_o + \Delta x$ may be obtained by taking the ratio t/T, where t is the total amount of time in which $x(t)$ falls inside the range $(x_o, x_o + \Delta x)$ during the total observation time T. This ratio will approach an exact probability description as T approaches infinity, or

$$\text{Prob}\left[x_o < x(t_o) \leqslant x_o + \Delta x\right] = \lim_{T \to \infty} \frac{t}{T} \qquad (7.3)$$

the probability density function is, by definition

$$p(x) = \lim_{\Delta x \to 0} \frac{1}{\Delta x} \left(\lim_{T \to \infty} \frac{t}{T}\right) \qquad (7.4)$$

and is always a real valued, non-negative function.

The probability that $x(t)$ falls inside the range (x_1, x_2) is given by

$$p(x_2) - p(x_1) = \text{prob}\left[x_1 < x(t) \leqslant x_2\right] = \int_{x_1}^{x_2} p(x)dx$$

The function $p(x)$ is known as the probability distribution function and is bounded by the values 0 and 1, such that

$$\text{Prob}\left[-\infty \leqslant x \leqslant \infty\right] = \int_{-\infty}^{\infty} p(x)\, dx = p(x = \infty) = 1$$

For many naturally occurring random processes, the plot of the probability density function $p(x)$ versus instan-

taneous value approximates a well known bell-shaped distribution. In fact the central limit theorem asserts that this distribution will result quite generally from the sum of a large number of independent random variables acting together (B17), the equation describing the distribution being of the form

$$p(x) = \frac{1}{\sigma\sqrt{2\pi}} \; e^{-\frac{(x - \bar{x})^2}{2\sigma^2}} \qquad (7.5)$$

where the random variable x is said to have a normal or Gaussian probability distribution. The above equation suggests that for a Gaussian noise, the probability laws governing the process are completely defined by its mean and variance. [Another useful distribution, known as the exponential distribution could describe some phenomena which are not normally distributed, such as the variance distribution over a given band. The probability density function in this case is given by

$$p(x) = \bar{x} \; e^{-\bar{x} \cdot x} \qquad x > 0 \; (\bar{x} > 0)$$

$$= 0 \qquad x < 0$$

and the distyribution is defined completely by the mean value $\bar{x}$.].

However, knowing the probability laws does not provide insight into the probability model which generated the data e.g. the interdependency of the data values at one time to that at another time. Such information is provided by an important function known as the autocorrelation function.

If τ is a displacement in time or lag, then the auto-correlation coefficient is obtained by taking the product of the values of the variable x at time t and t+ τ and then averaging over the observation time, or

$$R_x(\ \ ) = \lim_{T \to \infty} \frac{1}{T} \int_0^T x(t)\, x(t+\tau)\, dt \qquad (7.6)$$

The autocorrelation function constitutes a set of these coefficients calculated at different lags or time displacements. In general there is little point in calculating $R_x(\tau)$ for values of τ greater than T/4 [$R_x(\tau)$ is a declining function of lag τ]. A plot of $R_x(\tau)$ against lag τ is known as the correlogram which is a useful aid in interpreting the data.

In many scientific problems, one is interested in the relationship between one variable, x(t) and another variable y(t). As an example, consider the case where a radioactive trace is injected into a flow in a pipe and detected at two separate locations downstream along the pipe. By cross-correlating the information from the two stations, one is able, for instance, to determine the average velocity of the flow, and hence the name cross correlation technique. For the two processes x(t) and y(t), the cross correlation is defined by

$$R_{xy}(\tau) = \lim_{T \to \infty} \frac{1}{T} \int_0^T x(t)\, y(t+\tau)\, dt \qquad (7.7)$$

and

$$R_{yx}(\tau) = \lim_{T} \frac{1}{T} \int_0^T y(t)\, x(t+\tau)\, dt \qquad (7.8)$$

There is an extensive literature on statistical analysis of time series and the reader is referred to them for further details, e.g. Bendat (B17), Hannan (H21), Chatfield (C16), Otnes and Enochson (05).

So far we have looked into some of the techniques used to analyse time series in the time domain. However, some of the characters of the series may be better interpreted when studied in the frequency domain. Such an approach requires a knowledge of Fourier analysis which will not be considered in detail in this chapter. However Appendix (X) gives a simplified version of the technique and is intended to be helpful in explaining some of the results quoted in this chapter.

Given the autocorrelation function $R_x(\tau)$ of a process $x(t)$, the Fourier transform $S_x(f)$ and its inverse are defined as,

$$S_x(f) = \frac{1}{2\pi} \int_{-\infty}^{\infty} R_x(\tau)\, e^{-jw\tau}\, d\tau = \frac{2}{2\pi} \int_{0}^{\infty} R_x(\tau) \cos w\tau \; d\tau \qquad (7.9)$$

$$R_x(\tau) = \int_{-\infty}^{\infty} S_x(f)\, e^{jw\tau}\, dw \qquad (7.10)$$

and

$$w = 2\pi f$$

$S_x(f)$ is called the (auto) spectral density of the process $x(t)$ and gives the frequency composition of the data which in turn bears important relationships to the basic characteristics of the physical system involved. Sometimes the word power is added, i.e. the power spectral

density, which derives its name from the engineers use of the word in connection with the passage of an electric current through a resistance. For a sinusoidal input the power is directly proportional to the squared amplitude of the oscillations. The cross spectral density is given by a similar expression, namely

$$S_{xy}(f) = \frac{1}{2\pi} \int_{-\infty}^{\infty} R_{xy}(\tau)\, e^{-jw\tau}\, d\tau \qquad (7.11)$$

and

$$S_{yx}(f) = \frac{1}{2\pi} \int_{-\infty}^{\infty} R_{yx}(\tau)\, e^{-jw\tau}\, d\tau \qquad (7.12)$$

An important relationship is now obtained by applying the correlation theorem explained in Appendix (X) to the cross correlation function, i.e.

$$\int_{-\infty}^{\infty} R_{xy}(\tau)\, e^{-jw\tau}\, d\tau = X(f)\, Y(f)^* \qquad (7.13)$$

or in words, the Fourier transform of the correlation function of two functions x(t) and y(t) is equivalent to the complex multiplication of the separate Fourier transforms of the functions. The star (*) stands for complex multiplication.

But from equation (7.11), for the definition of $S_{xy}(f)$, we get,

$$S_{xy}(f) = X(f)\, Y(f)^* \qquad (7.14)$$

or the power cross spectral density of the two processes x(t) and y(t) can be calculated by first calculating the Fourier transform of each process and then performing a

complex multiplication. For the (auto) power spectral density, a similar relation is evolved, namely

$$S_{xx}(f) = X(f)\, X(f)^* \qquad (7.15)$$

This means that there are two methods available for calculating the power spectral density,

(i) Indirect Method: First calculate the auto (or cross) correlation then Fourier transform the results. This is known now as the Blackman-Tukey method.

(ii) Direct Method: Fourier transform the data then perform a complex multiplication to calculate a modulus which is proportional to the power density estimate. This method employs a special computational procedure known as the Fast Fourier Transform (abbreviated FFT) and is known as the FFT method.

The advantage of using the FFT (discovered in 1965) is the great savings in computing times especially for large data records. The common form of the FFT (used in the analysis here) requires the number of data points to be a multiple of 2. This may be achieved by either adding zero at the end of the data or by truncating the record such that the total number is a multiple of 2. For more detailed information a large number of books and papers are available, e.g. Otnes and Enochson (O5), Newland (N4), Brigham (B16), Bingham et al. (B19), etc.

7.2 PROBLEMS ARISING FROM ANALYSING DIGITISED TIME SERIES OF FINITE LENGTH

Time histories in general have a number of constraints imposed upon them by the nature of their origin and by the methods of observation and recording. Four main limitations are

(i) Record length is finite.

(ii) Range of data is restricted (recording instruments are sensitive only within a certain range).

(iii) Data are sampled.

(iv) Data are discrete (digitised to a finite precision).

Conditions (ii) and (iv) are mostly caused by the type of instruments being used, and although their recognition is important, their effects can be reduced to a negligible degree for most practical applications. For example in our case, the data acquisition system accepted signals within the range $\pm$ 1 volt, i.e. condition (ii), and also the signals were digitised to within 2 mv, i.e. condition (iv). More series problems arise because the function is not continuous, but sampled at discrete intervals, i.e. condition (iii), and also because the record length is finite, i.e. condition (i). These effects are normally known as aliasing and leakage respectively.

7.2.1 SAMPLING THEOREM

This theorem states that if the Fourier transform of

a function x(t) is zero for all frequencies greater than a certain frequency f_c and if it exists for lower frequencies, then the continuous function x(t) can be uniquely determined from a knowledge of its sampled values if the sampling interval Δt is such that

$$f_c = \frac{1}{2\Delta t} \qquad (7.16)$$

The frequency f_c is known as the 'Nyquist' or folding frequency. Failure to satisfy this condition will result in false peaks in the power spectrum, i.e. aliasing. These false peaks are actually higher frequency components in excess of f_c present in the signal x(t) which appear as lower frequency components in the fundamental frequency band $(-f_c < f < f_c)$ due to the fact that the sampling interval is not fine enough to describe these high frequency components. This is demonstrated in the sketch below where f_1 is the high frequency being sampled at the indicated equally spaced points and f_2 is the apparent (or aliased) frequency detected by this sampling.

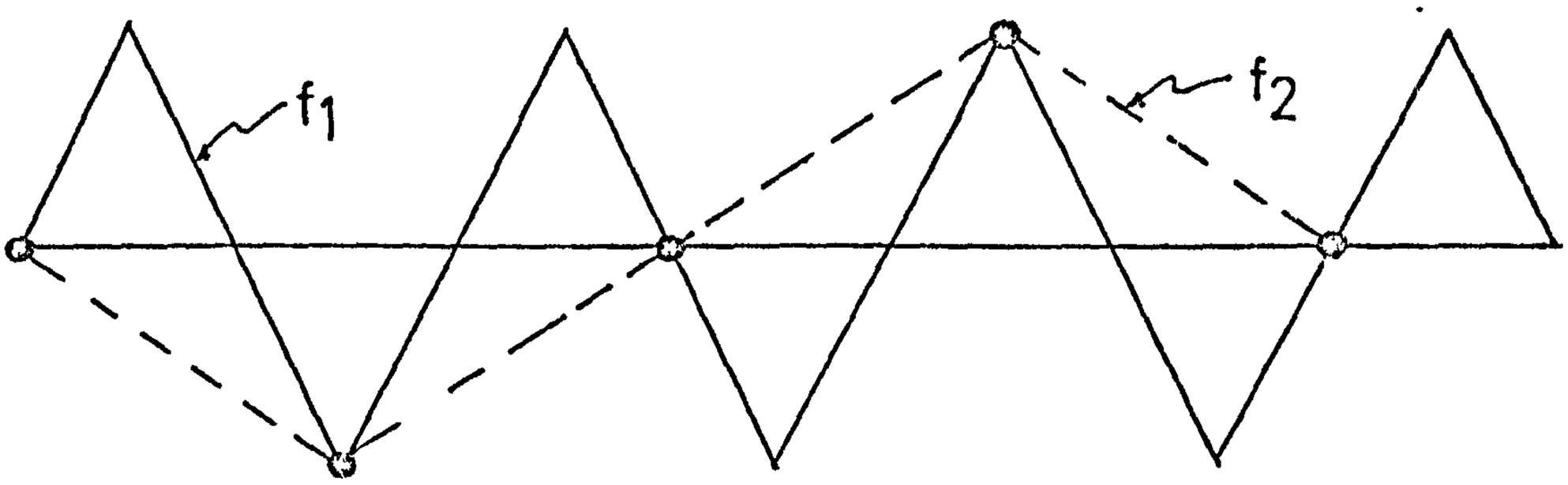

A more rigorous definition of aliasing is: in equally spaced data; two frequencies are said to be aliases of one another if sinusoides of the corresponding frequencies cannot be distinguished by their equally spaced values.

This condition occurs when

$$f_1 = \pm 2k\, f_c \pm f_2 \qquad k = 1,\ 2,\ 3, \text{--} \qquad (7.17)$$

These frequencies are aliases of one another, f_2 being the principal aliase.

In some cases visual inspection of a pilot sampled signal could give a rough idea about the frequency range possible. However, in other cases the only way to be certain that no aliasing will be present, may be to filter the time series (using a low pass filter at f_c) to remove intentionally all frequency components higher than f_c before collecting the data.

7.2.2 LEAKAGE

This is the most serious problem encountered when attempting to frequency analyse sampled time series and is caused by the way in which time domain truncation is seen from the frequency domain. Unfortunately, it will be present, one way or another, in all power spectral estimates. The power in the spectrum instead of being concentrated at a single point (impulse of zero width), is spread out over a much broader frequency range giving contributions of power to other frequencies present in the signal. The net result is a modification in power and hence a false power spectrum. Visualise an infinite process x(t) which has an autocorrelation function $R_x(\tau)$. The actual power spectral density $S_x(f)$ is

$$S_x(f) = \int_{-\infty}^{\infty} R_x(\tau)\, e^{-jw\tau}\, d\tau \qquad -\infty < f < \infty \qquad (7.18)$$

However, the process x(t) is only observed over the finite interval (-T, T) and hence the predicted power density is

$$\hat{S}_x(f) = \int_{-T}^{T} R_x(\tau)\ e^{-jw\tau}\ d\tau \qquad -T < \tau < T \qquad (7.19)$$

where the hat (^) stands for predicted or estimated value.

When viewed from the frequency domain, this truncation is equivalent to multiplying the actual estimates by a sin z/z function (Appendix X), i.e.

$$S_x(f) = 2 \int_{-\infty}^{\infty} S(f')\ \frac{\mathrm{Sin}\left[2\pi T\ (f-f')\right]}{\left[2\pi T\ (f-f')\right]}\ df' \qquad (7.20)$$

It is apparent that the actual estimates are different from the predicted ones, such that instead of an impulse (delta function) being detected at the frequency f, a sin z/z function is centred on each impulse and contributions of power (+ ve or -ve) from a large number of components of other frequencies are added. The function size z/z is shown below

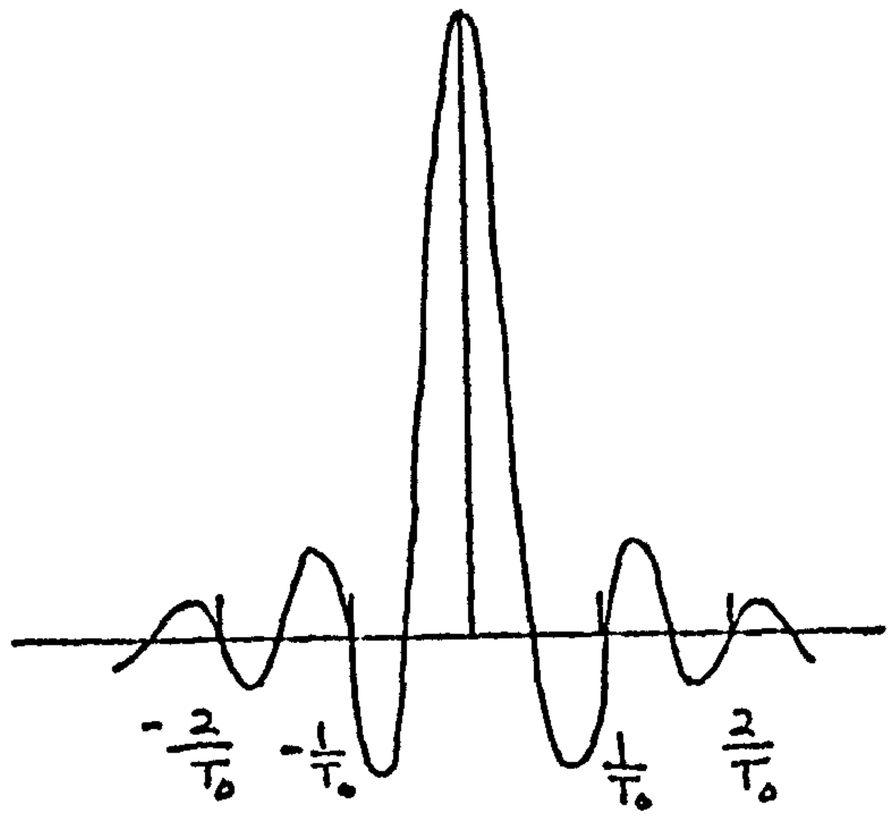

To make this clearer, let the function, assumed periodic, for the sake of argument, be sampled over a time which is a multiple of the period. Then the zeros of the

sin z/z function will coincide with the sample values which are separated by the reciprocal of the truncation time T_o (record length). In this case the discrete and continuous (actual) spectra are identical (i.e. no modification in spectrum). However, if the truncation time is not a multiple of the period (as is normally the case), then the frequency impulses will not coincide with the zeros of the sin z/z function and a false power is detected at frequencies other than the period. The power is said to have leaked to other frequencies through the infinite side lobes by an amount proportional to the area under each side libe as shown in the sketch above.

Half of the lobes are negative and could result in a negative estimate,(sometimes very large, depending on the spectrum), particularly since the height of the first two negative lobes is about one fifth of the main lobe. This is unsatisfactory since the average power is positive by definition.

7.2.3 LEAKAGE REDUCTION

To suppress the leakage problem, it is necessary to modify the box car (Appendix X) type of weighting in the time domain (or its equivalent Fourier transform in the frequency domain) so as to broaden the main lobe and decrease the effects of the side lobes. When leakage reduction procedures are carried out in the time domain, they are called windowing and when carried out in the frequency domain are called smoothing.

Some of these procedures are discussed now. Let $\bar{S}_k$ denote a calculated estimate at the k^{th} harmonic, then a better estimate is (B18),

$$
\begin{aligned}
S_o &= D_1 \bar{S}_o + 2D_o \bar{S}_1 && k = 0 \\
S_k &= D_o \bar{S}_{k-1} + D_1 \bar{S}_k + D_o \bar{S}_{k+1} && k = 1, 2, \ldots, m-1 \\
S_m &= D_1 \bar{S}_m + 2D_o \bar{S}_{m-1} && k = m
\end{aligned}
\qquad (7.21)
$$

where

	Hanning	Hamming
D_o	0.25	0.23
D_1	0.50	0.54

What we have done is smooth, or average, the power estimates using certain weighting constants and hence the word smoothing. The same results may be obtained if (Hanning procedure) the function

$$
\begin{aligned}
u_H(\tau) &= \tfrac{1}{2}\left(1 + \cos \frac{\pi \tau}{\tau_m}\right) && |\tau| < \tau_m \\
u_H(\tau) &= 0 && |\tau| > \tau_m
\end{aligned}
\qquad (7.22)
$$

where τ_m is the maximum lag to be calculated, is operated on the autocorrelation function (or the sampled data if τ and τ_m are replaced by t and T) before calculating the raw estimates. The function $u_H(\tau)$ is called a 'lag window' since it can be thought of as a window of variable transmission through which the process is observed and hence the word windowing. At both ends of the record the function is brought to zero, reducing potential discontinuities in the time domain.

Comparing the Hanning and the rectangular windows (see figure below) indicates that for the first window the main lobe is broader (twice the boxcar) and the side lobes are much smaller as is expected. The half power width for the Hanning and Hamming windows is $(1/\tau_m)$, where τ_m is the maximum lag.

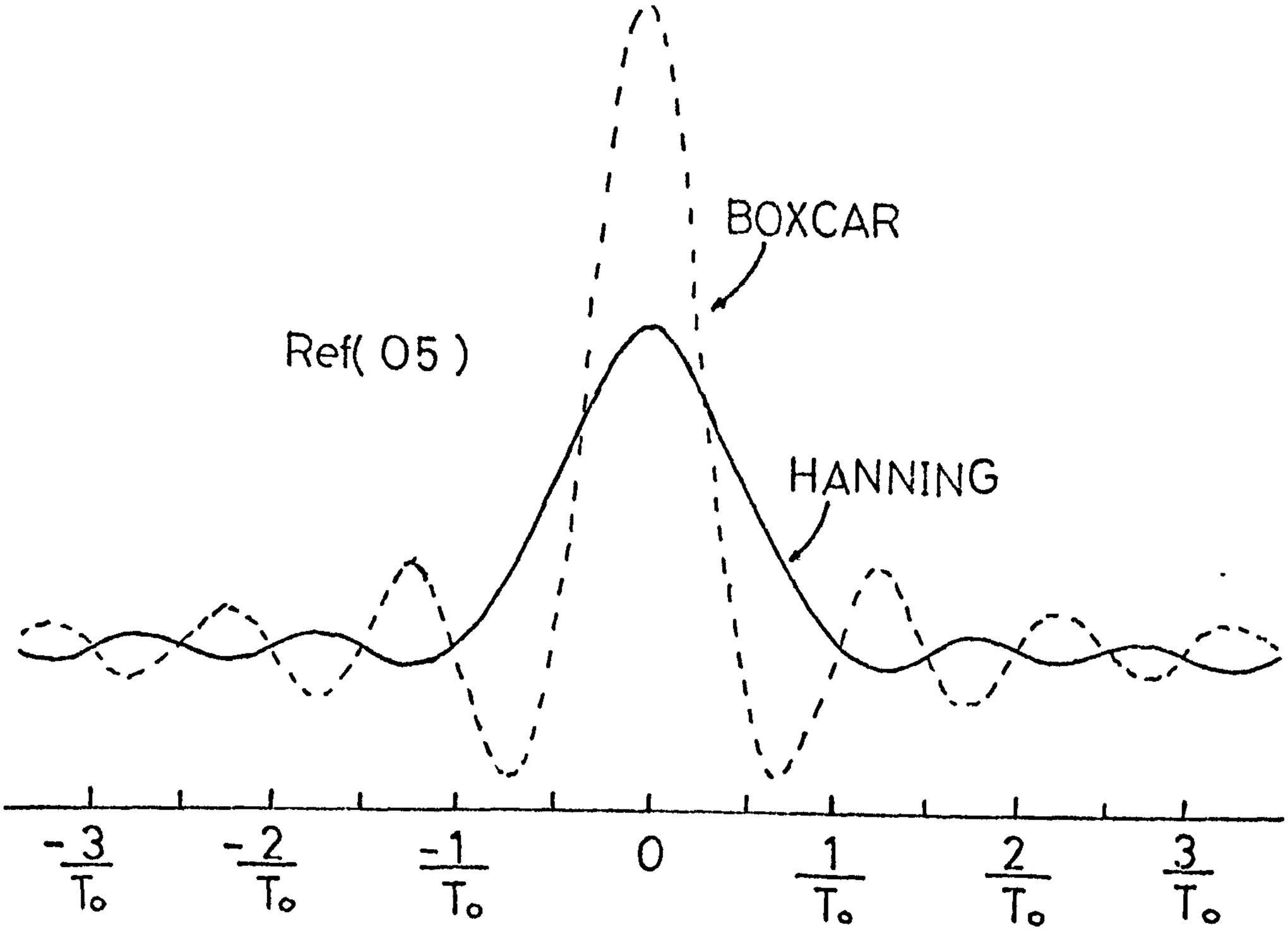

Parzen (P3) suggested a similar technique, but his window had the advantage that it did not give -ve estimates, i.e. the side lobes were always positive. This is a great comfort for engineers who are squeamish about seeing negative power estimates. The half power width is increased to $(1.3/\tau_m)$ i.e. resolution is reduced, and correspondingly the statistical variability is reduced.

Bingham et al (B19) suggested tapering the original sampled time series at both ends using a cosine taper over

1/10th of the data, at each end of the record. The smoothing filter shape is roughly triangular with the main lobe width being widened and the side lobe leakage suppressed, when compared to the Boxcar window. This procedure is recommended for use with the Fast Fourier transform technique mentioned earlier. One physical advantage of the tapering procedure is that only 20% of the data is modified while other procedures such as Hanning, Hamming, etc., modify the whole data to the extent that the resultant modified data hardly resembles the actual data as shown below.

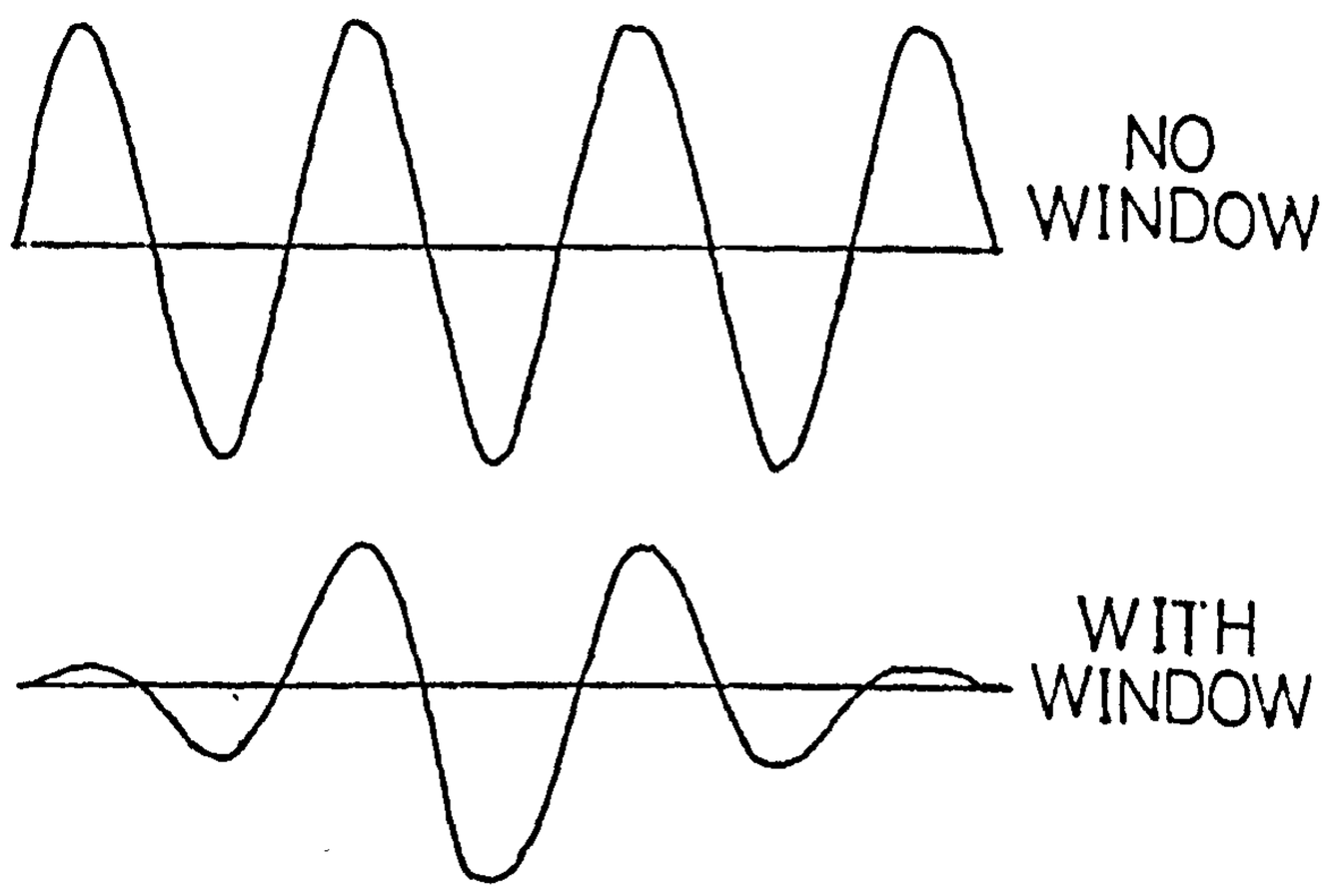

7.3 STATISTICAL RELIABILITY OF POWER SPECTRUM ESTIMATES

Statistical errors are defined as the uncertainty in the power estimates due to the amount of data gathered, the underlying probability nature of the data and the method used in deriving the desired parameters. It is very difficult to calculate an exact measure of the errors involved, however those based on white (uncorrelated) Gaussian noise analysis may be taken as guide lines since most random processes approach these conditions.

One way of discussing such errors is in terms of the

normalised standard error ϵ_o. For the direct method procedure, the normalised error is (05),

$$\epsilon^2 = 1 \qquad \text{for large N}$$

i.e. the standard deviation of the estimate is greater than or equal to the quantity being estimated. This means that the raw power densities are not consistent estimates of the actual value. The standard error is defined as the normalised error divided by the number of variables used to calculate a given estimate, or

$$\epsilon_o^2 = \frac{\epsilon^2}{2} = \frac{1}{2}$$

for the direct method, since two quantities (real and imaginary terms) are used to calculate a given power density estimate. However this problem can be overcome in practice by a sacrifice in resolving power, where M raw estimates are averaged to give a single but more reliable estimate. The standard error is reduced to

$$\epsilon_o = \frac{1}{\sqrt{2M}} \qquad (7.23)$$

and the band width of each estimate is broadened from $(1/N\Delta t)$ to $(M/N\Delta t)$, where Δt is the sampling time, and N is the total number of points per record.

A general expression for the normalised standard error in terms of the bandwidth, B_e (half power value) is

$$\epsilon_o^2 = \frac{1}{2B_eT}\ , \ T = \text{record length} \qquad (7.24)$$

For the correlation procedure (i.e. indirect method) the

band width

$$B_e = \frac{1}{m\Delta t} \qquad (7.25)$$

where m is the maximum number of lags.

Hence

$$\epsilon_o = \sqrt{\frac{m}{2N}} \qquad (7.26)$$

which explains why the maximum lag (m) is recommended not to exceed 5-10% of the record length (N).

Another way of discussing the statistical errors is by considering the components of the power spectrum estimates (square real and square imaginary terms) as a χ^2-variable (Appendix X) and to make use of that distribution to find a confidence interval for the estimate. If $S_x(f)$ is an estimate of the power density around the frequency f, then the confidence limits take the form,

$$\text{Prob}\left[A < S_x(f) \leqslant B\right] = q$$

where q is a fixed confidence level, normally 0.8, 0.9 or 0.95.

The above equation is interpreted as; with (100q)% confidence the true value of $S_x(f)$ lies between A and B. Let us define a quantity h, such that h = 1-q, then the parameters A and B known as the confidence limits are given by

$$A = \frac{n\,\hat{S}_x(f)}{\chi^2_{n,h/2}} \quad , \quad B = \frac{n\,\hat{S}_x(f)}{\chi^2_{n,1-h/2}} \qquad (7.27)$$

'n' is the equivalent number of degrees of freedom, and is

the number of variables used to calculate a given power estimate. For the direct Fourier transform calculations, n=2.

The χ^2 distribution function is plotted in Fig. 7.1 as a fraction of the estimated value against the equivalent number of degrees of freedom, which shows clearly that increasing the number of degrees of freedom narrows the uncertainty band. This suggests that in order to obtain a reliable estimate using the FFT method, smoothing is necessary to increase the equivalent number of degrees of freedom (at the expense of resolution). If M estimates are smoothed (averaged) to produce only one estimate, the equivalent number of degrees of freedom becomes

$$n = 2M \tag{7.28}$$

'n' can also be expressed in terms of the band width of the estimate, B_e as

$$n = 2 B_e T \tag{7.29}$$

Obviously, $B_e = (1/N\Delta t)$ for the FFT method without smoothing and $B_e = (M/N\Delta t)$ when smoothing over M estimates is carried.

For the correlation procedure, the band width of the estimates depends on the number of lags m, used to calculate the autocorrelation function, then

$$n = \frac{2N}{m} \tag{7.30}$$

Again the reason for restricting m to 5-10% of N is clear; it is to produce a higher equivalent number of

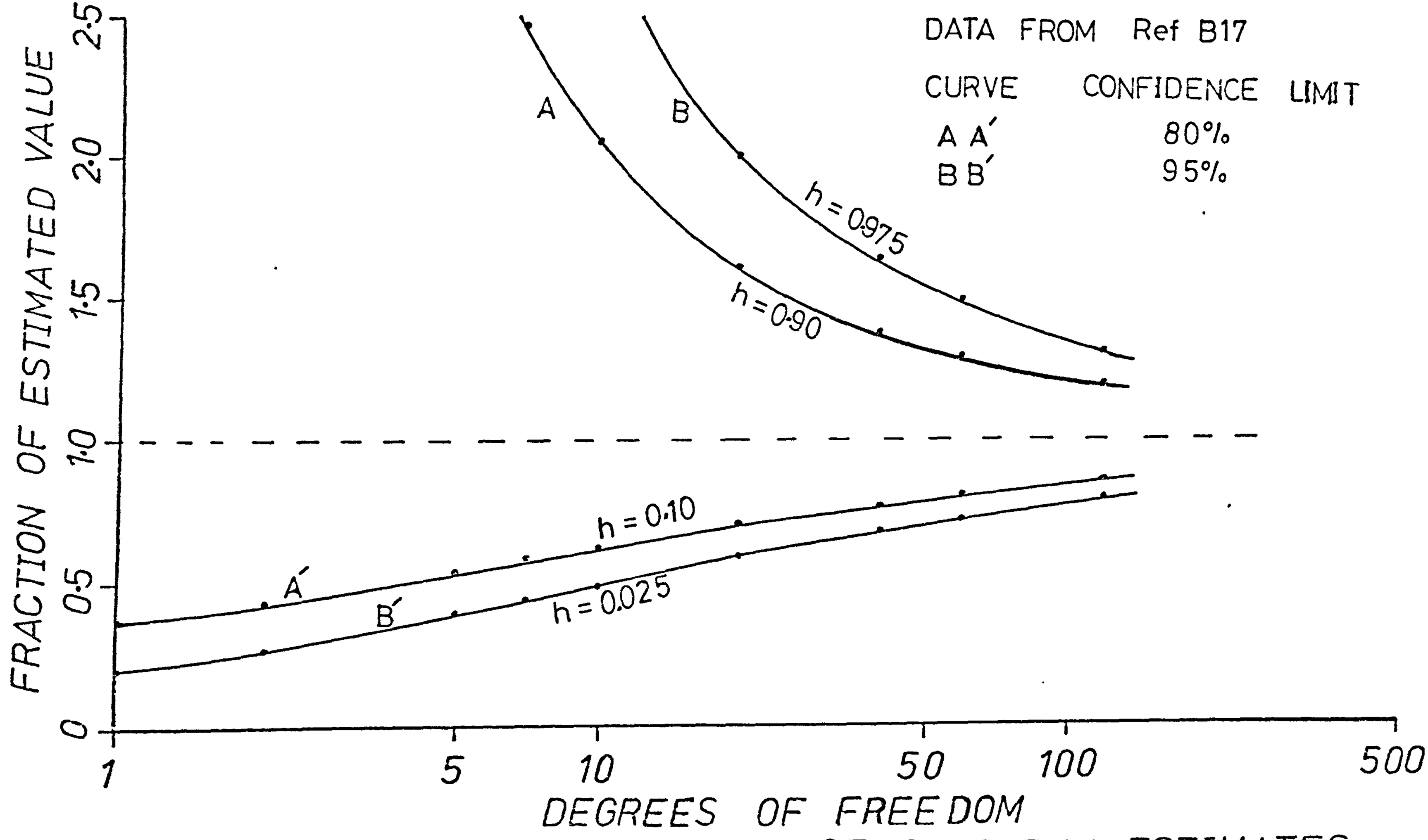

FIG. 7.1 STATISTICAL RELIABILITY OF SPECTRUM ESTIMATES

degrees of freedom, and hence higher stability.

7.4 SCOPE OF PRESENT ANALYSIS AND METHOD OF DATA COLLECTION

All the calculations were carried using the Strathclyde University ICL 1904S computer. Appendix X outlines the digital form of the equations and procedures used and also a listing of the different programs developed for these calculations.

For the void fraction data, the calculations involved determining

(i) the probability density function over a strip band $\Delta\alpha = 0.02$, as a function of the average void fraction in the band.

(ii) the power spectral density function as a function of frequency.

For each of the two sets of pressure measurement data, the calculations involved determining

(i) the probability density function of pressure over a strip band P = 10 mv as a function of the average pressure in the band.

(ii) the probability density function of the quantity $(p-\bar{p})^2$ over a strip ΔP^2 (equal to 100 mv^2) wide as a function of the average value of $(p-\bar{p})^2$ in the band, or

$$\frac{1}{M\Delta P}\sum_{i=1}^{M}(p_i - \bar{p})^2$$

which is a form of variance.

(iii) the power spectral density as a function of frequency.

(iv) The cross power spectral density and the cross correlation function as a function of frequency and time lag respectively.

A problem associated with the void fraction measurements was the low time constant of the void fraction sensor (0.1 sec). Hence the majority of the data were collected at a rate of 40 readings per sec which is $\sim$ 4 times the time constant of the unit with the hope that better results in terms of resolution would be obtained. However, the probability density function analysis carried on each single point of the record, and then on every 4th point showed almost identical results. In any case, the relatively high data collection rate was necessary for the analysis of the pressure signals.

Previous work on two phase pressure pulsations showed that the major frequencies detected were comparatively low, i.e. less than 5 Hz in general. For the purpose of this project it was thought that the highest frequency components would be within this limit too. However, to be on the safe side, the limit was taken up to 20 Hz which then determined the Nyquist or folding frequency f_c. The sampling time was thus

$$\Delta t = \frac{1}{2f_c} = \frac{1}{40} \text{ sec.}$$

or 40 readings taken per sec. This choice was supported by preliminary visual examination of some pilot records (displayed on V DU) and can also be seen by inspecting Figs. 5.10 to 5.14, which show the appropriate signals displayed on a time axis indicating that the major components are slow.

However, a few runs were carried out at a rate of 100 readings per sec (sampling interval 0.01 sec), or f_c = 50 Hz to help detect any higher components especially in the annular flow region where velocities are higher and accordingly higher frequency pulsations are more probable. However, power density analysis for such runs showed no additional higher frequency components and the highest significant frequency components detected were less than 5 Hz.

For these reasons, it was decided to use the sampling interval of 0.025 sec (rate of 40 readings per sec) which was considered reasonable when limitations of data storage and analysis computing time were taken into consideration. [Hubbard and Dukler (H6) took data readings at intervals of 0.032 sec but used intervals of 0.064 sec in their analysis]. A total of 4800 data points were collected per record corresponding to a 120 sec record length. Three channels were used (two for pressure and one for voidage) giving a total of approximately 15 K of store per run.

At the start of the power density calculations, an attempt was made to use the Blackman-Tukey method employing either Hanning or Hamming windows. Difficulties were experienced concerning negative power predictions which were severe in some cases. Thus it was decided to use the direct FFT method with the help of a fast Fourier transform subroutine given in Ref. (B16). Both, the power and cross power spectral density estimates were calculated using this

technique. A tapering window suggested by Bingham et al (B19) was applied to the data before performing the Fourier transformation. The raw spectrum estimates were then averaged over 10 estimates (M = 10) giving a total number of equivalent degrees of freedom of 20. The 80% confidence limits were calculated from Fig. 7.1 as follows:

$$q = 0.8, \quad h = 1 - q = 0.2$$

the confidence limits are

$$A = \frac{n\,\hat{S}(f)}{\chi^2_{n,h/2}} = \frac{n}{\chi^2_{n,0.1}}\,\hat{S}(f)$$

$$B = \frac{n\,\hat{S}(f)}{\chi^2_{n,1-h/2}} = \frac{n}{\chi^2_{n,0.9}}\,\hat{S}(f)$$

From Fig. 7.1, for n = 20 we get

$$A = 0.7\ S(f) \quad , \quad B = 1.6\ S(f)$$

then with 80% confidence, the true value of the power spectrum is within the following range,

$$0.7\ \hat{S}(f) < S(f) \leqslant 1.6\ \hat{S}(f)$$

After developing the program, it was checked by inputing two cosine functions of the form

$$x_r = \cos\frac{2\pi r}{N}\,k_1 + \cos\frac{2\pi r}{N}\,k_2$$

and studying the resulting spectrum estimates. The power spectrum showed two peaks at $(k_1/N\Delta t)$ and $(k_2/N\Delta t)$ with negligible leakage indicating the ability of the program to resolve the frequencies of the input signal.

For the cross correlation results, the calculations were based on implementing the direct definition of the function R_{xy}, i.e.

$$\hat{R}_{xyk} = \frac{1}{N-k} \sum_{i=0}^{N-1} x_i \, y_{i+k} \qquad k = 0, 1, \ldots m \qquad (7.31)$$

A similar result could have been arrived at (having calculated the unsmoothed raw cross power density with no tapering or windowing), by using an inverse Fourier transform on the raw power spectra. Sande (S22), however showed that the usual correlation function was not obtained by this procedure but rather a circular cross correlation functiou defined by

$$\hat{R}^{c}_{xyk} = \frac{N-k}{N} \left[\hat{R}_{xyk} + \hat{R}_{yx(N-k)} \right] \qquad (7.32)$$

The author found it easier to employ the direct definition (equation 7.31) of the correlation, which gives the positive part of the correlation only (i.e. time lag > 0). Further calculations are needed to arrive at the negative part, and was done using the equation

$$\hat{R}_{yxk} = \frac{1}{N-k} \sum_{i=0}^{N-1} y_i \, x_{i+k} \qquad k = 0, 1, \ldots m \qquad (7.33)$$

since

$$R_{xy}(-\tau) = R_{yx}(\tau) \qquad (7.34)$$

where τ is a time lag.

7.5 CHARACTERIZATION OF FLOW PATTERNS

In the following section the results of applying these discriminating criteria to the different flow patterns are

discussed separately. Because of the large number of graphs which resulted from the analysis, only few specimens are given in this Chapter (Figs. 7.2 to 7.7); the others are shown in Appendix Y.

7.5.1 ANALYSIS OF PRESSURE AND VOID FRACTION TRACES

The characterising criteria for the (local) void fraction and pressure signals are the shape of the trace, the size of the fluctuations and the frequency components present. However, the average value of the local void fraction measurement (0 to 1) adds to the diagnostic powers. It is worth mentioning here that in symmetrical systems, the local void fraction determined using a pencil beam normal to the tube centre line is equal to the overall mean void fraction at the measuring station. This is not the case for asymmetrical systems. However, in many of the asymmetric conditions encountered here, the difference between the average local void fraction and the overall mean void fraction (measured by the ionisation chamber, single shot method) was not great. In the data presented in Figs. Y1 to Y28, values of the overall mean void fraction $\bar{\alpha}$ are indicated for comparison with the local void fraction values α_{loc}.

Since the frequency response of the local void fraction unit is low, it is worth mentioning that this could result in a false indication being obtained when the pulsations are too fast for the instrument to detect.

Fig. Y1 shows the three signals for an empty tube condition, i.e. the zero readings of the pressure sensors

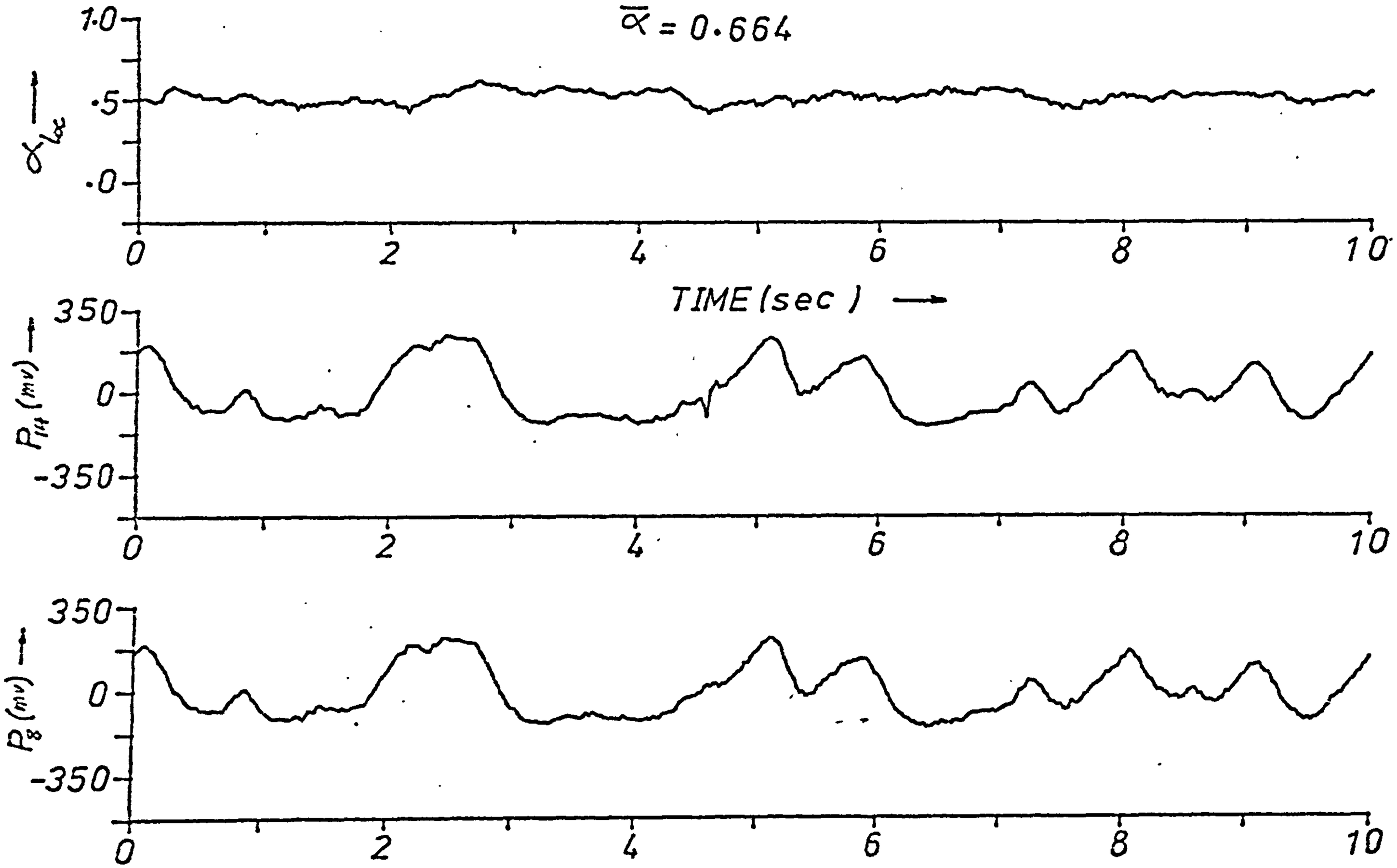

FIG. 7.2 TEST RUN 121405 (SLUG)
CODE (X)
PRESSURE AND VOID FRACTION SIGNAL TRACES

DISTORTED PAGES IN ORIGINAL

FIG. 7.3 PRESSURE PROBABILITY DENSITY RESULTS (CODE X)

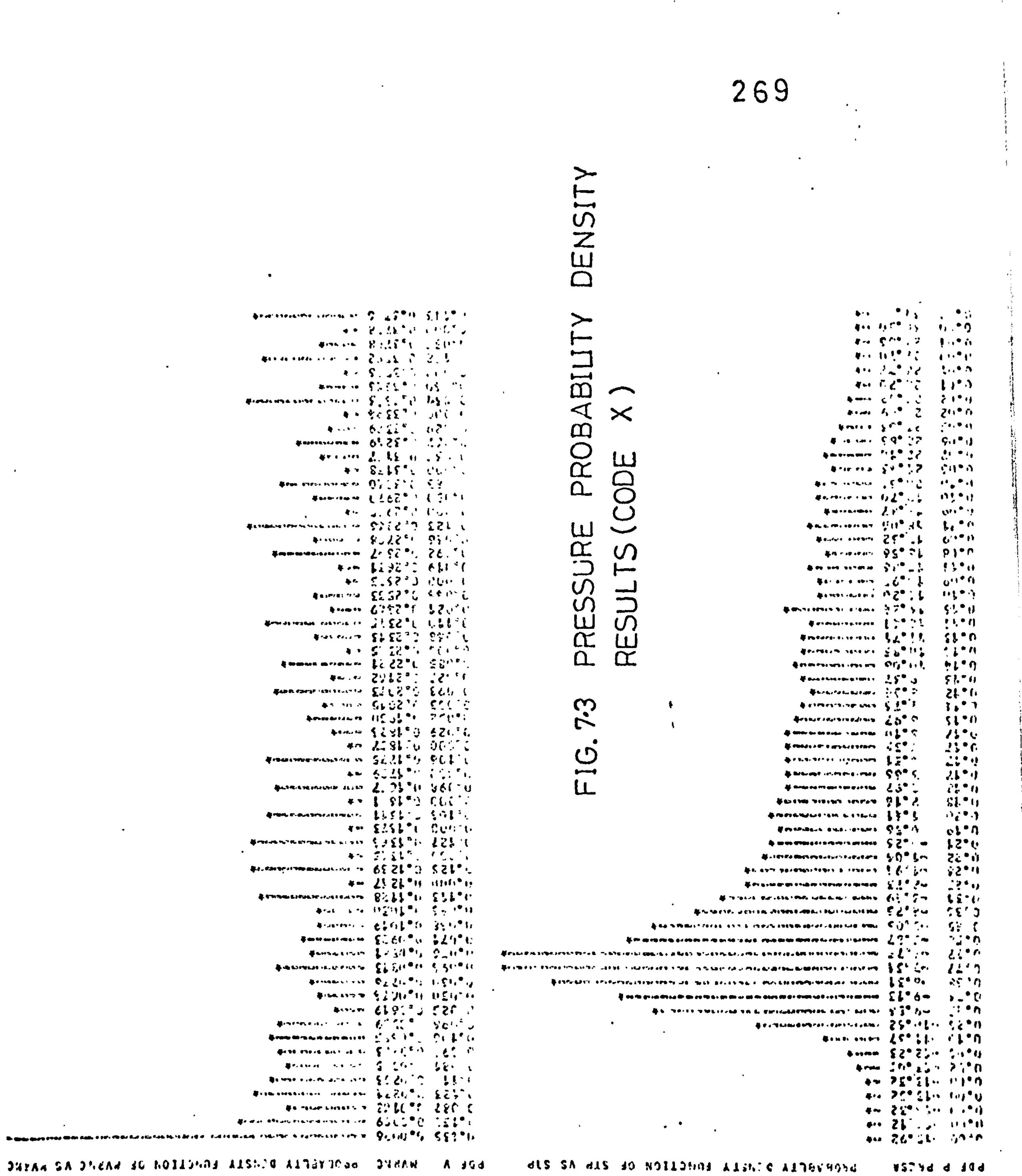

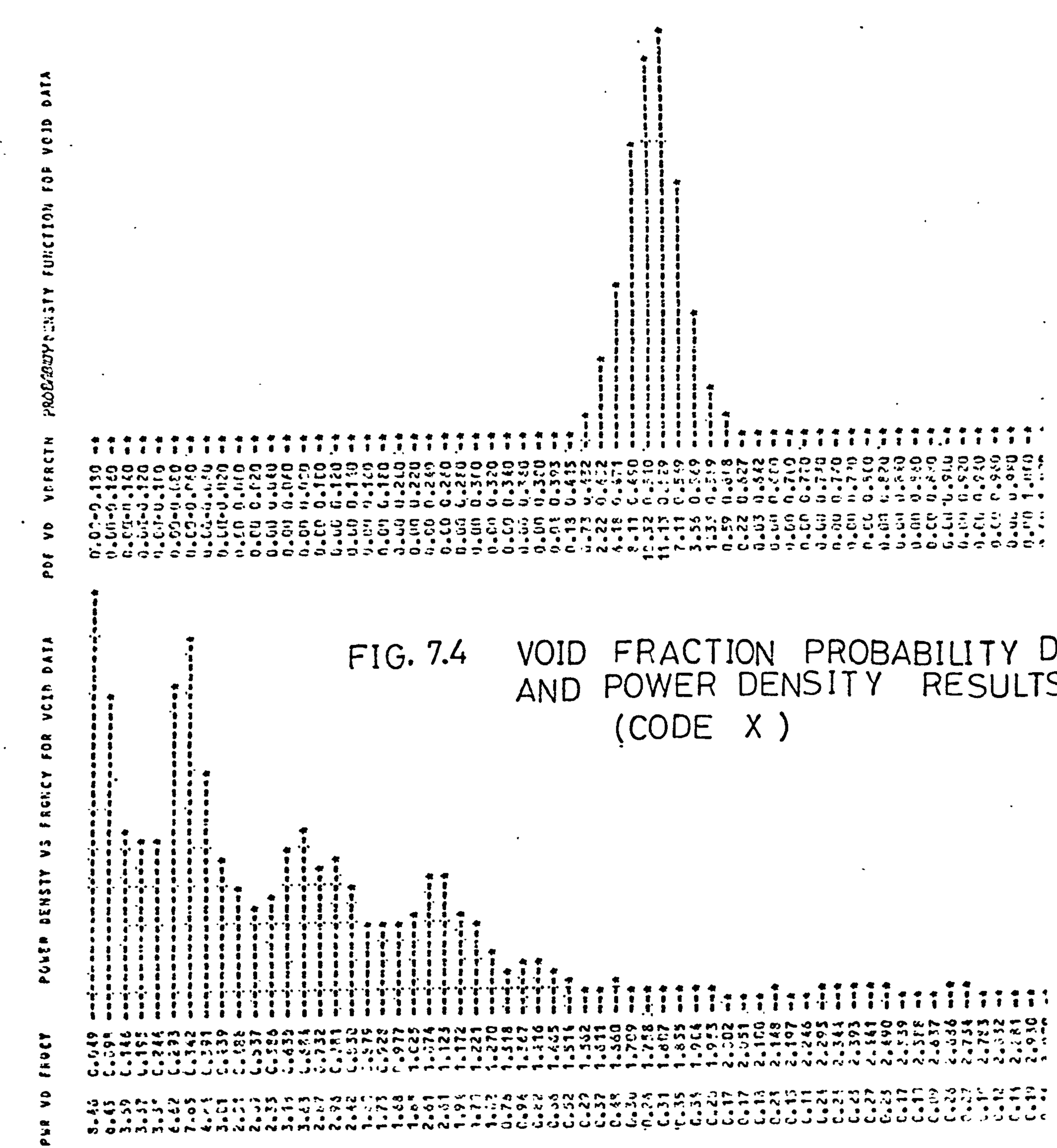

FIG. 7.4 VOID FRACTION PROBABILITY DENSITY AND POWER DENSITY RESULTS (CODE X)

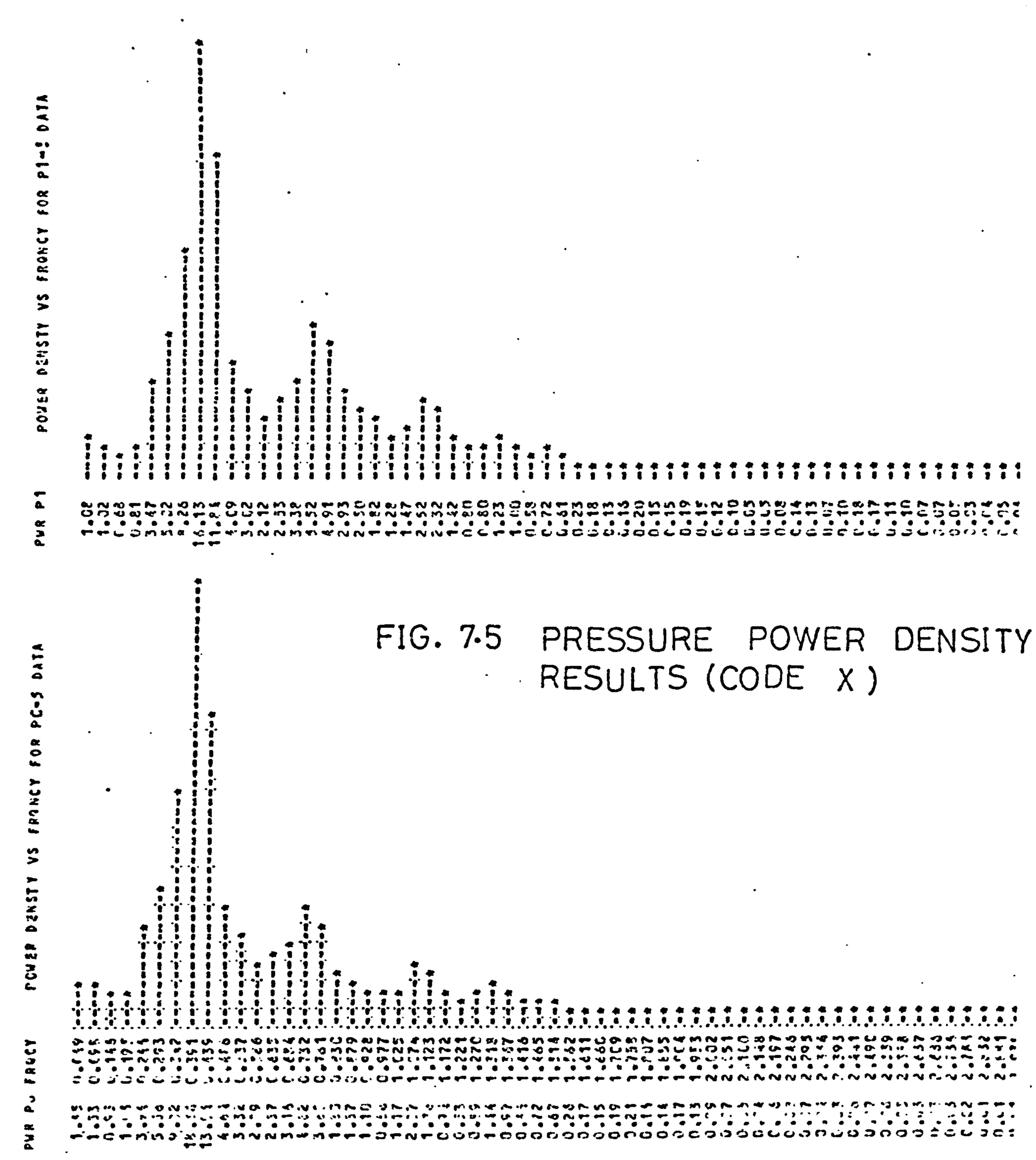

FIG. 7.5 PRESSURE POWER DENSITY RESULTS (CODE X)

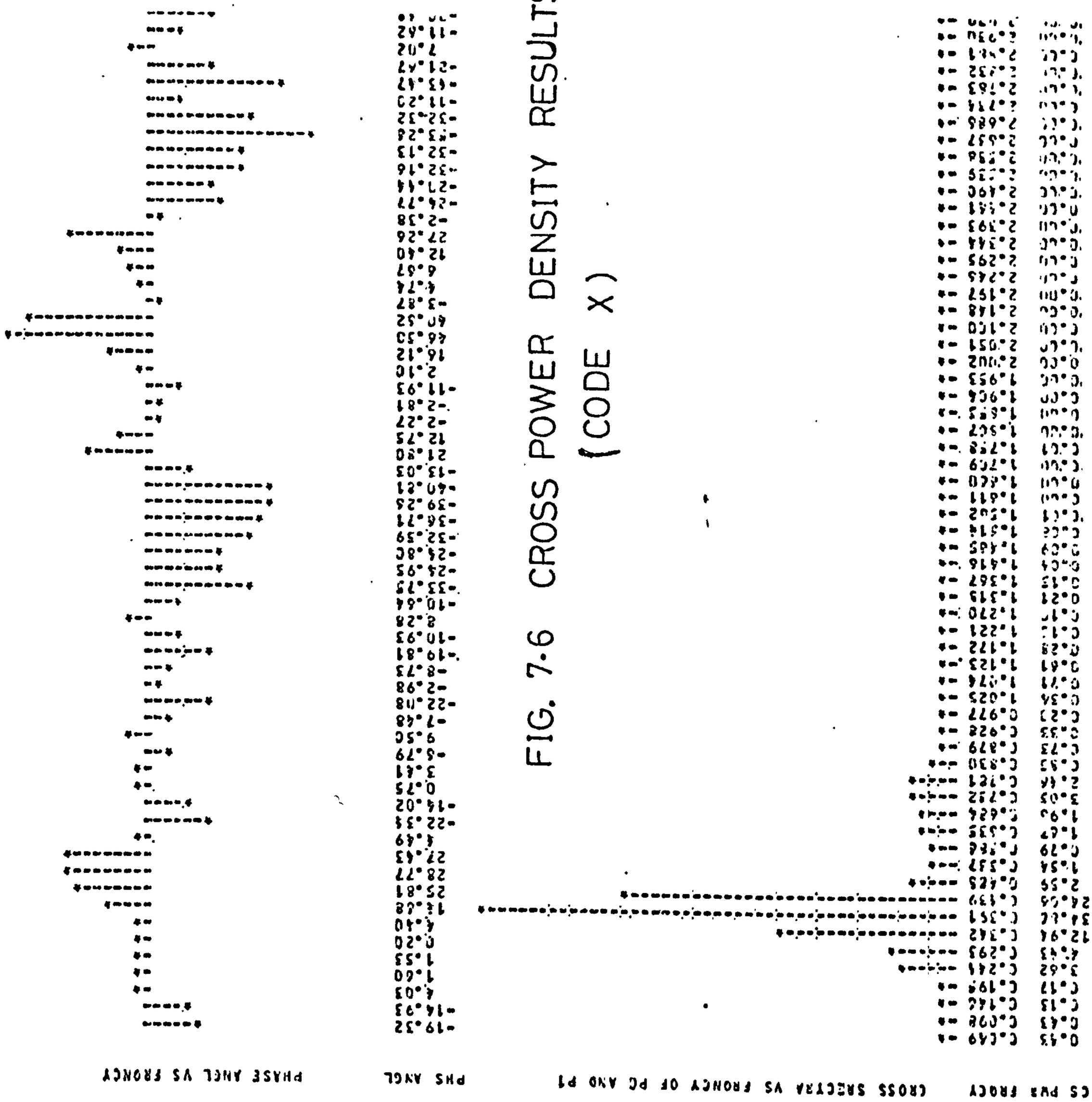
CROSS POWER DENSITY RESULTS
(CODE X)
CROSS SPECTRA VS FRQNCY OF PC AND P1
PHS ANGL
PHASE ANGL VS FRQNCY

FIG. 7.6

FIG. 7·7

TEST CODE X
CROSS CORRELATION
RESULTS

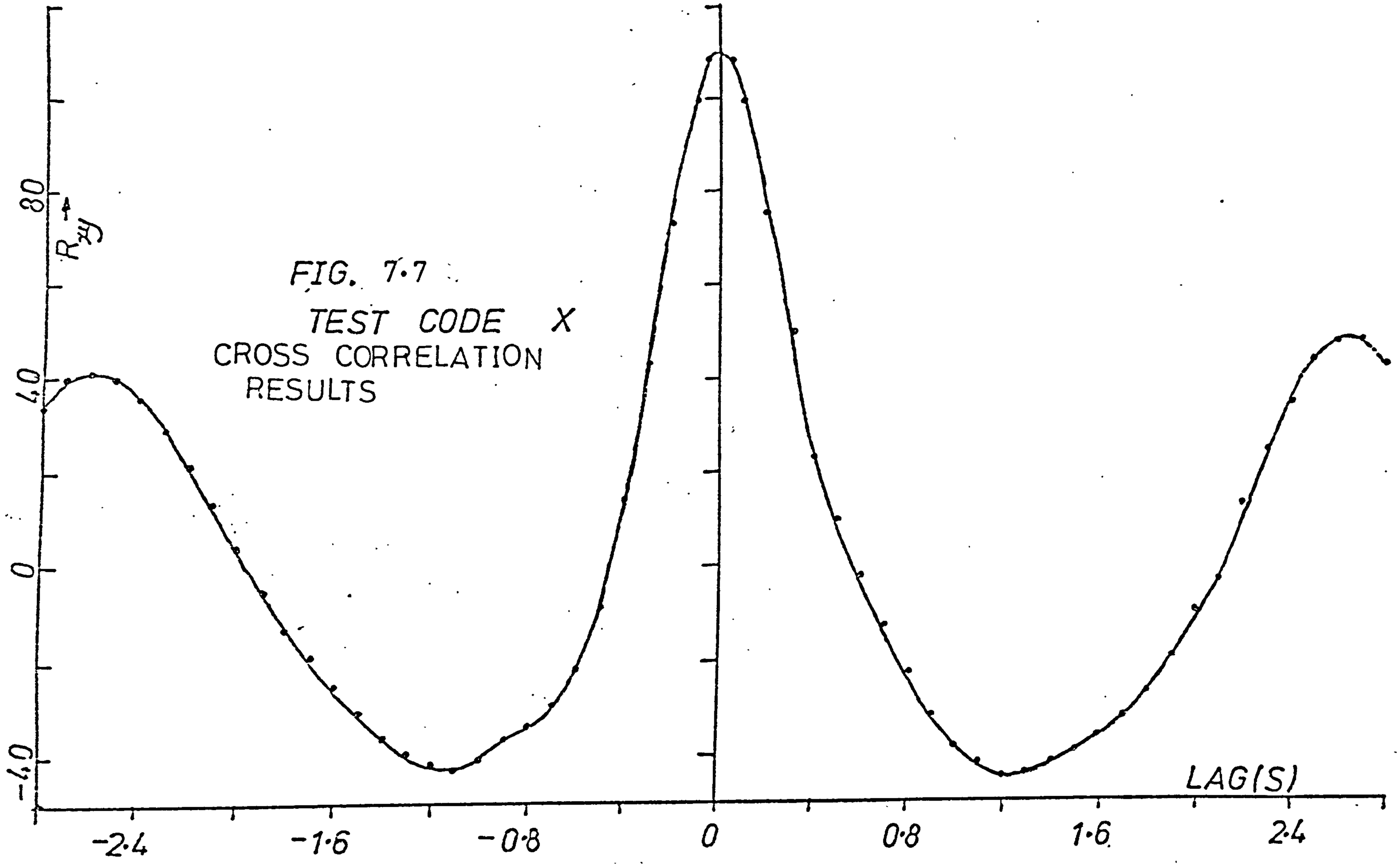

and the maximum reading of the void sensor. It is obvious that transducer P_8 (originally 5 v output at 100 psia) is less stable than transducer P_{14} (5 v output at 50 psia) which, probably is caused by the increase in the transducer amplifier gain of P_8 to produce an identical signal to that of P_{14} (i.e. 5 v output at 50 psia). This background noise will modify the actual pressure signal whenever the signal level is comparable in magnitude to that of the noise. This is clear by examining Fig. Y2 and Y3 for stratified and wavy flows plotted to the same scale of Fig. Y1. From visual observation, also from Fig.5.15 which gives the location of these points on the flow pattern map, the wavy flow condition is identified as belonging to the smooth, long wavelength type of wavy flow. The behaviour of the local void fraction signals and their average values are identical for both records.

The other wavy flow conditions (Figs. Y4 and Y5) show somewhat different trends in that the signals contain bigger and more defined pulses, also the local void fraction levels are much higher. These signals belong to the rough wavy conditions prior to the development of annular flow.

Figs. Y7 and Y10 display more or less identical signals in that they all show triangular shape pulses with high frequency components superimposed, also the local voidage level is high which is symptomatic of annular flow conditions.

Figs. Y12 to Y14, also Fig. Y16 show a distinct character is that the slow components of pressure are

predominant and appear in a form of square wave or a hump like shape. These correspond to slug type of flow as one would expect, with the slug formation being represented by a hump structure in the pressure and local void fraction traces. The pressure traces of Fig. Y15, on the other hand show some similarity to the annular flow traces, although the local void fraction traces are different and show clearly a slug type structure. Fig. Y17 was also identified visually as slug flow, but shows a somewhat different character, probably due to the higher slug frequency evident from the traces (void sensor is too slow to respond). However this run corresponds to the high air and water flow rates conditions where the flow structure becomes very milky in appearance, and difficult to distinguish.

It is interesting to note that in Figs. Y12 and Y13 there is almost no, or very little, time lag between the two pressure signals, which is rather strange considering the relatively low frequency of the pulses (c.f. Figs. Y14 and Y16). In addition, one might expect the local void fraction trace to show more visible and distinguished variations similar to those of Figs. Y14 to Y16. A possible explanation is that the slugs must have formed after the local void fraction measuring station (i.e. $>$ 12m from inlet). Visual observation supports this conclusion where the slugs were reported to have been formed at $>$ 12m from inlet (i.e. within 4m from exit).

Bubbly flows (Figs. Y19 and Y20) show both high and low frequency components and also display some similarity to annular flows (Figs. Y8 and Y10) and some slug flows (Fig. Y15), however they are different by virtue of the low local

voidage readings.

Plug flows (Figs. Y21 and Y22) also show high frequency components and some trends in their pressure signals are similar to that of annular flows. Their low local voidage level signal, however, show a slug type behaviour, as expected.

Fig. Y23 shows the condition corresponding to water flowing alone in the pipe at a superficial velocity of about 1.4 m/sec. The presence of high frequency components is very clear and probably explains their presence in plug flow traces of Fig. Y22 ($\sim$ 1.3 m/sec) and, to a lesser extent, in Fig. Y21 ($\sim$ 1 m/sec).

Figs. Y24 to Y27 show traces of some repeat tests detailed in Table 5-2 taken at the higher rate of 100 readings per sec whilst Fig. Y28 shows a repeat test taken at a lower rate of 10 readings per sec. These figures display the same features discussed earlier.

The above discussion demonstrates the usefulness of careful inspection and examination of the pressure and local void fraction pulsation traces and their magnitude in identifying the different flow patterns. At instances where the pressure signals failed to give a clear picture, the local voidage signal did so and vice versa.

In conclusion

(i) the stratified and smooth wavy flows show identical pressure and local voidage behaviour.

(ii) the rough wavy flows show more similarity to annular flows, than to stratified or smooth wavy flows.

(iii) Most slug flows display distinct trends and characteristics in both pressure and local void fraction behaviour as might be expected. Plug flows show similar local voidage behaviour.

7.5.2 PROBABILITY DENSITY ANALYSIS RESULTS

The basic approach here is based on characterising the magnitude of the pressure and local void fraction pulsations which, for the pressure sensing, is dependent on flow parameters (other than the flow pattern) such as fluid properties, system pressure behaviour and the level of pressure operation, etc., and hence is not as powerful as the local void fraction. In fact, similar flow patterns could show a wide range of pulsations (e.g. slug flow discussed above). Nevertheless the results presented in Section 7.5.1 suggest that a probability density approach based on both pressure and local void fraction signal should prove useful.

Figs.29 and 30 show the zero pressure reading probability density results for the two transducers which again reflects the higher background noise level of the P_8 transducer. The main features in these and other results for the two pressure records are almost identical, and hence only the results for the more stable transducer are discussed. Fig. Y58 shows the tube empty condition probability density results for the local void fraction sensor together with the power density plot which will be discussed later. The results show some randomness, as expected at this γ -ray intensity, however the lower the

local voidage (smaller intensity of the γ -ray beam) the higher the random errors will be which reach its maximum at zero local voidage. This is clearly seen from Fig. Y80 which gives the results for the tube full condition, i.e. zero local void fraction. The results indicate finite probabilities even at $\alpha \pm 0.1$.

Fig. Y31 and Y32 show narrow probability distributions similar to those of Fig. Y30, indicating small pressure fluctuations. The local void fraction (Figs. Y59 and Y60) behaves in a similar fashion with its average value falling near 0.4. These belong to stratified and smooth wavy flows.

Rough wavy flows show relatively narrow probability density distributions for pressure (Figs. Y33 and Y34), but display different local void fraction behaviour (Figs. Y62 and Y61) with an average value greater than 0.7.

Annular flows (Figs. Y36 to Y39) show a wider pressure probability band and, expectedly, the variance starts to show the familiar J-shape distribution which tails off comparatively quickly. The void fraction results (Figs. Y64 to Y67), however show narrow bands concentrated at $\alpha > 0.7$, corresponding to the range of occurrence of annular flows.

Figs. Y41 to Y43 show a very distinct characteristic where the pressure probability band is quite wide. Expectedly the variance does not die down quickly, corresponding to slug type flows. Figs. Y44 to Y46, although belonging to slug flow, show probability band widths similar to those of annular flows.

The local void fraction probability graphs for slug flows might be expected to show a two hump distribution, one corresponding to the liquid slug and the other to the air plug. As mentioned above, if the slug frequency is high, the sensor is not able to respond to these effects. Also if the slug is frothy, then the flow structure becomes more homogeneous.

Figs. Y69 to Y71 show comparatively wide bands with the results of the first two graphs showing only one bump. This was probably due to the slugs forming near but after, the void fraction station as explained earlier. The conditions of Fig. Y71 nearly produced a two hump structure while those of Figs. Y72 and Y73 show clearly such a behaviour. These figures correspond to the conditions of Figs. Y44 and Y45 where pressure behaviour showed trends similar to that of annular flow. The results in Fig. Y74 show a comparatively narrow band at voidage level less than 0.4, similar to those of stratified and smooth wavy flows.

The results in Figs. Y48 and Y49 show relatively narrow pressure probability bands, but the local void fraction results (Fig. Y76 and Y77) show wide probability bands concentrated near $\alpha_{loc.} = 0.1$. These were identified visually as bubbly flows.

The results in Figs. Y50 and Y51 were identified as belonging to plug flows and these show trends similar to wavy flow, i.e. relatively sharp bands. However, the corresponding local void fraction results show identical behaviour to that of slug flow.

The results given in Figs. Y53 to Y57 for pressure and Figs. Y81 to Y85 for local void fraction belong to the repeat tests and are identical to their sister graphs discussed above.

Generally speaking, although the results of the pressure probability graphs do not always agree with those of the local void fraction, both seem to compensate for each other and in fact more information could be gained about the system. However, the local void fraction sensor appears to be the more powerful tool, especially when local effects are important. For example, while the pressure pulsations for some tests showed a slug type behaviour, the local void fraction did not. The range and size of the local pressure fluctuation at a point is influenced by the overall pressure behaviour of the system, and not local effects only.

In conclusion the results of the probability density study confirms the comments given at the end of section 7.5.1.

7.5.3 POWER SPECTRAL DENSITY ANALYSIS RESULTS

The local void fraction results given in Figs. Y58 to Y85 are discussed first bearing in mind that the usefulness of the technique is limited due to the following factors,

(i) the slow response time of the apparatus.

(ii) the superposition of a random noise on the actual signal.

Condition (ii) suggests that if the variations in local void fraction are small or random then the resulting power

density distribution will show similar trends to that of noise. Of all the flow patterns encountered, one would expect slug and plug flows and perhaps smooth wavy flows (i.e. big changes in α) to show different trends, if the variations in the local void fraction are within the response time of the apparatus.

Fig. Y58 shows the results for the tube empty condition ($\alpha = 1$) and here the spectrum is due entirely to random noise. Fig. Y80 gives the results for the tube full condition ($\alpha = 0$) and again the spectrum is due to the random noise. The spectrum of a random noise is flat by definition but, due to the limited time of observation, the above result approximates to such a condition with Fig. Y80 being flatter due to the higher noise level.

Fig. Y60 shows a high power near zero frequency, suppressing all the noise components present in the signal. This corresponds to smooth wavy flows. Stratified flow results (Fig. Y59) also shows a high power near zero frequency, but are not large enough to suppress the power due to the random noise at other frequencies.

Figs. Y61 and Y62 produced identical results to that for the tube empty condition, i.e. random noise with comparatively higher power being given to lower frequencies. These correspond to the rough wavy flow conditions where the local void fluctuations are expected to show small variations, not enough to suppress the noise bands.

Annular flow results (Figs. Y64 to Y68) show similar trends since the fluctuations are expected to be small too.

Figs. Y69 and Y70 indicate a clear depression in the power at high frequencies (spectrum tails off quickly) with more power being given to low frequencies. This is a reflection of the bigger variations in local void fraction as is seen from the width of the probability density results in the same figures. These correspond to the conditions where the slugs were formed near, but after, the local void fraction sensor. Figs. Y71 to Y73 display a wide range of structures characterised by severe depression in power at high frequencies and a band like spectrum, corresponding to slug flow conditions.

Fig. Y74 displays an almost flat spectrum corresponding to a noise-like signal. This was identified as slug flow but, as can be seen from the probability density results, the variations in local void fraction are small and do not approximate to the expected two hump structure.

Figs. Y76 and Y77 produce similar trends and correspond to bubbly flow conditions.

As expected, plug flows (Figs. Y78 and Y79) show spectra with more defined structures, characterised by severe suppression of power at high frequencies, similar to those of slug flows.

The results of Figs. Y81 to Y85 for the repeat tests supports the conclusions that signal like data produce power spectral results that tail off very quickly, i.e. very little power at high frequencies. For other flow conditions the spectrum declines relatively slowly giving more power to high frequencies. This means that such a technique is useful for characterising slug and plug type of flows, and

probably smooth wavy flows too.

We next turn to discuss the power spectral density results for the pressure signals. In each figure, the bottom plot gives the P_8 transducer results, while the top ones give that for P_{14}.

Fig. Y86 shows the power spectral density results for the two transducers background noise. The P_8 transducer has $\sim$ 34% of the power concentrated near zero frequency indicating that a zero impulse will be detected whenever the noise level is comparable to the signal. For the P_{14} transducer the power observed is $\sim$ 7%. It is worth mentioning that a zero impulse will also be detected if,

(i) the transducers start to drift such that the apparent signal is a superposition of the actual signal and a term bt, where b is a constant, and t stands for time. In this case the constant b could be determined (from the slope of the signal plotted versus time) and the trend then removed.

(ii) the signal is modulated by a low frequency component. To remove this, a rough estimate of the low component period is obtained from the original trace, then the record is divided into several sections, (equal nearly to the period) and the average value of the signal calculated in each and removed from the data in that particular section. Hence the name 'moving average'.

(iii) the power leaks from higher frequencies.

Visual observation of the traces showed that (i) and (ii) were negligible for most of the data and the leakage reduction technique was employed in the calculations to reduce (iii). Another important factor affecting the accuracy of the analysis is the frequency response function of the whole unit, i.e. from the sensing element to the ADC unit of the data acquisition system, which must be flat. However, there is no easy way by which one can perform such a check. The manufacturers claims that the unit is feasible up to 5 kHz, and the cutoff frequency of the co-axial cables carrying the signal were found experimentally to be in excess of 1 kHz, with a flat response below that.

Stratified flow results (Fig. Y87) reflect the transducer characteristics (Fig. Y86), since the size of the pressure pulsations are comparable to the noise.

The results for the smooth wavy flow condition (Fig. Y88) reflect the features of stratified results, however they also show peaks near $\sim$ 3 Hz and $\sim$ 10 Hz. The presence of the peaks suggests that up to 10 waves pass the transducer per sec, which contradicts visual observations. The author cannot ignore the fact that the 10 Hz component could be due to aliasing of the 50 Hz mains signal which is superimposed on the actual data, or

$$f_{alise} = \pm 2k\, f_c \pm 50 = \pm 40k \pm 50 \text{ Hz}, \quad k = 1, 2, 3, ..$$

$$= \pm 10 \text{ Hz}$$

This could have been caused by some bad earthing corresponding to that particular record, and will be ignored in the discussion.

Fig. Y89 shows more power at the high frequency side of the spectrum especially for the P_{14} results. Fig. Y90 show some power at high frequencies with most of the power being concentrated at the low frequency side. The author cannot discount the probability of having some exit effects interference as one might guess by inspecting the results given in Fig. Y89 for the P_{14} transducer.

Annular flow results in general show some high frequency components and display a wide variety of structures, such as a broad band (Fig. Y92), a narrow band (Fig. Y93), or even a multiband (Figs. Y91, Y94 and Y95).

Slug flow results (Figs. Y97 to Y101) are characterised by a more defined spectra which tails off quickly producing almost negligible power at high frequencies. The only exception is probably the results of Fig. Y99.

The results of Fig. Y102 indicate a large zero frequency components which suppress all other frequencies. This is caused by the presence of some low frequency components superimposed on the signal which can be seen by inspecting the original pressure traces (Fig. Y17), especially for the P_8 transducer. The reason for the presence of such low frequency component is unknown, however it was observed only in this test which corresponds to the highest air and water flowrates.

Fig. Y103 which corresponds to transition from bubbly to frothy slug shows spectra which cannot be distinguished from annular flow ones.

The spectra displayed by bubbly flows (Figs. Y104 and

Y105) are similar to those of slug flow in that negligible power is present at high frequency components, however the power is more uniformly displayed among the frequencies in the band (Fig. Y105).

Figs. Y106 and Y107 show the results for plug flows which display trends found in both slug and annular flows. Fig. Y107 shows a $\sim$10 Hz component.

Fig. Y108 is the pressure spectrum for the water flowing alone in the pipe at U_{sf} = 1.4 m/sec and also shows a $\sim$ 10 Hz component. These could be due to aliasing of the mains signal which is superimposed on the actual data as explained earlier.

The repeat test results (Figs. Y109 to Y113) support the above comments. In conclusion

(i) stratified and smooth wavy flows show similar trends

(ii) rough wavy flows show high frequency components and behaviours similar to annular flows

(iii) bubbly and slug flows produce negligible power at high frequencies.

7.5.4 CROSS POWER SPECTRAL DENSITY RESULTS

This analysis isolates only those common frequency components present in the two pressure signals and the equivalent of such procedures in the time domain produces what is known as the cross correlation technique. The cross power density results are shown in Figs. Y114 to Y141 in terms of the modulus (bottom plot) and the phase angle (top plot).

The transducer background signals show ~ 90% of the power being concentrated near zero frequency (Fig. Y141).

The stratified and smooth wavy results (Figs. Y115 and Y116) also show high power concentrated at very low frequencies. The peak near 10 Hz (Fig. Y116) is ignored as explained earlier.

Fig. Y117 shows considerable power at high frequencies while Fig. 118, although displaying some high frequency components, shows most of the power concentrated at low frequencies. These belong to rough wavy flow conditions.

Most of the annular flows show a wide range of spectra, from single peaked (Fig. Y121) to multipeaked Figs. Y120, Y122 and Y123) concentrated at low and mid frequency. With the exception of Fig. Y120, most of the peaks are relatively broad.

Slug flows are mostly single peaked (Figs. Y125, Y126, Y128 and Y129), or sometimes double peaked (Fig. Y127) mostly at low frequencies. The only exception is Fig. Y127 which displays comparatively high power at mid frequencies similar to those of Fig. Y121 for annular flows.

The results of Fig. Y130 reflect the problems that could arise in frequency analysis especially after examining the original traces (Fig. Y17) where the presence of a high frequency component is obvious.

Bubbly flow results may display similar trends to those of slug flows (Fig. Y132), or broader low frequency bands (Fig. Y133) approaching the condition of flat spectrum.

Fig. Y134 shows a slug character while Fig. Y135 shows a bubbly character and both belong to plug flows.

The repeat tests results (Figs. Y137 to Y141) produced consistent trend to the original test data.

In conclusion, whilst certain flow patterns show similar trends there appears to be some which show different characteristics. Nevertheless, some general conclusions can be drawn as follows.

(i) Stratified and wavy flows show similar trends with the power mostly concentrated near zero frequency.

(ii) Annular and rough wavy flows produced a wide range of frequencies and were the only flows to show high frequency components. Most of the spectra were multipeaked.

(iii) Slug, plug and bubbly flow in general produced low frequency components other than zero which could be a narrow band (most slug flows) or two or more broad bands (plug and bubbly flows).

7.5.5 CROSS CORRELATION ANALYSIS RESULTS

Before starting the discussion of these results, it must be borne in mind that the cross correlation function is a continuous function of time, and the author took the liberty of connecting the points plotted in Figs. Y142 to Y170 by a smooth curve. This is a standard procedure (unless there are reasons to believe the opposite, as shown in one example later on).

Fig. Y142 gives the results of correlating the two transducers' noise record which show an oscillating

character similar to that of a sin z/z function, and hence the process is a band limited one (Appendix X). This is indeed the case as was shown earlier (Fig. Y114), where around 90% of the power was concentrated in the band 0 - 0.05 Hz.

The results plotted in Figs. Y143 and Y144 also show similar trends, but to a lesser extent, reflecting the tendency of such patterns to produce the equivalence of a relatively narrow band process.

The rough wavy results (Figs. Y145 and Y146) show symmetrical correlations which indicate that the pressure time histories detected by the two transducers are identical. They also show that the pressure signal at P_{14} leads that at P_8. The positive correlations indicate that an increase in P_{14} causes an increase in P_8.

Annular flow data (Figs. Y147 to Y151), show symmetrical positive correlations at low water flow rates and symmetrical negative correlations at high water flowrates. They also indicate clearly that the pressure signal at P_{14} leads that at P_8, which means that the signals collected were largely due to the system pressure behaviour rather than local effects; and that the pulsations of the system pressure were caused by the exit.

In slug flows, however, the local pulsations are high compared to exit disturbances, and also the discontinuities in the phase when more than one slug is present, attenuate pressure propagation phenomena. One would not expect such flows to produce symmetrical correlations because more than

one slug could exist in the pipe at one time, and besides a slug could form anywhere. Accordingly, a multipeaked structure might be expected as shown in Figs. Y155 to Y157. Figs. Y153 and Y154 show symmetrical correlations and indicate that the pressure signal at P_8 leads that at P_{14}, or is in phase with it. This means that the slugs could have formed between the local void fraction station (i.e. 12m from inlet) and the P_{14} station (i.e. 14m from inlet) or even after it. The results of Fig. Y158, showed a multipeak structure, but the effect of a sin z/z function cannot be eliminated due to the relatively high power found near zero frequency (Fig. Y102).

Bubbly flows show symmetrical correlations, both negative (Fig. Y160) and positive (Fig. Y161). Also both showed that P_{14} leads P_8, but with a comparatively larger time lag than that of annular flows indicating lower sonic velocity in the latter case.

Plug flows also show both negative (Fig. Y162) and positive (Fig. Y163) correlations, multiple or single peaked but less symmetric. However the way in which Fig. Y162 is plotted actually filters out the higher frequency component which otherwise would have appeared as shown in Fig. Y164. This component corresponds to f $\sim$ 10 Hz and this was present also in the pressure record for water flowing alone in the pipe at nearly the same superficial velocity. However mains interference as explained earlier cannot be excluded.

Fig. Y165 gives the results for water flowing alone in

the pipe which shows symmetrical positive correlation with P_8 leads P_{14} by small time lag as expected.

The results given in Fig. Y166 to Y170 for the repeat tests confirms the comments mentioned earlier.

It is interesting to estimate the pressure signal propagation velocity (which is, at least, related to the velocity of sound) which can be obtained from the ratio of the distance between the two sensing points and the time lag between the signals. The time lag can be obtained from the cross correlation graphs (where symmetrical characteristics were obtained) as the displacement of the peak from the zero time axis. A normal procedure would be to fit a quadratic equation to the curve near the peak and use this to determine the exact location of the peak. However, for the purpose of this exercise, it was thought sufficient to estimate the time lag directly from the graphs.

(i) Single Phase Water Flow:

Here it is to be expected that the pressure signal propagation velocity is close to the value of the sonic velocity in water and, from Fig. Y165, the average time lag of $\leqslant$ 0.005 sec gives a sonic velocity $\geqslant$ 1198.6 m/sec, which confirms this (water velocity is taken as $\sim$ 1.4 m/sec).

(ii) Bubbly Flows:

In two phase flows, in general, the sonic velocity is much less than that in either phase, this being partly caused by the phase discontinuities in the flow structure. From Figs. Y160 and Y161, the average

time lag $\simeq$ 0.075 - 0.085 sec and hence the corresponding pressure propagation velocity is $\simeq$ 74.6-84 m/sec (mean mixture velocity is taken as $\sim$ 4 m/sec).

By considering bubbly flow as a fluid with average properties, i.e. homogeneous flow and for $\rho_f c_f^2 \gg \rho_g c_g^2$, and $\rho_f \gg \rho_g$ (i.e. air-water mixture near atmospheric pressure), we have (Ref. W1),

$$C_{tp}^2 = \frac{\rho_g}{\rho_f} \frac{C_g}{\alpha(1-\alpha)} \qquad (7.35)$$

Substituting the values from Table 5-2, for test runs code E and D, we get

$$C_{tp} \simeq 48.8 - 52.6 \text{ m/sec}$$

where C_g is the sonic velocity in air taken as 331.4 m/sec.

The slightly higher values obtained from the experimental graphs can perhaps be explained by the fact that the bubbly flow observed experimentally was not completely homogeneous (as required by equation 7.35) but had much less bubble concentration near the bottom of the pipe.

(iii) Annular Flows:

For annular flows (and indeed for all separated flows) it is difficult to visualise the propagation phenomena, nevertheless one can estimate the pressure signal propagation velocity using the same procedure. From Figs. Y166 to Y168, the average time lag of $\simeq$0.012 - 0.016 sec gives a pressure propagation

velocity relative to the mixture of $\simeq$ 375-500 m/sec (with an air velocity of $\sim$ 25 m/sec). This is higher than the velocity of sound in air alone and the following comments are relevant in explaining this.

Henry et al (H5) found that, in stratified flow, the velocity of pressure wave propagation was equal to the sonic velocity of air, no matter whether the pressure pulse was initiated in the gas or the liquid phase. However their simulated slug flow data (air-water mixture) showed velocities always greater than the sonic velicity in air and approaching that of liquid at low voidages. Evan et al (E3) found that in annular flows, the propagation was primarily through the core, and that the axial inhomogeneities there produced a wide variation in the measured acoustic velocity.

In spite of these difficulties, it can be seen that the pressure pulsation data also offer possibilities in the field of sonic velocity measurements in addition to flow pattern determination.

In conclusion, and apart from its usefulness in estimating pressure signal velocities, the following flow pattern effects were noticed.

(i) stratified and smooth wavy flow showed a superimposed oscillatory function indicating a strong band limited process behaviour.

(ii) annular and rough wavy flows showed symmetric correlations with small time lags.

(iii) slug and plug flows showed less symmetrical, but more multipeaked correlations. Bubbly flows, whilst showing a symmetrical correlation, had time lags much greater than those for annular flows.

The analysis of results presented in sections 7.5.1 to 7.5.5 showed that certain flow patterns did show similar trends in general and can be grouped in one category. However there were few exceptions, where results did not tie in with the general character of the respective flow pattern. In addition there were problems associated with the stability of the P_8 transducer and the low time constant of the local void sensor. Nevertheless, when the local void fraction and pressure results were combined, produced a powerful tool which identified flow patterns adequately.

In general the following groups of flow patterns showed much of a similarity within themselves.

(i) stratified and smooth wavy.

(ii) annular and rough wavy.

(iii) slug, plug and probably bubbly.

CHAPTER 8 THEORETICAL ANALYSIS

CHAPTER 8 THEORETICAL ANALYSIS

The experimental results presented earlier in Chapter 6 clearly showed the effects of flow pattern on the friction multiplier and void fraction data obtained. It was also apparent that only three main groups of flow patterns required to be considered and identified in order to define the different effects. (These findings were consistent with the 'preliminary' results obtained from the flow pattern sensors, presented in Chapter 7.)

In this chapter these three main groups of flow patterns are defined, or characterised, on the basis of discontinuities or transitions in the experimental pressure drop and void fraction characteristics, the groups being (i) Separated Flows, (ii) Intermittent Flows, (iii) Annular Flows.

Thereafter, the transition regions, or boundaries between the groups are defined on the basis of a wave stability model. The ability to identify the particular flow regime obtaining under a particular set of conditions then allows flow pattern dependent pressure drop and void fraction correlations to be developed and compared with experimental data.

8.1 CHARACTERISATION OF FLOW PATTERN GROUPS OR REGIMES

In order to characterise the individual flow patterns into flow pattern groups, several different plots of the experimental data were made (with the individual flow patterns identified) and these are shown in Figs. 8.1 to 8.5.

Fig. 8.1 shows a plot of the homogeneous two phase friction multiplier ϕ^2_{fo} versus the experimental ϕ^2_{fo} value with the effects of liquid and gas flow rates identified. As can be seen, for each particular water flow rate the characteristic is divided into two separate parts, e.g. 'A' and 'AA', 'C' and 'CC', etc., connected by a hypothetical dotted line for convenience of identification. One part of each characteristic contains particular flow pattern data e.g. 'A' contains stratified and smooth wavy data, while 'AA' contains rough wavy and annular data. 'C' contains plug and slug flow data whereas 'CC' contains only annular flow data.

These characteristics suggest the flow pattern grouping for the data covered should be

(i) Separated Flows: i.e. stratified and smooth wavy

(ii)Intermittent Flows: i.e. bubble, plug and slug

(iii)Annular Flows: i.e. rough wavy and annular.

This flow pattern grouping is confirmed in Fig. 8.2 where the experimental two phase friction multiplier ϕ^2_{fo} is plotted to a base of mass dryness fraction and in Fig. 8.3 to 8.5 where the void fraction α is plotted against volume fraction β or air volume flowrate Q_g. In all cases, transitions or discontinuities are obtained with the various parts of the characteristics being flow pattern dependent.

It is worth mentioning that some slug flow points appear in the part of the characteristics attributed to annular and rough wavy flows. On checking these points

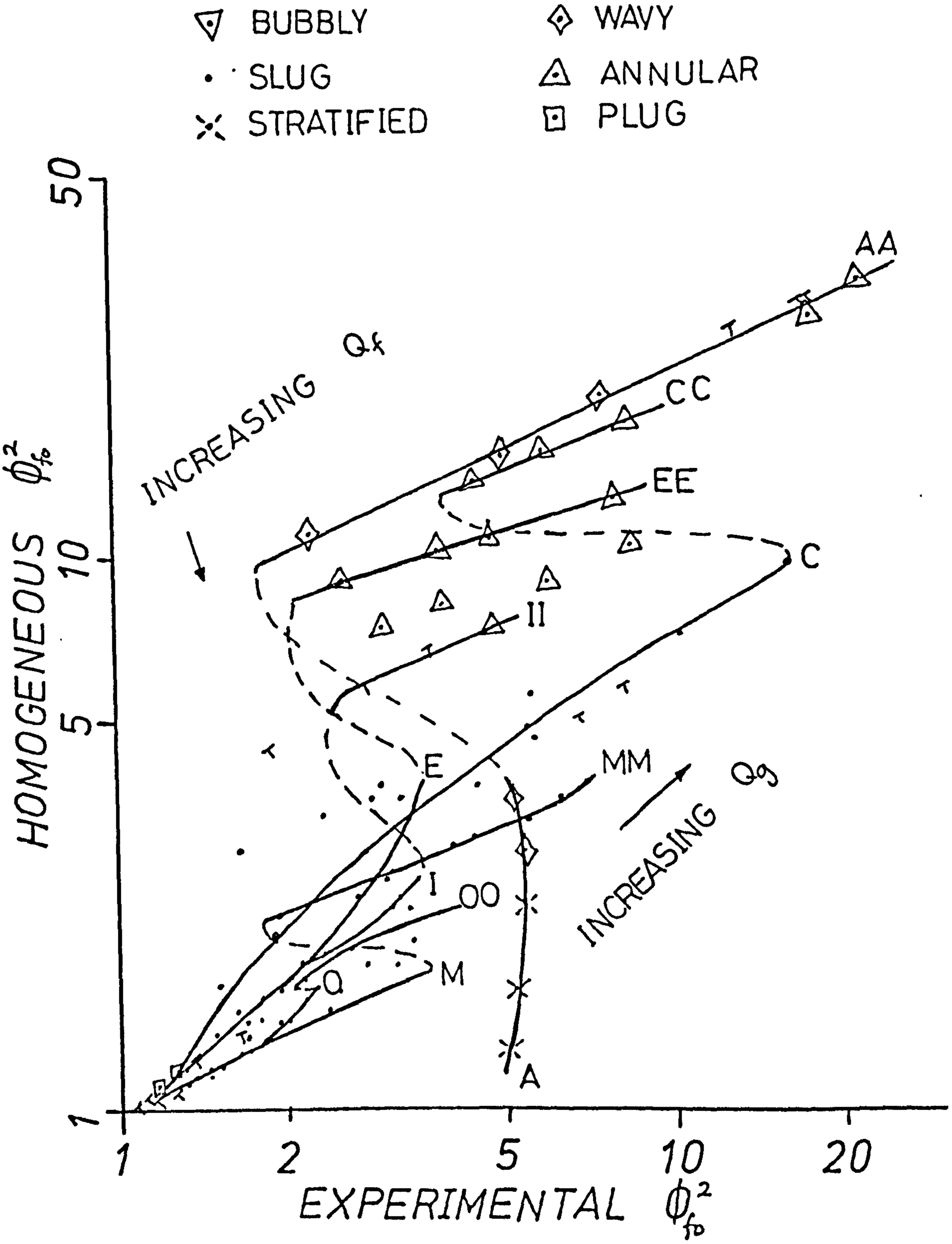

FIG. 8·1 COMPARISON BETWEEN EXPERIMENAL AND HOMOGENEOUS FLOW MODEL SHOWING EFFECT OF WATER FLOWRATE

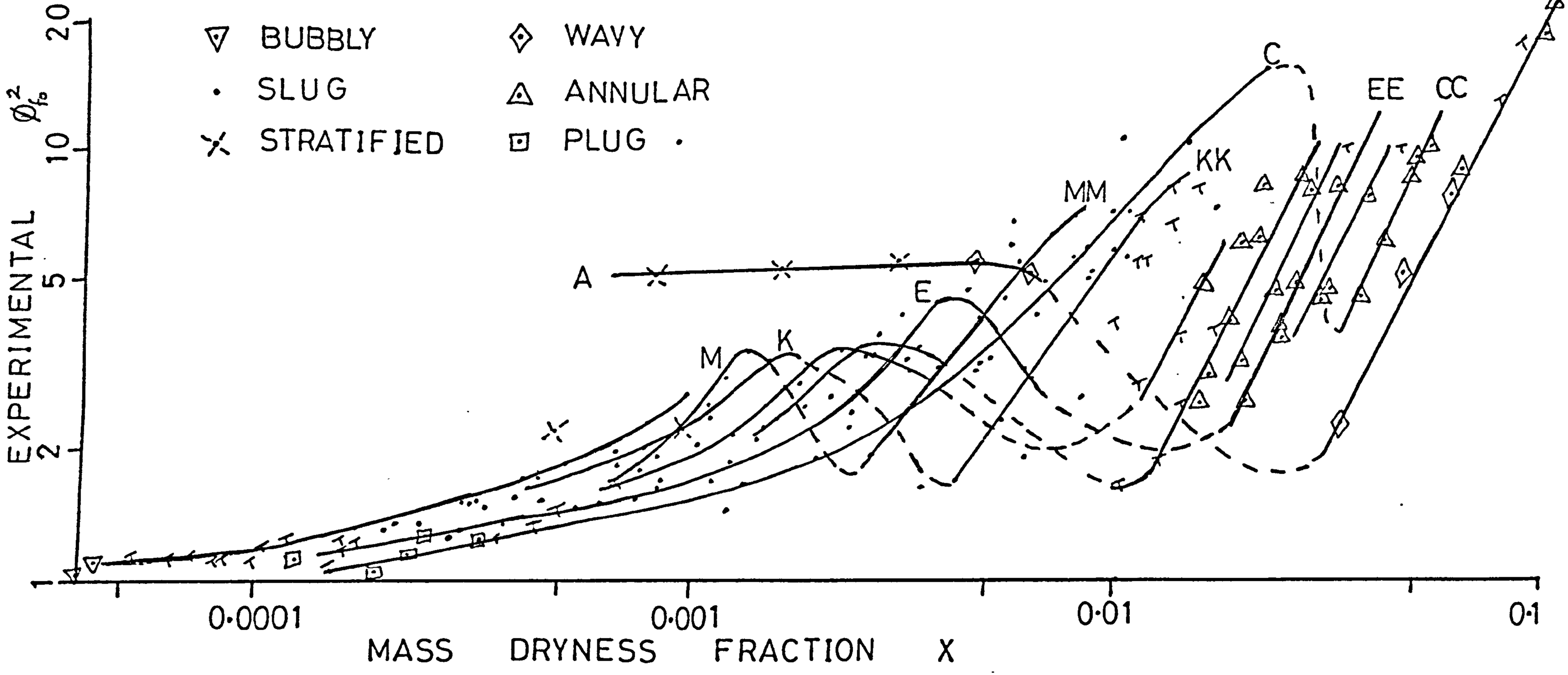

FIG. 8·2 $\phi_{fo\ EXP.}^2$ VS MASS DRYNESS FRACTION SHOWING WATER FLOWRATE EFFECTS FOR PHASE 2 DATA

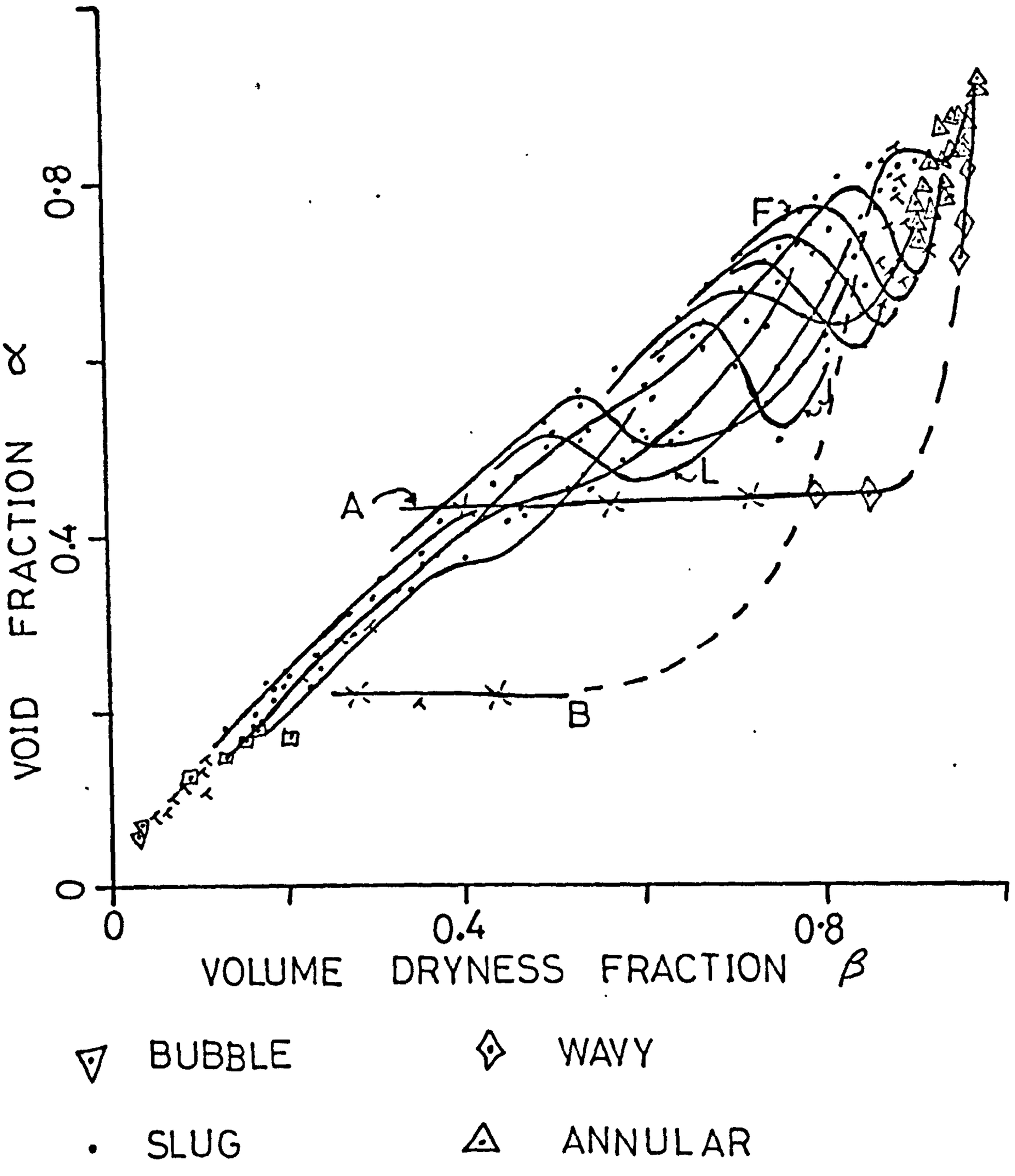

FIG. 8·3 VOID FRACTION VS INPUT VOLUME FRACTION SHOWING WATER FLOWRATE EFFECT FOR PHASE 2 DATA

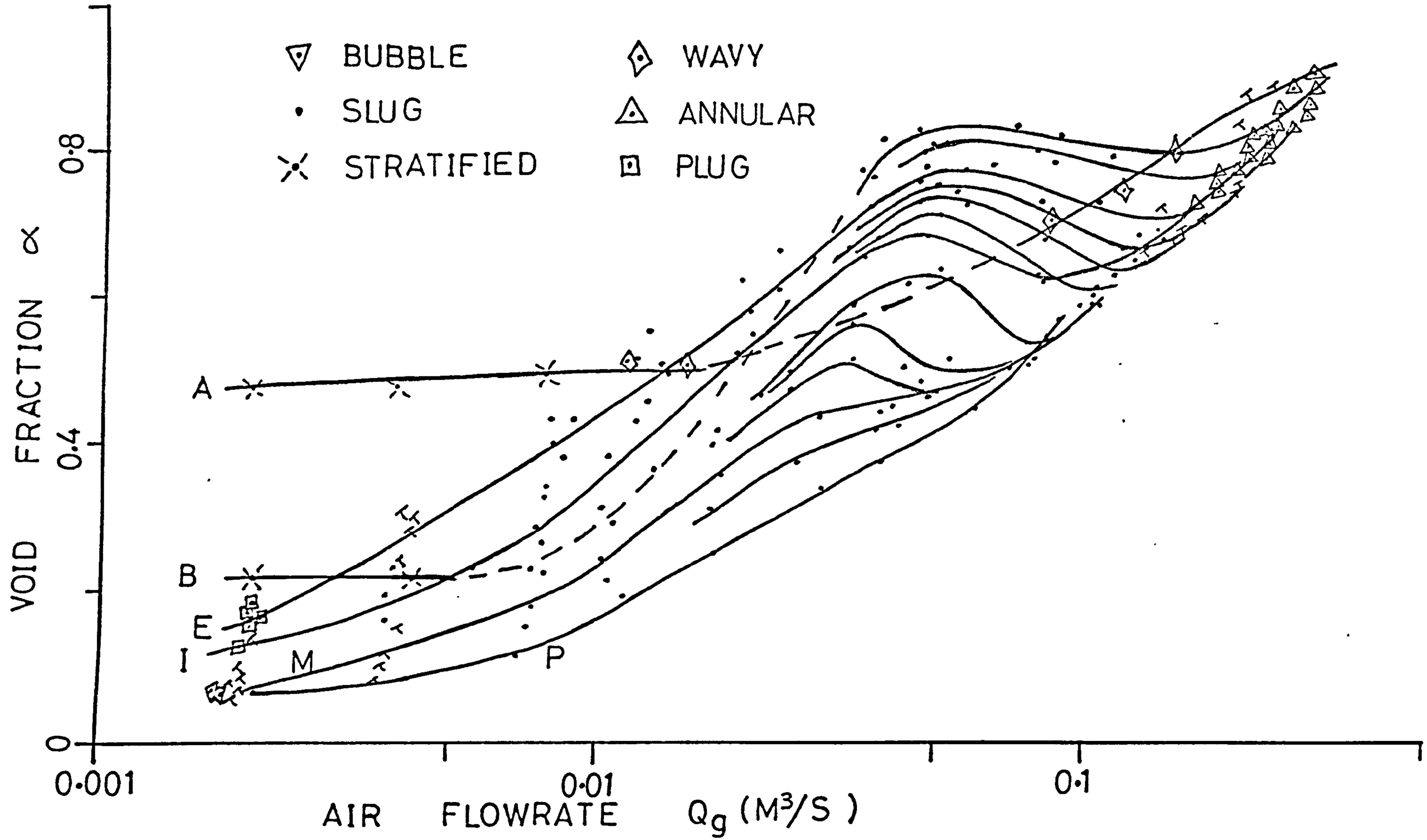

FIG. 8.4 VOID FRACTION VS AIR FLOWRATE SHOWING EFFECT OF WATER FLOWRATE FOR PHASE 2 DATA

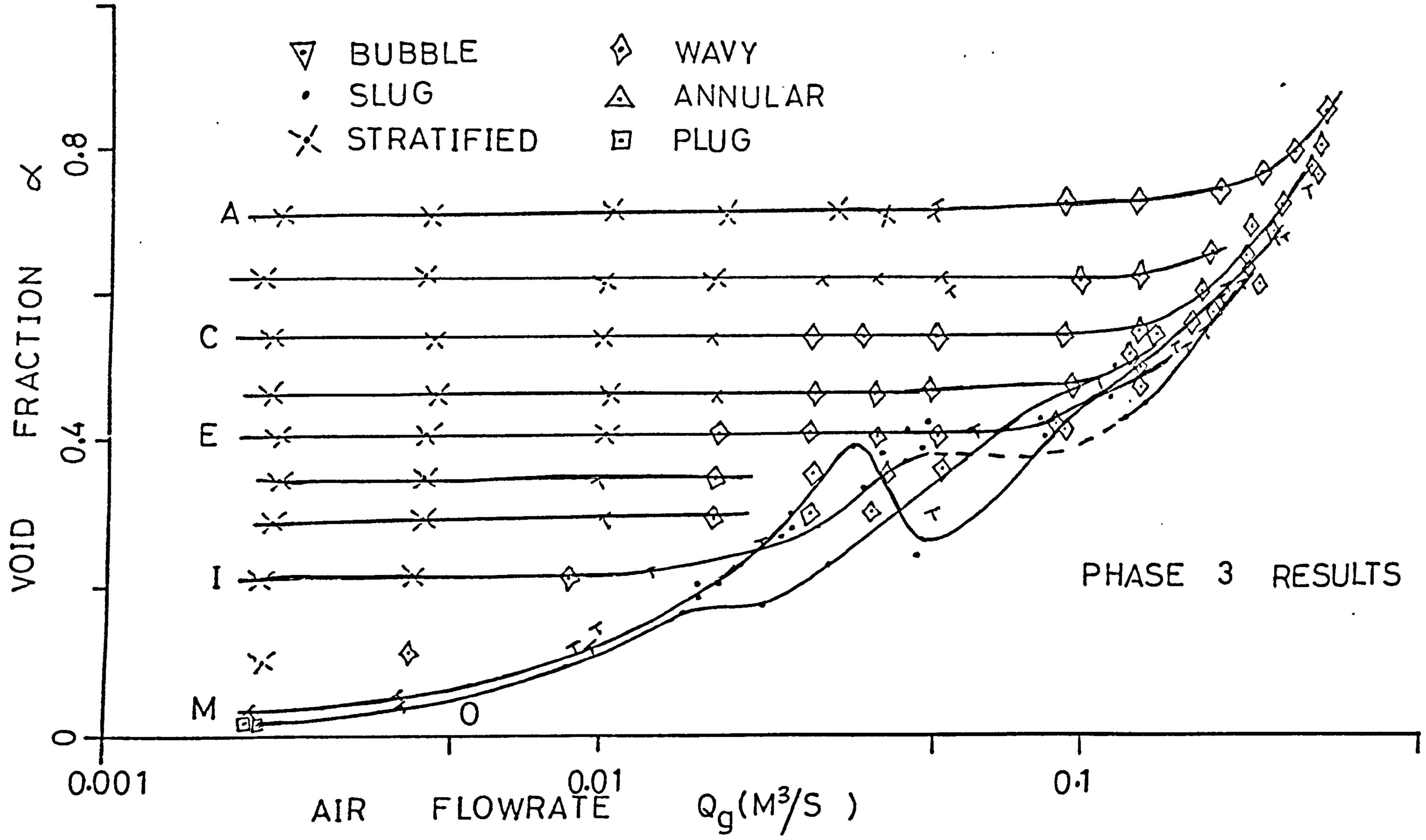

FIG. 8.5 VOID FRACTION VS AIR FLOWRATE SHOWING EFFECT OF WATER FLOWRATE FOR PHASE 3 DATA

(which were identified visually as slug flows), the flow had the appearance of thick clouds of droplets rather than slugs of liquid. This emphasises the subjectiveness of flow pattern identification by visual means.

Another point worth noting is that at very high water flowrates the transition between intermittent flows and annular flows is not nearly so sharp and the shapes of the respective parts of the characteristics are fairly similar, e.g. 'O' and 'OO' in Fig. 8.1 and 'p' in Fig. 8.4.

It was mentioned in Chapter 5 that some differences in the flow patterns obtained from the Phase 1 and Phase 2 were observed, this being attributed to the difference in entry conditions produced by the double 90^{o} bend and the mixing device respectively. Consequently, in the subsequent analysis, the Phase 2 and Phase 3 data are mainly used (mixing device at test section entry) since these produced the more stable flow conditions.

8.2 PREDICTION OF FLOW PATTERN TRANSITIONS

In this section the transition boundaries between the three flow pattern groups are defined and evaluated on the basis of a simple wave stability model. These boundaries are

(i) Intermittent - Separated Flow boundary

(ii) Intermittent - Annular Flow boundary

(iii) Separated - Annular Flow boundary

At this stage it is worth mentioning some features observed visually regarding the mechanisms involved near the transition boundaries, which might help in the

development of the theoretical model.

8.2.1 VISUAL OBSERVATIONS AT THE TRANSITION BOUNDARIES

(A) Intermittent - Separated Flow Boundary: This boundary normally occurred at comparatively low air and water flow-rates. Sometimes a large wave was observed to traverse the whole length of test section without blocking the air passage. However an increase in air flowrate would cause slugging and, once a slug was formed, the liquid level remaining in the pipe was very small but built up with the continuous supply of water until the combination of liquid level and air velocity necessary for wave growth was met again. In this case the water level, and hence the water flowrate, was relatively low. At much lower water flow-rates, the slug flow pattern was by-passed into rough wavy and annular flows. Thus it appeared that a minimum liquid level was required for the formation of a slug, provided other conditions were satisfied.

On the other hand, when the liquid level was high (i.e. at relatively high water flowrates) only small disturbances (or small amplitude waves) were needed to block the air passage and form a slug or plug type of flow.

In general the slug could have formed at any point along the test section, the important parameters apparently being air velocity and liquid level in the pipe.

(B) Intermittent - Annular Flow Boundary: This transition normally occurred at much higher air flowrates and over a wider and higher range of water flowrates. Consider the

case of a developed slug flow in the pipe at low air and water flowrate conditions. It was observed that, on increasing the air flowrate, the slug started to form further and further downstream from the mixer. After the mixer, a rough wavy (probably misty-wavy) flow prevailed with a fast moving liquid layer at the bottom of the pipe. As the liquid moved downstream its depth increased (liquid level became higher) and its velocity decreased causing relatively higher amplitudes waves to appear on the surface until a slug was formed. When the air flow was increased further, the point where the slug was formed moved downstream. This indicated that a certain combination of water level and air velocity was required before a slug could form.

A point was reached where a slug was not able to form in the available length of test section. The flow at this stage was wavy-misty indicating the start of annular flows.

At higher water flowrates, the waves were sheared by the flowing gas to form a thick cloud of droplets, normally in the second half of test section. At even higher water flowrate conditions, the above mechanisms were less apparent due to the difficulty in identifying the flow structure which had a very foggy and milky appearance.

8.2.2 THEORETICAL MODELS

The experimental observations mentioned above suggest that a realistic model could be based on a wavy flow situation with a wave stability criterion. Such a model is developed and discussed with respect to the different

transitions. The model is developed for flow in a rectangular channel to avoid the complexities involved with a circular channel, at this stage.

Consider the presence of a solitary wave in a rectangular channel as shown below. No limitations are imposed on the shape of the wave or on the mechanism of its

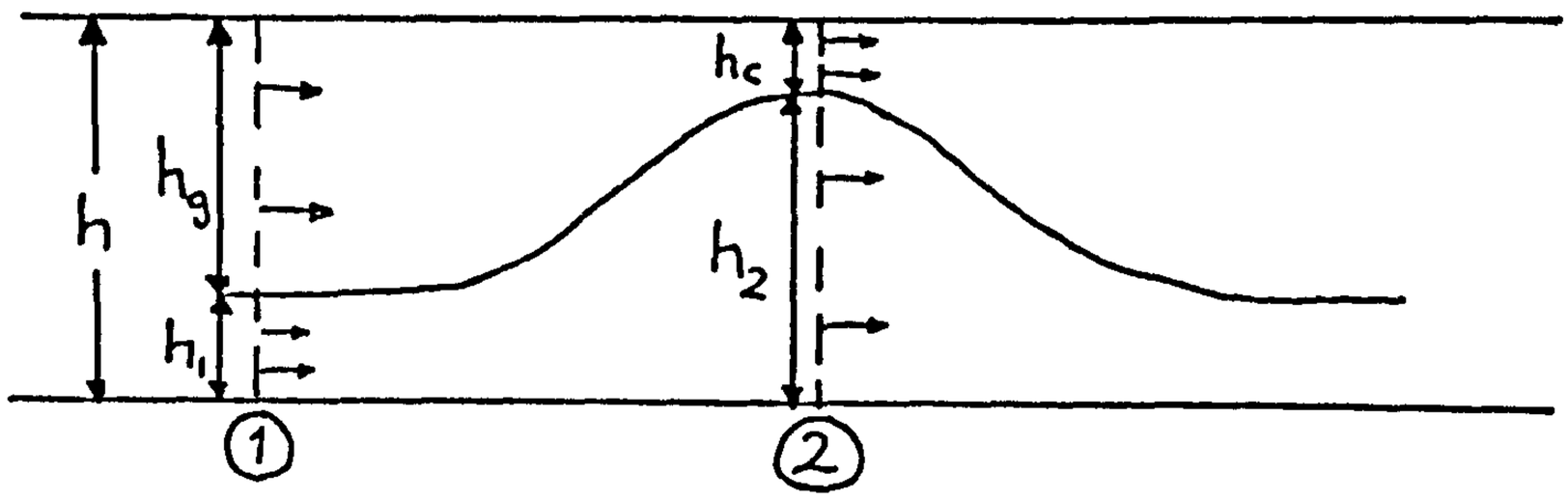

formation. Consider also two sections 1 and 2, with section 1 clear of the wave disturbance and section 2 at the wave crest; the gas and liquid velocities at these sections are then unidirectional. Now consider two points at the interface at sections 1 and 2, one on the gas phase side and the other on the liquid phase side of the interface. Assume that the local velocities U_{loc}, can be related to the mean phase velocity U (i.e. across the part of the C/S occupied by the particular phase) through a factor k, i.e.

$$(U_f)_{loc} = k_f U_f \qquad (8.1)$$

$$(U_g)_{loc} = k_g U_g \qquad (8.2)$$

where $U_f = \frac{Q_f}{A_f}$ and $U_g = \frac{Q_g}{A_g}$.

If the wave velocity is neglected (this will be true at least for low liquid levels) then the following equations

can be written

(i) Bernoulli's equation for the liquid phase

$$p_1 + \tfrac{1}{2}\rho_{f_1}(k_{f_1} U_{f_1})^2 + \rho_f g h_1 = p_2 + \tfrac{1}{2}\rho_{f_2}(k_{f_2} U_{f_2})^2 + \rho_{f_2} g h_2 \tag{8.3}$$

(ii) the phase continuity equation for the liquid phase

$$h_1 U_{f_1} \rho_{f_1} = h_2 U_{f_2} \rho_{f_2} \tag{8.4}$$

(iii) Bernoulli's equation for the gas phase

$$p_1 + \tfrac{1}{2} \rho_{g_1}(k_{g_1} U_{g_1})^2 = p_2 + \tfrac{1}{2} \rho_{g_2} (k_{g_2} U_{g_2})^2 \tag{8.5}$$

(iv) the phase continuity equation for the gas phase

$$(h - h_1) \rho_{g_1} U_{g_1} = (h - h_2) \rho_{g_2} U_{g_2} \tag{8.6}$$

From equation (8.3) and since $\rho_{f_1} \simeq \rho_{f_2} = \rho_f$,

$$p_1 - p_2 = \tfrac{1}{2} \rho_f k_{f_1}^2 U_{f_1}^2 \left[\left(\frac{k_{f_2} U_{f_2}}{k_{f_1} U_{f_1}} \right)^2 - 1 \right] + \rho_f g h \left(\frac{h_2}{h_1} - \frac{h_1}{h} \right) \tag{8.7}$$

From equation (8.5),

$$p_1 - p_2 = \tfrac{1}{2} \rho_{g_1} k_{g_1}^2 U_{g_1}^2 \left[\frac{\rho_{g_2}}{\rho_{g_1}} \left(\frac{k_{g_2} U_{g_2}}{k_{g_1} U_{g_1}} \right)^2 - 1 \right] \tag{8.8}$$

Substituting in equation (8.7) yields

$$\rho_{g_1} k_{g_1}^2 U_{g_1}^2 \left[\frac{\rho_{g_2}}{\rho_{g_1}} \left(\frac{k_{g_2} U_{g_2}}{k_{g_1} U_{g_1}} \right)^2 - 1 \right] = \rho_f k_{f_1}^2 U_{f_1}^2 \left[\left(\frac{k_{f_2} U_{f_2}}{k_{f_1} U_{f_1}} \right)^2 - 1 \right] + 2 \rho_f g h \left(\frac{h_2}{h} - \frac{h_1}{h} \right) \tag{8.9}$$

Let us assume that the wave becomes unstable and develops into a slug when the air gap between the wave crest and the top of the channel wall reaches a critical value, h_c; also that the liquid level is sufficient to supply the necessary amount of liquid to form the slug. The value of h_c is then expected to depend on the equilibrium air gap in the channel, as was shown experimentally by Kordyban (K9).

Thus from equation (8.6), and since $h_c = h - h_2$,

$$h(1 - \frac{h_1}{h}) \rho_{g_1} U_{g_1} = h_c \rho_{g_2} U_{g_2}$$

hence

$$\frac{U_{g_2}}{U_{g_1}} = \frac{\rho_{g_1}}{\rho_{g_2}} \frac{\alpha}{\alpha_c} \qquad (8.10)$$

where $\alpha_c = \frac{h_c}{h}$ and $1 - \alpha = \frac{h_1}{h}$ for the rectangular channel.

Also from equation (8.4),

$$\frac{U_{f_2}}{U_{f_1}} = \frac{h_1}{h_2} = \frac{1 - \alpha}{1 - \alpha_c} \qquad (8.11)$$

Let $k_{g_o} = \frac{k_{g_2}}{k_{g_1}}$ and $k_{f_o} = \frac{k_{f_2}}{k_{f_1}}$, then substituting in equation (8.9) gives

$$\rho_{g_1} k_{g_1}^2 U_{g_1}^2 \left[\frac{\rho_{g_1}}{\rho_{g_2}} k_{g_o}^2 (\frac{\alpha}{\alpha_c})^2 - 1 \right] = \rho_f k_{f_1}^2 U_{f_1}^2$$

$$\left[k_{f_o}^2 (\frac{1 - \alpha}{1 - \alpha_c})^2 - 1 \right] + 2 \rho_f gh(\alpha - \alpha_c) \qquad (8.12)$$

Dividing by $\rho_f gh$, and rearranging, gives

$$\frac{U_{f_1}^2}{gh} k_{f_1}^2 \left[k_{f_o}^2 \left(\frac{1-\alpha}{1-\alpha_c}\right)^2 - 1 \right] = \frac{U_{g_1}^2}{gh} k_{g_1}^2 \frac{\rho_{g_1}}{\rho_f}$$

$$\left[\frac{\rho_{g_1}}{\rho_{g_2}} k_{g_o}^2 \left(\frac{\alpha}{\alpha_c}\right)^2 - 1 \right] - 2(\alpha - \alpha_c)$$

But since $U_{f_1} = \frac{U_{sf_1}}{1-\alpha}$, $U_{g_1} = \frac{U_{sg_1}}{\alpha}$, $Fr_f = \frac{U_{sf}^2}{gh}$ and $Fr_g = \frac{U_{sg}^2}{gh}$, then the above equation can be written as,

$$Fr_f \frac{k_{f_1}^2}{(1-\alpha)^2} \left[k_{f_o}^2 \left(\frac{1-\alpha}{1-\alpha_c}\right)^2 - 1 \right] = Fr_g \frac{k_{g_1}^2}{\alpha^2} \frac{\rho_{g_1}}{\rho_f} \left[k_{g_o}^2 \left(\frac{\alpha}{\alpha_c}\right)^2 \frac{\rho_{g_1}}{\rho_{g_2}} - 1 \right]$$

$$- 2(\alpha - \alpha_c)$$

Rearranging again

$$Fr_f = \frac{(1-\alpha)^2 \alpha}{1 - k_{f_o}^2 \left(\frac{1-\alpha}{1-\alpha_c}\right)^2} \left\{ \left(\frac{\sqrt{2}}{k_{f_1}}\right)^2 \left(1 - \frac{\alpha_c}{\alpha}\right) - \frac{Fr_g}{\alpha^3} \left(\frac{k_{g_1}}{k_{f_1}}\right)^2 \frac{\rho_{g_1}}{\rho_f} \left[\frac{\rho_{g_1}}{\rho_{g_2}} k_{g_o}^2 \left(\frac{\alpha}{\alpha_c}\right)^2 - 1 \right] \right\} \qquad (8.13)$$

The experimental results of Kordyban (K9) indicated the existence of a relationship between h_g, the mean 'air channel' depth, and h_w, the wave height necessary to cause slugging. In addition, for air gaps greater than a particular value (i.e. liquid level too low) no slugging was observed. His relationship was linear and could be expressed in the form,

$$h_w = k(h - h_1) \cdot \quad \text{where} \quad k < 1$$

or

$$\frac{h_w}{h} = k\alpha \qquad (8.14a)$$

where k is a constant.

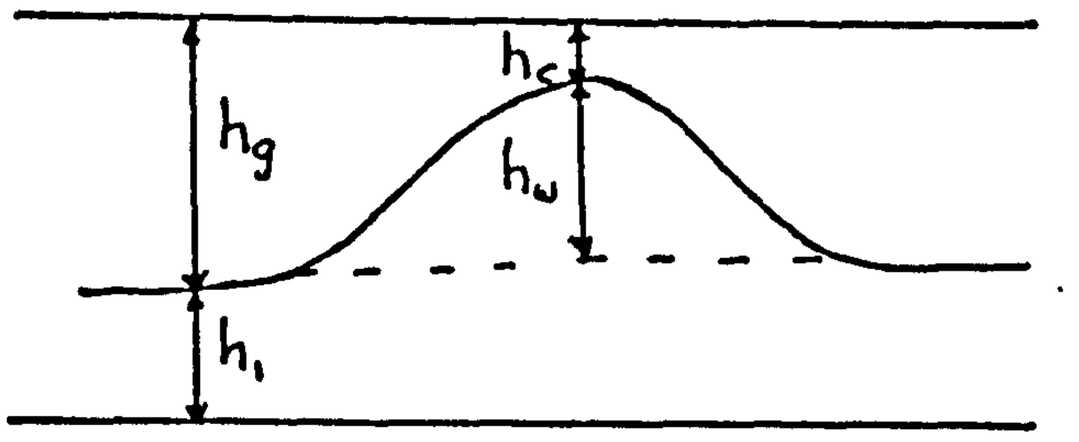

But $h_g = h - h_1 = h_c + h_w$

$$\therefore \frac{h_w}{h} = \alpha - \alpha_c \qquad (8.14b)$$

From equation (8.14a),

$$\alpha_c = (1-k)\,\alpha = k_1 \alpha \qquad (8.14c)$$

where $k_1 = 1-k$

Substituting equattion (8.14c) into equation (8.13) gives

$$Fr_f = \frac{(1-\alpha)^2 \ \alpha}{1-k_{f_o}^2 \left(\frac{1-\alpha}{1-k_1\alpha}\right)^2} \left[\left(\frac{\sqrt{2}}{k_{f_1}}\right)^2 (1-k_1) - \left(\frac{k_{g_1}}{k_{f_1}}\right)^2 \left(\frac{\rho_{g_1}}{\rho_f}\right) \frac{Fr_g}{\alpha^3} \left(\frac{\rho_{g_1}}{\rho_{g_2}} \left(\frac{k_{g_o}}{k_1}\right)^2 - 1 \right) \right] \qquad (8.15)$$

which is the equation determining the condition of stability of the wave.

To simplify equation (8.15), certain assumptions regarding the k_{f_o} (i.e. k_{f_2}/k_{f_1}) and k_{g_o} (i.e. k_{g_2}/k_{g_1}) factors (introduced earlier to relate the local velocities at the interface to the mean phase velocities) are required. It is reasonable to assume the velocity profiles in the liquid and gas phases at section 1 are identical to the respective profiles at section 2, which then sets k_{f_o} and k_{g_o} to unity. A precise definition of the phase velocity profiles is needed to evaluate k_{f_1} and k_{g_1}, which are expected to be constants.

The term outside the brackets in equation (8.15), i.e.

$$f(\alpha) = \frac{(1-\alpha)^2\,\alpha}{1 - \left(\frac{1-\alpha}{1-k_1\alpha}\right)^2} \qquad (8.16)$$

is fairly complex and a simpler expression might be obtained by calculating the term, for different k_1 values, over the possible range of α values as detailed in Table 8-1 below.

k_1 / α	$f(\alpha)$ in equation (8.16)					k_1 / $1-\alpha$
	0.9	0.8	0.7	0.6	0.5	
0.1	3.71	1.88	1.276	0.972	0.79	.9
0.2	2.66	1.38	0.951	0.738	0.61	.8
0.4	1.19	0.65	0.471	0.382	0.329	.6
0.6	0.394	0.235	0.184	0.158	0.143	.4
0.7	0.184	0.118	0.096	0.086	0.08	.3
$k=1-k_1$	0.1	0.2	0.3	0.4	0.5	

Table 8-1 Range of $f(\alpha)$ for different k and α values.

Fig. 8.6 shows a plot of $f(\alpha)$ versus $(1-\alpha)$ and, as can be seen, the term $f(\alpha)$ can be expressed by an equation of the form

$$f(\alpha) = \frac{(1-\alpha)^2\,\alpha}{1 - \left(\frac{1-\alpha}{1-k_1\alpha}\right)^2} = f(k)\,(1-\alpha)^{2n}$$

$$2.72 \leqslant 2n \leqslant 2.12$$

Equation (8.15) then becomes

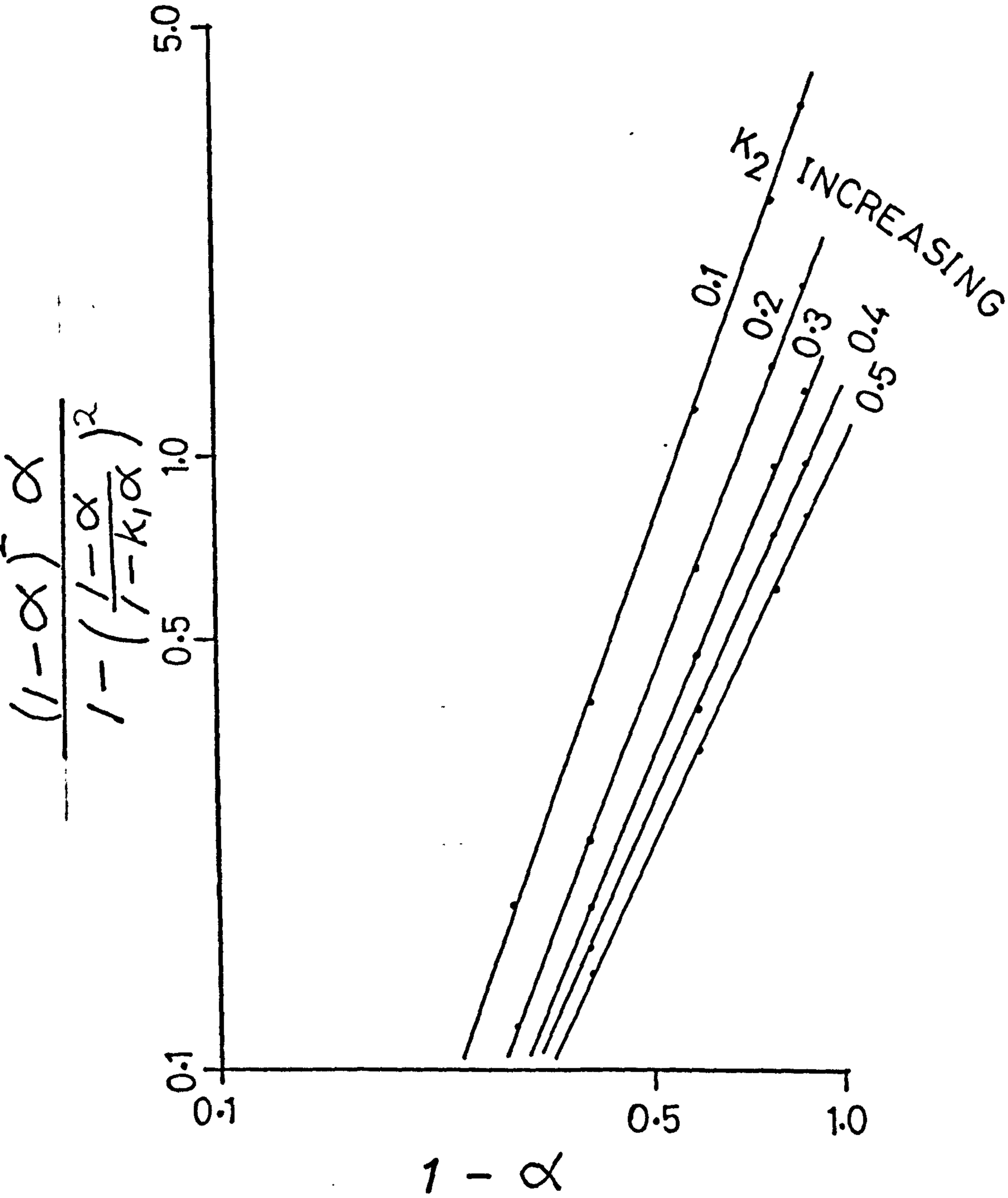

FIG.8.6 THE DEPENDENCE OF THE TERM IN EQUATION (8.16) ON $(1-\alpha)$

$$Fr_f = f(k)(1-\alpha)^{2n}\left[\left(\frac{\sqrt{2}}{k_{f_1}}\right)^2 (1-k_1) - \left(\frac{k_{g_1}}{k_{f_1}}\right)^2 \left(\frac{\rho_{g_1}}{\rho_f}\right) \frac{Fr_g}{\alpha^3} \left(\frac{\rho_{g_1}}{\rho_{g_2}} \left(\frac{1}{k_1}\right)^2 - 1\right)\right] \qquad (8.17)$$

which is the criterion for wave stability.

8.2.2.1 INTERMITTENT - SEPARATED FLOW TRANSITION

The problem of determining this boundary is reduced to that of being able to predict the occurrence of slug (or plug) flows, as explained in section 8.2.1. If the liquid level is sufficient to supply the amount necessary to form the slug, then equation (8.17) can be used to determine the transition. The term inside the R.H. square bracket is fairly complicated; however, a close examination reveals that one of the terms contains the factor ρ_g/ρ_f, which is very small for the air-water system being considered and could perhaps be neglected. To check this point, information about the terms inside the bracket are required, which include the void fraction, gas Froude number, etc. Table 8-2 gives the experimental transition boundary results for Phase 2 and Phase 3 deduced from Figs. 8.7 and 8.8.

At the transition it was difficult to measure the void fraction because of the highly fluctuating nature of the flow, hence the data collected just prior to the transition (i.e. separated flow points) were used and these are shown in Table 8-3 and plotted in Fig. 8.9 on

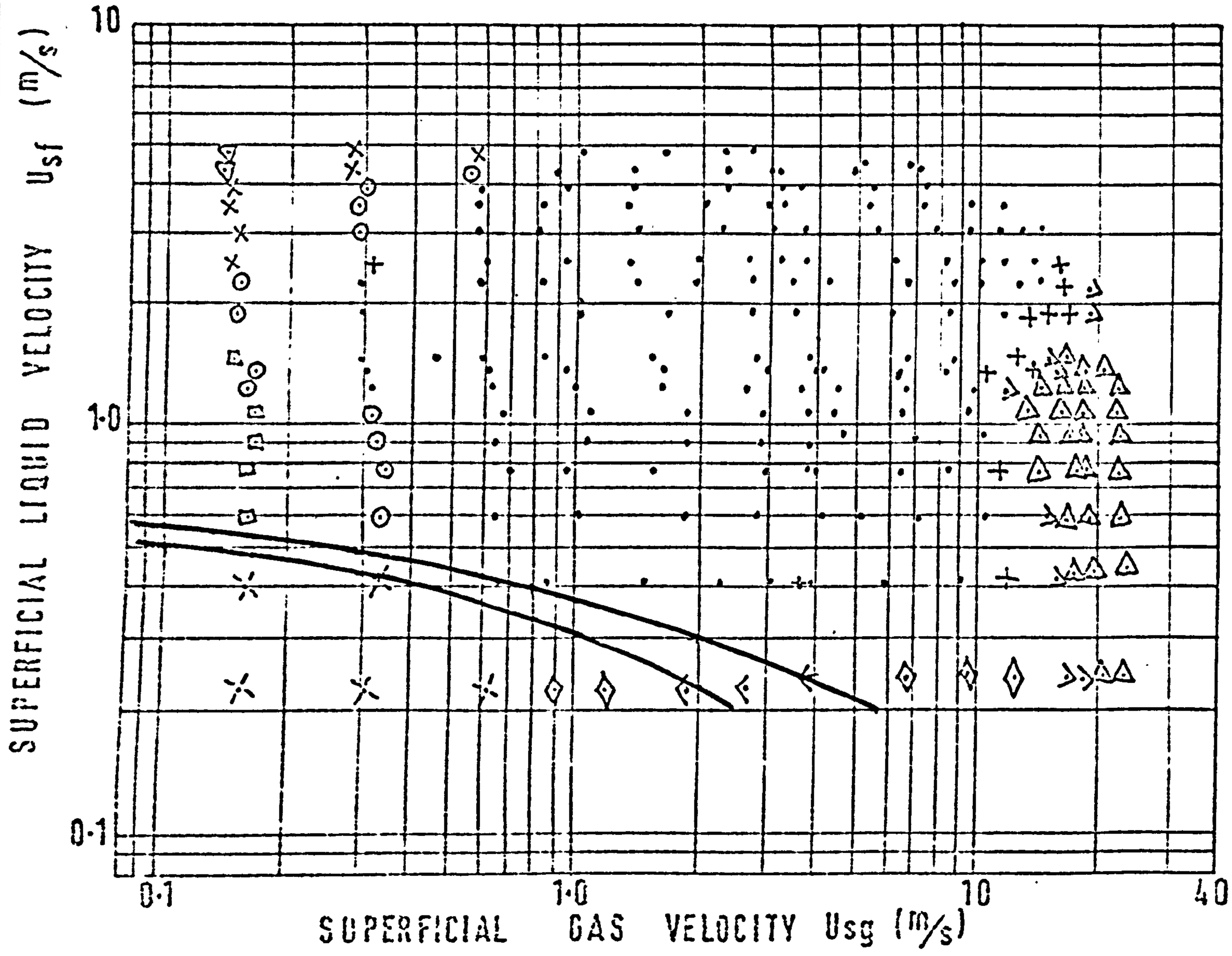

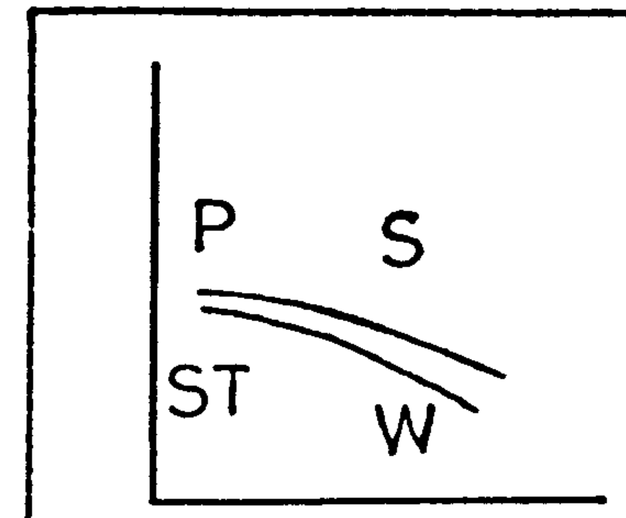

P : PLUG

S : SLUG

ST : STRATIFID

W : WAVY (SMOOTH)

FIG. 8·7 PHASE 2 FLOW PATTERN MAP

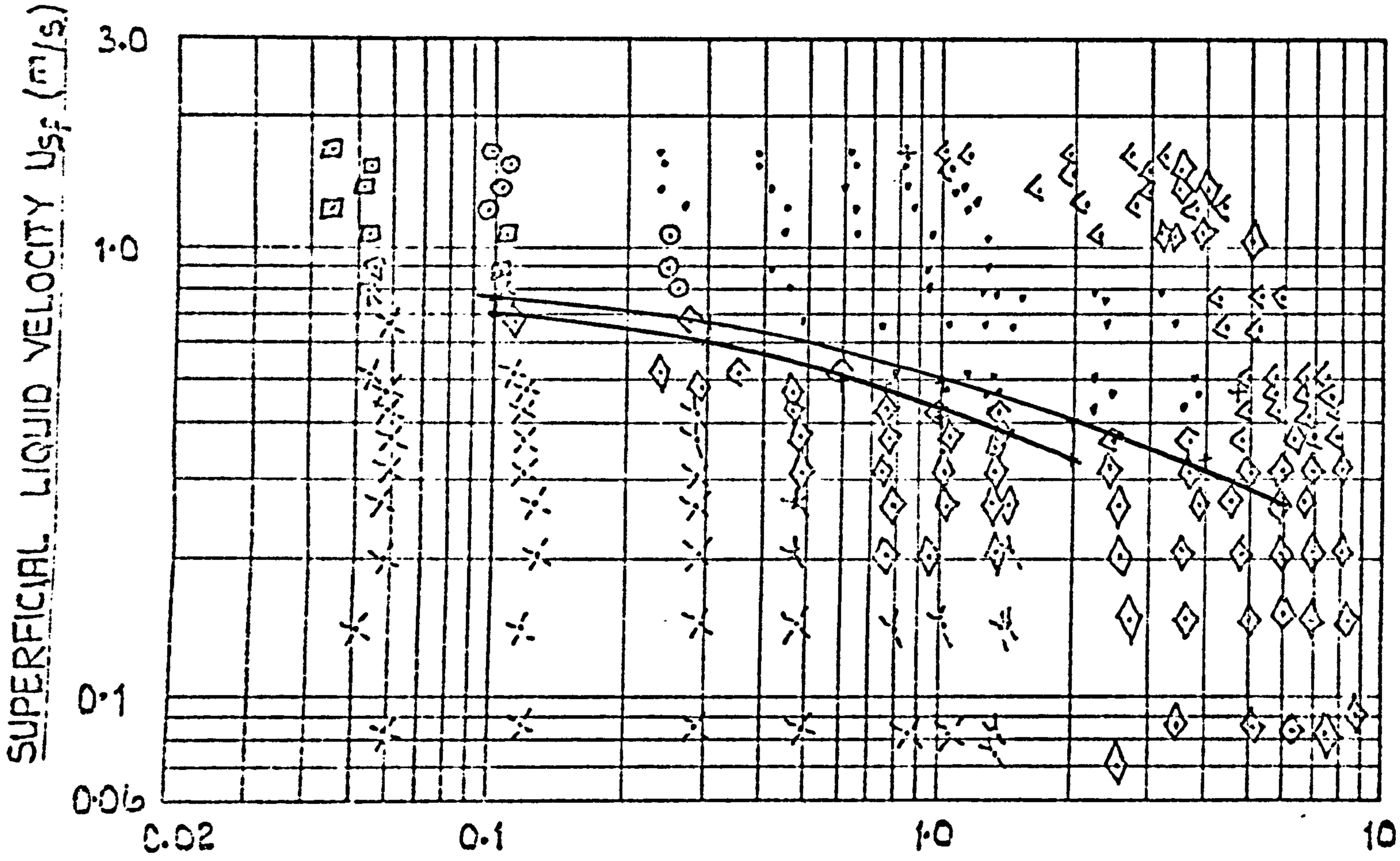

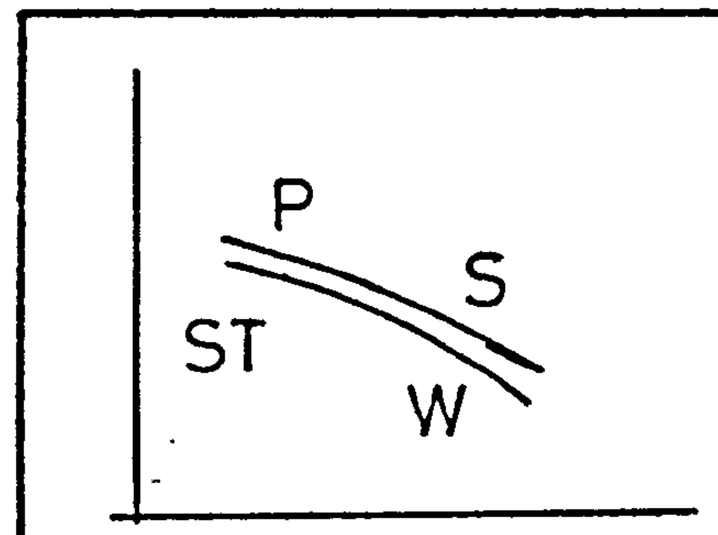

P : PLUG

S : SLUG

ST : STRATIFIED

W : WAVY (SMOOTH)

FIG. 8·8 PHASE 3 FLOW PATTERN MAP

	U_{sf} (m/s)	U_{sg} (m/s)	$1 - \beta$	α
Slug Boundary				
(A) Phase 2				
	0.55	0.10	0.846	0.154
	0.48	0.30	0.615	0.220
	0.40	0.80	0.333	0.320
	0.30	2.0	0.131	0.460
	0.23	4.0	0.054	0.570
	0.20	5.5	0.035	0.610
(B) Phase 3				
	0.74	0.10	0.881	0.150
	0.67	0.30	0.691	0.190
	0.58	0.60	0.492	0.260
	0.50	1.0	0.335	0.320
	0.41	2.0	0.170	0.430
	0.33	4.0	0.076	0.530
	0.26	6.0	0.042	0.610
Separated Boundary				
(A) Phase 2				
	0.50	0.10	0.833	0.160
	0.42	0.30	0.583	0.230
	0.33	0.80	0.292	0.345
	0.22	2.0	0.099	0.500
(B) Phase 3				
	0.70	0.10	0.875	0.145
	0.60	0.30	0.667	0.200
	0.50	0.60	0.455	0.270
	0.42	1.0	0.296	0.340
	0.33	2.0	0.142	0.450

Table 8-2 Transition boundaries determined from the flow pattern maps for Phases 2 and 3.

the basis of $(1 - \alpha)$ versus $(1 - \beta)$. Most of the data points correspond to wavy flow conditions, and hence the measured void fractions *could* overestimate the (actual)

Test No.	$1 - \alpha$	$1 - \beta$
(A) Phase 2		
052101	0.546	0.160
112101	0.778	0.560
(B) Phase 3		
032806	0.785	0.687
022906	0.884	0.859
130807	0.700	0.360
040907	0.756	0.510
011507	0.653	0.215

Table 8-3 Experimental test points prior to slugging.

equilibrium liquid level in the pipe required by theory. However, it is thought that the use of these values is a fair approximation. The data in Fig. 8.9 show a reasonable linear relationship which can be expressed as

$$(1 - \alpha) = k_3 \, (1 - \beta)^m \qquad (8.18a)$$

and this relationship was used to evaluate the void fractions for the transition boundaries given in Table 8-2.

Calculations were carried out to evaluate the two terms in the R.H. square bracket of equation (8.17) assuming $k_1 \simeq 0.75$ (using Kordyban results), $k_{f_1} \simeq k_{g_1} = 1$,

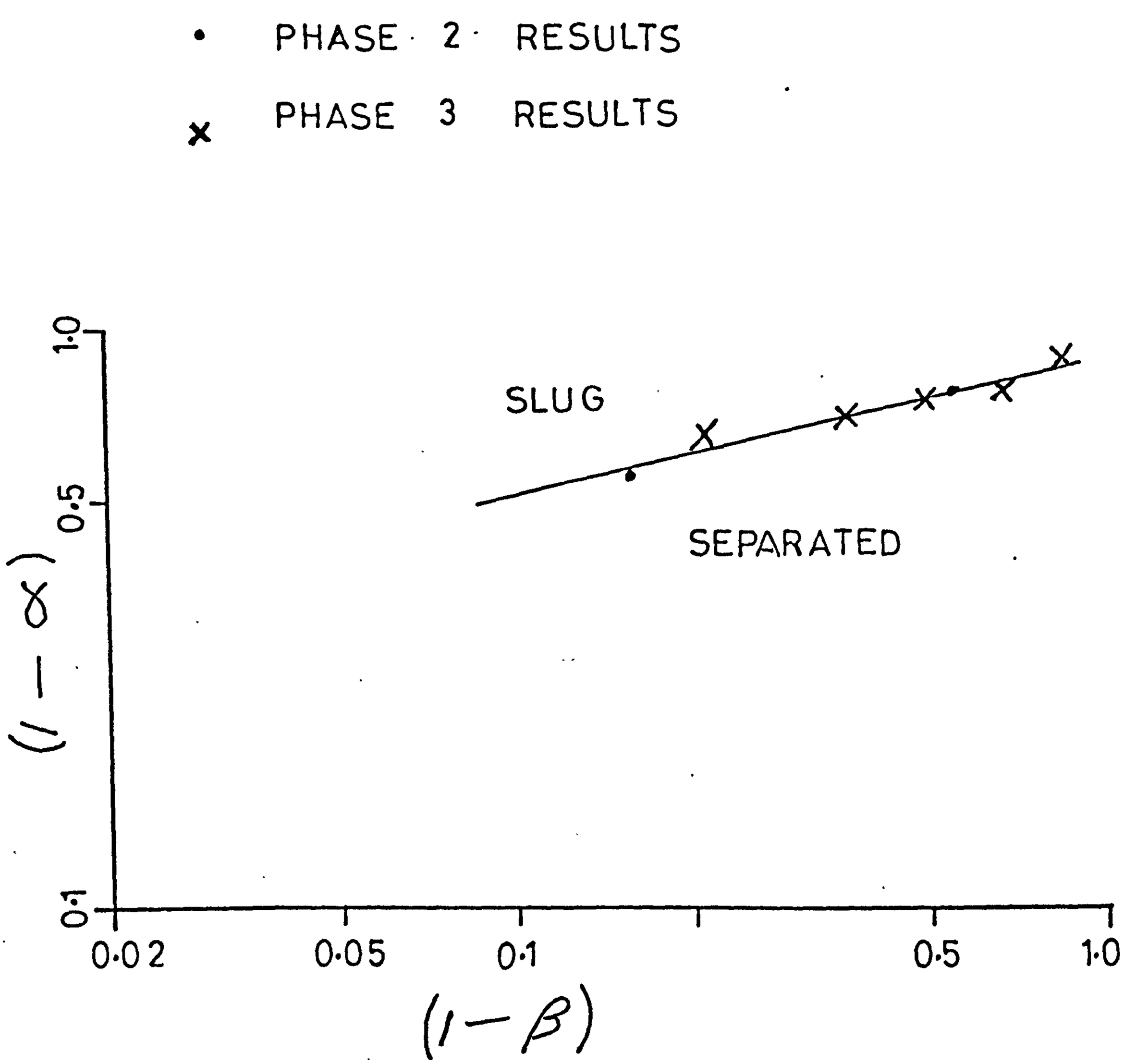

FIG. 8.9 VOID FRACTION CORRELATION FOR THE SLUG – SEPARATED TRANSITION TRANSITION

and $\rho_{g_1} = \rho_{g_2}$. These calculations are shown in Table 8-4 and show that the second term is generally negligible compared to the first. Hence equation (8.17) can be written in the more compact form

$$Fr = f(k) k_2 (1 - \alpha)^{2n} \tag{8.19}$$

where $k_2 = \left(\frac{\sqrt{2}}{k_{f_1}}\right)^2 (1 - k_1) \simeq 0.5$

In view of equation (8.18a), the above equation becomes

$$Fr_f^{\frac{1}{2}} = \left[f(k)\, k_2\, k_3\right]^{\frac{1}{2}} (1 - \beta)^{mn} \tag{8.20}$$

Fig. 8.10 shows a plot of $Fr_f^{\frac{1}{2}}$ versus $(1 - \beta)$ for the data given in Table 8-2. As expected the transition zone occurs over a band of conditions; on one side separated flow exists and on the other intermittent flow exists. The relationships are linear on the log plot and can be expressed as

$$Fr_f^{\frac{1}{2}} \simeq 0.50 (1 - \beta)^{0.31} \quad \text{Intermittend flow side of the boundary} \tag{8.21a}$$

$$Fr_f^{\frac{1}{2}} \simeq 0.47 (1 - \beta)^{0.39} \quad \text{Separated flow side of the boundary} \tag{8.21b}$$

and are the transition equations recommended for the Separated-Intermittent transition.

From equation (8.21a) for the condition of definite transition to intermittent flows,

$$mn = 0.31 \tag{8.22}$$

and by using the results of Fig. 8.6 for the range of realistic values of 'n', i.e.

	U_{sf} (m/s)	U_{sg} (m/s)	$F_{rg}^{\frac{1}{2}}$	α	ψ^*	γ^*	
Slug Boundary							
(A) Phase 2							
	0.55	0.10	0.09	0.154	0.002	0.500	
	0.4	0.8	0.717	0.32	0.015	0.500	
	0.2	5.5	4.93	0.61	0.100	0.500	extreme case
(B) Phase 3							
	0.74	0.10	0.068	0.150	0.001	0.500	
	0.26	6.0	4.1	0.61	0.069	0.500	
Separated Boundary							
(A) Phase 2							
	0.50	0.10	0.09	0.160	0.002	0.500	
	0.22	2.0	1.793	0.500	0.024	0.500	
(B) Phase 3							
	0.70	0.10	0.068	0.145	0.001	0.500	
	0.33	2.0	1.365	0.450	0.019	0.500	

$$\psi^* = \left(\frac{k_{g_1}}{k_{f_1}}\right)^2 \left(\frac{\rho_{g_1}}{\rho_f}\right) \frac{F_{rg}}{\alpha^3} \left[\frac{\rho_{g_1}}{\rho_{g_2}} \left(\frac{1}{k_1}\right)^2 - 1\right]$$

$\left(\frac{1.2}{1000}\right) \frac{F_{rg}}{\alpha^3} \left(0.778\right)$, for $k_{g_1} = k_{f_1} = 1$, $\rho_{g_1} = \rho_{g_2}$, $k_1 = 0.75$, $\rho_{g_1} = 1.2 \frac{kg}{m^3}$ and $\rho_f = 1000 \frac{kg}{m^3}$

$$\gamma^* = \left(\frac{\sqrt{2}}{k_{f_1}}\right)^2 (1 - k_1) = 0.50 \text{ for } k_1 = 0.75, \; k_{f_1} = 1$$

Table 8-4 Check calculations for the terms in the R.H. square bracket of equation (8.17)

• PHASE 2 RESULTS

× PHASE 3 RESULTS

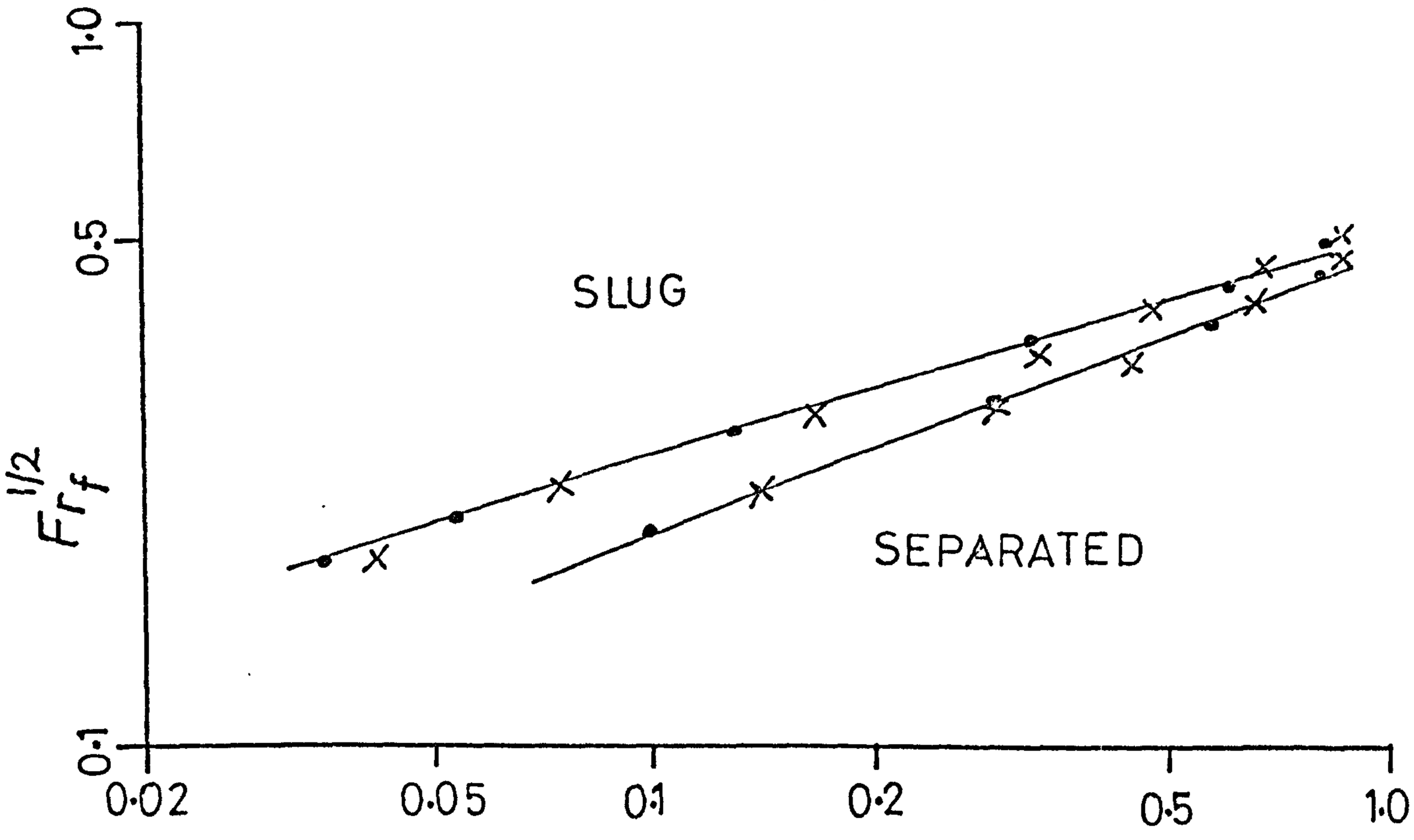

FIG. 8·10 SLUG SEPARATED TRANSITION CORRELATION

$$1.36 \leqslant n \leqslant 1.06 \qquad (8.23)$$

the range of values 'm' can take is, from equation (8.22),

$$0.228 \leqslant m \leqslant 0.292 \qquad (8.24)$$

Using the results of Fig. 8.9, equation (8.18a) can be rewritten as

$$(1 - \alpha) = 0.88\ (1 - \beta)^{0.24} \qquad (8.18b)$$

or $$m = 0.24 \qquad (8.25)$$

which agrees with equation (8.24). From equations(8.22) and (8.25), we get

$$n \simeq 1.29\ , \text{ and } \quad 2n \simeq 2.58 \qquad (8.26)$$

and from Fig. 8.6, this value of '2n' corresponds to $k \simeq 0.20$ which compares favourably with the Kordyban (K9) results which showed a value of $k \simeq 0.25$.

Whilst most of the work found in the literature involved a gas Froude number type of correlation (e.g. Wallis and Dobson, W3), most of the experimental data published (shown by the flow pattern maps given in Chapters 2 and 6) showed the separated-intermittent transition to be more sensitive to the liquid Froude number. Nevertheless, the gas Froude number dependency is also implied in equations (8.21) since the quantity $(1 - \beta) \equiv Fr_f/(Fr_f + Fr_g)$ if the Froude numbers are based on superficial velocities.

8.2.2.1 SEPARATED - ANNULAR FLOW TRANSITION

The wave stability model gives the conditions at which the wave becomes unstable and tends to grow. However,

if the liquid level is not high enough to supply the necessary amount of liquid required to form the slug, then, although the wave is probably unstable, the slug cannot form. Instead, air drag causes rough wavy flow to appear indicating the start of the annular regime.

Little data was available to check this criteria and in fact only those of Phase 3 could be used since few test points were taken near this transition. Because of the subjectiveness of visual identification, the changes in the void fraction characteristics shown in Fig. 8.5 were used as an indication of the transition and, as can be seen, the transition is fairly gradual. Table 8-5 gives the experimental data at the start of the transition, also the quantity $\dot{\psi}^*$ (see Table 8-4).

Test No.	$1-\alpha$	$1-\beta$	U_{sg} (m/s)	U_{sf} (m/s)	$\dot{\psi}^*$
051207	.229	.0132	6.35	.085	0.039
041307	.339	.0287	5.0	.148	0.038
111307	.433	.0548	3.59	.208	0.031
021407	.529	.093	2.6	.266	0.029
091407	.573	.114	2.431	.314	0.034

Table 8-5 Experimental test points from Phase 3 data at the smooth-rough wavy transition predicted from Fig. 8.5. For the meaning of $\dot{\psi}^*$ refer to Table 8-4.

Check calculations similar to those carried out in section 8.2.2.1 showed the term inside the R.H. square bracket of equation (8.17) to be a constant. The results of Table 8-5 plotted in Fig. 8.11 on the basis of $(1-\alpha)$ versus $(1-\beta)$ indicate that the conditions at the transition can be approximately expressed by an equation of the form

$$(1-\alpha) = k_4 (1-\beta)^p \qquad (8.27a)$$

Equation (8.17) can then be written in a form similar to equation (8.20) or

$$Fr_f^{\frac{1}{2}} \simeq \left[f(k) k_2 k_4\right]^{\frac{1}{2}} (1-\beta)^{np} \qquad (8.28a)$$

Using the results of the data plotted in Fig. 8.12, i.e. liquid Froude number versus $(1-\beta)$, the above equation can be re-written as

$$Fr_f^{\frac{1}{2}} = 0.71 (1-\beta)^{0.56} \qquad (8.28b)$$

or $$pn = 0.56 \qquad (8.29)$$

The results of Fig. 8.11, indicate that equation (8.27a) may be re-written as

$$(1-\alpha) = 1.5 (1-\beta)^{0.43} \qquad (8.27b)$$

i.e. $$p = 0.43 \qquad (8.30)$$

Hence from equation (8.29), we get

$$n = 1.3 \text{ , and } \quad 2n = 2.6 \qquad (8.31)$$

which is within the values of '2n' suggested by equation (8.23), i.e.

$$1.36 \leq n \leq 1.06 \qquad (8.23)$$

PHASE 3 DATA

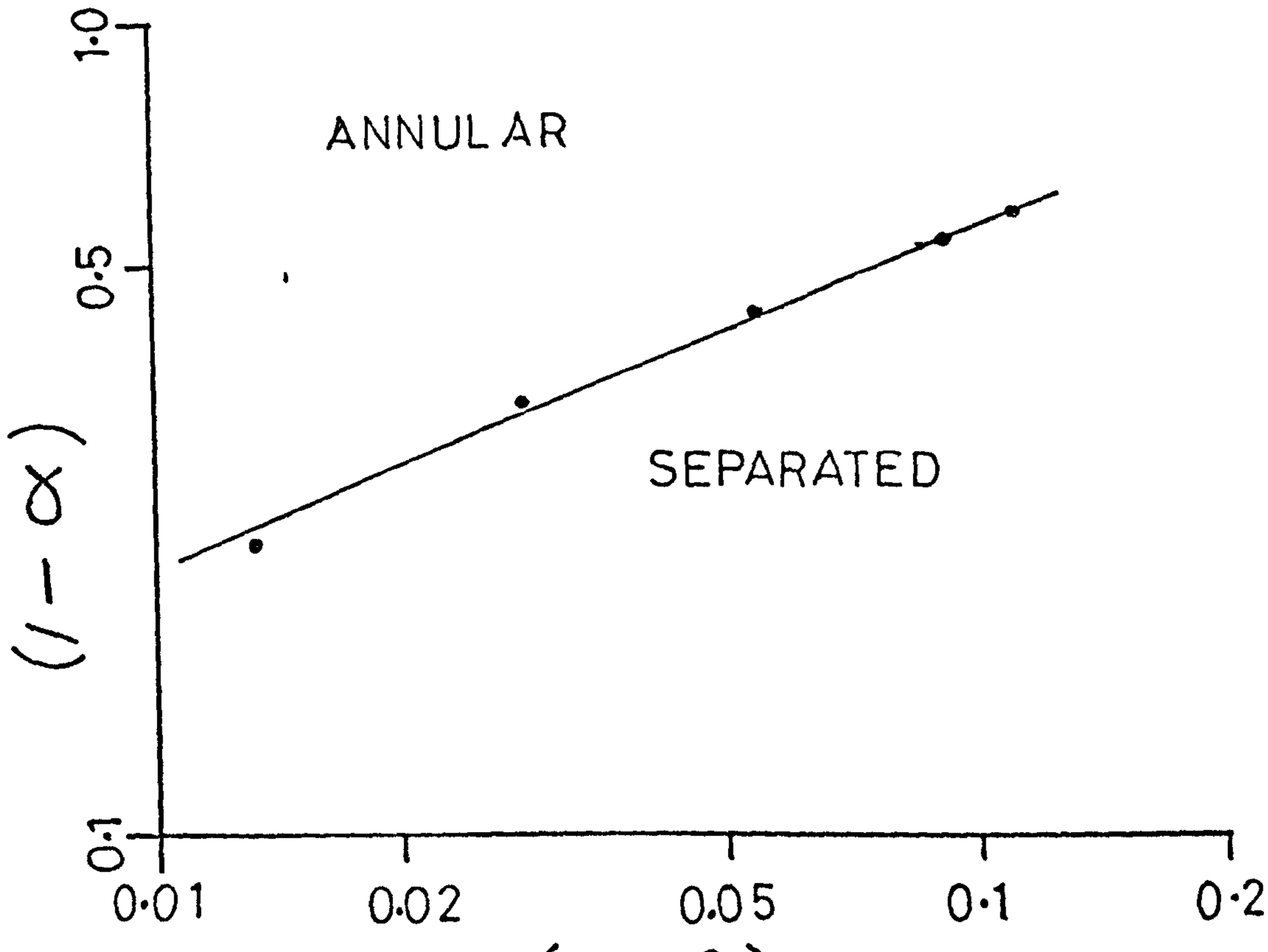

FIG. 8·11 VOID FRACTION CORRELATION FOR THE ANNULAR-SEPARATED TRANSITION

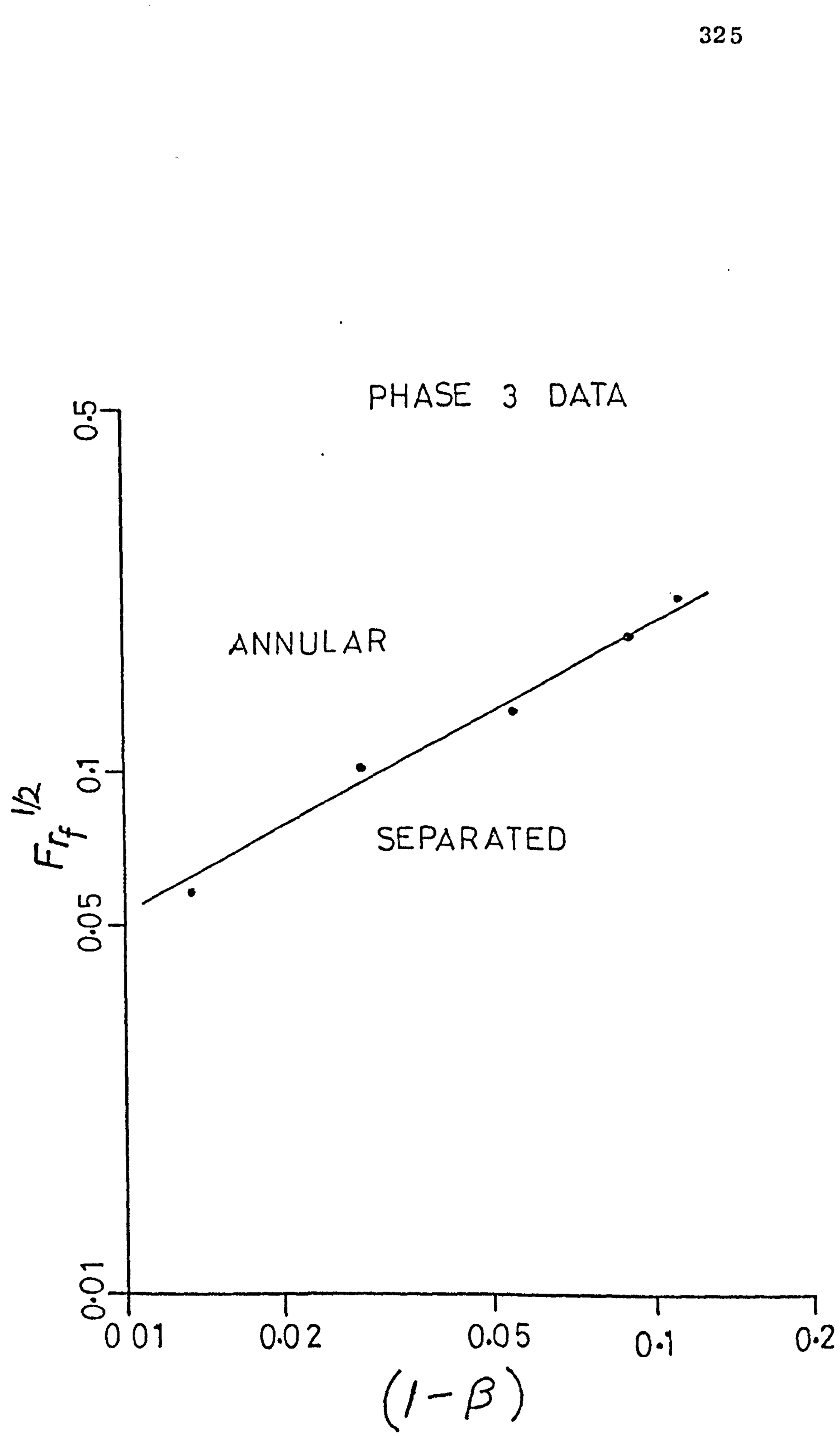

FIG. 8.12 ANNULAR – SEPARATED TRANSITION CORRELATION

Equation (8.28b) determines the condition for the transition from smooth wavy (separated regime) to rough wavy (annular regime) flows, and the solution of this equation and equation (8.21b) for the separated-intermittent transition will determine the conditions below which slug flow will not exist. This is given by

$$1 - \beta \simeq 0.09 \quad \text{or} \quad Fr_f^{\frac{1}{2}} \simeq 0.18 \tag{8.32}$$

A similar result could have been arrived at using a simple physical criteria for the minimum liquid level necessary for the slug to form. It might be expected that the minimum liquid level (corresponding to $1 - \alpha$) would require to be half the channel height. This can be explained as follows; when a finite amplitude wave begins to grow, as a result of aerodynamic suction over its crest, liquid must be supplied from the film adjacent to the wave. If the wave is approximated by a sinusoid, then, when the level is above the centre line, the peak of the wave will reach the top before the trough reaches the bottom, and slug flow can develop. When the liquid level is below the centre line, the inverse will happen and slug development is less possible.

This sinusoid simulation is perhaps too idealised, however it does seem to agree with the findings of equation (8.32), i.e. $(1 - \beta) \simeq 0.09$, as can be seen from Fig. 8.9 where this value of $(1 - \beta)$ corresponds to a $(1 - \alpha)$ value of $\simeq 0.5$.

8.2.2.3 INTERMITTENT - ANNULAR FLOW TRANSITION

The experimental observations presented in section 8.2.1, together with those presented in Chapter 2 indicated that various complicated mechanisms could be present at this transition, such as droplet formation by wave shearing, film formation by droplet deposition or other mechanisms. In general, the data in the literature suggest that this transition would be more sensitive to a gas Froude number, rather than a liquid Froude number, type of correlation (steep boundary lines on U_{sf} versus U_{sg} co-ordinates). However, while this could be true, a simple hypothetical experiment would indicate that the liquid Froude number is also important. Visualise a situation where annular flow exists in a horizontal pipe at given gas and liquid flow-rates. Then by decreasing the gas flowrate, keeping liquid flowrate constant, one might expect the film thickness (at the bottom of the pipe) to increase until a condition is met where waves on the surface become unstable and develop into slugs.

The importance of the liquid Froude number in this transition could have been arrived at by dimensional analysis (at least for our test conditions) as follows. The development of a given flow pattern is dependent on such parameters as liquid and gas flowrates, properties of the phases, pipe diameter, inclination, etc. However, for our test conditions the properties were kept constant, and although the flows were in horizontal pipes, the gravity

component was important as was found in section 8.2.2.1 for the separated-intermittent transition. Hence the following possible combinations emerge

$$U_f = f(U_g,\ D,\ g) \qquad (8.33a)$$

or $$U_f = f(U_{sg},\ g) \qquad (8.33b)$$

or $$Fr_f = f(Fr_g) \qquad (8.33c)$$

Other possible correlations could involve β or $1 - \beta$ since,

$$\beta = \frac{Fr_g^{\frac{1}{2}}}{Fr_g^{\frac{1}{2}} + Fr_f^{\frac{1}{2}}} \quad \text{and} \quad 1 - \beta = \frac{Fr_f^{\frac{1}{2}}}{Fr_f^{\frac{1}{2}} + Fr_g^{\frac{1}{2}}}$$

where the Froude numbers are defined on the basis of superficial velocities.

One form could be

$$Fr_f = f(1 - \beta) \qquad (8.34)$$

To facilitate plotting a general flow pattern map for the air-water system being considered here, the form of correlation shown in equation (8.34) will be used here. In doing so it is recognised that, in general, a dependence on fluid properties may have to be superimposed on top of this.

Because of the subjectiveness of visual observations in determining this boundary, the transition in the characteristics of Fig. 8.2 for the pressure drop multiplier and Fig. 8.4 for the void fraction were used to determine the transition band. These data are given in Table 8.6 and plotted in terms of $(1 - \alpha)$ versus $(1 - \beta)$ in Fig. 8.13,

using only the pressure drop measurements before and after the transitions in the characteristics of Fig. 8.2. Fig. 8.14 also shows these data, together with those of the void fraction transition in Fig. 8.4, plotted to the co-ordinates suggested by equation (8.34). The stable annular flow boundary and the stable slug flow boundary may, approximately, be correlated by equations of the form

$$Fr_f^{\frac{1}{2}} = 5.2\ (1-\beta)^{0.72} \qquad \text{annular flow side of the boundary} \qquad (8.35a)$$

$$Fr_f^{\frac{1}{2}} = 4.2\ (1-\beta)^{0.89} \qquad \text{slug flow side of the boundary} \qquad (8.35b)$$

It is important to note that these equations are only applicable to the system considered here and that extrapolation should be done with care.

As mentioned in section 8.1, the transition between intermittent and annular flows becomes less sharp on increasing the liquid flowrate. At the highest water flow-rate conditions (onset of bubbly flows) no discontinuity appeared in the characteristics of Figs. 8.1 to 8.4, indicating no change in flow mechanisms, i.e. annular flow did not develop, but rather a homogeneous type flow prevailed. This was observed to occur at superficial liquid velocities $\sim$ 4 m/s and hence the value is taken as the condition for the onset of homogeneous flows. This corresponds to the 127 mm (5") ID pipe only and extrapolation to higher diameters should be done with caution.

A general flow regime map can now be plotted for the separated-intermittent-annular transitions based on the

Table 8.6

Test No.	Diagnosis	U_{sf} (m/s)	U_{sg} (m/s)	$1 - \alpha$	Pattern
070901	P1, V1	2.2837	2.6576	.431	2
080901	V2	2.2708	3.3487	.491	2
150901	P1	2.5959	1.971	.523	2
160901	V1	2.6016	2.6496	.481	2
170901	V2	2.5818	3.184	.542	2
061201	V1	3.0977	2.2583	.561	2
071201	P1, V2	3.1142	3.0298	.553	2
152301	V1	1.0858	3.7007	.24	2
072601	V1	1.253	3.632	.263	2
162601	V1	1.3709	3.9826	.281	2
022801	V1	.4184	5.8205	.158	2
013001	P1, V1, V3	.4254	9.042	.20	2
010502	P2	.4389	17.393	.172	5
020202	V1	.5918	7.1062	.176	2
030202	P1, V2	.5918	10.5206	.203	2
040202	V3	.5918	15.2002	.218	52
010602	P2	.5868	16.9269	.188	5
080202	P1, V1	.7716	6.3477	.194	2
090202	V2	.7791	8.5405	.262	2
100202	V3	.7828	11.2775	.274	25
110202	P2	.7753	14.8669	.220	5
010302	P1	.945	4.511	.220	2
020302	V1	.9325	6.9035	.211	2
030302	V3	.9388	10.3016	.309	2
040302	P2	.9357	14.3691	.235	5
060302	P1, V2	1.0804	4.351	.246	2
080302	V3	1.0804	9.5064	.332	2
090302	P2	1.0912	13.306	.271	5
010402	P1, V2	1.22	4.4624	.271	2
030402	V3	1.2342	9.1942	.364	2
040402	P2	1.2413	11.9488	.317	52
060402	P1, V2	1.3794	4.0187	.290	2
080402	V3	1.3666	8.3617	.385	2

Contd.

Test No.	Diagnosis	U_{sf} (m/s)	U_{sg} (m/s)	$1 - \alpha$	Pattern
090402	P2	1.3666	10.4346	.336	25
011802	P1, V1	1.4826	3.7801	.313	2
021802	V2, V3	1.4675	6.521	.370	2
041802	P2	1.4922	12.4797	.302	25
081802	P1, V1	1.9252	3.9988	.359	2
091802	V3	1.9061	6.0507	.492	2
101802	P2	1.9099	8.4298	.392	2
012002	V3	2.2773	4.2071	.483	2
022002	P2	2.2708	6.683	.448	2
012302	V3	2.5733	3.6751	.512	2
022302	P2	2.5618	6.1726	.482	2
112302	P2	3.1072	5.5719	.497	2

Table 8-6 Phase 2 results for the slug/annular boundary deduced using transition points indicated by Figs. 8.2 and 8.4.

Key

P1 : Last possible pressure drop measurement in slug flow.

P2 : First possible pressure drop measurement in annular flow.

V1 : Last possible void fraction measurement in slug flow.

V2 : Void fraction in the transition zone.

V3 : Minimum void fraction value measured before it starts to increase again.

$$F_{rf}^{\frac{1}{2}} = \frac{U_{sf}}{\sqrt{gD}} \quad , \quad 1 - \beta = \frac{U_{sf}}{U_{sf} + U_{sg}}$$

PHASE 2 DATA

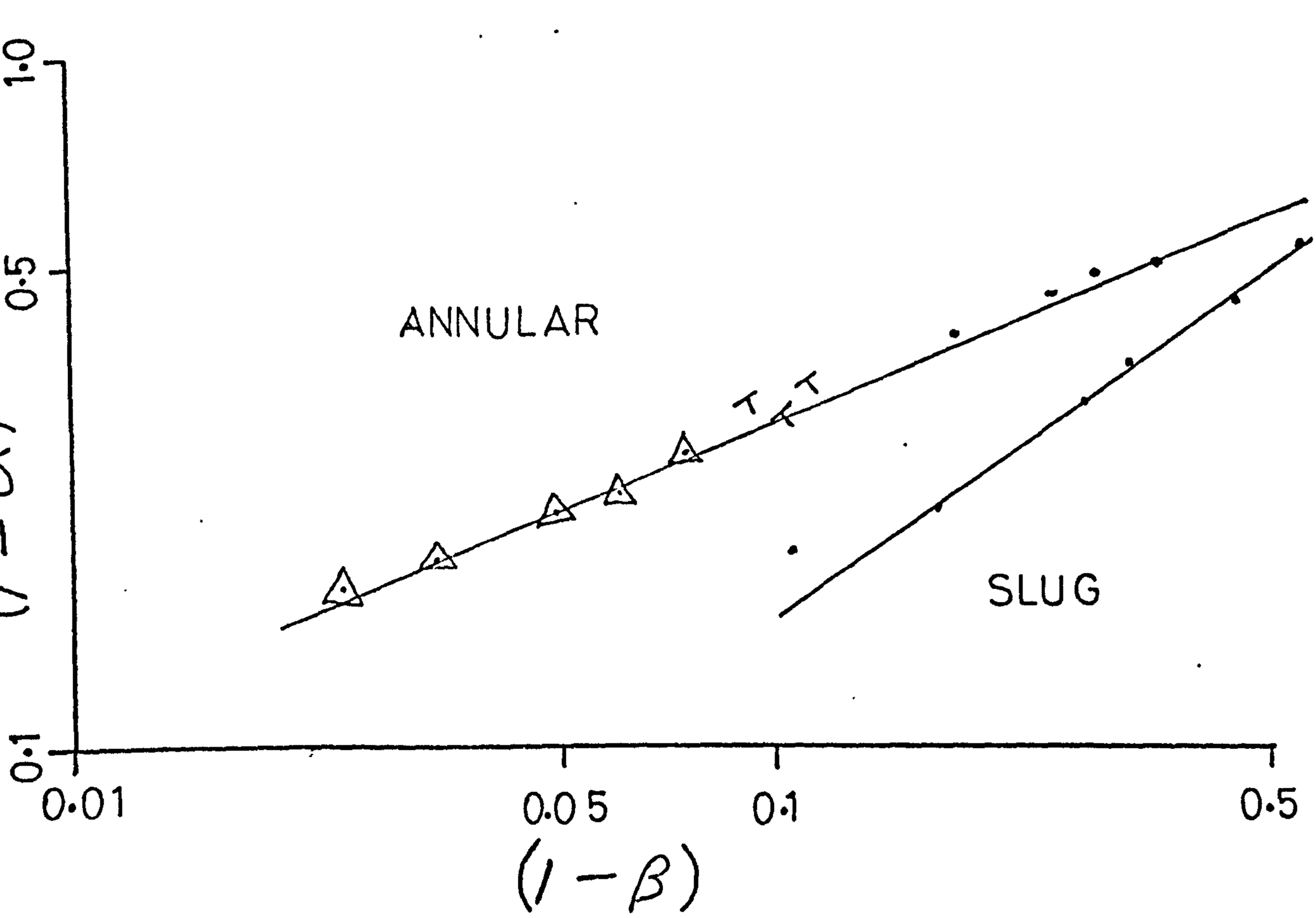

△ ANNULAR
• SLUG
T TRANSITION

USING TRANSITION POINTS INDICATED BY FIG 8·2

FIG. 8.13 VOID FRACTION CORRELATION FOR THE SLUG-ANNULAR TRANSITION

PHASE 2 DATA

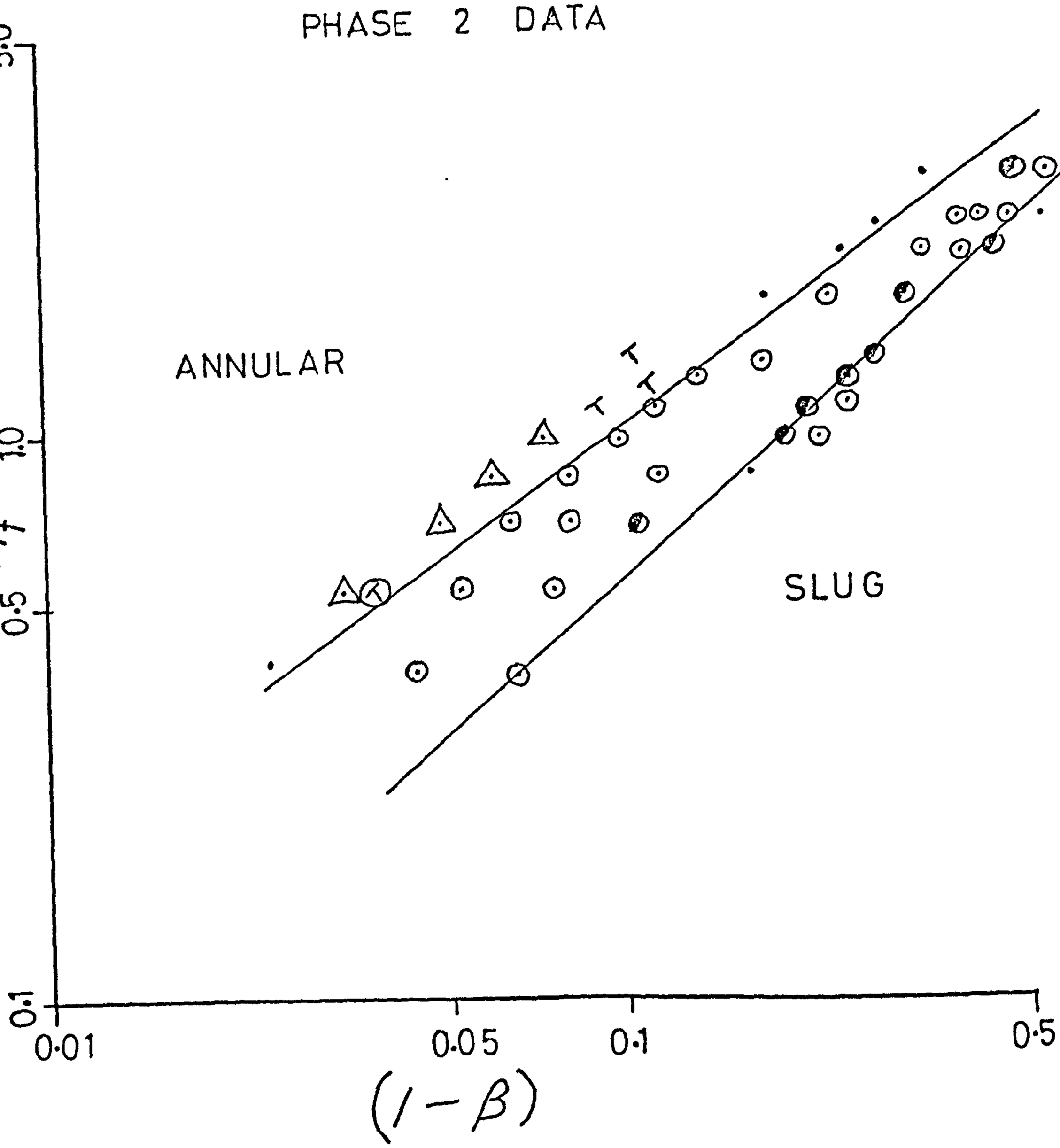

△ ANNULAR
• SLUG
T TRANSITION
} PRESSURE DROP READING POSSIBLE

o VOID FRACTION READING CHANGES

⊙ VOID FRACTION READING CHANGES AND PRESSURE DROP MEASUREMENTS POSSIBLE

FIG. 8.14 SLUG-ANNULAR TRANSITION CORRELATION

dimensionless group $Fr_f^{\frac{1}{2}}$ and 1 - β suggested by the wave stability theory. Using the experimental results (i.e. Fig. 8.10, 8.12 and 8.14), the map is shown in Fig. 8.15 with all of the transition boundaries being reduced to simple straight lines on a log-log scale. The map is also presented in Fig. 8.16, but on the basis of different coordinates of $Fr_f^{\frac{1}{2}}$ versus $(1-\alpha)$, also suggested by the theory.

These boundaries were transferred to the Phase 2 map plotted on coordinates of superficial velocities and are shown in Fig. 8.17. The striking feature in this figure is the negative slope of the intermittent-annular transition boundary. Most of the transition data available in the literature showed a positive slope for this boundary (see flow pattern maps in Chapters 2 and 6), although these were mostly based on visual observations, which has been shown to be inadequate. The only transition data identified by more objective means was that of Choe et al (C6), which also showed a negative slope, as can also be seen from their line plotted in Fig. 8.17 for comparison. They used a pressure transducer to detect slug flows through the pressure pulsations characterising such flows.

It is interesting to note (as a consequence of this negative slope) that at a given air velocity (Fig. 8.17) or a given void fraction (Fig. 8.16) the flow pattern can change from intermittent to annular flow by increasing the water flowrate (i.e. liquid Froude number). This may be explained by considering the case of a developed slug flow

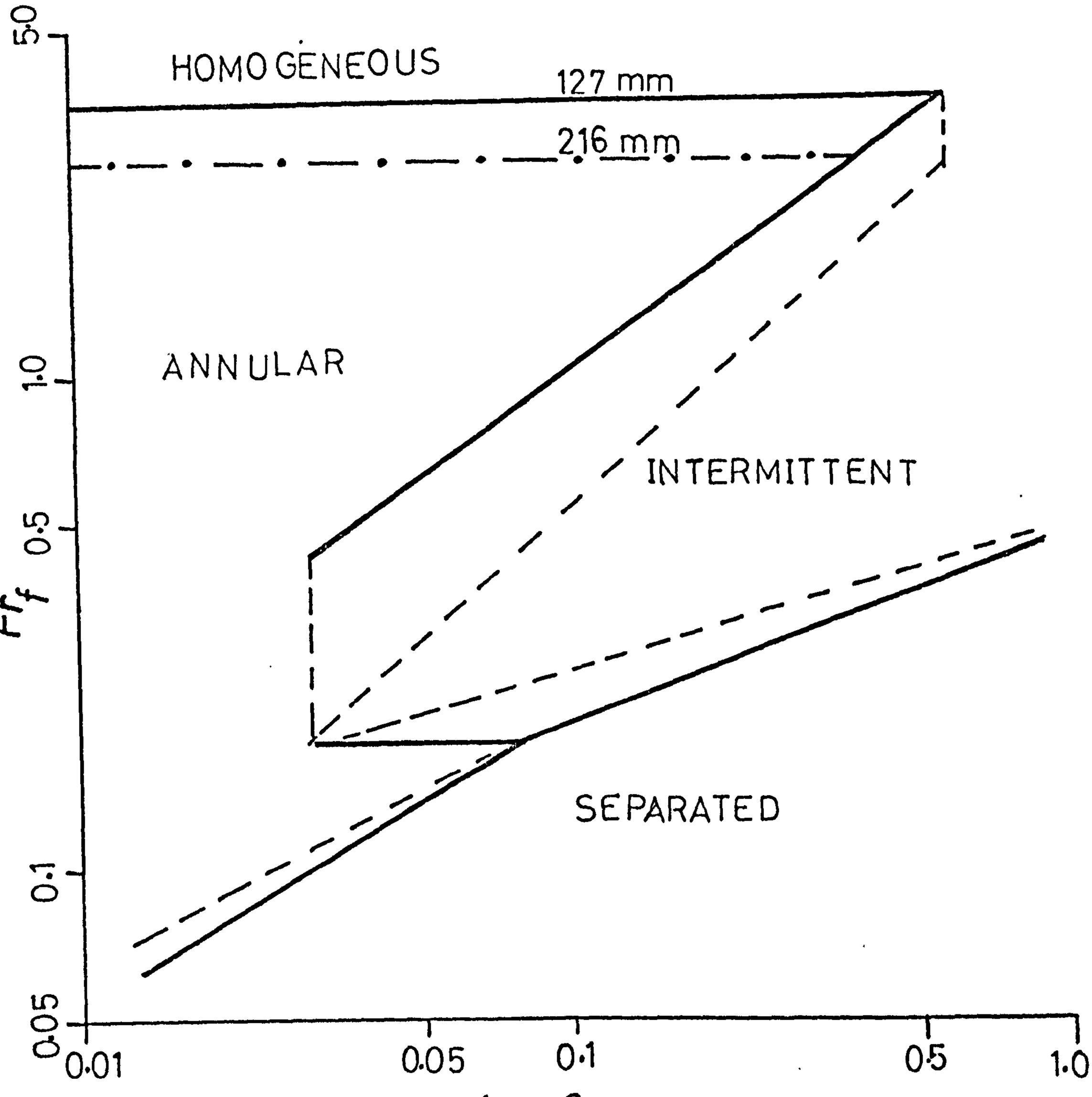

FIG. 8.15 PROPOSED FLOW PATTERN MAP

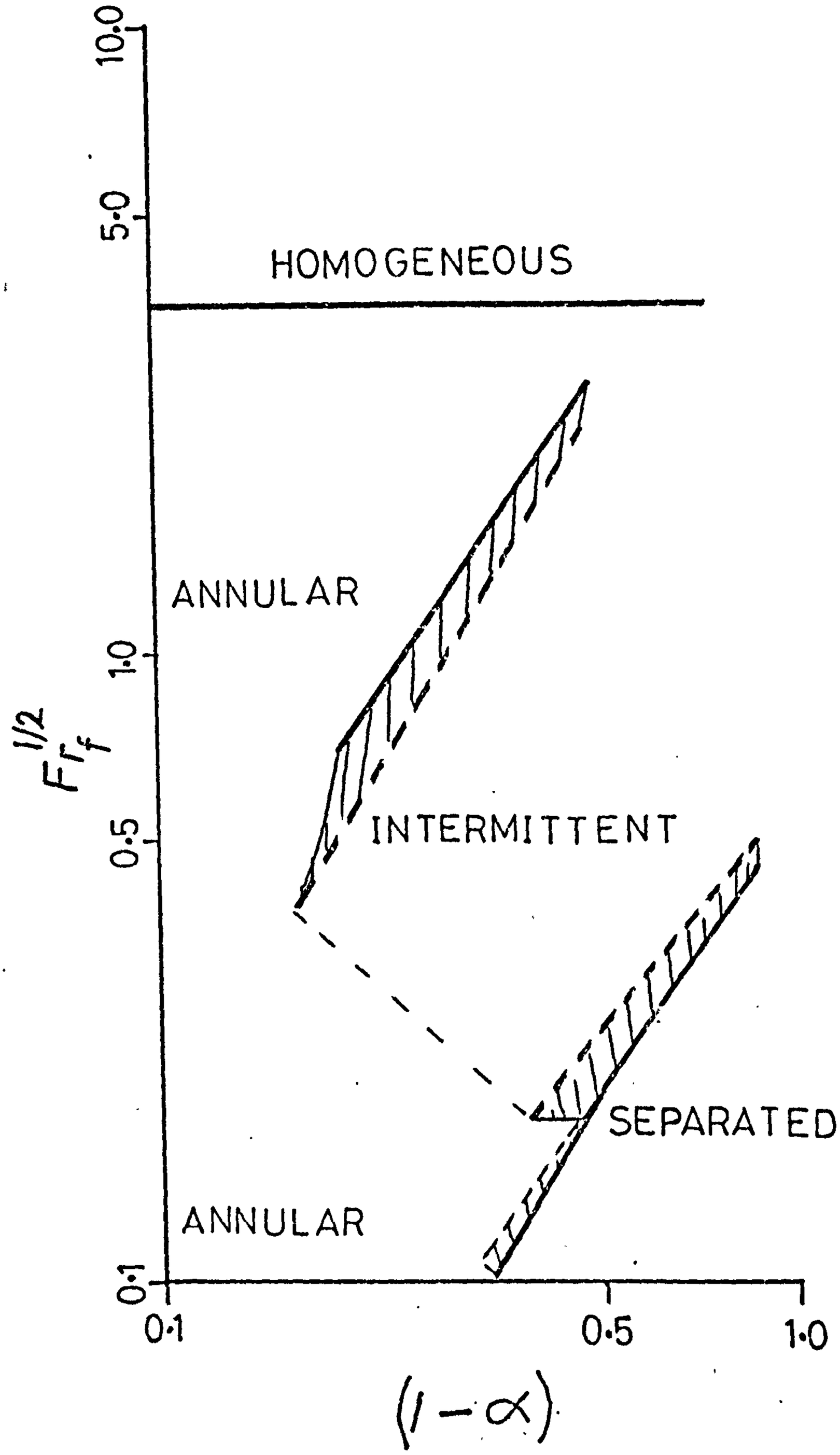

FIG. 8.16 PROPOSED FLOW PATTERN MAP

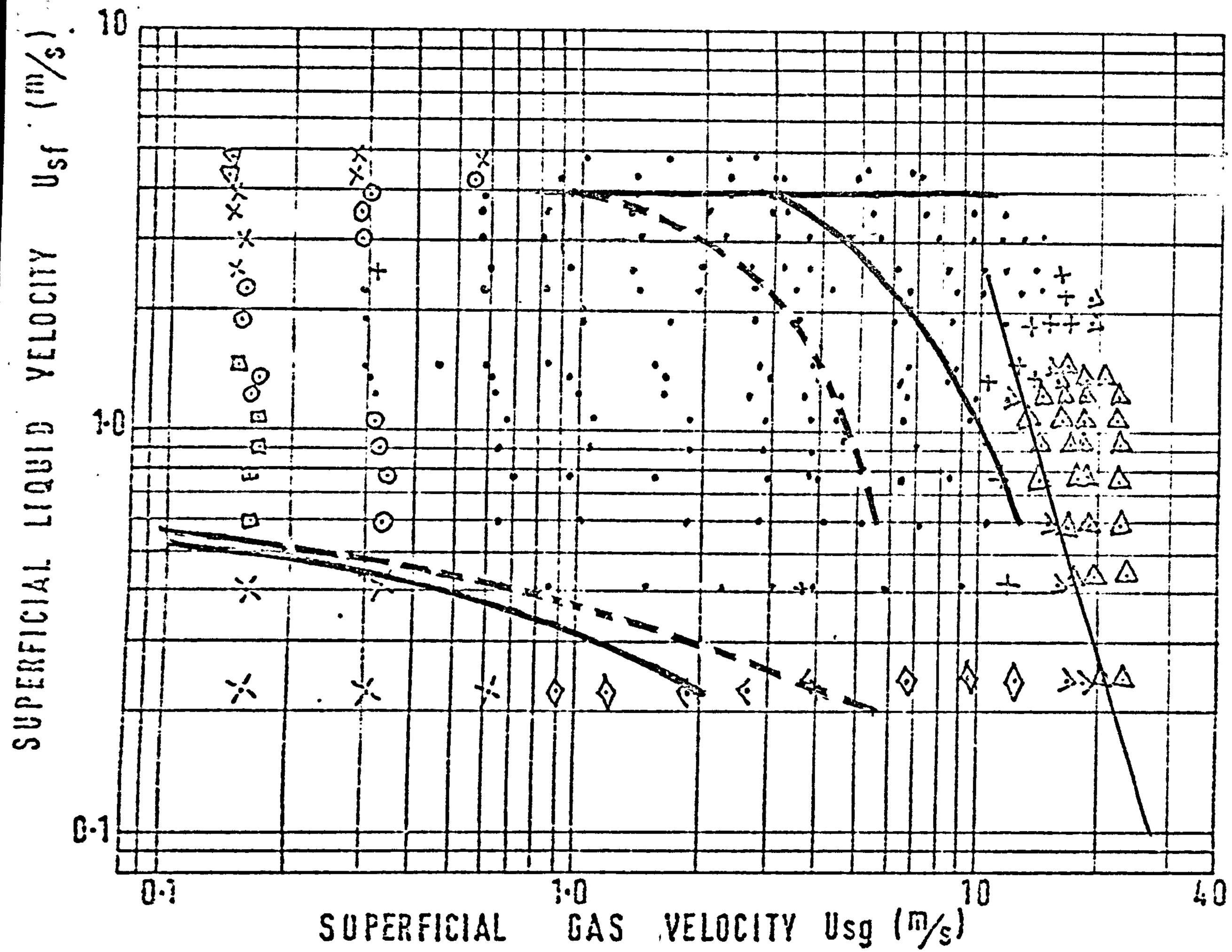

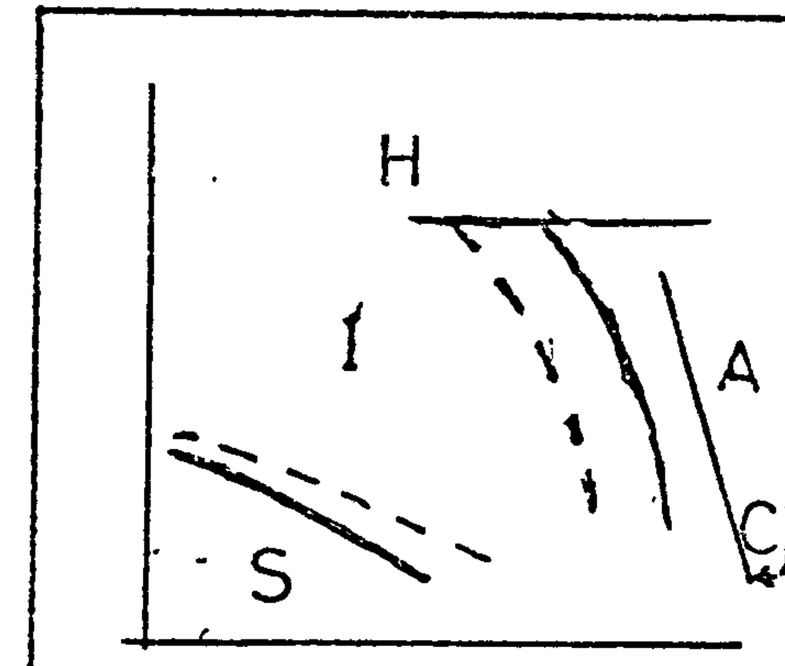

H HOMOGENEOUS

I INTERMITTENT

S SEPARATED

A ANNULAR

CH. CHOE ET AL LINE

FIG. 8.17 COMPARISON BETWEEN THE PHASE 2 AND THE PROPOSED MAPS

△ ANNULAR
• SLUG
◇ WAVY
⊡ PLUG
✕ STRATIFIED
▽ BUBBLY

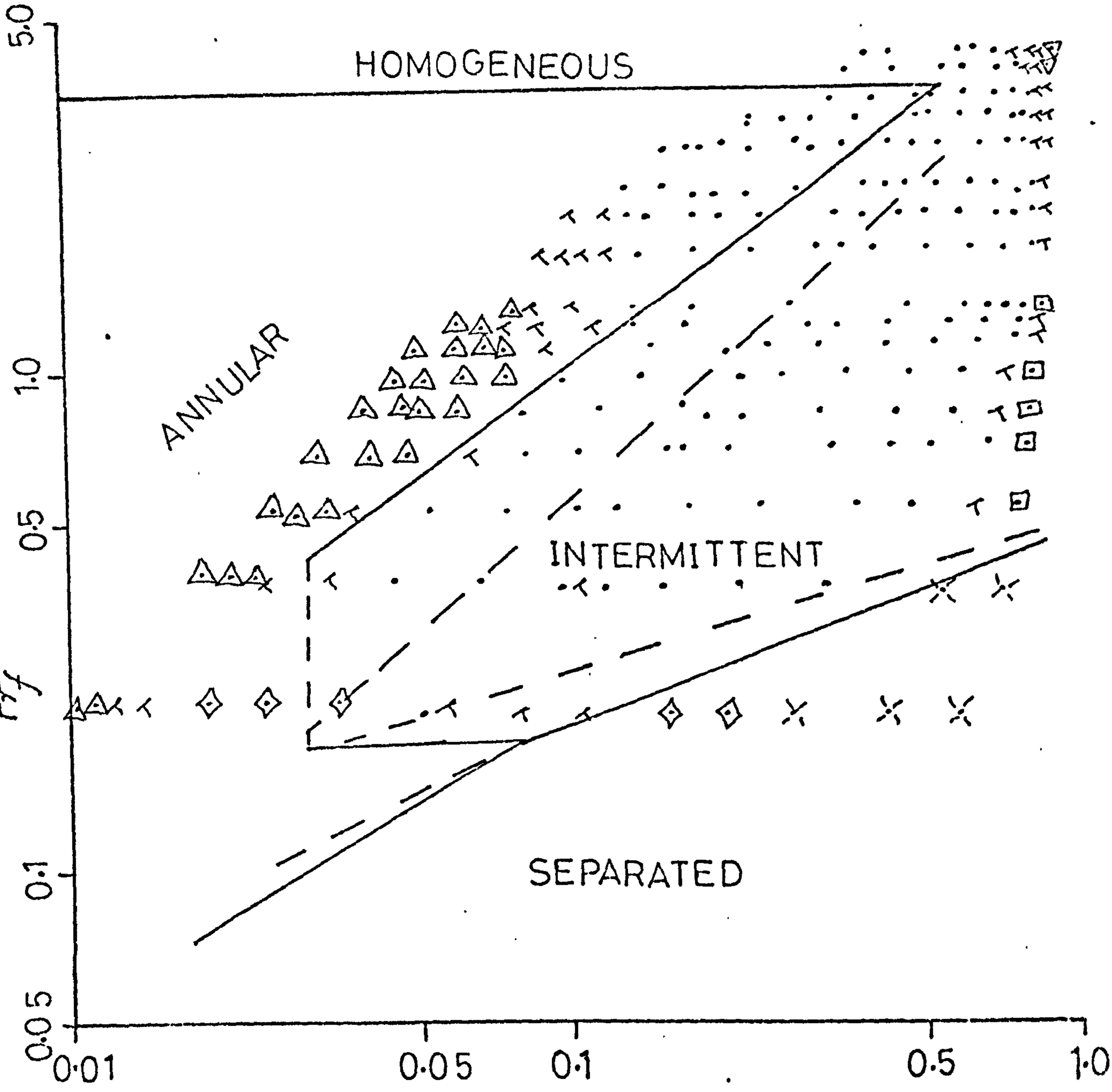

FIG 8.17A COMPARISON OF PHASE 2 RESULTS WITH THE PROPOSED MAP

in a horizontal pipe. The pressure drop across the slug is then balanced by the friction at the tube wall. Now by keeping the void fraction constant and increasing liquid flowrate, simply means faster moving liquid, and hence faster moving slugs. A point is reached where the pressure drop across the slug is much larger than that due to wall friction and the slug is accelerated to higher velocity, and finally broken down into droplets by the force of the flowing gas.

8.3 PRESSURE DROP PREDICTION

8.3.1 ANNULAR FLOWS

In large diameter pipes, annular flows deviate appreciably from the ideal case of 'uniform thickness annulus'. Instead, a superimposed stratification exists whereby a very thick liquid layer appears at the bottom of the pipe with a negligibly thin layer at the top. In this section, a simple model is first developed on the basis of a uniform annulus and then an attempt is made to introduce the superimposed stratification effect on the basis of experimental observations.

Consider the case of annular flow in a horizontal pipe with droplets in the core. If 'D' is the internal diameter of the pipe and $\bar{\delta}$ is the average film thickness, then

$$\bar{\delta} = \tfrac{1}{2} (D - d) \qquad (8.36)$$

and

$$\alpha = \frac{A_g}{A} = k_c \frac{d^2}{D^2} \tag{8.37}$$

where d is the average core diameter, and k_c is a factor introduced to allow for the presence of droplets in the core (assumed homogeneous hereafter) which is given by

$$k_c = \frac{Q_g}{Q_c} = \frac{Q_g}{Q_g + Q_e} \leqslant 1 \tag{8.38}$$

The fraction of the total liquid volume flowrate which is entrained is given by

$$k_e = \frac{Q_e}{Q_f} \tag{8.39}$$

which could be a function of gas flowrate, properties, etc. Obviously k_c and k_e are interrelated through the gas and liquid flowrates, i.e. from equations (8.38) and (8.39)

$$k_c = \frac{1}{1 + k_e \frac{Q_f}{Q_g}} \tag{8.40}$$

Neglecting acceleration effects then, from the sketch below, a force balance on the core gives

$$\frac{\sum \text{force}}{\text{volume of mixture}} = 0$$

$$\frac{(-\frac{\partial p}{\partial Z} \Delta Z) \frac{\pi}{4} d^2}{(\frac{\pi}{4} D^2) \Delta Z} - \frac{(\pi d) \bar{\tau}_i \Delta Z}{(\frac{\pi}{4} D^2) \Delta Z} = 0 \tag{8.41a}$$

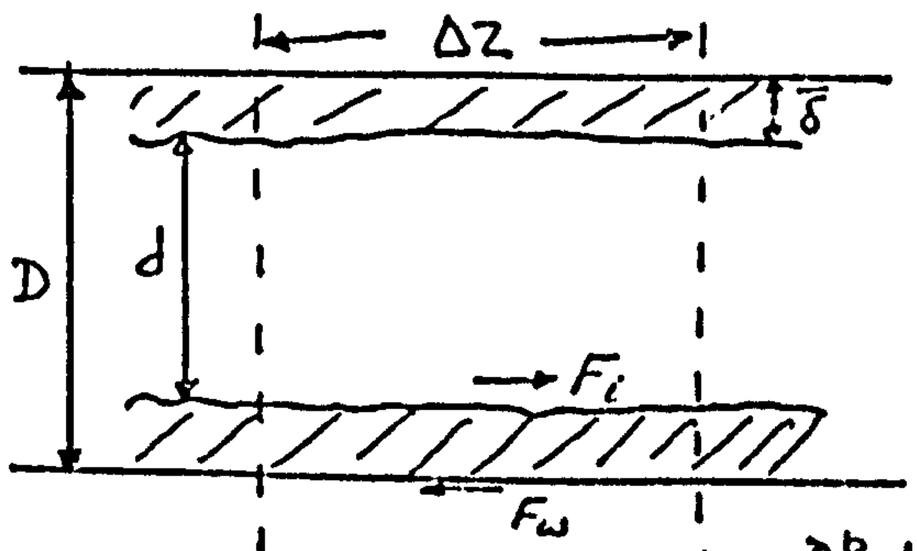

where $\bar{\tau}_i$ is the average interfacial shear stress.

$$\therefore -\frac{\partial p}{\partial Z} = \frac{4\overline{\tau}_i}{D}\left(\frac{D}{d}\right)$$

or from equation (8.37),

$$-\frac{\partial p}{\partial Z} = \frac{4\overline{\tau}_i}{D}\sqrt{\frac{k_c}{\alpha}} \qquad (8.41b)$$

For the liquid film,

$$\frac{\left(-\frac{\partial p}{\partial Z}\Delta Z\right)\frac{\pi}{4}(D^2 - d^2)}{\left(\frac{\pi}{4}D^2\right)\Delta Z} + \frac{(\pi d)\ \overline{\tau}_i\ \Delta Z}{\left(\frac{\pi}{4}D^2\right)\Delta Z} - \frac{(\pi D)\,\overline{\tau}_{wf}\,\Delta Z}{\left(\frac{\pi}{4}D^2\right)\Delta Z} = 0 \qquad (8.42a)$$

where $\overline{\tau}_{wf}$ is the average wall shear stress.

$$\therefore -\frac{\partial p}{\partial Z} = \frac{4\overline{\tau}_{wf}}{D}\frac{1}{\left(1-\frac{\alpha}{k_c}\right)} - \frac{4\overline{\tau}_i}{D}\frac{\sqrt{\frac{\alpha}{k_c}}}{\left(1-\frac{\alpha}{k_c}\right)} \qquad (8.42b)$$

Substituting for $\left(-\frac{\partial p}{\partial Z}\right)$ from equation (8.41b) gives

$$\frac{\overline{\tau}_i}{\overline{\tau}_{wf}} = \sqrt{\frac{\alpha}{k_c}} \qquad (8.43)$$

If τ_{wf_l} is taken to represent the 'all liquid' condition wall friction shear stress (i.e. with the liquid component flowing alone), then

$$-\left(\frac{\partial p}{\partial Z}\right)_{f_l} = \frac{4\tau_{wf_l}}{D} \qquad (8.44)$$

Utilising equations (8.44), (8.43) and (8.41b) gives

$$\phi_f^2 = \frac{(-\partial p/\partial Z)}{(-\partial p/\partial Z)_{f_l}} = \frac{\overline{\tau}_{wf}}{\tau_{wf_l}} \qquad (8.45)$$

As detailed in Appendix Z for annular flow conditions, the two phase friction multiplier can be expressed as

$$\phi_f^2 = \frac{(1 - k_e)^{2-n} \left(1 + \sqrt{\frac{\alpha}{k_c}}\right)^n}{\left(1 - \frac{\alpha}{k_c}\right)^2} \qquad (8.46)$$

which requires an entrainment correlation.

It is easily shown that

$$\phi_{f_o}^2 = \phi_f^2 (1 - x^2) \frac{\lambda_{f_1}}{\lambda_{f_o}} \qquad (8.47)$$

where λ_{f_1} and λ_{f_o} are the friction factors based on the water component flowrate and the total mixture flowrate, respectively, flowing alone in the tube.

Because of the relatively low qualities covered by the experimental data (Fig. 8.2) and because $\lambda_{f_1} > \lambda_{f_o}$ (due to $Re_{f_1} < Re_{f_o}$), the approximation $\phi_{f_o}^2 \simeq \phi_f^2$ can be made without introducing significant error.

The experimental $\phi_{f_o}^2$ results for Phase 2 tests are plotted against $(1 - \alpha)$ in Fig. 8.18. The data show a similar trend to that suggested by equation (8.46) but with the values much lower than the zero entrainment line (i.e. $k_c = 1$, $k_e = 0$). The influence of water flowrate is clear and is such that the higher the water flowrate the closer is the agreement with the zero entrainment line.

It was thought unwise at this stage to use existing entrainment correlations to evaluate k_c and k_e since the data available generally refer to small diameter pipes and very thin films.

The void fraction α is not normally known and a correlation in terms of, say, the mass dryness fraction (as suggested by Fig. 8.2) is necessary. This effect can

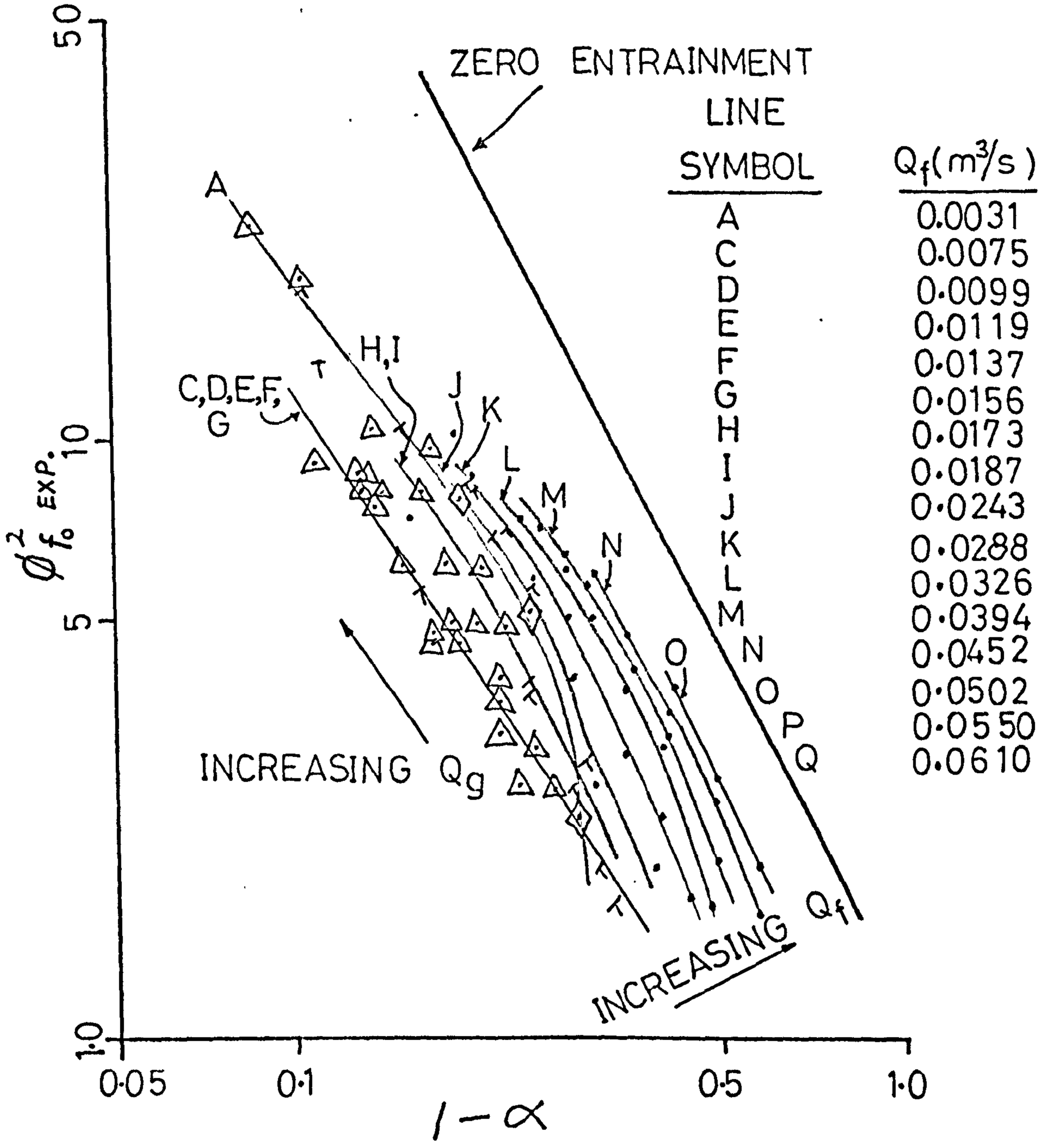

FIG. 8.18 $\phi^2_{f_o\,EXP.}$ VS $(1-\alpha)$ FOR ANNULAR FLOW WITH WATER FLOWRATE EFFECT SHOWN

be seen in the plot of $\phi^2_{f_o}$ versus x shown in Fig. 8.19, where straight lines are obtained with slopes ranging from $\sim$2 at the lowest water flowrate to $\sim$1 at the highest water flowrate. This indicates that a possible correlation could take the form

$$\phi^2_{f_o} = f(Q_f)\ x^n \qquad (8.48)$$

where 'n' and $f(Q_f)$ are functions of at least water flowrate (as shown in Figs. 8.19 and 8.20) and possibly diameter also.

Most horizontal annular flows are asymmetric (to a certain degree) even in relatively small diameter pipes ($\sim$1" - 2" ID). This behaviour is amplified in the bigger pipes, due to larger gravity effects, and this results in much thicker films at the bottom of the pipe than at the top. The experimental data of Whalley et al (W6) indicated that, for annular flows, the inferface roughness increases with film thickness, which in turn means a rougher interface at the bottom than at the top. The visual observations carried out in this project reinforced this conclusion and showed that (at least at relatively low water flowrate) the film at the top part of the tube was smooth compared to the bottom part which was very rough. This, in effect, means that the interfacial friction factor at the bottom is higher than at the top and suggests that the interfacial friction shear stress is higher at the bottom (see also section 2.6.3, part b). This effect is shown schematically in the sketch below, where the total interfacial shear force per unit length is given by

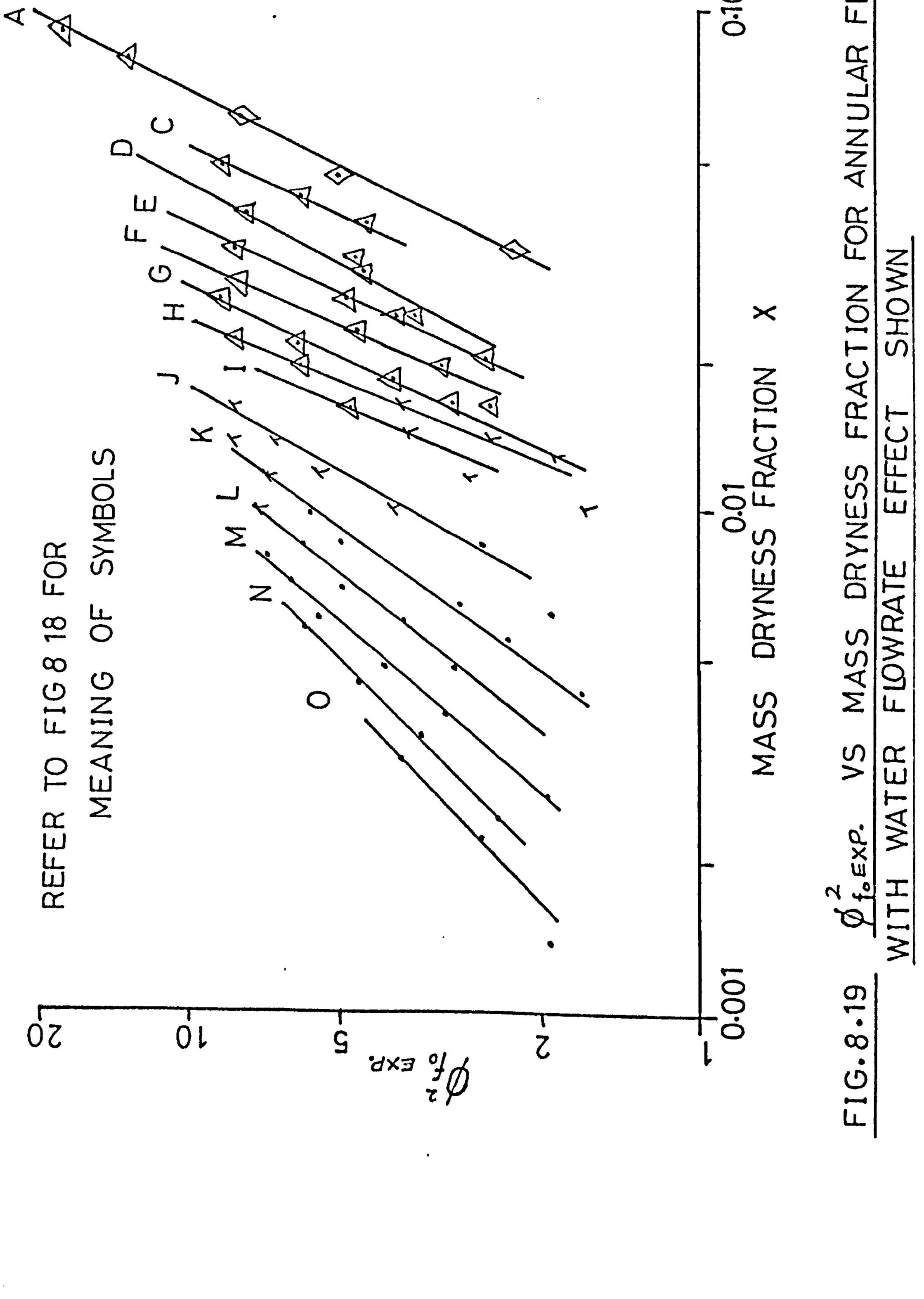
REFER TO FIG 8 18 FOR MEANING OF SYMBOLS
A
B
C
D
E
F
G
H
I
J
K
L
M
N
O
0·10
0.01
0.001
MASS DRYNESS FRACTION X
$\phi^2_{fo\,exp.}$ VS MASS DRYNESS FRACTION FOR ANNULAR FLOW WITH WATER FLOWRATE EFFECT SHOWN
$\phi^2_{fo\,exp.}$
1
2
5
10
20

FIG.8.19

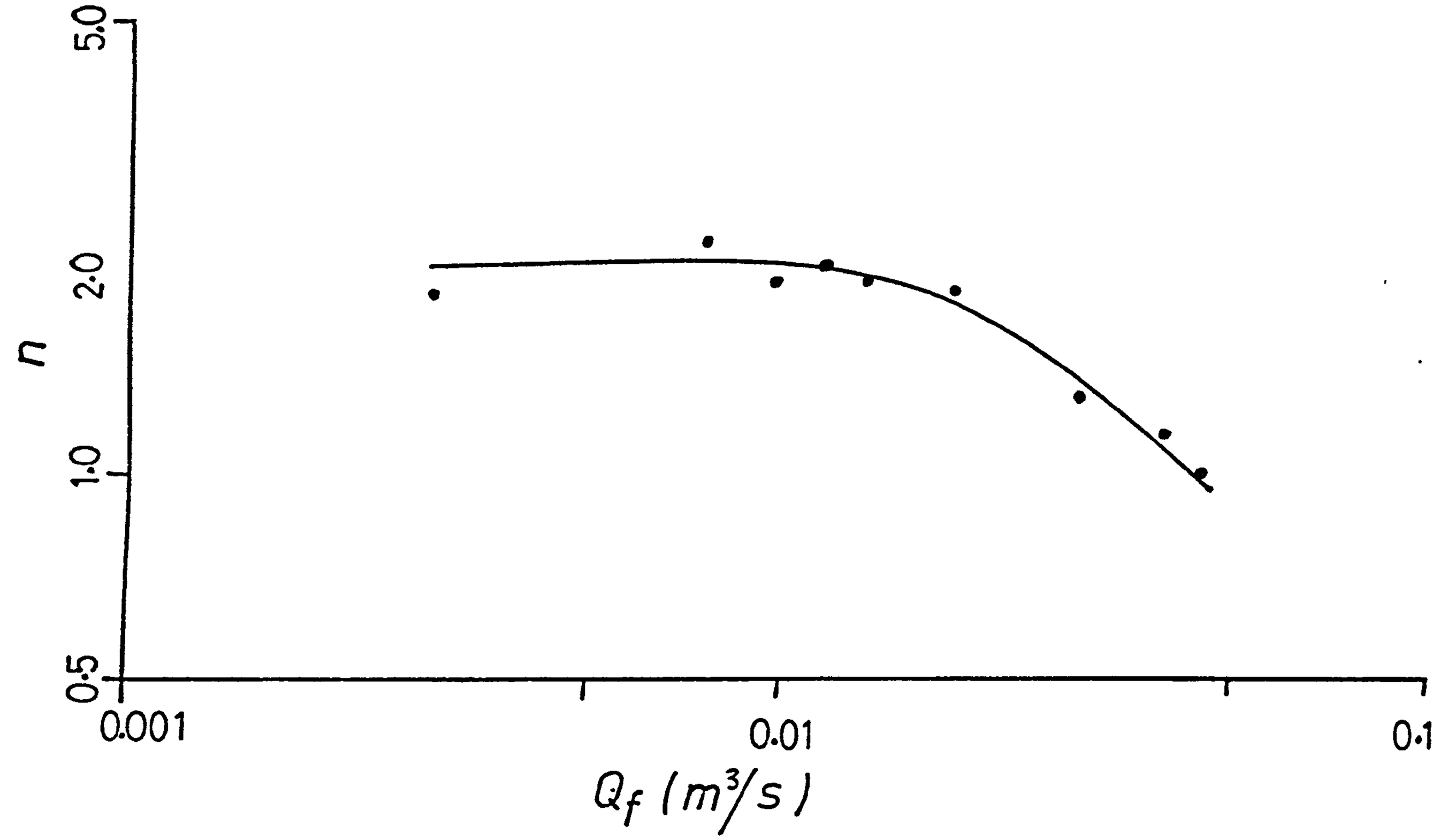

FIG. 8·20 THE DEPENDENCE OF THE EXPONENT IN EQUATION (8·48) ON WATER FLOWRATE

$$F_i = \int_0^{2\pi} \tau_i(\theta)\, r\, d\, \theta \qquad (8.49a)$$

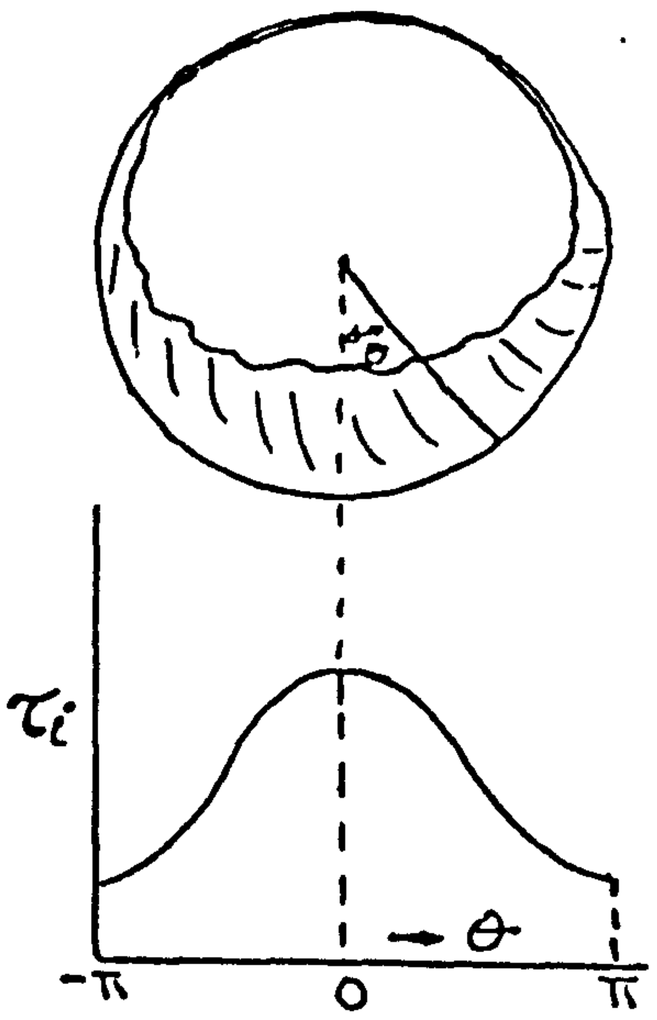

or

$$F_i = \bar{\tau}_i \pi\, d \qquad (8.49b)$$

where 'd' is the average core diameter, and $\bar{\tau}_i$ is the average interfacial shear stress given by

$$\bar{\tau}_i = \frac{1}{\pi d} \int_0^{2\pi} \tau_i(\theta)\, r\, d\, \theta \qquad (8.49c)$$

For the case of uniform film thickness (at the same flow conditions and total film C/S area), the shear stress is constant over the interface and the total shear force is then

$$F_{iu} = \tau_{iu} \pi\, d \qquad (8.50)$$

In this idealised situation (which is approached in small diameter pipes) the whole interface will be rough and it is likely that

$$\bar{\tau}_i < \tau_{iu} \qquad (8.51)$$

which, in view of equation (8.41b), might explain the low friction multipliers obtained for such flows when compared to the different correlations (mostly based on small diameter data) examined in Chapter 6. This explanation presupposes that beyond certain film thickness value, an increase in the film thickness will cease to cause appreciable increase in roughness (analogous to the behaviour in rough pipes). The experimental data showed

that for most of the conditions covered the film thickness at the bottom of the pipe could be as high as $\sim$ 25 mm ($\sim$1") or even higher as compared to a maximum value of $\sim$0.7 mm covered by the Whalley et al results.

Further work is needed along these lines to determine a correction effect for this asymmetric behaviour.

It was mentioned earlier (Chapter 6) that the large diameter tube data showed appreciable stratification and change in level effects which tended to produce different, and probably smaller, pressure drop values if the measurements were taken at tapping points other than those at the bottom of the tube. For the annular flow data being considered here, centre line tappings were used. These data might include some change in level effects due to asymmetry but these are probably small compared to the total pressure gradient.

8.3.2 INTERMITTENT FLOWS

The results given in Fig. 8.2 indicated that the behaviour of most slug, plug and bubbly flow points was fairly similar. Furthermore, the void fraction data presented in Chapter 6 (Fig. 8.3) also showed such points to cluster near the zero slip line, suggesting a possible correlation in terms of a homogeneous model with appropriately weighted mixture viscosity.

Using a trial and error solution, a homogeneous model based on a "viscosity of particle suspensions" suggested by Happel (H22) and corrected for mass velocity effects, i.e.

$$\mu_H = (1 + 5.5\beta)\left(\frac{G}{4300}\right)^{\beta} \qquad (8.52)$$

was used correlated the Phase 2 data within + 50% and -12.5% (Fig. 8.21) with a tendency for over prediction. Weisman and Choe (W4) also found it necessary to use correlations that predicted mixture viscosities much higher than that of the liquid in order to correlate the homogeneous flow data.

Using equation (8.52) in conjunction with a homogeneous flow model, however, under predicted the Phase 3 results (Fig. 8.22) by a maximum 50%. It is difficult to explain why this should be so, because of the limited conditions covered and the small amount of data collected, however change of level effects may be at least partly responsible and these in turn are a function of diameter.

8.3.3 SEPARATED FLOWS

It was shown in Chapter 6 that, for separated flows, the pressure drop measured in the gas phase differed from that measured in the liquid phase, due to the presence of a hydraulic gradient. One then ponders the physical meaning of such measurements and how they contribute to the total pressure drop which in turn requires some postulation for its prediction. To clarify these points a simple exercise was carried out as shown below with further details given in Appendix Z.

Consider a rectangular, horizontal duct of width B and height H in which steady state separated flow exists such that the liquid level decreases downstream, thus

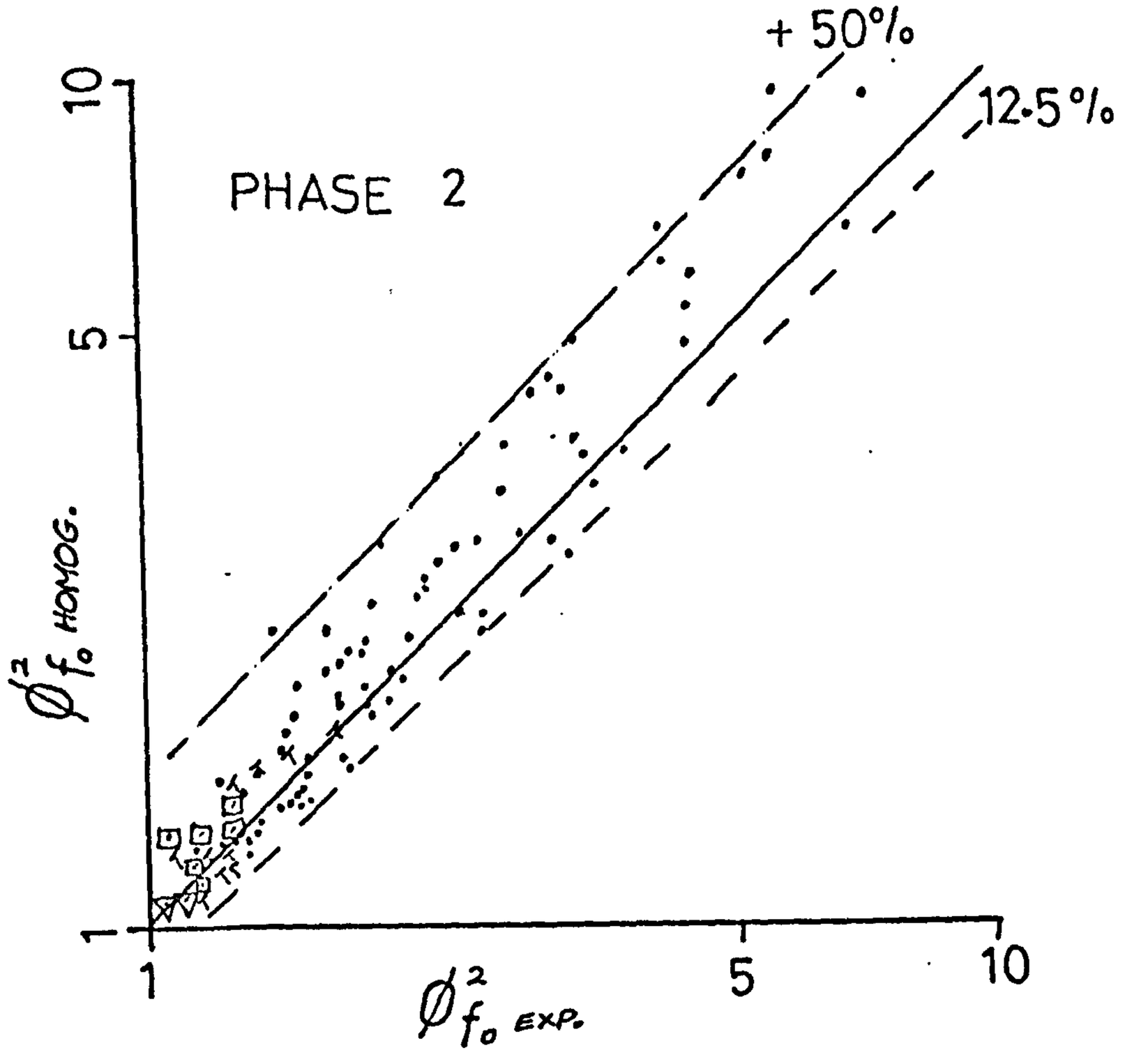

FIG. 8.21 COMPARISON BETWEEN EXPERIMENTAL AND HOMOGENEOUS FLOW MODEL FOR PHASE 2 INTERMITTENT FLOW DATA

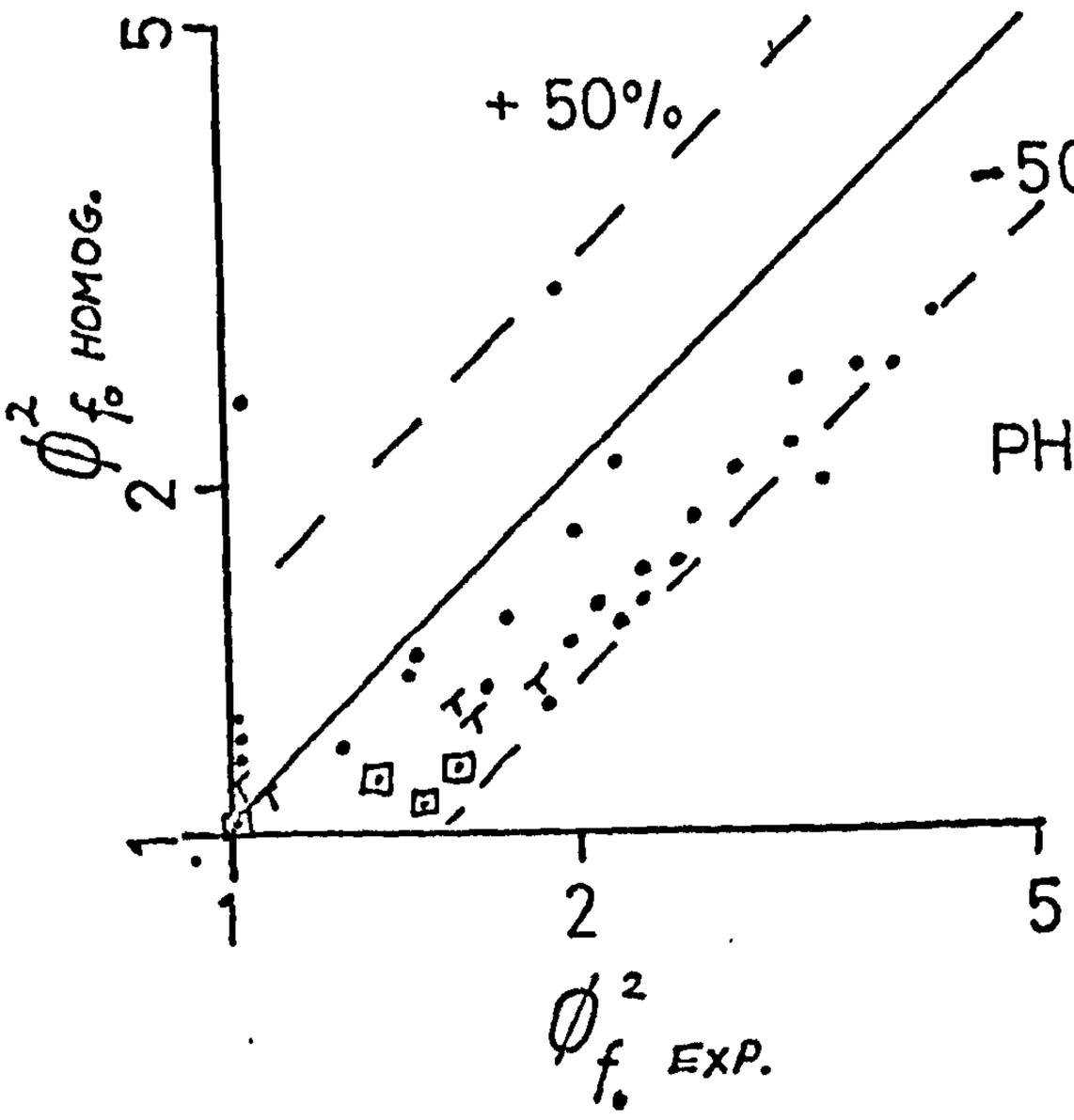

FIG. 8.22 COMPARISON BETWEEN EXPERIMENTAL AND HOMOGENEOUS FLOW MODEL FOR PHASE 3 INTERMITTENT FLOW DATA

simulating the conditions encountered in large diameter pipes. Variations in liquid density are neglected.

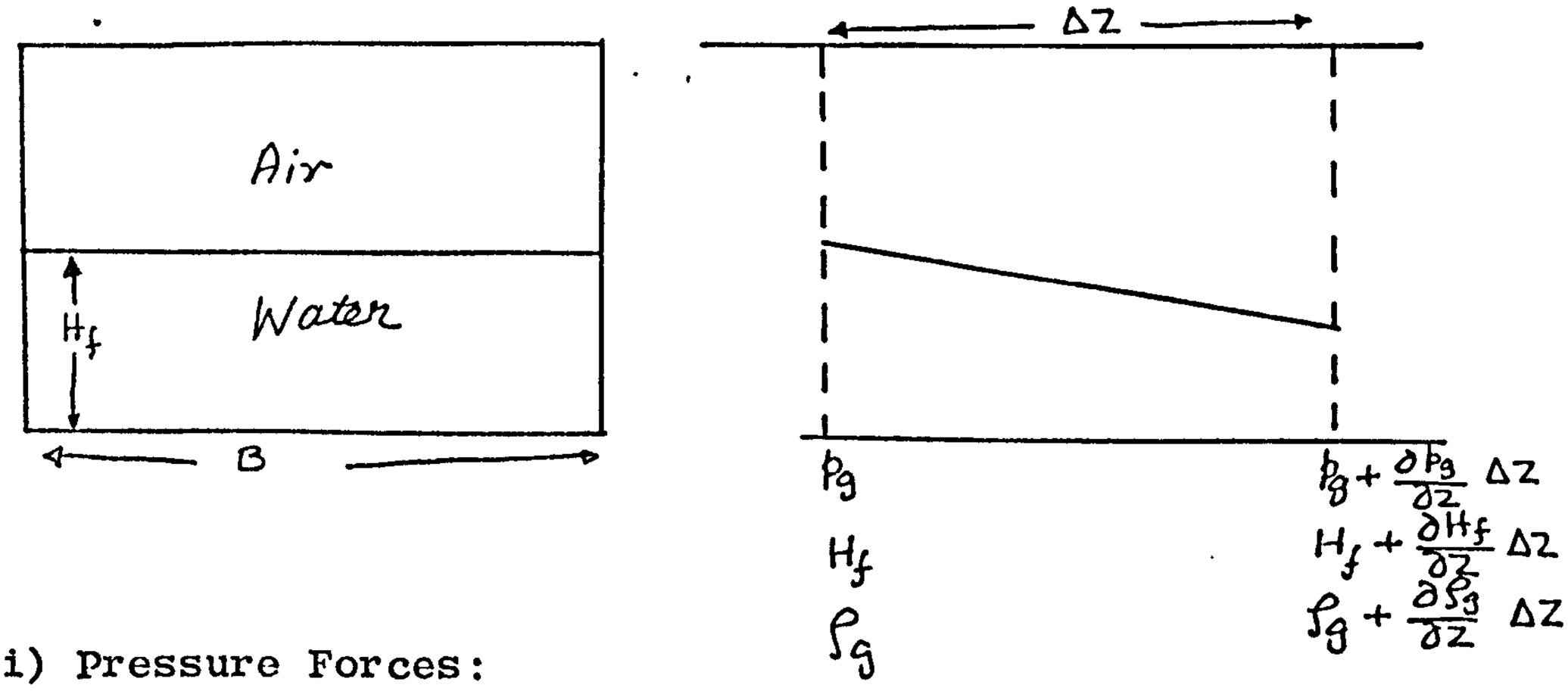

(i) Pressure Forces:

Net pressure force in direction of motion =

$$- HB \frac{\partial p_g}{\partial Z} \Delta Z - \rho_f g B \frac{\partial H_f}{\partial Z} (H_f + \tfrac{1}{2} \frac{\partial H_f}{\partial Z} \Delta Z) \Delta Z \qquad (8.53)$$

(ii) Frictional Forces:

Net friction force in direction of motion =

$$- F_{wg} - \frac{\lambda_f M_f^2}{8 \rho_f B^2 H_f^2} \left[1 - \frac{1}{H_f} \frac{\partial H_f}{\partial Z} \Delta Z \right] \left[B + 2H_f + \frac{\partial H_f}{\partial Z} \Delta Z \right] \qquad (8.54)$$

where λ_f is the wall friction factor (Appendix Z).

(iii) Rate of Change in Momentum:

Total rate of change in momentum

$$= \frac{\partial}{\partial Z} (M_g U_g + M_f U_f) \Delta Z$$

$$= \frac{\partial}{\partial Z} (M_g U_g) \Delta Z - \frac{M_f^2}{\rho_f B H_f^2} \frac{\partial H_f}{\partial Z} \Delta Z \qquad (8.55)$$

Conservation of momentum for the combined flow gives

$$- BH \frac{\partial p_g}{\partial Z} \Delta Z - \rho_f g B \frac{\partial H_f}{\partial Z} \left[H_f + \tfrac{1}{2} \frac{\partial H_f}{\partial Z} \Delta Z \right] \Delta Z - F_{wg}$$

$$- \frac{\lambda_f M_f^2}{8 \rho_f B^2 H_f^2} \left[1 - \frac{1}{H_f} \frac{\partial H_f}{\partial Z} \Delta Z \right] \left[B + 2H_f + \frac{\partial H_f}{\partial Z} \Delta Z \right] \Delta Z$$

$$= \frac{\partial}{\partial Z} (M_g U_g) \Delta Z - \frac{M_f^2}{\rho_f B H_f^2} \frac{\partial H_f}{\partial Z} \Delta Z \qquad (8.56)$$

Applying the conservation of momentum to the gas phase alone gives

$$B p_g \frac{\partial H_f}{\partial Z} \Delta Z - BH \frac{\partial p_g}{\partial Z} \Delta Z + BH_f \frac{\partial p_g}{\partial Z} \Delta Z + B \frac{\partial p_g}{\partial Z} \Delta Z \frac{\partial H_f}{\partial Z} \Delta Z$$

$$- F_{wg} - \frac{\lambda_{ig}}{8} \rho_g (U_g - U_f)^2 B \Delta Z = \frac{d}{dZ} (M_g U_g) \Delta Z \qquad (8.57)$$

where λ_{ig} stands for the interfacial friction factor (Appendix Z).

Substituting in equation (8.56) and rearranging gives

$$B \frac{\partial p_g}{\partial Z} \Delta Z \left[H_f + \frac{\partial H_f}{\partial Z} \Delta Z \right] - \frac{M_f^2}{\rho_f B H_f^2} \left[\frac{\partial H_f}{\partial Z} \Delta Z - \right.$$

$$\left. \frac{\lambda_f}{8B} (1 - \frac{1}{H_f} \frac{\partial H_f}{\partial Z} \Delta Z)(B + 2H_f + \frac{\partial H_f}{\partial Z} \Delta Z) \right] -$$

$$B \frac{\partial H_f}{\partial Z} \Delta Z \left[p_g + \rho_f g (H_f + \tfrac{1}{2} \frac{\partial H_f}{\partial Z} \Delta Z) \right] + \frac{\lambda_{ig}}{8} \rho_g (U_g - U_f)^2 B \Delta Z$$

(8.58)

Carrying out the same procedure for circular pipes is much more complex as indicated in Appendix Z.

Two simple cases can be considered

(A) <u>No change in level</u>:

This means $\frac{\partial H_f}{\partial Z} = 0$ and equation (8.58) reduces to

$$\Delta p_g = \frac{\partial p_g}{\partial Z} \Delta Z = - \frac{\lambda_f M_f^2}{8 \rho_f B^2 H_f^3} (B + 2H_f) - \frac{\lambda_{ig}}{8H_f} \rho_g (U_g - U_f)^2 \Delta Z \qquad (8.59)$$

i.e. the pressure drop in the gas consists of 'liquid wall friction' and 'interfacial friction' components.

Thus pressure tapping points in the gas phase (top of tube) can be related to,

(a) gas wall friction plus interfacial friction, or

(b) liquid wall friction plus interfacial friction (equation 8.59) or

(c) gas wall friction = liquid wall friction if interfacial friction is neglected.

(d) If pressure tappings in the liquid phase (bottom of tube) then the measured pressure drop p_f is given by

$$\Delta p_f = \Delta p_g + \rho_f g \frac{\partial H_f}{\partial Z} \Delta Z = \Delta p_g$$

(B) <u>With change in liquid level</u>

This means $\frac{\partial H_f}{\partial Z} \neq 0$, and from equation (8.58)

$$\Delta p_g = \frac{- \lambda_f M_f^2 (B + 2H_f)}{8 \rho_f B^3 H_f^2 (H_f + \frac{\partial H_f}{\partial Z} \Delta Z)} + \frac{\lambda_f M_f^2 \frac{\partial H_f}{\partial Z} \Delta Z (1 + \frac{B}{H_f})}{8 \rho_f B^3 H_f^2 (H_f + \frac{\partial H_f}{\partial Z} \Delta Z)}$$

$$+ \frac{\frac{\partial H_f}{\partial Z} \Delta Z}{(H_f + \frac{\partial H_f}{\partial Z} \Delta Z)} \left[\frac{M_f^2}{\rho_f B^2 H_f^2} - p_g - \rho_f g (H_f + \tfrac{1}{2} \frac{\partial H_f}{\partial Z} \Delta Z) \right]$$

$$+ \frac{\lambda_{ig}}{8} \frac{\rho_g (U_g - U_f)^2 \Delta Z}{(H_f + \frac{\partial H_f}{\partial Z} \Delta Z)} \qquad (8.60)$$

i.e. the pressure drop in the gas consists of 'liquid wall

friction', 'additional' wall friction (liquid) due to variation in level, 'change in liquid momentum' due to change in level, 'change in gas pressure' due to change in level, 'change in liquid pressure' due to change in level, and 'interfacial friction'.

Thus the pressure tapping points in the gas phase (top of tube) can be related to

(a) gas wall friction plus interfacial effect plus gas acceleration effects, or

(b) liquid wall friction plus interfacial effects, plus a number of change in level effects which may or may not be significant.

(c) If liquid wall friction effects are desired (in order to effect some evaluation of the net friction ΔP in terms of gas wall friction and liquid wall friction) then the Δp_g measured value may require modification.

(d) If pressure tapping points are situated in the bottom of the tube, i.e. in the liquid phase, then the measured pressure drop p_f is given by

$$\Delta p_f = \Delta p_g + \rho_f g \frac{\partial H_f}{\partial Z} \Delta Z \qquad (8.61)$$

Hence the change in liquid level $\frac{\partial H_f}{\partial Z}$ can be found from

$$\frac{\partial H_f}{\partial Z} = \frac{\Delta p_f - \Delta p_g}{\rho_f g \Delta Z} \qquad (8.62)$$

where ΔZ is the distance between the measuring points,

Δp_g is the pressure difference measured with top taps

and Δp_f is the pressure difference measured with bottop taps.

Equation (8.58) suggests that, in order to effect a theoretical solution, the term $\frac{\partial H_f}{\partial Z}$ must be known. While this could have been calculated using equation (8.62), it was thought unwise to extrapolate equation (8.60) to the round tube conditions (in view of the complexities encountered in Appendix Z; also no information was available on the liquid level in the pipe).

For the case of stratified flow where there is a change in liquid level, i.e. where the Δp_g and Δp_f values are not equal, a postulation regarding the overall friction pressure gradient must be made. Since it is essentially based on wall friction, it seems reasonable to weight this on the respective phase wetted perimeters, i.e.

$$\left(\frac{\Delta p}{\Delta Z}\right) = \frac{\Delta p_g}{\Delta Z}\left[\frac{B + 2(H - \bar{H}_f)}{2(H + B)}\right] + \frac{\Delta p_f}{\Delta Z}\left[\frac{B + 2\bar{H}_f}{2(H + B)}\right] \quad (8.63)$$

where $\bar{H}_f$ is the average liquid level between the measuring stations.

The experimental pressure drop data (top and bottom tappings) are plotted in Fig. 8.23 in terms of the liquid friction multiplier and mass dryness fraction. The differences in magnitudes between the two pressure drop readings are significant except perhaps in the high quality range (i.e. high air flowrate, and hence the transition to rough wavy flow conditions) where the effects of changes in level become less important. Also the trends are completely different with the top pressure tapping results

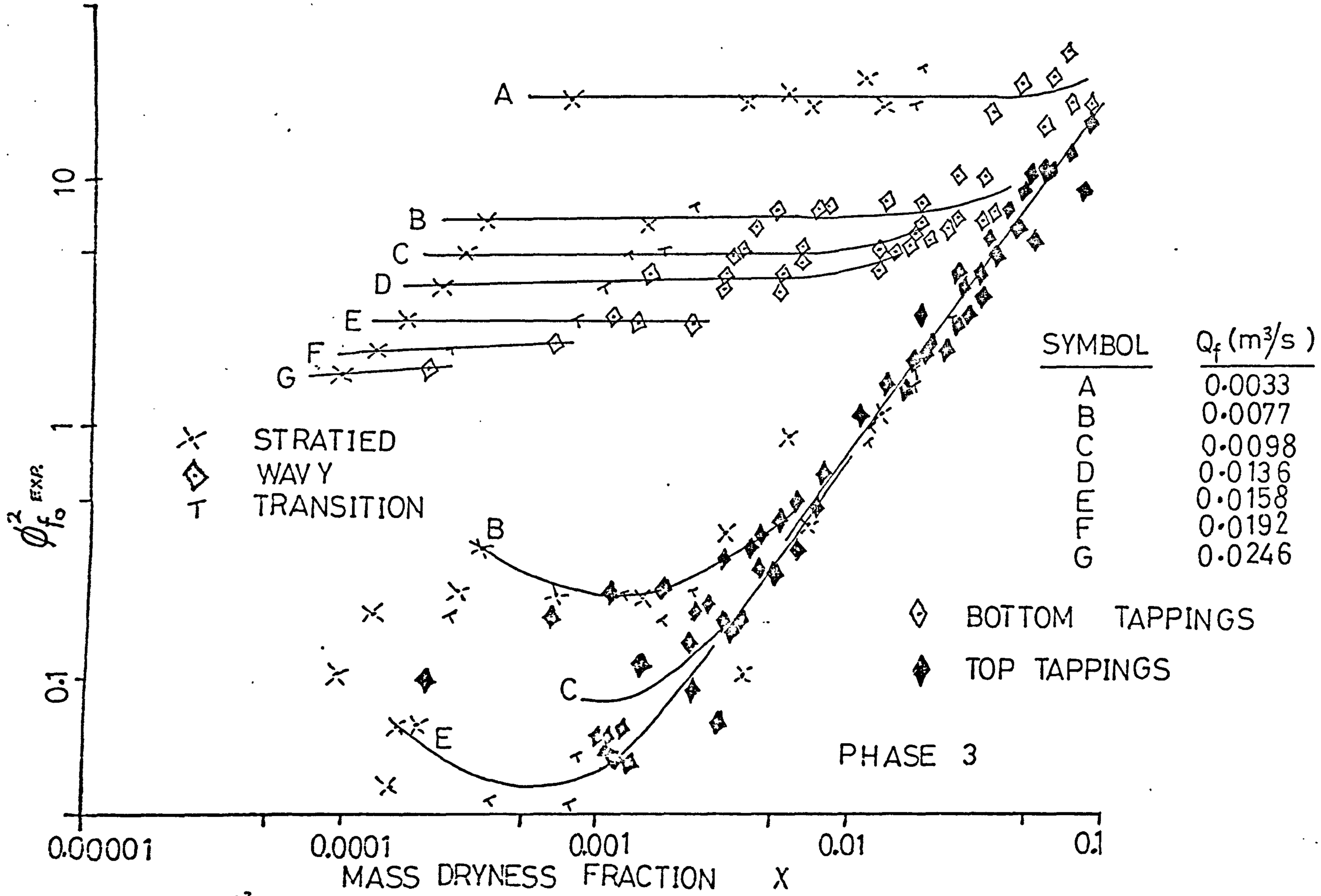

FIG. 8·23 $\phi^2_{f_{lo}}$ EXP. VS MASS DRYNESS FRACTION FOR TOP AND BOTTOM TAPPING SHOWING WATER FLOWRATE EFFECT

showing an almost negligible water flowrate effect contrary to the bottom pressure tapping results where such effects are large reflecting a significant liquid level influence.

The two phase friction multipliers based on top pressure tapping points data, and shown in Fig. 8.23, can be reasonably expressed by

$$\phi^2_{f_o \text{ gas}} = 583.4\ x^{1.44} \qquad (8.64)$$

By plotting the friction multiplier results based on the bottom tappings measurements (i.e. the horizontal lines in Fig. 8.23) against water flowrate, the following relation was obtained (Fig. 8.24)

$$\phi^2_{f_o \text{ liquid}} = 0.0139\ Q_f^{-1.28} \qquad (8.65)$$

An attempt was made to calculate a weighted two phase multiplier based on equation (8.63), the weighting factor being replaced by that for round tubes, i.e. using liquid wetted perimeter divided by the tube perimeter calculated from known void fraction values and geometrical relationships for the tubes. The results are shown in Fig. 8.25, plotted to a base of mass dryness fraction, and reflect, in general, the trends found in the bottom tapping measurement results, but with lower multiplier values. The high quality results reflect the influence of the top pressure tapping point measurement results and correspond to the transition conditions at rough wavy flows.

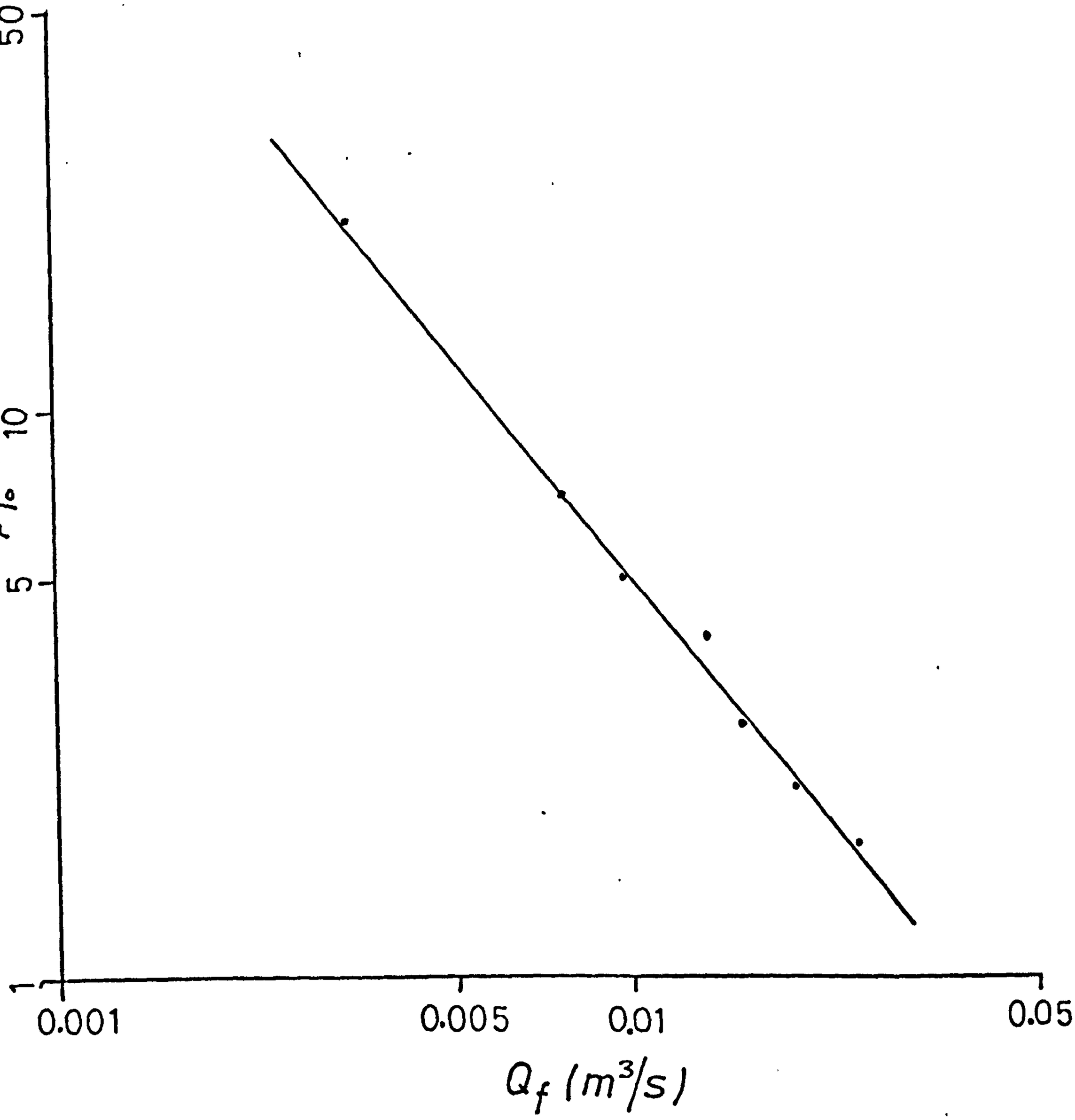

FIG. 8.24 EFFECT OF WATER FLOWRATE ON THE PRESSURE DROP MEASURED AT THE BOTTOM TAPPING POINTS

FOR MEANING OF SYMBOLS

REFER TO FIG. 8-23

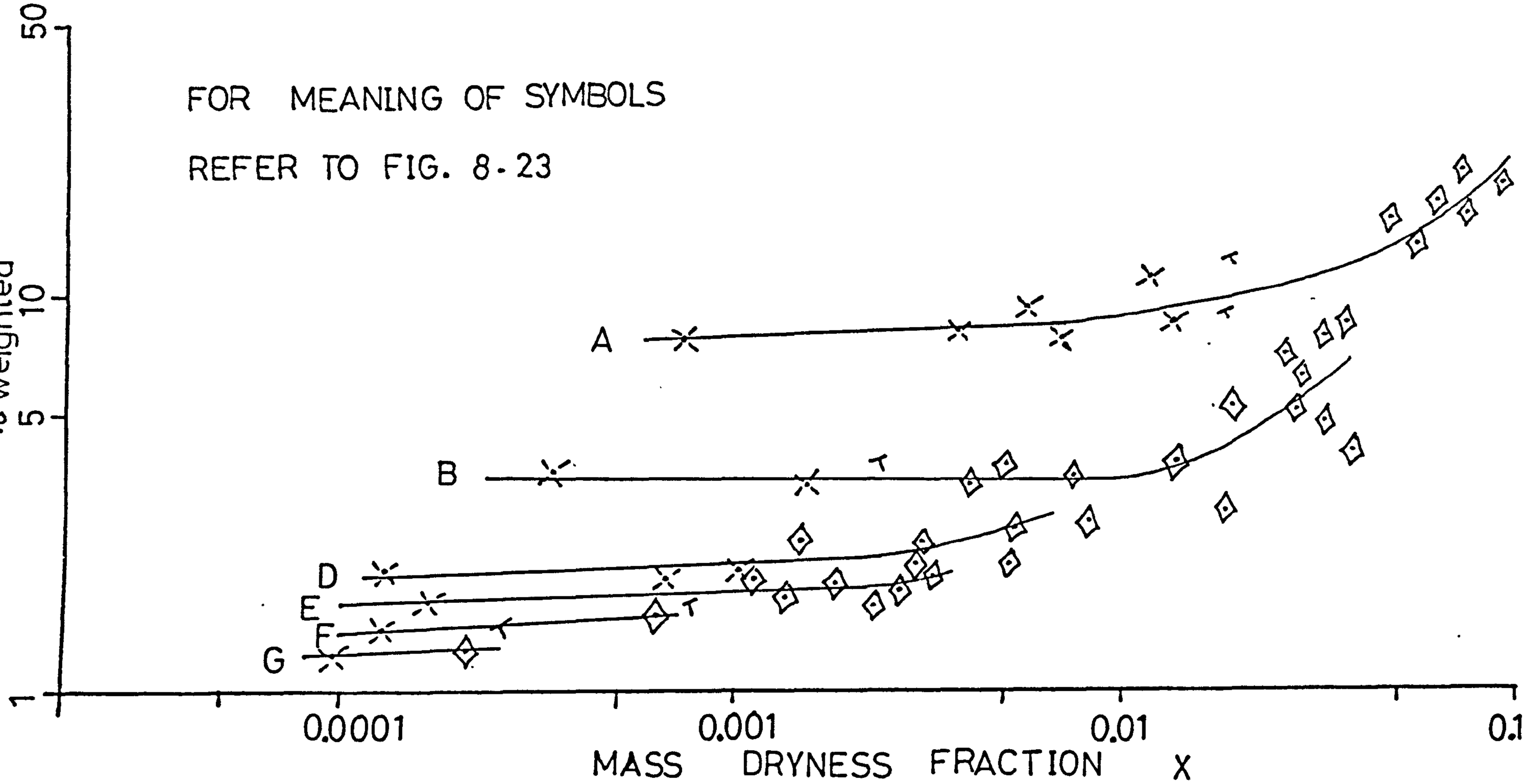

FIG·8·25 WEIGHTED TWO PHASE FRICTION MULTIPLIER FOR SEPARATED FLOW

8.4 VOID FRACTION PREDICTION

8.4.1 ANNULAR FLOWS

As indicated in Figs. 8.4 and 8.5 previously a plot of void fraction against air flowrate correlated the annular and rough wavy flow data and this is confirmed in Fig. 8.26 where a reasonable correlation is obtained for these data in isolation. A further plot of the void fraction data to a base of gas Reynold's number (for both Phase 2 and Phase 3 tests) is shown in Fig. 8.27. As can be seen the data for both tests can be represented by the expression

$$\alpha = 0.267\ (\ln Re_g) - 2.377 \qquad (8.66)$$

to within $\pm$ 10% approximately, indicating that the Reynold's number is an important variable for void fractions in annular flow. Using the gas Reynold's number accounts for diameter effects.

Such data could also be correlated in terms of the flow distribution parameter (R3), i.e.

$$U_g = K\ U_H + K\ U_R \qquad (8.67)$$

where $U_H = \frac{Q_t}{A} = U_{sg} + U_{sf} \equiv$ homogeneous flow velocity and U_R is a relative velocity term $\equiv U_g - U_H$.

Fig. 8.28 shows a plot of the gas velocity U_g versus the homogeneous flow velocity U_H which results in a distribution parameter $K \sim 1$ (45^o slope) and a relative velocity $U_R \simeq 2.5 \rightarrow 4.5$ m/sec (intercept). At low mixture velocities some points deviate from this relationship indicating a slug type of flow with a higher distribution parameter. The value of unity obtained for the distribution

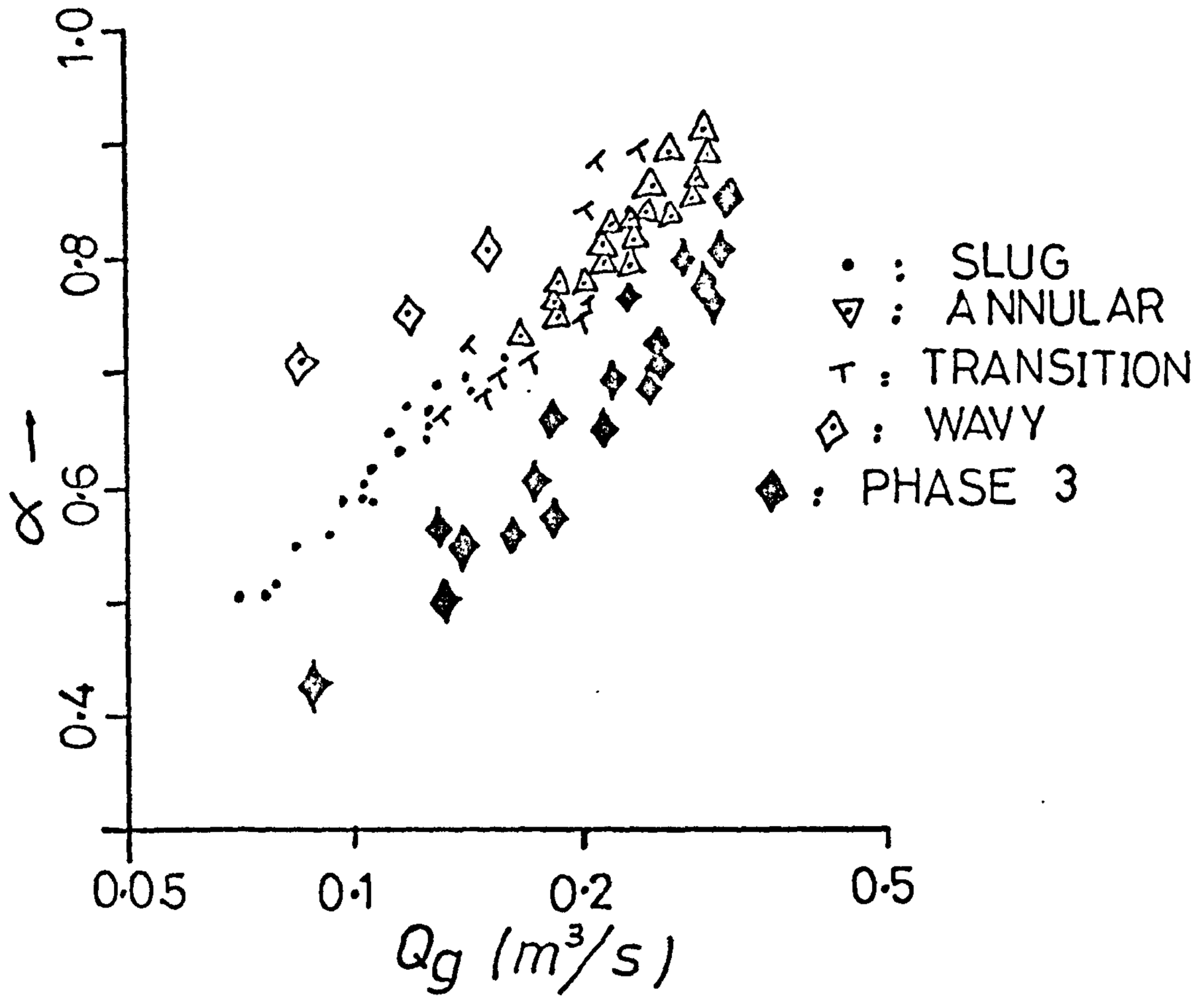

FIG. 8.26 VOID FRACTION CORRELATION FOR ANNULAR FLOW

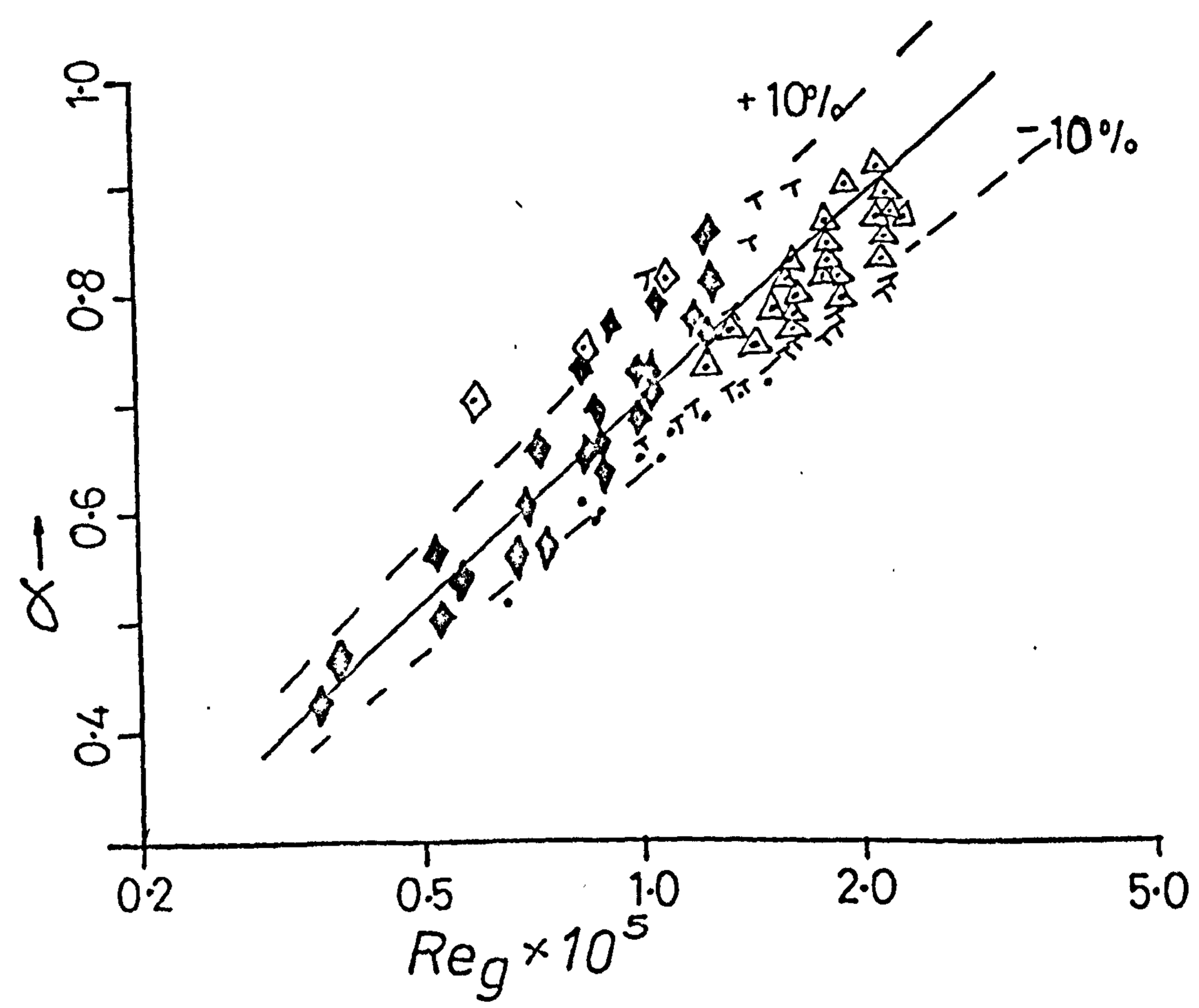

FIG. 8·27 VOID FRACTION CORRELATION FOR ANNULAR FLOW

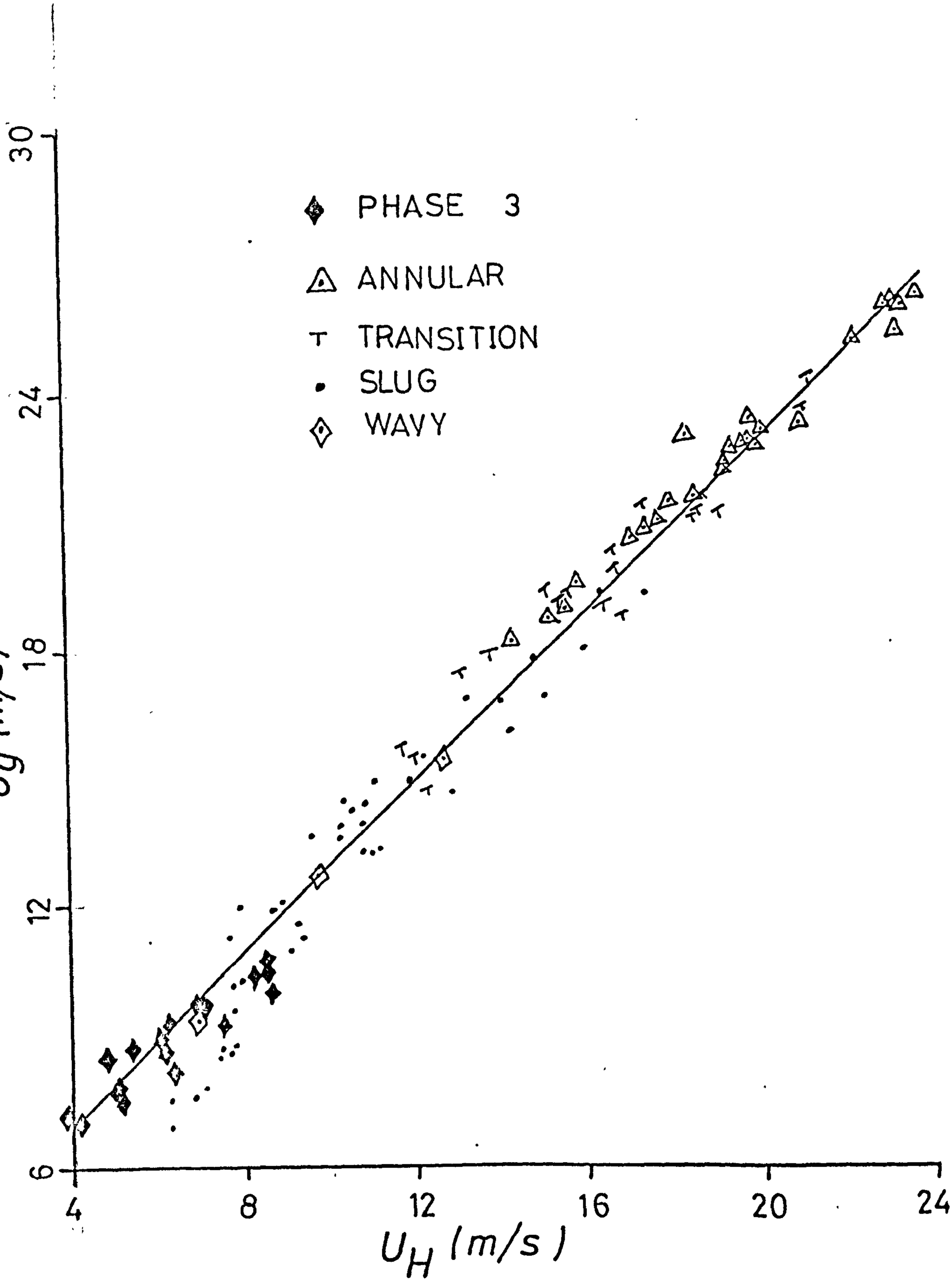

FIG. 8.28 EVALUATION OF THE DISTRIBUTION PARAMETER FOR ANNULAR FLOW

parameter is equal to the value found by Zuber et al (Z3) for such flow in vertical pipes, and suggests that the gas occupies most of the cross-section in these annular flows. Thus an alternative method of obtaining the void fraction, resulting from Fig. 8.28 and equation 8.67 is

$$\alpha = \frac{U_{sg}}{U_H + 3} \qquad (8.68)$$

8.4.2 INTERMITTENT FLOWS

A possible correlation for these flows could perhaps be obtained from a plot of α versus β since, for such flows, the slip ratio is normally close to unity. Fig. 8.29 shows such a plot for the Phase 2 data and indicates this to be a reasonable correlation. Phase 3 deviates from the above behaviour as discussed previously in Chapter 6. A plot similar to that suggested by equation (8.67) indicated the expected linear relationship but with a stronger water flowrate effect and this is shown in Fig. 8.30. Here the distribution parameter ranges from $\sim$1.14 at the lowest water flowrate to $\sim$1.54 at the highest one corresponding to frothy slug flows. This is again in agreement with the results of Zuber et al (Z3) for vertical flows. The low air flowrate conditions show some different trends characterised by higher values of the distribution parameter. At these conditions, the top part of the tube was occupied by air most of the time and this might have caused some errors resulting from the use of a horizontal γ -ray beam (i.e. shone parallel to the plane of the phase separation) rather than a vertical beam. Such a procedure was found to overpredict the void fraction for stratified types of flow.

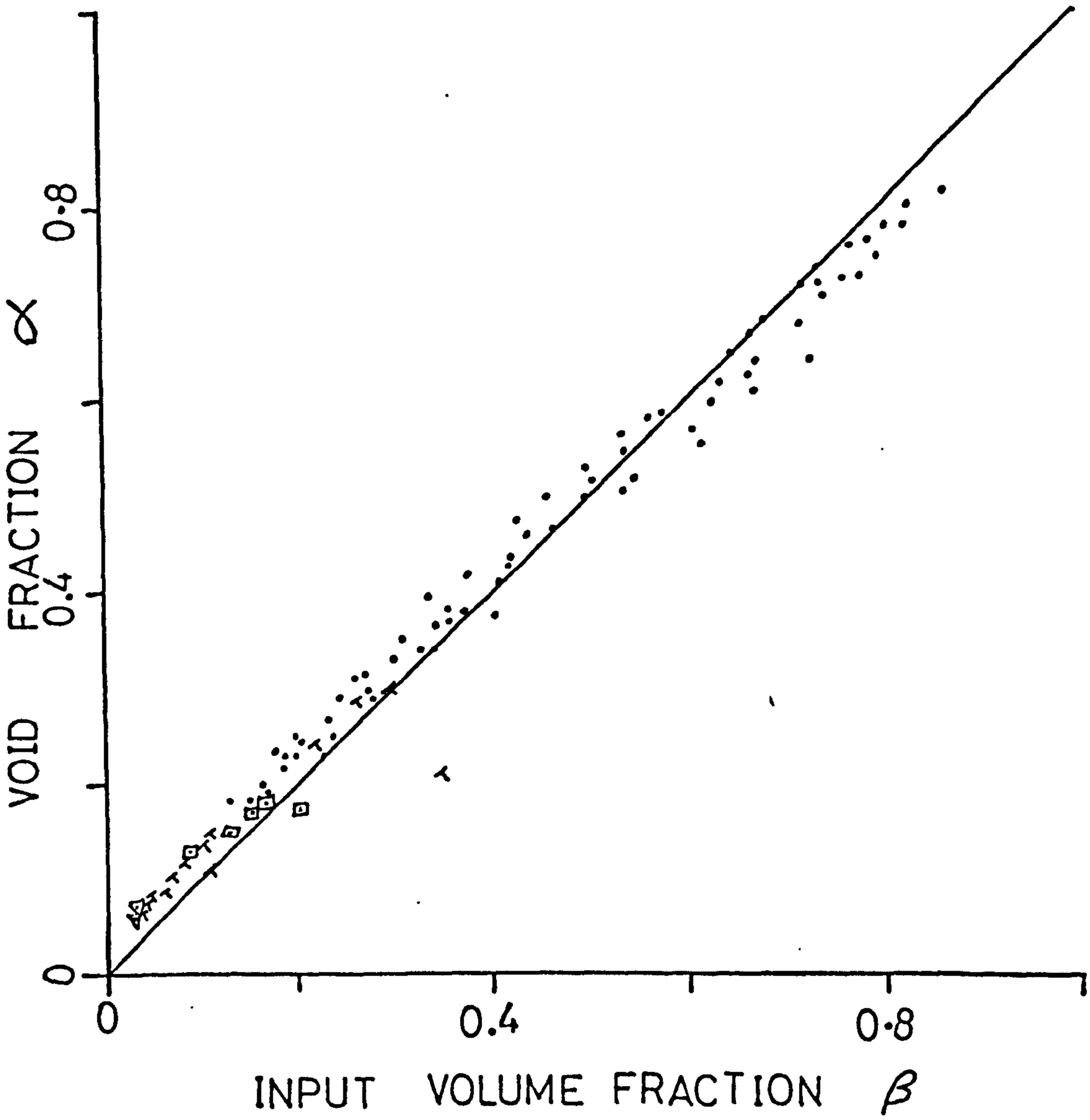

FIG. 8.29 VOID FRACTION CORRELATION FOR INTERMITTENT FLOW

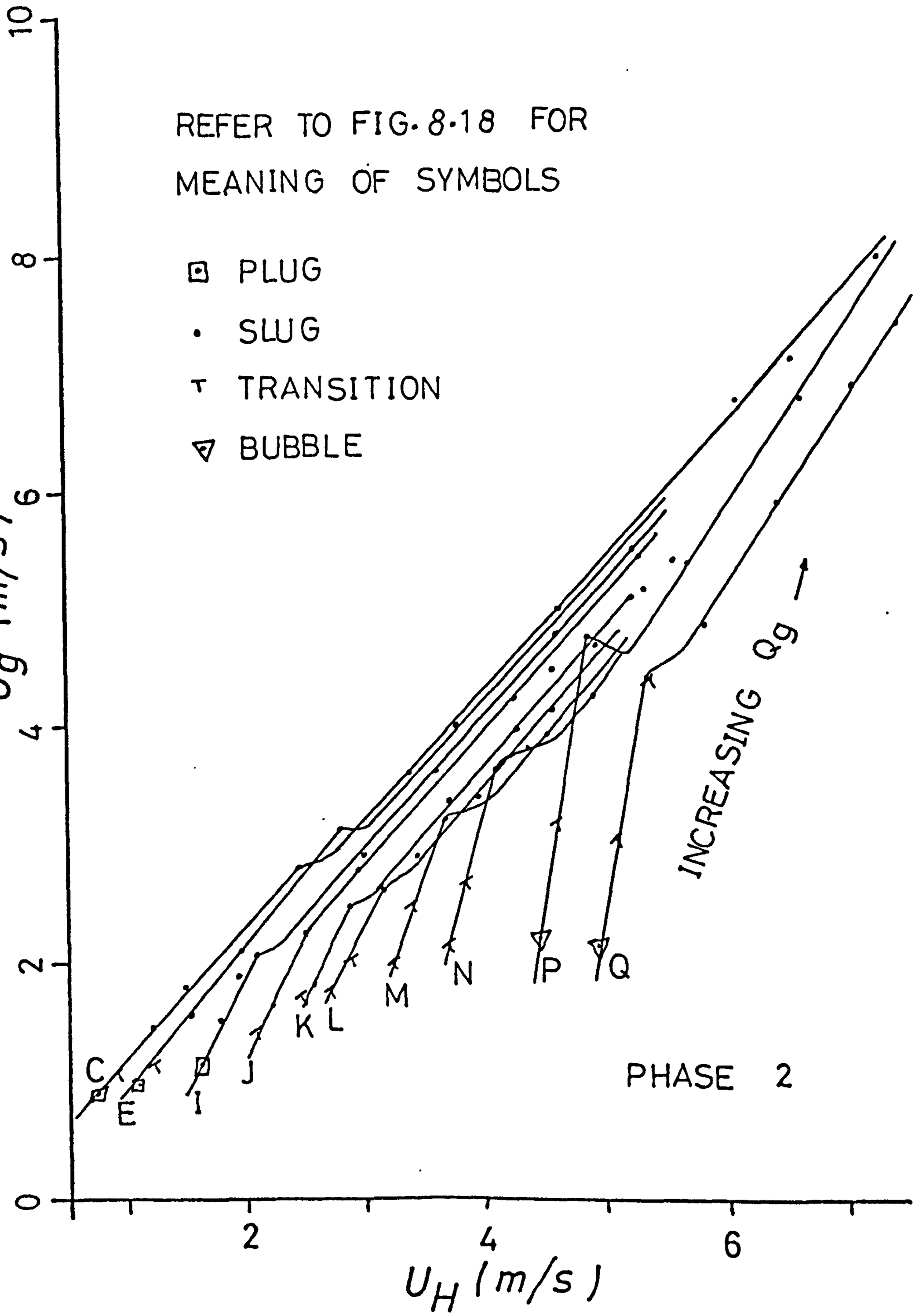

FIG. 8·30 EVALUATION OF THE DISTRIBUTION PARAMETER FOR INTERMITTENT FLOW (WATER FLOWRATE EFFECT SHOWN)

The Phase 3 results are plotted to the same coordinates of U_g and U_H and shown in Fig. 8.31. The scatter in the data may be explained in terms of the errors in the averaging of the electrometer reading which was highly fluctuating due to the low slug frequencies covered by the test condition as discussed earlier in Chapter 6.

8.4.3 SEPARATED FLOW

The results of Fig. 8.5 indicated the possibility of using water flowrate to correlate the void fraction data. While this was true for each tube, it was not possible to correlate both sets of data (i.e. Phase 2 and 3) with one correlation. A plot of α against liquid Froude number (based on water superficial velocity) produced a reasonable single correlation of the results as shown in Fig. 8.32 indicating that the Froude number is an important variable for void fractions in separated flows. Using the Froude number accounts for diameter effects. On this plot because of the small amount of data collected in the Phase 2 tests, some Phase 1 data were also included. The data plotted refer to stratified and smooth wavy flows.

A plot of air velocity against homogeneous mixture velocity U_H for the Phase 3 data is shown in Fig. 8.33 and indicates some interesting behaviour. The effect of water flowrate on the distribution parameter is pronounced and such that higher water flowrates produce higher values of distribution parameter (i.e. steeper slopes) with values between 1.4 and 4.3. The 127 mm (5") tube data (Phases 1 and 2) show similar behaviour (Fig. 8.34) with roughly

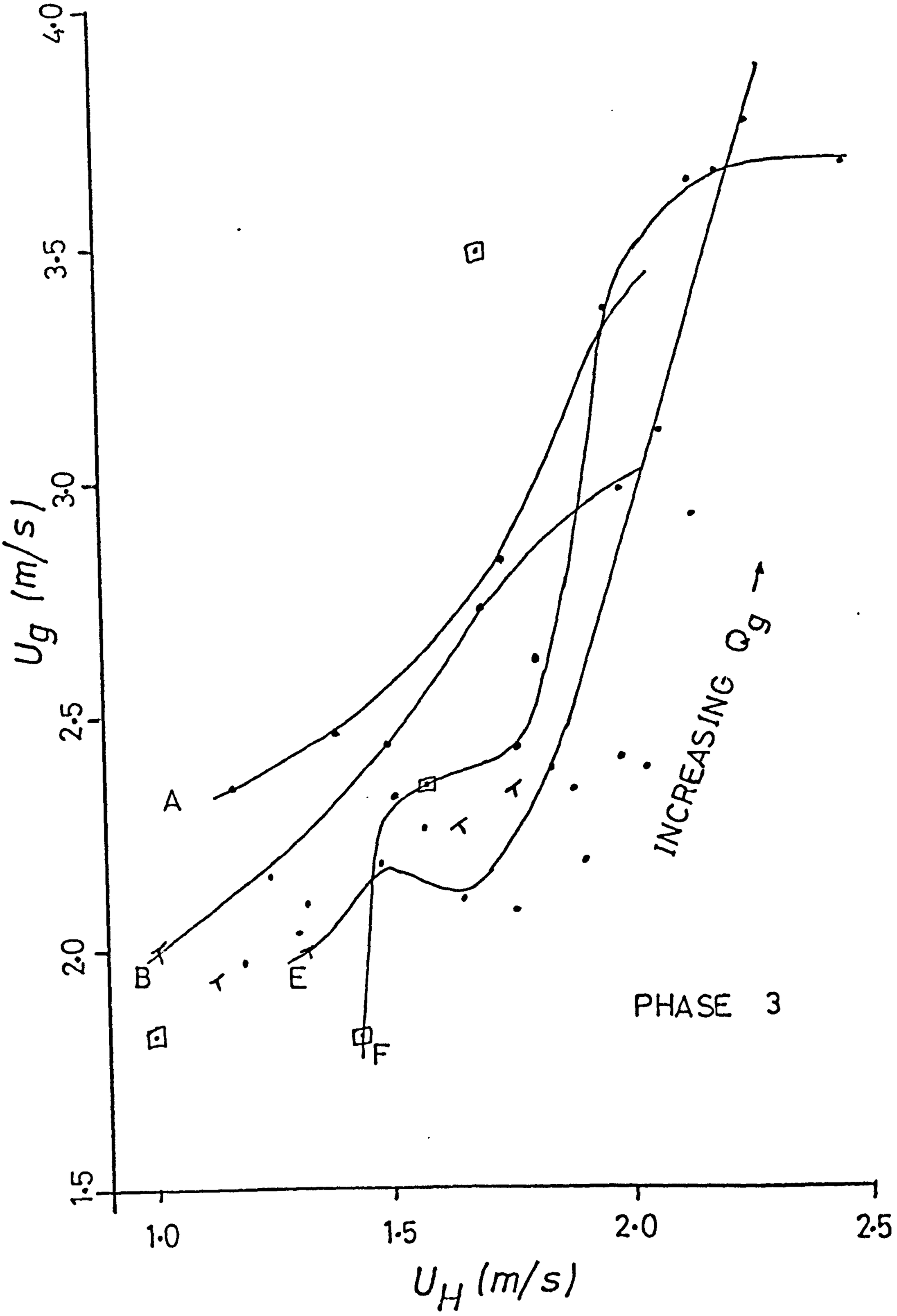

FIG. 8.31 EVALUATION OF THE DISTRIBUTION PARAMETER FOR INTERMITTENT FLOW

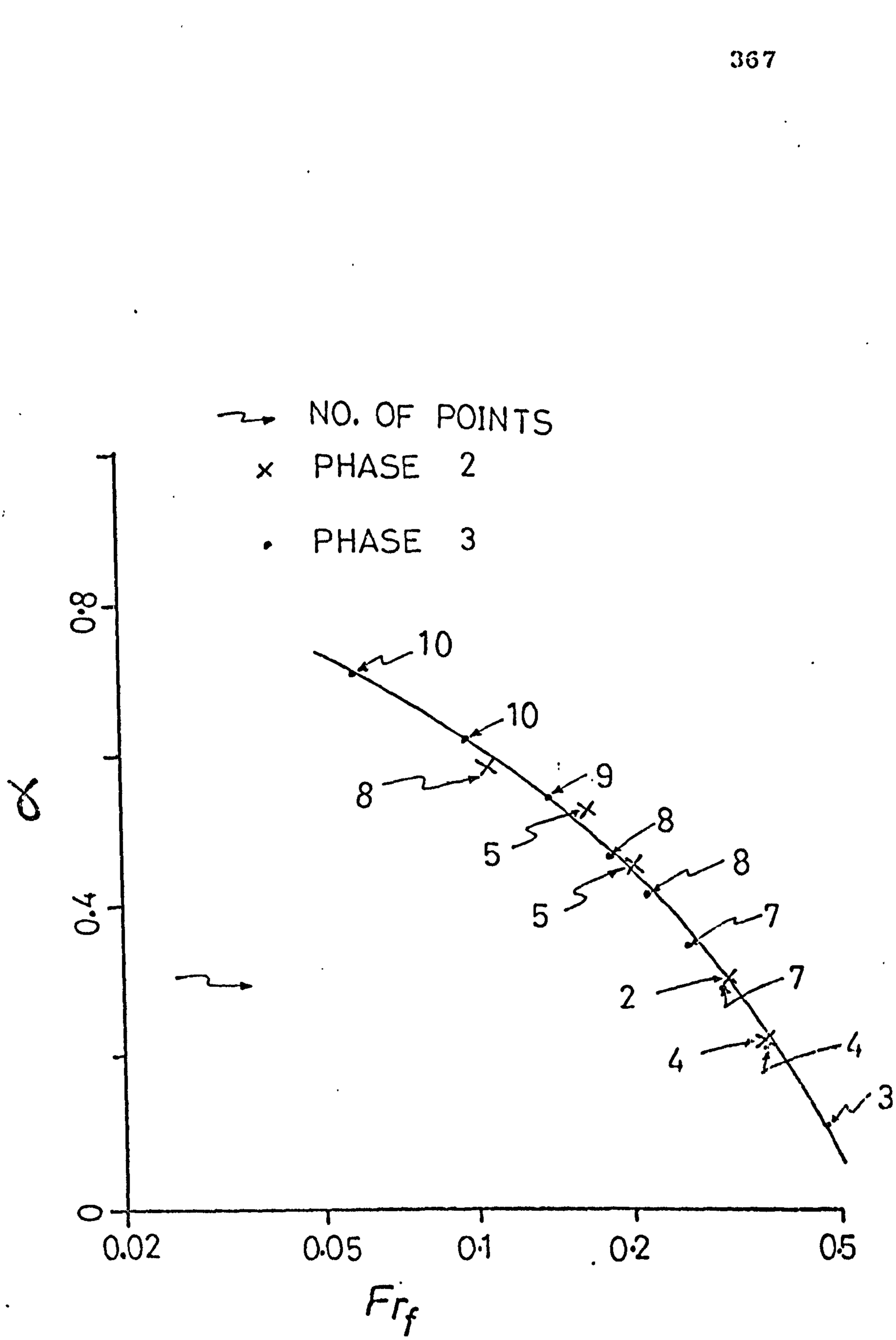

FIG. 8-32 VOID FRACTION CORRELATION FOR SEPARATED FLOW

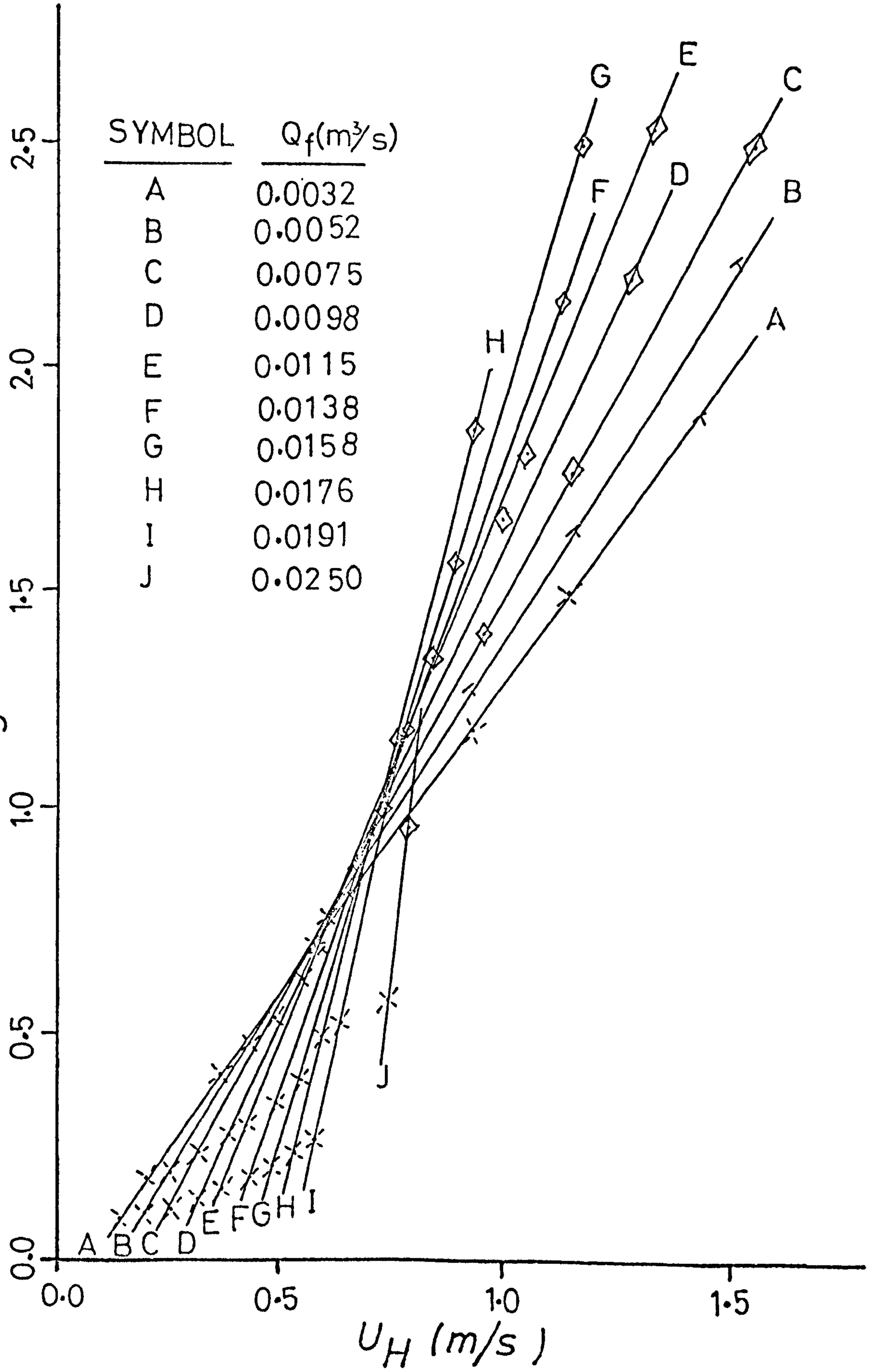

FIG. 8.33 EVALUATION OF THE DISTRIBUTION PARAMETER FOR SEPARATED FLOW WITH WATER FLOWRATE EFFECT SHOWN (PHASE 3)

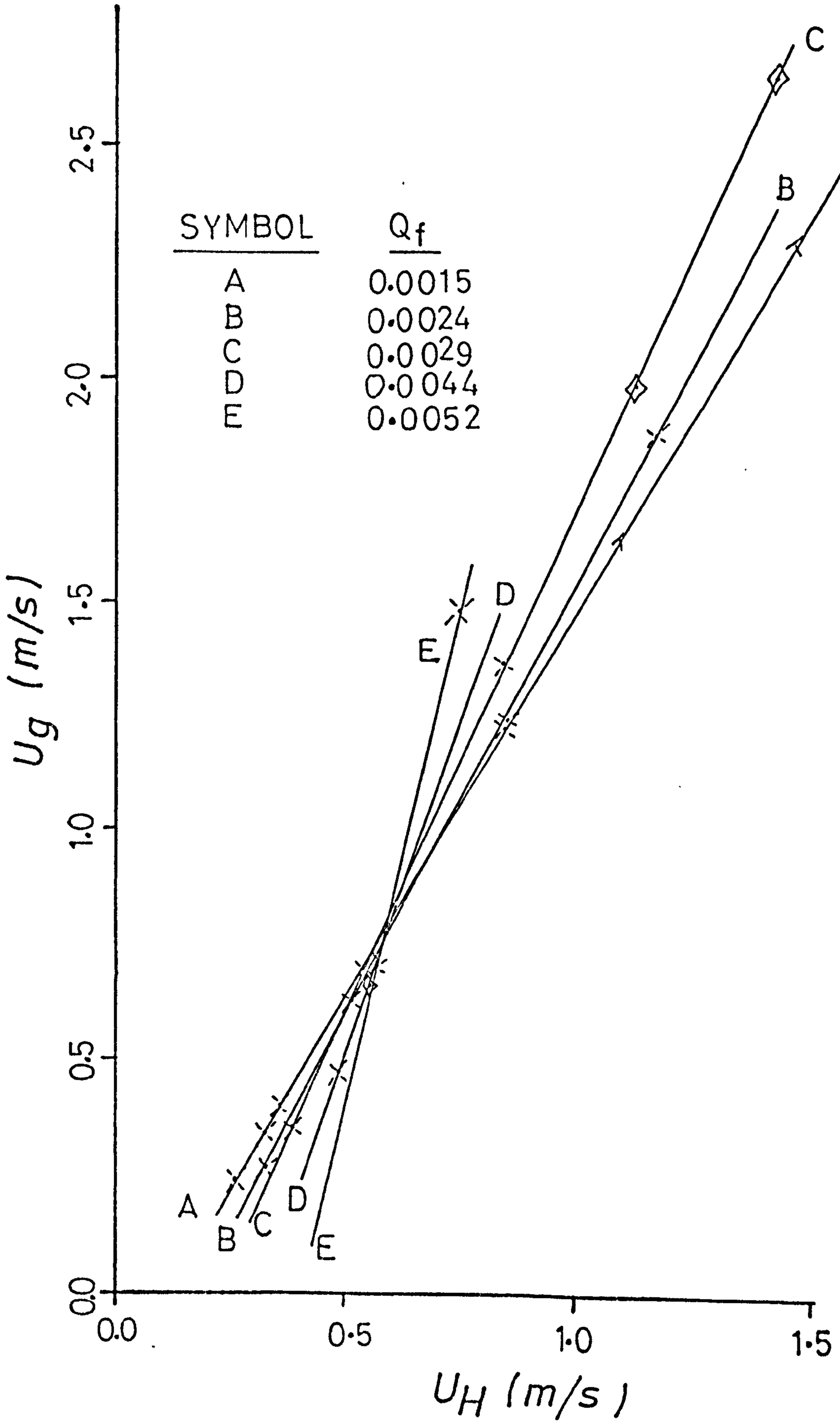

FIG. 8.34 EVALUATION OF THE DISTRIBUTION PARAMETER FOR SEPARATED FLOW WITH WATER FLOWRATE EFFECT SHOWN (PHASE 2)

the same range of distribution parameter. A reasonable correlation for the distribution parameter is obtained for the two tube sizes by plotting K against the liquid Froude number (based on liquid superficial velocity) as shown in Fig. 8.35. It should be noted that increasing the water flowrate effects an increase in the distribution parameter and also increases the liquid level. Hence the high 'K' values cannot be interpreted as indicating concentrations near the wall or near the centre line of the tube. For separated flows, the distribution parameter loses its usual meaning in that sense, and should, perhaps, be thought of in terms of the liquid level in the pipe, i.e. the higher the distribution parameter, the higher the liquid level.

An attempt was made to correlate the slip data for Phase 2 and Phase 3 in Figs. 8.36 and 8.37 which show a plot of the slip factor against input volume fraction β. Both sets of data showed some slip factors < 1 which is more pronounced in the 216 mm tube data (corresponding to stratified flow points).

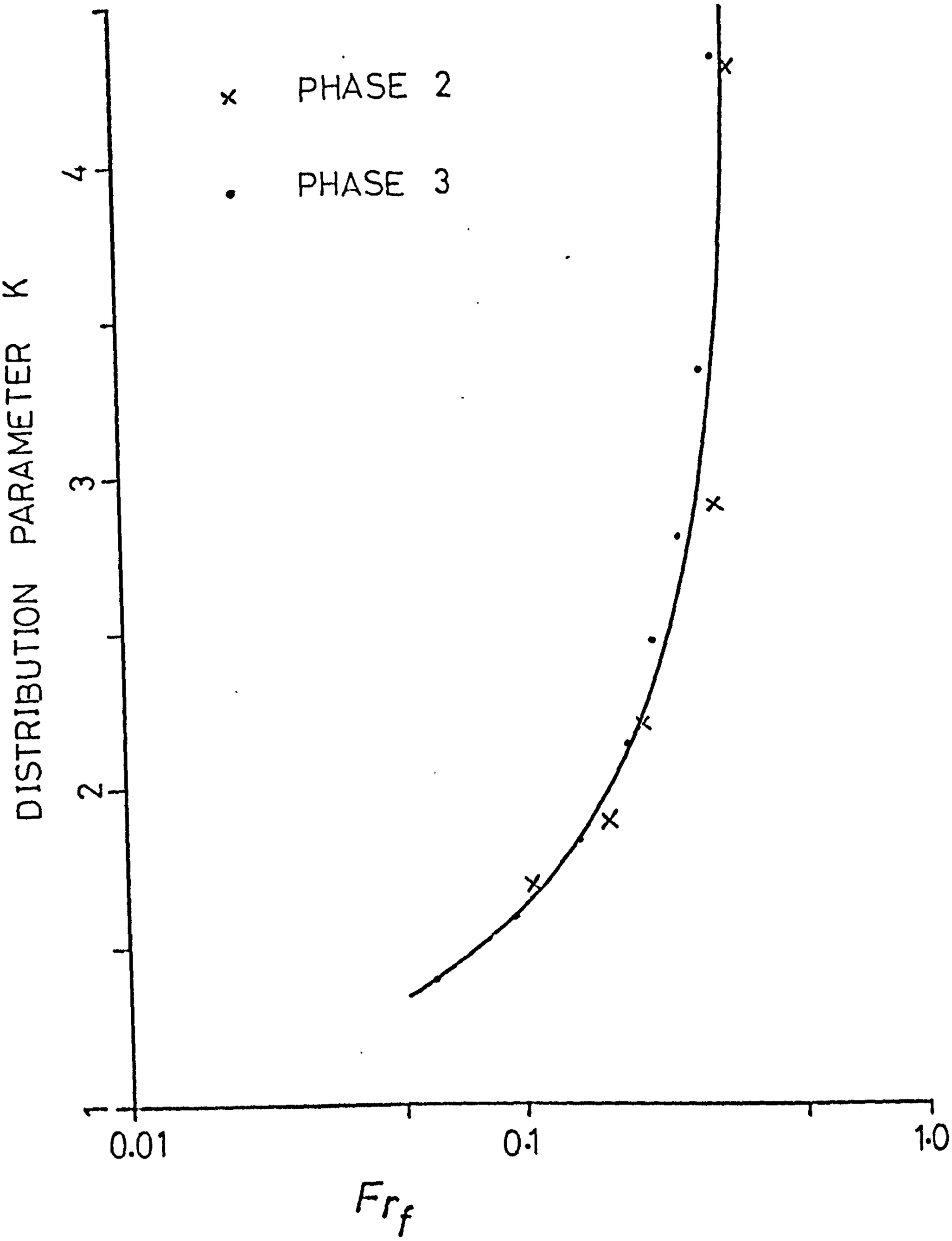

FIG. 8.35 EFFECT OF THE LIQUID FROUDE NO. ON THE DISTRIBUTION PARAMETER FOR SEPARATED FLOW

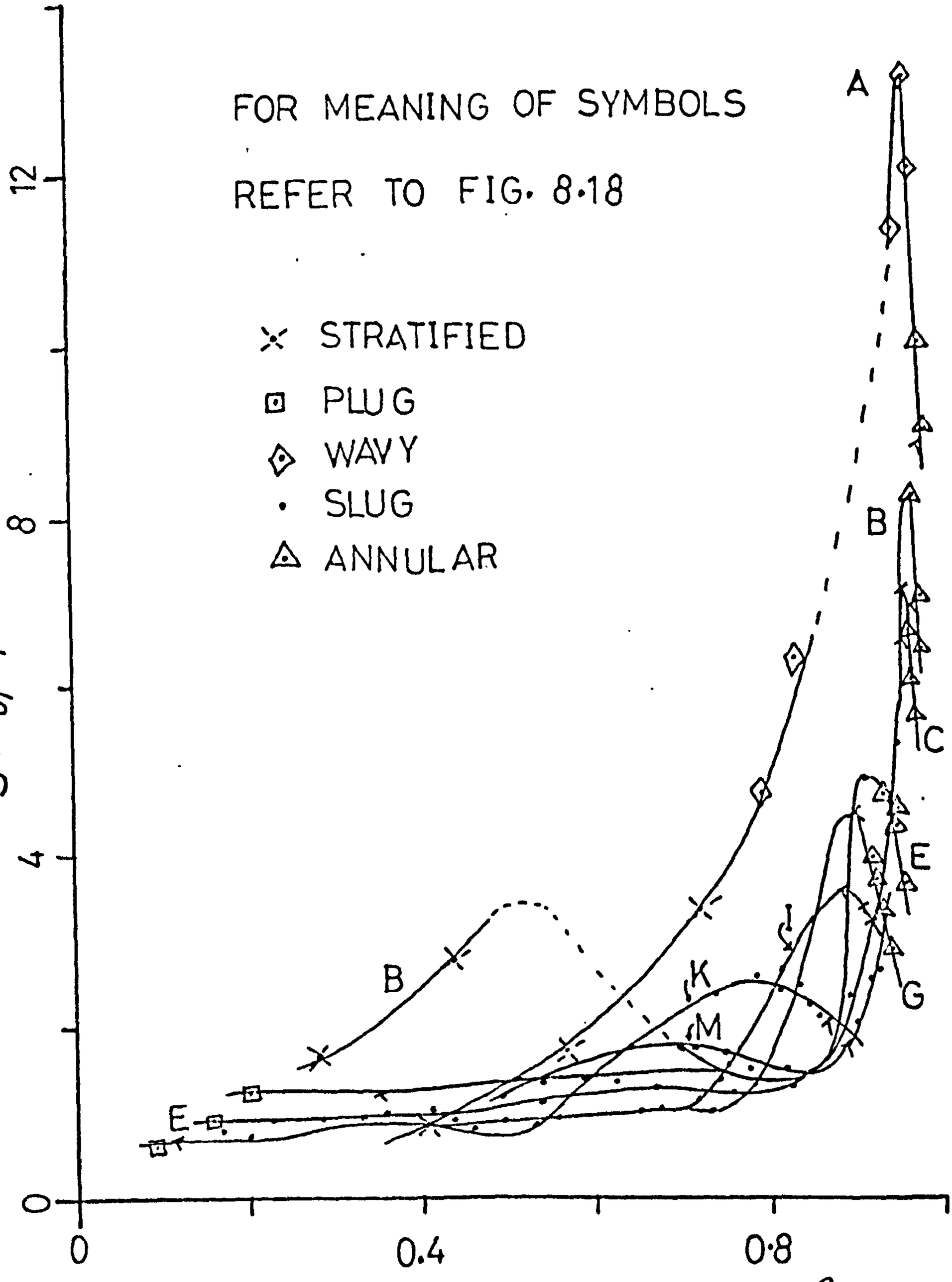

FIG. 8·36 THE DEPENDENCE OF THE SLIP FACTOR ON β WITH WATER FLOWRATE EFFECT SHOWN (PHASE 2)

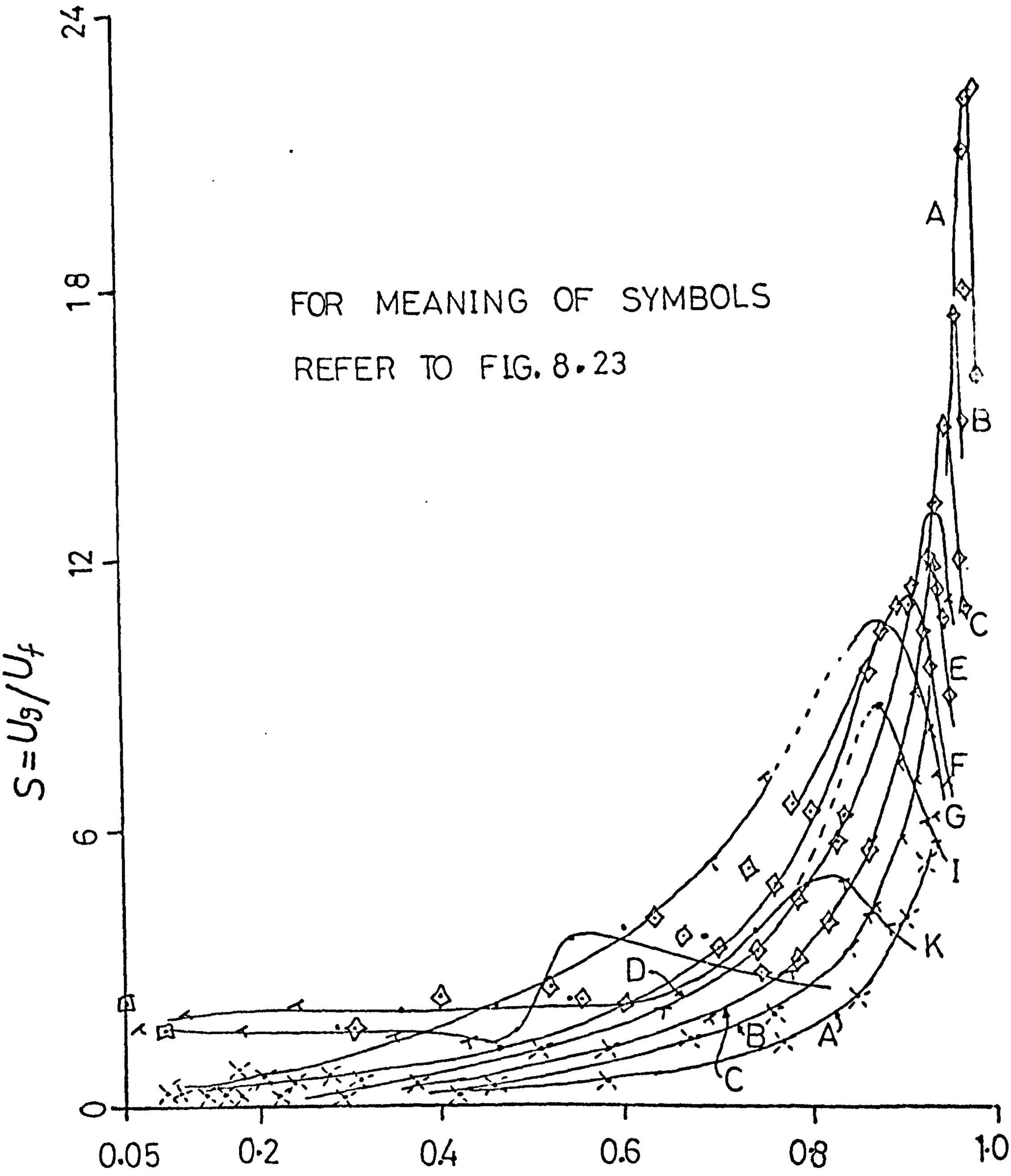

FIG. 8.37 THE DEPENDENCE OF THE SLIP FACTOR ON β WITH WATER FLOWRATE EFFECT SHOWN (PHASE 3)

CHAPTER 9 CONCLUSIONS AND RECOMMENDATIONS

CHAPTER 9 CONCLUSIONS AND RECOMMENDATIONS

9.1 CONCLUSIONS

1. For two phase flow in large diameter tubes, satisfactory correlation of the pressure drop and void fraction results requires a flow pattern dependency and this in turn requires the transitions between flow regimes to be defined adequately.

2. Flow pattern maps in general are of limited value, partly due to the inadequacy of the arbitrary two co-ordinate map system normally used to define all of the flow pattern transitions. However, the data presented here do indicate that, with the largest tube, the effect of tube diameter is to move the boundaries to lower superficial gas velocities and higher superficial liquid velocities, with a widening of the wavy flow region. Flow pattern transitions are not sharp, but as observed visually, are fairly gradual.

3. None of the friction pressure drop correlations studied predict pressure drop adequately for the tubes tested. Correlations which include directly the effect of flow pattern seem necessary.

4. There is more scope in large diameter tubes for flow separation and stratification with accompanying variation in liquid level along the tube. This makes the siting of pressure tapping points important and complicates the interpretation of the pressure drop data.

5. The need for objective assessment of the flow pattern is clear, and the pressure and local void fraction

variation measurements pr sented show promise as a useful technique for this purpose, especially when analysed statistically. The development of these probes should be continued.

6. The pressure drop and void fraction data, supported by the statistical analysis results of the pressure and the local void fraction pulsations, indicate that only three main flow regimes manifest themselves in horizontal two phase flow in large diameter pipes. These are

(i) Separated Flows (stratified and smooth wavy).

(ii) Annular Flows (annular, annular-mist and rough wavy).

(iii) Intermittent Flows (plug, slug and bubbly).

7. The problem of predicting the main flow regimes is reduced to that of predicting intermittent flow boundaries. A simple theoretical model based on the stability of a large wave resulted in the dimensionless map co-ordinates $F_{rf}^{\frac{1}{2}}$ and $1-\beta$, which predicted the experimental results reasonably well. Pressure drop and void fraction were subsequently correlated successfully in terms of these flow regimes.

8. The settling lengths required in two phase flow are strongly dependent on flow pattern, but are generally greater than the corresponding single phase flow lengths. The extremes are slug type flows which require very long settling lengths (often much greater than L/D = 75) and stratified type flows which settle fairly quickly.

9. In large diameter tubes, slip factors in bubble and plug type flows are approximately unity but can be

slightly less. Much higher slip factors are found in annular and slug type flows. The slip factors in stratified and wavy type flows are strongly dependent on air flow rate.

10. The effect of a horizontal return bend (two 90^{o} bends separated by 1m pipe) in general was to change the flow mode and behaviour especially with annular flows. This could explain, in part, some of the difficulties encountered in correlating the two phase flow data.

9.2 RECOMMENDATIONS

9.2.1 CORRELATIONS

The following correlations are recommended for use over the range of conditions covered by this work.

1. FLOW PATTERNS

(i) Separated-Intermittent Flow Regimes Boundary occurs at

$$Fr_f^{\frac{1}{2}} = 0.47(1-\beta)^{0.39}$$ Separated flow side of the boundary

$$Fr_f^{\frac{1}{2}} = 0.50(1-\beta)^{0.31}$$ Intermittent flow side of the boundary

with

$$Fr_f^{\frac{1}{2}} > 0.18$$

(ii) Separated-Annular Flow Regimes Boundary occurs at

$$Fr_f^{\frac{1}{2}} = 0.71(1-\beta)^{0.56}$$

with

$$Fr_f^{\frac{1}{2}} < 0.18$$

(iii) Annular-Intermittent Flow Regimes Boundary occurs at

$$Fr_f^{\frac{1}{2}} = 5.2(1-\beta)^{0.72}$$ Annular flow side of the boundary

$$Fr_f^{\frac{1}{2}} = 4.2(1-\beta)^{0.89}$$ Slug flow side of the boundary

with $(1-\beta) > 0.03$

2. PRESSURE DROP

(i) Annular Flow:

The results of Figs. 8.18 and 8.19 (for the 127 mm nominal bore pipe).

(ii) Intermittent Flow:

A homogeneous model based on the following mixture properties

$$\rho_m = \beta \rho_g + (1 - \beta) \rho_f$$

$$\mu_m = (1 + 5.5\beta) \left(\frac{G}{4300}\right)^{\beta}$$

and for the 127 mm (5") nominal bore pipe.

(iii) Separated Flow:

The 216 mm (8.5") nominal bore pipe results,

top tappings

$$\phi^2_{f_o gas} = 583.4 \; x^{1.44}$$

bottom tappings

$$\phi^2_{f_o liquid} = 0.0139 \; Q_f^{-1.28}$$

3. VOID FRACTION

(i) Annular Flow:

$$\alpha = 2.67(\ln Re_g) - 2.377$$

or

$$\alpha = \frac{U_{sg}}{U_H + 3}$$

(ii) Intermittent Flow:

$$\alpha = \beta$$

for the 127 mm (5") nominal bore pipe.

(iii) Separated Flow:

The results of Fig. 8.32.

9.2.2 FUTURE WORK

1. More data are needed in large diameter tubes with possibly longer test sections, particularly with the 216 mm (8.5") pipe, and over wider test conditions to include the very high flowrates regions of annular and bubbly flows.

2. Further development of the 'void fraction and pressure' probes for objective flow pattern measurements could be carried along the following lines:

(i) Use identical and possibly more stable transducers (noise level below $\pm$ 2 mv) with the existing data acquisition system.

(ii) Conduct tests with different separation distances between the two pressure transducers.

(iii) Attempt to improve the time constant of the void fraction probe.

3. Further investigation is needed into the problem of pressure drop prediction for the three flow regimes in general, and for the separated flow regime (i.e. stratified and smooth wavy) in particular.

REFERENCES

A1. Alves, G.E.

Co-current liquid/gas flow in a pipeline contactor.

Chem. Engng. Progress, vol. 50, No. 9, pp.449-456, 1954.

A2. Armand, A.A.

The resistance during the movement of a two phase system in horizontal pipes.

Izv, VTI. Vol. 15, No. 1, pp.16-23, 1946. English Translation: N.L.L., M882, Boston, Spa. York.

A3. Al-Sheikh, J.N., Saunders, D.E. and Brodkey, R.S.

Prediction of flow patterns in horizontal two phase pipe flow.

Can. J. Chem. Engng. Vol. 48, pp.21-29, 1970.

A4. Alves, G.E.

Experience with industrial co-current liquid/gas pipelines.

Symposium on Multi-phase flow systems, Univ. of Strathclyde, paper F1, I. Chem. E. Symp. Series No. 38 (1974).

A5. Akagawa, K., Hamaguchi, H., Sakaguchi, T.

Studies on the fluctuation of pressure drop in two phase slug flow.

Bull. J.S.M.E., Vol. 14, No. 71, part I, pp.447-454, part II, pp.445-461; part III, pp.462-469, (1971).

A6. Akagawa, K. and Sakaguchi, T.
Fluctuation of void ratio in two phase flow.
Bull. J.S.M.E., Vol. 9, No. 33, pp.104-120 (1966).

A7. Andeen, G.C. and Griffith, P.
Trans. ASME, Ser. C., J. heat transfer, Vol. 90, p.211, 1968.

A8. Aziz, K. and Govier, G.W.
Horizontal annular mist flow of natural gas-water mixtures.
Can. J. Chem. Engng. Vol. 40, pp.51-59, 1962.

A9. Agrawal, S.S., Gregory, G.A. and Govier, G.W.
An analysis of horizontal stratified two phase flow in pipes.
Can. J. Chem. Eng., Vol. 51, No. 3, pp.280-286, 1973.

A10. Anderson, R.J. and Russell, T.W.F.
Film formation in two phase annular flow.
AIChE J, Vol. 16, No. 4, pp.626-633, 1970.

A11. Alia, P., Cravarolo, L. et al.
Liquid volume fraction in adiabatic two-phase vertical upflow in a round conduit.
Report No. R-105, CISE Segrate (Milano), 1965.

A12. Alves, G.E.
Co-current liquid gas pipeline contactors
Chem. Engng. Prog. Vol. 66, No. 7, pp.60-67, 1970.

A13. Anderson, G.H. and Hills, P.D.
Two phase annular flow in tube bends.
Symp. Multi-phase Flow Systems, Univ. of Strathclyde, paper J1, I. Chem. E. Symp. Series, No. 38, 1974.

B1. Baxandell, P.B. and Thomas, R.
The calculation of pressure gradients in high rate flowing wells.
J. Pet. Tech., pp.1023-1028, 1961, AIME 222.

B2. Bergelin, O.P. and Gazley, C.
Co-current gas/liquid flow. Pt. 1, flow in horizontal tubes.
Proc. H.T. Fluid Mech. Inst., A.S.M.E. (1949), Berkeley, Calif., pp.5-18.

B3. Baker, O.
Designing for simultaneous flow of oil and gas.
Oil and Gas J., Vol. 53, No. 12, pp.185-195 (July 1954).

B4. Baker, O.
Multiplan flow in pipelines.
Oil and Gas J., pp.156-167 (Nov. 1958).

B5. Bergles, A.E., Lopina, R.F. and Fiori, M.P.
Critical heat flux and flow pattern observations for low pressure water flowing in tubes.
Trans. A.S.M.E., J. Heat Transfer, Vol. 89, pp.69-74 (1967).

B6. Beattie, D.R.H.
Two phase pressure losses - flow regime effects and associated phenomena.
Aust. A.E.C. Lucas Heights, May 1971,
I.S.B.N.O. 642.99420X-: AAEC/TM 589.

B7. Baroczy, C.J.

A systematic correlation for two phase pressure drop.

Chem. Engng. Prog., Symp. Series, Vol. 62, No. 64, pp.232-249 (1966).

B8. Bankoff, S.G.

A variable density single fluid model for two phase flow with particular reference to steam/water flow.

J. Heat Transfer, Trans. A.S.M.E., vol. 82, No. 2 (1960) pp.265-272.

B9. Baldima, O.M. and Peterson, D.F.

Item 15 in "Problems of heat transfer and hydraulics of two phase media", by S.S. Kutateladze, Pergamon Press, London (quoted in R3).

B10. Beattie, D.R.H.

Two phase flow structure and mixing length theory Nuclear Engng. and Design, Vol. 21, pp.46-64, 1972.

B11. Borishansky, V.M., Paleev, I.I.

Some problems of heat transfer and hydraulics in two phase flows.

Int. J. Heat Mass Transfer, Vol. 16, pp.1072-1085, (1973).

B12. Butterworth, D. and Pulling, D.J.

A visual study of mechanisms in horizontal air/water flow.

AERE - M2556, 1972.

B13 Baroczy, C.J.

Correlation of liquid fraction in two phase flow with application to liquid metals.

Chem. Engng. Prog. Symp. Ser. No. 57, Vol. 61, pp.179-191, Heat transfer, Boston.

B14. Baker, O.

Effect of hills on two phase pressure drop.

Oil and Gas Journal, Vol. 55, No. 45, p.150, 1957.

B15. Birks, J.B.

Scintillation Counters.

Pergamon, Oxford, 1964.

B16. Brigham, E.O.

The fast Fourier transform.

Prentice-Hall, Inc., 1974.

B17. Bendat, J.S. and Piersol, A.G.

Random data: analysis and measurement procedures.

Wiley-Interscience, 1971.

B18. Blackman, R.B. and Tukey, J.W.

The measurement of power spectra.

Dover Publications, Inc., New York, 1958.

B19. Bingham, C., Godfrey, M.D. and Tukey, J.W.

Modern techniques of power spectrum estimation

IEEE transactions on Audio and Electroacoustics

Vol. Au-15, No. 2, June 1967.

C1. Choe, W.G. and Weisman, J.

Flow patterns and pressure drop in co-current vapor-liquid flow. A state of the art report. Univ. of Cincinnati, Ohio (Sept. 1974).

C2. Collier, J.G.

Two phase gas-liquid pressure drop and void fraction. A review of the current position. Paper No. B1, presented at the 1974 European Two Phase Flow Conference.

C3. Collier, J.G.

Convective boiling and condensation. McGraw-Hill Comp., 1972.

C4. Coney, M.W.E. and Fisher, S.A.

Flow visualization studies of air/water flowing in a bend and a horizontal tube.

Part 1: Flow regimes and published work C.E.G.B., C.E.R.L., RD/L/N165/70 (1970)

Part 2: Detailed description and analysis C.E.G.B., C.E.R.L., RD/L/N173/70 (1970).

C5. Cichy, P.T. and Russel, T.W.F.

Two phase reactor design tubular reactor. Reactor model development. Ind. & Engng. Chem. Vol. 61, No. 8, pp.6-14, Aug. 1969.

C6. Choe, W.G., Weinberg, L., and Weisman, J.

Observation and correlation of flow pattern transitions in horizontal cocurrent gas/liquid

flow.

Presented to Two Phase Flow and Heat Transfer Symposium-Workshop, Ft. Lauderdale, Florida (1976).

C7. Chisholm D. and Laird, A.D.K.

Two phase flow in rough tubes.

Trans. A.S.M.E., Vol. 80, No. 2, pp.276-286 (1958).

C8. Chisholm, D. and Sutherland, L.A.

Prediction of pressure gradient in pipeline systems during two phase flow.

Fluid Mech. and Meas. in Two Phase Flow Systems. Proc. Inst. Mech. Engrs. 1969-70, Vol. 184, Pt. 3C, paper No. 4, pp.24-32.

C9. Cichy, P.T. and Russel, T.W.F.

Two phase reactor design. Tubular reactor. Reactor model development.

Ind. Engng. Chem., Vol. 61, No. 8, pp.6-14, Aug. 1969.

C10. Chisholm D.

The influence of viscosity and liquid flowrate on the phase velocities during two phase flow.

NEL Report No. 33, 1962.

C11. Chenoweth, J.M. and Martin, M.W.

A pressure drop correlation for turbulent two phase flow of gas/liquid mixtures in horizontal pipes.

Pet. Refiner, Vol. 34, No. 10, pp.151-155, 1955.

C12. Chisholm, D.

A theoretical basis for the Lockhart-Martinelli correlation for two phase flow.

Int. J. Heat & Mass Transfer, Vol. 10, pp.1767-1778, 1967.

C13. Chisholm, D.

Pressure gradients due to friction during the flow of evaporating two phase mixtures in smooth tubes and channels.

Int. J. Heat and Mass Transfer, Vol. 16, pp.347-358, 1973.

C14. Cohen, L.S. and Hanratty, T.J.

Effect of waves at gas-liquid interface in a turbulent air flow.

J. Fluid Mech., Vol. 31, Pt. 3, pp.467-479, 1968.

C15. Chisholm, D.

Research note: void fraction during two phase flow.

J. Mech. Engng. Sci., Vol. 15, No. 3, pp.235-236, 1973.

C16. Chatfield, C.

The analysis of time series: theory and practice.

Chapman and Hall, 1975.

D1. Dukler, A.E., Wicks, M. and Cleveland, R.G.

Frictional pressure drop in two phase flow. Part A. A comparison of existing correlations for pressure loss and hold up.

A.I.Ch.E.J. Vol. 10, No. 1, pp.38-43 (1964).

D2. De Gance, A.E. and Atherton, R.W.
Chemical Engineering aspects of two phase flow.
Part 1, Introduction.
Chem. Engng. Vol. 77, pp.135-139 (March 1970).

D3. Part 2. Phase equilibria, flow regimes, energy loss.
Chem. Engng., Vol. 77, pp.151-158 (April 1970).

D4. Part 3. Transferring heat in two phase systems.
Chem. Engng., Vol. 77, pp.113-120 (May 1970).

D5. Part 4. Horizontal flow correlations
Chem. Engng., Vol. 77, pp.95-103 (July 1970).

D6. Part 5. Mechanical energy balance
Chem. Engng., Vol. 77, pp.119-126 (Aug. 1970).

D7. Part 6. Vertical and inclined flow correlations
Chem. Engng., Vol. 77, pp.87-94 (Oct. 1970).

D8. Davis, M.R.
Pressure fluctuations in a vapor liquid mixture flow.
Int. J. Heat and Mass transf., Vol. 16, pp.2043-2054, 1973.

D9. Dukler, A.E.
Eleventh Advanced Seminar - two phase gas/liquid flows.
A.I.Ch.E. Meeting, New York, Nov. 1967 (quoted in D3).

D10. Dukler, A.E., Wicks, M., et al.
Frictional pressure drop in two phase flow.
Part B. An approach through similarity analysis.
AIChE J, Vol. 10, No. 1, pp.44-51, 1964.

D11. Duns, H.Jr. and Ros, N.C.J.
Vertical flow of gas and liquid mixtures in wells.
Proc. Sixth World Pet. Cong. Frankfurt, pp.451-465, Vol. II, 1963.

D12. Davis, E.J.
Interfacial shear measurements for two phase gas liquid flow by means of preston tubes.
Ind. Engng. Chem. Fund., Vol. 8, pp.153-159, 1969.

E1. Evans, R.G., Gouse, S.W. and Bergles, A.E.
Pressure wave propagation in adiabatic slug/annular - mist two phase gas/liquid flow.
Chem. Engng. Sci. Vol. 25, No. 4 (1970), pp. 569-582.

E2. Eaton, B.A., Andrews, D.E., et al.
The prediction of flow patterns, liquid holdup and pressure losses occurring during continuous two phase flow in horizontal pipelines.
Trans. Soc. Pet. Engrs. A.I.M.E., Vol. 240, pp.815-828 (1967), J. of Pet. Tech., Vol. 18, No. 7, pp.815-828 (1967).

E3. Evans, R.G., Gouse, S.W., and Bergles, A.E.
Pressure wave propagation in adiabatic slug/annular/mist two phase gas/liquid flow.
Chem. Engng. Sci., Vol. 25, No. 4, (1970), pp.569-582.

E4. Ellis, S.R. and Gay, B.

The parallel flow of two fluid streams: interfacial shear and fluid-fluid interaction.

Trans. Instn. Chem. Engrs. Vol. 37, p.206, 1959.

E5. Etchells, A.W. III.

Stratified horizontal two phase flow in pipe.

Ph.D. thesis, University of Delaware, 1970.

F1. Fohrman, M.J.

The effect of the liquid viscosity in two phase two component flow.

Argonne National Lab., Report No. A.N.L. - 6356 (1960).

F2. Francher, G.H. and Brown, K.E.

Prediction of pressure gradient for multiphase flow in tubing.

Soc. Pet. Eng. J., pp.59-69, Trans. AIME, p.228, 1963.

F3. Fisher, S.A. and Hopley, C.E.

Axial view studies of air/water mixtures flowing in a vertical 90^{o} and horizontal tube.

CEGB Report No. RD/L/N266/71, 1971.

F4. Flanigan, O.

Effect of uphill flow on pressure drop in design of two phase Gathering Systems.

Oil and Gas J., Vol. 56, No. 10, p.132, 1958.

F5. Faires, R.A. and Parks

Radioisotope laboratory techniques

Butterworths, 3rd edition, 1973.

G1. Govier, G.W. and Aziz, K.

The flow of complex mixtures in pipes.

Van Nostrand Reinhold Comp. 1972.

G2. Gouse, S.W.

An index to the two phase gas/liquid flow literature.

M.I.T. Report No. 9 (1966).

G3. Govier, G.W. and Omer, M.M.

The horizontal pipeline flow of air/water mixtures.

Can. J. Chem. Engng., Vol. 40, pp.93-104 (1962).

G4. Govier, G.W.

Developments in the understanding of the vertical flow of two fluid phases.

Can. J. Chem. Engng., Vol. 43, pp.3-10 (1965).

G5. Greskovich, E.J., Shrier, A.L., et al.

True gas content for horizontal gas/liquid flow.

Ind. Engng. Chem. Fundamentals, Vol. 8, No. 3, 1969, pp.591-593.

G6. Groothuis, H. and Hendal, W.P.

Heat transfer in two phase flow.

Chem. Engng. Sci., Vol. 11, pp.212-220, 1959.

G7. Gould, T.L., Tek, M.R. and Katz, D.L.

Two phase flow through vertical, inclined or curved pipe.

J. Pet. Tech. Aug. 1974, pp.915-926.

G8. Griffith, P. and Lee, K.S.

The stability of an annul s of liquid in a tube.

Trans. A.S.M.E.J. Basic Engng., pp.666-672, 1964.

G9. Gazley, C.Jr.

Co-current gas-liquid flow.

III. Interfacial shear and stability.

Paper presented at Inst. Fluid Mech. Ht. transf.

June, 1949, pp.29-40.

G10. Gregory, G.A. and Scott, D.S.

Int. Symp. Research Co-current Gas/liquid Flow,

Univ. of Waterloo, Sept. 1968, proc. p.633

(quoted in G1).

G11. Gregory, G.A. and Scott, D.S.

Correlation of liquid slug velocity and frequency

in horizontal co-current gas-liquid slug flow.

AIChE J, Vol. 15, No. 6, pp.933-935, 1969.

G12. Greskovich, E.J. and Shrier, A.L.

Pressure drop and hold up in horizontal slug flow.

AIChE J, Vol. 17, No. 5, pp.1214-1219, 1971.

G13. Gill, L.E., Hewitt, G.F. and Lacey, P.M.C.

Data on the upwards annular flow of air-water

mixtures.

Chem. Eng. Sci. Vol. 20, p.71.

G14. Gardner, G.C. and Neller, P.H.

Phase distributions in flow of an air-water

mixture round bends and past obstructions at

the wall of a 76 mm box tube.

Fluid Mech. Measurements in two phase flow systems,

Proc. Inst. Mech. Engrs, 1969-70, Vol.184, Pt.3C,

pp.93-101.

G15. Gregory, G.A.

Comments on the prediction of liquid hold up for gas liquid f ow in inclined pipes.

Can. J. Chem. Engng. Vol. 52, pp.463-467, 1974.

G16. Guzhov, A.I., Mamayev, A.A. and Odishariya, G.E.

A study of transportation in gas-liquid systems.

Paper presented at the 10th International Gas Conf. Hamburg, 1967.

G17. Greskovich, E.J. and Cooper, W.T.

Correlation and prediction of gas-liquid holdups in inclined upflows.

AIChE.J, Vol. 21, No. 6, pp.1189-1192, 1975.

H1. Hewit, J.F., and Hall Taylor, N.S.

Annular two phase flow.

Pergamon, Oxford, 1970.

H2. Hoogendoorn, C.J.

Gas/liquid flow in horizontal pipes.

Chem. Engng. Sci. Vol. 9, (1959), pp.205-217.

H3. Hoogendoorn, C.J. and Buitlarr, A.A.

The effect of gas density and gradual vaporisation on gas/liquid flow in horizontal pipes.

Chem. Engng. Sci. Vol. 16, (1961), pp.208-221.

H4. Hosler, E.R.

Flow patterns in high pressure two phase (steam/water) flow with heat addition

9th National Heat Transfer Conference, A.I.Ch.E.-

A.S.M.E., Seattle (1967), Preprint 22, Chem. Engng. Progress Symp. Series, Vol. 64, No. 82, pp.54-66 (1968).

H5. Henry, R.E., Grolmes, M.A. and Fauske, H.K.
Propagation velocity of pressure waves in gas/liquid flow.
Univ. of Waterloo, pp.1-17, Sept. 1968.

H6. Hubbard, M.G., and Dukler, A.E.
Characterisation of flow regimes for horizontal two phase flow. Pt. I.
Proc. 1966 Heat Transfer and Fluid Mechanics Inst. (Santa Clara, Calif.), pp.100-121.

H7. Hughmark, G.A.
Pressure drop in horizontal and vertical co-current gas-liquid flow.
I. and E.C. Fundamentals, Vol. 2, No. 4, 1963, pp.315-321.

H8. Huey, C.T. and Bryant, R.A.A.
Isothermal homogeneous two phase flow in horizontal pipes.
A.I.Ch.E. J, Vol. 13, No. 1, pp.70-77 (1967).

H9. Hughmark, G.A.
Holdup in gas-liquid flow.
Chem. Engng. Progress, Vol. 58, No. 4, pp.62-65, 1962.

H10. Hughmark, G.A. and Pressburg, B.C.
Holdup and pressure drop with gas-liquid flow in a vertical pipe.
A.I.Ch.E. J, Vol. 7, pp.677-682, 1961.

H.11 Hagedorn, A.R. and Brown, K.E.
Experimental study of pressure gradients occurring during continuous two phase flow in small diameter vertical conduits.
J. Pet. Tech., pp.475-484, Trans. AIME, p.234, 1965.

H12. Hughmark, G.A.
Heat transfer in horizontal annular gas liquid flow.
Chem. Engng. Progress Symp. Ser. No. 57, Vol. 61, Heat transfer-Boston.

H13. Hewitt, G.F.
Disturbance waves in annular two phase flow.
Fluid Mech. Measur. Two Phase flow systems.
Proc. Inst. Mech. Engrs, 1969-70, Vol. 184, Pt. 3C, pp.142-150, paper 18.

H14. Hughmark, G.A.
Film thickness, Entrainment and pressure drop in upward annular and dispersed flow.
AIChE J, Vol. 19, No. 5, pp.1062-1065, 1973.

H15. Hughmark, G.A.
Holdup and heat transfer in horizontal slug gas-liquid flow.
Chem. Engng. Sci., Vol. 20, pp.1007-1010, 1965.

H16. Hubbard, M.G.
An analysis of horizontal gas liquid slug flow.
Ph.D. thesis, Univ. of Houston, Texas, 1965.

H17. Hubbard, M.G. and Dukler, A.E.

Flow model for horizontal gas-liquid slug flow.

Paper presented at the 65th National Meeting of the AIChE, Tampa, Fla., 1968 (quoted in G1).

H18. Hooker, H.H. and Popper, G.F.

A Gamma-ray attenuation method for void fraction determination in steam-water mixtures.

ANL-5766, 1958.

H19. Harms, A.A. and Forrest, C.F.

Dynamic effects in radiation diagnosis of fluctuating voids.

Nuclear Sci. Engng. Vol.46, pp.408-413, 1971.

H20. Hutchinson, P. and Whalley, P.B.

A possible characterisation of entrainment in annular flow.

A.E.R.E. - R7126.

H21. Hannan, E.J.

Time series analysis.

Science paperbacks and Methuen and Co. Ltd., 1960.

H22. Happel, J.

J. Appl. Phys., Vol. 28, pp.1288-1292, 1957.

I1. Ishagai, S., Yamane, M. and Roko, K.

Measurement of the component flows in a vertical two phase flow by making use of the pressure fluctuation.

Bull. J.S.M.E., Vol. 8, No. 31, pp.375-390, (1965).

I2. Ishii, M. and Grolmes, M.A.
Inception criteria for droplet entrainment in two phase co-current film flow.
AIChE J, Vol. 21, No. 2, pp.308-318, 1975.

I3. Isbin, H.S., Rodriguez, H.A., et al.
Void fractions in two phase flow.
AIChE J, Vol. 5, No. 4, pp.427-432, 1959.

J1. Johnson, H.A. and Abou-Sabe, A.H.
Heat transfer and pressure drop for turbulent flow of air/water mixtures in a horizontal pipe.
Trans. A.S.M.E., vol. 74, pp.977-987, 1952.

J2. Johannessen, T.
A theoretical solution of the Lockhart and Martinelli flow model for calculating two phase pressure drop and holdup.
Int. J. Heat and Mass Transfer, Vol. 15, pp.1443-1449 (1972).

J3. Jones, O.C. Jr. and Zuber, N.
The inter-relation between void fraction fluctuating and flow patterns in two phase flow.
HTFS 1772, March 1974.

J4. Jepsen, J.C.
Mass transfer in two phase flow in horizontal pipelines.
AIChE J, Vol. 16, No. 5, pp.705-711, 1970.

K1. Kotohiko, Sekoda, Sato, Y. and Kariya, S.

Horizontal two phase air water flow characteristics in the disturbed region due to 90° bend.

J. Soc. Mech. Eng. 1969, 35(289), 2227-2233,

NEL TT2237.

K2. Kosterin, S.I.

An investigation of the influence of the diameter and the position of a tube on the hydraulic resistance and the structure of flow of gas/liquid mixtures.

IZV.AKAD, NAUK, Obd. Tekh. Naut. No. 12 (1949) pp.1824-1831, HTFS. 6802.

K3. Krasiakova, L.I.

Some characteristics of the flow of a two phase mixture in a horizontal pipe.

Zhur. Tekh. Fiz., Vol. 22, No. 4 (1952) pp.654-669. Soviet Technical Phys. (translated).

K4. Knowles, C.R.

The effect of flow patterns on pressure loss in multiphase horizontal flow.

M.Sc. Thesis, Univ. of Texas, Austin (1965),

H.T.F.S. 13549.

K5. Kozlov, B.K.

Regimes and types of flow for an air/water mixture in vertical tubes.

Styrikovich "Hydrodynamics and heat transfer during boiling in high pressure boilers". pp.7-18. Moskow Akad. Nauk, SSSR (1955): Translation A.E.C. tr-4490.

K6. Kodirka, A.A.

Two phase heat transfer with gas injection through a porous boundary surface.

ANL-6862, 1964. (quoted in C3).

K7. Kutateladze, S.S., Nakoryakov, V.E., et al.

Spectral characteristics of vertical two phase flow.

Soviet physics-Doklady, Vol. 16, No. 9, March 1972, pp.718-719.

K8. Kordyban, E.S. and Ranov, T.

Mechanism of slug formation in horizontal two phase flow.

Trans. A.S.M.E.J. Basic Engng., pp.857-864, 1970.

K9. Kordyban, E.

The transition to slug flow in the presence of large waves.

Brief Communication M.F. 129(L) - pp.1-5.

K10. Kordyban, E.

Interfacial shear in two phase wavy flow in closed horizontal channels.

J. Fluids Engng., Vol. 96, p.97, 1974.

K11. Kordyban, E.S.

A flow model for two phase slug flow in horizontal tubes.

J. Basic Engng. Transaction of ASME, pp.613-618, 1960.

K12. Knudsen, J.G. and Katz, D.L.

Fluid dynamics and heat transfer.

McGraw-Hill Book Co., New York, 1958 (quoted in G1).

L1. Lockhart, R.W. and Martinelli, R.C.
Proposed correlations of data for isothermal two phase, two component flow in pipes.
Chem. Engng. Prog. Vol. 45. No. 1, pp.39-48 (1949) (HTFS61)..

L2. Lunde, K.E.
Heat transfer and pressure drop in two phase flow.
Chem. Engng. Symp. Ser. Vol. 57, No. 32 (1961), pp.104-110.

L3. Lackme, C.
Some statistical properties of two phase flow in vertical tubes.
Proc. Symp. on two phase flow, Univ. of Exeter, (1965), paper D201-213, Vol. II.

L4. Levy, S.
Prediction of two phase pressure drop and density distribution from mixing length theory.
Trans. ASME, J. Heat Transfere, May 1963, pp. 137-152.

L5. Levy, S.
Steam slip - theoretical predictions from momentum model. J. of heat transfer, Trans. A.S.M.E., pp.113-124, May 1960.

L6. Lawson, J.D. and Brill, J.P.
A statistical evaluation of methods used to predict pressure losses for multiphase flow in vertical oil well tubing.
J. Petroleum Tech., pp.903-914, Aug. 1974.

L7. Levy, S.

Theory of pressure drop and heat transfer for annular steady state two phase, two component flow in pipes.

Second Midwestern Conf. Fluid Mech. Ohio State Univ. Columbus, Ohio, 1952, proc. p.337 (quoted in G1).

L8. Levy, S.

Prediction of two phase annular flow with liquid entrainment.

Int. J. Heat Mass Transfer, Vol. 9, pp.171-188, 1966.

L9. Littlefield, T.A. and Thorley, N.

Atomic and nuclear physics.

Van Nostrand Comp. Ltd., 2nd edition, 1968.

M1. Mologin, M.A.

Types of flow of gas/liquid mixtures in horizontal pipes.

Dokl. Akad. Nauk. SSSR, Vol. 94, No. 5, (1954) pp.807-810, AERE LIB/TRANS. 479.

M2. Mandhane, J.M., Gregory, G.S. and Aziz, K.

A flow pattern map for gas/liquid flow in horizontal pipes.

Int. J. Multi-phase Flow, Vol. 1, No. 4, pp. 537-553 (1974).

M3. McAdams, W.H., et al.

Vaporisation inside horizontal tubes. II. Benene-oil mixtures.

Trans. ASME, Vol. 64, p.193, 1942.

M4. Martinelli, R.C. and Nelson, D.B.

Prediction of pressure drop during forced circulation boiling of water.

Trans. ASME, Vol. 70, 1948, pp.695-702.

M5. Muscettola, M.

Two phase pressure drop - comparison of the 'Momentum exchange model and Martinelli and Nelson's correlation with experimental measurements.

A.E.E.W.-R 284, UKAEA - Reactor Group, 1963.

M6. McManus, H.N. Jr.

Local liquid distribution and pressure drops in annular two phase flow.

ASME paper No. G1-HYD-20.

M7, Moeck, E.O. and Stachiewicz, J.W.

Droplet interchange model for annular-dispersed, two phase flow.

Int. J. Heat Mass transfer, Vol. 15, pp.637-653, 1972.

M8. Moussalli, G. and Chawla, J.M.

Void fraction and pressure drop in bubbly flow.

Paper presented at the 1974 European Two Phase Flow Conference.

M9. McComas, S.T.
J. Basic Eng., Trans. ASME, Scr. D., Vol. 89, p.847, 1967, (quoted in G1).

M10. McComas, S.T. and Eckert, E.R.G.
J. Appl. Mech., Trans. ASME, Ser. E, Vol. 30, p.765, 1965, (quoted in G1).

M11. Maddock, C., Lacey, P.M.C. and Patrick, M.A.
The structure of two phase flow in curved pipe. Inst. Chem. Engrs. Symp. Ser. No. 38, Multiphase flow systems, Symposium held at the Univ. of Strathclyde, Vol. II, paper J2, pp.1-21.

M12. Martinelli, R.C., Boelter, M.K., et al.
Isothermal pressure drop for two-phase two-component flow in a horizontal pipe. Trans. ASME, pp.139-151, Feb. 1944.

N1. Nishikawa, K., Sekoguchi, K. and Sukano, T.
Relationship between pulsating pressure and flow pattern in upward two phase flow. Bull. J.S.M.E., Vol. 12, No. 54, pp.1410-1416 (1969).

N2. Neal, L.G. and Bankoff, S.G.
A high resolution resistivity probe for determination of local void properties in gas/liquid flow.
A.I.Ch.E.J., Vol. 9, No. 4, p.490, 1963.

N3. Newland, D.E.
An introduction to random vibrations and spectral analysis. Longman 1975.

O1. Oliver, D.R. and Wright, S.J.

Pressure drop and heat transfer in gas/liquid slug flow in horizontal tubes.

Brit. Chem. Engng., Vol. 9, No. 9, pp.590-596 (1964).

O2. Orkiszewski, J.

Predicting two phase pressure drops in vertical pipe.

J. Pet. Tech., pp.829-838, Trans. AIME, p.240, 1967.

O3. Ower, E. and Pankhurst, P.C.

The measurement of air flow.

Pergamon Press, 1966.

O4. Overman, R.T. and Clark, H.M.

Radioisotope Techniques.

McGraw-Hill, 1960.

O5. Otnes, R.K. and Enochson, L.

Digital time series analysis.

John Wiley and Sons, 1972.

P1. Petrick, M.

Two phase air-water flow phenomena.

ANL 5787, 1958.

P2. Poettmann, F.H. and Carpenter, P.G.

The multiphase flow of gas, oil and water through vertical flow strings with application to the design of gas lift installations.

Drill. and prod. pract. API (1952), 257.

P3. Parzen, E.

Mathematical considerations in the estimation of spectra.

Technometrics, Vol. 3, pp.167-190, 1961.

Q1. Quandt, E.R.

Analysis of gas/liquid flow patterns.

Chem. Engng. Symp. series, Vol. 61, No. 57, 1965.

R1. Richardson, B.L.

Some problems in horizontal two phase two component flow.

Argome National Lab. Report No. ANL-5949 (1958).

R2. Reid, R.C., Reynolds, A.B., et al.

Two phase pressure drop in large diameter pipes.

A.I.Ch.E.J., Vol. 3, No. 3, pp.321-324 (1957).

R3. Rooney, D.H., Bradford, A.M. and Cornwell, R.S.

Void fraction and friction effects in horizontal steam/water flows.

Multiphase flow systems, Symposium. The Institute of Chem. Engrs. Symp. Series No. 38, Vol. II, Paper No. 33, Univ. of Strathclyde.

R4. Ros, N.C.J.

J. Petrol. Technol., Vol. 13, p.1037, 1961.

(quoted in G1).

R5. Russell, T.W.F., Etchells, A.W., et al.
Pressure drop and hold up in stratified gas-liquid flow.
AIChE J, Vol. 20, No. 4, pp.664-669, 1974.

R6. Russell, T.W.F. and Lamb, D.E.
Flow Mechanism of two phase annular flow.
Can. J. Chem. Engng., Vol. 43, pp.237-245, 1965.

S1. Simpson, H.C., Rooney, D.H., et al.
Flow patterns in two phase flow Part 1: literature survey and design recommendations for gas liquid flows in closed channels.
HTFS DR 41, AERE-R8120, Sept. 1975.

S2. Sekoguchi, K., Sato, Y., and Kariyaraki, A.
The influences of mixers, bends and exit sections on horizontal two-phase flow.
Proc. Int. Symp. in co-current gas/liquid flow.
Univ. of Waterloo (Sept. 1968) (HTFS 6214).
Also in Trans. Jap. Soc. Mech. Eng. 1969, 35(279), 2234-2242, N.E.L.T.T 2235.

S3. Soliman, H.M. and Azer, N.Z.
Visual studies of flow patterns during condensation inside horizontal tubes.
5th Int. Heat Transf. Conf. Tokyo (1974), paper CS 1.6, Vol. III, pp.241-245.

S4. Sakaguchi, T., Akagawa, K., et al.
Transient behaviour of air/water two phase flow in a horizontal tube.
A.S.M.E. Preprint No. 73-WA/HT-21 (1973).

S5. Schicht, H.H.
Flow patterns for an adiabatic two phase flow of water and air within a horizontal tube.
VERAH. TECH. Vol. 3, No. 4, (1969), pp.153-163.
C.E.G.B., C.E. Transl. No. 5472 (1971).

S6. Scott, D.S.
Properties of co-current gas/liquid flow.
Advances in Chem. Engng. Vol. 4, pp.199-277, 1963.

S7. Sato, T., Minamiyama, T.,
Study of heat transfer in boiling two phase channel flow. Part 1. Flow patterns in a boiling channel.
Heat transfer Japanese Res. No. 4. pp.1-30 (1972).

S8. Soliman, H.M. and Azer, N.Z.
Flow patterns during condensation inside a horizontal tube.
A.S.H.R.A.E. Trans. Vol. 77, part 1, pp.210-224, (1971).

S9. Simpson, H.C., Rooney, D.H. and Callander, T.M.S.
Transient effects in two phase bubbly down flow.
European two phase flow meeting, Harwell 3rd-7th June, 1974.

S10. Simpson, H.C., Rooney, D.H.

Depressurisation effects on a Freon 113 circulating loop.

Paper No. A3, European two phase flow group meeting, Erlanger, 31st May-4th June, 1976.

S11. Sternling, C.V.

Lecture to meeting of A.I. Chem. E. Dec. 1965 (quoted in C1).

S12. Smith, S.L.

Void fractions in two phase flow: A correlation based upon an equal velocity head model.

Proc. Inst. Mech. Engrs. Vol. 184. Pt. 1, No. 36, pp.647-664, 1969-1970.

S13. Sher, N.C. and Green, S.J.

Boiling pressure drop in thin rectangular channels.

Chem. Engng. Prog. Symp. Ser. 55(23). pp.61-71, 1959.

S14. Smith, T.N. and Tait, R.W.F.

Interfacial shear stress and momentum transfer in horizontal gas liquid flow.

Chem. Eng. Sci. Vol. 21, p.63, 1966.

S15. Schlichting, H.

Boundary layer theory.

McGraw-Hill Book Co., New York, 1968.

S16. Shaw, R.

The measurement of static pressure

J. Fluid Mech., Vol. 7, p.550, 1960.

S17. Sterling, C.V.

Lecture to meeting of AIChE (Dec. 1965). Quoted in Cl.

S18. Smith, A.V.

A fast response multi-beam X-ray absorption technique for identifying phase distributions during steam water blowdowns.

J. Br. Nucl. Energy Soc., Vol. 14, pp.227-235, 1975.

S19. Simpson, H.C. and Rooney, D.H.

Void Fraction prediction under saturated conditions.

NEL Report No. 386.

S20. Simpson, H.C., Rooney, D.H., et al.

Flow pattern and pressure drop studies.

Report No. 1: Results from phase 1 tests.

Report No. 2: Results from phase 2 tests.

Report No. 3: Results from phase 3 tests.

Report No. 4: Concluding report on flow pattern and pressure drop studies in large diameter tubes.

Submitted in accordance with Research Contract RD/1065/014 to the Department of Industry (National Engineering Laboratory).

S21. Simpson, H.C., Rooney, D.H., et al.

Two phase flow in large diameter horizontal tubes.

Paper A6, European Two Phase Flow Group Meeting, Grenoble, 6th-9th June 1977.

S22. Sande, G.

On an alternative method for calculating covariance functions.

Princeton Computer Memorandum, Princeton, N.J.

T1. Taitel, Y. and Dukler, A.E.

A model for predicting flow regime transitions in horizontal and near horizontal gas/liquid flow.

A.I.Ch.E., J. Vol. 22, No. 1, pp.47-55, 1976.

T2. Tong, L.S.

Boiling heat transfer and two phase flow.

Wiley and Sons, 1965.

T3. Traviss, D.P. and Rohsenow, W.M.

Flow regimes in horizontal two phase flow with condensation.

A.S.H.R.E. J., April 1973, pp.31-39.

T4. Turner, J.M. and Wallis, G.B.

Report No. NYO-3114-6, 1965 (quoted in W1).

T5. Taitel, Y. and Dukler, A.E.

A theoretical approach to the Lockhart-Martinelli correlation for stratified flow.

Brief Communication: MF 76-P.P.1-5.

T6. Thom. J.R.S.

Prediction of pressure drop during forced circulation boiling of water.

Int. J. Heat Mass transfer, Vol. 7, pp.709-724, 1964.

T7. Turner, J.M.

Ph.D. thesis, Dartmouth College, Hanove , N.H., 1966 (quoted in W1).

V1. Van Thanh Nguyen and Spedding, P.L.

Two phase flow: The concept of semiparity and equivalent transport properties of fluids.

A.I.Ch.E. J, Vol. 19, No. 3, pp.652-654, 1973.

V2. Vermeulen, L.R. and Ryan, J.T.

Two phase slug flow in horizontal and inclined tubes.

Can. J. Chem. Engng., Vol. 49, pp.195-201, 1971.

W1. Wallis, G.B.

One dimensional two phase flow.

McGraw Hill Comp., 1969.

W2. White, P.D. and Huntingdon, R.L.

Horizontal cocurrent two phase flow of fluids in pipelines.

The Petroleum Engr., Vol. 27, No. 9, (1955), D10-D45.

W3. Wallis, G.B. and Dobson, J.E.

The onset of slugging in horizontal stratified air/water flow.

Int. J. Multiphase Flow., Vol. 1, No. 1, pp.173-193 (1973).

W. Weisman, J. and Choe, W.G.

Methods for calculation of pressure drop in cocurrent gas liquid flow.

Paper presented at "Two phase flow and heat transfer symposium - Workshop". Ft. Lauderdale, Florida 1976.

W5. Wicks, M. III, and Dukler, A.E.

Entrainment and pressure drop in cocurrent gas-liquid flow. 1. Air-water in horizontal flow.

A.I.Ch.E. J., Vol. 6, No. 3, p.463, 1960.

W6. Whalley, P.B., Hewitt, G.F. and Hutchinson, P.

Experimental wave and entrainment measurements in vertical annular two-phase flow. Symposium on Multi-phase flow systems, Univ. of Strathclyde, Paper A1, I. Chem. E. Symp. Series No. 38 (1974).

Y1. Yagi, S. and Kato, Y.

Chem. Eng. (Japan), 18, 2, (1954) (quoted in I3).

Z1. Zahn, W.R.

A visual study of two phase flow while evaporating in horizontal tubes.

Trans. A.S.M.E. J. Basic Engng., Vol.86, pp.417-429 (1964).

Z2. Zuber, N. and Findlay, J.A.

Average volumetric concentration in two phase flow systems.

Trans. A.S.M.E. J. Heat Transf., Vol. 87, Series C, pp.453-468, 1965.

Z3. Zuber, N., Staub, F.W., et al.

Steady state and transient void fraction in two phase flow systems - final report for the program of two phase flow investigation.

Vol. I, II, GEAP-5417, Jan. 1967.

U.S. Atomic Energy Commission Contract AT(04-3) - 189, Project Agreement 35.